The rates and mechanisms of Fe(II) oxidation in a passive vertical flow reactor for the treatment of ferruginous mine water

A thesis submitted for the Degree of Doctor of Philosophy

By

Andrew Barnes, BSc(Hons), MSc

School of Engineering, Cardiff University.

September 2008

ProQuest LLC
789 East Eisenhower Parkway
P.O. Box 1346
Ann Arbor, MI 48106-1346

DECLARATION

This work has not previously been accepted in substance for any degree and is not concurrently submitted in candidature for any degree.

Signed ..... (candidate) Date 24/4/09

STATEMENT 1

This thesis is being submitted in partial fulfilment of the requirements for the degree of PhD (insert MCh, MD, MPhil, PhD etc, as appropriate)

Signed ..... (candidate) Date 24/4/09

STATEMENT 2

This thesis is the result of my own independent work/investigation, except where otherwise stated.
Other sources are acknowledged by explicit references.

Signed ..... (candidate) Date 24/4/09

STATEMENT 3

I hereby give consent for my thesis, if accepted, to be available for photocopying and for inter-library loan, and for the title and summary to be made available to outside organisations. 4/4/09

Signed ..... (candidate) Date 24/4/09

STATEMENT 4: PREVIOUSLY APPROVED BAR ON ACCESS

I hereby give consent for my thesis, if accepted, to be available for photocopying and for inter-library loans **after expiry of a bar on access previously approved by the Graduate Development Committee.**

Signed ..... (candidate) Date 24/4/09

Acknowledgements

I would like to thank Professor Keith Williams, Dr Devin Sapsford and Dr Matt Dey for their continuous support throughout this period of study. I would also like to thank my parents, family and partner, without whom I wouldn't have got this far. I would also like to thank Jeffery Rowlands and Ravi Mitha whose assistance has been essential throughout.

Abstract

This thesis presents the methodology and results of research undertaken into the rates and mechanisms of iron oxidation both in field and laboratory environments. The field based aspects of the research entailed the collection and analysis of hydrological, hydrogeochemical, and mineralogical data from two parallel treatment systems. Both systems were treating identical ferruginous, circum-neutral, coal-mine drainage, from the Taff Merthyr site, South Wales. During this study a novel pilot scale passive Vertical Flow Reactor (VFR) was trialled against a conventional settlement lagoon and the performance of both systems was compared.

The second research aspect focuses on the determination of heterogeneous Fe(II) oxidation rates under laboratory conditions. Experiments were carried out under varying pH, and catalytic surface concentration and type. An analytical method was developed which allowed for the determination of both dissolved and sorbed Fe(II).

The results of the field study have shown that the VFR system is capable of removing Fe at a rate greatly in excess of a conventional settlement lagoon. This therefore drastically reduces the treatment area required. In addition, due to the heterogeneous method by which the VFR operates (passing mine-water down through a bed of ochre solid), highly efficient manganese removal was also achieved.

The laboratory study has shown that significant catalysis of Fe(II) oxidation can be achieved under mildly acidic pH conditions making Fe(II) oxidation (and therefore passive mine-water treatment) feasible under these conditions. Evidence is also presented for the adsorption of non-oxidisable Fe(II) onto Fe(III) (hydroxy)oxides under mildly-acidic pH conditions. A comparison was then made between field and laboratory results and a conceptual model was produced to describe the observed adsorption and oxidation characteristics.

I. Table of Contents

II. List of Tables

III. Table of Figures

1 Introduction

In anoxic surface and ground waters both Fe and Mn are stable in solution and are mobilised as the reduced divalent Fe(II) and Mn(II) ions over a very broad pH range. On mixing with oxic waters, or equilibration with atmospheric oxygen, oxidation of the divalent ions to the sparingly soluble Fe(III) and Mn (III,IV) forms leads to the precipitation of voluminous oxides and (hydroxy)oxides (termed (hydroxy)oxides here). Although not toxic in the conventional sense, Fe and Mn are pollutants because the (hydroxy)oxides can be detrimental to aquatic ecosystems smothering the fauna and flora. Dissolved Fe and Mn also implants a metallic taste in drinking-water, and precipitation of Fe(III) and Mn(III,IV) (hydroxy)oxides can lead to furring of domestic and industrial water supply pipe and staining of laundry. For these reasons it is preferable to remove dissolved Fe and Mn from contaminated waters prior to further use, or release into the environment.

Cardiff University has developed a treatment system for the removal of contaminants (principally Fe and Mn), from polluted waters. The Vertical Flow Reactor system (VFR) harnesses the processes of auto catalysis via "ochre accretion" and auto filtrationto enhance natural attenuation processes.

This thesis describes the methods employed and presents the results collected, during the operation of a field scale VFR pilot plant. The VFR is located at the Taff Merthyr mine water treatment wetland in South Wales, UK. In addition the results of a parallel laboratory study are also presented. The laboratory study attempts to increase the understanding of the mechanisms of heterogeneous Fe oxidation.

1.1 Thesis aims

This thesis is written to read conventionally. However the study was split primarily into two sections running in parallel.

These were, firstly:

- the design and operation of a pilot scale, field based, mine water treatment system, and secondly;
- a laboratory investigation into the rates and mechanisms of iron oxidation within such a treatment system.

For this reason the thesis is split into field based and laboratory based work.

1.1.1 Field investigation aims

These were to:

- document the design and construction of a field scale VFR system,
- present the results of the physical, mineralogical and geochemical characterisation of the VFR and lagoonal ochre precipitates,
- present the results collected from the performance and geochemical monitoring of the field scale VFR pilot plant,
- compare the performance of a VFR system to that of a conventional settlement lagoon, treating identical mine waters,
- detail the longevity and performance constraints of a VFR system, and
- discuss the VFR performance in terms of Fe and Mn oxidation and removal rates.

1.1.2 Laboratory investigation aims

These were to:

- present the results from a series of laboratory based experiments looking at the mechanisms of heterogeneous iron oxidation,
- identify the mechanisms involved in heterogeneous oxidation of iron, and
- compare laboratory rates and mechanism with those identified in the field VFR.

1.2 Organisation of the thesis

Chapter 2 describes both active and passive treatment principles. This focuses primarily on treatment systems for iron removal having a direct influence on the development of the VFR system. The chemistry of minewater generation is also discussed with particular emphasis on the Taff Merthyr site.

Chapter 3 describes the geochemistry of Fe, particularly relevant to the mine water environment which is compared, where possible, to Mn geochemistry. Particular focus is lent to the redox chemistry of iron.

Chapter 4 gives an account of the VFR design, construction and operation.

Chapter 5 details the field monitoring and analysis methods employed during the monitoring of the VFR pilot plant and Taff Merthyr lagoons.

Chapter 6 details the methods used in the characterisation of the ochre precipitates collected from the VFR pilot plant and Taff Merthyr lagoons.

Chapter 7 presents the results of the physical, geochemical and mineralogical characterisation of the VFR pilot plant and Taff Merthyr settlement lagoonal ochre.

Chapter 8 presents the results of the performance monitoring of the VFR pilot plant and Taff Merthyr settlement lagoons. Details are given of the hydrological and geochemical performance. The results are then discussed in terms of system longevity and contaminant removal rates.

Chapter 9 details the methods employed during the laboratory investigation into the geochemical mechanisms of homogeneous and heterogeneous Fe oxidation.

Chapter 10 presents the results obtained of the geochemical mechanisms of iron oxidation in the laboratory. The results are then discussed in terms of iron

adsorption and oxidation of adsorbed iron species. An attempt is then made to compare laboratory mechanisms with those of the VFR field reactor.

Chapter 11 present the conclusion and recommendation for future work compiled from the current study.

2 Treatment principles for iron and manganese removal

2.1 Introduction

This chapter briefly discusses mine water pollution in terms of its causes and consequences. It then discuses the aspects of mine water chemistry and in particular the ranges of chemical characteristics reported. Particular attention is paid to the hydrogeochemical characteristics of the abandoned Taff Merthyr colliery site, South Wales, UK, as this is the chosen location for the mine water treatment system trialled in the current study. Finally it deals with the treatment principles of mine water clean-up with particular emphasis on "passive" treatment of circum-neutral ferruginous mine drainage relevant to the current study.

Section 2.2: The mine water problem – gives a brief description of minewater generation and the problems faced by mine water pollution in terms of environmental impacts and treatment.

Section 2.3: Mine water chemistry – gives a brief overview demonstrating the varied nature of mine water pollution and the problems this causes in devising passive treatment options. The minewater chemistry of the Taff Merthyr site is then discussed in caomparisonto other UK coal mine waters.

Section 2.5: Treatment principles – outlines the basic treatment principles for treatment of polluted mine drainage.

Section 2.6: Treatment technologies – describes the passive treatment technologies relevant to the current VFR project.

2.2 The mine water problem

Acid Mine Drainage (AMD) and Acid Rock Drainage (ARD) are terms used to describe water that has been acidified, and polluted with metals and sulfate during sulfide mineral oxidation (principally pyrite). In many cases (but not always, as the polluted drainage can be from natural erosion and weathering) the causes of the pollution are anthropogenic, with the exposure of pyrite to oxidising environments through mining activity (both historic and current). The term ARD is therefore preferred to encompass both anthropogenic and natural sources.

AMD and ARD imply that the drainage is "acidic". This can be misleading as, in many cases, pyrite mineralisation can be hosted in, or underlie carbonate rocks (especially in coal deposits in which the depositional environment is such that coal beds are interbedded with marine limestone's and carbonate rich clastic rocks). Dissolution of carbonate rocks adds a degree of acid buffering capacity (determined experimentally as alkalinity), to the surrounding groundwater. This acts to neutralise the acidity produced during pyrite oxidation producing sulfate and metaliferous waters with circum-neutral pH. In these circumstances, typical of UK coal mine drainage, the term "mine water pollution" is used to encompass polluted waters issuing from mine (including coal mine) sources.

The causes and consequences of mine water pollution have been intensely studied over the past thirty years since the problem was first acknowledged in the USA in the 1970's. Up to this point pollution was rarely an issue and was a "fact of life". The type locality for historic mining pollution in the European Union (EU) is the Rio Tinto region in the south west of Spain.

UK mining has a legacy of some 2000 years (since Roman occupation). However, since the start of the industrial revolution in the 17th Century, a significant increase in mine production (both metal and coal) coupled with a lack of knowledge and regulation of environmental and human impacts, has resulted in extensive, un-tempered mine water pollution. Living with the

impacts of mine water pollution in the UK was a way of life in former mining communities with ochre stained and biologically barren rivers being common place.

Since the 1980s, increasing emphasis has been placed on the cleanup of the UK river systems as a result of public, Non Government Organisation (NGO) opposition. This has resulted regulatory change and the implementation of numerous projects to treat polluted mine water discharges and to introduce a "polluter pays" policy (absent from the UK mining industry up to 31-12-1999) to help prevent and control future pollution incidents.

Recently a number of regulatory publications have been issued regarding mine water pollution in the USA (Hedin et al, 1994; EPA, 2000), Canada (MEND, 1996), and the EU (PIRAMID, 2003; Betlem et al, 2004).

2.3 Mine Water generation and evolution

2.3.1 Overview of mine water generation

Mine water discharges are the result of rebounding groundwater after the cessation of dewatering pumping at mine sites. Dewatering is necessary in the majority of mines as it is common place to exploit mineral reserves that are found at or below the water table. In the cases where dewatering is necessary significant drawdown of the water table will occur in the localised area forming a cone of depression around the mine site. The maximum depth of the water table during pumping will be governed by the mine sump. In the case of coal mine depression of the water table is not always localised as coal deposits generally occur within regional coal fields. In these examples many collieries may be actively dewatering in which case several cones of depression may overlap and the cessation of pumping at one colliery may not necessarily mean that the groundwater will recover fully.

Most mineral resources (with the exception of diamonds and iron ore) occur alongside accessory sulfide minerals formed under reducing conditions (be this in carboniferous swamps or in hydrothermal fluids). During mine

dewatering metal sulfide minerals are exposed to atmospheric oxygen and oxidise to releasing sulfate and metals in to solution. By far the most common metal sulfide mineral is pyrite (FeS_2) which upon oxidation release dissolved Fe(II), sulfate and acidity into solution (the mechanisms of this are discussed further in Section 2.4.1). Further oxidation of dissolved Fe(II) and precipitation of Fe(III) (hydroxy)oxides leads to the generation of further acidity.

2.3.2 Mine water generation at the Taff Merthyr colliery

The Taff Merthyr colliery was one of the last deep mines to be developed in the South Wales coalfield. Sinking of the two 580m deep shafts was begun in 1922 by the Taff Merthyr steam coal company. These were completed in 1924 and production commenced in 1926. Extraction was from the Seven Feet seam but later deepening of the two shafts to 640m in 1974 lead to mining of the Five Feet Gellideg seam (this was later abandoned in 1988, Welsh Coal Mines, 2009; and references therein). The Taff Merthyr colliery was one of the most productive in South Wales and on the 30th of October 1992, after much public opposition, was the last of the British Coal Boards deep mines to close. Demolition was completed in 1994 (Coal Authority, 2002)

Mining was by way of long wall methods which lead to large areas of fractured roof rock and localised reactivation along historic fault sections. The generalised geology of the coal measures include the coal measures themselves, overlying seat earths (often with root systems), overlying siltstones and shale's. The shale's and siltstones are often pyritic as are the coal measures which begin to oxidise on exposure to atmospheric oxygen.

Opperational dewatering of the Taff Merthyr colliery lead to localised depression of the water table and was accompanied by a more regional depression within the South Wales coalfield area. After the downturn of the UK coal industry, mine closures lead to the cessation of dewatering and a generalised regional groundwater rebound (see Figure 2-1).

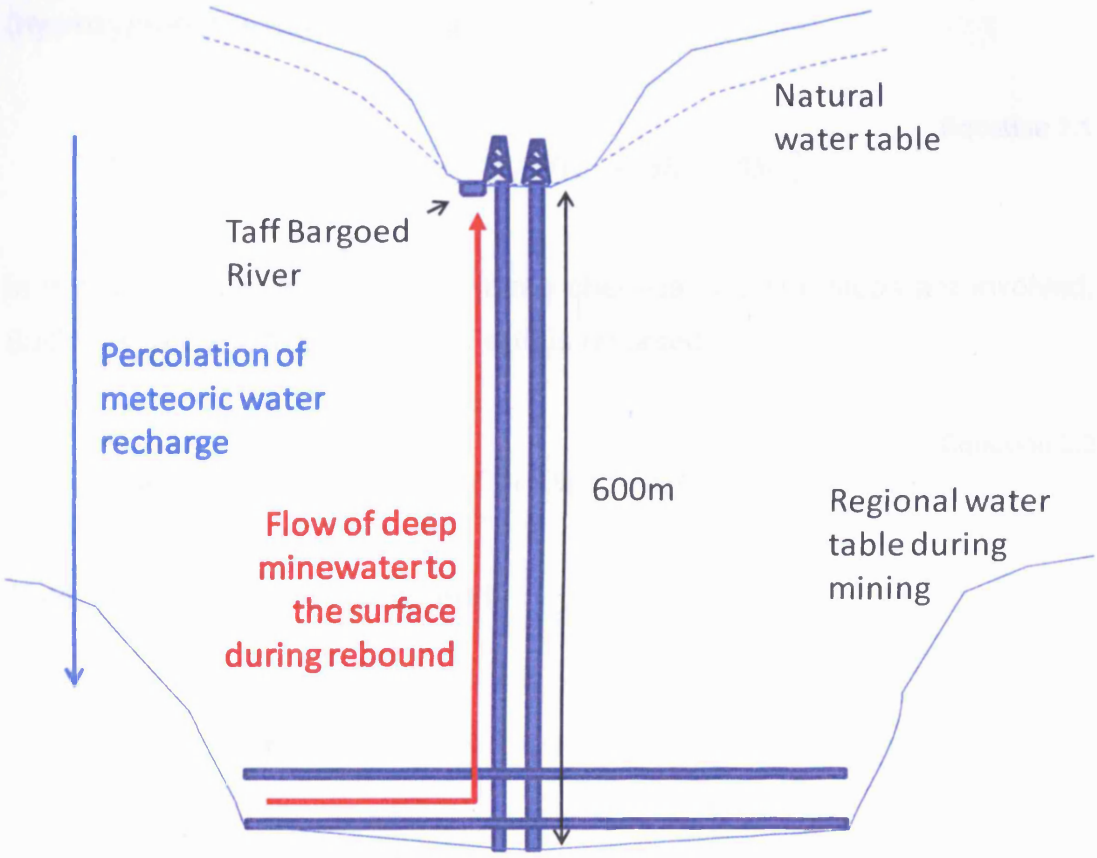

Figure 2-1: Schematic cross section of the Taff Merthyr colliery showing mine water characteristics

At Taff Merthyr dewatering continued until 1992 and surface discharges were not evident until November 2004. Rebound of the water table led to mine water breakthrough with ferruginous circum-neutral water discharging at a combined flow rate up to 120 L sec^{-1} from two culverts draining the capped shafts (Coal Authority, 2002).

2.4 Mine water chemistry

2.4.1 Sulfide oxidation

Oxidation of sulfide occurs in all sulfide minerals on exposure to oxygen. However, it is only the oxidation of pyrite (FeS_2) (the most common metal sulfide) that is net-acid producing forming ARD. Above a pH of ~ 3, Fe(III) hydrolyses and precipitates as Fe(III) oxides, hydroxides, and oxyhydroxides

(termed simply Fe(III) (hydroxy)oxides from this point forward). The overall reaction for the oxidation of pyrite and the precipitation of Fe as Fe(III) (hydroxy)oxides is (Langmuir, 1997):

Equation 2.1

$$4FeS_2 + 15O_2 + 10H_2O \rightarrow 4FeOOH_{(S)} + 16H^+ + 8SO_4^{2-}$$

In this overall reaction, a total of three chemical reaction steps are involved. Sulfide is oxidised to sulfate and Fe(II) is released:

Equation 2.2

$$2FeS_2 + 7O_2 + 2H_2O \rightarrow 2Fe^{2+} + 4SO_4^{2-} + 4H^+$$

Secondly Fe(II) is oxidised to Fe(III):

Equation 2.3

$$4Fe^{2+} + O_2 + 4H^+ \rightarrow 4Fe^{3+} + 2H_2O$$

Finally Fe(III) precipitates as Fe(III) (hydroxy)oxide:

Equation 2.4

$$Fe^{3+} + 2H_2O \rightarrow FeOOH_{(S)} + 3H^+$$

As shown in Equation 2.1, the overall reaction is net-acid generating producing 4 moles of protons for every mole of pyrite oxidised. This results in an overall acidification of the system. Below a pH of 3, dissolved concentrations of Fe(III) become significant and precipitation of Fe(III) (hydroxy)oxides (as shown in Equation 2.4) becomes negligible. At this pH the Fe(III) ion takes over as the primary sulfide oxidising agent in accordance with the following reaction:

Equation 2.5

$$FeS_2 + 14Fe^{3+} + 8H_2O \rightarrow 15Fe^{2+} + 2SO_4^{2-} + 16H^+$$

In the absence of bacteria (Sapsford, 2003 and references therein) and below pH 6, the reaction shown by Equation 2.3 proceeds extremely slowly. As Equation 2.3 is the rate determining step the replenishment of the Fe(III)

"pool" would in theory cease. However, acidophilic bacteria (such as *Thiobacillus* ferroxidans, Herbert, 1999) are capable of rapidly oxidising Fe(II) to Fe(III) under these conditions and therefore the reaction can continue.

2.4.2 Neutralisation reaction

Acidity produced during the oxidation of pyrite can effectively be consumed by the dissolution of some mineral constituents (see Bowell et al, 1997). Although Fe and Mn secondary mineral phases (e.g. goethite and ferrihydrite) are highly effective acidity regulators around pH 3 (Langmuir, 1997), Ca and Mg carbonate minerals are the only phases capable of readily neutralizing acidity and producing a mine water of circum-neutral pH.

The higher the concentration of CO_3 dissolved within the mine water, the higher is the capacity of the mine water to resist pH change due to the addition of protons (Stumm and Morgan, 1996). A measure of the pH buffering capacity is generally determined by an acid titrationto a set pH which is termed "alkalinity". Alkalinity is generally measured as the concentration of $CaCO_3$ required to react completely with the amount of added acid (for example, mg L^{-1} as $CaCO_3$).

2.4.3 Net-alkalinity and net-acidity

If a particular mine water's measured alkalinity is greater than the mine waters calculated acidity (see Hedin et al, 1994), then the mine water can be classified as net-alkaline (PIRAMID, 2003). Vice versa, if a mine waters measured alkalinity is lower than the calculated acidity, the mine water is net-acidic. The acidity of the mine water can be calculated in accordance with Hedin et al (1994) as follows:

Equation 2.6

$$Acidity_{calc} = 50\left[\left(\frac{2Fe^{2+}}{56}\right)+\left(\frac{3Fe^{3+}}{56}\right)+\left(\frac{2Mn}{55}\right)+\left(\frac{3Al^{3+}}{27}\right)+\left(1000e^{-pH}\right)\right]$$

where $Acidity_{calc}$ is the calculated acidity in mg L^{-1} as $CaCO_3$. In this way, a net-acid mine water can be initially circum-neutral in pH if its load of Fe and Mn is in the reduced form. This is generally the case for circum-neutral mine-waters where micro-aerobic conditions persist at the mine portal. On exposure to atmospheric O_2, oxidation of the reduced Fe (and Mn) in accordance with Equation 2.3 leads to precipitation of Fe(III) (hydroxy)oxides and associated production of acidity as shown in Equation 2.4. The inherent buffering capacity measured titrimetrically as "alkalinity" is then consumed by the acidity produced.

2.4.4 Mine Water Chemistry at the Taff Merthyr site

Table 2-1 give the average mine water chemistry determined at the distribution weir of the Taff Merthyr treatment scheme. The data was collected during the duration of the current study over a two year period and the raw data is given in Appendix 2.2. The Taff Merthyr minewater is of circum-neutral, net alkaline type with moderate concentrations of iron and manganese but does not contain any other elements of concern. Iron concentrations have decreased from an Initial high of 25 mg/L in 1994 (Coal Authority, 2002).

Table 2-1: Average mine water composition recorded at the distribution weir to the Taff Merthyr site

Analyte	Units	Mean value	SD
Temperature	°C	11.62	± 0.57
pH		6.93	± 0.23
Eh	mV	170.4	± 40.79
Ec	μScm^{-1}	797.0	± 69.98
Dissolved O_2	mg L^{-1}	3.5	± 0.93
Alkalinity	mg L^{-1} as $CaCO_3$	244.18	± 9.08
SO_4^{2-}	mg L^{-1}	226.33	± 21.35
Fe(II)	mg L^{-1}	6.33	± 1.26
Filtered Fe	mg L^{-1}	8.89	± 1.26
Total Fe	mg L^{-1}	9.51	± 2.87
Filtered Mn	mg L^{-1}	0.8	± 0.08
Total Mn	mg L^{-1}	0.82	± 0.08
Ca	mg L^{-1}	101.58	± 8.18
Mg	mg L^{-1}	42.11	± 2.66
K	mg L^{-1}	13.04	± 1.3
Na	mg L^{-1}	15.87	± 1.85
Si	mg L^{-1}	4.78	± 0.44
Sr	mg L^{-1}	0.59	± 0.13

2.4.5 Comparison of Taff Merthyr and other minewater's

The average Taff Merthyr minewater determined in the current study (see Table 2-1) has been compared to chemistries of other minewater's from the South Wales, Scotland and Durham coalfields. This was done to determine how representative Taff Merthyr is of typical mine water discharges and if the use of the Taff Merthyr site was justified in this respect.

Figure 2-2 compares net alkalinity (calculated in accordance with Hedin et al, 1994) and pH determined at 82 sites across the UK. These have been sub-divided in to their representative coalfield. Taff Merthyr is indicated separately as a red diamond.

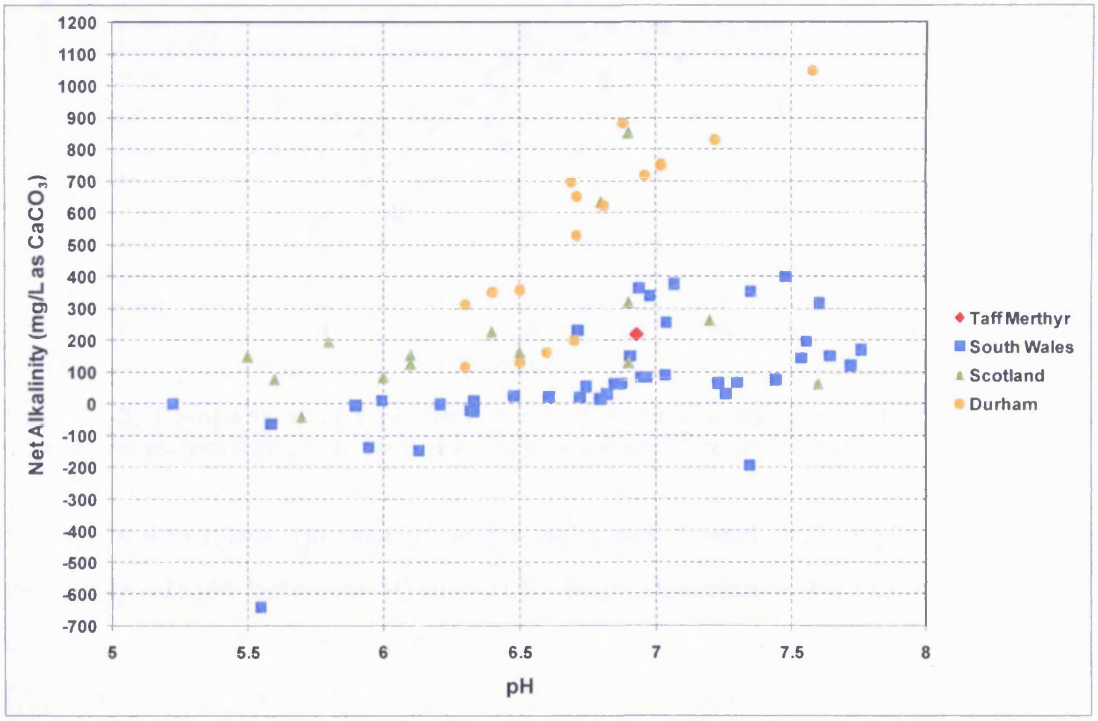

Figure 2-2: Comparison of pH and Net Alkalinity in Taff Merthyr and other mine waters (data courtesy of Ben Rees personal communication)

It is evident that the range of pH conditions determined for most emerging coal mine waters lies between 5.5 to 8 (circum-neutral to mildly acidic). Also with the exception of 9 sites, all are net-alkaline. It is also evident that the Durham sites are generally lower pH and alkalinity and the Scottish sites are generally higher alkalinity. The South Wales sites generally exist within a fairly

narrow alkalinity range but exhibit pH conditions that span the two observed extremes.

Figure 2-3 compares total iron and sulfate concentrations within the same group of samples. It is evident that a fairly log: log linear relationship exists between these two parameters.

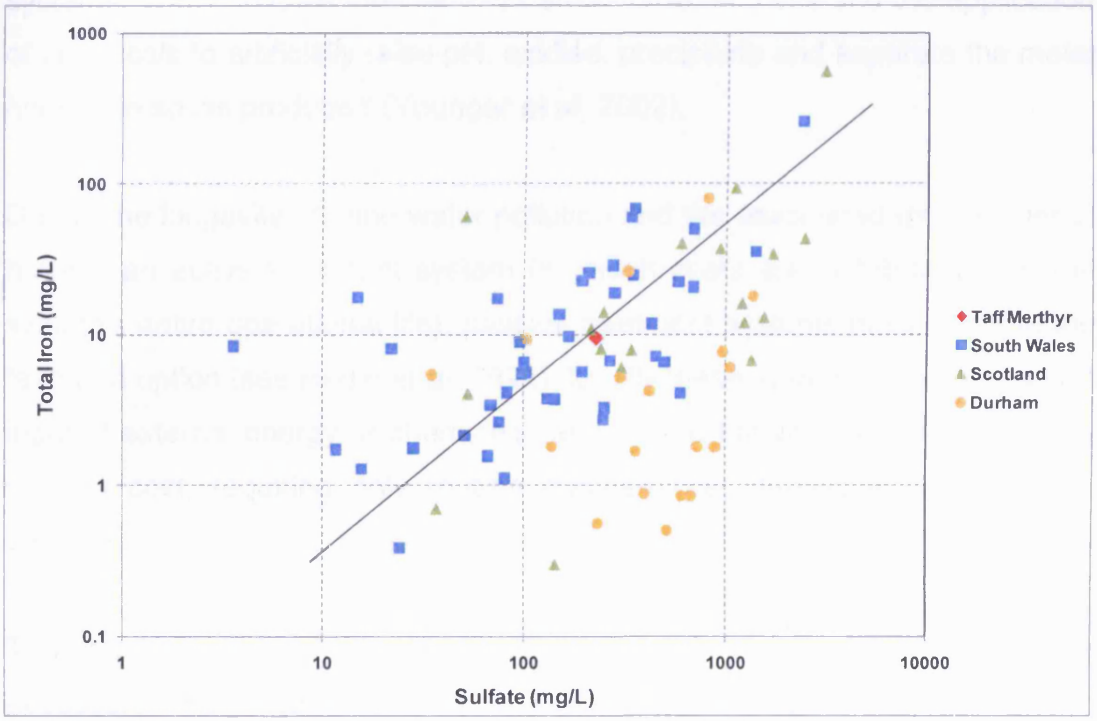

Figure 2-3: Comparison of total iron and sulfate concentrations in Taff Merthyr and other mine waters (data courtesy of Ben Rees personal communication)

Iron concentrations generally range between 1 and 100 mg/L and sulfate generally ranges between 10 and 2000 mg/L. Generally the Durham coalfield lies outside of this trend with a general high sulfate / low iron range. The Scottish mines generally show the highest sulfate and generally high iron contents.

Based on the key environmentally sensitive parameters of Fe, pH, alkalinity, and sulfate (as well as Mn) the Taff Merthyr site is representative of a wide range of coal mine water chemistries within the UK.

2.5 Treatment principles

Due to the varied chemistry of mine drainage, the design of treatment systems is generally undertaken on a site specific basis. Treatment can be "active", "passive" or "hybrid" (incorporating elements from either active or passive technologies). Until the 1990's all proven technologies for the treatment of mine drainage were, what is now called "active treatment" systems. These involve the use of external power sources and the application of chemicals to artificially raise pH, oxidise, precipitate and separate the metal hydroxide solids produced (Younger et al, 2002).

Due to the longevity of mine water pollution and the associated expenditure of running an active treatment system (in which costs are distributed over the system's entire operational life), passive treatment systems have become the favoured option (see Hedin et al, 1994). Ideally these systems have no human input of external energy or chemicals, and should theoretically have very low running cost, requiring only routine maintenance, de-sludging and sludge disposal.

True passive systems should ideally rely solely on gravity to supply the necessary energy for treatment and any chemical agent (e.g. limestone, compost etc) is placed in the system during construction and only requires periodic replacement. Hybrid systems incorporate feature of both passive and active treatment. For instance the Ynysarwed system in south Wales (UK) is an example of a hybrid system using active treatment to remove the bulk of the metal load and to add alkalinity. However this system discharges into an aerobic reed-bed wetland for final polishing of the effluent.

There are also numerous examples of predominantly passive treatment systems that use pumps to raise the raw mine water (known as pumped-passive systems) to a level where passive treatment can be undertaken under gravity flow. Examples of pumped passive systems can be seen at Taff Merthyr in south Wales, Whittle in England and Cuthil in Scotland (see Coal Authority, 2002). There are also examples of largely passive systems where

external chemical dosing is employed for either pH modification or for chemical oxidation.

Generally, for net acid waters an initial treatment step is required in which the pH of the minewater is increased (if the mine water is initially acidic), and in which additional alkalinity is added to the system. This is usually undertaken by contacting the minewater with carbonate rock (usually limestone). This dissolves into the water increasing the inherent buffering capacity.

Several systems are generally used for this (PIRAMID, 2003; and references therein):

- Compost wetlands and subsurface sulfate reducing systems – use of organic substrate to precipitate metal contaminates as sulfides. Alkalinity is also increased due to the action of Sulfate Reducing Bacteria (SRB) which metabolise SO_4^{2-} and release HCO_3^-.
- Oxic Limestone drains (OLDs) – minewater flows through an open channel containing crushed limestone.
- Reducing and Alkalinity Producing Systems (RAPS) – minewater flows down through a bed of organic substrate (usually compost) and then passes through an underlying bed of crushed limestone. The organic substrate reduces Fe(III) to Fe(II) preventing "armouring" of the limestone substrate (as discussed in the following section).
- Anoxic Limestone Drains (ALDs) – the minewater discharge is sealed from the atmosphere at source and passes through a limestone bed sealed from the atmosphere.
- Permeable Reactive Barriers (PRBs) – groundwater contaminated with ARD is passed through a buried trench containing reactive material (such as compost and limestone) to add alkalinity.

After passing through one of (or a sequence of) these systems, the minewater should (ideally) be both net-alkaline and have a circum-neutral pH.

Passive treatment to remove the contaminant load is now relatively simple, and examples of the common technologies are (PIRAMID, 2003):

- Aerobic wetland – a system of (usually) constructed wetlands planted with reed beds. Treatment principles are primarily to slow down the water flow and allow settling of Fe, Mn and other metals precipitated as hydroxides. The reed beds also act as filters sifting suspended particulates. Some attenuation of dissolved contaminants is also achieved by direct root uptake.
- Settlement lagoons – large constructed basin which allows water velocities to decrease to a point where settlement of particulate Fe and Mn precipitates is possible. These systems are commonly placed upstream of constructed wetlands for upfront Fe removal and to extend the lifetime of the constructed, aerobic wetland.
- Surface Catalysed Oxidation Of Ferrous Iron (SCOOFI) – SCOOFI systems use the autocatalytic oxidation of Fe(II) (as discussed in section 3.8) to oxidise Fe(II) to Fe(III) and "accrete" the resulting precipitate to the surface of existing oxide. The system uses high surface area support media on which the reaction takes place.
- Sand filters – sand filters have frequently been used for removing Fe and Mn from potable water supplies. However, they are not generally used in the treatment of minewater due to maintenance costs and frequencies.

Of these treatment systems, those most relevant to the VFR systems will be discussed in detail in section 2.6.

2.5.1 Reporting of treatment system performance

2.5.1.1 Hydraulic retention time

The Hydraulic Retention Time (HRT) is the measure of the average length of time that a unit of liquid remains in a body of liquid. HRT is related to the flow rate of effluent through a water body by the following equation:

Equation 2.7

$$HRT = \frac{V}{Q}$$

Where HRT is the hydraulic retention time in units of time, V is the pore volume of the water body in units of volume, and Q is the volumetric flow rate in units of volume over time. In mine water treatment scenarios HRT is used to describe the average amount of time that a unit of mine water remains in a treatment system of a certain volume. The HRT required differs markedly for different treatment systems especially between active and passive systems as the retention time required for passive treatment is far greater than that required for active treatment. In accordance with Equation 2.7 this equates to a much larger volume and due to the nature of passive treatment systems, the volume can only be delivered by increasing the surface of the treatment area and not its depth. Therefore, the selection of an active treatment option is usually only undertaken when the implementation of a passive treatment system is not feasible due to the chemistry of a particular discharge or due to the large land take and possibly considerable costs incorporated into the construction of a passive system.

2.5.1.2 Area adjusted contaminant removal rates

The most common way of reporting treatment system performance is using an area-adjusted contaminant removal rate (R_A) as devised by Hedin et al (1994). This is simply the mass of a contaminant removed per unit area per unit time and is most commonly reported as g m^{-2} day^{-1} (PIRAMID, 2003). The use of R_A values are also indispensable in the design of passive treatment systems as they offer a robust method of wetland sizing using values stipulated by Hedin et al (1994) from monitoring of a range of passive wetland systems in the USA. For known raw-mine water flow rates, contaminant loadings and target concentrations, the sizing formula in the general form reported by Younger et al (2002) can be used:

Equation 2.8

$$A = \frac{Q_d(C_i - C_t)}{R_A}$$

where A is the required wetland area (m^2), Q_d is the mean daily flow rate (m^3 day^{-1}), C_i is the mean daily influent contaminant concentration (mg L^{-1}), C_t is the concentration of contaminant in the final discharge (mg L^{-1}) and R_A is the area-adjusted contaminant removal rate (g m^{-2} day^{-1}). The R_A value used in the calculation will be dependent on the chemistry of the discharge and the chosen treatment system. R_A values do not give an indication of the total contaminant removal as a very high R_A value can be attained for systems that discharge well above required discharge limits but have a very high initial contaminant load or that treat very high flows. It is important that R_A values are reported with ancillary information such as treated and untreated contaminant concentrations or untreated contaminant concentrations and % removal.

Application of R_A values for Fe removal allows easy comparison of different system's performance and is often used directly in system sizing. Hedin et al (1994) gave values of 10 g m^{-2} day^{-1} for wetland systems that were to meet regulatory guideline values for Fe discharge concentrations and 20 g m^{-2} day^{-1} for systems where only "reasonable improvement" is required. However, due to the large variation in mine water chemistry and the associated variation in Fe oxidation, settling and removal rates can only really be transferred across like for like systems. For instance Hedin et al (1994) found a range of R_A values between 6 and 42 g m^{-2} day^{-1} over a sample of 6 wetlands indicating inconsistencies in passive wetland performance due to site specific issues. Reported R_A values for Mn removal are generally in the range of 0.5 to 1 g m^{-2} day^{-1} (Hedin et al, 1994) using conventional aerobic wetlands.

2.6 Treatment technologies relevant to the VFR system

To date a number of government-led initiatives have driven studies to be undertaken to determine the feasibility and design of passive treatment systems. The most important publications are (from Canada) Mine Environment Neutral Drainage (MEND) review of passive systems for mine site drainage (MEND, 1996) and (from the EU) the Passive In-situ Remediation of Acidic Mine / Industrial Drainage (PIRAMID), Engineering

guidelines for the passive remediation of acidic and/or metaliferous mine drainage and similar wastewater (PIRAMID, 2003).

This section will give a brief overview of treatment technologies relevant to the current research. Therefore, emphasis is given to the treatment of ferruginous mine waters using only passive technologies.

2.6.1 Settlement lagoons and aerated reed-bed wetlands

Settlement lagoons and aerobic (reed-bed) wetlands are widely used for the treatment of circum-neutral, net-alkaline, ferruginous mine water by the removal of the Fe load as Fe(III) (hydroxy)oxides. Although these treatment systems are only effective at treating, net-alkaline mine waters, this can include mine waters that have previously passed through a RAPS, ALD, or OLD (or equivalent) systems (see section 2.4.3).

Aerobic reed-bed wetlands are suitable for the polishing of ferruginous mine waters with Fe concentrations less than 5 mg L^{-1} (PIRAMID, 2003). At concentrations greater than this, reed growth may be inhibited, and / or the reed-bed will rapidly clog due to precipitation of ochre (Fe(III) (hydroxy)oxides). For concentrations of Fe greater than 5 mg L^{-1}, up-front Fe removal is advised in the form of a settlement lagoons designed such that the discharging mine water has a total Fe concentration below 5 mg L^{-1}.

2.6.1.1 Settlement lagoon sizing

Sizing of settlement lagoons is commonly done using one of three "rule of thumb" guidelines (PIRAMID, 2003). These are:

- using a nominal HRT of 48 hours,
- sizing based on 100 m^2 of lagoon per L sec^{-1} of mine water flow, and
- assuming an iron removal rate of 10 g m^{-2} day^{-1}.

In addition, the UK Coal Authority (see Parker, 2003) has identified a linear relationship between the percentage reduction in influent iron concentration and the nominal HRT as follows:

Equation 2.9

$$\%Fe_{removed} = 2HRT$$

where %Fe is the % reduction in the inlet Fe concentration across the system and HRT is the hydraulic retention time in hours.

2.6.1.2 Applicability to Cardiff University's VFR system

The VFR system is designed as an upfront Fe remover and it is hoped that this system alone should, in some circumstance, be able to fully replace the conventional settlement lagoons and aerobic reed bed wetland configuration. In addition, the Taff Merthyr mine water treatment system in South Wales (UK) is the chosen site for the installation of a field-scale VFR treatment system. At this site, mine water is currently treated by up-front settlement lagoons followed by a series of aerobic reed bed wetlands (Coal Authority, 2002). This site is therefore ideal for performance comparisons to be made between these two systems.

2.6.2 Reducing and Alkalinity Producing Systems (RAPS)

First described by Kepler and McCleary (1994), RAPS (formally termed Sequential Alkalinity Producing Systems (SAPS)) are design to add alkalinity and raise the pH of net-acid mine waters by the dissolution of carbonate mineral and by the release of bicarbonate by Sulfate Reducing Bacteria (SRB) (PIRAMID, 2003).

Conventionally, a RAPS system is constructed as a vertical flow system in which the mine water flows down through a compost layer prior to flowing through a limestone gravel bed (see Figure 2-4). The compost layer is designed to create strongly reducing conditions in which all oxygen is consumed and Fe(III) is reduced to Fe(II). The compost layer should be between 0.15 and 0.6 m in thickness (Watzlaf et al, 2003) and can be

composed of an assortment of materials (for example, municipal waste compost, cow manure and straw etc, see PIRAMID, 2003 and references therein).

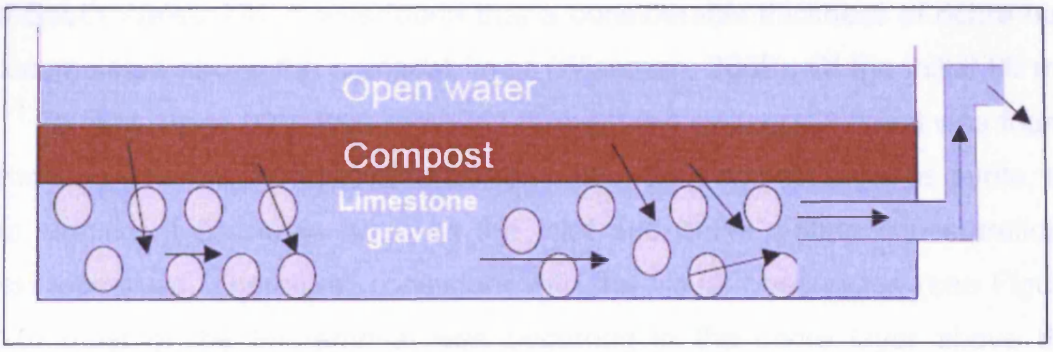

Figure 2-4: Schematic cross section through a conventional RAPS system. (after PIRAMID, 2003)

The primary purpose of the compost layer in a RAPS system is to reduce the dissolved Fe(III) load to Fe(II) in order to prevent "armouring" of the reactive limestone media as pH is elevated. The limestone layer is ideally 0.5 to 1 m thick (PIRAMID, 2003 and references therein) and composed of 25 to 50 mm particles.

Although conventionally RAPS systems are constructed as layered systems (see Figure 2-4), a number of different configurations have been trialled. These included a system in which the gravel and compost constituents are completely mixed (e.g. Younger et al, 2003), and where the compost and gravel layers are side by side (e.g. Jarvis and England, 2002).

RAPS sizing is usually based on a hydraulic retention time in the gravel layer. A limestone layer hydraulic retention time of approximately 14 hours is recommended (PIRAMID, 2003 and references therein).

2.6.2.1 Removal of iron as Fe(III) (hydroxy)oxides in RAPS systems

As mentioned previously, RAPS systems are designed primarily to add alkalinity and increase pH and secondly to remove metals (including Fe) as sulfides. Some RAPS systems, particularly those used to treat circum-neutral

(although net-acidic) mine water have been found to remove Fe as Fe(III) (hydroxy)oxides on the surface of the compost bed. An example of a RAPS system operating in this manner is the Whitworth A RAPS at the Pellena site in South Wales, UK. It was found that a considerable thickness of ochre had accumulated above the compost layer (Wiseman, 2002). Of the initial 60 mg L^{-1} Fe load, up to 90% was removed through the system. Of this it was found that only minimal Fe removal occurred within the compost layer as pyrite, as no significant decrease between the inlet and outlet sulfate concentrations was observed. Therefore, consistent with the visual observation (see Figure 2-5) most of the Fe removal was occurring in the ochre layer above the compost.

Figure 2-5: Whitworth A RAPS system showing ochre precipitation on compost surface

2.6.2.2 Permeability restraints of RAPS systems

Due to the potential for the permeability of a RAPS system to decrease with time a freeboard of greater than 1.5 m is recommended (Younger et al, 2002). In the case of a RAPS system that is actively precipitating Fe as Fe(III) (hydroxy)oxides above the compost layer, the permeability is likely to

decrease much more rapidly (e.g. Dey and Williams, 2000; Reilly, 2001) as the ochre is likely to have a much lower hydraulic conductivity than the compost substrate. Dey and Williams (2000) showed the lifetime of the Whitworth A RAPS system would be markedly reduced by ochre precipitation.

2.6.2.3 Applicability to the VFR system

The design concept for the VFR treatment system described within this thesis (see Dey et al, 2003) is based on observations made of the Whitworth A RAPS. It is thought that the ochre layer above the RAPS compost substrate acts to remove Fe by the process of ochre accretion (Burke and Banwart, 2002) and similar in concept to the "SCOOFI" process (Younger, 2000; Jarvis and Younger, 2001) as described in section 2.6.4.

2.6.3 Sand filters for iron and manganese removal

Slow sand filters have been used for the treatment of water for potable supplies since the turn of the 19th century and have demonstrated successful treatment of waters with naturally elevated levels of Fe and Mn (Huisman and Wood, 1974). The design, construction and operation of slow sand filters is covered in detail by Huisman and Wood (1974) and the basic design is shown in Figure 2-6.

The basic design of a sand filter is an under-drained fine sand bed on a gravel support through which raw water is passed under gravity. A supernatant water reservoir is kept above the filter bed to allow for fluctuations in flow and to provide the necessary driving head. The filter bed in a potable water supply system is highly biologically active with the surface layer developing a "Schmutzdecke", (a gelatinous biofilm matrix of bacteria, fungi, protozoa, Rotifera and Diatoms) which acts to break down organic contaminants and micro filter particulates. Downward flow velocities in fine sand filters are normally between 0.1 and 0.4 m hr^{-1}.

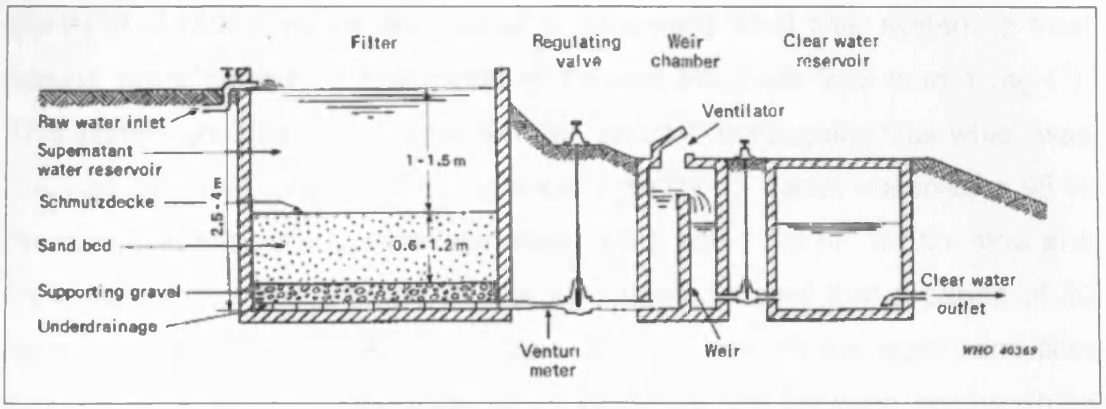

Figure 2-6: Schematic of a typical slow sand filter (from Huisman and Wood, 1974)

Rapid sand filters or "roughing" filters are built to the same general design as the slow sand filter shown in Figure 2-6 but use a larger grade sand (usually 0.5 to 3 mm diameter) and downward flow velocities are 20 – 50 times faster than slow sand filters. Rapid sand filters are capable of removing Fe and Mn from water actively (by filtration of Fe and Mn (hydroxy)oxide flocs formed during active aeration and lime addition) but also passively by autocatalytic and possibly microbial oxidation (see Søgaard et al, 2000). The existences of Gallionealla like stalks were clearly evident in electron-micrographs of the recovered filter cake. As will be discussed in Chapter 3, the influence that the microbial catalysed Fe(II) oxidation has on the overall Fe(II) oxidation rate is not clear. Although effective at removing Fe (and to some extent Mn), the high backwash frequency of rapid sand filters is too frequent to be used for conventional passive treatment of mine water.

2.6.3.1 Small scale sand filters for iron and manganese removal

The problem of Fe and Mn in potable supplies in the developing countries has led to the installation and trial of small scale sand filters for use with hand pumps (see Andersson and Johansson, 2002 and references therein). Andersson and Johansson (2002) compared up-flow and down-flow filter systems of these types. Using up front "trickle-tray" aerators they showed promising results at circum-neutral pH, with up to 95 % total Fe removal with a residence time of 60 minutes and dissolved O_2 concentrations less than 3.5 mg/L.

Pacini et al (2005) trailed the use of a composite sand filter system to treat natural water containing low levels of Fe and Mn (both less than 1 mg l^{-1}). This system consisted of a trickle aerator, an up-flow roughing filter which was followed by either slow sand or rapid sand filtration. Pacini observed a 95 % removal efficiency with vertical velocities of 0.5 and 12 m hr^{-1} for the slow and rapid sand filters respectively. It was also demonstrated that a period of 30 days for the up-flow roughing filter and 15 - 30 days for the rapid sand filter and 90 days for the slow sand filters could be left between backwashing (however this would be reduced in moderate to high Fe situations). The rapid sand filter used in a Danish potable water treatment plant as studied by Søgaard et al (2000), treated 10 mg l^{-1} of Fe at a vertical velocity of 11.6 m hr^{-1}. This plant required a backwash frequency of 28 hr.

2.6.3.2 Applicability to the VFR system

Sand filters used for the removal of Fe and Mn from potable water supplies function in an almost identical fashionto the current VFR system. However, the VFR system does not contain a sand filter. Instead it uses a gravel support and relies exclusively on auto-filtration of ochre particulates and "ochre accretion" (Burke and Banwart, 2002) in Fe removal.

2.6.4 Ochre accretion and SCOOFI systems for Fe removal

In the UK there are many examples of near acid to circum-neutral mine water discharges (see Section 2.4.5 and Banks et al, 1997). Banks et al (1997) observed that ochre deposition in the receiving watercourses was generally continuous and extensive, despite there being no suspended ochre in the water column. The preferential precipitation of ochre (mainly Fe(III) (hydroxy)oxides) on surfaces is thought to be due to adsorption of Fe(II) onto pre-existing ochre particles, followed by rapid "auto-catalytic" oxidation forming new solid. This mechanism has been termed "ochre accretion" by Burke and Banwart (2002).

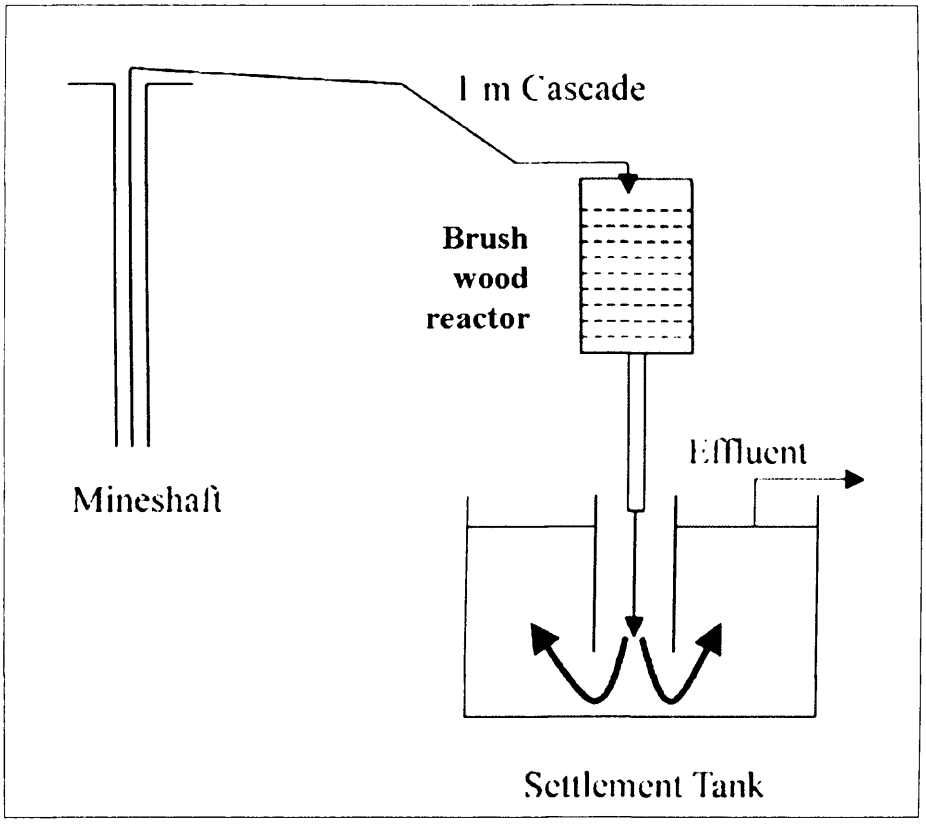

Figure 2-7: Schematic of Best and Aikmans treatment system as used at Kames colliery (taken from Burke and Banwart, 2002; as described by Best and Aikman, 1983)

An early study by Best and Aikman (1983), attempted to harness the process of ochre accretion for mine water treatment. They used a reactor filled with brush wood as a high surface area medium (see Figure 2-7). Mine water was then allowed to flow vertically through this, under unsaturated conditions.

In a system developed by Younger (2000), the process of ochre accretion was adapted for use under both saturated (Younger, 2000) and unsaturated (Jarvis and Younger, 2001) flow conditions. The generic system was termed "SCOOFI" (the Surface Catalysed Oxidation Of Ferrous Iron). In SCOOFI reactors, high surface area media, for example, limestone gravel, steel slag or commercial trickling filter media can be used as support media. Accretion of ochre onto the support media acts to present a highly catalytic surface for the oxidation of Fe(II) that has been adsorbed from the passing mine water. A more detailed discussion of the rates and mechanism of Fe(II) oxidation, catalysed by Fe(III) (hydroxy)oxide surfaces is given in Section 3.8.

Geochemical modelling of an unsaturated SCOOFI reactor was attempted by Burk and Banwart (2002). They used the geochemical modelling code Steadyql (Furrer et al, 1989; 1990) and described the adsorption of Fe(II) to the accreting ochre surface using the surface species described by Zhang et al (1992). A second order rate constant as stipulated by Wehrli (1990) (using the results of Tamura et al 1976b) was used to model the oxidation rate of the Fe(II) surface species.

2.6.4.1 Applicability to the VFR system

The SCOOFI process harnesses "ochre accretion" to enhance the Fe(II) oxidation rate. This mechanism is also used in the VFR system. However, the SCOOFI and VFR systems differ in the way the accreting ochre is supported. In the SCOOFI system, ochre accretes around a high surface area support medium (e.g. steel slag, trickling filter media) whilst in the VFR system the ochre is self supporting and the available surface area is not limited to the surface area of the support media.

3 Iron oxidation chemistry

3.1 Introduction

Iron forms the most abundant transition metal in the earth's crust at 5 wt% (Hem, 1963). However, at circum-neutral pH and in most oxic surface waters the dissolved concentration of Fe does not reflect its crustal abundance. This is due to the low solubility of the hydrolysis products of its stable oxidised forms.

The abiotic oxidation of Fe(II) by dissolved oxygen can proceed along two parallel pathways, firstly homogeneous oxidation in a solution containing no surfaces, and secondly via heterogeneous oxidation in a suspension. Under these conditions the Fe(II) oxidation rate is highly pH dependant with the half life varying from minutes at pH 7 to years at pH 2. Under conditions of low pH or low concentrations of oxygen where the abiotic rate is low, the reaction may be greatly accelerated by the presence of lithotrophic bacteria that facilitate the reaction. Also the presence of mineral surfaces and especially Fe(III) (hydroxy)oxides can have a catalytic effect on the reaction rate under conditions where solute surface interactions are favourable.

Several previous authors have reviewed the literature of Fe(II) oxidation kinetics (Sung and Morgan, 1980; Davison and Seed, 1983; Millero 1985; Wehrli 1990; Stumm and Sulzberger, 1992; Stumm, 1997). However, there is a vast pool of recent work that has not been compiled. This chapter critically reviews the extensive back catalogue of literature and data on the subject of Fe(II) oxidation with specific emphasis on heterogeneous abiotic oxidation kinetics and mechanism. The emphasis is to drive the discussion relative to Cardiff University's VFR mine water treatment system. This is designed to use heterogeneous catalysis of Fe(II) oxidationto enhance its Fe removal performance.

The chapter is organised into the following sections:

Section 3.2: The Hyber Weiss cycle and oxygen reduction – gives an overview of the role dissolved oxygen plays in the oxidation reactions of Fe(II).

Section 3.3: Abiotic homogeneous Fe(II) oxidation – discusses the rates and mechanisms of homogeneous Fe(II) oxidation and gives details of rate expressions devised by previous authors.

Section 3.4: Iron (and manganese) hydrolysis – describes the characteristics of dissolved Fe and Mn hydrolysis and the effects hydrolysis has on the oxidation kinetics (and redox potential) of dissolved iron.

Section 3.5: Fe ligand complexes – discusses the effects various ligand's have on the oxidation kinetics of Fe(II)

Section 3.6: Homogeneous kinetic consideration of Fe(II) oxidation in mine water scenarios – describes the passive treatment technologies relevant to the current VFR project.

Section 3.7: Interfacial chemistry of Fe(II) on metal (hydroxy)oxide surfaces – summarises the solid / liquid interfacial process including, adsorption, Interfacial Electron Transport and surface charge effects.

Section 3.8: Surface catalysed oxidation of Fe(II) – describes the rates and mechanisms discussed in the literature for abiotic heterogeneous Fe(II) oxidation

Section 3.9: Microbial Fe(II) oxidation – summarises the microbial Fe(II) oxidation process in mine water treatment scenarios.

Section 3.10: Chapter summary.

3.2 The Hyber Weiss cycle and oxygen reduction

Oxygen is the most prevalent oxidising agent in the natural environment. For this reason it is most often harnessed in mine water treatment for the oxidation of Fe(II) (and Mn(II)) to Fe(III) which precipitates rapidly at circum-neutral pH (between pH 5 and 8) as sparingly soluble Fe(III) (hydroxy)oxides.

The stoichiometry for the oxidation of Fe(II) by aqueous O_2 to Fe(III) (hydroxy)oxide (FeOOH), is in accordance with the reaction proposed by Stumm and Lee (1961):

Equation 3.1

$$4Fe(II) + O_2 + 6H_2O \leftrightarrow 4FeOOH + 8H^+$$

in which reduction of each mole of O_2 consumes four moles of electrons. This is in accordance with the reaction sequence proposed by Haber and Weiss (1934):

Equation 3.2

$$[a]...O_2 + e^- \leftrightarrow O_2^{\bullet -}$$
$$[b]...O_2^{\bullet -} + e^- \leftrightarrow H_2O_2$$
$$[c]...H_2O_2 + e^- \leftrightarrow HO^{\bullet} + H_2O$$
$$[d]...HO^{\bullet} + H^+ + e^- \leftrightarrow H_2O$$

in which the rate determining step was confirmed by Wehrli (1990) to be the initial reduction of O_2 by Fe(II) (step a). Wehrli (1990) calculated the reduction potentials of the four reduction steps of O_2 from standard E° data from Bielski et al (1985), and Sawyer and Valentine (1981). This showed that, because the super-oxide radical is a powerful reducing agent (Table 3.1), and therefore the first reduction step from the di-oxygen molecule to the super-oxide radical is endergonic.

Table 3.1: Values of E°, ΔG° and Log K for the one electron steps in the reduction of $O_{2(aq)}$

Reaction	Oxygen species formed	E° [a] Volts	ΔG° [b] kJ mol^{-1}	Log K [b]
$[a]...O_2 + e^- \leftrightarrow O_2^{\bullet -}$	Superoxide radical	-0.16	15.5	-2.7
$[b]...O_2^{\bullet -} + e \leftrightarrow H_2O_2$	Hydrogen Peroxide	1.72	-165.9	29.1
$[c]...H_2O_2 + e \leftrightarrow HO^{\bullet} + H_2O$	Hydroxyl radical / Water	0.99	-95.3	16.7
$[d]...HO^{\bullet} + H^+ + e \leftrightarrow H_2O$	Water	2.53	-244.9	42.9

[a] *Standard electrode potentials E_H° (V) calculated from Gibbs free energy change of the reaction ΔG° (J mol^{-1}) values reported in Stumm and Morgan (1996) using relationship $E_H^{\circ} = \Delta G^{\circ}/nF$ where n is the charge number of the reaction and F is the Faraday constant.*
[b] *Values from Stumm and Morgan (1996) Table 11.1.*

3.3 Abiotic homogeneous Fe(II) oxidation

The abiotic oxidation of Fe(II) by dissolved O_2 can proceed along two parallel pathways, firstly via homogeneous oxidation in solution and secondly via heterogeneous oxidation in association with mineral surfaces. Kinetics of homogeneous Fe(II) oxidation are known to be highly pH dependant (Stumm and Lee, 1961; Singer and Stumm, 1968; Tamura et al, 1976a; Sung and Morgan, 1980; Davison and Seed, 1982; Millero, 1985; Millero et al, 1987).

3.3.1 Empirical Fe(II) oxidation rate laws

At circum-neutral pH, the empirical rate law shown in Equation 3.1 has been most commonly verified for synthetic solutions (Stumm and Lee, 1961; Singer and Stumm, 1970; Ghosh, 1974; Tamura et al, 1976a; Millero et al, 1987), fresh lake water (Davidson and Seed, 1983) and seawater (Kester et al, 1975). It has been demonstrated that the reaction is first order with respect to [Fe(II)] and pO_2 and second order with respect to $\{OH^-\}$.

This is shown in the following equation:

Equation 3.3

$$R = \frac{-d[Fe(II)]}{dt} = k_{pOH}[Fe(II)]pO_2\{OH^-\}^2$$

where R is the oxidation rate in M sec^{-1}, [ ] signifies concentration (M), pO_2 is the partial pressure of O_2 (atm), $\{OH^-\}$ signifies the OH^- ion activity in M and k_{pOH} is the rate constant in M^{-2} atm^{-1} sec^{-1}. In the previous works listed above (excluding Sung and Morgan, 1981, who used OH^- ion concentration converted using a calculated value of the activity coefficient), OH^- activity was used to derive rate constants. This was calculated from experimentally determined pH (usually determined using a glass electrode and NBS buffer system) using Equation 3.4:

Equation 3.4

$$\{OH^-\} = \frac{K_w}{\{H^+\}}$$

where K_w is the temperature dependant dissociation constant for water (Davison and Seed, 1983) and $\{H^+\}$ is the hydronium ion activity in M and is related to pH via the equation:

Equation 3.5

$$pH = -\log_{10}\{H^+\}$$

In this respect Equation 3.3 can be re-written in the H^+ form as follows:

Equation 3.6

$$R = -\frac{d[Fe(II)]}{dt} = \frac{k_{pH}[Fe(II)]pO_2}{\{H\}^2}$$

where k_{pH} is related to k_{pOH} by the square of the dissociation constant of water and becomes M^2 atm^{-1} sec^{-1}.

Stumm and Lee (1961) found that, in using Equation 3.3, the Fe(II) oxidation reaction has an apparent activation energy of zero. However, it was also evident that, at a fixed pH, the oxidation rate was highly temperature dependant. This is due to the variation of K_w with temperature and the associated variation in the $\{OH^-\}$. If the rate law is used in the form of Equation 3.6, activation energies of 96 kJ mol^{-1} (Stumm and Lee, 1961), 105 ± 25 kJ mol^{-1} (Sung and Morgan, 1980), and 125 ± 2 kJ mol^{-1} (Millero et al, 1987) have

been calculated. This indicates significant temperature dependence of the oxidation rate.

It is also applicable to substitute pO_2 (atm) with either $\{O_2\}$ or $[O_2]$ (M). In this case k_{pH} becomes k'_{pH} in M sec^{-1} and k_{pOH} becomes k'_{pOH}. The k' forms are related to the k forms by Henrys law constant (K_H) for oxygen ($K_H = 1.26 \times 10^{-3}$ M atm^{-1} at 25°C). To transform to $\{O_2\}$, an estimated activity coefficient for oxygen must be used. The transformed expression is shown in Equation 3.7 and Equation 3.8.

Equation 3.7

$$R = \frac{-d[Fe(II)]}{dt} = \frac{k'_{pH}[Fe(II)][O_2]}{\{H^+\}^2}$$

Or alternatively, in the OH^- form:

Equation 3.8

$$R = \frac{-d[Fe(II)]}{dt} = k'_{pOH}[Fe(II)][O_2]\{OH^-\}^2$$

Equation 3.3, Equation 3.6, and Equation 3.7 are valid only between pH 5 and 8. It is evident that the rate dependence on $\{OH^-\}$ or $\{H^+\}$ changes with pH from $R \propto \{OH^-\}^2$ or $\{H^+\}^2$ at circum-neutral pH to $R \propto \{OH^-\}$ or $\{H^+\}$ below pH 5 and to $\{OH^-\}$ or $\{H^+\}$ independence below pH 3. Above pH 3 and below pH 5 the reaction appears to be first order with respect to $\{H^+\}$ and Fe(II) (Holluta and Kolle, 1964). The rate expression can be written as:

Equation 3.9

$$R = \frac{-d[Fe(II)]}{dt} = \frac{k[Fe(II)][O_2]}{\{H^+\}}$$

where k is in M^{-2} sec^{-1}.

Below pH 3 the oxidation rate was found to be independent of $\{H^+\}$ and the general rate expression can be described as:

Equation 3.10

$$R = \frac{-d[Fe(II)]}{dt} = k[Fe(II)]^n[O_2]$$

where n is the reaction order with respect to [Fe(II)] and depends on the ionic medium. n has been reported as 1st order in solutions of phosphoric acid (Cher and Davidson, 1955), pyrophosphoric acid (King and Davidson, 1958) and Hydrochloric acid (Posner, 1953) and 2nd order in solutions of sulphuric acid (McBain, 1901; Lamb and Elder, 1931), nitric acid (Pound, 1939) and perchloric acid (George, 1954). k can be M^{-1} sec^{-1} if n = 1 or M^{-2} sec^{-1} if n = 2.

Millero (1985) recognised that the observed rate dependence could be explained by the parallel oxidation of the Fe(II) hexaquo[1] and hydroxo[2] complexes with the rate attributed to each species increasing in the order Fe(II), $Fe(OH)^+$ and $Fe(OH)_2^0$.

3.3.2 Composite Fe(II) oxidation rate laws

Work undertaken by Singer and Stumm (1970), Tamura et al (1976a), Millero (1985) and later Wehrli (1990) has shown that the high pH dependence on the oxidation rate of Fe(II) by oxygen can be expressed as the parallel oxidation of the different Fe(II) hydrolysis products. This is in accordance with the rate expression devised by Wehrli (1990) using data from Singer and Stumm (1970) and Millero (1987) and adapted by Burke and Banwart (2002) as in Equation 3.11:

Equation 3.11

$$R = \frac{-d[Fe(II)]}{dt} = \sum(k_i[Fe(II)_i])[O_2]$$

[1] Iron complexed by six water molecules $Fe(H_2O)_6^{2+}$

[2] Iron complexed by six water molecules, one or more of which has been de-protonated $Fe(H_2O)_{6-n}(OH)_n^{2-n}$

where $[Fe(II)_i]$ is the concentration of the individual Fe(II) species in M, k_i is the individual second order rate constant for the oxidation of the associated Fe(II) species by O_2 in M^{-1} sec^{-1} and $[O_2]$ is the dissolved oxygen concentration in M.

An alternative composite rate expression has been devised by Whitney-King (1998) (see also Santana-Casiano, 2000 and 2004) as in Equation 3.12:

Equation 3.12

$$R = \frac{-d[Fe(II)]}{dt} = (4\sum k_{\alpha i}\alpha[Fe(II)_i])[O_2][Fe(II)]$$

where $\alpha[Fe(II)_i]$ is the ionic fraction of each Fe(II) species in the solution and a function of the ionic media, $k_{\alpha i}$ is the second order rate constant for oxidation by oxygen in M^{-1} sec^{-1} and the factor 4 reflects the stoichiometry of Fe(II) oxidation by oxygen. $[O_2]$ is the oxygen concentration in M and [Fe(II)] is the total Fe(II) concentration in M. $k_{\alpha i}$ is related to k_i in Equation 3.12 by the following relationship:

Equation 3.13

$$If.....\alpha[Fe(II)_i][Fe(II)] = [Fe(II)_i]$$

$$Then.....4\sum k_{\alpha i} = \frac{\sum k_i}{4}$$

The corresponding second order rate constants for Fe(II) species (as determined by separate researchers) are presented in Table 3.2. In addition Mn(II) species are displayed for comparison.

In the case of both Equation 3.11 and Equation 3.12 the $[Fe(II)_i]$ concentration can be determined from [Fe(II)] using the relevant stability constants and $\alpha[Fe(II)_i]$ = 1/ [Fe(II)].$[Fe(II)_i]$. It should be noted that due to the nature of the composite rate laws the reported 2nd order rate constants are only valid when used with the appropriate stability constants for the individual Fe(II) species used in their initial determination. This should be kept in mind when calculating Fe(II) oxidation rates using rate constants reported in the literature. When applied to thermodynamic datasets included with geochemical

modelling software, the contributionto the overall Fe(II) concentration by individual species may vary affecting the overall rate.

Table 3.2: Second order rate constants reported for Fe(II) and Mn(II) species

	2^{nd} order rate constant (k_i) (Log M^{-1} sec^{-1}) at 25°C in pure water (as in Equation 3.12)					
Source	**A**	**B**	**C**	**D**	**E**	**F**
Fe species						
Fe^{2+}	-5.1	-6.04	-5.1	-2.7	-1.06	
$FeOH^{+}$	1.4	0.84	1.4	0.7	1.38	
$Fe(OH)_2^{0}$	6.9	5.94	6.89	6.9	4.91	
$FeHCO_3^{+}$		<0.12		-2.5	-2.38	
$FeCO_3^{0}$		<-0.4		-2.5	-1.23	
$Fe(CO_3)_2^{2-}$		4.04		4.0	2.41	
$Fe(CO_3)(OH)^{-}$		2.22		2.2	0.24	
$FeCl^{+}$				-2.7		
$FeSO_4^{0}$				-2.7		
Fe-Phthalate				-3.0		
Fe-Salicylate				4.04		
Mn species						
Mn^{2+}						< -9.39
$MnOH^{+}$						-1.18
$Mn(OH)_2$						1.92
$Mn(CO_3)_2^{2-}$						-0.49
Fe(II) surface species						
$(\equiv FeO)_2Fe^{\#}$	0.7					
$\equiv FeOFe^{+}$			0.69			
$\equiv FeOFeOH^{0}$			0.69			
Mn(II) surface species						
$(\equiv FeO)_2Mn^{*}$	-0.16					
$(\equiv AlO)_2Mn^{*}$	-1.55					

A = As reported in Wehrli (1990)
B = Whitney-King (1998)
C = Burk & Banwart (2002)
D = Santa-Casino et al (2004)
E = Santa-Casino et al (2005)
F = Morgan (2005)
** = After Davies and Morgan (1989)*
 # = Determined by Wehrli (1990) using data from Tamura et al (1976b) for Fe(II) oxidation on goethite
" = Converted from the form of k_i as used in Equation 3.11

3.3.2.1 Activation energy considerations in the composite rate laws

The effect of temperature on the individual second order rate constants used in the composite rate laws (Equation 3.11 and Equation 3.12) is unclear. A re-

working of previously reported rate data with respect to Fe speciation and conversion using either of the composite rate laws may allow the identification of any variation in k_i with temperature and therefore the calculation of activation energies for the individual Fe(II) species.

3.3.3 Ionic strength effects

Sung and Morgan (1980) reported that iron oxidation rate decreases with increasing Ionic strength. This is shown in Table 3.3 in which the rate constants are reported in the form of Equation 3.8.

Table 3.3: Effect of varying ionic strength on Fe(II) oxidation rate constants

Ionic strength (M)	k ($M^{-3}sec^{-1}$)
0.009	5.29×10^{14}
0.012	4.10×10^{14}
0.020	3.80×10^{14}
0.040	2.90×10^{14}
0.060	2.38×10^{14}
0.110	1.59×10^{14}

Sung and Morgan (1980)

3.4 Iron (and manganese) hydrolysis

Baes and Mesmer (1976) published an exhaustive compilation of available experimental data on cation hydrolysis. In their account the hydrolysis reaction is typically written in the H^+ form as in Equation 3.14.

Equation 3.14

$$M(H_2O)_6^{+y} + nH_2O \leftrightarrow M(H_2O)_5(OH)_n^{(y-n)} + nH_3O^+$$

although Stumm and Morgan (1996) state that the reaction can equally be written in the OH^- form:

Equation 3.15

$$M(H_2O)_6^{+x} + nOH^- \leftrightarrow M(H_2O)_5(OH)_n^{(x-n)} + nH_2O$$

The hydrolysis constants for the above reactions would therefore be:

Equation 3.16

$$K_1 = \frac{[Me(H_2O)_5(OH)_n^{(x-n)}].[H_3O]^n}{[Me(H_2O)_6^{+x}]}$$

and

Equation 3.17

$${}^{\bullet}K_1 = \frac{[Me(H_2O)_5(OH)_n^{(x-n)}]}{[Me(H_2O)_6^{+x}].[OH^-]^n}$$

where K_1 and ${}^{\bullet}K_1$ are the hydrolysis constant, [ ] denotes the concentration of the individual species in molar, Me is a divalent metal ion. As is conventional, the concentration of H_2O is presumed to be unity (in low ionic strength solutions) and K_1 and $^*K_1$ are therefore related by the dissociation constant for water K_w via:

Equation 3.18

$$K_1 = {}^{\bullet}K_1 K_w$$

Future reference to the hydrolysis constants and hydrolysis reactions will always be in the H^+ form (Equation 3.14 and Equation 3.16). Also, in the above examples, the waters of hydration and the full notation for the hydronium ion are included. These will be omitted from future reference for clarity.

3.4.1 Fe hydrolysis

The Fe(II) and Fe(III) oxidation states of iron are stable over broad regions of redox potential and pH commonto the aqueous environment. The Fe(II) ion only hydrolyses slightly before precipitation of $Fe(OH)_2$ or Fe_3O_4 (magnetite) with Fe(II) forming the dominant species up to pH 9 (Baes and Mesmer, 1976). The associated equilibrium constants at 25°C are listed in Table 3.4.

Fe(III) hydrolyses more fully with hydrolysis of the hexaquo ion beginning at pH 1 (Baes and Mesmer, 1976). Comparison is made between Mn(II) hydrolysis constants which are generally lower than those of Fe(II) which means that relative proportions of each hydrolysed Mn(II) species will be lower for a given pH.

In aqueous solutions under acidic conditions Fe(II) and Fe(III) ions form the hexaquo complexes $Fe(H_2O)_6^{2+}$, and $Fe(H_2O)_6^{3+}$. Dative covalent bonding around the positive metal centres causes the hydrogen of the water molecules to become more electro positive; this in turn leaves them more open to be removed to protonate a hydroxide ion in solution.

3.4.2 Mn hydrolysis

A detailed account of the hydrolysis of aqueous Mn was compiled by Baes and Mesmer (1976). They state that the Mn(II) valence is the most stable aqueous oxidation state for the metal under conditions typical of the earth's surface. It is also indicated that the Mn(III) and Mn^{7+} valances do also occur in solution and are important for the chemistry of the element. However, Mn(III) readily precipitates as sparingly soluble MnOOH or mixed valance Mn_3O_4 at circum-neutral pH (Baes and Mesmer, 1976). In additionto this under conditions where Mn(III) can exist in solution, it is unstable and is easily reduced to Mn(II) or disproportionates to Mn(II) and $Mn(IV)O_{2(s)}$ (Baes and Mesmer, 1976) following the reaction:

Equation 3.19

$$2Mn(III) + 2H_2O \leftrightarrow Mn(II) + MnO_{2(S)} + 4H^+$$

No significant aqueous chemistry of Mn(IV) exists as MnO_2 (pyrolusite in its crystalline form) is extremely insoluble.

Table 3.4: Fe and Mn hydrolysis constants at 25°C in pure water

Hydrolysis product	Hydrolysis constants (log K_{OH})[a]			
	Fe(II)	Mn(II)	Fe(III)	Mn(III)
$M^{+y}OH^{(y-1)}$	-9.5	-10.59	-2.19	0.0 – 0.7[c]
$M^{+y}(OH)_2^{(y-2)}$	-20.57[d]	(-22.2)[b]	-5.67	
$M^{+y}(OH)_3^{(y-3)}$	-31	(-34.8)[b]	-12.56[d]	
$M^{+y}(OH)_4^{(y-4)}$	-46	-48.3	-21.6	

Note: Polymer species omitted as their contribution is negligible under metal concentrations representative of natural waters.
[a] All values from Baes and Mesmer (1976) as summarised from experimental data unless otherwise stated.
[b] Values estimated by Baes and Mesmer (1976) from a regular progression of stepwise formation constants
[c] Range of values as reported by Diebler and Sutin (1964), Wells and Davies (1967) and Fackler and Chawla (1964) and summarised by Baes and Mesmer (1976)
[d] In accordance with Wateq4F.dat dataset included with PhreeqC

3.4.2.1 Mn(II) hydrolysis

The hydrolysis of Mn(II) is summarised here following the account given by Baes and Mesmer (1976). It is noted that experimentally determined hydrolysis constants are only available for the $MnOH^+$ (Perrin, 1962) and $Mn(OH)_4^{-2}$ (Fox et al, 1941 recalculated by Baes and Mesmer, 1976) hydrolysed species. Baes and Mesmer (1976) also reported the formation of Mn_2OH^{3+} and $Mn_2(OH)_3^+$ polymer species. The existence of these polymer species has largely been discounted in natural waters. This is due to the very high concentrations of Mn(II) used in the experiments as compared to natural levels. Calculations by Morgan (2005) showed that, in the pH range 8 to 9, the stability constants proposed for these two species would give total Mn(II) concentrations in 15 fold excess of the measured $Mn(OH)_2$ solubility. For this reason these two species have been emitted from further discussion.

Hydrolysis constants for the species $Mn(OH)_2^o$ and $Mn(OH)_3^-$ were determined by Baes and Mesmer (1976) assuming a "regular progression of the stepwise formation constants" between the experimentally determined constants for the $MnOH^+$ and $Mn(OH)_4^{-2}$ species.

3.4.3 Comparison of Fe and Mn hydrolysis

Table 3.4 lists the equilibrium hydrolysis reaction constants for Fe and Mn 2+ and 3+ valence states, at 25^0C, in pure water. Polymer species have been omitted in all cases as their contribution is negligible under the metal concentrations representative of natural waters.

The first hydrolysis constant for the Mn(III) valance state has been included for comparison although the range of experimentally determined values (Diebler and Sutin, 1964; Wells and Davies, 1967 and Fackler and Chawla, 1964) are several orders of magnitude higher than those determined for Fe(III) and Cr^{3+}. Baes and Mesmer (1976) indicated that the unusually high values could be a consequence of some form of polymerised Mn(III) rather than formation of the $MnOH^{2+}$ species.

3.4.4 Discrepancies in Fe stability constants in thermodynamic and geochemical datasets

Comparisons of reported stability constants for Fe(II) and Fe(III) species in pure and natural waters have been examined extensively by Millero et al (1995). In the calculation of Fe(II) oxidation rates using either of the devised composite rate laws (Equation 3.11 or Equation 3.12) it is necessary to determine Fe(II) chemical speciation. This is most easily achieved using chemical speciation codes such as PhreeqC, Minteq, and WateQ4F. In order to determine geochemical speciation the above codes must be used in conjunction with a specified thermodynamic database of stability constants. Unfortunately, there is not a universally agreed thermodynamic dataset incorporating all the available data for Fe(II) speciation. The available datasets often show some variation in the stability constants of the Fe(II) and Fe(III) species, and also discrepancies often occur in the inclusion or exclusion of individual complexes. Geochemical modelling work conducted in the current work uses the PhreeqC (Parkhurst and Appello, 1999) modelling, using the Wateq4F geochemical database (Ball and Nordstrom, 1991) as given in Table 3.5.

3.5 Fe ligand complexes

As well as hydrolysis of the Fe(II) hexaquo ion, complex formation with various other ligand's has been shown to markedly effect the observed Fe(II) oxidation rate (Stumm and Lee, 1961; Ghosh et al, 1966; Jobin and Ghosh, 1972; Ghosh, 1974; Theis and Singer, 1974; Tamura et al, 1976a; Sung and Morgan, 1980; Miles and Brezonik, 1981; Davison and Seed, 1983; Liang et al, 1993; Whitney-King, 1998; Santana-Casiano et al, 2000, 2004; and Wolthoorne et al, 2004). In addition Fe(II) ligand interactions have been used to explain lower observed rates in seawater than in fresh water (Millero et al, 1987).

At circum-neutral pH many ligands have the effect of reducing the oxidation rates of Fe(II) due to competition with Fe(II) and by reducing the ionic fraction of the fast reacting hydrolysed Fe(II) species (see references above). Sung and Morgan (1980) and references therein, demonstrate that under acidic conditions, high sulfate concentrations appear to increase the oxidation rate of Fe(II) by dissolved O_2. This can be attributed to a higher oxidation rate attributed to the $FeSO_4^o$ and $FeHSO_4^+$ species than the extremely slow reacting Fe(II) hexaquo ion.

A number of dissolved chemical species act as homogeneous catalysts in the oxidation of Fe(II) (in additionto various heterogeneous catalysts e.g. Fe(III) (hydroxy)oxide), these include Cu(II), Co(II) and Mn(II) ions (Stumm and Lee, 1961), PO_4^{3-} and F^- (Tamura et al, 1976a, Sung and Morgan, 1980), and citric acid (Theis and Singer, 1974, Miles and Brezonik, 1981). Liang et al (1993) found that although the effects of natural organic matter, fulvic acid and polyglutamate were undetectable at atmospheric O_2 concentrations, they showed rate enhancement effects at low partial pressures of O_2.

Table 3.5: Equilibrium constants for Fe and Mn species used in this study (values at 25^{0}C in pure water)

	Equilibrium constants (log K_{eq})[a]		
	Fe(II)	**Mn(II)**	**Fe(III)**
$M^{+y}CO_3^{(y-2)}$	5+.69[c]	4+.4[d]	9+.72[b]
$M^{+y}HCO_3^{(y-1)}$	+1.47[c]	+1.27[d]	
$M^{+y}(CO_3)_2^{(y-4)}$	7+.45[c]	5+.7[d]	
$M^{+y}OHCO_3^{(y-1)}$	-4.025[c]	-6.1[d]	
$M^{+y}SO_4^{(y-2)}$	2+.25	2+.25	4+.04
$M^{+y}HSO_4^{(y-1)}$	+1.08		2+.48
$M^{+y}(SO_4)_2^{(y-4)}$			5+.38
$M^{+y}Cl^{(y-1)}$	+0.14	+0.61	+1.48
$M^{+y}Cl_2^{(y-2)}$		+0.25	2+.13
$M^{+y}Cl_3^{(y-3)}$		-0.31	+1.13
$M^{+y}Cl_4^{(y-4)}$			
$M^{+y}F^{(y-1)}$	+1.0	+0.84	6+.2
$M^{+y}F_2^{(y-2)}$			+10.8
$M^{+y}F_3^{(y-3)}$			+14.0
$M^{+y}PO_4^{(y-3)}$			
$M^{+y}HPO_4^{(y-2)}$	3+.6		5+.43
$M^{+y}H_2PO_4^{(y-1)}$	2+.7		5+.43
$M^{+y}NO_3^{(y-1)}$			
$M^{+y}(NO_3)_2^{(y-2)}$		+0.6	
$M^{+y}(HS)_2^{(y-2)}$	8+.95		
$M^{+y}(HS)_3^{(y-3)}$	+10.99		
$M^{+y}Acetate^{(y-1)}$	-3.47[b]		
$M^{+y}(Acetate)_2^{(y-2)}$	-7.03[b]		
$M^{+y}(Acetate)_3^{(y-3)}$			

[a] *All values from Wateq4F dataset (Ball and Nordstrom, 1991) as included with PhreeqC Version 2.13.2 (USGS, 2007) unless stated otherwise*
[b] *Value from LLNL dataset*
[c] *Values reported by Whitney-King (1998)*
[d] *Values reported by Morgan (2005)*

A number of substances have been shown to retard the oxidation rate, most notably sulfate and chloride anions (Tamura et al, 1976a, Sung and Morgan, 1980 see Table 3.6) as well as tannic and hummic acids (Theis and Singer, 1974, Miles and Brezonik, 1981). Looking at rate accelerating and retarding effects in a mechanistic way (using the composite rate law approach) it becomes apparent that the observed rate effects are largely relative. For example, regarding sulfate, this is shown to retard the overall oxidation rate at circum-neutral pH (Tamura et al, 1976a, Sung and Morgan, 1980) but increase the rate in the acidic pH range (Sung and Morgan, 1980). This is because the sulfate ligand, complexes the Fe(II) ion across a broad pH range. At circum-neutral pH this has the effect of lowering the relative concentrations of the fast reacting hydrolysed surface Fe(II) species (therefore reducing the overall oxidation rate). In comparison sulfate complexation in the acidic pH range has the effect of increasing the Fe(II) oxidation rate as the sulfate speciated Fe(II) ion oxidises more rapidly than the Fe(II) hexaquo ion which dominates in lower pH conditions.

Table 3.6: Effects of some common ligands on the Fe(II) oxidation rate constants

Anions	Conc, M	k ($M^{-3}sec^{-1}$)*	k ($M^{-3}sec^{-1}$)#
ClO_4^-	0.1	2.38×10^{14}	
	0.5		7.4×10^{13}
NO_3^-	0.1	2.04×10^{14}	
Cl^-	0.1	1.63×10^{14}	1.16×10^{14}
	0.25		2.50×10^{13}
	0.50		2.12×10^{13}
$H_3SiO_4^-$	0.0012	1.63×10^{14}	
Br^-	0.1	1.36×10^{14}	
I^-	0.1	1.36×10^{14}	
SO_4^{2-}	0.033	1.36×10^{14}	
	0.165		1.03×10^{13}

** Tamura et al, (1976a), # Sung and Morgan (1980)*

King (1998), and Santa-Casiano et al (2004 and 2005) have shown that carbonate ions also have a similar effect on Fe(II) oxidation rate due to individually attributed oxidation rates of separate species. Individual second order rate constants are given in Table 3.2 for the Fe(II) carbonate species $FeHCO_3^+$, $FeCO_3$, $Fe(CO_3)_2^{2-}$ and $Fe(CO_3)(OH)^-$. Of these the $FeHCO_3^+$ and $FeCO_3$ species are slower reacting than the $Fe(CO_3)_2^{2-}$ and $Fe(CO_3)(OH)^-$

species (however the calculated second order rate constant has been shown to vary between researchers). The relative proportion of these species is strongly pH dependant and is reflected in the overall oxidation rate.

3.6 Homogeneous kinetic considerations of Fe(II) oxidation in mine water scenarios

As was shown in the Section 3.5 the solution chemistry and in particular the Fe(II) – ligand interactions play a fundamental role in determining the observed Fe(II) oxidation rate. In the natural environment water bodies are geochemically complex with a wide distribution of ions and molecules, therefore the speciation and associated oxidation kinetics of Fe(II) will vary from one local to the next. The chemistry of mine water discharges is generally characterised by elevated sulfate concentrations with respect to normal groundwater and in the case of circum-neutral discharges by high carbonate concentrations which may affect Fe(II) oxidation by ligand interaction. Kirby and Elder Brady (1998) found that large discrepancies between rates measured in the field at mine water discharges and rates reported in the literature were evident especially at low pH. This has been attributed to biotic processes and the presence of lithotrophic acidophilic bacteria such as *Thiobacillus* sp. *Thiobacillus* sp catalyse the oxidation of Fe(II) in the pH region 2 to 5. They effectively increase the pseudo first order rate constant by up to eight orders of magnitude from the homogeneous abiotic rate (see Figure 3-6, Section 3.10)

3.6.1 Common errors incurred during kinetic experiments

Davison and Seed (1983) gave a critical review of reported circum-neutral Fe(II) oxidation rate constants with regards to common errors incurred during the measurement procedure. They concluded that under carefully controlled experimental conditions any error incurred in the calculation of previously reported rate constants due to [Fe(II)] measurement and / or pO_2 measurement could be minimised. However, at circum-neutral pH where the oxidation rate is dependent on $\{OH^-\}^2$, the measurement of pH (and therefore the calculation of $\{OH^-\}$) would have an optimistic accuracy of $^+/_-$ 0.1 units

which would result in a theoretical range in calculated rate constants of $7.8x10^{14}$ – $1.9x10^{15}$ $M^{-2}atm^{-1}sec^{-1}$ assuming a mean experimental constant of $1.2x10^{15}$ $M^{-2}atm^{-1}sec^{-1}$. It is also important to consider error incurred during pH measurement due to the stirring effect, and (during heterogeneous Fe(II) oxidation experiments) due to the suspension effects.

3.7 Interfacial chemistry of Fe(II) on metal (hydroxy)oxide surfaces

3.7.1 Fe and Mn mineral precipitates

Under redox conditions where divalent Fe and Mn are stable, the dissolved concentrations of the metal ions are controlled principally by the solubility of their associative hydroxide. Therefore solubility is strongly pH dependant. In the presence of significant dissolved carbonate, the precipitation of divalent Fe and Mn as CO_3 minerals (siderite and rhodochrosite respectively) significantly reduces the solubility of the divalent species with respect to pH. When sulfate is present under strongly reducing conditions FeS and MnS mineral precipitation takes place.

At circum-neutral pH, and with increasing redox potential the dissolved concentration of Fe (and to some extent Mn) is determined by the solubility's of oxide and oxyhydroxide minerals. First to precipitate are the mixed valance "spinel" type minerals or "Fe green rusts", however, with a further increase in redox potential the precipitation of sparingly soluble oxides, hydroxides and (hydroxy)oxides occurs.

Figure 3-1 shows the Eh and pH stability regions for the systems Fe and Mn – O – H reproduced from Takeno (2005). The diagrams where produced by Takeno (2005) using the geochemists workbench software (Bethke, 2005), and the default thermo.dat database file based on the Lawrence Livermoor National Laboratory data set, 0.3245r46.

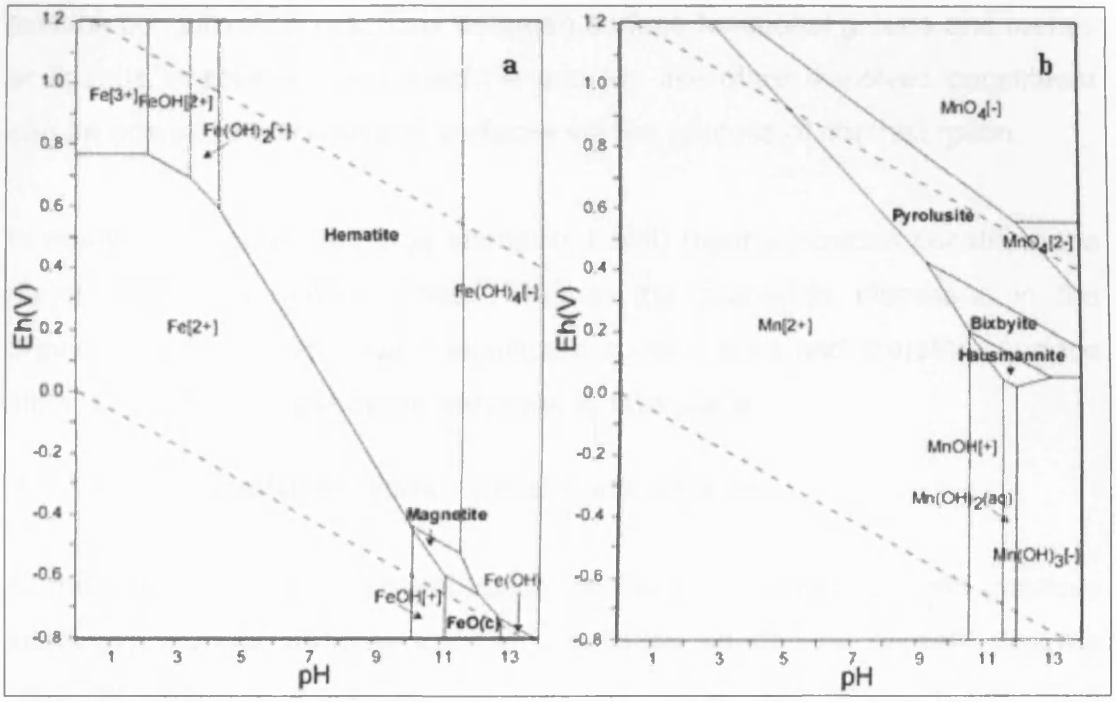

Figure 3-1: Eh – pH diagram of the system (a) Fe-O-H and (b) Mn-O-H. ∑ Fe or Mn = 10^{-10} M, 295.15°C, 10^5 Pa

Reproduced from Takeno (2005), constructed using Geochemists Workbench software (Bethke, 2005) using the default thermo.dat database file based on the Lawrence Livermoore National Laboratory dataset 0.3245r46.

In general, at pH below 9.5, the divalent Fe and Mn ions are highly soluble and do not readily form salts or hydroxide precipitates apart from in highly concentrated solutions. The solubility of higher valence Fe and Mn (hydroxy)oxide type minerals is highly pH dependant, increasing with decreasing pH. At lower pH conditions (typical of ARD) in which sulfate and metal concentrations are elevated, it is common for Fe hydroxy sulfate minerals to be the dominant solid phase. Iron precipitation at a low pH may include various cation-Jarosites and Schwertmannite minerals as well the Fe(III) (hydroxy)oxide goethite.

3.7.2 Chemisorption reactions of Fe and Mn on mineral surfaces

Adsorption is the accumulation of matter at the solid-water interface (Stumm and Morgan, 1996). Chemisorption or surface coordination (Stumm and Morgan, 1996) is the process of forming surface coordinative bonds during

surface complexation reactions between surface functional groups and metals or ligands in solution. Dissolved Fe and Mn like other dissolved constituent can be adsorbed onto mineral surfaces via the process of chemisorption.

In many mine water discharge scenario, Fe(III) (hydroxy)oxides constitute the major secondary mineral phase. Due to the properties discussed in the previous section they present significant surface area and therefore surface sites for surface complexation reactions to take place.

3.7.2.1 Fe adsorptionto hydrous metal oxide surfaces

At the termination of the crystal lattice (at the solid solution or solid gaseous interface), mineral surfaces expose unsatisfied bonds and present discrete sites for chemical reactions with ions and molecules from solution. The exposure of these sites causes a net charge to develop at the surface. In the case of Fe(III) (hydroxy)oxides (and metal oxides and hydroxides in general) surfaces are terminated in oxide groups and are often written as $\equiv SO^-$ where S denotes an individual surface site.

Iron oxides and (hydroxy)oxides form geochemically important minerals at the Earth's surface due to their abundance, reactivity and high surface area. The presence of these minerals has a marked effect on the longevity of Fe(II) and associated oxidising agents. Of particular Interest is the catalytic effect observed on the oxidation of Fe(II) in the presence of Fe(III) (hydroxy)oxide surfaces as these often form the reaction product and make the reaction autocatalytic in nature and generally show a catalytic effect greatly in excess of other non-Fe oxides and hydroxides (Tamura et al, 1976b, 1980; Sung and Morgan, 1980; Sarikaya, 1980, 1990; Robinson et al, 1981; Tufekci and Sarikaya, 1996, 1998; Tufekci et al, 2000; Demir and Tufekci, 2002; Park and Dempsey, 2005). Also of particular interest to the scope of this thesis is the association of Fe(III) (hydroxy)oxides with ferruginous mine drainage where they form the dominant solid phase at the redox front.

3.7.3 Electric double layer theory and electrostatic adsorption models

Due to inherent imperfections of the solid crystal lattice and termination of bonds at a mineral surface, minerals carry an inherent surface charge. Electric Double Layer (EDL) theory describes how this charge generates an electrostatic potential in contact with a solution that declines rapidly away from the surface. EDL theory also assumes that an excess of counter-ions (ions of opposite charge) exist near the surface (Langmuir, 1997).

Dzomback and Morel (1990) found that two types of surface adsorption sites were required to adequately describe the adsorption of cations onto the surface of hydrous ferric oxide (HFO). The type 1 or strong sites have a high affinity for cations and are not seen to adsorb anions. The type 2 or weak sites are capable of adsorbing both cations and anions and have a much lower affinity than type 1 sites for cation adsorption. Although type 1 sites have an extremely high affinity for cations they make up only 2.5 % of the total adsorption sites on HFO. Unlike other authors (Zhang et al, 1992; Charlet et al, 1998; Liger et al, 1999; Vikesland and Valentine, 2002) the generalized two layer model used in Dzomback and Morels study did not require the inclusion of a monohydrolyzed surface species to fit adsorption data for any of the cations studied. However this study did not incorporate any data for Fe(II) adsorption. Appelo et al (2002) optimized the data from Liger et al (1999) to include the strong and weak sites described by Dzomback and Morel (1990).

3.7.4 Surface charge and zeta potential

As mentioned previously the surfaces of Fe(III) (hydroxy)oxides carry inherent electrical charges due to unsatisfied bonds and chemisorption of specific determining ions. The zeta potential (ζ) is the potential drop that exists between the shear plane and the bulk solution surrounding a charged particle. ζ is related to the particle charge, which in the case of Fe(III) (hydroxy)oxides is determined by chemisorbed ions, and the thickness of the EDL which is inversely proportional to the concentration and valence of the electrolyte (Eckenfelder, 2000). Due to a number of assumptions that must be invoked

and problems with results interpretation, ζ can not be directly related back to the magnitude of the surface potential (Dzombak and Morel, 1990) but is useful in determining the stability of the particles, the closer the ζ is to zero the more likely particles are to coagulate to form flocs.

3.7.5 Interfacial Electron Transfer and Fe(II) fixation

It has been recognised that charge delocalisation or Interfacial Electron Transfer (IET) can occur between adsorbed Fe(II) and structural Fe(III) of Fe(III) (hydroxy)oxides (see Wehrli, 1990; and Jeon et al, 2003; and references therein) analogous to inner-sphere electron transfer between the Fe(II) / Fe(III) hexaquo complexes in weak acid solutions. Recent studies using the ^{57}Fe isotope specificity of Mossbauer spectroscopy have largely confirmed the existence of IET between adsorbed Fe(II) and underlying structural Fe(III).

Williams and Scherer (2004) presented spectroscopic evidence for electron transfer between adsorbed Fe(II) and structural Fe(III) in goethite, hematite and ferrihydrite at circum-neutral pH. By doping $^{56}Fe(III)$ iron oxide surfaces with $^{57}Fe(II)$ they observed the formation of a $^{57}Fe(III)$ surface layer in the absence of a solution phase oxidising agent. $^{57}Fe(II)$ adsorbed onto rutile and aluminium oxide did not show any conversionto $^{57}Fe(III)$. The observed oxidation was attributed to Fe(II) / Fe(III) IET. A further study by Larese-Casanova and Scherer (2007) looked in more detail at the adsorption of $^{57}Fe(II)$ onto hematite and found that the observed $^{57}Fe(II)$ / $^{57}Fe(III)$ conversion was evident up to an estimated monolayer coverage of adsorbed $^{57}Fe(II)$ on the hematite surface. This study also revealed that formation of a truly adsorbed $^{57}Fe(II)$ occurred only after estimated monolayer surface coverage had been achieved. Desorption experiments showed that only Fe(II) adsorbed after the point at which monolayer surface coverage had been achieved could be extracted by re-suspension in Fe(II) free buffer. They state that at low Fe(II) concentrations "Fe(II) species are transient and quickly undergo IET with structural Fe(III) in hematite" and presumably in goethite and ferrihydrite. It is also apparent that once monolayer surface coverage and IET of $^{57}Fe(II)$ to $^{57}Fe(III)$ has been achieved further IET is prevented. It is not

clear why monolayer surface coverage prevents further IET but Larese-Casanova and Scherer (2007) hypothesise that the band gap within the newly formed surface layer may be less conducive to further IET than the original Fe(III) (hydroxy)oxide.

Silvester et al (2005) showed that $^{57}Fe(II)$ adsorbs onto goethite and HFO in agreement with a thermodynamic model which allowed for the formation of two Fe(II) surface species, those of $\equiv FeOFe^{+}$ and $\equiv FeOFeOH^{o}$. However, Mossbauer spectroscopy revealed that the surface $^{57}Fe(II)$ was almost completely converted to $^{57}Fe(III)$ despite the presence of a viable solution phase oxidising agent and it was thought that the observed oxidation must be due to IET with the underlying hematite Fe(III) centres.

Is the IET Fe(II) that has been transferred to the bulk solid available to reduce aqueous and adsorbed oxidising agents? Evidence from Williams and Scherer (2004) appears to show that it is not. Goethite was exposed to Fe(II) without the presence of a solution phase oxidising agent in order for potential IET to take place. The suspension was then filtered and the Fe(II) doped goethite was re-suspended in buffer solution. $ArNO_2$ was then added as the oxidising agent. In a control experiment where aqueous Fe(II) had not been removed the $ArNO_2$ was reduced, in the filtered experiment $ArNO_2$ was not reduced despite the presence of IET Fe(II). On addition of Fe(II) back into the reactor $ArNO_2$ reduction proceeded immediately at a rate comparable with that in the control experiment. Park and Dempsey (2005) found that during Fe(II) oxidation by dissolved oxygen in the presence of HFO a portion of sorbed Fe(II) was consistently recoverable once all dissolved Fe(II) had been oxidised. This was attributed to IET Fe(II). Currently to date this is the only study that has shown the presence of potential IET Fe(II) "post" oxidation with a solution phase oxidising agent.

Gregory et al (2004) studied the heterogeneous reduction of hexahydro-1,3,5-trinitro-1,3,5-triazine (RDX) by Fe(II) in the presence of magnetite (Fe_3O_4) surfaces. It was found that magnetite greatly accelerated the rate of reduction of RDX and that negligible reduction was observed in solutions of Fe(II) and

RDX without magnetite and also in suspensions of RDX and magnetite but without Fe(II). This shows that the magnetite surface is an effective catalyst for RDX reduction by Fe(II) and also that the structurally bound Fe(II) of the spinel structure of magnetite is not a viable reducing agent for RDX. Vikesland and Valentine (2002) studied the reduction of monochloramine by Fe(II) in the presence of various Fe(III) (hydroxy)oxides surfaces. They found that, on an area adjusted basis the catalytic activity of the studied solids decreased in the order magnetite > goethite >> lepidocrocite > hematite >> ferrihydrite. The resulting oxides were shown to be able to reduce nitrobenzene but only in the presence of dissolved Fe(II).

Table 3.7: Previous work showing evidence for Interfacial Electron Transfer (IET) and or dual Fe(II) surface species

Theory	Supporting author
Interfacial Electron Transfer (IET)	Williams and Scherer (2004), Park and Dempsey (2005), Silvester et al (2005), Larese-Casanova and Scherer (2007), Jeon et al (2003)
Dual Fe(II) surface species	Liger et al (1999), Charlet et al (1998), Zhang et al (1992), Silvester et al (2005).

Pecher et al (2002) observed that the pseudo first order rate constant for the reduction of halogenated alkanes by Fe(II) in the presence of goethite increased as a function of pre-equilibration contact time (t_{eq}) between the goethite and Fe(II) before oxidant addition. It was found that the rate increased from t_{eq} = 0 and then levelled off after 20 hours. Pecher et al used 1,10-phenanthroline to desorbe surface bound Fe(II) from goethite and found that in an anoxic suspension of goethite (25 m^2dm^{-1}) and aqueous Fe(II) (1mM) that the amount of non phenanthroline desorbable Fe(II) increased from 9 to 14 μmol m^{-2} over 20 hours indicating a connection between the increasing observed reduction rates and the increase in non desorbable sorbed Fe(II). Pecher et al attributed this to the rearrangement of initially sorbed Fe(II) surface species to more reactive surface species with equilibrium time. It was also found that the surface adsorption model was the

best fit to all the adsorption data. However, it is also stated that heterogeneous electron transfer is unlikely at the goethite / Fe(II) interface as structural Fe(III) in goethite is stabilised by structural oxygen contrary to the recent spectroscopic evidence (Williams and Scherer 2004, Silvester et al 2005, Larese-Casanova and Scherer 2007)

3.8 Surface catalysed oxidation of Fe(II)

3.8.1 Empirical rate constants

Tamura et al (1976b) studied the heterogeneous oxidation of Fe(II) by dissolved O_2 in the presence of amorphous $Fe(OH)_3$ and found the rate expression in Equation 3.20 is best used to best describes the observed rate:

Equation 3.20

$$R = \frac{-d[Fe(II)]}{dt} = -\left(\frac{d[Fe(II)]}{dt} + \frac{d[Fe(II)_{ads}]}{dt}\right)$$

$$= \left(k + k'[Fe(III)]\right)[Fe(II)_{Tot}]$$

in which

$$k = k_O[O_2][OH^-]^2$$

$$k' = k_S \frac{K}{\{H^+\}}$$

$$k_S = k_{SO}[O_2]$$

where $Fe(II)_{Tot}$ signifies total Fe(II) (both dissolved and adsorbed), Fe(II) is dissolved Fe(II), $Fe(II)_{ads}$ is adsorbed Fe(II). [ ] signifies concentration in M apart from [Fe(III)] which is the concentration of amorphous $Fe(OH)_3$ in mg l^{-1}. k and k_s are pseudo first order rate constants in sec^{-1}. k' is the surface corrected rate constant in $mg^{-1}l$ sec^{-1}. k_o is the real rate constant for the homogeneous oxidation of Fe(II) which is $2.3x10^{14}$ M^{-3} sec^{-1}. k_{so} is the real

rate constant for the heterogeneous reaction determined to be 73 M^{-1} sec^{-1}. Finally K is the equilibrium constant for the adsorption of Fe(II) onto amorphous $Fe(OH)_3$ which was determined to be $2.51x10^{-10}$ mol mg^{-1}, k_o, k_{so} and K where determined in 0.1 M $NaClO_4$ – 0.01 M $NaHCO_3$ solutions at 25°C. It should be noted that the above rate expression is valid only were the dissolved concentration of Fe(II) is in large excess of the adsorbed concentration of Fe(II).

The equilibrium constant for the adsorption of Fe(II) onto Fe(III) is related to the ratio of sorbed Fe(II) to total Fe(II) by the equation:

Equation 3.21

$$\frac{[Fe(II)_{sorbed}]}{[Fe(II)_{tot}]} = \frac{K[Fe(III)]}{[H^+]}$$

Sung and Morgan (1980) used the Tamura et al (1976b) rate expressionto model autocatalytic oxidation of Fe(II) by the reaction product (HFO). They converted the [Fe(III)] expression from mg l^{-1} to M using a value of 107 g mol^{-1} for HFO thus converting the reported equilibrium constant K from $2.51x10^{-10}$ mol mg^{-1} to the dimensionless value of $1.41x10^{-5}$. They found reasonable agreement between the rate predicted using the Tamura et al (1976b) rate constant for heterogeneous oxidation and their own experimental data (in a 0.5 M $NaClO_4$ – 0.005 M $NaHCO_3$ solution at 25°C) with k' of 3.53 and 6 M^{-1} sec^{-1} respectively. Sung and Morgan also experimented in different ionic mediums and found k' to be higher (24 M^{-1} sec^{-1}) in 0.5 M NaCl – 0.005 M $NaHCO_3$ as compared to Na_2SO_4 and $NaClO_4$. On infra red spectrophotometric analysis of the reaction products they found distinct ClO_4^- and SO_4^{2-} peaks whereas Cl^- peaks (can you have Cl peaks on FTIR – probably not!) where not discovered suggesting an interaction of the ionic media with the precipitate.

Park and Dempsey (2005) studied the heterogeneous oxidation of Fe(II) by trace amounts of O_2 in the presence of HFO. In this study either 25 minutes or 24 hours of anoxic pre-equilibration were allowed between the dissolved Fe(II)

and suspended HFO. It was found that upon addition of oxygen, the pseudo first order Fe(II) oxidation rates appeared to be an order of magnitude higher than the equivalent rates calculated using the Tamura et al (1976b) determined heterogeneous rate law. The rate was also found to be dependent on the concentrations of both sorbed and dissolved Fe(II).

Equation 3.22

$$R = \frac{-d[Fe(II)]}{dt} = k[Fe(II)_{diss}][Fe(II)_{sorbed}][O_2]$$

Where $[Fe(II)_{diss}]$ and $[Fe(II)_{sorbed}]$ are the concentrations of dissolved and sorbed Fe(II) in M and k is the rate constant with units of M^{-2} s^{-1} and an average value of 2.03 (± 0.63) $x10^7$ M^{-2} s^{-1}.

Park and Dempsey attributed the higher rates found in their study as compared to the Tamura et al (1976b) study to either the low O_2 conditions or to anoxic pre-equilibration time. In additionto this it should also be noted that the pseudo first order k values reported by Park and Dempsey where calculated from the $[Fe(II)_{diss}]$ whilst the Tamura et al rates were determined from total [Fe(II)]. In addition Park and Dempsey used Fe(III) and Fe(II) Cl^- salts in their study and as mentioned before the selection of background electrolyte can have a marked effect on the catalytic effect with ClO_4^- and SO_4^{2-} anions inhibiting the surface rate (Sung and Morgan, 1980). Since $NaClO_4^-$ was used in the Tamura studies this would lead to an under-calculation of the rate when applied to a study such as Park and Dempsey's in which Cl^- was the background anion. Using the k' value reported by Sung and Morgan for catalytic oxidation in a 0.5 M NaCl solution of 24 M^{-1} sec^{-1} it is possible to back-calculate a value for K and / or k_{so} which would give a tentative figure for oxidation in a NaCl solution using Equation 3.23.

Equation 3.23

$$K = \frac{(k'[H^+])}{(k_{SO}[O_2])}$$
$$= \frac{(24M^{-1}\sec^{-1}6.3x10^{-8}M)}{(73M^{-1}\sec^{-1}2.2x10^{-4}M)}$$
$$= 9.3x10^{-5}$$

The numeration is consistent with Equation 3.20 with the changes applied by Sung and Morgan (1980). It should also be noted that back-calculating K or k_{so} gives the same output when applied to the Park and Dempsey data in the calculation of the pseudo first order rate. Figure 3-2 shows the predicted pseudo first order rates (k_{Tamura} sec^{-1}) for the Park and Dempsey study calculated using a) the original and b) the corrected values for K in the Tamura et al (1976b) rate expression (x axis). These have been plotted against the measured pseudo first order rate data (k_{mod} sec^{-1}) from the Park and Dempsey study.

The buffer systems used in the Tamura et al and Park and Dempsey studies differ as Tamura et al used a $NaHCO_3 - CO_2$ buffer whilst Park and Dempsey used Na-PIPES buffer. It has been shown that the presence of measurable dissolved carbonate greatly inhibits the adsorption of Fe(II) onto goethite and it is presumed that this is because the Fe(II)-carbonate complexes do not adsorb as readily to the Fe(III) (hydroxy)oxides as the Fe(II) hexaquo and hydroxo complexes (Vikesland and Valentine, 2002). Although un-quantified, the effect this would have on the Tamura et al (1976b) (Equation 3.20) heterogeneous rate constant, which was determined in a 0.1M $NaClO_4$ - 0.01M $NaHCO_3$ solution would be to under-calculate the adsorption of Fe(II) onto HFO when applied to a system void of significant carbonate such as Park and Dempsey's study. The horizontal red line in Figure 3-2 indicates unity between the Park and Dempsey experimental values and the predicted values using the Tamura et al rate law. Adjustment of the K value used to calculate the data set B from $9.43x10^{-5}$ to $3x10^{-4}$ brings the experimental verses predicted values to unity, which equates to a change from 0.78 mg Fe(II) per mole of HFO to16.8 mg Fe(II) per mole of HFO. A further study by Tamura and co-workers (Tamura et al, 1980) investigated the catalytic effect on Fe(II) oxidation by lepidocrocite and goethite (α and γ FeOOH) and compared the results with amorphous $Fe(OH)_3$.

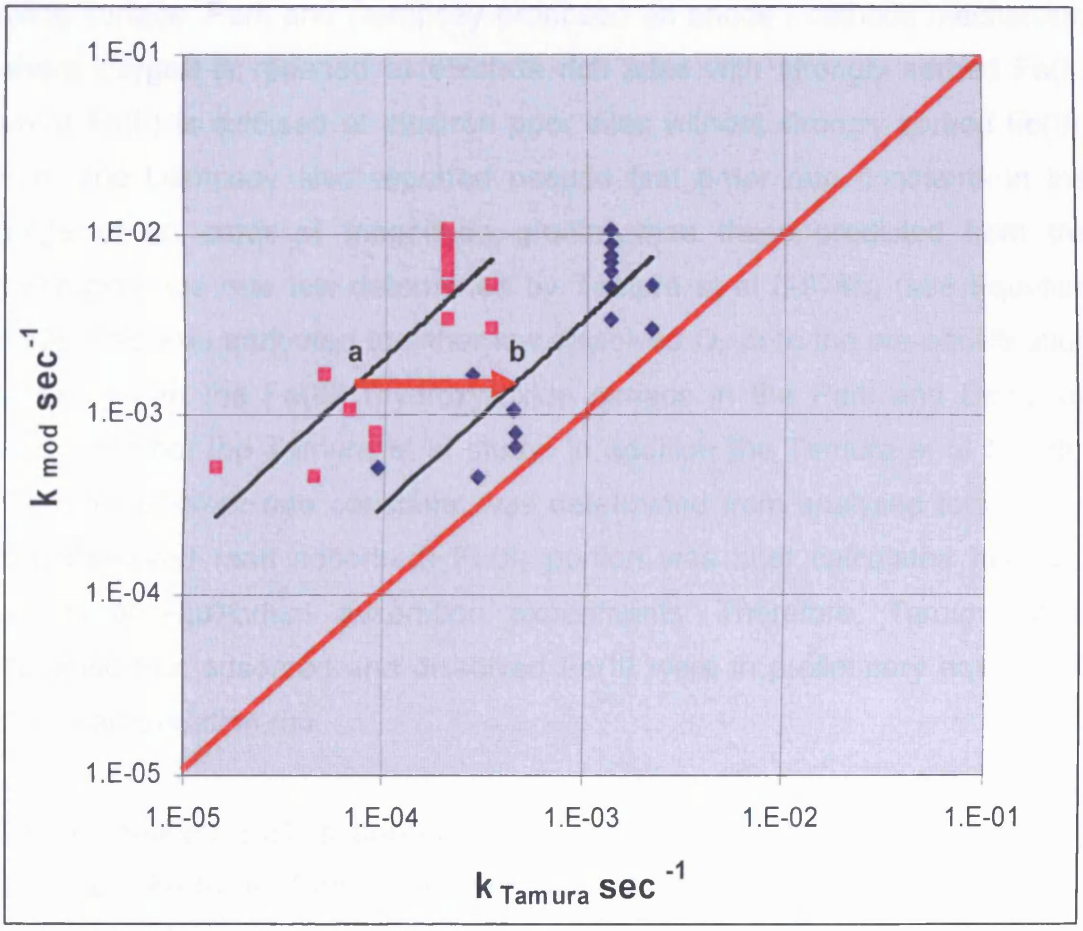

Figure 3-2: Comparison of pseudo first order oxidation rate constants for Fe(II)

k_{mod} determined by Park and Dempsey (2005) with predicted rate using Tamura et al (1976b) rate law (Equation 3.20) with a) determined using Tamura et al (1976b) rate constant in NaClO4 solution (pink points) and b) the corrected values for K in the Tamura et al (1976b) rate expression (blue points)

In Park and Dempsey's (2005) study of the rates of oxidation of Fe(II) by low partial pressures of oxygen in the presence of freshly precipitated HFO. An extraction method for Fe(II) was used (as described by Jean et al, 2003) for the determination of total and dissolved Fe(II), in conjunction with the analytical method as devised by Tamura et al (1974). Using this method they found it possible to report both dissolved Fe(II) and also sorbed Fe(II) (which was the difference between total and aqueous concentrations). It was found that during oxidation experiments, the amount of measurable sorbed Fe(II) remained constant whilst the dissolved Fe(II) was completely depleted. This behaviour was attributed to discrete, structurally different sites on the iron

oxide surface. Park and Dempsey proposed an anode / cathode mechanism where oxygen is reduced at electron rich sites with strongly sorbed Fe(II) whilst Fe(II) is oxidised at electron poor sites without strongly sorbed Fe(II). Park and Dempsey also reported pseudo first order rate constants in the range of an order of magnitude greater than those predicted from the heterogeneous rate law determined by Tamura et al (1976b) (see Equation 3.20). This was attributed to either low dissolved O_2 or to the pre-equilibration of Fe(II) with the Fe(III) (hydroxy)oxide surface in the Park and Dempsey study and not the Tamura et al study. In addition the Tamura et al (1976b) pseudo first order rate constants was determined from analysed total Fe(II). The dissolved (and adsorbed) Fe(II) portion was later calculated from the results of equilibrium adsorption experiments. Therefore, Tamura et al assumed that adsorbed and dissolved Fe(II) were in preliminary equilibrium during an oxidation run.

When Equation 3.20 is applied to the measured values of dissolved and adsorbed Fe(II) in Park and Dempsey (2005) study, an artificially low prediction of the heterogeneous oxidation rate may occur (as compared to Park and Dempseys (2005) actual observed rate). This is due to the assumption by Tamura et al (1976b; 1980), that preliminary equilibrium occurs between dissolved and surface Fe(II) species. Park and Dempsey showed that equilibrium between sorbed and dissolved Fe(II) is not reached during an oxidation run, and that significant sorbed Fe(II) remains on the surface despite almost complete oxidative removal of dissolved Fe(II).

Zhang et al (1992) and Liger et al (1999) showed that the existence of two types of Fe(II) surface species best explain the observed adsorption of Fe(II) on lepidocrocite and haematite respectively. They described two surface species:

Equation 3.24

$$\equiv FeOH + Fe(II) \leftrightarrow \equiv FeOFe^{+} + H^{+}$$

$$\equiv FeOH + Fe(II) + H_2O \leftrightarrow \equiv FeOFeOH + 2H^{+}$$

Liger et al (1999) also studied the effect of pH on the reduction rate of U(VI) by Fe(II) in the presence of Hematite (α-Fe_2O_3). It was shown that the rate of U(VI) reduction followed a linear dependence on [≡FeOFeOH°] (Figure 3-3) and also that reduction only occurred at a pH above which the ≡FeOFeOH surface species became significant despite the presence of significant adsorbed Fe(II) (presumably as ≡FeOFe$^+$).

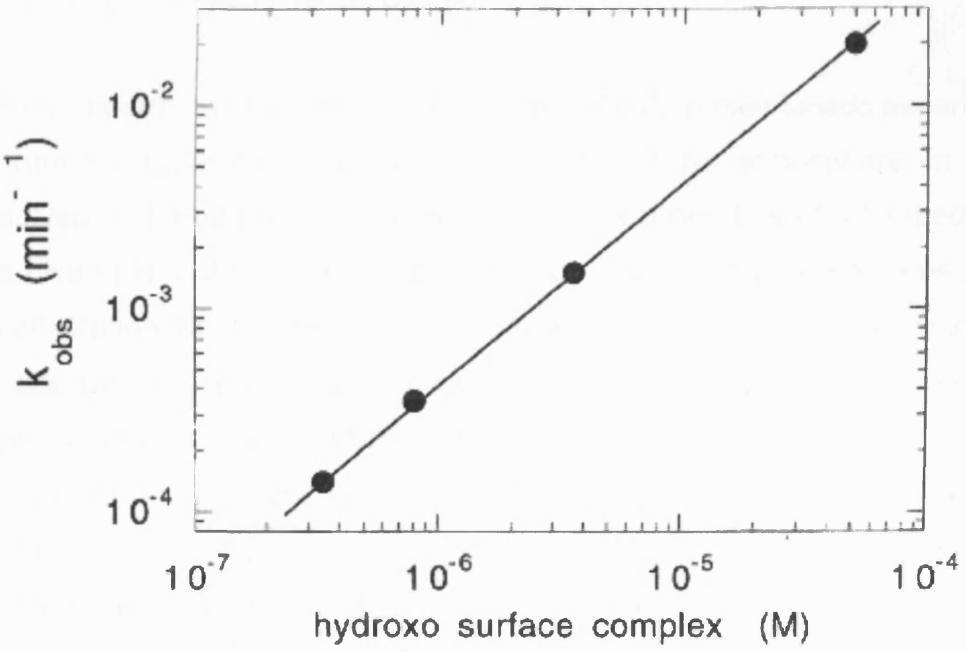

Figure 3-3: Plot of the pseudo first order rate of reduction of U(VI) in min^{-1} by Fe(II) against the calculated concentration of the surface complex ≡FeOFeOH (from Liger et al, 1999)

The pseudo-first-order rate constant for U(VI) reduction by Fe(II) in the presence of hematite nanoparticles depends linearly on the concentration of the hydroxo surface complex.

Charlet et al (1998) further investigated this and showed that the ≡FeOFeOH species could also be employed to explain the oxidation of some organic pollutants. However, Wehrli (1990) attributed a pseudo first order oxidation rate for Fe(II) by dissolved O_2 in the same order of magnitude for adsorbed Fe(II) as for the FeOH$^+$ species (calculated from kinetic data from Tamura et al, 1976b; Singer and Stumm, 1970; and Millero et al, 1987). Wehrli (1990) predicted the redox potentials of adsorbed Fe(II) from data published by Tamura et al (1976b) as follows:

Equation 3.25

$$(\equiv FeO)_2 Fe^{+} + e^{-} \leftrightarrow (\equiv FeO)_2 Fe^{II} \quad \ldots\ldots\ldots\ldots E^{o} = 0.36V$$

$$or \equiv FeOFeOH^{+} + e^{-} \leftrightarrow \equiv FeOFeOH \quad \ldots\ldots\ldots\ldots E^{o} = 0.36V$$

$$FeOH^{+}_{(aq)} + e^{-} \leftrightarrow FeOH^{2+}_{(aq)} \quad \ldots\ldots\ldots\ldots E^{o} = 0.34V$$

It is evident that the calculated redox potential is very similar to that predicted for the aqueous $FeOH^+$ redox couple.

Tamura determined the amount of adsorbed Fe(II) in their kinetic experiments by running separate adsorption runs under a N_2 atmosphere in which dissolved and total Fe(II) was determined. The proportion of adsorbed Fe(II) at a given pH in the kinetic experiment was taken to be the same as that in the adsorption run. Liger et al (1999) showed that it is the ≡FeOFeOH surface species which is readily oxidised by UO_2^{2+} and that the ≡$FeOFe^+$ species is largely unreactive, and that the proportion of each species varies with pH. Tamura et al (1976b) did not measure the surface area of the iron hydroxides or the surface concentration of Fe(II) during their oxidation experiments. Therefore, when Wehrli came to estimate a surface rate constant for $Fe(II)_{ads}$ the total adsorbed Fe(II) using the Tamura et al (1976b) data, the amount of reactive $Fe(II)_{ads}$ (≡FeOFeOH) may have been underestimated. In this case the rate determined by Wehrli may be an underestimation of the true rate attributed to the ≡FeOFeOH species.

Dempsey et al (2002) conducted experiments to test the theory presented by Tufekci and Sarikaya (1996) that [Fe(III)] above 600 mg/L did not increase the oxidation rate of Fe(II). Tufekci and Sarikaya (1996) used initial [Fe(II)] of 3 mg/L in all of their heterogeneous oxidation experiments to minimise any autocatalytic effects and [Fe(III)] of 0 – 600 mg/L. Dempsey et al (2002) used 1 – 700 mg/L Fe(III) and found a linear relationship between k_{tot} and Fe(III) concentration. They concluded that the heterogeneous rate law devised by Tamura et al (1976b) still applied and that the results presented by Tufekci and Sarikaya (1996) were misleading and could well be a factor of floc

formation as indicated by Tufekci and Sarikaya themselves. However, Dempsey et al (2002) used 85 mg/L Fe(II) in their experiments which equates to an Fe(III) Fe(II) ratio of 8.23, this compares to a ratio 100 for Tufekci and Sarikaya's work. For Dempsey et al to have replicated the kinetic ceiling effect that was seen by Tufekci and Sarikaya it may have been necessary to use 8500 mg/L Fe(III) to mimic the same Fe(III) / Fe(II) ratio.

Tufekci and Sarikaya (1996) results did show a linear relationship between k_{tot} / [Fe(III)] up to 50 mg/L of Fe(III), this equates to an [Fe(III)] / [Fe(II)] ratio of 16.6 assuming that this ratio is interchangeable it can be assumed that Dempsey et al also would see a linear increase in k_{tot} with Fe(III) concentrations up to an Fe(III) / Fe(II) ratio of 16.6 or an Fe(III) concentration of 1411 mg/L; over double that used in their oxidation experiments.

3.8.2 Heterogeneous oxidation mechanisms

Several researchers have found that two surface Fe(II) species (those of $\equiv FeOFe^{+}$ and $\equiv FeOFeOH^{o}$) are required to best fit experimental data for the adsorption of Fe(II) on lepidocrocite (Zhang et al, 1992), goethite (Coughlin and Stone, 1995), magnetite (Charlet et al, 1998) hematite, and ferrihydrite (Liger et al, 1999).. Of these two species Liger et al (1999) found the rate of reduction of U(VI) by Fe(II) adsorbed on hematite to be directly proportional to the modelled concentration of the $\equiv FeOFeOH^{o}$ surface species and not to the overall concentration of surface Fe(II) (as demonstrated in Figure 3-3). This indicates that the $\equiv FeOFeOH^{o}$ species was a more viable reducing agent than $\equiv FeOFe^{+}$.

It is known that heterogeneous electron transfer can occur between adsorbed Fe(II) and underlying Fe(III) centres of Fe(III) (hydroxy)oxide minerals (Stone and Morgan, 1987; Wehrli, 1990). Studies by Williams and Scherer (2004), Silvester et al (2005) and Larese-Casanova and Scherer (2007) have found spectroscopic evidence for heterogeneous electron transfer between adsorbed Fe(II) and underlying Fe(III) and in the case of Silvester et al (2005) and Larese-Casanova and Scherer (2007) that almost all adsorbed Fe(II) undergoes heterogeneous electron transfer with the underlying Fe(III) centres

forming a surface Fe(III) layer which could possibly dispel the use of the conventional surface model for adsorption of Fe(II) onto Fe(III) (hydroxy)oxides and for the prediction of surface catalysed oxidation rates. It should also be noted that Larese-Casanova and Scherer (2007) only detected truly adsorbed Fe(II) species after calculated monolayer surface coverage had been exceeded. The presence of residual surface bound Fe(II) on Fe(III) (hydroxy)oxide surface (as found in the study of Park and Dempsey, 2005) is consistent with the theory of IET, and the formation of Fe(II) that it is unavailable for oxygen reduction. However, the residual Fe(II) could also be attributed to the formation of an un-reactive strongly bound $\equiv FeOFe^{+}$ species and to significant hysteresis in surface species equilibration. Further insight may be gained by long term oxidation of surface bound Fe(II) to determine its stability or by using a stronger oxidising agent.

Intrinsic stability constants determined by acid base titrations of Fe(II) solutions in the presence of Fe(III) (hydroxy)oxide will not have taken into account the process of heterogeneous electron transfer (Nano and Strathmann, 2006) as evidenced by Williams and Scherer (2004), Silvester et al (2005) and Larese-Casanova and Scherer (2007). It is also possible that during adsorption experiments, the observed proton release (that is generally attributed to the formation of a hydrolysed Fe(II) surface species) may be due to hydrolysis of the newly formed surface Fe(III) species formed by IET with adsorbed Fe(II). This is feasible as the log of the first hydrolysis constant for Fe(III) in solution is -2.19 as compared to -9.5 for Fe(II) (Baes and Mesmer, 1976) and a similar relationship would be expected for adsorbed Fe(III) and Fe(II) species. This is supported by Dzombak and Morel (1990) who found that, generally, no hydrolysed surface species were required to model divalent transition metal cation adsorption by hydrous ferric oxide. In contrast trivalent Cr(III) on HFO (Dzombak and Morel, 1990) and Al(III) on lepidocrocite (Zhang et al, 1992) does require the addition of a hydrolysed surface species.

Barry et al (1994) studied the heterogeneous catalytic oxidation of Fe(II) on Fe_2O_3, TiO_2, MnO_2, Al_2O_3 and SiO_2 and found that on an area adjusted basis, oxidation rates on Fe_2O_3, TiO_2 and MnO_2 were approximately equal and three

orders of magnitude greater than those for Al_2O_3 and SiO_2. Nano and Strathmann (2006) determined surface complexation parameters for Fe(II) on TiO_2, Al_2O_3 and AlOOH and found adsorption onto TiO_2 was best described by single site adsorption with two surface Fe(II) species $\equiv TiOFe^+$ and $\equiv TiOFeOH^o$ in agreement with surface Fe(II) species found on Fe(III) (hydroxy)oxides. On AlOOH and Al_2O_3 however no evidence was found for the hydrolysed surface species. The above evidence would appear to support the surface species mechanism and the reactivity of the hydrolysed surface Fe(II) species unless IET also takes place on TiO_2. However Nano and Strathmann (2006) found complete recovery of all adsorbed Fe(II) after acidificationto pH 4.5 indicating that no IET had taken place. However, they also state that TiO_2 enhances the surface hydrolysis of many other divalent metal ions. It should also be noted that Fe_2O_3, TiO_2 and MnO_2 can all act as semi conductors (Stumm and Morgan, 1996). Clearly further work needs to be done to understand the role of heterogeneous electron transfer and also to determine if the observed titration data are due to a) formation of $\equiv FeOFeOH^o$ surface species or b) the extent to which electron transfer has occurred.

Following this previous discussion reliance of the surface catalysed rate on the concentration of the hydrolysed Fe(II) surface species as observed by Liger et al (1999) could be due to the increasing degree of thermodynamic stability of magnetite or other mixed valence Fe (hydroxy)oxides as indicated by Jeon et al (2003) and an increasing degree of electron transfer in the newly formed Fe (hydroxy)oxides phase which would support the semiconductor mechanism.

3.9 Microbial Fe(II) oxidation

It has been demonstrated in field studies by Kirby and Elder Brady, (1998) that, in circum-neutral mine waters (pH 6 to 7), under moderate O_2 (approximately 4.5 mg/L) field determined Fe(II) oxidation rates are within one-half an order of magnitude of the predicted rate calculated using the Stumm and Lee's (1961) homogeneous abiotic rate law and the verified rate constant stated by Davison and Seed (1983) (Equation 3.3). A study by Søgaard et al (2000) of Danish water treatment plants reported Fe(II)

oxidation rates at circum neutral pH and with O_2 concentrations < 3 mg/L up to 60 times greater (Figure 3-5) than calculated using Stumm and Lee rate law and Davison and Seed's rate constant (Figure 3-4). The elevated rate has been attributed to microbial catalysis by neutrophilic lithotrophic Fe(II) oxidising bacteria (principally *Gallionella ferruginea*).

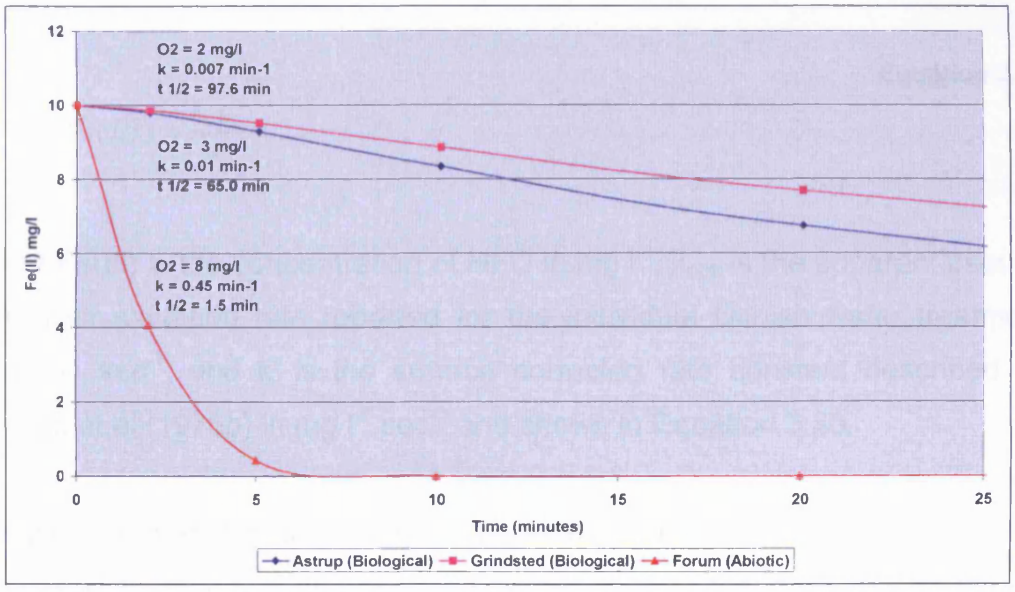

Figure 3-4: Modelled Fe(II) oxidation rates in three Danish potable water treatment plants as described by Søgaard et al (2000).
Modelled using abiotic rate constant as determined by Davison and Seed (1983) ($k=1.89x10^{14}$ $M^{-3}sec^{-1}$)using 10 mg L^{-1} Fe(II).

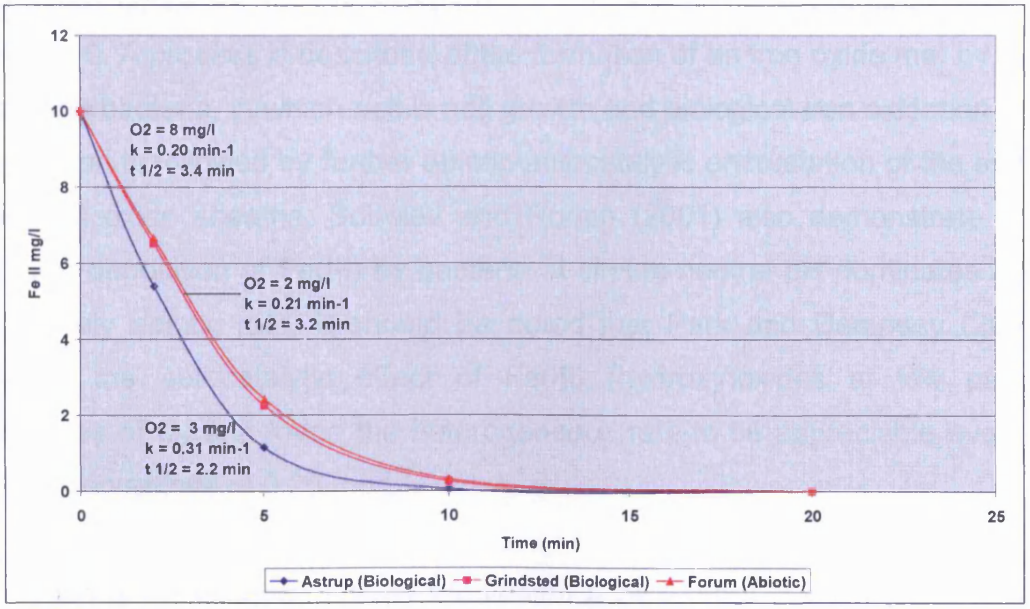

Figure 3-5: Fe(II) oxidation rates in three Danish potable water treatment plants for 10 mg L^{-1} Fe(II)calculated using actual field rate constants determined by Søgaard et al (2000) for the individual treatment plant.
Rate constants used; Astrup ($k=5.49x10^{15}$ $M^{-3}sec^{-1}$), Grindsted ($k=5.68x10^{15}M^{-3}sec^{-1}$) and Forum ($k=1.89x10^{14}$ $M^{-3}sec^{-1}$)

These results are questionable however, as abiotic heterogeneous catalysis is neglected. Calculations using the Tamura et al (1976b) heterogeneous rate law suggest that approximately 174 mg l^{-1} (Grinstead) and 295 mg l^{-1} (Astrup) of ferric precipitates would be required to produce similar observed oxidation rates using the expression derived from Equation 3.26:

Equation 3.26

$$Fe(III) = \frac{k_{obs}}{k'}$$

where Fe(III) is the concentration of HFO in mg l^{-1}, k_{obs} is the apparent pseudo first order oxidation rate reported for the individual Danish water treatment works in sec^{-1}, and k' is the surface corrected rate constant described by Tamura et al (1976b) in mg l^{-1} sec^{-1} and shown in Equation 3.20.

Anderson and Pederson (2003) studied the growth of *Gallionella ferruginea* biofilms in pumped ground water and described O_2, Eh and pH growth ranges of 0.5 – 3.5 mg/L, 130 – 250 mV and 7.2 - 7.6 pH units. Emerson and Weiss (2004) found iron oxide flocs in a Fe(II) rich wetland composed mainly of *Leptothrix ochracea* and *Gallionella ferruginea* sheaths at pH ranges between 5.8 and 6. A process is described of the formation of an iron oxide mat by iron oxidising bacteria, in which active cell growth and biological iron oxidation and deposition is followed by further abiotic autocatalytic encrustation of the spent bacterial oxide sheaths. Sobolev and Roden (2001) also demonstrate that suboxic deposition of Fe(III) by bacteria at circum-neutral pH dominates over the purely abiotic rate. It should be noted that Park and Dempsey (2005) studied the autocatalytic effect of Fe(III) (hydroxy)oxides at low partial pressures of O_2 and found the heterogeneous rate to be appreciable even at O_2 concentrations of 0.25 mg/L.

Emerson and Revsbech (1994) formulated a zero-order reaction rate for the oxidation of Fe(II) by neutrophilic Fe oxidising bacteria (0.7 – 1.35×10^{-9} mol (Fe(II)), cm^3 (Bacteria), $hour^{-1}$) at O_2 concentrations between 0.16 – 1.3 mg/L. This rate was used by Burke and Banwart (2002) in the modelling of Fe(II) removal in a passive engineered ochre accretionary reactor. The bacterial

effect was found to be negligible as the model was based on optimising oxygenation and promoting abiotic oxidation.

Other attempts to model passive mine water treatment schemes at both acidic and circum-neutral pH (Kirby and Elder Brady 1998, Kirby et al 1999, Dempsey et al, 2001) have neglected to include the possibility of neutrophilic microbial Fe(II) oxidation, though Kirby and Elder Brady (1998) and Kirby et al (1999) include rates associated with *Acidithiobacillus ferrooxidans,* which are well known to catalyze the oxidation of Fe(II) to Fe(III) under aerobic acidic conditions at rates up to 6 orders of magnitude greater than the purely abiotic rate alone (see Figure 2.3).

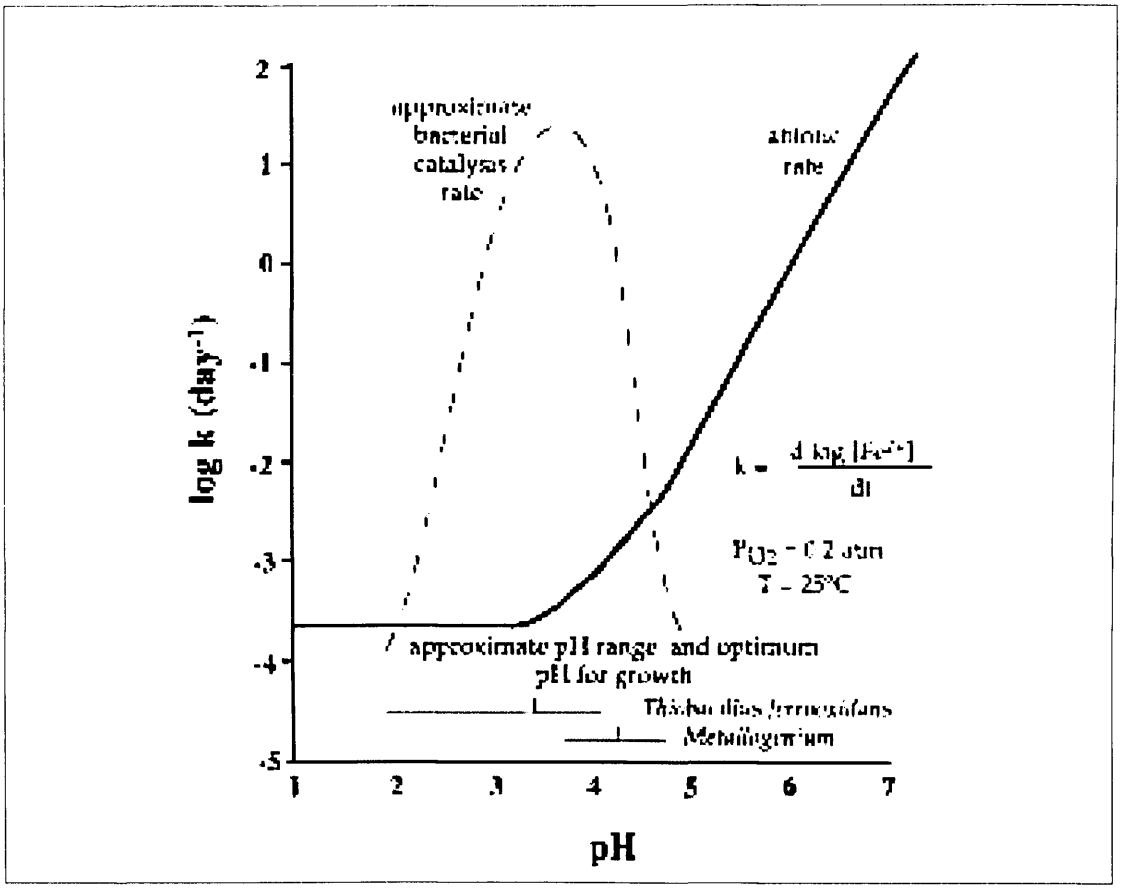

Figure 3-6: Schematic plot showing abiotic and biotic pseudo first order rate constants (in days^{-1}) for Fe(II) oxidation by oxygen, against pH

From Kirby and Elder Brady (1998), using data from Singer and Stumm (1970), and Waddell (1978)

3.10 Chapter summary

Chapter 3 has reviewed the literature concerning the oxidation of Fe(II) by dissolved oxygen in aqueous solution, with and without the presence of surface catalysts. An attempt has also been made to highlight the significance of microbial activity in the reaction. The chapter can be summarised as follows:

- The rate of homogeneous oxidation of Fe(II) is highly pH dependant. At pH between 5 and 8, the oxidation rate is inversely dependant on the square of the activity of the hydronium ion. Below pH 5 and above pH 3 this reduces to a linear dependence and below pH 3 the reaction appears to be largely independent of pH.
- The pH dependence of Fe(II) oxidation has been explained by previous investigators as the parallel oxidation of the various hydrolysed Fe(II) species. Hydrolysis (and some ligand complexation) promotes oxidation by decreasing electron density and facilitating electron transfer between the Fe(II) centre and the O_2 molecule.
- Fe(II) oxidation is autocatalytic with the reaction product at circum-neutral pH, (Fe(III) (hydroxy)oxide), acting as an effective catalyst.
- Previous research has found that significant sorbed Fe(II) remains on the surface of freshly precipitated Fe(III) (hydroxy)oxide, despite the presence of O_2. This indicates that a portion of the adsorbed Fe(II) is not available for the reduction of dissolved O_2. This has been attributed to heterogeneous, Interfacial Electron Transfer (IET) between the Fe(III) (hydroxy)oxide surface and the sorbed Fe(II). In addition this is backed in the literature by significant spectroscopic evidence.
- The mechanisms of Fe(II) surface catalysis are not currently well understood. Two theories have been presented in the literature as follows:
    1. The surface species mechanism – Reliant on fast reacting surface Fe(II) species.

2. The semi conductor mechanism – Reliant on Interfacial Electron Transfer, and the Fe(III) (hydroxy)oxide surface acting as a semiconductor.

- Microbial Fe(II) oxidation is limited to the oxic acidic and sub-oxic circum-neutral zones where purely abiotic oxidation rates are limited either by low- pH or O2 availability. Although there is a wealth of microscopic evidence for the existence of circum-neutral Fe(II) oxidising bacteria they often exist in, or actively precipitate an Fe(III) (hydroxy)oxide substrate.

4 Pilot plant design and construction

4.1 Introduction

The objective of the EPSRC-funded research project was to design, construct and operate a pilot scale Vertical Flow Reactor (VFR) using a gravel bed as a support media for ochre accretion. Previous small scale trials have shown that the system shows promising removal efficiencies (see Dey and Williams, 2000) and lends itself well to field scale operation. The chapter is split into the following sections:

Section 4.2 VFR design concept evolution – describes how the VFR design went from the initial concept into its current state as a field scale pilot plant.

Section 4.3 Pilot plant design – gives details of the design of the current field scale pilot plant.

Section 4.4 Site selection – describes the criteria used during the site selection for the VFR field trial and gives details of the chosen site.

Section 4.5 Construction – gives a step by step account of the VFR construction and commissioning.

4.2 VFR design concept evolution

Current best practice for the passive treatment of net-alkaline ferruginous mine effluent is up front pre-treatment, usually involving aeration followed by settling lagoons and then a final polishing in aerobic reed bed wetlands (Dey et al, 2003). The pre-treatment step is designed to remove 30 to 50 % of the iron load in order to a) reduce the stress on the polishing reed bed biota b) enhance the longevity of the system and reduce clogging of the polishing reed bed and c) allow easy removal and disposal of the precipitated ochre. It should also be noted that the inclusion of a settlement lagoon is generally

required for all passive treatment systems at some point (Sapsford et al, 2005). For instance in a passive system for the treatment of net acidic mine drainage a Reducing and Alkalinity Producing System (RAPS) or an Anoxic Limestone Drain (ALD) would generally be included prior to a settlement lagoon in order to add alkalinity and raise the pH to facilitate Fe(II) oxidation. In either case in order to attain 30 to 50 % iron removal a settlement lagoon will require a large surface area and generally achieve below 10 g m^{-2} day^{-1} iron removal (PIRAMID, 2003).

The design concept for the VFR treatment system evolved after observations made of the Gwenffrwd RAPS in South Wales. It was seen that a considerable portion of the iron load was being removed above the RAPS system as Fe(III) (hydroxy)oxides as opposed to being removed within the compost substrate via sulfide precipitation (Dey and Williams, 2000). It was thought that the mechanism of iron removal was via a process of catalytic oxidation and ochre accretion onto existing ochre particles. This gave rise to the development of an interesting alternative design concept to conventional pre-treatment offering enhanced removal efficiencies and reduced land take. Similar in theory to the "SCOOFI" process (Jarvis and Younger, 2001 and Burke and Banwart, 2002) but developed independently and unlike the SCOOFI process does not depend on a support media for iron accretionto take place. In contrast ochre accretion is allowed to take place above a gravel support forming an ochre bed through which mine water can flow vertically.

The design concept was initially trialled at the circum-neutral and net-alkaline Worsley Delph mine water discharge in Manchester, UK on behalf of Mouchal Parkman (Dey and Williams, 2001). The Worsley Delph reactor consisted of a 30 x 30 x 30 cm tank lined with an under-drained sand bed support for the accreting ochre bed. The trial ran for one week with the raw water pumped into the system using a small 12 V caravan pump. Preliminary results were promising as shown in Table 4.1 with up to 90 % total Fe removal and R_A values for total Fe between 18 and 48 g m^{-2} day^{-1}.

On the strength of the Worsley Delph trial a further field trial was undertaken at the Taff Merthyr mine water treatment wetland in South Wales (UK). The discharge is circum-neutral, net-alkaline and has an average total Fe load of 10 mg L^{-1} of which 6 mg L^{-1} is Fe(II). At peak the discharge flow rate can reach 180 L sec^{-1}. The VFR consisted of a 1 m^3 Intermediate Bulk Container (IBC) with a 100 mm bed of pea gravel in the base. A discharge pipe was connected to the base drain tap with a swan neck discharge to maintain the water level as shown in Figure 4-1.

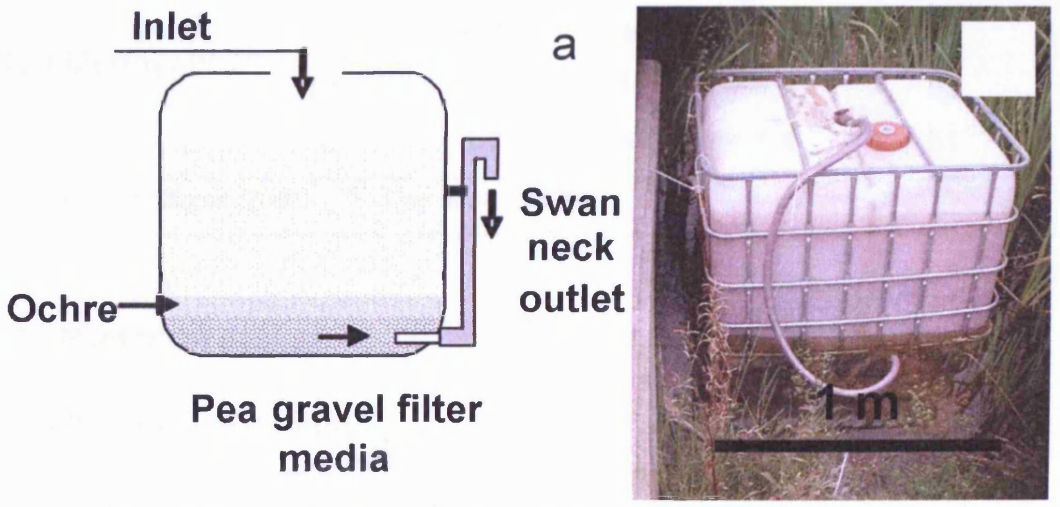

Figure 4-1: Taff Merthyr-Intermediate Bulk Container (IBC) field trial a) schematic b) photograph (from Sapsford et al, 2005).

This was then fed with water from the distribution channel of the Taff Merthyr settlement lagoon via a siphon tube. The performance of the IBC VFR at Taff Merthyr was promising with up to 93% total Fe removal with a nominal HRT of 6.3 hours equating to a R_A value for total Fe of 32 g m^{-2} day^{-1} and a variation of 26 – 79 g m^{-2} day^{-1} was observed. Table 4.1 gives details of the Worsely Delph and Taff Merthyr-IBC performances. The promising results of the two trials prompted the development of the design of a pilot-scale VFR. The aim was to demonstrate that the system is feasible for adaptationto full scale mine water treatment projects. On this basis a research proposal was submitted to the EPSRC and funding won for the design and construction of a pilot-scale VFR.

Table 4.1: Performance of the Worsely Delph and Taff Merthyr-Intermediate Bulk Container (IBC) field trials

Trial	Total iron (mg L^{-1})	pH	Flow rate (L hr^{-1})	Retention time (hr)	Iron removal (%)
Worsley Delph#	14	6-7	2	23.0	97
	14	6-7	4	11.5	95
	14	6-7	6	7.7	94
Taff Merthyr IBC*	10	6-7	135	6.7	81
	10	6-7	144	6.3	93
	10	6-7	171	5.3	88
	10	6-7	648	1.4	51

Dey and Williams (2001) * *Dey et al (2003)*

4.3 Pilot plant design

4.3.1 Design criteria

The design criteria listed in Table 4.2 were used as a basis for the VFR design. The basic design concept was identical to the small scale field trials at Worsley Delph and Taff Merthyr. The VFR would consist of two sections, a down-flow treatment section that would receive the raw mine water which was separated from an up-flow section by a baffle wall. The treatment section would be underlain by a gravel support bed onto which the ochre could accrete. This would be under-drained to the up-flow section in which a water level control structure was situated.

Table 4.2: VFR design criteria

Criteria	Justification
Ease of construction	Pilot plant design will allow construction by University research team with limited technical expertise.
Ease of up scaling	Should be designed with full scale construction in mind allowing adaptation of pilot scale design concepts to full scale construction and operation.
Ease of geochemical sampling and performance monitoring	Due to the research nature of this project and that extensive sampling will be undertaken, the design should include suitable systems for sampling and flow monitoring.
Hydraulic simplicity	Flow within the system should be kept as simplistic as possible to allow easy geochemical and hydrodynamic modelling.
Adaptability	Should be a flexible enough design to allow the trial of differing support medias and head characteristics for research purposes.
Budget	The cost of the build was limited by the constraints of the EPSRC funding.

4.3.2 Choice of materials

Due to the mass of the tank it was necessary to construct a reinforced concrete "raft" foundation the design of which was determined by Mouchel Parkman. For the construction of the main tank, three alternatives where considered:

1. A reinforced concrete tank, poured in-situ
2. A hollow concrete block wall tank with internal steel reinforcement and concrete filled.
3. A prefabricated galvanised pressed steel sectional tank on a reinforced concrete base.

Costs were determined for the construction of each tank type and viability was determined in terms of ease of construction and suitability in accordance with the design guidelines in Table 4.2. It was shown that a galvanised pressed steel sectional tank supplied by Horseley Bridge Tanks (part of the Balmoral

tanks group) formed the best possible material in terms of a cost / functionality basis. Using the constraints of this construction material the final design is as shown schematically in Figure 4-2.

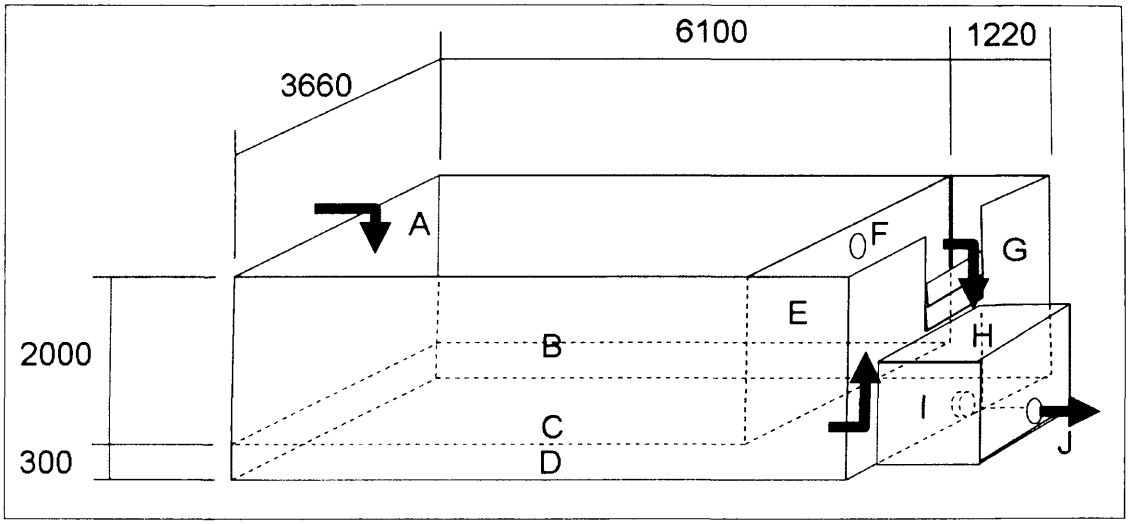

Figure 4-2: VFR tank schematic (not to scale) with approximate measurements in mm.

Where A = Raw mine water inlet B = Down-flow treatment chamber C = Gravel bed (see Figure 4.4 for details) D = Under-drain E = Up-flow chamber F = Treatment chamber overflow G = Weir level control structure H = Discharge collection chamber I = Gate valve from up-flow chamber to discharge collection chamber J = Outflow to stream

4.3.3 Under-drain design

The VFR is designed around an under-drained gravel bed as described earlier. Three different concepts where considered for the gravel support and drainage system:

1. System of slotted drainage pipes buried within the gravel medium and connecting to a central flexible swan neck tube the height of which could be adjusted to alter the driving head
2. Gravel bed underlain by a thick bed of large cobbles with a high hydraulic conductivity. Mine water would flow down through the gravel bed and then unhindered through the cobble support medium under a baffle wall and over a control structure

3. Fully suspended plenum floor design in which the gravel bed is placed above a mesh floor supported above the base of the VFR by a system of concrete pillars

The plenum and cobble supported gravel beds would present the most uniform horizontal flow conditions. It was decided that of these the plenum floor design would give the easiest calculation of water volume below the gravel bed and lent itself most readily to hydrodynamic modelling due to flow simplicity. Figure 4-3 shows a cross section through the VFR gravel bed as it appears during the second year of operation.

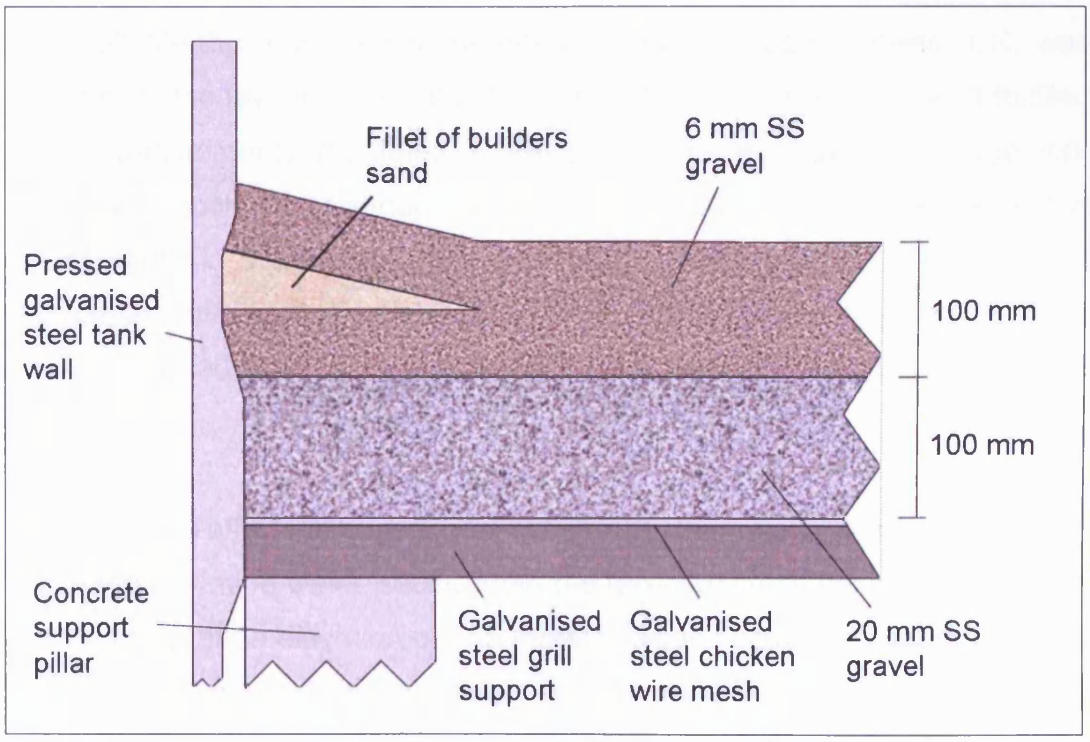

Figure 4-3: Cross section through the VFR gravel bed as it appears during the second year of operation

Where SS is sandstone

For the first year of operation a 100 mm thick bed of 20 mm sandstone gravel chips were used, in the second year a further 100 mm of 6 mm gravel chips where placed over the top of the existing 20 mm gravel in accordance with Figure 4-3. Also during the emplacement of the 20 mm gravel bed a fillet of builders sand approximately 100 mm wide (as shown in Figure 4-3) was

placed around the tank edges to curtail short circuiting / edge effects that were seen with the 20 mm gravel. It should also be noted that, in an attempt to prevent short circuiting / edge effects towards the end of the first year of operation using the 20 mm gravel a series of rags where placed around the edges of the tank to plug the gaps between the tank wall and the ochre / gravel bed. It was decided to use rags after they had proved useful in plugging of leaks around the outflow weir boards.

4.4 Site selection

4.4.1 The Taff Merthyr site

The Taff Merthyr mine water treatment scheme in South Wales, UK, was selected as the favourable locationto construct the VFR pilot plant as it fulfilled all the requirements stipulated in the siting criteria (Table 4.3, page 83). Figure 4-4 shows the regional location of the Taff Merthyr site in relationto the city of Cardiff in South Wales. The treatment scheme is located on the site of the former Taff Merthyr colliery (UKGR ST 103 990) which closed in 1993. The colliery had two 600 m shafts which were filled and capped shortly after closure.

The existing Taff Merthyr treatment scheme is a pumped / passive system in which the raw mine water issuing from the two capped shafts is collected in a central sump at an elevation of 155 meters Above Ordinance Datum (mAOD) and pumped to a distribution weir at 167 mAOD. The distribution weir subdivides the flow into four settlement lagoons via separate aeration cascades as shown in Figure 4-5 and Figure 4-6.

Figure 4-7 shows a cartoon schematic of the raw mine water collection, pumping and distribution systems. The distribution weir subdivides the flow in the following manner, lagoons L1 and L2 each take 30 % and lagoons L3 and L4 each take 20 %. Each lagoon is designed with a minimum 24 hours HRT (Coal Authority, 2002) and is intended to remove upwards of 50 % of the Fe load. After the initial pumping stage each treatment leg is entirely passive.

Final polishing of the mine water is undertaken by a series of reed bed wetlands in which *Typha latifolia* and *Phragmites astralis* form the majority of planted reed species, discharge to the receiving waters (the river Bargoed Taff) is consistently below the UK Environment Agency discharge limit of 1 mg L^{-1} for total Fe (Coal Authority, 2002).

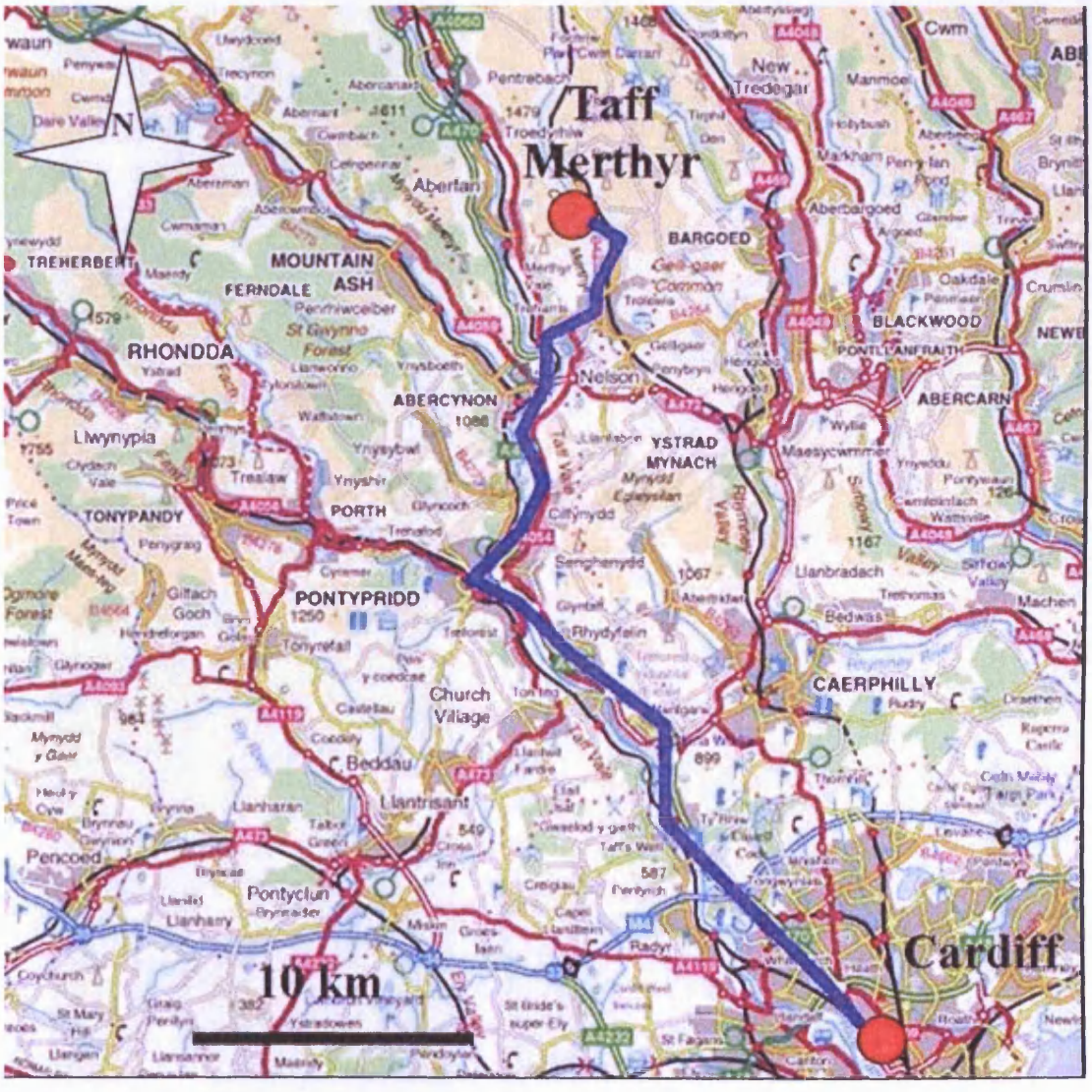

Figure 4-4: Map showing the location of the Taff Merthyr site in relationto the city of Cardiff, South Wales, UK.

The route marked in blue is 34 km. Map courtesy of Ordnance survey through the Edina Digimap service (2007).

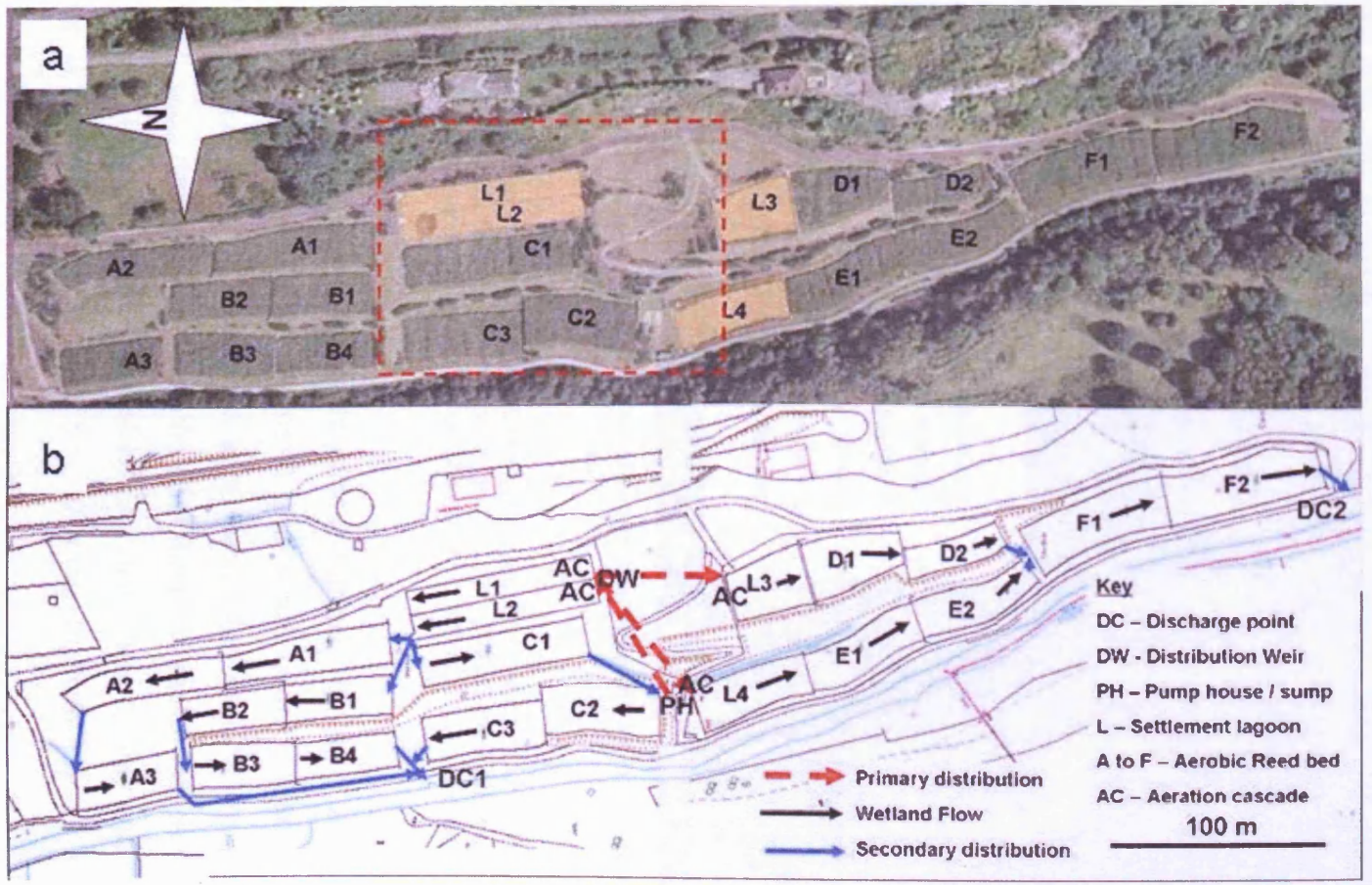

Figure 4-5: a) Aerial photograph and b) map of the Taff Merthyr site showing details of the settlement lagoons and aerobic reed-bed wetlands

Base image courtesy of Google Earth (2006), The geo information group (2007) and Europa Technologies (2007). Map courtesy of EDINA DigiMap service (2007). PH = pump house and sump, DW=distribution weir, AC=aeration cascade and L=settlement lagoon, DC=discharge point, letters A to F indicate individual reed-bed.

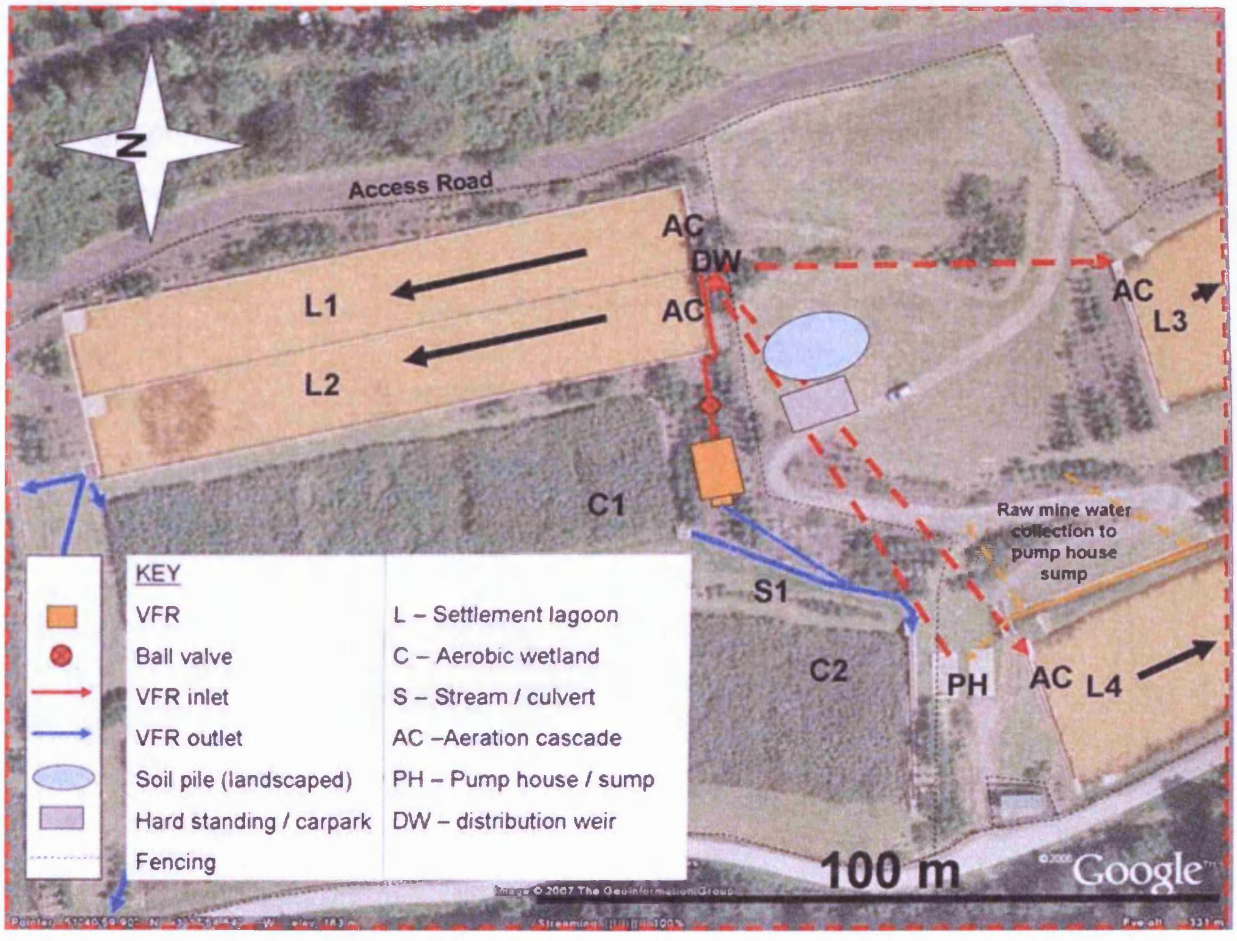

Figure 4-6: Exploded image of the Taff Merthyr site highlighted in Figure 4-5 showing VFR location and pump / distribution system

Base image courtesy of Google Earth (2006), The geo information group (2007) and Europa Technologies (2007). PH = pump house and sump, DW=distribution weir, AC=aeration cascade and L=settlement lagoon, DC=discharge point, letters A to F indicate individual reed-bed.

The pumping equipment consists of four pumps. Pumps 1 and 3 are ABS 1541A M90/4-22 EX, and pumps 2 and 4 are larger capacity ABS 2005 M185/4. The pumping capacities at a static head of 12.23 m are 49.6 and 105.9 L sec^{-1} respectively. Pumping operation and maintenance is carried out by Engenica (a Thames Water subsidiary) and currently only one of each size pump is in operation at any one time with the duplicate pumps kept as back up.

The pumps are activated by two float switches as shown in Figure 4-8 located in the raw mine water collection sump and pump chamber. Float switch a) is at a lower level than switch b) and activates one of the low capacity pumps.

Float switch b) is at a higher level and activates either one of the high capacity pumps. In this way the smaller pumps do the majority of the pumping with the larger pumps assisting during very high mine water flow conditions.

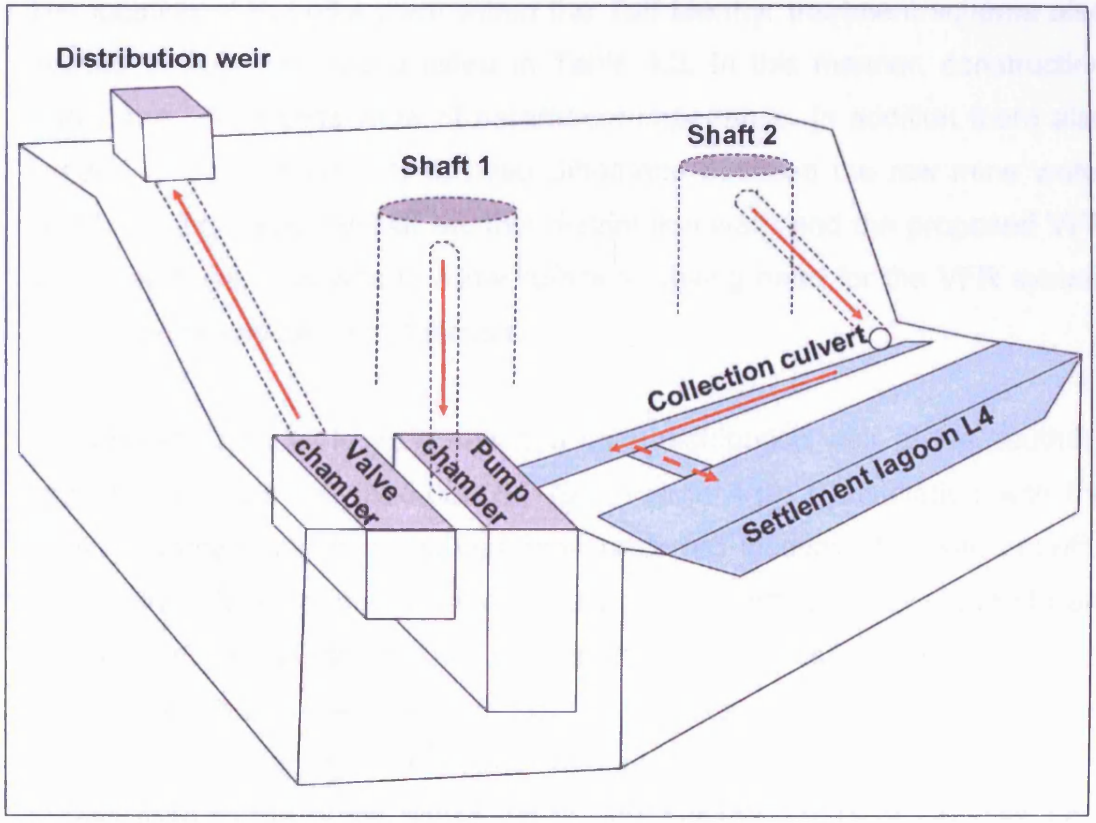

Figure 4-7: Schematic of the Taff Merthyr raw mine water collection and distribution system

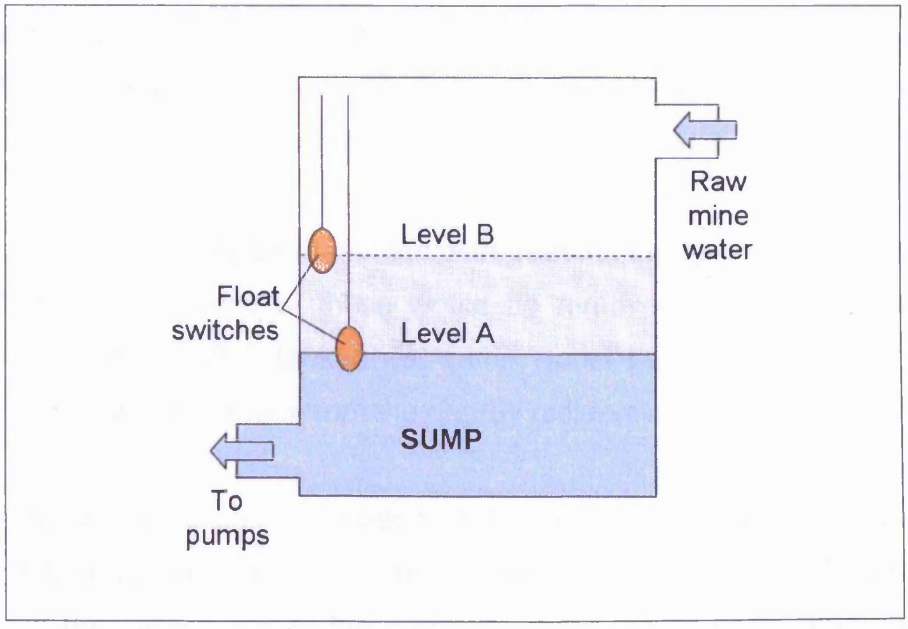

Figure 4-8: Schematic of the Taff Merthyr raw mine water collection sump and float switches

4.4.2 Pilot plant location

The location of the pilot plant within the Taff Merthyr treatment scheme also needed to fulfil the criteria listed in Table 4.3. In this manner, construction works and site access were of paramount importance. In addition there also needed to be at least 3 m of head difference between the raw mine water supply (in this case the Taff Merthyr distribution weir) and the proposed VFR discharge point. This was to allow sufficient driving head for the VFR system and the proposed aeration cascade.

The chosen site was located near the main distribution weir at the southern end of lagoon L2 and reed-bed C1 (see Figure 4-6). Consultation with the Coal Authority found that this was their preferred location. The site benefits from being close to the main distribution weir and an ideal downstream discharge point (the stream linking C1 and C2 reed beds). There was 3 m of head drop between the two points which was ideal for the VFR driving head requirements. The site was adjacent to the gravel track linking the main access road to the pump house which was suitable for HGV vehicles and, additionally a large area of open ground (50 m E-W x 100 m N-S), approximately 20 m to the south of the site was available for use. This was used for constructing a hard standing (car parking area and lorry turning circle) and also for the storage of excavation waste ready for landscaping.

The site had previously been planted with trees during the landscaping of the Taff Merthyr site. Some of these would be removed to make way for the construction of the VFR tank whilst some would be used to form a visual barrier shielding the system from the nearby residential property.

An alternative site would have been on the area of open ground marked in Figure 4-6 as the location of the soil pile. However, construction at this point would not be feasible due to the proximity of the buried rising main from the pump house to the distribution weir and would have a higher visual impact

due to the lack of tree cover. Construction would have required more pipe work both into and out of the system some of which would have to pass under the gravel access track causing further complications.

Table 4.3: VFR siting criteria

Criteria	Justification
Easy access from Cardiff University	To minimise travel times and expenses during routine sampling and construction.
Mine water chemistry typical of UK coal mine effluents	To allow proving of the VFR on a representative discharge enabling the most rapid conversion from pilot scale to full scale operation.
Existence of proven conventional treatment system for comparison of performance	Necessary to enable evaluation of VFR performance against existing systems.
Suitable space for construction	Enough free land for VFR treatment system including car-parking and for the movement of men and mobile plant during construction and decommissioning.
Well prepared access roads from main highway to construction site	To allow easy access for mobile plant, and HGV vehicles during construction and decommissioning.
Suitable head difference between raw discharge and receiving water	Necessary to provide enough driving head for VFR system to work.

4.5 VFR construction

4.5.1 Site survey, marking out and making safe

The proposed site was surveyed using a Laser Range Theodolite (LRT). Using this, the footprint of the excavation was marked out on the ground using a surveyor's tape measure and line marking spray paint. The area was then cordoned off with high visibility orange barrier fencing and secured with 1.3 m steel fencing pins. The appropriate warning signage was distributed around the area in order to make the dangers of access to the site clear to the public.

Figure 4-9: Site safety

4.5.2 Vegetation clearance and Excavation

In order for mobile plant to gain access to the site it was necessary to remove a 10 m section of chain wire fence. The wire fence was rolled back and the post stored for reinstatement after the project was completed. During construction this fence was replaced with the same orange barrier fencing as used to cordon off the back of the site at the end of each day.

A CASE CX130 back hoe and a Benford PS5000 dumper were hired with drivers from Ivor Thomas and Son, Neath, UK. Using the back hoe the vegetation was cleared from the work area. Wherever possible the trees were removed with root balls intact so that they could be replanted after work had been completed. An area of approximately 20 m (E-W) by 10 m (N-S) was cleared for the working area. A section of turf 5 m (E-W) by 10 m (N-S) was removed from beside the access road adjacent to the site to construct the hard standing area which would later be covered with 100 mm of sub base.

The back hoe was used to dig a 0.5 x 0.5 x 10 m trench from the south-west corner of L2 in Figure 4-6 to the start of the proposed aeration cascade. At this point the excavation was expanded to 2.5 m width for a further 5 m. A further trench was excavated from the discharge point into the receiving stream (S1 Figure 4-6) linking aerobic reed beds C1 and C2, at a level from the surface at the discharge point to the proposed overflow catchment at a

depth of 1.7 m. This trench was lined with approximately 150 mm of un-compacted sub-base.

The area for the main tank base was excavated to the dimensions of 10 x 6 x 1.7 m. The ground conditions were mainly as expected with made ground making up a majority of the site. However during the excavation of the main tank a large section of approximately 300 mm thick unbroken reinforced concrete was found at a depth of approximately 0.7 m. This slowed down progress and needed to be broken with a pneumatic hammer mounted on the backhoe prior to it being excavated as shown in Figure 4.11. It was also found that a buried retaining wall was situated at the eastern edge of the main tank excavation running parallel to the tank wall, this was left in place as it acted as a retaining wall between the deep (1.7 m) main tank excavation and the shallower (0.5 m) excavation of the aeration cascade base. This also meant that no support was required at the eastern edge of the main excavation. The sides of the main excavation were battered down to prevent slope failure as shown in Figure 4.12.

Figure 4-10: View looking west across the excavation showing the use of the pneumatic hammer to break the reinforced concrete slab.

Photograph courtesy of Dr Devin Sapsford, 12/04/05.

Figure 4-11: Looking east across the finished excavation ready for delivery of Type 1 sub-base.

Author (left) and Dr Mathew Dey (right). Photograph courtesy of Dr Devin Sapsford.

4.5.3 Foundations

The foundation design was drawn up and finalized by Mouchel Parkman engineers and consisted of reinforced concrete on a compacted sub-base. The sub base was 200 mm Type 1 sub-base compacted with 3 passes of a vibrating tamper plate (Hewden hire, Cardiff). Sectional plywood shuttering reinforced with 50 x 50 mm pine was constructed at the University to a depth of 300 mm and to the dimensions of 8800 x 4900 mm. The sectional shuttering was transported to site and bolted together ontop of the sub-base (see Figure 4-12). Once in place the shuttering was secured with 500 mm pegs of 20 mm diameter re-bar hammered on the outside of the shuttering.

The reinforcement consisted of two layers of A393 mesh reinforcement with the first layer spaced 50 mm from the sub-base with the second layer 200 mm above this. A further 50 mm was allowed above the second layer and the top of the shuttering. In the main tank each layer of reinforcement consisted of four sheets of A393 mesh (dimensions 2.4 x 4.8 m) with a 300 mm overlap. The same reinforcement was followed for the aeration cascade but leaving only 100 mm spacing between each layer of mesh and a single sheet above and below.

Figure 4-12: View facing east of the assembly of the ply-wood shuttering, ready for layering of the reinforced mesh and concrete pour.

Foreground Prof Keith Williams. Background Author (right) Dr Mathew Dey (left). The unearthed concrete retaining wall is just visible at the back of the excavation Photograph courtesy of Dr Devin Sapsford.

Figure 4-13: View facing east during the first pour of concrete onto the sub-base, shuttering-mesh assembly.

Photograph courtesy of Dr Devin Sapsford.

C40 concrete was used as stipulated by Mouchel Parkman and supplied pre-mixed by Minimix Ltd (now part of the Lafarge group). A spread of the concrete over the entire base was made easier by the use of a 5.5 m^3 capacity lorry with a 15 m placing conveyor as shown in Figure 4-13, in total 15 m^3 of concrete was laid in the first pour and was tamped off and levelled to

the top of the shuttering by Cardiff University personnel. The base was then left for 48 hours to go off.

4.5.4 Tank construction

A sectional steel tank was purchased from Horseley Bridge Tanks and consisted of square galvanised hot pressed steel sections 1.22 x 1.22 m in diameter (see Figure 4-14). The sections were externally flanged and manufactured in accordance with BS1564, 1975 Type 1. The finished tank dimensions were 7.32 x 3.66 x 2.44 m with a baffle wall 1.22 m from the discharge end which finishing 350 mm short of the base. This was to allow water flow down through the gravel bed and under the baffle wall. The tank was supplied without a base and was set in 150 mm of concrete poured above the reinforced concrete base as shown in Figure 4-15. A 100 mm gate valve was installed 200 mm from the base of the central panel at the discharge end to allow drainage of the system. The upper central panel was completely removed to allow for the installation of a weir structure. In addition the upper central panel of the baffle wall would also have a 100 mm diameter cut out 100 mm from the top to allow overflow.

The tank was constructed by a construction team from Horseley and was bolted together with water tight seals made by rubber gaskets between the individual sections. The tank was braced internally at the top and middle levels by galvanised steel angle bar which is a standard design feature of the sectional steel tank. This consisted of lateral stiffeners in the middle of the tank and 45^0 stiffeners in the corners as shown in Figure 4-16.

The inside of the tank was braced at the base with five 150 x 20 mm timbers across its width which had been notched at the base to allow the installation of sampling tubing which can be seen in Figure 4-16. The timber braces would give a surface to tamp to for the second pour of concrete as well as preventing flex in the sides of the tank. Figure 4-15 shows the completed tank assembly after coating with an acid etch solution to roughen the surface of the steel. The gasket seals were further waterproofed with beads of black mastic

and then the entire inside of the tank and the timber braces were coated with a bituminous paint to prevent leakage, corrosion, rot (in the case of the timbers) and to further increase the water proofness of the tank.

Sampling tubing was installed consisting of a series of sixteen 10 mm flexible plastic tubes threaded through the spare bolt holes at the base of the discharge end of the tank. The tubes where then threaded under the timber braces to rise at pre determined locations as shown in Figure 4-16. Using two elbow connectors a snorkel-like end was attached to prevent blockage during the concrete pour or a build up of sediment during operation.

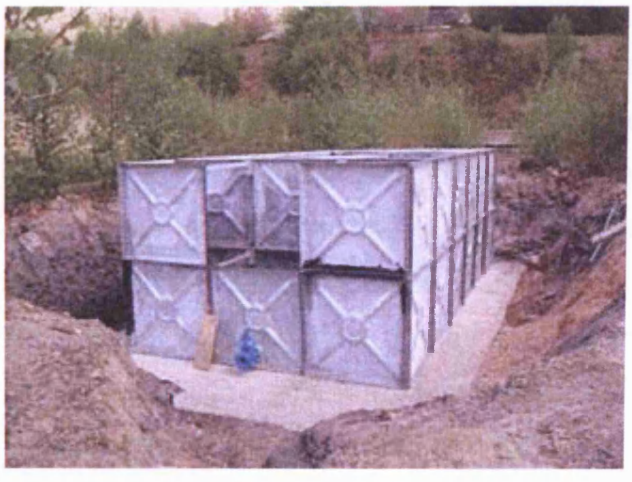

Figure 4-14: View facing east of the exterior of the assembled steel tank
The dull surface is due to the acid etch applied prior to painting with bituminous paint. The baffle wall and gate valve are clearly visible. Photograph courtesy of Dr Devin Sapsford.

Figure 4-15: View facing west of the inside of the sectional steel tank (looking towards the discharge end)
The wooden struts, sample tubes, steel cross members and the gap below the baffle wall can be seen. Photograph courtesy of Dr Devin Sapsford.

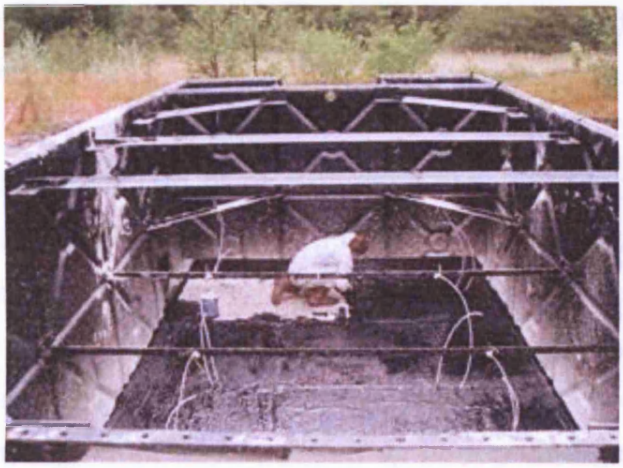

Figure 4-16: View facing west of the inside of the tank after the second concrete pour
The concrete is being coated with bituminous paint to minimise seepage. The sample tubes can clearly be seen protruding from the concrete base. Photograph courtesy of Dr Devin Sapsford.

The second pour of C40 concrete was made once the bituminous paint had dried and consisted of 150 mm depth inside and outside of the tank. This pour would act to anchor the tank sides and also form the impermeable base to the tank and was tamped down internally to the surface of the timber braces. It should also be noted that the sampling tubes were buried in the concrete base. After a further 48 hour curing period, a coating of bituminous paint was applied to the concrete floor of the tank forming a waterproof layer above the concrete and adjoining the tank walls (see Figure 4-16). Any large cracks that formed during contraction of the concrete were filled with black mastic to prevent leakage. The finished tank consisted of two sections the larger (6.1 x 3.66 m) would form the treatment end and would be fitted with a plenum floor and under drained to the smaller (1.22 x 3.66 m) "clean" end with the outlet weir. Once the coat had dried the VFR was filled a quarter full with water using a petrol pump (Hewden hire, Cardiff) to check for visible seepage.

4.5.5 Construction of the plenum floor, gravel bed and outlet weir

The plenum floor in the treatment tank was constructed of fifteen 1.2 x 1 m galvanised steel grates with yield strengths of 20 kN m^{-2} (Arco Redman). It was necessary to cut the central gratings to reduce the width and allow them to fit in the tank. This was done using an oxyacetylene torch and ends where cut bare steel was exposed were treated with bituminous paint to prevent

corrosion. Extra stiffening was also supplied to the cut ends in the form of lengths of aluminium box section.

To support the floor concrete block work was constructed in the base of the tank (see Figure 4-17), the desired height of 300 mm was attained by building one block on its side and another ontop upright. These were fixed in place with cement mortar and positioned so that the corners of the gratings were supported at each point. The grating was laid on the block work and the sampling tube arrangement was threaded up through the grates as shown in Figure 4-18. The bed design would incorporate initially a 100 mm layer of 20 mm sandstone gravel to be placed above the plenum floor to form the ochre bed support, in order to prevent this from falling through the grating a layer of 10 mm galvanised "chicken wire" was fastened to the grating using zip ties and was also used to mould to the contours of the inside of the tank walls to prevent the gravel from falling through. The finished bed is shown in Figure 4-18 looking into the tank from above and in Figure 4-19 looking from underneath the finished bed. It should be noted that at the beginning of the second year of operation a further 100 mm of 6 mm sandstone gravel was added to the top of the initial layer of 20 mm gravel.

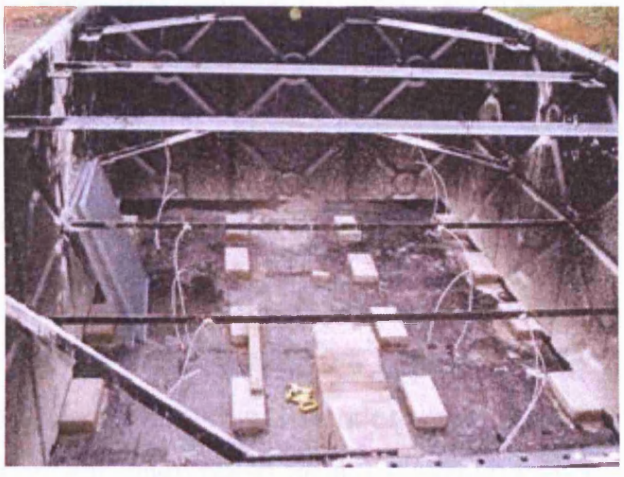

Figure 4-17: View facing west of the concrete block support arrangement for the plenum floor

Photograph courtesy of Dr Devin Sapsford.

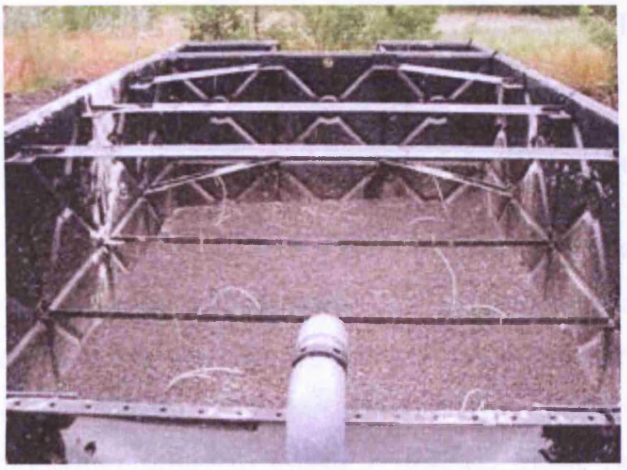

Figure 4-18: View facing west of the finished plenum floor with the 100 mm thick bed of 20 mm sandstone gravel.

The finished inlet pipe is also visible in the foreground. Photograph courtesy of Dr Devin Sapsford.

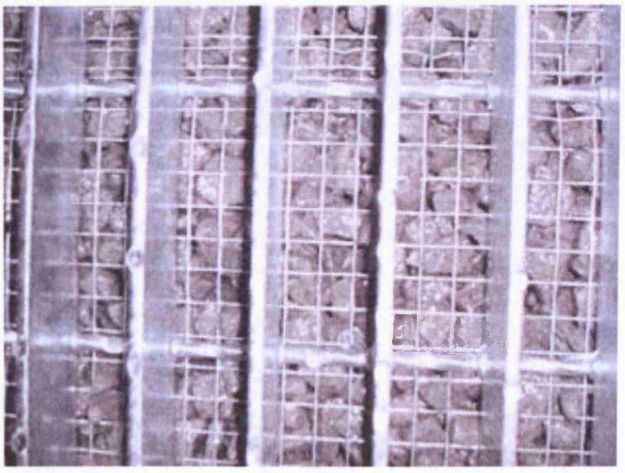

Figure 4-19: Looking up through the plenum floor showing the steel grill, chicken wire and gravel layers.

Photograph courtesy of Dr Devin Sapsford.

The corners of the channel section were sealed with Evo-Stik Liquid Metal® to prevent leakage. Figure 4-20b shows the completed weir. The weir boards were constructed of 25 x 150 mm pine timber with a 90° V-notch cut out of the top two boards, the tank level could be set by adding or removing boards as necessary. The V-notch section was constructed from two timber sections bolted together allowing a 250 mm deep V-notched sectionto be removed. Water overflowing from the V-notch would flow freely into the discharge

chamber. The white material in between the weir boards in Figure 4-20b is sealing putty left over from the sealing of the tank.

4.5.6 Building the discharge chamber and outflow pipe

The outflow pipe consisted of 110 mm internal diameter brown PVC push fit soil pipe in 4 m lengths joined with double socket soil pipe couplers. The pipe assembly was packed in sub-base in the base of the outlet trench with a slight overhang at the discharge end into the stream. The level of the pipe was checked by pouring water down to check it drained freely before he trench was backfilled. The discharge chamber end of the pipe was allowed to rest 200 mm onto the reinforced concrete base.

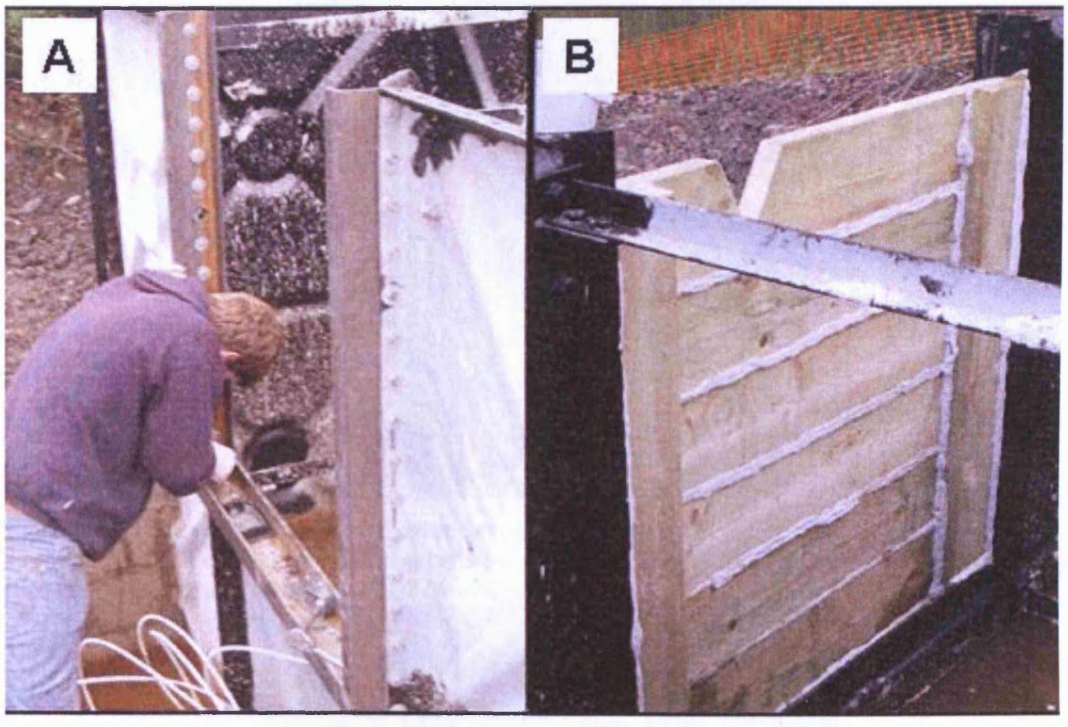

Figure 4-20: a) Attachment of the mild steel box section weir support at the discharge end of the tank, b) Completed weir showing the V-notch and putty used for sealing the weir boards.
Author pictured. Photograph courtesy of Dr Devin Sapsford

The discharge chamber was constructed from a single layer of high density concrete blocks as shown in Figure 4-21 and supported internally with step structures constructed in block work to aid access to the chamber. The finished dimensions were 1.32 m wide x 1.96 m long x 0.86 m deep. Once

backfilling around the chamber was complete two 20 x 50 x 1960 mm double channel section, galvanised steel girders were fixed to the tops of the walls adjacent to the tank walls with plugs and screws. This would be used to support two 1.2 x 1 m galvanised steel grates to cover the chamber and prevent access as shown in Figure 4-22. The right hand grate had a section removed to allow access to the gate valve using a adapted key fitting. The sampling tubes where threaded up through the grate and secured into an adapted strong box. Each of the sampling tubes were fitted with a ball valve at this end to allow flow control during sampling. The area outside the discharge chamber was backfilled with unused sub-base material to allow good drainage and reduce the pressure on the retaining walls.

Figure 4-21: Construction of the discharge chamber.
The sampling pipe arrangement can be seen rising up against the tank wall. *Dr Mathew Dey pictured. Photograph courtesy of Dr Devin Sapsford.*

Figure 4-22: View looking east of the finished discharge chamber showing the galvanised steel grating.
Photograph courtesy of Dr Devin Sapsford

4.5.7 Building the inflow pipe and aeration cascade

The inflow pipe was to be tapped directly into the weir plate of the Taff Merthyr distribution weir (see Figure 4-23). The sequence of photographs in Figure 4-24 shows the route taken by the feed pipe. A 100 mm internal class C ABS pipe (rated to 9 bar) with cemented joints was used to prevent leakage. The pipe was secured to the inside of the L2 aeration cascade and was then buried in a hand dug trench along the south edge of the L2 settlement lagoon distribution channel. A further two angles where inserted as the pipe dropped into the main trench leading to the aeration cascade base at which point an ABS ball valve was fitted.

Figure 4-23: Insertion of the VFR feed pipe into the distribution weir

Photos courtesy of Dr Devin Sapsford Mr Jeff Rowlands (Light blue) and Author (Black)

The initial design incorporated an aeration cascade constructed of high density concrete blocks onto the reinforced concrete base. Building was commenced and was near completion when it suffered vandalism and was largely destroyed. Due to the relatively high dissolved O_2 of the pumped mine water (3-4 mg/L), it was decided not to rebuild the aeration cascade and inlet pipe was plumbed directly into the VFR as it was decided that removing the aeration cascade would reduce further tampering with the system. Working on these principles the existing pipe was extended along the base of the concrete up to the tank wall where an elbow was inserted and a vertical

section inserted. The pipe assembly was finished with a "swan neck" section over the tank side forming the inlet and secured with a heavy duty pipe clip bolted to the tank as shown in the final image of Figure 4-24.

Figure 4-24: Sequence of photographs showing the feed pipe from the distribution weir to the VFR inlet

Photos courtesy of Dr Devin Sapsford Mr Jeff Rowlands (Light blue) and Author (Black)

4.5.8 Finishing and landscaping

To complete the VFR construction the back hoe and dumper were used to back fill around the tank and over the inlet and discharge pipes. The trees that were removed during the initial site clearance where re-planted and the

original fencing was reinstated with the fence posts set in post crete. In additionto this a gate was installed at the edge of the gravel path to allow access to the site and was locked with a chain and standard Coal Authority lock. Excess sandstone gravel was used to form a path from the gate to the VFR and along the southern edge. This was edged with stones and allowed visitors access. The soil and construction waste pile was capped with the removed topsoil and later landscaped (curtsey of the Coal Authority) being seeded with grass. The soil around the tank was not seeded but was covered in compost mulch (Cardiff University, Carmarthen composting centre) and left to self seed.

4.5.9 Alterations to the VFR during operation

The VFR remained largely unaltered during the first year of operation apart from the addition of a 5 mm grey acrylic weir plate that was fitted behind the existing VFR weir boards. The weir plate was designed to prevent leakage that was occurring between the weir boards.

Figure 4-25: Using cotton rags to block short-circuiting pathways around the tank walls

Professor Keith Williams pictured. Photograph courtesy of Dr Devin Sapsford.

The VFR was operated and monitored between the 17th of June 2005 and the 13th of May 2007 (a total of two years) after commissioning. Initially the gravel bed support consisted of a 100 mm layer of 20 mm diameter sandstone

gravel. Operation of the pilot plant using this support medium continued between the 17th of June 2005 and the 25th May 2006. On the 16th of May 2006 the tank was drained and wet cotton rags were placed around the edge of the tank as shown in Figure 4-25, in an attempt to curtail the short-circuiting observed during the first year of operation.

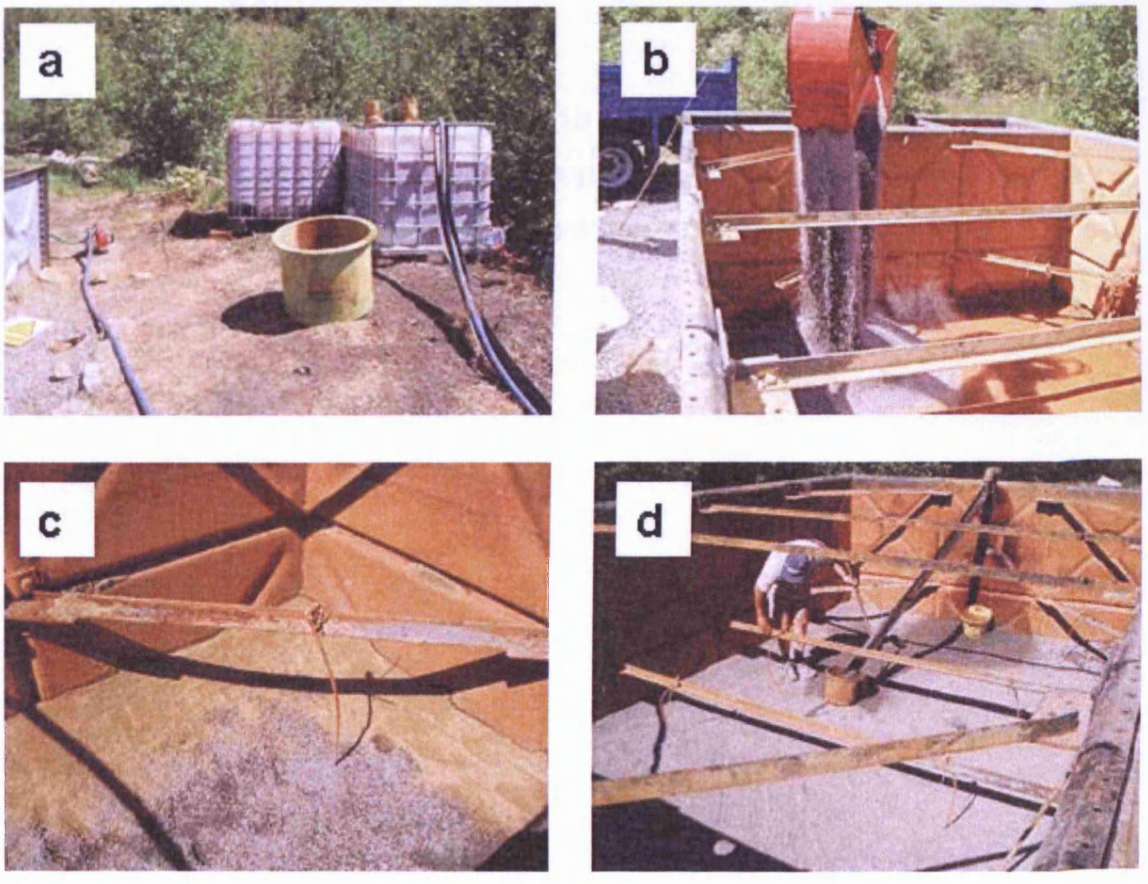

Figure 4-26: Sequence of photos showing the installation of the 6 mm gravel bed

a) the ochre removal pump, b) the delivery of 6 mm gravel, c) installation of the fillet of builders sand, d) the finished 6 mm gravel bed Prof Keith Williams pictured in bottom right. Photographs courtesy of Dr Devin Sapsford

The pilot plant was drained on the 25th of May 2006 in order that the accumulated ochre could be removed and an additional 100 mm layer of 6 mm sandstone gravel could be added. This was placed above the original 100 mm of 20 mm gravel using the procedure described as follows:

1. VFR drained until the freatic surface is approximately 50 mm above the ochre bed.

2. The ochre was then shovelled by hand into a large (approximately 250 L) fibreglass tub positioned on the gravel bed. Water was then added to the ochre slurry as required to make a suspension of a consistency suitable for pumping with a small petrol two stroke centrifugal pump.
3. The pump lifted the ochre suspension over the top of the VFR and into two empty IBC's.

During the second year of operation a 10 L bucket was suspended beneath the inlet swan neck. This was initially to prevent scour of the bed during the second year as water levels were kept to a minimum.

5 Field sampling – materials and methods

5.1 Introduction

The following chapter describes the materials and methods used in the hydrological and geochemical monitoring of the VFR and settlement lagoons. The chapter is split into the following sections:

Section 5.2: Flow rates and head determination – gives the details of the methods used in the determination of flow rates and determining head difference (water depth) in the VFR and settlement lagoons.

Section 5.3: Geochemical sampling methods – gives details of the methods used in the determination of geochemical and electrochemical field parameters including analytical methods.

Section 5.4: Field oxidation rates – gives the details of the methods used in the determination of homogeneous oxidation rates of Fe in the field.

Section 5.5: Field sampling protocols – Gives details of the sampling protocols followed during the VFR monitoring program

Section 5.6: Decommissioning and final sampling – describes how the VFR was decommissioned at the end of the sampling period and details how ochre was collected for analysis.

5.2 Flow rates, head and permeability determination

5.2.1 Flow rate determination for the VFR

The measurement of flow rate through a mine water treatment system of known volume allows for the calculation of HRT and contaminant removal rates consequently forming an integral part of any monitoring program. With the VFR, flow rates were measured using the volumetric container and stopwatch technique as reported in Wolkersdorfer (2006) in which the time taken to fill a container of known volume is used to calculate the flow rate as follows:

Equation 5.1

$$Q = \frac{V}{\Delta t}$$

Were Q is the flow rate (L sec^{-1}), V is the volume of the container (L) and t is the time taken to fill the container (sec). In the case of the VFR a 10 L bucket was used and calibrated using a 1000 mL measuring cylinder. In each case between 5 and 10 measurements were taken and the mean was used for further calculations. It was found that the standard deviation of all readings was within ± 10 % of the mean value. It has been reported that this method of flow measurement is very accurate when the time taken to fill the container is greater than 10 seconds and in the case of the VFR a 10 L bucket was used which therefore is accurate with flows less than or equal to 1 L sec^{-1} (PIRAMID, 2003).

For the first three months of VFR operation Q was monitored at the inlet to the VFR, this proved to be problematic as the inlet flow was not always constant and therefore did not represent the mean flow through the VFR. This can be explained by the switched pumping system at the Taff Merthyr site described in the previous chapter which pumps to the distribution weir from which the inlet pipe to the VFR was tapped. During times of low mine water discharge flows (usually during the summer months) pumping was intermittent and

therefore the flow to the VFR was also intermittent and did not reflect the mean flow through the VFR system. After the first three months of operation, VFR flow rates were recorded at either the discharge over the weir into the collection chamber or at the outfall into the receiving stream thus giving a point measure of the system "smoothed" flow rate.

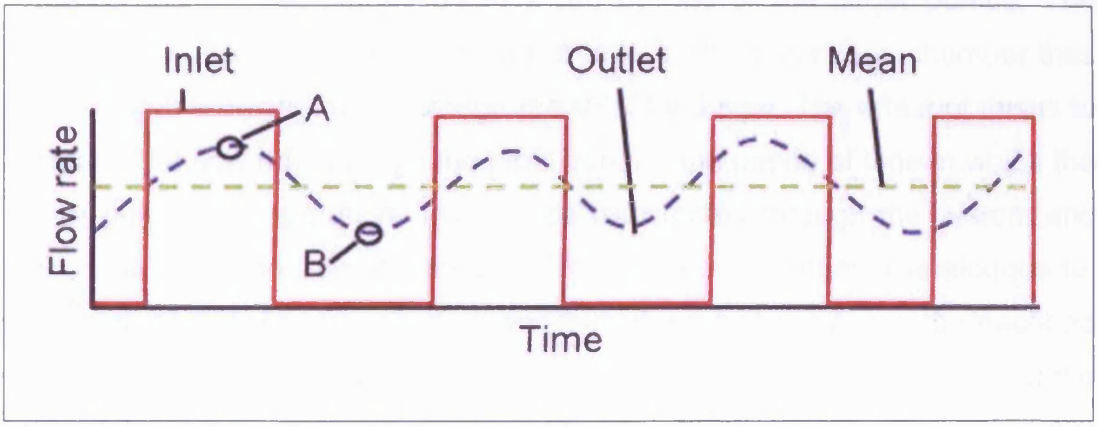

Figure 5-1: Schematic chart illustrating the effect of flow smoothing on an intermittent flow through a water body with time

Inlet = Flow rate recorded at the inlet, Outlet = Flow rate recorded at the outlet, Mean = The mean flow rate through the water body. Points A and B demonstrate the variability from the mean in flow rates calculated from spot measurements taken at different times.

Figure 5-1 shows how an intermittent flow at the inlet to a water body is effectively smoothed during flow through the water body. This effect was observed for the settlement lagoons L1 and L2 during intermittent pumping and presumed to hold true for the VFR system. During this research the variation in the flow rate measured at the VFR discharge over an extended period was not determined. It has been presumed that a spot measurement of flow rate at the VFR discharge is representative of the mean flow through the VFR system. However, Figure 5-1 demonstrates that during times of intermittent pumping (and therefore inlet flow), a spot measurement can deviate from the mean flow rate by an amount defined by variance of the data. In absence of a true measure of the standard deviation, a deviation of ± 10 % from the mean point measurement has been allowed in quoting discharge values as mean VFR flow rates. It should also be noted that seasonal variations will occur in the standard deviation from the discharge flow with the value being minimal during winter months where pumping is constant and

being maximal during summer months where pumping is intermittent.

During times of high mine water flow and therefore constant pumping there can be a variation in flow at the VFR inlet due to a variation in the driving head at the distribution weir. This is associated with the continuous operation of either of the smaller pumps being aided by one of the larger pumps. The associated water surge raises the water level in the distribution chamber thus increasing the driving head through the VFR feed pipe. The effect of this is to increase the flow rate through the pipe work for the period of time in which the larger pump is in operation. This will be transmitted through the system and will cause deviation from the mean VFR flow rate in a manner analogous to, (although of a lesser magnitude than) that of intermittent pumping described previously. The ± 10 % deviation applied to point measurements of flow at the VFR discharge is assumed to account for the variations from the mean VFR flow rate due to this affect.

Determination of mean VFR flow rates from the first three months of operation in which only VFR inlet flows were recorded during pumping was attempted as follows. Using weekly pump run totals (the hours worked by each pump) for the Taff Merthyr site an average weekly ratio of pumps onto pumps off was determined as follows:

Equation 5.2

$$P_R = \frac{H_{P1}}{W_H}$$

where P_R is the weekly pumping time on / off ratio, H_{P1} is the time in hours pumped by either pump 1 or 3 and W_h is the total number of hours in a week. Using the value of P_R it is possible to crudely correct for the effect that the pump down time has on the overall mean flow through the VFR using measurements taken at the VFR inlet during pumping, simply by the relationship:

Equation 5.3

$$Q_{Mean} = Q_{Inlet} P_R$$

where Q_{MEAN} is the mean flow through the VFR (L sec^{-1}), Q_{INLET} is the flow measured at the inlet to the VFR during flow on conditions (L sec^{-1}) and P_R is the weekly pumping ratio.

It is also apparent that there is a lag time between cessation of pumping and cessation of flow into the VFR. This can be attributed to the draining under falling head conditions of two distinct reservoirs above the level of the VFR inlet. The reservoirs are:

1. The volume of the distribution weir chamber below the base of the V-notch and above the base of the VFR feed pipe
2. The volume of the VFR feed pipe work above the VFR inlet level

After commissioning mine water flow rates through the VFR were measured at the discharge from the VFR into the receiving stream (conduit from reed bed C1 (see Figure 4-6) using a plastic 10 L bucket calibrated using a 1 L measuring cylinder. The time to fill to 10 L was then recorded with a stopwatch. In each case the mean of at least 5 readings were taken to determine the average flow rate.

5.2.2 Flow rate determination for L1 and L2 lagoons

Flow rates for the Taff Merthyr settling lagoons were determined via two methods. Firstly flow rates were calculated using weekly pumping hours run and flow rates for the individual pumps as follows:

Equation 5.4

$$Q_L = 0.6\sum\left(Qi\left(\frac{t_{pi}}{t_w}\right)\right)$$

where Q_L is the combined flow rate for the L1 and L2 settlement lagoons (L sec^{-1}), the subscript $_i$ can be either of the four pumps, Q_i is the flow rate

attributed to each pump (L sec^{-1}), $t_{p/}$ is the weekly pumping total attributed to each pump (hours) and t_w is the total hours in a week. The factor 0.6 represents the share of the total flow entering the L1 and L2 lagoons. Flow rates for pump on times were approximated from the manufacturers pumping curves (see Appendix 2) and the pumping head data of 12.23 m taken from the site plan (height between pump level and the top of the distribution weir V-notch. No attempt was made to correct for variation from ideal pump flow rates due to a drop in pump efficiency with wear or by constrictions in the pipe work due to ochre accretion.

The second method for the determination of the combined flow for the L1 and L2 lagoons was using the subsurface or 0.9 x V-Max method from maximum channel flow velocities determined with a vane flow meter near the water surface (U.S. Department of the Interior – Bureau of reclamation, 2001). The flow is calculated as follows:

Equation 5.5

$$Q_l = fVA$$

where Q_L is the flow rate (m^3 sec^{-1}), V is the central channel velocity (m sec^{-1}), A is the cross sectional area of the channel (m^2) and f is the factor for average velocity in area which can vary between 0.85 and 0.95, however a value of 0.9 is commonly used (Marsh McBirney, 2007). In addition it was found that using the value of 0.9 for f resulted in the best correlation between flow rates determined using the subsurface method and values determined using the pumping hours.

5.2.3 VFR head measurement

The hydraulic head difference was routinely measured between the treatment and up-flow sections of the VFR. Measurement was made using a tape measure from the phreatic surface and the tank top datum on either side of the baffle wall.

The head difference was calculated as follows:

Equation 5.6

$$\Delta H = H_t - H_l$$

where ΔH is the head difference (m), H_T is the water level below the tank top on the treatment side (m) and H_U is the water level below the tank top on the up-flow side (m).

5.2.4 VFR permeability calculations

Due to the nature of the VFR it was not possible to directly measure the thickness of the accreting ochre bed to calculate the true coefficient of permeability using Darcy's Law which states that:

Equation 5.7

$$K = \frac{Q}{\left(\frac{\Delta H}{L}\right)A}$$

where K is the coefficient of permeability in m sec^{-1}, Q is the flow rate in m^3 sec^{-1}, A is the cross sectional area of the ochre bed in m^2, ΔH is the head loss across the bed in m and L is the thickness of the bed in m. In the absence of bed thicknesses a Bed Thickness Independent (BTI) coefficient of permeability K_L in sec^{-1} (Sapsford, 2007) can be calculated as follows:

Equation 5.8

$$K_l = \frac{Q}{\Delta HA}$$

This is related to the true coefficient of permeability by the expression:

Equation 5.9

$$K = K_L L \ .$$

5.3 Geochemical sampling methods

5.3.1 Determinations of temperature, pH and Eh

Temperature, pH and Oxidation Reduction Potential (ORP) where determined using a Hanna Instruments HI-991003 which uses a glass electrode for pH and a platinum electrode for ORP combined with a single gel reference electrode. The instrument also has Automatic Temperature Compensation (ATC) to correct the measured pH to a theoretical reading at 25°C.

pH calibration was carried out at ambient temperature in the field using pH(25°C) 7.01 and 4.01 NIST certified buffers in accordance with the manufacturer's guidelines (which state that pH calibration should be carried out using fresh buffer solution, without stirring and as near as possible to the ATC temperature of 25°C). Under ideal conditions an error of ± 0.02 pH units from the absolute value should be obtained as stipulated in the manufacturer's guidelines. However, it was often found that after calibration in the field, the instrument would deviate by as much as ± 0.05 pH units away from the pH 7.01 buffer concentration when re-immersed. It should also be noted that field measurements themselves will affect the accuracy of the measurements due to the introduction of potential effects such as stirring and suspension effects as documented fully in Galster (1991). Therefore a conservative error of ± 0.1 pH units has been applied to field readings.

With ORP determination the manufacturer's states an accuracy of ± 1 mV which is used as a real error. In order to correct ORP readings to true system Eh readings a correction of + 200 mV was added to the ORP measurement to allow for the Ag / AgCl reference electrode in a gel stabilised saturated KCl electrolyte.

Temperature measurement should be accurate to ± 0.5 °C as stated in the manufacturer's guidelines and is used as a real error.

5.3.2 Field dissolved oxygen measurement

Dissolved Oxygen was determined with a Hanna Instruments HI-9142 portable dissolved oxygen meter. This featured ATC and one point calibration at 100 % saturation in moist air. All calibration procedures were in accordance with the manufacturer's guidelines and were carried out in the field at ambient temperature.

The instrument gave a readout in parts per million (ppm) which was taken to be directly comparable to mg L^{-1}, which assumes a density of water equal to 1000 kg m^{-3}. Corrections where not made for either barometric pressure or salinity. Accuracy was stated as $\pm$ 0.1 ppm in the manufacturer's guidelines and this was taken as absolute.

5.3.3 Field electrical conductivity measurement

Electrical conductivity was measured using one of three instruments, a Mettler Toledo MC126, a Hannah Instruments HI-933000 or a Mettler Toledo X Mate Pro. In each case the instruments were calibrated in accordance with the manufacturers guidelines with either NIST certified buffers at 1413 μScm^{-1} (to 25°C). Alternatively an in house buffer was made using Analytical Reagent (AR) grade KCl, made up to 0.01 M with 18.2 MΩ H_2O and standardised against NIST certified buffer. In the case of the MT MC126 meter, a two point calibration at zero (in air) and 1413 μScm^{-1} was performed (at a reference temperature of 25°C).

5.3.4 Measurements using flow cell

During sampling from the VFR sample ports a Waterra Sheffield flow-though cell (as shown in Figure 5-2) was used. This minimised atmospheric contact and ensured a consistent flow past the probes. The flow through cell consists of a number of separate cell chambers joined together, the probes are then inserted and the cell assembly was attached to the sampling ports by a length of PVC tubing which was sealed to the pipe work with a rubber pressure seal assembly as shown in Figure 5-3.

Figure 5-2: VFR sample port monitoring using a Waterra Sheffield flow through cell and hand held meters

5.3.1 Field determination of Fe(II), total Fe and sulfate

When indicated the field determination of Fe(II), total Fe and sulfate was carried out in the field using a Hach DR-890 colorimeter and Hach reagent powder pillows. Ferrous powder pillows for 25 ml samples for the determination of Fe(II) and FerroVer powder pillows for 10 ml samples for the determination of total Fe were used. A standard adjust was performed using the FerroVer method and a commercially available 1000 mg L^{-1} Fe standard. This was diluted to 1 mg L^{-1} by pipetting 1 mL of standard into a 1 L class A volumetric flask and diluting to 1 L with deionised water. Both Fe(II) and total Fe methods use phenanthroline for the determination of Fe. The procedure has a maximum range of 3 mg L^{-1} and an estimated detection limit of 0.03 mg L^{-1} under ideal laboratory conditions. For samples that were found to be over range, deionised water was used to dilute the sample in a measuring cylinder and the appropriate correction factor was applied to the analytical concentration.

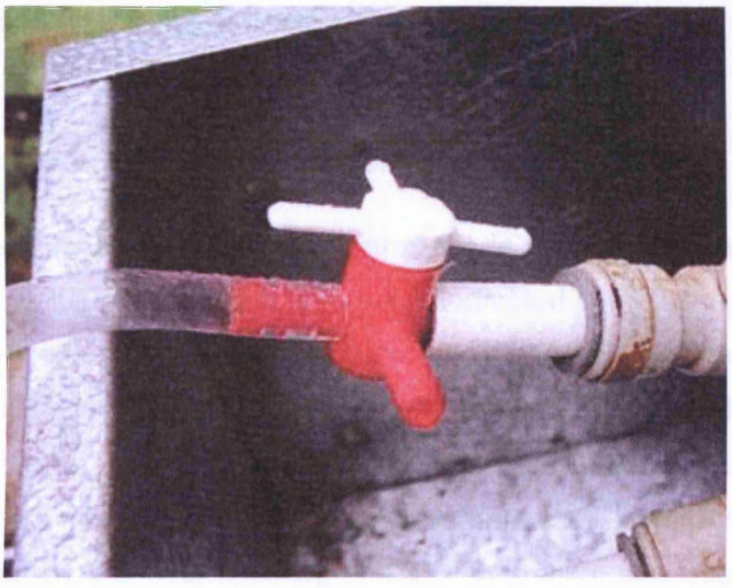

Figure 5-3: Detail of the pressure fitting connecting the flow cell to the sample ports

Sulfate was also determined with the Hach meter using SulfaVer reagent powder pillows for 10 ml samples. In each case the procedures listed in the Hach DR-890 water analysis handbook were followed. Precision and accuracy where not determined for this method.

5.3.2 Field determination of alkalinity

Prior to 29-7-2005 alkalinity was determined using a HACH Alkalinity test kit. In this, dilute H_2SO_4 is added drop wise using a pipette to the sample containing a bromocresol green methyl red indicator powder pillow. Due to the nature of the test, precision and accuracy are low.

After 29-7-2005 a Hach 16900 digital titrator using a 1.600 N H_2SO_4 cartridge and bromocresol green methyl red indicator powder pillows were used. Titrations where conducted on 0.45 μm filtered samples to remove any solid carbonate phases. 100 mL of filtered sample was used and measured using a measuring cylinder. Titrations were conducted to a light violet -grey end point at pH 4.8 and alkalinity was read directly from the titrator counter in mg L^{-1} as $CaCO_3$. Precision is defined by the accuracy of the plunger thread but is presumed to be within ± 10 % of the stated value. Prior to measurement it was made sure that any air bubbles were removed from the delivery tube and

any excess acid was removed with deionised water before the counter was reset.

5.3.3 Filtration and sample preservation

Water samples were taken for metals analysis in Cardiff University's CLEER laboratory using ICP-AES. When filtration is indicated samples were filtered in the field using either a Perspex filtration kit with a vacuum hand pump or Millipore Swinnex syringe filter holders and either 20 or 60 mL disposable Plastipak syringes. In each case Whatman 0.45 μm cellulose nitrate membrane filters where used unless otherwise stated. Between filtrations the filter kit was rinsed with deionised water and a fresh filter was used each time. Samples were preserved for ICP-OES analysis of metals with 1 mL of 10 % HNO_3 per approximately 25 mL of sample to a pH less than 2. 10 % HNO_3 was made by diluting concentrated trace analysis grade (Fisher Scientific) HNO_3 with deionised water. When total is indicated, this is taken to mean the sample preserved without filtration.

5.3.4 Cation analysis

Dissolved metal analysis of preserved samples was conducted in the CLEER facility using Inductively Coupled Plasma – Optical Emission Spectroscopy (ICP-OES). The instrument used was a Perkin Elmer Optima 2100 DV with an AS90 plus auto-sampler and a PC running WinLab 32 software. An initial sweep of all elements against a deionised water blank for the Taff Merthyr mine-water revealed the significant detectable metals:

Ca, Fe, K, Mg, Mn, Na, Si, Sr and Zn

Further ICP analysis of field samples was conducted on the above metal suite. In each case analysis was calibrated against a set of three standards made up from commercially available 1000 mg L^{-1} standards in additionto a 2 % HNO_3 blank. The standards were made up by diluting down by a factor of 10 from the highest standard. Standards where run during analysis after every 10 samples as unknowns to check calibration accuracy. The commercial standards are certified as ± 0.2 % of the stated concentration and dilutions

are presumed to be accurate to within ± 10 %. In most cases the determined value read within ± 10 % of the standard concentration. However in a small minority of cases significant drift did occurred and the accuracy dropped to ± 15 %. Therefore an error of ± 15 % should be used when interpreting the results.

Table 5.1: Variation in triplicate total field metal samples analysed using ICP-OES on three separate occasions

09/01/2006	Fe	Mn	Ca	K	Mg	Na	Si	Sr
	mg L^{-1}	mg L^{-1}	mg L^{-1}	mg L^{-1}	mg L^{-1}	mg L^{-1}	mg L^{-1}	mg L^{-1}
1	8.89	0.79	99.90	12.43	45.52	15.88	4.92	0.63
2	8.81	0.77	99.97	12.19	42.89	15.55	4.86	0.62
3	8.92	0.77	99.46	12.21	42.56	15.50	4.83	0.62
mean	**8.87**	**0.78**	**99.78**	**12.28**	**43.66**	**15.64**	**4.87**	**0.62**
SD	**0.046**	**0.009**	**0.226**	**0.109**	**1.324**	**0.169**	**0.037**	**0.005**
Range	**0.11**	**0.02**	**0.51**	**0.24**	**2.96**	**0.38**	**0.09**	**0.01**
% Range	**1.24**	**2.58**	**0.51**	**1.95**	**6.78**	**2.43**	**1.85**	**1.60**

05/05/2007	Fe	Mn	Ca	K	Mg	Na	Si	Sr
	mg L^{-1}	mg L^{-1}	mg L^{-1}	mg L^{-1}	mg L^{-1}	mg L^{-1}	mg L^{-1}	mg L^{-1}
1	7.07	0.72	88.39	12.03	37.76	13.60	3.92	0.58
2	7.16	0.72	92.12	12.11	38.84	13.75	3.91	0.58
3	7.08	0.72	88.59	12.10	38.60	13.63	3.94	0.58
mean	**7.11**	**0.72**	**89.70**	**12.08**	**38.40**	**13.66**	**3.92**	**0.58**
SD	**0.04**	**0.00**	**1.71**	**0.04**	**0.46**	**0.06**	**0.01**	**0.00**
Range	**0.09**	**0.00**	**3.73**	**0.08**	**1.08**	**0.15**	**0.03**	**0.01**
% Range	**1.28**	**0.56**	**4.16**	**0.66**	**2.81**	**1.10**	**0.69**	**0.86**

31/01/2006	Fe	Mn	Ca	K	Mg	Na	Si	Sr
	mg L^{-1}	mg L^{-1}	mg L^{-1}	mg L^{-1}	mg L^{-1}	mg L^{-1}	mg L^{-1}	mg L^{-1}
1	7.68	0.77	99.97	12.19	42.89	15.55	4.86	0.62
2	7.66	0.77	99.49	12.21	42.56	15.50	4.83	0.62
3	7.3	0.73	96.35	11.85	41.75	15.10	4.71	0.6
mean	**7.55**	**0.76**	**98.60**	**12.08**	**42.40**	**15.38**	**4.80**	**0.61**
SD	**0.17**	**0.02**	**1.61**	**0.17**	**0.48**	**0.20**	**0.06**	**0.01**
Range	**0.38**	**0.04**	**3.62**	**0.36**	**1.14**	**0.45**	**0.15**	**0.02**
% Range	**5.04**	**5.29**	**3.67**	**2.98**	**2.69**	**2.93**	**3.13**	**3.26**
where % range is = to 100/mean x range								

Variation between field triplicates was assessed on three separate occasions (see Table 5.1). In each case, the range (as a percentage of the mean value) did not exceeded 7 % and was well within the ± 15 % analytical error.

5.4 Field oxidation rates

Field Fe(II) oxidation rates were determined by Dr Devin Sapsford (see Sapsford, 2007). Experiments were conducted in 10 L plastic buckets and pH, temperature and dissolved O_2 concentrations were monitored using portable field meters as shown in Figure 5-4 and Figure 5-5. During an experimental run time was recorded on a stop watch and total and filtered water samples were taken at 10 minute intervals and preserved with H_2SO_4 for analysis of Fe(II) in the laboratory. A 12 V compressor was used to supply compressed air to the reactors via an aeration apparatus constructed from 8 mm internal diameter push fit plastic tubing. A ring section was used to fit at the base of the reactors this was perforated with pin holes in order to supply a diffuse bubble air supply to reactor mixture. The air line was split two ways to allow two reactors to be used at any one time.

A number of different experiments were conducted to test different scenarios of homogeneous and heterogeneous oxidation under aerated and un-aerated conditions as described in Table 5.2.

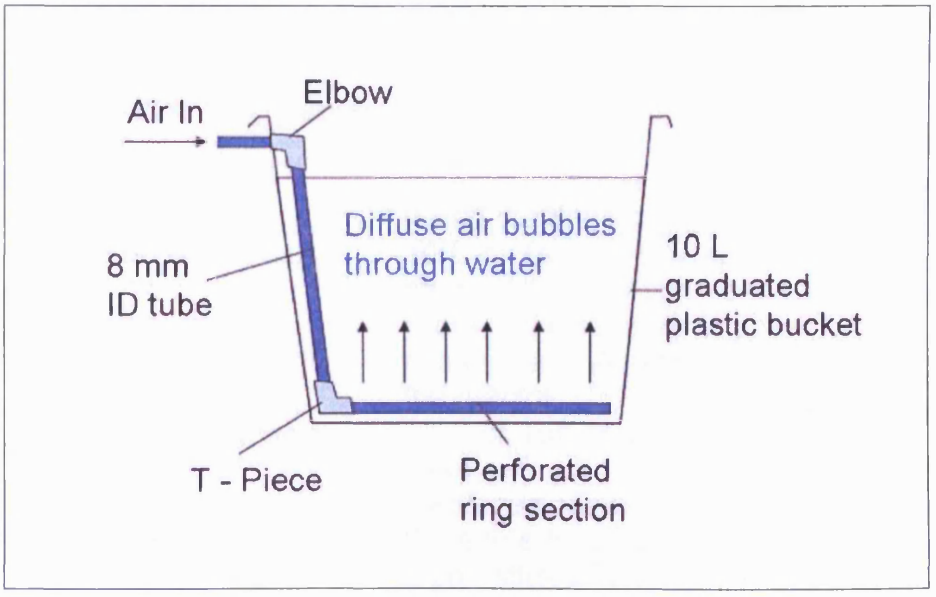

Figure 5-4: Schematic of field oxidation rate reactor

Figure 5-5: Fe(II) oxidation rates being determined in the field

Table 5.2: Description of field oxidation rate experiments

Experiment	Description
Un-aerated homogeneous	10 L of Taff Merthyr mine water collected from base of L2 aeration cascade, no further aeration. Simple stirring of reactor prior to taking readings and samples.
Aerated homogeneous	10 L of Taff Merthyr mine water collected from base of L2 aeration cascade, reactor aerated with compressed air supplied by portable 12 V compressor. Aeration acted to thoroughly stir the reactor.
Aerated heterogeneous	10 L of Taff Merthyr mine water collected from base of L2 aeration cascade, to this a measured amount of ochre solids collected from the same location was added. The reactor was then stirred and aerated with the 12 V compressor and ring aerator.

5.5 Sampling protocols

5.5.1 VFR Sampling protocols

VFR routine sampling was done, where possible, on a weekly to fortnightly basis. The intensity of the routine sampling varied over the duration of VFR operation and the choice of measured parameters was based on the stability and importance of each measurement. Minimal readings consisted of electrochemical measurements (pH, temperature, ORP and dissolved O_2) and collection of unfiltered and filtered acidified samples. This level of sampling combined with discharge or corrected inlet flow and head measurements was adequate for regular monitoring of the VFR performance. On a more intensive routine sampling trip, total Fe, Fe(II), SO_4^{2-} and alkalinity were also determined.

The monitoring of the VFR sample ports was carried out on four occasions during VFR operation. In each case, electrochemical geochemical field parameters were taken as well as acidified samples (total and filtered) for metal analysis.

5.5.2 Lagoon monitoring

The settlement lagoons were monitored on a regular basis on most site visits for the first year of VFR operation. After the first year only occasional monitoring was performed. Lagoon sampling consisted of, where possible, a full sweep of parameters to mirror the VFR monitoring. From May 2005 to January 2006 three sampling points were utilised, the distribution weir, the base of the L1 aeration cascade and the combined L1 and L2 discharges. From March 2006 onwards only the distribution weir and the combined L1 and L2 discharges were monitored representing the inlet and outlet to the combined settlement lagoons respectively.

Electrochemical parameters and field analytes (Fe(II), total Fe, Alkalinity, Sulfate and suspended solids) where monitored for the first four months of pilot plant operation (July to October 2005) to give a background to the

receiving water course. Due to the consistency of the data it was not deemed necessary to monitor after this point.

On the 17th of October 2005 a depth profile along settlement lagoon L1 was conducted using a white plastic tube marked with notches at 0.5 cm intervals. It was found that the rough notches cut into the tube effectively picked up the ochre allowing the depth to be read from the top of the ochre marked section. The total water depth was also taken at this point and readings were taken at roughly 3 meter intervals in the centre of the lagoon.

On the 4th of October 2005 a survey of the variation in the chemical characteristics of the mine water at the distribution weir was conducted. Electrochemical field parameters as well as total samples for metal analysis were taken at 60 second intervals across four on off pump cycles. The aim of this exercise was to check the validity of point measurements at the distribution weir.

On the 21st of December 2005 the flow rate was monitored at the combined discharge from settlement lagoons L1 and L2 using the 0.9 x V-max method over an extended time period. The aim of this exercise was to detect any variation in the flow rate and therefore the extent of flow smoothing as described in Sections 5.3 and 5.4. The flow velocity was determined using a vane flow meter.

5.5.3 Full Taff Merthyr treatment site survey

On the 11th of November 2005 a full sampling and monitoring sweep of the Taff Merthyr site was conducted. During this time electrochemical and geochemical field parameters as well as total and filtered samples for metal analysis were collected from pre-designated sampling locations. In addition flow measurements were taken using a vane flow meter in channel sections in accordance with the method given in Section 5.2. On the same day a full analysis of the VFR was conducted including sample ports and in tank surface water measurements. Sampling points were located at the discharges from

each of the treatment units (settlement lagoons, reed beds etc) and from the distribution weir.

In addition a traverse was conducted along the L2 settlement lagoon at a distance of 2.5 m from the edge at 10 m interval using a remote pull syringe device and a float. This enabled sampling at different depths 0.3 and 0.8 m below the surface, total samples for metals were taken as well as temperature measurements.

5.6 Decommissioning and final sampling

5.6.1 General

The VFR was decommissioned on 14-5-2007. The tank was partially drained and an ochre depth survey was carried out, ochre samples were then taken for further characterisation. In order to decommission and drain the VFR without over stressing the ochre bed it was decided to drain the tank over a 24 hour period. The inlet valve was closed and the outlet valve was opened slightly to allow a slow release of water. The following day on arrival at the tank the outlet valve was closed with the water level lying approximately 5 cm above the surface of the ochre bed.

A survey of ochre bed depth was carried out using a 10 mm internal diameter PVC tube which had etched notches to collect ochre and indicate ochre depth. The same system was used for determining ochre depth in the L1 settlement lagoon. The VFR treatment tank was divided into a grid 20 x 20 cm squares and a string was passed across the width of the tank and held taught with weights on either side. The string was marked at 20 cm intervals widthways and a transect was made at each point recording a) apparent ochre depth and b) height from gravel surface to the top of tank (string line) the string was then moved 20 cm length ways along the treatment tank and the procedure was repeated until a full grid had been completed. It should be noted that on occasions the plastic tube used for ochre depth measurements lifted cores of ochre which were removed and retained in 30 mL steralyn

bottles for analysis. The remainder of the water was then drained from the tank over a period of approximately 30 minutes. Following this ochre samples were taken for the following testwork:

- Bulk samples (25 L) for Specific Cake Resistance (SCR) tests, ochre density and solids content.
- 250 mL samples for zeta potential analysis diluted with mine water.
- 250 mL samples for sequential extractions and total acid digest and BET measurements.

Finally a small trench was dug through the ochre to the gravel bed in order to obtain photographs of the bed profile. A core was taken with an improvised piston corer devised by Dr Devin Sapsford (Cardiff University) in which the end of a 60 mL disposable PlastiPak polyethylene syringe was removed so it could be inserted into the ochre bed whilst retracting the syringe plunger so as to keep it at the level of the ochre surface.

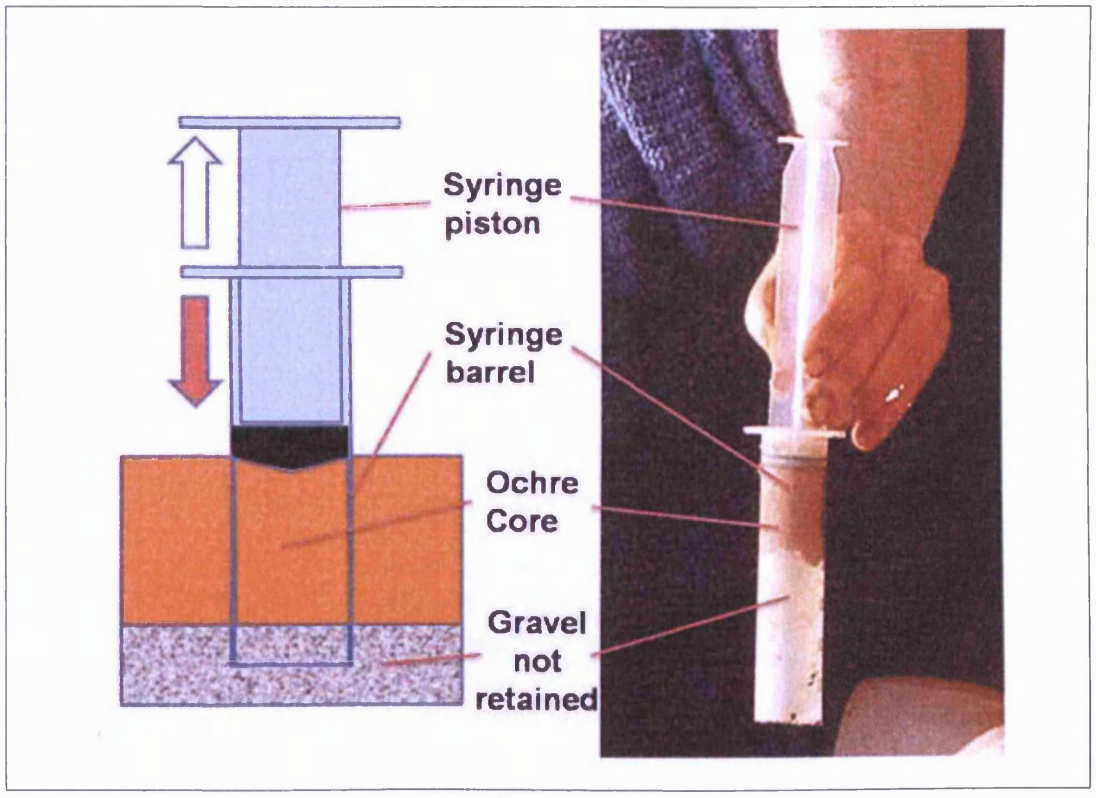

Figure 5-6: Piston corer devised by Dr Devin Sapsford

The ochre was sufficiently competent that a 45 mm thick core could be removed Vertical depths are approximate as the core was roughly sliced into 3 mm thick sections, therefore each data point represents the average value of the 3 mm section and is positioned at the vertical centre of the section depth.

6 Methods of field and synthetic ochre characterisation

6.1 Introduction

Due to the importance of the ochre bed in the operation of the VFR system it was deemed necessary to further investigate the properties of the ochre recovered from the field and its synthetic counterparts. A full characterisation of the field ochre was undertaken to determine its physical, mineralogical, geochemical and surface electrochemical properties. Further to this, a study of ochre / Fe(II) interactions was conducted (see chapter 8 and 9) in which synthetic goethite (Bayferrox 930, Lannexes) was used in a laboratory investigation. Therefore some of the characterisation procedures used here were also undertaken on the Bayferrox 930. The chapter is split into the following sections:

Section 6.2: Sample storage – describes the method of ochre storage prior to preparation for analysis

Section 6.3: Physical properties – describes the materials and methods used for the physical characterisation of the ochre. This includes density determination, visual identification, surface area measurements, and determination of Specific Cake Resistance (SCR)

Section 6.4: Mineral characterisation – describes the methods used in the identification of crystalline mineral phases by X-Ray Diffraction (XRD).

Section 6.5: Geochemical characterisation – describes the methods used for the geochemical characterisation of the ochre. This includes whole sample assay and sequential extractions.

Section 6.6: Zeta potential and Iso Electric Point – describes the experimental methods used for the determination of the electrokinetic characteristics and charging behaviour of the ochre.

6.2 Sample storage

Generally preparation of ochre samples for geochemical, physical and mineralogical characterisation involved drying the sample prior to further use. Once the ochre sample is dried, no further alterationto the mineral phase should occur (unless drying is conducted at temperatures exceeding 105 °C). Drying of samples was undertaken within 48 hours of sample collection. For test work that required the use of a wet sample (e.g. zeta potential determination and SCR testing), measurements were taken as soon after sample collection as possible (within 48 hours for zeta potential readings). The remaining bulk samples were stored at room temperature and open to the atmosphere.

6.3 Physical properties

6.3.1 Solids content, density and voids ratio

Measured volumes of ochre sludge collected from the Taff Merthyr VFR bed on the 14th of May 2007 were weighed and dried to determine the following physical characteristics, bulk density, dry density, voids ratio and dry solids content as a volume percentage and as a weight percentage.

Bulk density was determined as follows:

Equation 6.1

$$\rho_b = \frac{W_w}{V_w}$$

Where ρ_b is the bulk density in g cm^{-3}, W_w is the wet mass of the sludge in g and V_w is the wet sludge volume in cm^3.

The dry density of the solid was determined as follows:

Equation 6.2

$$\rho_d = \frac{W_d}{V_d}$$

Where ρ_d is the dry density in g cm^{-3}, W_d is the dry mass of the sludge in g determined after drying for 6 days at 105 °C and V_d is the dry sludge volume in cm^3 determined by the equation.

Equation 6.3

$$V_d = V_w - V_{H2O} = V_w - (W_w - W_d)$$

in which V_{H2O} is the volume of water in cm^3 and is approximately equal to the mass of water when the density is taken to be 1 g cm^{-3}. The voids ratio (R_V) was determined as follows:

Equation 6.4

$$R_V = \frac{V_W}{V_{H2O}}$$

The determination of the dry solids content of the ochre as a volume percentage of the initial wet solids volume (% v/v) was determined as follows:

Equation 6.5

$$\%(v/v) = \frac{100}{V_w} V_d$$

Finally the determination of the dry solids content of the ochre as a weight percentage of the initial wet solids weight (% w/w) was determined as follows:

Equation 6.6

$$\%(w/w) = \frac{100}{W_w} W_d$$

6.3.2 Surface area determination

Surface areas were obtained on samples of field ochre and the synthetic Fe(III) (hydroxy)oxide Bayferrox 930 (Lanexes, Germany) after drying at 105°C for 24 hours. The BET N_2 gas adsorption method (Brunauer, Emmett and Teller, 1938) was used and analysis was performed using a Micrometrics Gemini instrument at Cardiff University, School of Chemistry. The error incurred in such a measurement is taken to be ± 10 % (Dr S Taylor, personal communication).

6.3.3 Specific Resistance to Filtration

Specific Resistance to Filtration (SCR) tests were carried out by Dr Devin Sapsford on samples of VFR bed ochre collected on the final sampling day. A Svedala piston press (see Figure 6-1) was used for SCR determination and four successive tests at a fixed 5 Bar pressure were carried out on 500 mL sub-samples of ochre bed sludge.

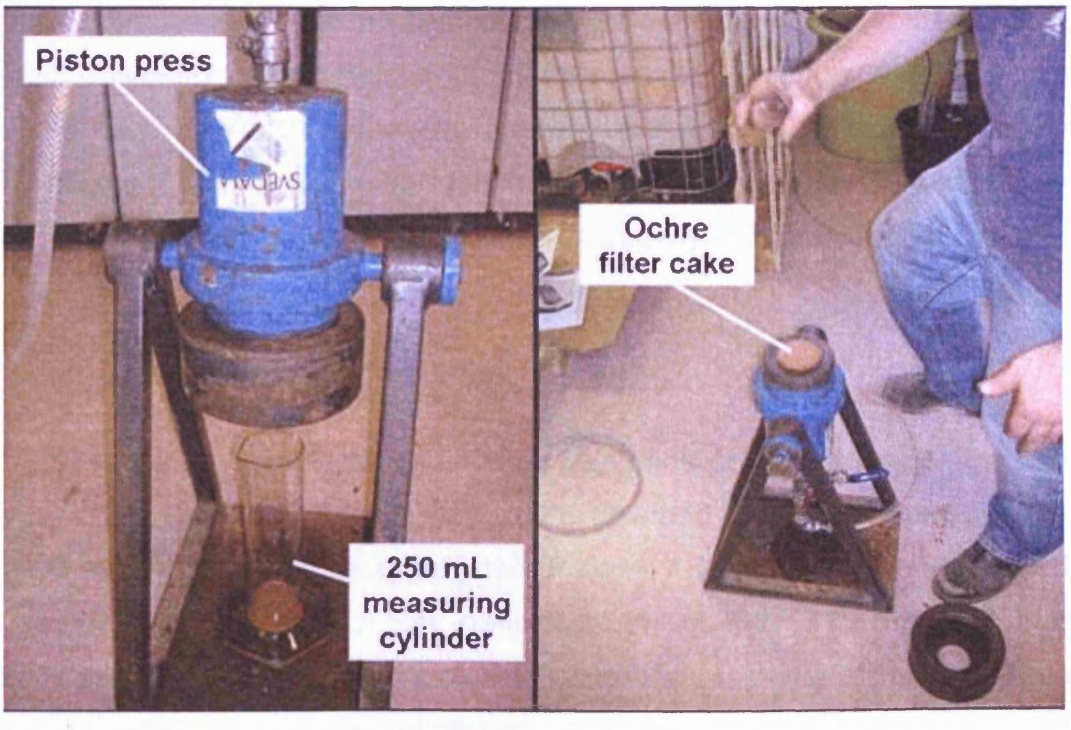

Figure 6-1: Apparatus used in SCR tests

During filtration the volume of filtrate was recorded against time at 10 second intervals. These data, together with the filter cake characteristics, were analysed using the general filtration equation for constant pressure and area as given in Coulson et al (1991):

Equation 6.7

$$\frac{t}{V} = \left(\frac{\alpha\mu CV}{2A^2\Delta P}\right) + \left(\frac{\mu Rm}{A\Delta P}\right)$$

where t is the time in sec, V is the volume of filtrate in m^3, C is the dry filter cake mass per unit volume of filtrate in kg m^{-3}, α is the specific cake resistance in m kg^{-1}, ΔP is the pressure drop in Pa, μ is the viscosity of the liquid (0.001 Pas), A is the filtration area (0.0045 m^2) and Rm is the resistance of the filtration material in m^{-1}.

6.3.4 Light and electron microscopy

Visual characterisation of the field ochre was carried out by Dr Sapsford at Cardiff University using a Reichert Jung microscope with a maximum of 400 x magnification. The microscope was fitted with a Polyvar MET camera to allow still imaging. Scanning Electron Microscopy (SEM) work was carried out by Bangor University; School of Microbiology (Courtesy of Prof B. Johnson et al).

6.4 Mineralogical characterisation

Mineral characterisation was undertaken using fine powder X-Ray Diffraction (XRD). Samples of ochre collected from the filter bed of the VFR were dried at 105 °C for 24 hours and disaggregated. Powder XRD patterns were obtained using a Philips PW3830 X-Ray generator, Philips PW1710 diffractometer controller and X Pert High Score plus software. Patterns where compared to a software database and / or published data. The details of the instrument settings are listed in Table 6.1

Table 6.1: Settings used during X-Ray Diffraction characterisation

Scan Parameter	**Setting**
X-ray generator	Philips PW3830
Diffractometer controller	Philips PW1710
Scan Axis	Gonio
Start position [°2Th]	5.01
End position [°2Th]	79.99
Step size [°2Th]	0.02
Scan step time [s]	0.5
Scan type	Continuous
Offset [°2Th]	0
Divergence slit type	Automatic
Irradiated length [mm]	10
Specimen length [mm]	10
Receiving slit [mm]	0.05
Measurement temperature [°C]	0
Anode material	Cu
K-Alpha1 [A]	1.54060
K-Alpha2 [A]	1.54443
K-Beta [A]	1.39225
K-A2 / K-A1 ratio	0.5
Defractor type	PW1710
Goniometer radius [mm]	173
Dist focus divergence slit [mm]	91
Search Parameter	**Setting**
Library software	X-pert Hi score plus
Method	Minimum second derivative
Minimum significance	2
Minimum tip width	0.01
Maximum tip width	1
Peak base width	2
Correction method	Automatic
Bending factor	5
Use smoothed input data	Yes
Granularity	20

6.5 Geochemical characterisation

6.5.1 Whole Sample Digestion

Complete digest of ochre samples was carried out using approximately 0.1 g of dry (105°C for 24 hours) sample, weighed accurately to 4 figures using an analytical balance. 10 mL of aqua regia consisting of 1 part concentrated HNO_3 to 3 parts concentrated HCl was used as the digest medium and the sample was digested in a Perkin Elmer P1200 microwave.

6.5.2 Carbon and sulphur analysis

Total carbon and total sulfur were determined on 1 g samples of dry field ochre. Samples were analysed using a SC144DR Leco Furnace. Analysis using this instrument is accurate to within ± 10 %

6.5.3 Sequential extraction

A four stage sequential extraction was undertaken by Dr Sapsford (Cardiff University) as used previously (Sapsford, 2003) and adapted from Dold (2001). Analysis was conducted on samples of dry field ochre and synthetic iron oxide (Bayferrox 930 and 947; Lanexes, Germany) in accordance with the following procedure. 0.1 g of powdered sample was accurately weighed on a 4 figure analytical balance. Extractions were carried out sequentially on the weighed sample in polypropylene disposable test tubes. Phase separation was achieved by centrifugation at 3500 rpm for 20 minutes. The centrifugate was decanted and retained for analysis using ICP-OES prior to the next extraction stage. The four extraction stages consisted of:

1. **Deionised water leach** - 20 mL of deionised water for 1 hour centrifuged and analysed for Ca and Mg.
2. **Exchangeable fraction** – 10 mL of 1M ammonium acetate, pH 4.5 for 2 hour centrifuged and analysed for Ca, Mg, Al, Co, Cr, Fe, Mn, Ni, Pb and Zn.

3. **Poorly crystalline Fe and Mn oxides and (hydroxy)oxides** - 10 mL of 0.2 M ammonium oxalate, pH 3, darkness for 1 hour. Centrifuged and analysed for Ca, Mg, Al, Co, Cr, Fe, Mn, Ni, Pb and Zn.
4. **Crystalline Fe and Mn oxides and (hydroxy)oxides** – 10 mL of 0.2 M NH_4 – Oxalate, pH 3, light, 80 °C for 2 hours. Centrifuged and analysed for Ca, Mg, Al, Co, Cr, Fe, Mn, Ni, Pb and Zn.

6.6 Zeta potential and Iso Electric Point

Zeta potential (ζ) characteristics were determined for samples of field ochre obtained from the VFR during the second year of operation and for samples of washed synthetic goethite powder (Bayferrox 930) for comparison. Using potentiometric titrations of pH and determining ζ at different pH values, it was possible to determine the surface charging characteristics of the pH of the Iso Electric Point (IEP) and the relationship between pH and sign of the surface charge. Furthermore the result could be used to give an indication of particle stability in differing media.

6.6.1 Apparatus

Zeta potential measurements were made using a Malvern Instruments, Zeta Sizer Nano (Z) (see Figure 6-2) and disposable polystyrene capillary cells. A calibration check was conducted prior to running a titration using a Malvern instruments -50 mV ζ standard and running the diagnostic operating procedure.

Ochre suspensions were titrated in a 500 mL polyethylene beaker and mixed with a PTFE magnetic stirrer bar. Temperature was controlled at 25 ± 0.1 °C by submerging the titration vessel in a Grant water bath. pH and temperature were monitored using a Hanna pH213 meter coupled with HI 1131B glass-body combination pH electrode. pH was calibrated in accordance with the manufacturers guidelines using commercially available pH 4.01 and 7.01

buffers which were stored in the water bath to allow calibration at the operating temperature.

6.6.2 Materials and methods

ζ characteristics were determined for suspensions of Bayferrox 930 and ochre obtained from the VFR during the second year of operation. The pH of the Iso Electric Point (IEP) was determined by fast titration of suspensions with 0.1 or 0.01 N HNO_3 from an initial alkaline to circum neutral pH. $NaNO_3$ was used as an indifferent background electrolyte for the synthetic goethite suspension and titrations were performed in electrolyte concentrations of 0.1, 0.01 and 0.001 M. In addition, one titration was performed on a goethite suspension of 0.1 N $NaNO_3$ and an estimated quantity of $NaHCO_3$ (between 0.5 and 1 g L^{-1}). The VFR field ochre was diluted and titrated in Taff Merthyr mine water. The following methodology applies for the titration of field ochre and Bayferrox 930:

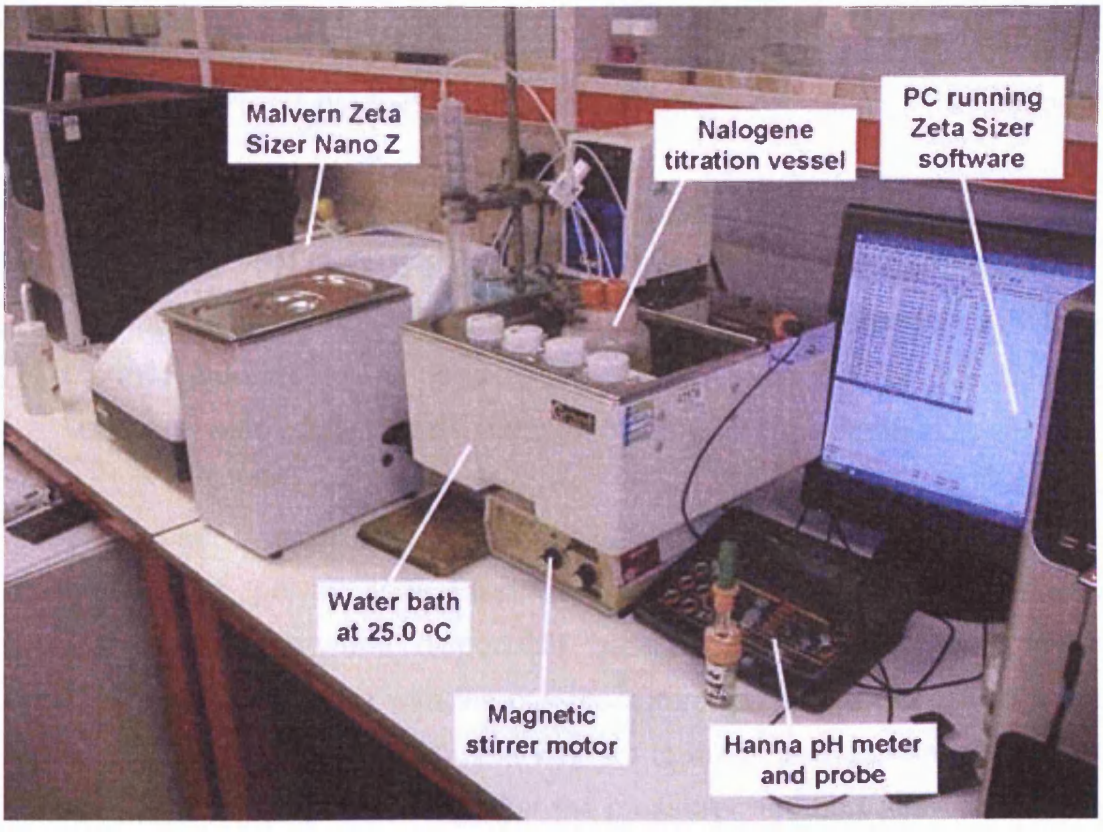

Figure 6-2: Zeta titration apparatus

- Goethite titration - 100 mg goethite was added to a 500 mL polyethylene volumetric flask containing either 4.245, 0.4245 or 0.0424 g of $NaNO_3$ equating to 0.1, 0.01 or 0.001 M ionic strength and made up to mark with deionised water.
- Field ochre titration - Ochre slurry collected from the Taff Merthyr VFR was pipetted into a beaker containing 500 mL of Taff Merthyr mine water. Ochre was added until a milky consistency was attained
- Goethite bicarbonate titration – A "tip of a spatulas worth" of $NaHCO_3$ was added to a suspension of 100 mg Bayferrox 930 in 500 mL of 0.1 M $NaNO_3$.
- The Suspension was decanted into a 500 mL polyethylene beaker containing a PTFE coated magnetic stirrer and placed in a water bath at 25°C ontop of a stirrer plate to equilibrate. Temperature, pH and Ec where monitored.
- Goethite titration - Immediately before the start of the titration the initial pH of the suspension was raised to approximately 10.5 by the drop-wise addition of 0.1 N NaOH.
- Field ochre and goethite bicarbonate titration– No initial pH adjustment was made.
- A rapid titration was then conducted by the addition of 0.1 N ($pH > 8.5 < 5.5$) and 0.01 N ($pH > 5.5 < 8.5$) HNO_3 drop-wise to attain *p*H increments of approximately 0.25 pH units to an end *p*H of approximately 3.5. The term rapid titration is used to describe a maximum of 10 minutes between acid addition and ζ measurement for pH equilibration.

At each pH set point an aliquot of suspension was removed from the beaker using a 20 mL polyethylene PlastiPak syringe. This was injected into a Malvern clear polystyrene disposable capillary ζ cell. The ζ was then determined in accordance with the manufacturers guidelines using Malvern's M3 PALS technique. The instrument was set to take the mean value of 1000 separate readings at each point. After the measurement had been taken, the measurement aliquot was injected back into the reaction vessel. The pH was then readjusted and the procedure repeated.

7 Results: Ochre characterisation

7.1 Introduction

Chapter 7 presents the result of ochre characterisation test-work conducted on ochre samples from the Taff Merthyr lagoons and VFR systems. Physical, mineralogical and geochemical test-work was conducted and where possible a comparison is made between lagoons and VFR ochres. The Chapter is split into the following sections:

Section 7.2: Physical characterisation – presenting and discussing the results of physical test work on the VFR and lagoon ochre including density and solids content, microscopy, surface area determination, filtration and electrokinetic characteristics.

Section 7.3: Mineralogical characterisation – presenting results obtained using X-Ray Diffractionto determine the mineralogy of the ochre in the VFR and settlement lagoons. This is then discussed in terms of mineral formation pathways.

Section 7.4: Geochemical characterisation – presenting the results obtained from geochemical analysis the VFR and lagoon ochre including acid digest and sequential extraction.

Section 7.5: Chapter summary and conclusions

7.2 Physical characteristics

7.2.1 Visual inspection

Figure 7.1 shows a photographic cross section through the VFR ochre bed taken on the 14/6/07. On initial inspection the 6 mm gravel bed appeared clean and free from ochre armouring or visual staining. The overlying ochre

bed was found to be 4 to 7 cm thick and supported above the gravel bed rather than incorporated within it.

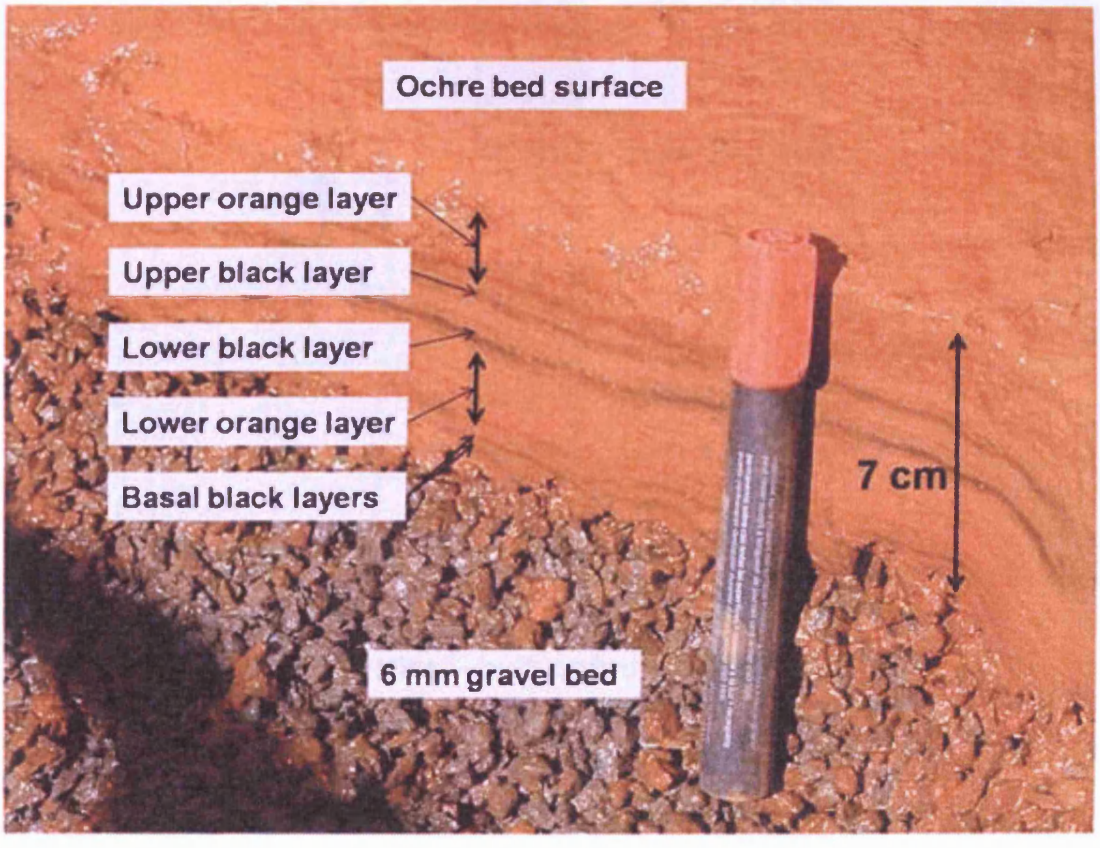

Figure 7-1: Photographic cross section through the 6 mm VFR ochre bed

A series of layers could be identified in the bed cross section, the bulk of the bed consisted of an orange ochre with the consistency of estuarine mud which was inter-dispersed with thin dark grey to black more competent crust like layers which could be removed as thin flakes. The layering of the bed was irregular and four distinct layers were evident as indicated in Figure 7-1 and Figure 7-2. Figure 7-2 shows a schematic cross section through the ochre bed showing the approximate depths of the dark layers and the approximate total depth of the bed at this point.

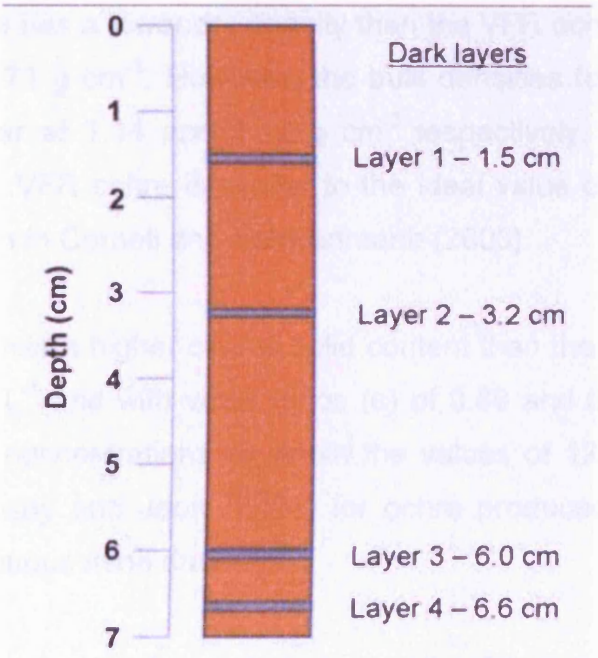

Figure 7-2: Schematic cross section through the 6 mm VFR ochre bed

7.2.2 Physical properties – bulk ochre sludge

Table 7.1 shows the physical properties determined from the VFR and lagoonal ochres as sampled on the 14/6/07. Only single tests were carried out for each of the materials and therefore no estimation of error can be given. Both dry and bulk densities were determined by oven drying of a measured volume of settled sludge as described fully in section 6.3.

Table 7.1: Physical properties of the VFR and lagoonal ochre

Determinant	Units	Lagoon[a]	VFR[b]
Bulk density	g cm^{-3}	1.14	1.12
Dry density	g cm^{-3}	2.34	3.71
Solids content	g L^{-1}	251	150
	% (w/w)	21.96	14.48
	% (v/v)	10.76	4.58
	% (w/v)	25.13	15.01
Voids ratio		0.89	0.95
Fe solids content	g L^{-1}	79.23	80.41

[a] Sample collected from south west corner of L2 lagoon near distribution channel on 14/6/2007. [b] Bulk sample from VFR ochre bed collected on 14/6/2007.

The lagoonal ochre has a lower dry density than the VFR ochre at 2.34 g cm^{-3} as compared to 3.71 g cm^{-3}. However, the bulk densities for both the ochre sludge's are similar at 1.14 and 1.12 g cm^{-3} respectively. The dry density determined for the VFR ochre is similar to the ideal value of 3.96 g cm^{-3} for ferrihydrite as given in Cornell and Schwertmann (2003).

The lagoon ochre has a higher overall solid content than the VFR with values of 251 and 150 g L^{-1} and with voids ratios (e) of 0.89 and 0.95 respectively. Both ochre solids concentrations lie within the values of 12 and 25 % (w/v) reported by Dempsey and Jeon (2001) for ochre produced during passive treatment of ferruginous mine drainage.

Although the lagoonal ochre has a higher overall solids content it also has a lower dry weight iron concentration which will be shown in section 7.4.1. This results in wet sludge iron concentrations being almost identical explaining the low dry density of the lagoonal ochre as compared to the VFR ochre.

7.2.3 Physical properties – vertical VFR profile

An ochre core was extracted from the centre of the VFR bed primarily for determination of chemical composition but also allowed the determination of solids content with depth. Using this method, a solids bed profile was constructed as shown in Figure 7-3A. In addition, using the VFR ochre dry density, the solids content in g L^{-1} was determined as shown in Figure 7-3B.

It was found that the solids content of the VFR bed increased with increasing depth through the bed. It was also evident that the solids content shown in the bed profile is higher than that reported for the bulk VFR ochre, (even at the surface of the ochre bed) with values of 165 g L^{-1} as compared to 150 g L^{-1}. As the bulk VFR sludge was collected in a 15 L container, significant disturbance of the ochre sludge during sampling may have occurred which may have resulted in loss of some of the bed packing even though test work was conducted on settled samples. The ochre core was removed as a largely undisturbed sample and therefore no loss of bed packing is expected.

Therefore the solids contents determined from the bed core will be representative of the actual bed solids contents at that depth. From Figure 7-3B the following relationship can be determined:

Equation 7.1

$$SC = \frac{d + \beta}{k}$$

where SC is the solids concentration in g L^{-1}, d is the ochre depth in cm, β is a constant with the value of 6.67 cm, and k is the slope of the relationship between d and SC with a value of 0.04 g^{-1} L cm^{-1}.

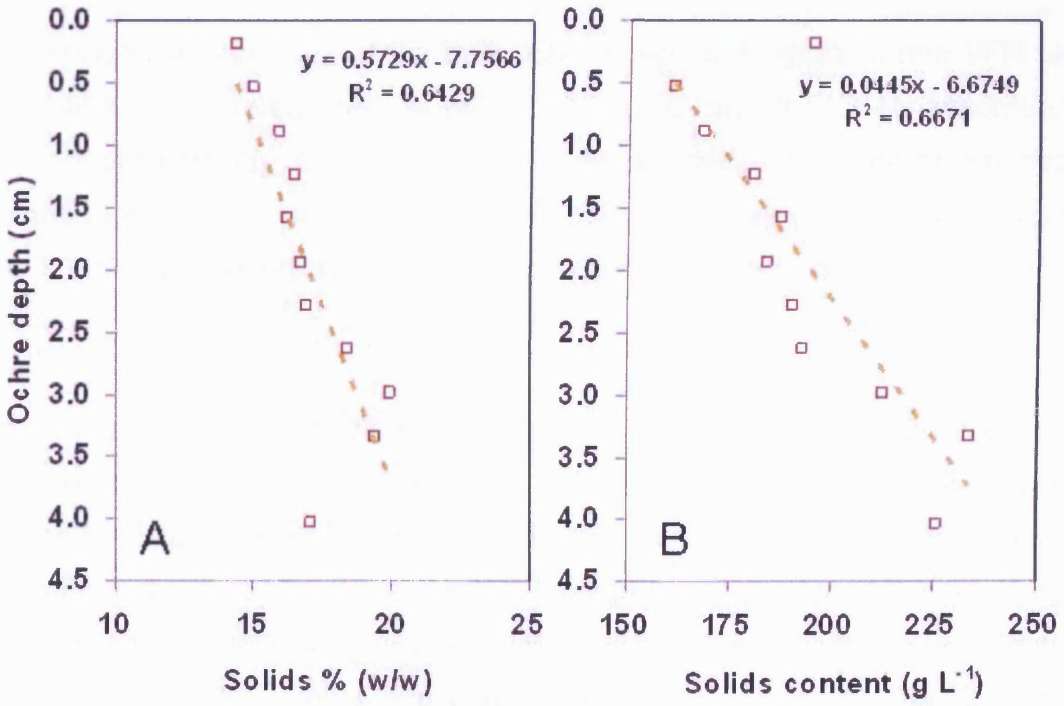

Figure 7-3: A) % (W/W) solids and B) solids content (g L^{-1}) with depth in the 6 mm VFR ochre

If the observed increase in solids content is a true reflection of the bed profile and not due to seepage of water from the base of the ochre core, it can be attributed to three possible processes:

1. Compaction of filter cake due to weight of overburden and downward movement of filtrate will lead to a lower voids ratio and a higher solids

content.

2. Accretion of dissolved constituents onto homogeneously precipitated ochre particulates. For example older ochre and therefore deeper ochre will have had a longer time period for ochre accretion and therefore particle volume will increase, voids ratio will decrease, bulk density and solids content will increase.
3. The formation of more thermodynamically stable particulates via Ostwold ripening (see Ratke and Voorhees, 2002). The degree to which transformation will occur depends on the time since initial particle formation and therefore depth within the ochre bed.

7.2.4 Specific surface area of dry ochre

The specific surface area of the bulk ochre collected from the 6 mm VFR on the 14/6/07 was determined as 247 ± 24.7 m^2 g^{-1} using BET-N_2 adsorption (School of Chemistry, Cardiff University). Surface areas were not determined for the lagoon ochre or the 20 mm VFR ochre. However, it is assumed that the 20 mm VFR ochre would not differ in particle size from the 6 mm VFR ochre.

The surface area reported here is within the range of 200 to 400 m^2 g^{-1} as reported by Cornell and Schwertmann (2003) from assessment of literature values for natural samples. However, the specific surface area determined for the VFR ochre is at the lower end of the range of readings determined by Dzombak and Morel (1999) and below the 600 m^2 g^{-1} recommended by Davis and Leckie (1978), Luoma and Davis (1983), and references therein, and used by Dzombak and Morel (1999) for modelling surface complexation on freshly precipitated ferrihydrite.

Ferrihydrite forms particulate aggregates and becomes micro-porous due to intra particulate porosity (Cornell and Schwertmann, 2003). Due to the nature of the ferrihydrite aggregates, the surface area is a reflection of the aggregate surface area as the N_2 gas used in the BET method may not be able to penetrate fully into the aggregate pores. However, the N_2-BET determined

surface area reported here is assumed to be a true reflection of the available surface area of the ochre in the VFR bed.

7.2.5 Light microscopy

Figure 7-4 shows a transmission light micrograph of an ochre sample collected from the 6 mm VFR bed on the 14/05/07. The scale bar is 100 µm. It is possible to make out loose ochre flocs up to 100 µm in diameter. Also evident are elongate strands up to 100 µm in length and less than 5 µm in width.

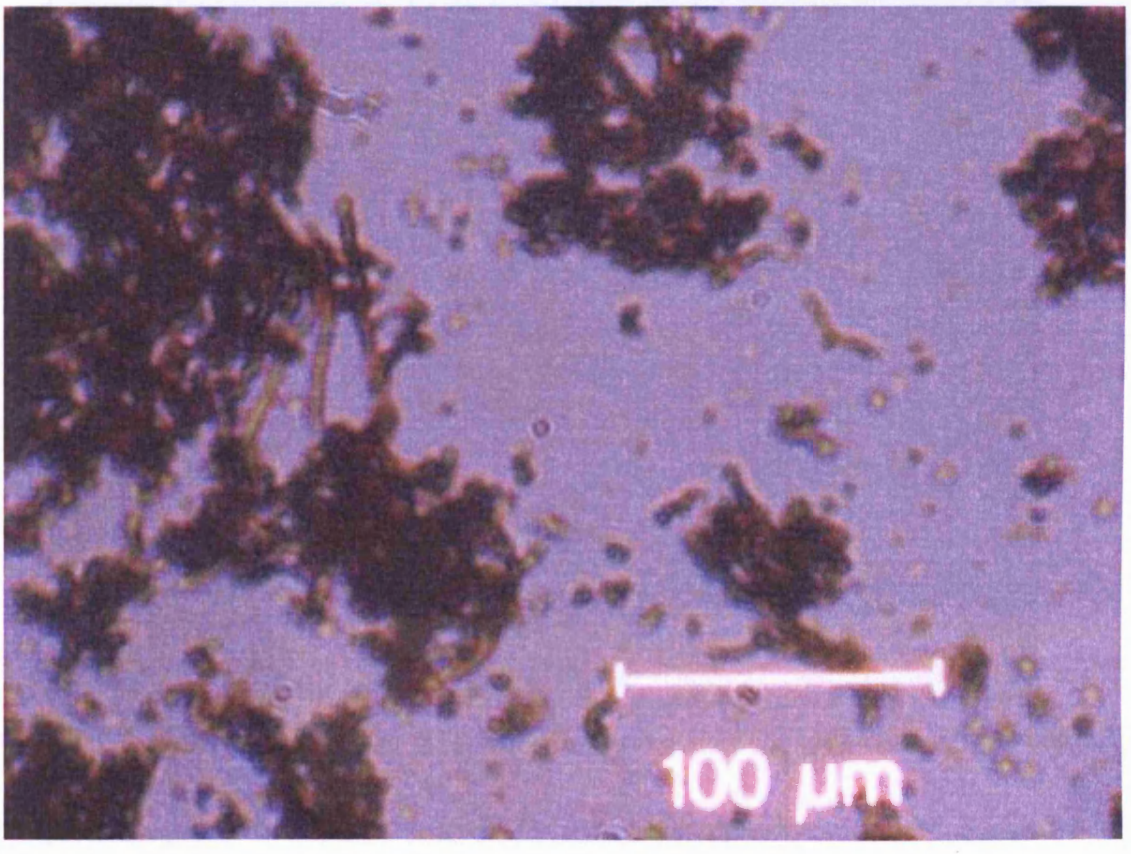

Figure 7-4: High magnification light micrograph showing the ochre "flocs"

7.2.6 Electron microscopy

Figure 7-5 and Figure 7-6 show Scanning Electron Microscopy (SEM) images of ochre collected from the 20 mm VFR ochre bed on the 02/06/06. In each case the scale bar at the top left is equal to 5 µm. No clear crystalline

structure can be identified in the images apart from rough edged platy like crystal of approximately 5 µm in diameter. The lack of any distinguishable crystal structure is consistent with the largely amorphous 2-line ferrihydrite determined in XRD in section 7.3. There is a large size range with individual particulates of < 0.1 µm in diameter to aggregates of > 10 µm. In addition the optical light micrographs show individual flocs up to 100 µm. Aggregates are globular in nature and appear to be made up of individual particles of approximately 0.5 µm in diameter.

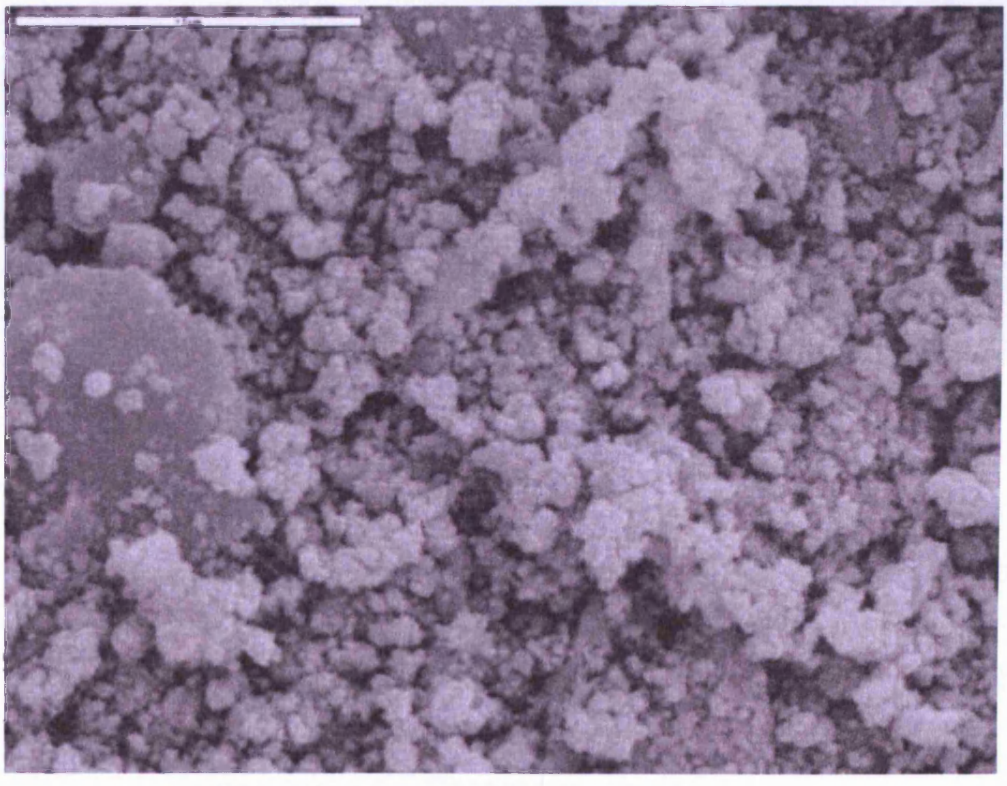

Figure 7-5: SEM image of the VFR ochre showing globular aggregates and platy crystals

Scale bar = 5 µm

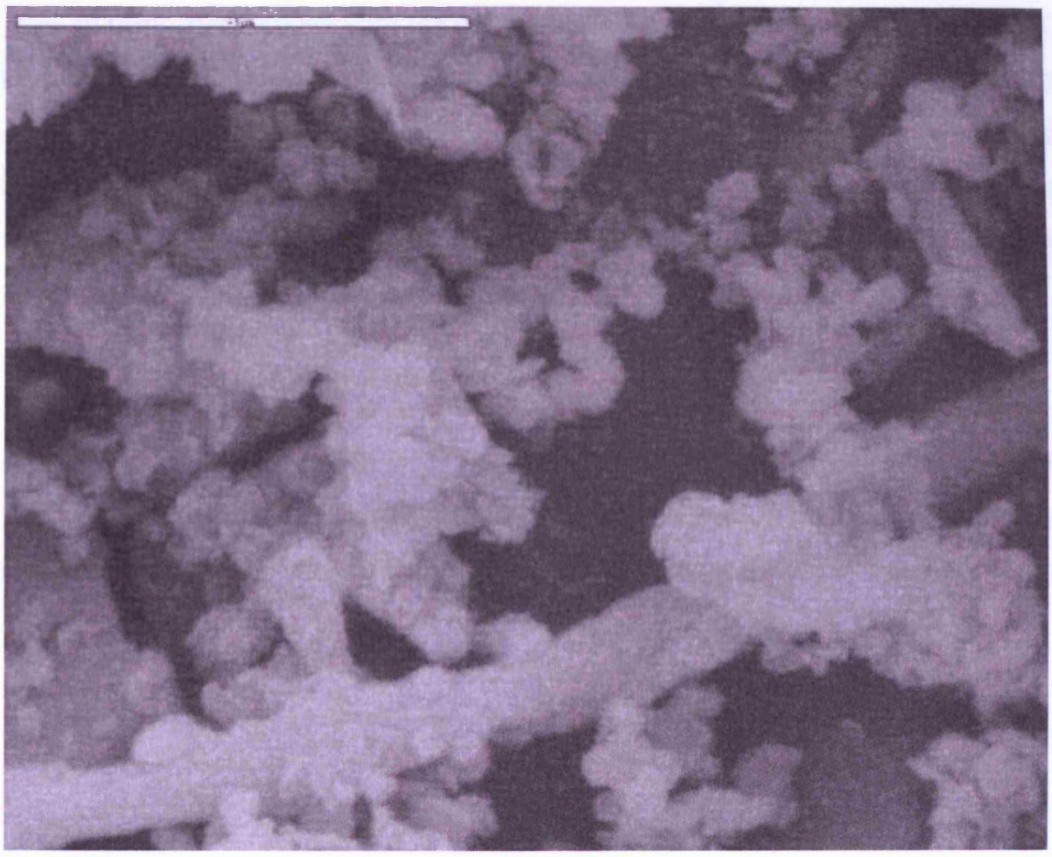

Figure 7-6: SEM image of VFR ochre showing helixical strand

Scale bar = 5µm

These images have been compared with images taken of ochre produced in sand filters from Søgaard et al, (2000 and 2001). The sand filters were used for the treatment of ferruginous circum-neutral ground water by microbial induced oxidation of Fe(II) and precipitation as ochre. Helixical strands were prolific in the images taken by Søgaard et al (2000 and 2001) and were described as encrusted exopolymer stalks of the iron oxidising bacteria *Gallionella ferruginea*. Closer inspection of the light microscope image in Figure 7-4 shows that the strands are prolific and a concentration of 3 to 5 strands per 100 x 100 µm square. This equates to $5x10^8$ strands per m^2 and, taking a conservative estimate for the slide monolayer surface coverage of 100 µm, equates to an approximate concentration of $5x10^{11}$ strands per L^{-1} of ochre.

A preliminary microbiological study conducted by Bangor University (UK) (Bangor, 2007) suggested that the observed stalks described by Søgaard et al (2000 and 2001) as *Gallionella ferruginea* are typical of fungal rhizomes. However, the microbial community of the VFR ochre is currently being characterised further by Newcastle University. This should give a definite answer to the origins of the observed strands.

7.2.7 Zeta potential measurements

Figure 7-7 shows zeta potential (ζ) against pH for a sub-sample of 6 mm VFR ochre collected on the 05/01/07 and analysed on the 08/01/07. The ochre was titrated with HNO_3 in the supernatant mine water, at 25°C, between pH 2.5 and 7.7.

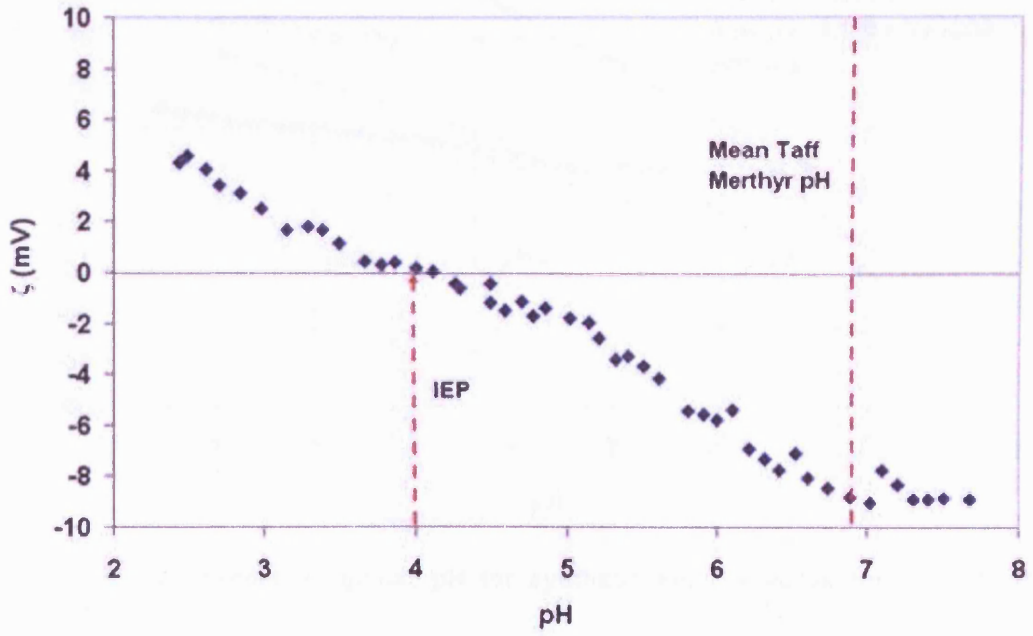

Figure 7-7: Zeta potential against pH for the 6 mm VFR ochre

The Iso Electric Point (IEP) was determined at pH 4 for the 6 mm VFR ochre. The ζ determined at the mean pH of the Taff Merthyr mine water (pH 6.9) was – 8.5 mV which corresponds with the maximum magnitude determined in the pH range studied. In addition there is a linear relationship between pH and ζ between pH 2.5 and 7 and above pH 7 no further change in ζ is seen.

Figure 7-8 shows ζ against pH for the VFR ochre (as shown in Figure 7-7) compared with samples of synthetic Fe(III) (hydroxy)oxide titrated in $NaNO_3$ and $NaNO_3$ / $NaHCO_3$ solutions. Synthetic Fe(III) (hydroxy)oxide indicated as goethite in Figure 7-8 are of commercially available synthetic goethite powder pigment (Bayferrox 930, Lanxess) previously washed as described in section 9.2.2.2, and 0.1, 0.01 and 0.001 M indicate the concentrations of $NaNO_3$ electrolyte used. The series "Goethite 0.1 M + $NaHCO_3$" shows the titration of goethite in 0.1 M $NaNO_3$ electrolyte together with approximately 0.01 M $NaHCO_3$. All titrations were performed using the method as described in section 6.6.

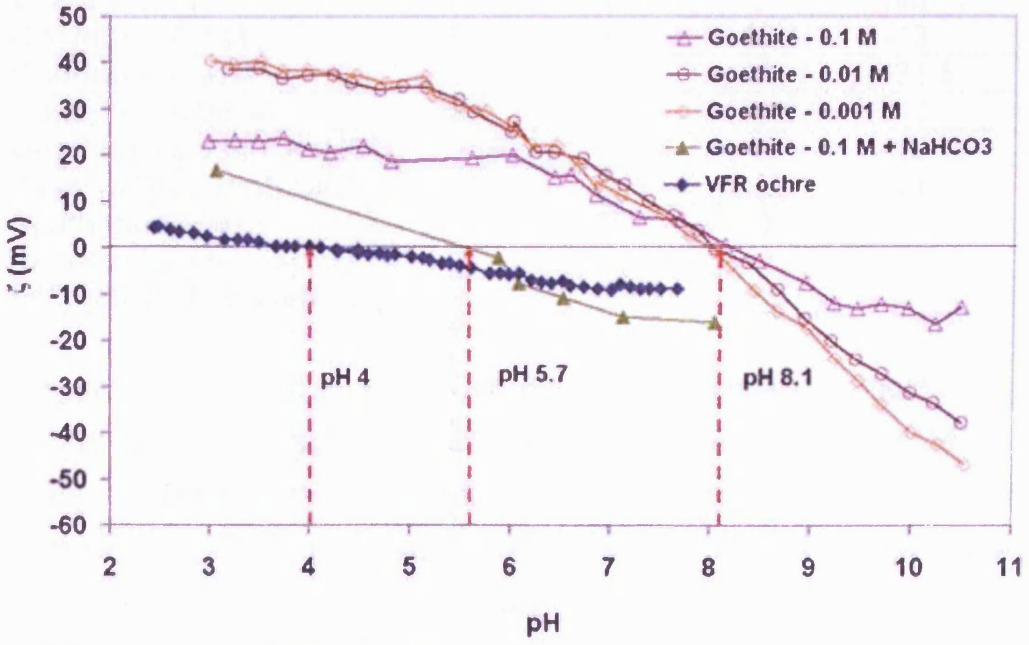

Figure 7-8: Zeta potential against pH for synthetic Fe(III) (hydroxy)oxide in $NaNO_3$ solutions

Table 7.2 summarises the IEP and values of ζ determined at pH 4, 7 and 10 for the VFR ochre and synthetic Fe(III) (hydroxy)oxide. Table 7.2 also shows the results of similar titrations by Dempsey and Jeon (2001) for comparison. An IEP of pH 8.1 was determined for the washed goethite titrated in indifferent $NaNO_3$ electrolytes. This therefore represents the Pristine Point of Zero Charge (PPZC) in the absence of specifically adsorbed ions (Stumm and Morgan, 1996). However strict CO_2 free conditions were not used in this study

and even though attempts were made to limit CO_2 adsorption into the titration mixture (see section 6.6.2) it is possible that minor levels of dissolved CO_2 species may influence the IEP as indicated in studies by Evans et al (1979), Zeltner et al (1988) and Villalobos and Leckie (2000). With increasing electrolyte concentration a reduction can be seen in the magnitude of the ζ determined at a particular pH. For instance, at pH 10 the ζ determined for the goethite used in this study in 0.1, 0.01 and 0.001 M $NaNO_3$ electrolyte were -13, -31.5 and -40 mV respectively.

Table 7.2: Summary of results of zeta potential pH titrations

	IEP pH	ζ pH 4 mV	ζ pH 7 mV	ζ pH 10 mV
VFR 6 – ochre	4	0	-9	n/d
Goethite – 0.1 M	8.1	21.2	15.4	-13
Goethite – 0.01M	8.1	37.1	11	-31.5
Goethite – 0.001M	8.1	38.5	11.2	-40
Goethite – 0.1 M + $NaHCO_3$	~5.7	~16.8	-15	n/d
Passive HB – High $CaCO_3$ [b]	~3.5	-2.5	n/d	n/d
Synthetic Fe(III) (hydroxy)oxide – Fe(III)chloride pH 8 NaOH	8	35	10	-30

The series Goethite 0.1 M + $NaHCO_3$ in Figure 7-8 shows a reduction of the IEP to pH 5.7 but no significant difference is seen in the magnitude of ζ at high pH conditions where a magnitude of -15 mV at pH 8 is comparable to that of Goethite in 0.1 M $NaNO_3$ at pH 10 and in both cases the ζ titration curve levels before these points indicating no further increase in ζ above this pH. The IEP determined for the field ochre sample (determined as largely amorphous ferrihydrite using XRD analysis – see section 7.3) is at pH 4 which is 4 pH units lower than the average PPZC determined for ferrihydrite by Dzombak and Morel (1990) from analysis of literature values in which a mean value of 8 and a range of 7.9 to 8.2 was found.

The IEP shift and low ζ magnitude observed in the VFR ochre is consistent with results reported by previous authors. Zänker et al (2003) determined very low IEP of pH 2.6 in partially diluted mine waters and a low magnitude ζ of -7.5 mV at pH 5.6, the recorded pH of the water body. The water chemistry

was characterised by high sulfate, Ca, carbonate and silicate concentrations and also 2.6 mg L^{-1} of organic matter. A study by Davies et al (2002) of Si adsorptionto Fe(III) (hydroxy)oxide found that Si did cause a lowering of the IEP and could be invoked to account for the negative ζ seen in the Taff Merthyr study and the Zänker et al (2003) study. However, Davies et al (2002) found Si concentrations an order of magnitude greater than those seen at Taff Merthyr were necessary to lower the IEP of ferrihydrite to pH 5. Therefore Si cannot be invoked to explain the observed Taff Merthyr IEP shift.

Liang et al (1993a) reported negative ζ in the order of -20 mV for Fe(III) (hydroxy)oxides precipitated after oxygenation of an aquifer containing Fe(II) at circum-neutral pH. On further study (Liang et al, 1993b) it was found that at circum-neutral pH the presence of 0.5 – 2 mg L^{-1} of natural organic matter significantly lowered the observed electrophoretic mobility (analogous in sign to ζ) of freshly precipitated Fe(III) (hydroxy)oxide from positive to negative. However Liang et al (1993a,b) did not determine the IEP of the Fe(III) (hydroxy)oxide precipitates and therefore a direct comparison cannot be drawn between their study and the results given here.

Dempsey and Jeon (2001) conducted ζ measurements on ochre samples taken from mine drainage sites in Pennsylvania, USA and found IEP as low as pH 3.5 and found that the magnitude of the ζ was below ± 10 mV. They attributed the low ζ to suppression of the diffuse layer in the presence of high concentrations of Ca^{2+} in the mine water and the IEP shift to high concentrations of sulfate. It was found that ζ titration of synthetic Fe(III) (hydroxy)oxide in the presence of SO_4^{2-} but without Ca^{2+} present showed a similar IEP shift to that found in titrations of field samples but that the magnitude of the ζ was much greater at a given pH. Similarly titrations of synthetic Fe(III) (hydroxy)oxide without Ca^{2+} or SO_4^{2-} showed an IEP at pH 7.8 and ζ greater than ± 30 mV at pH conditions below 4 and or greater than 10.

In the present study it has been found that the presence of HCO_3 can significantly reduce the IEP of synthetic goethite to pH 5.7 but cannot account for the observed IEP of the VFR ochre. In light of the data presented by Dempsey and Jeon (2001) it seems likely that the major controls over the IEP of Fe(III) (hydroxy)oxide particles and overall ζ magnitude in circum-neutral mine water is the potentially determining ion SO_4^{2-} and the divalent counter-ion Ca^{2+} respectively. It should also be expected that Mg^{2+} will add to the total counter-ion effect. The effect dissolved organic matter has on IEP in the Taff Merthyr VFR is unclear and the concentration of dissolved organic matter was not determined.

High concentrations of Ca^{2+} and Mg^{2+} in the Taff Merthyr mine water lead to suppression of the magnitude of negative ζ to a value below -10 mV. A general rule of thumb is that a particle sol is stable if the ζ is greater than ± 30 mV. Below this a sol becomes increasingly unstable and the likelihood of particle coagulation and settling increases. The low ζ determined for the VFR ochre in the Taff Merthyr mine water indicates that freshly precipitated Fe(III) (hydroxy)oxide particles are relatively unstable and will rapidly coagulate. This is in agreement with the SEM images in Figure 7-5 and Figure 7-6 in which aggregates of individual particles can clearly be seen. Dempsey (1995) (and later Bullen, 2007) demonstrated, that in active mine water treatment using the High Density Sludge (HDS) process, that the lowest density sludge is often produced when ζ is closest to zero and the primary precipitate is destabilised forming dendritic flocs. However, in passive treatment a low ζ will enhance coagulation and settling rate in a traditional settling lagoon and also help to maintain a high surface area and bed permeability in a VFR system.

It should be noted that the ζ of the ochre particulates precipitated in mine water discharges may change significantly on entering a receiving water course with an appreciably different chemistry. If the receiving watercourse has a much lower ionic strength than the mine water this could result in an increase in the magnitude of the ζ and formation of a stable suspension and increased particulate transportation.

7.2.8 Filtration characteristics

Three constant pressure filtration tests were run on samples of the 6 mm VFR ochre collected on the 14/6/2007 to determine the filtration characteristics of the ochre with specific relevance to future removal and dewatering in a full scale treatment scenario. Figure 7-9 shows the time / volume in sec m^{-3} against volume of filtrate for the three tests. Specific Cake Resistance (SCR) was calculated for each of the tests using the universal filtration equation in the form used by Bullen (2007). In each case SCR values were computed using the slope of the linear part of the line presented in Figure 7-9 which equates to a maximum filtrate volume of 175 mL.

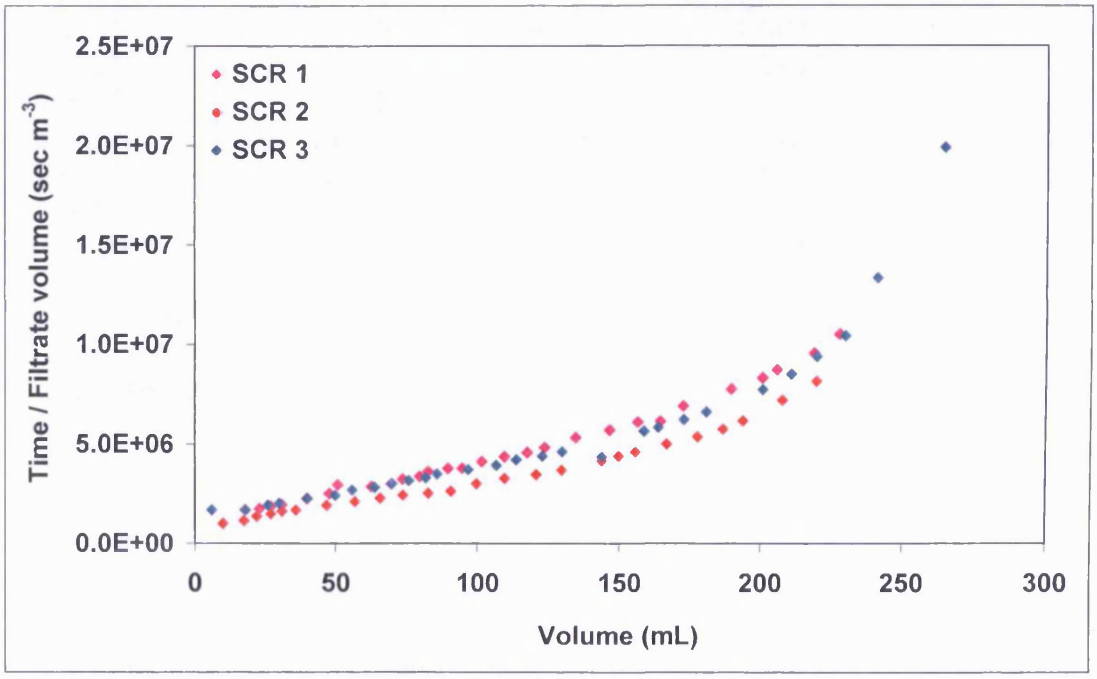

Figure 7-9: Time / filtrate volume against cumulative volume recorded in SCR tests

Table 7.3 summarises the results of the three tests and compares the results obtained here with the results of SCR tests on sludge from active mine water treatment systems as given in Bullen (2007) and for active and passive systems as given by Dempsey and Jeon (2001). SCR results of sludge

produced from iron in Tap Water during Single Pass[1] treatment (TW – SP), iron in Tap Water during High Density Solids treatment (TW – HDS) and using real Acid Rock Drainage during HDS treatment (ARD – HDS) are shown for the Bullen (2007) study. Results of sludge collected from two locations of a ARD Passive treatment Wetland site (ARD - PW 1 and ARD - PW 2) and identical ARD using Single Pass treatment (ARD – SP) are given for the Dempsey and Jeon (2001) study.

Table 7.3: Summary of SCR test results and comparison with literature data

Test	Initial solids % (w/w)	Cake solids % (w/w)	Specific cake resistance Gm kg^{-1} [a, b]
VFR 1[a]	21.08	34.36	4,983[a]
VFR 2[a]	20.59	35.52	4,370[a]
VFR 3[a]	20.59	40.81	4,927[a]
Mean	20.75	36.90	4,760
SD	0.23	2.81	276.72
% SD	1.11	7.61	5.81
TW - SP[b]	1	8.9	52,800
TW - HDS[b]	8.4	44.5	1,230
ARD - HDS[b]	32.3	76.3	1
ARD – PW 1[c]	19.1		430
ARD – PW 2[c]	20		20
ARD - SP[c]	1		260-1250

[a] *This study*
[b] *Bullen (2007)*
[c] *Dempsey and Jeon (2001)*

The mean SCR value for the VFR sludge is 4760 Gm kg^{-1} with a % SD of 5.81. This is an order of magnitude lower than the value obtained by Bullen (2007) for single pass active treatment sludge of 52800 Gm kg^{-1}. This was obtained from the active treatment of ferruginous water using chemical dosing for pH manipulation and polymer flocculent additionto aid coagulation and settling. It should also be noted that the initial solids content is much higher in the VFR sludge at 20.75 % (w/w) than the 1 % (w/w) of the single pass sludge.

[1] Active mine and waste water treatment in which Fe is removed by pH manipulation and aeration. Resulting ochre sludge is then removed from the system and is not-recirculated unlike the High Density Sludge (HDS) process in which sludge is recirculated.

The SCR value obtained by Bullen (2007) for High Density Solids (HDS) sludge produced from iron in tap water is 4 x lower than that produced in the VFR at 1230 Gm kg^{-1}. It should be noted however that the initial solids content of the VFR ochre is over twice that of the HDS test which is only 8 % (w/w) whilst the cake solids contents are comparable at 36.9 and 44.5 % (w/w) respectively. Comparison of the HDS produced from real Acid Rock Drainage (ARD) with the results of the VFR single pass and HDS iron in tap water results show a difference of 3 orders of magnitude between the SCR of the tap water HDS and the ARD HDS.

The results obtained by Dempsey and Jeon (2001) are one to two orders of magnitude lower than those obtained for the VFR ochre which could be due to the lower pressure used in the Dempsey and Jeon (2001) filtration test. An attempt to correct Dempsey and Jeon (2001) values using their reported coefficient of compressibility resulted in only minor increases in reported SCR values. Although the mine water was circum neutral in the Dempsey and Jeon (2001) study it had a considerably higher Fe(II) load than the Taff Merthyr mine water with values between 94 and 245 mg L^{-1} as opposed to 6.3 mg L^{-1} in the Taff Merthyr mine water. In such cases of high Fe(II) concentrations, surface concentration of Fe(II) on Fe(III) (hydroxy)oxide will be much greater than at lower Fe(II) concentrations in accordance with the law of mass action giving rise to increased surface oxidation and particle accretion. It is therefore possible that this effect would be similar to formation of HDS in active treatment at alkaline pH with high ζ and therefore possibly be responsible for the observed filtration characteristics. In contrast, the lower iron concentrations observed in the Taff Merthyr mine water may lead to respectively lower surface Fe concentrations. This may potentially form less dense flocs.

7.3 Mineralogical characterisation

This section presents the results and discusses the mineralogy of the ochre in the Taff Merthyr settlement lagoons and VFR. Characterisation of mineral

phases was conducted using X-Ray Diffraction (XRD) analysis of homogenised powdered samples.

7.3.1 Fe mineralisation

Figure 7-10 and Figure 7-11 show XRD traces for the 20 mm VFR and the 6 mm VFR. In each case the XRD traces are displayed as plots of total counts against goniometric angle °2Theta (°2θ). Both 20 mm and 6 mm VFR ochres show undulose peaks at 35 and 62.5 °2θ. This is characteristic of the largely amorphous Fe(III) (hydroxy)oxide, 2-line ferrihydrite (Cornell and Schwertmann, 2003).

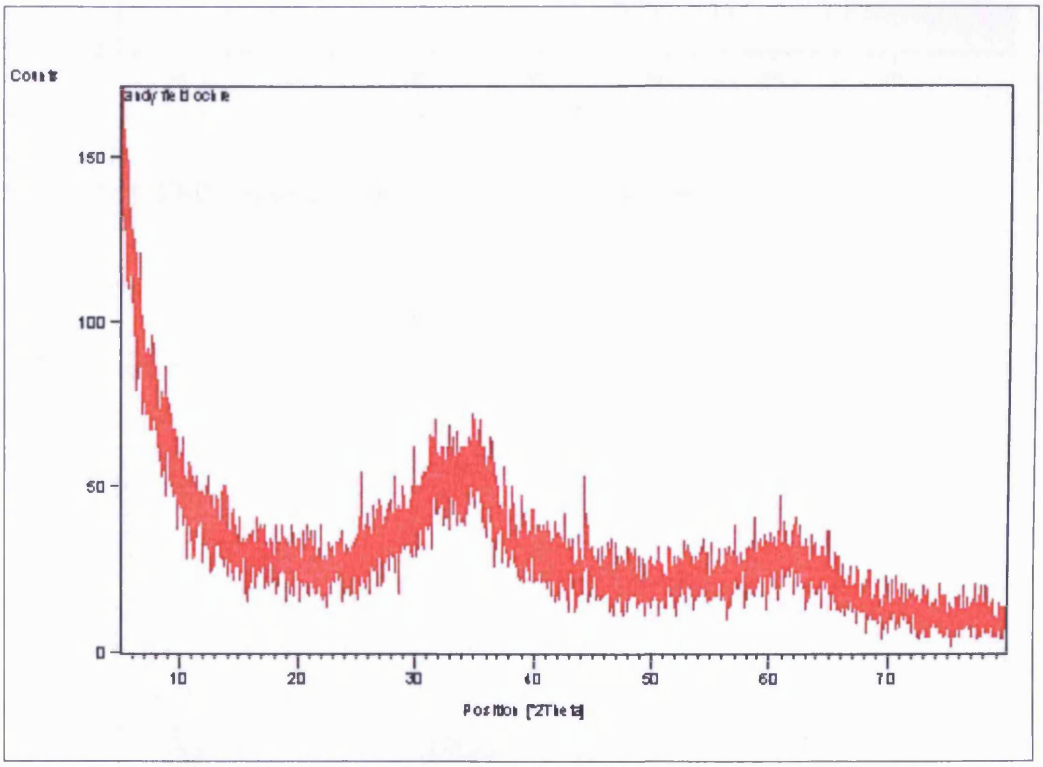

Figure 7-10: XRD trace determined for 20 mm VFR ochre

Figure 7-12 shows the XRD trace for ochre collected from the distribution channel into the L2 lagoon taken on the 10/7/05. In agreement with the VFR ochre samples shown in Figure 7-10 and Figure 7-11 the trace shows characteristic undulose peaks typical of 2-line ferrihydrite.

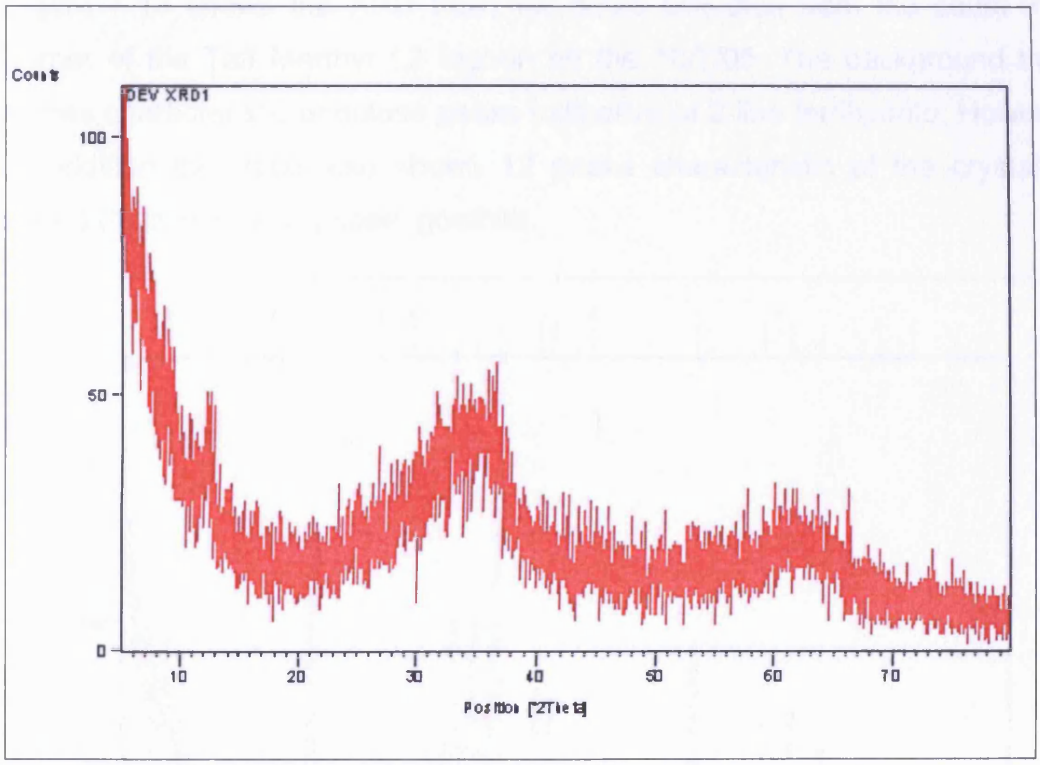

Figure 7-11: XRD trace determined for 6 mm VFR ochre

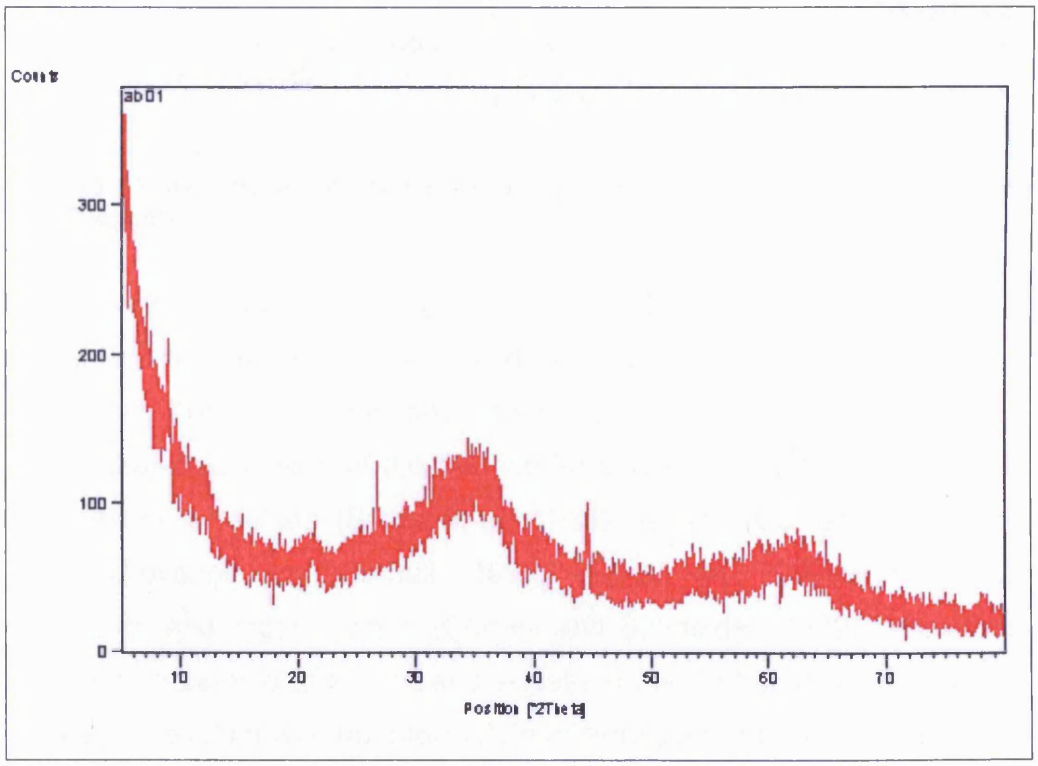

Figure 7-12: XRD trace determined for ochre collected from the L2 lagoon distribution channel

Figure 7-13 shows the XRD trace for ochre collected from the south west corner of the Taff Merthyr L2 lagoon on the 10/7/05. The background trace shows characteristic undulose peaks indicative of 2-line ferrihydrite. However, in addition the trace also shows 12 peaks characteristic of the crystalline Fe(III) (hydroxy)oxide phase, goethite.

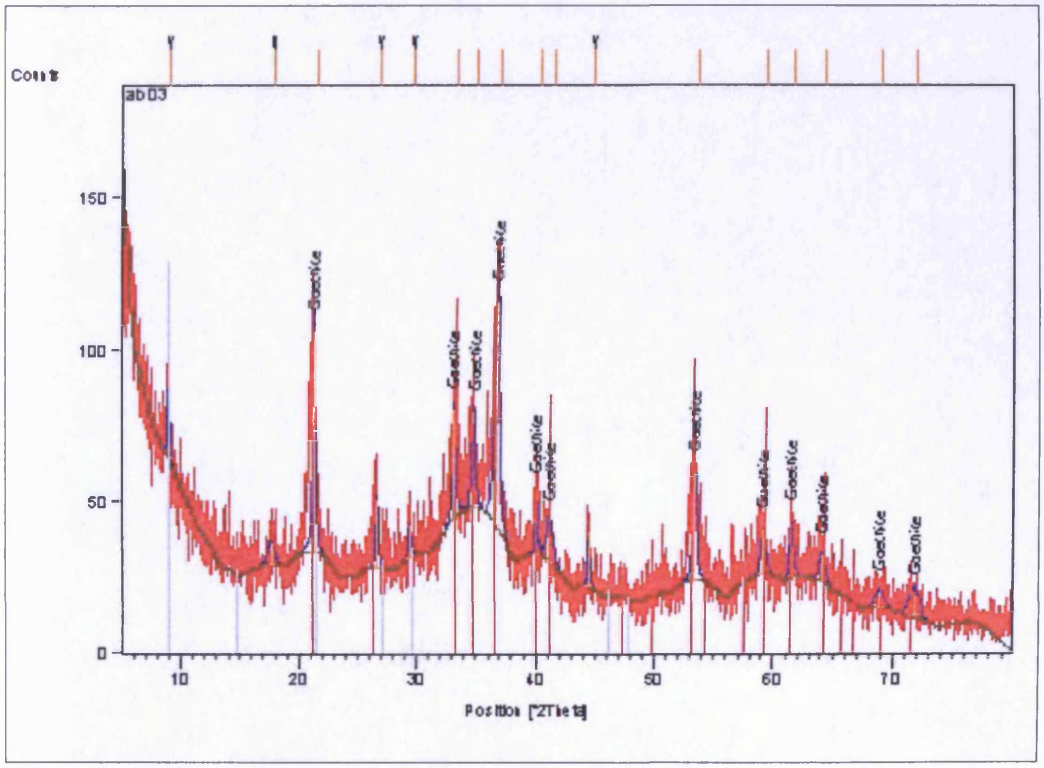

Figure 7-13: XRD trace determined for ochre collected from the south west corner of the L2 lagoon

In previous laboratory investigations it has been found that ferrihydrite is unstable in the presence of dissolved Fe(II) and rapidly transforms to goethite (Park and Dempsey, 2005 and references therein). However, it has been shown that stabilisation of the ferrihydrite phase can be achieved due to co-precipitation of sulfate (Brady et al, 1986), silicate (Cornell and Schneider, 1989, Giovanoli and Cornell, 1992; Cornell and Schwertmann, 2003), phosphate and organic acids (Cornell and Schneider, 1989). Therefore, the confirmed presence of sulfate and silicate in the Taff Merthyr mine water can be used to explain why transformation of ferrihydrite to goethite is not seen in the VFR and distribution channel ochres. This explanation does not however explain why goethite is observed in the L2 lagoon.

Figure 7-14 shows a photograph of ochre collected from the south west corner of the L1 lagoon on the 14/6/07. A photograph insert showing the orange colour of the VFR ochre is included in the top right corner for colour comparison. It was found that the L1 ochre was olive green in colour rather than the orange colour traditionally associated with Fe(III) (hydroxy)oxide ochres. It was also found that a colour change from olive green to orange occurred on exposure of lagoonal ochre to the atmosphere.

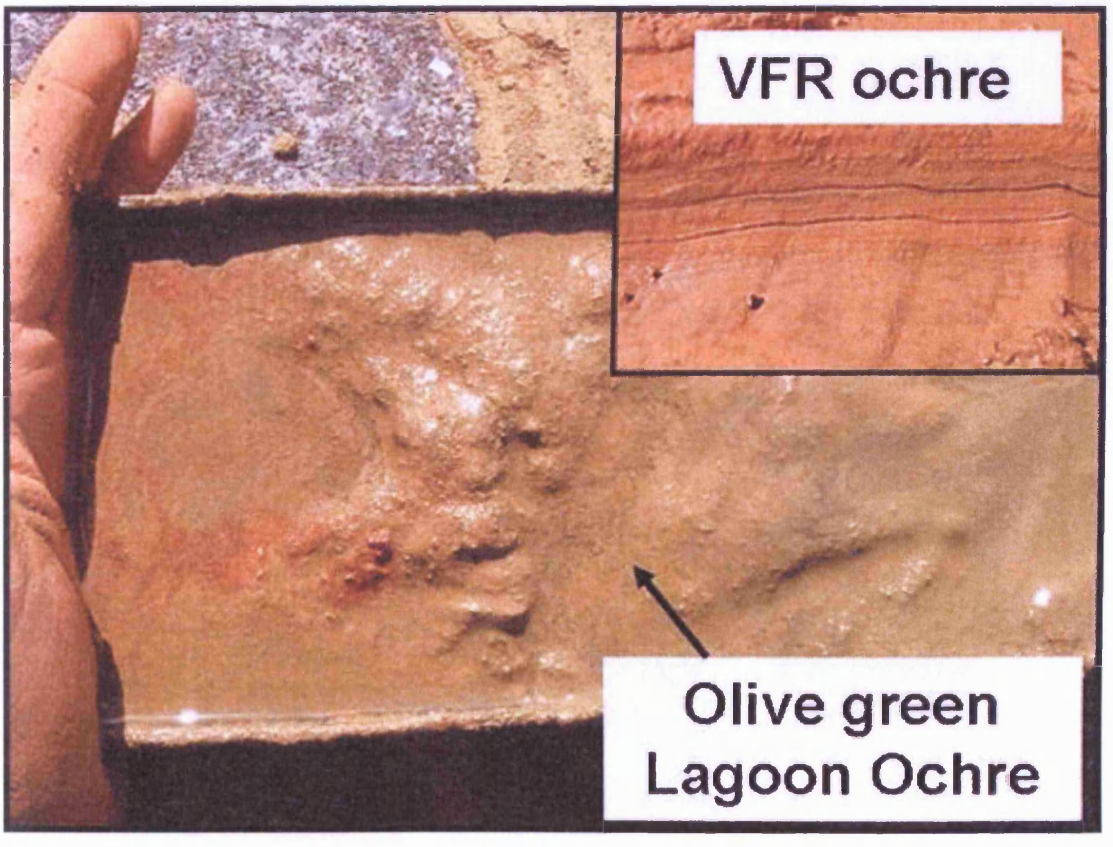

Figure 7-14: Photograph of olive green ochre collected on the 14/6/07. Insert shows the VFR ochre for comparison

The olive green colour of the lagoon ochre is indicative of the formation of reducing conditions at the base of the settlement lagoon and the possible presence of green rust. Bioreduction of Fe(III) (hydroxy)oxide minerals and the formation of green rust is well documented (O'Loughlin et al, 2007 and references therein). It is also known that oxidation of green rust in the presence of carbonate at pH between 5 and 7 results in formation of goethite (Cornell and Schwertmann, 2003). This may give a logical route for the

formation of the goethite as identified in Figure 7-13. This is despite the increased stability of ferrihydrite with respect to more crystalline phases as discussed previously and the proposed formation pathway is illustrated in Figure 7-15. Likewise formation of goethite will not occur by this mechanism in either the distribution channel or the VFR ochre bed as oxic conditions will inhibit ferrihydrite bioreduction.

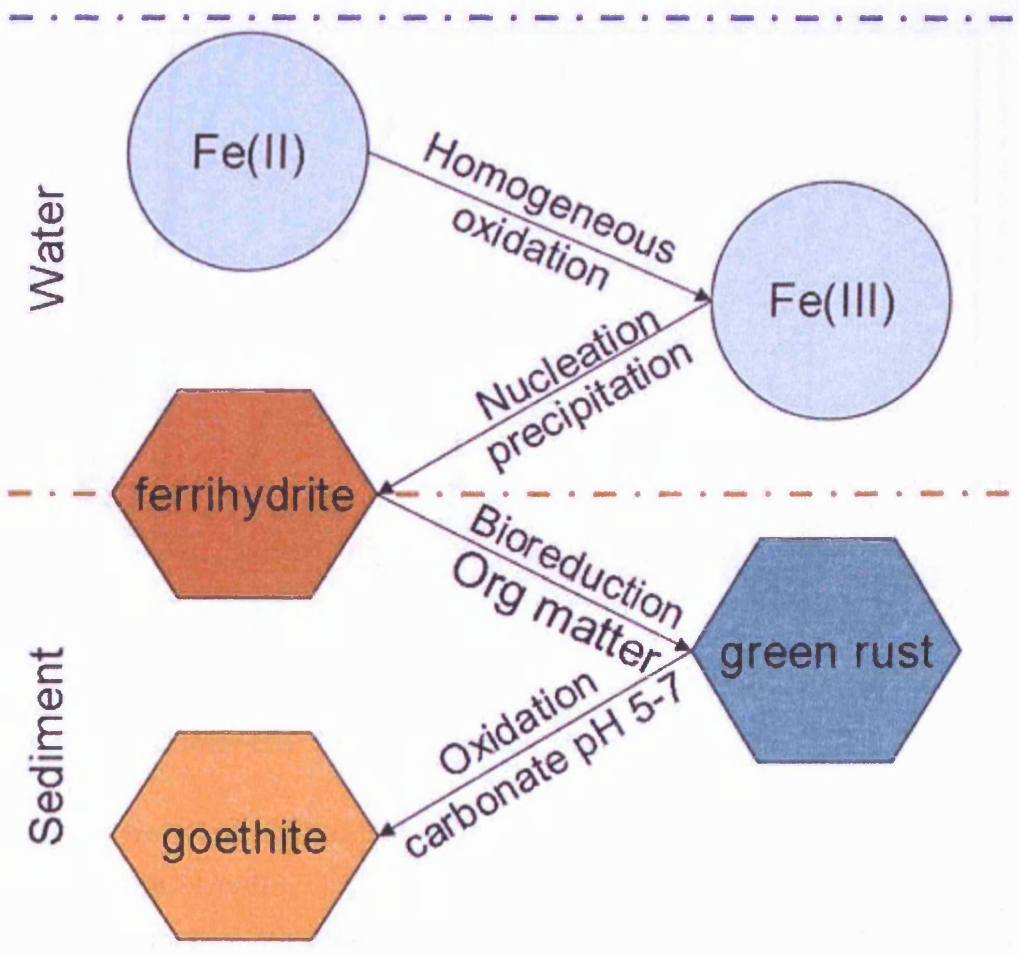

Figure 7-15: Pathways for the formation of goethite in the settlement lagoons

Hexagons = solid phase, circles = dissolved phase, Org matter = organic matter, Concept from Cornell and Schwertmann (2003).

7.3.2 Mn mineralisation

Figure 7-16 shows the XRD trace obtained for second year VFR ochre following a 2 N HCl extraction. Using this extraction, the ferrihydrite phase

dissolves almost completely as is evident in loss of the characteristic undulose peaks at 35 and 62.5 °2θ. The remaining non-acid extractable phase consists of a dark grey to black solid and shows peaks consistent with barium manganese oxide hydrate ($Ba_2Mn_{14}O_{27}.xH_2O$) and birnessite ($(Na,Ca)_{0.5}(Mn(IV),Mn(III))_2O_4 \cdot 1.5H_2O$), with peak matches of 40 and 35 % respectively.

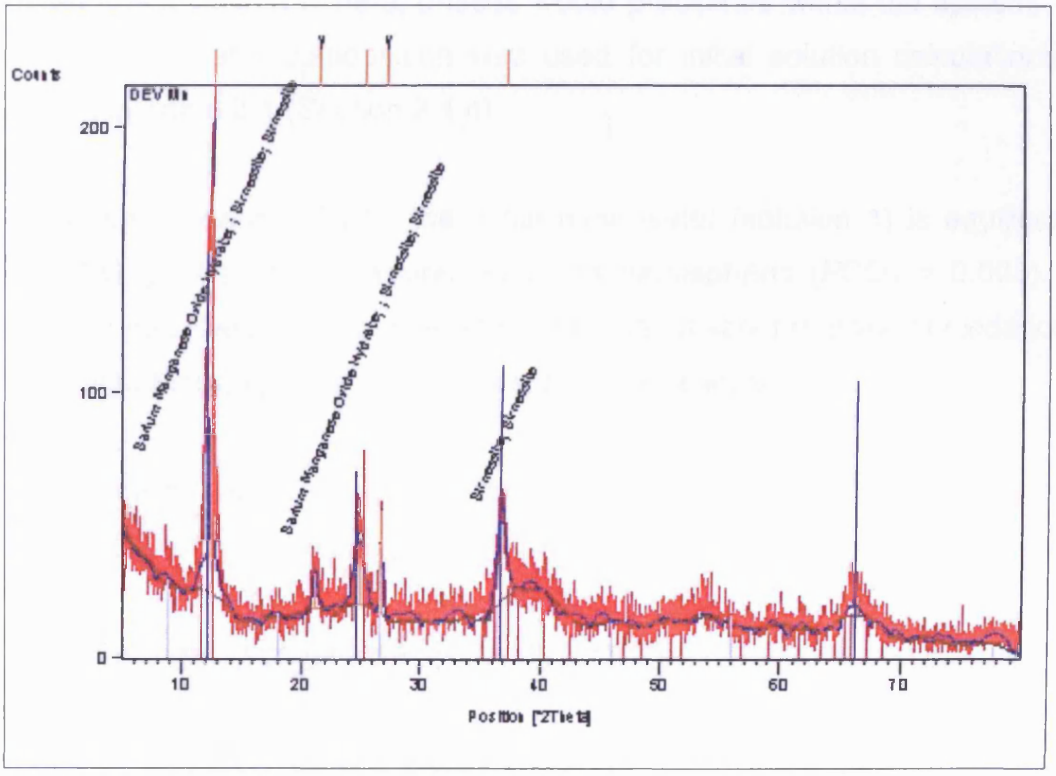

Figure 7-16: XRD trace after 2 N HCl extraction of 6 mm VFR ochre

Due to the sensitivity of powder XRD analysis, mineral phases that constitute less than approximately 1 % of the total solid are not detectable. Therefore the Mn containing mineral phases as evident in Figure 7-16 after acid extraction are not detectable in the bulk VFR ochre XRD trace. The XRD analysis is consistent with the formation of dark mineral bands within the VFR ochre bed (See Figure 7-1) which are shown to be elevated in manganese (Mn) as discussed in section 7.4. It is also evident that these mineral phases are resistant to 2 N HCl extraction.

7.3.3 Calcite mineralisation

Precipitation of $CaCO_3$ may be expected given the high alkalinity of the Taff Merthyr mine water and degassing of CO_2 on atmospheric exposure. PhreeqC (Parkhurst and Appello, 1999) modelling, using the Wateq4F geochemical database (Ball and Nordstrom, 1991), was undertaken to determine if $CaCO_3$ mineral phases would precipitate within the system. The mean mine water composition was used for initial solution calculations as shown in Table 2-1 (Section 2.4.4).

In the first scenario (TM1), the initial mine water (solution 1) is equilibrated with $CO_{2(g)}$ at partial pressures equal to atmospheric (PCO_2 = 0.003). In addition dissolved O_2 was omitted from the input script to prevent oxidation of Fe(II) and Mn(II) species. The input script is as follows:

The following script shows the PhreeqCI input for simulation TM1. The full PhreeqCI input and output script are given in Appendix 4.

```
TITLE Taff Merthyr CO2 equilibration (TM1).
SOLUTION 1 Mean Taff Merthyr DW composition
    temp      11.6
    pH        6.93
    pe        3.0171 ###pe=Eh*0.0177###
    redox     pe
    units     mg/L
    density   1
    Si        4.78
    K         13.04
    Na        15.87
    Ca        101.58
    Mg        42.11
    Mn        0.8
    Sr        0.59
    Cl        10
    S(6)      226.33 as SO4
    Alkalinity 297.7286 as HCO3
    Fe(2)     6.3
    Fe(3)     2.59
    -water    1 # kg

EQUILIBRIUM_PHASES 1
    CO2(g)    -2.523 10       ###SI CO2(g)=LogPCO2 in Air###
    Fe(OH)3(a) 0 10

end
```

The following is a summary of the PhreeqCI output script for the initial solution calculations for simulation TM1:

```
----------------------------Description of solution----------------

                                    pH  =   6.930
                                    pe  =   3.017
                        Activity of water  =   1.000
                           Ionic strength  =  1.440e-002
                       Mass of water (kg)  =  1.000e+000
                     Total carbon (mol/kg)  =  6.241e-003
                        Total CO2 (mol/kg)  =  6.241e-003
                      Temperature (deg C)  =  11.600
                    Electrical balance (eq)  = -2.029e-006
 Percent error, 100*(Cat-|An|)/(Cat+|An|)  =  -0.01
                                Iterations  =  10
                                   Total H  = 1.110177e+002
                                   Total O  = 5.553342e+001

--------------------------------Redox couples-----------------------

      Phase               SI log IAP  log KT[1]

      Aragonite         -0.51   -8.77   -8.26  CaCO3
      Calcite           -0.36   -8.77   -8.42  CaCO3
----------------------------------------
Beginning of batch-reaction calculations.
----------------------------------------
```

The following is a summary of the PhreeqCI output script after equilibration with atmospheric CO_2 during simulation TM1.

```
----------------------------Description of solution----------------

                                    pH  =   7.876
                                    pe  =  -1.040
                        Activity of water  =   1.000
                           Ionic strength  =  1.429e-002
                       Mass of water (kg)  =  1.000e+000
                 Total alkalinity (eq/kg)  =  4.836e-003
                        Total CO2 (mol/kg)  =  4.928e-003
                      Temperature (deg C)  =  11.600
                    Electrical balance (eq)  = -2.029e-006
 Percent error, 100*(Cat-|An|)/(Cat+|An|)  =  -0.01
                                Iterations  =  17
                                   Total H  = 1.110176e+002
                                   Total O  = 5.553065e+001

----------------------------Distribution of species----------------
```

[1] Where SI = IAP/KT and SI is the Saturation Index, IAP is the Ion Activity Product, and KT is the solubility product. When SI is greater than 1 the solution is oversaturated with respect to the stated mineral phase

```
Phase              SI log IAP  log KT

Aragonite           0.42   -7.84   -8.26  CaCO3
Calcite             0.58   -7.84   -8.42  CaCO3
Dolomite            0.92   -15.84  -16.76  CaMg(CO3)2


------------------
End of simulation.
------------------
```

Modelling has shown that mine water equilibration with atmospheric CO_2 results in an increase in system pH from ~ 6.9 to ~7.86. In addition both aragonite and calcite $CaCO_3$ polymorphs, are oversaturated. However, no direct evidence for crystalline $CaCO_3$ phases (either calcite or aragonite) were identified in XRD in either the lagoonal or VFR ochre. This may indicate that $CaCO_3$ phases if present are at concentrations below 1 wt% in the solid.

7.4 Geochemical characterisation

7.4.1 Whole sediment analysis – Bulk solids

Whole sediment analysis was conducted on three samples of year 2 VFR ochre: VFR 6 Core, VFR 6 Bulk and VFR 6 Bulk 2 and two samples of lagoonal ochre: year 1 lagoon and year 2 lagoon respectively. All VFR samples and the year 2 lagoon sample were collected on the 14/6/07. The year 1 lagoon ochre was collected on the 10/7/05.

Carbon and sulfur were determined by combustion and Infra-Red detection using a Leco element analyser. All other elements were determined using strong acid digestion followed by elemental analysis using ICP-AES. The constituents are reported as their concentrations corrected as common oxides unless indicated otherwise. FeHyd indicates the concentration of iron (Fe) as ferrihydrite using the formula $Fe_2O_30.5(H_2O)$ and the formula weight of 169 g $mole^{-1}$. Manganese is reported as Mn(III)OOH in the absence of evidence for Mn(IV) phases, for example pyrolusite, in XRD analysis. Silicon concentrations were not determined in the acid digest but previous whole sediment analysis of the Taff Merthyr ochre has shown Si to constitute approximately 40 mg g^{-1} of the dried solid equating to a SiO_2 concentration of 85 mg g^{-1} or 8.5 %. This is supported by the proportion of Si removed by the 6

mm VFR system (see section 8.6). SiO_2 is assumed to make up the difference between the mass of the sum of the measured constituents and the total dry ochre mass. SiO2# therefore indicates the inferred concentration of SiO_2 determined from mass balance.

Figure 7-17 shows the concentrations of the major components CaO, FeHyd, CO_2, MnOOH, and SiO2# in the Taff Merthyr ochres. It can be seen that FeHyd makes up the predominant mineral phase at a concentration of approximately 800 mg g^{-1} in all samples besides the Yr 2 Lagoon ochre. In this case FeHyd makes up 580 mg g^{-1} of dry solid. However, it should be noted that, once normalised in terms of wet ochre solids concentrations, the concentrations of Fe as ferrihydrite are 121.6 and 119.8 g dm^{-1} in the 6 mm VFR and lagoonal sludges respectively.

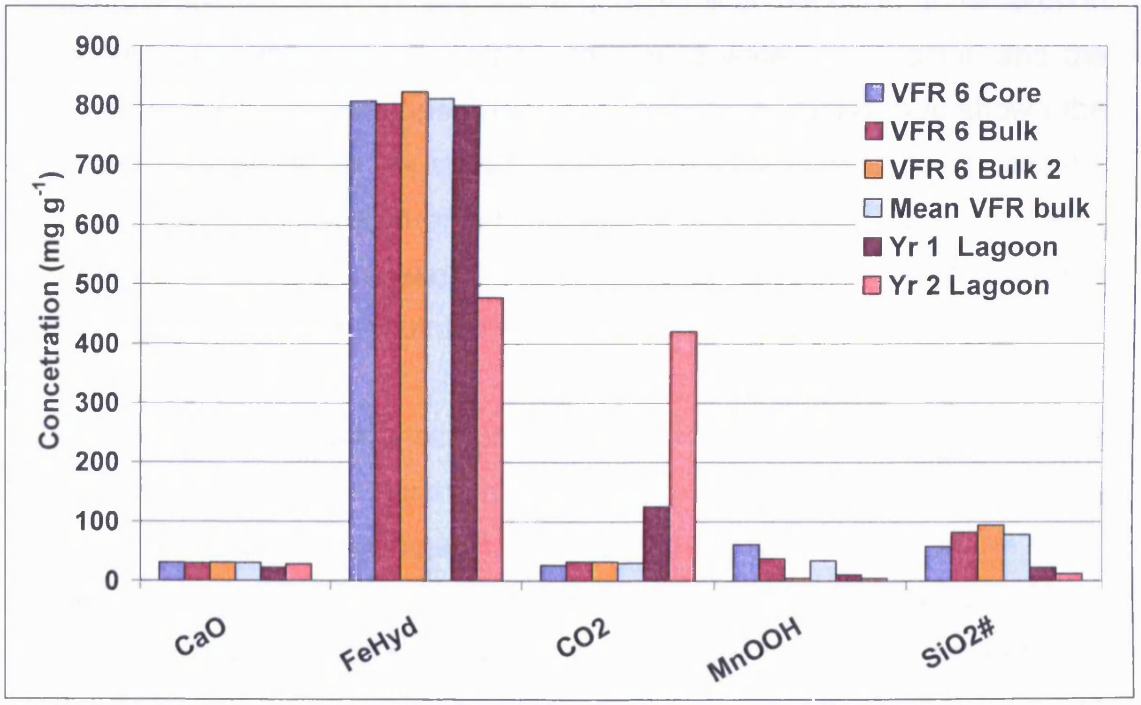

Figure 7-17: Comparison of major components in the bulk 6 mm VFR and lagoon ochre

Concentrations of Ca as CaO are fairly uniform in all samples with mean values of 28 mg g^{-1}. C as CO_2 has a mean value of 30.5 mg g^{-1} in the three 6 mm VFR samples. However, CO_2 is considerably higher in both the Yr 1 and Yr 2 lagoonal ochres with values of 124 and 420 mg g^{-1} respectively. Mn as MnOOH is shown to be generally higher in the VFR ochre than the lagoon ochre with a mean value of 35 mg g^{-1} and an order of magnitude range from 5

to 61.5 mg g^{-1}. MnOOH concentrations in the lagoon ochres were 10 and 5 mg g^{-1} for Yr 1 and Yr 2 respectively.

The uniform distribution of Ca within the data indicates that the high C content of the lagoonal ochre is not due to precipitation of $CaCO_3$. In the absence of elevated Ca, the elevated C content in the ochre bed may be attributed to a number of possible sources:

1) Direct precipitation of siderite ($FeCO_3$).
2) Accumulation of organic matter.
3) Presence of hydroxy-carbonate green rust in the ochre bed.

PhreeqC (Parkhurst and Appello, 1999) geochemical modelling undertaken in this study, using the average Taff Merthyr mine water composition and the Wateq4F geochemical database (Ball and Nordstrom, 1991), has shown the emerging mine water to be slightly oversaturated with respect to siderite. However, direct precipitation of siderite seems unlikely due to the slow rates of siderite precipitation (Jimenez-Lopez and Romanek, 2004) as compared to Fe(II) oxidation at circum-neutral pH.

The organic and inorganic carbon content of the lagoonal ochre was not determined separately in this study and therefore it is not possible to directly determine the presence of organic matter in the ochre. However, of the three possible sources listed above a combination of source 2 and 3 would fit in with the goethite formation pathway described in Section 7.3. The presence of hydroxy-carbonate green rust alone could not account for the high C values in the Yr 2 lagoonal ochre as the mole ratio of Fe to C is 6:1 (Hansen, 1989; Williams and Scherer, 2000) equating to 0.036 g(C) g^{-1}(Fe). Therefore organic C appears to be the only likely C source capable of accounting for the high C concentration seen in the lagoonal ochre. Origins could include animal faeces, plant matter, windblown dust and possibly coal particulates suspended in the mine water.

Figure 7-18 shows the concentrations in mg g^{-1} of the minor constituents aluminium, potassium, magnesium, sodium, sulfur, zinc and the total trace constituents (others) as their relative oxides in the VFR and lagoonal ochre. Interestingly, the elevated concentrations of C in the lagoonal layers as shown in Figure 7-17 is accompanied by elevated Al, K, and Mg but is depleted in Zn.

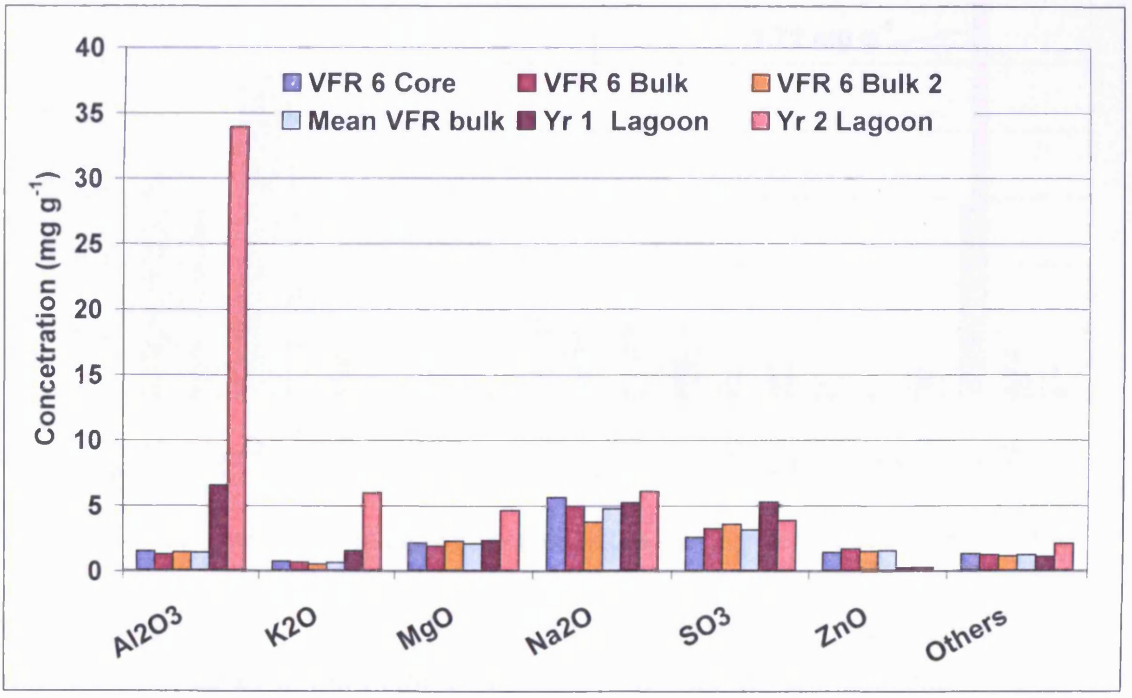

Figure 7-18: Comparison of minor components in the bulk 6 mm VFR and lagoon ochre

Figure 7-19 shows the concentrations in mg g^{-1} of trace constituents arsenic, barium, cobalt, nickel, lead, chromium, copper, molybdenum, titanium and thallium in the VFR and lagoonal ochre. It can be seen that the lagoonal ochre is depleted in As, Ba, Co, Ni and Tl but concentrated in Ti and Cu.

The elevated concentrations of Al, K, Mg and Ti could plausibly be explained by either atmospheric fallout of windblown dust or settling of solid particulates close to the distribution channel. In either case these elements form major constituents in many common soil and rock forming minerals. It should also be noted that the solid sample taken in the VFR was not in close proximity to the inlet pipe and therefore may not contain the same solid particulates that

may have settled below the inlet pipe. If settlement of suspended particulate minerals and coal fines is responsible for the above observations their origin could either be due to wash out from the mine workings or sediment washed into the Taff Merthyr mine water collection culvert during rainfall events.

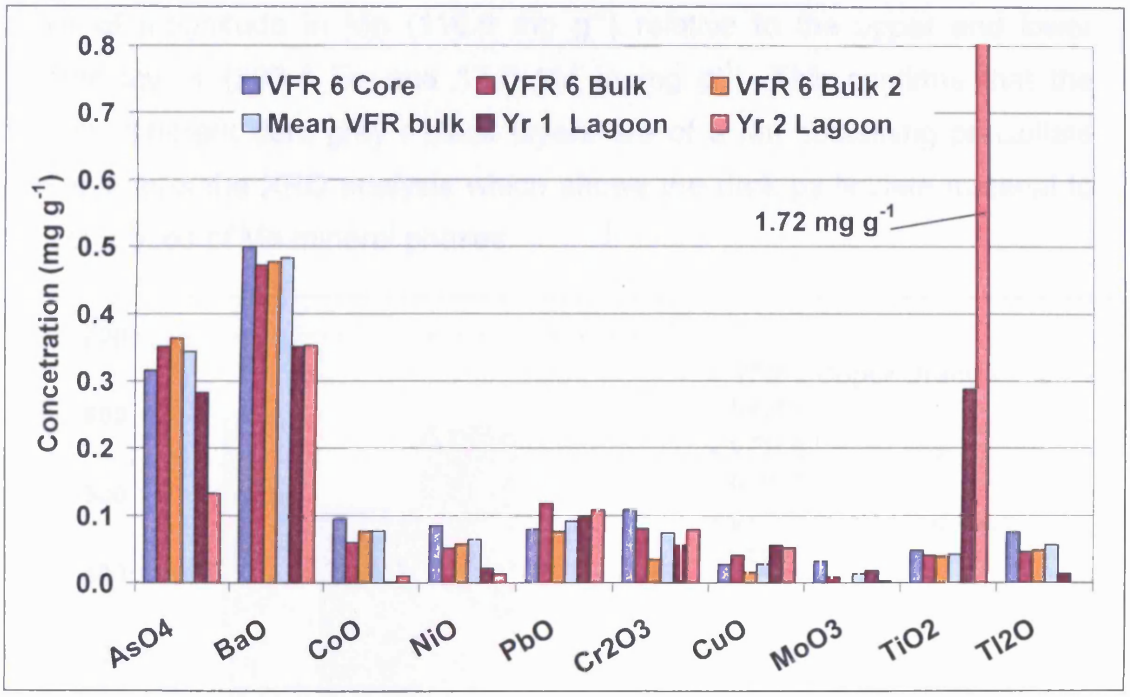

Figure 7-19: Comparison of trace components in the bulk 6 mm VFR and lagoon ochre

Mn, Si (inferred), As, Ba, Co, Ni, Zn and Tl all appear to be concentrated in the VFR ochre in comparisonto the lagoonal ochre. Concentration of the major constituents Mn and Si can be supported by removal data from VFR water samples (see sections 8.4 and 8.6), however all other analytes were below detection in the water samples apart from Zn. Slight contamination of Zn from the plenum floor made interpretation of Zn removal from water samples impossible and therefore Zn is not discussed further.

7.4.2 Whole sediment analysis – Bed profile

Further characterisation of three visually different layers in the 6 mm VFR ochre bed was undertaken in order to determine any variation in chemical characteristics. The upper orange, lower black and bottom orange layers as shown in Figure 7-1 were sub-sampled. The samples then underwent strong acid digestion followed by elemental analysis using ICP-AES.

Figure 7-20 and Table 7.4 show the proportion of the major redox sensitive metals, Fe and Mn as the proportion of dried solid. It can be seen that the lower black layer is depleted in Fe (486.6 mg g^{-1}) and concentrated by an order of magnitude in Mn (116.6 mg g^{-1}) relative to the upper and lower orange layers (596.4 Fe and 17.6 Mn in mg g^{-1}). This confirms that the visually different dark grey / black layers are of a Mn containing precipitate and supports the XRD analysis which shows the dark particulate material to be composed of Mn mineral phases.

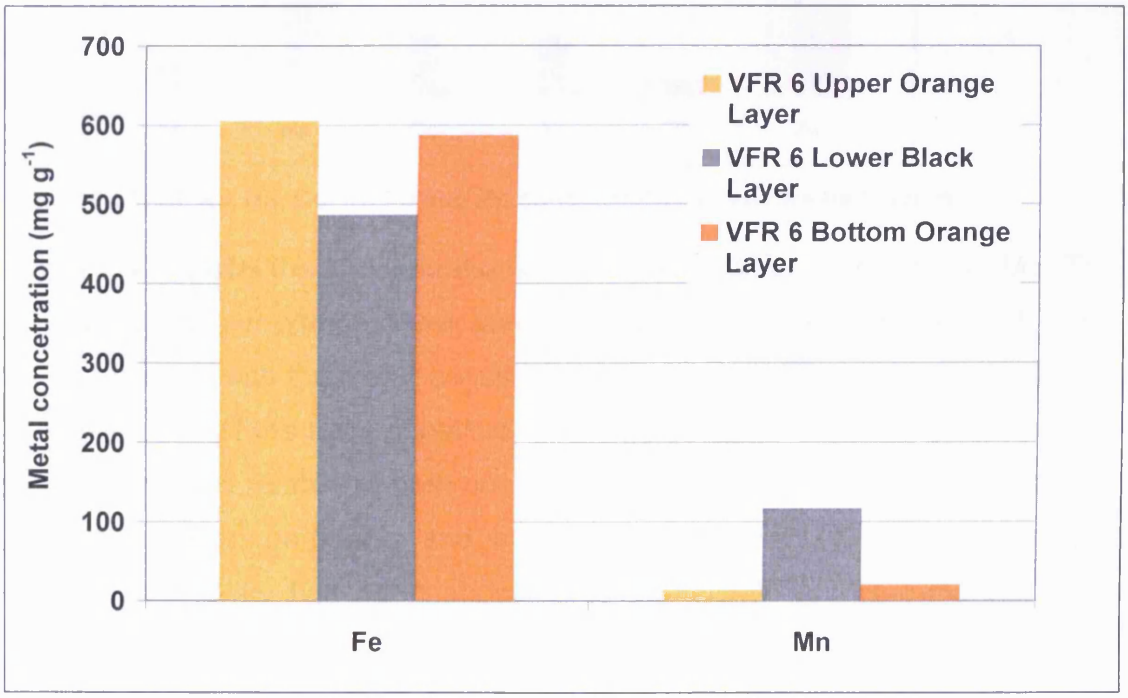

Figure 7-20: Fe and Mn concentrations in ochre bed layers

Table 7.4: Variation in Mn and Fe in ochre solids

As mg g^{-1}	Fe	Mn
Mean orange layers	596.4	17.63
Lower Black Layer	486.6	116.6

Figure 7-21 shows the concentration of the minor constituents Al, As, Ba, Co, Ni, Pb and Zn in mg g^{-1} of dried solid for the upper orange, lower black and bottom orange layers of the VFR bed. It is evident that the concentrations of

all of these analytes apart from As and Pb, are elevated in the lower black layer as compared to the upper and lower orange layers.

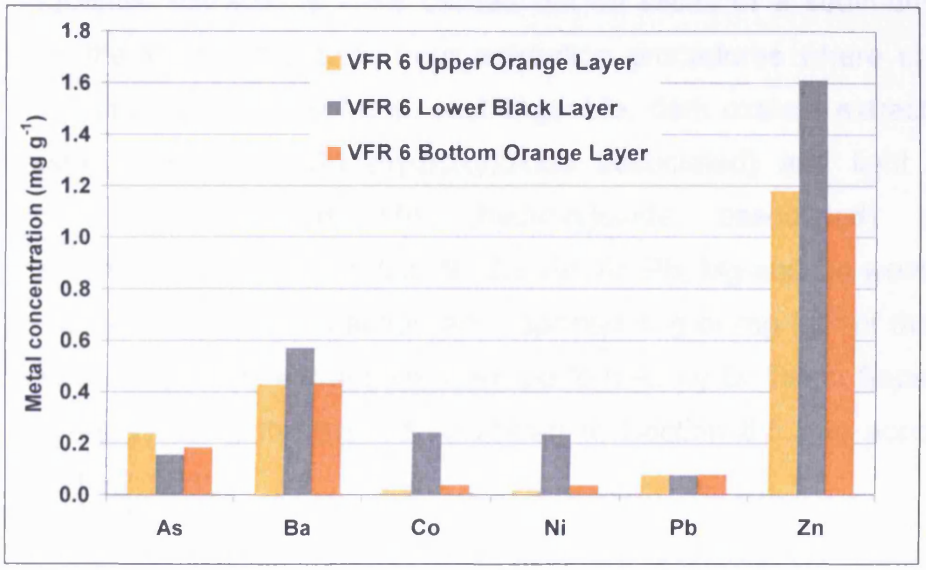

Figure 7-21: Al, As, Ba, Co, Ni, Pb and Zn concentrations in ochre bed layers

Figure 7-22 shows the concentrations of the trace constituents Cr, Cu, Mo, Ti and Tl in the upper orange, lower black and bottom orange layers. As with the trend observed with the minor constituents as shown in Figure 7-22, elevated concentrations of the trace constituents Cr, Cu, Ti and Tl can be seen in the lower black layer relative to both orange layers. These findings are consistent with trace metal portioning and scavenging by Mn(III,IV) (hydroxy)oxide mineral phases as has been shown to occur in soil and sub-marine Mn nodules.

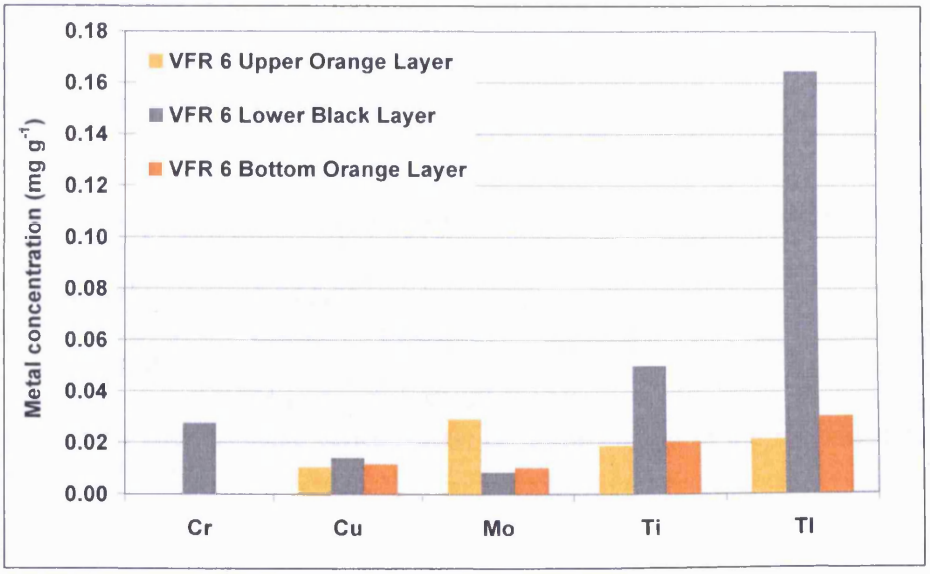

Figure 7-22: Cr, Cu, Mo, Ti and Tl concentrations in ochre bed layers

7.4.3 Sequential extraction – bed profile

Sequential extractions were carried out on slices of a sediment core taken from the VFR ochre bed. Four extraction procedures where undertaken to determine the water soluble, exchangeable, dark oxalate extractable (poorly crystalline Fe and Mn (hydroxy)oxide associated) and light hot oxalate (crystalline Fe and Mn (hydroxy)oxide associated) constituents. Concentrations of Mn, Cr, Co, Ni, Zn, Fe, Al, Pb, Mg and Ca were determined in eluate from each extraction and reported in g or mg kg^{-1} of the initial dried ochre. Sequential extractions were performed by Dr Devin Sapsford (Cardiff University) using the procedure shown in Section 6.5.3 in accordance with Sapsford (2003).

Figure 7-23 to Figure 7-27 show the sequential extraction results as total extracted for all metals. However, in this case of Ca and Mg, the water soluble fraction is given and the light hot oxalate fraction is not. From initial inspection of the data it is evident that most of the analyte is extracted during either the exchangeable or dark oxalate extractable leach apart from Al where a significant portion is extracted in the hot light oxalate leach.

As dark oxalate is capable of dissolving only poorly crystalline Fe and Mn (hydroxy)oxides, this indicates that there is little to no crystalline Fe and Mn oxides present supporting the mineralogical findings in Section 7.3. On the basis of variability with depth it is possible to characterise the analytes into three categories as shown in Table 7.5.

Table 7.5: Classification of analytes based on variability with depth through the 6 mm VFR ochre bed

Variability	Analyte	%[#]
Low	Zn, Fe, Pb, Ca	< 35
Intermediate	Mg	> 35 < 80
High	**Mn**, Cr, Co, Ni, Al	> 80

[#] *Minimum total extracted concentration as a percentage of the maximum determined total extracted concentration.*

Of the analytes which exhibit highly variable characteristics with depth Mn (see Figure 7-23a) is most prevalent with concentrations varying between 5 and 55 g kg^{-1}. Other analytes in this category are only detectable in mg kg^{-1} concentrations. Also apparent is that the variability of Mn, Cr, Co and Ni is almost completely due to variation in the dark oxalate extractable portion. The peaks in the high variability analytes can be roughly associated with the dark Mn mineral enriched bands as depicted in Figure 7-1 and Figure 7-2.

Figure 7-25a and b show the concentrations of Zn and Fe with depth through the VFR bed. In both cases the exchangeable portion is relatively high with initial proportions of 60 and 40 % exchangeable for Zn and Fe respectively with the remainder made up by the dark oxalate extractable portion. It is also evident that the exchangeable portion decreases with ochre depth which may be caused by increased particulate aggregation with depth and a reduction in specific surface area in accordance with the process of Ostwold ripening (Ratke and Voorhees, 2002).

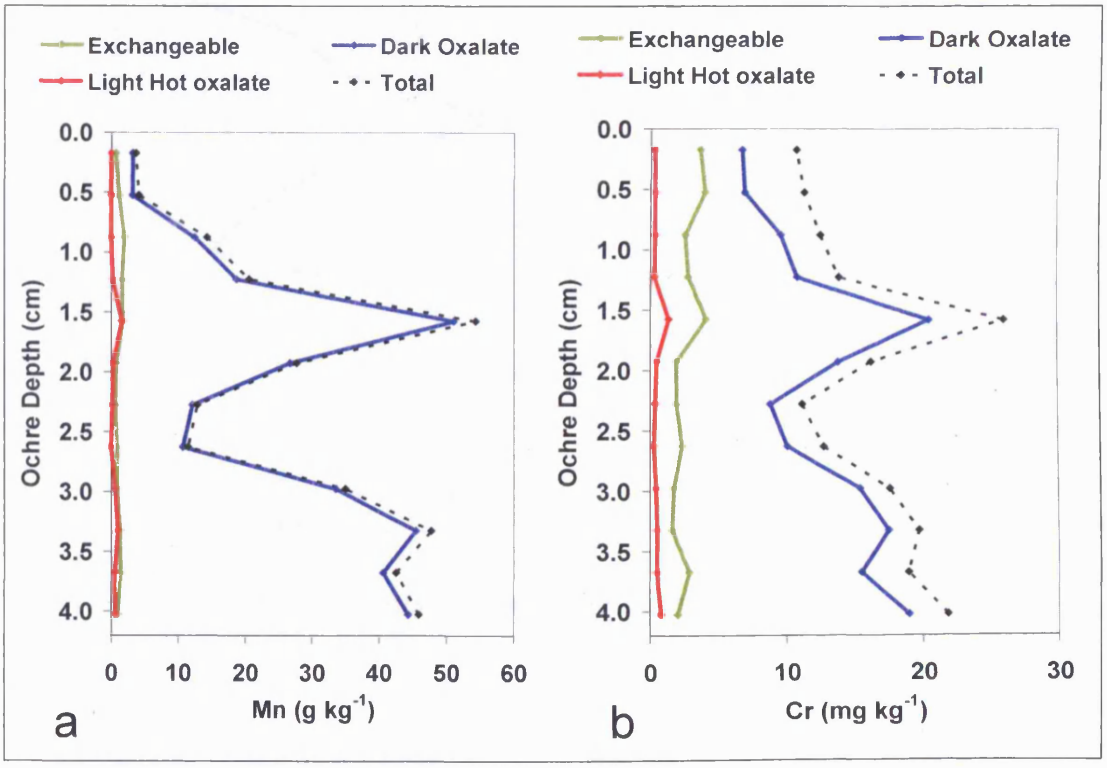

Figure 7-23: a) Mn sequential extraction and b) Cr sequential extraction

Figure 7-26a shows the concentration of Al with depth. Al is the only analyte which exhibits both the characteristics of the Mn associated elements and also a strong dependence on the light hot oxalate extraction. It is postulated that substitution of Al in the Mn oxide structure may increase its resistance to reductive dissolution by oxalate.

Figure 7-26b shows the variation in Pb concentration and demonstrates little variation with depth and is almost all associated with the dark oxalate extraction. Pb does not appear to be associated with the hydrous Mn oxide phase and therefore must form either a co-precipitate or substituting ion with ferrihydrite. Substitution of Pb with poorly crystalline Fe(III) (hydroxy)oxides has been identified previously (Strawn et al, 2006)

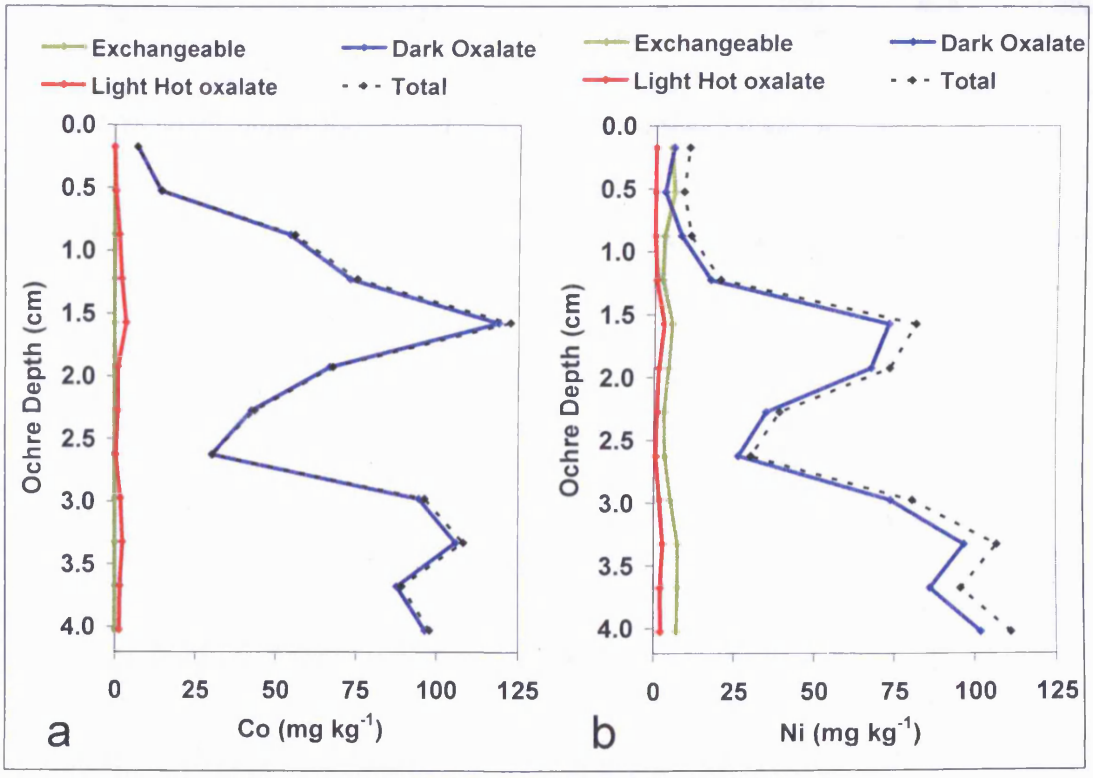

Figure 7-24: a) Co sequential extraction and b) Ni sequential extraction

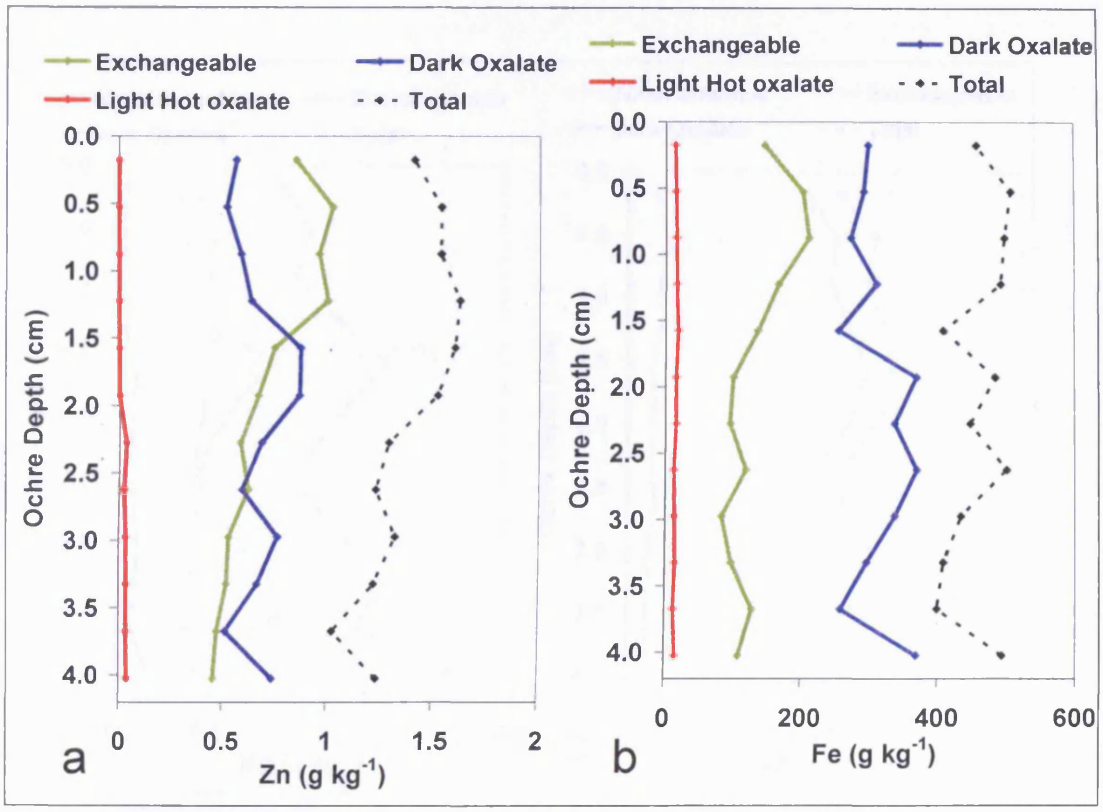

Figure 7-25: a) Zn sequential extraction and b) Fe sequential extraction

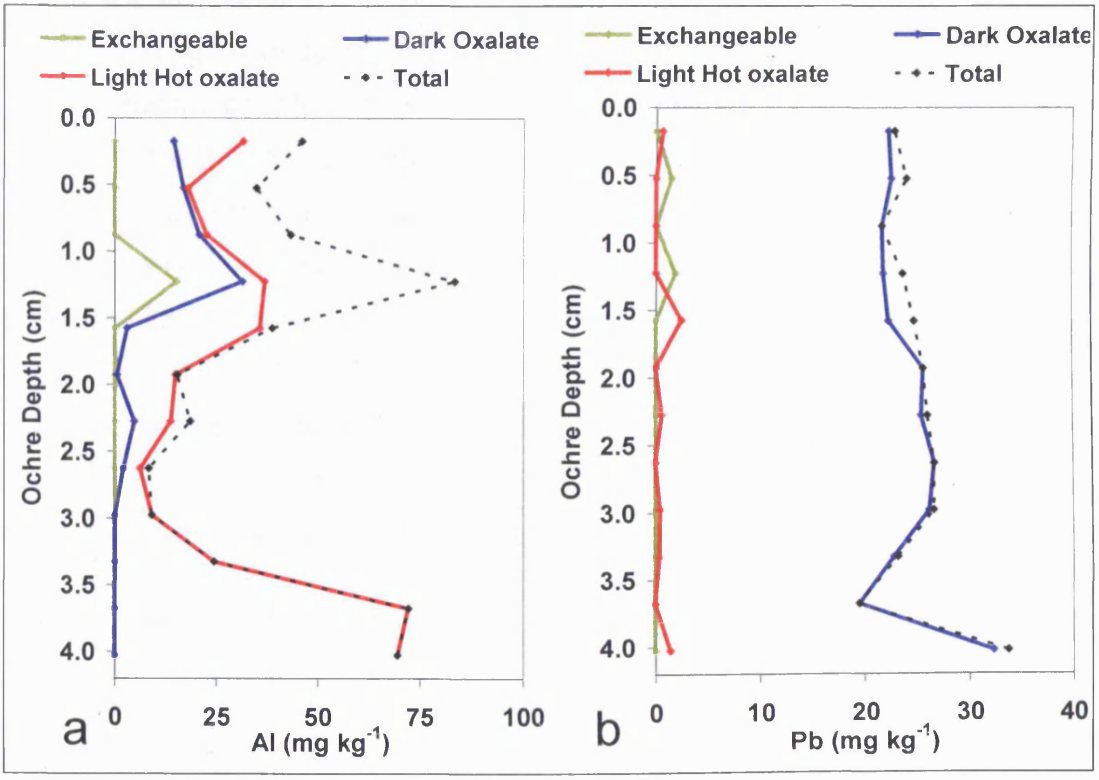

Figure 7-26: a) Al sequential extraction and b) Pb sequential extraction

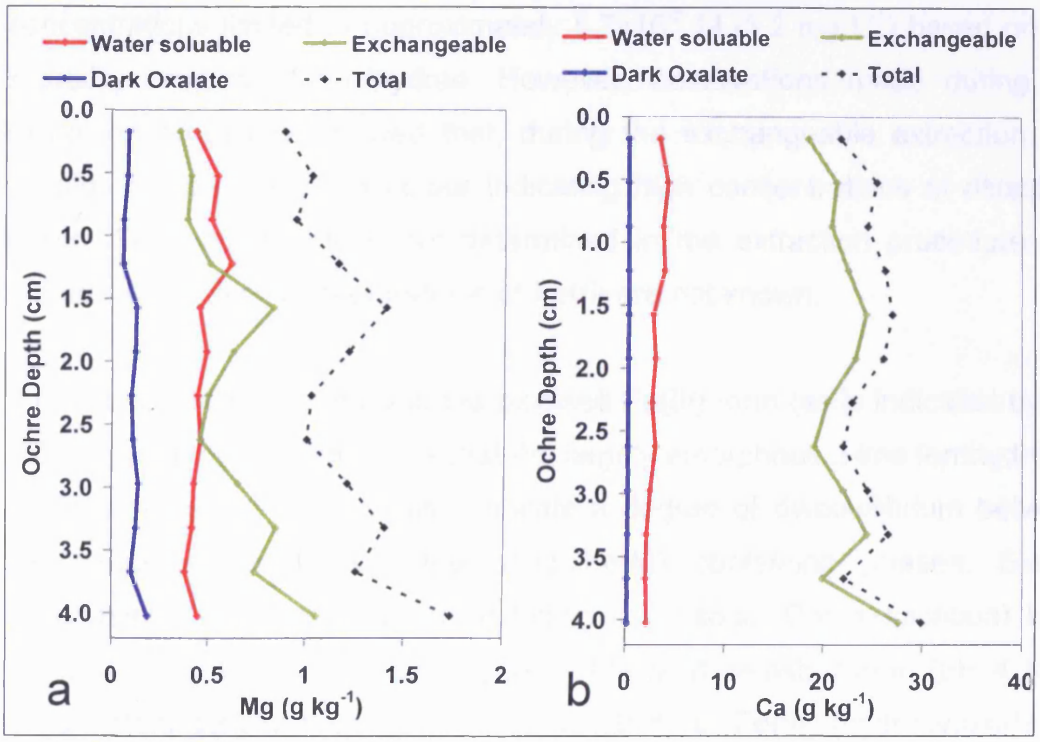

Figure 7-27: a) Mg sequential extraction and b) Ca sequential extraction

Finally Figure 7-27a and b show the variations in the concentrations of Mg and Ca in g kg^{-1} with depth. In each case the water soluble portion is shown in red, the exchangeable in green and the dark oxalate extraction in blue. The water soluble portion appears to show a slight decrease with depth while the dark oxalate fractions show little variation in both Mg and Ca. The Mg exchangeable fraction shows a variation typical of Mn association indicating a possible high adsorption affinity for hydrous Mn oxide. The Ca exchangeable fraction does not show a strong variation with depth however it should be indicated that the exchangeable leach used here is capable of dissolving $CaCO_3$ and therefore this is not conclusive to either Ca or Mg adsorbed to either ferrihydrite or hydrous Mn oxide mineral phases.

7.4.4 Exchangeable Fe(II)

The high portion of exchangeable Zn is expected as Zn adsorbs strongly to ferrihydrite with an adsorption edge at pH ~5 (Dzombak and Morel, 1990). The concentration of exchangeable Fe is unusually high. It would be reasonable to explain the high exchangeable Fe concentrations via desorption

of adsorbed Fe(II) as the solubility of Fe(III) at pH 4.5 is negligible, with concentrations limited to approximately $5.7x10^{-5}$ M (3.2 mg L^{-1}) based on the solubility product of ferrihydrite. However, observations made during the extraction procedure showed that, during the exchangeable extraction, the solution turned orange in colour indicating high concentrations of dissolved Fe(III). Fe speciation was not determined in the extraction procedure and therefore dissolved concentrations of Fe(II) are not known.

If the observed Fe is mostly in the oxidised Fe(III) form (as is indicated by the colour), then this demonstrates that the largely amorphous 2-line ferrihydrite is particularly fissile. It would also indicate a degree of disequilibrium between the dissolved Fe(III) and the solid Fe(III) containing phases. Similar observations (Colorado School Of Mines – Personal Communication) have found that Fe(III) precipitates only very slowly in weakly acidic (pH 4 to 5) mine-waters despite the apparent low solubility of Fe(III) (hydroxy)oxides at this pH. Therefore dissolution of ferrihydrite formed at circum-neutral pH (and therefore out of equilibrium at pH 4.5) will not result in the immediate precipitation of more stable phases (e.g. goethite). It is therefore expected that some disequilibrium due to kinetic restraints is responsible for the dissolution of 22 to 40 % of the total ochre Fe at pH 4.5.

7.5 Chapter 7 summary and conclusions

This chapter has presented the data for the characterisation of ochre collected from the Taff Merthyr settlement lagoons and VFR pilot plant in terms of its physical, mineralogical and geochemical properties. It is possible to draw the following conclusions:

- The lagoon ochre wet solids content is higher than that of the VFR ochre sludge, but it was found that both sludges had almost identical Fe contents due to differences in the Fe proportions in the dry ochre.
- The specific cake resistance of the 6mm VFR ochre is lower than that of single pass active treatment sludge and within the same order of

magnitude as that determined in the high density sludge active treatment process.

- Iron concentration normalised as ferrihydrite in the dry VFR ochre, makes up 80 % of the total whilst only making up 48 % of the lagoon ochre. This was accompanied by a higher dry density of the VFR ochre than the lagoon ochre.
- PhreeqC modelling has demonstrated that the Taff Merthyr mine-water is oversaturated with respect to the carbonate mineral phases aragonite, calcite and dolomite upon equilibration with atmospheric CO_2. In addition modelled atmospheric equilibration with respect to $CO_{2(g)}$ acts to increase pH and supersaturate calcium carbonate mineral phases.
- 40 % of the lagoonal ochre carbon content was not calcium related whilst 100 % of the VFR ochre carbon content was Ca related
- The VFR ochre has a specific surface area of 247 m^2 g^{-1} measured using N_2-BET method. This compares well with ochre surface areas determined in previous research.
- In cross section the VFR bed contained four distinct dark grey layers. Geochemical and mineralogical characterisation of these layers have shown them to contain elevated manganese concentrations and to have XRD peaks associated with barium manganese oxide hydrate and birnessite. It was also found that as well as Mn, the elements Tl, Ti, Cr, Co, Ni, Zn and Ba were also elevated within these layers.
- The bulk of the VFR ochre was found to be largely amorphous 2-line ferrihydrite under XRD. No conversion of the VFR ferrihydrite to goethite was detected. This is thought to be due to the inhibitory effect of Si and SO_4^{2-} ions in the mine-water.
- Conversion of ferrihydrite to goethite was evident in the lagoonal ochre. Suspected reducing conditions in the lagoonal ochre opens a possible pathway for the formation of goethite via bio-reduction of ferrihydrite to green rust followed by re-oxidation and re-crystallisation as goethite.
- The zeta potential of VFR ochre was found to be -8.5 mV at the pH of Taff Merthyr mine water (pH 6.9). In addition the IEP was found to be at pH 4. The low IEP in relationto PPZC is thought to be due to sulfate

adsorptionto the ferrihydrite surface. The low magnitude of the zeta potential is thought to be due to the prevalence of divalent counter ions. The low magnitude of zeta potential means particle aggregation is likely as is seen under electron and light microscope.

8 Pilot plant results

8.1 Introduction

The following chapter presents and describes the results obtained during the operation of the VFR pilot plant and settlement lagoons. Recorded data values are plotted against the time in days since the 4/5/05, the date sampling commenced. Data for the combined L1 and L2 lagoons were gathered from the first day. VFR monitoring did not commence until the 17/6/05 and therefore the first data gathered for the VFR is on day 44. The chapter is split into the following sections:

Section 8.2: Hydraulic characteristics – presents the recorded hydraulic data for flow and head difference.

Section 8.3: Fe removal – presents and discuses the recorded total, filtered and ferrous "Fe(II)" iron concentrations.

Section 8.4: Mn removal – presents and discuses the recorded total Mn concentrations.

Section 8.5: Temperature, pH, Eh, dissolved O_2, and alkalinity parameters – presenting and discussing the recorded electrochemical parameters.

Section 8.6: Metals concentrations – presents the data for the detectable non redox sensitive analytes in the Taff Merthyr mine water.

Section 8.7: VFR system longevity and performance – discusses the sizing requirements for a VFR system and determines the necessary de-slugging interval and system longevity. Bed depths and hydraulic conductivity are then discussed.

Section 8.8: Kinetic assessment of iron and manganese removal – discusses the removal of Fe and Mn within the lagoons and the VFR in terms of the chemical rates and mechanisms.

Section 8.9: Chapter summary and conclusions

8.2 Hydraulics

8.2.1 Flow rates

Figure 8-1 shows the lagoon flow rates in L sec^{-1} against the time in days since sampling started. Each data point is the calculated total volume pumped since the previous visit, divided by the time since the previous visit. Therefore flow rate is representative of the mean flow rate during this time period. Also shown is the cumulative through-put in m^3 determined directly from the pumping hours run.

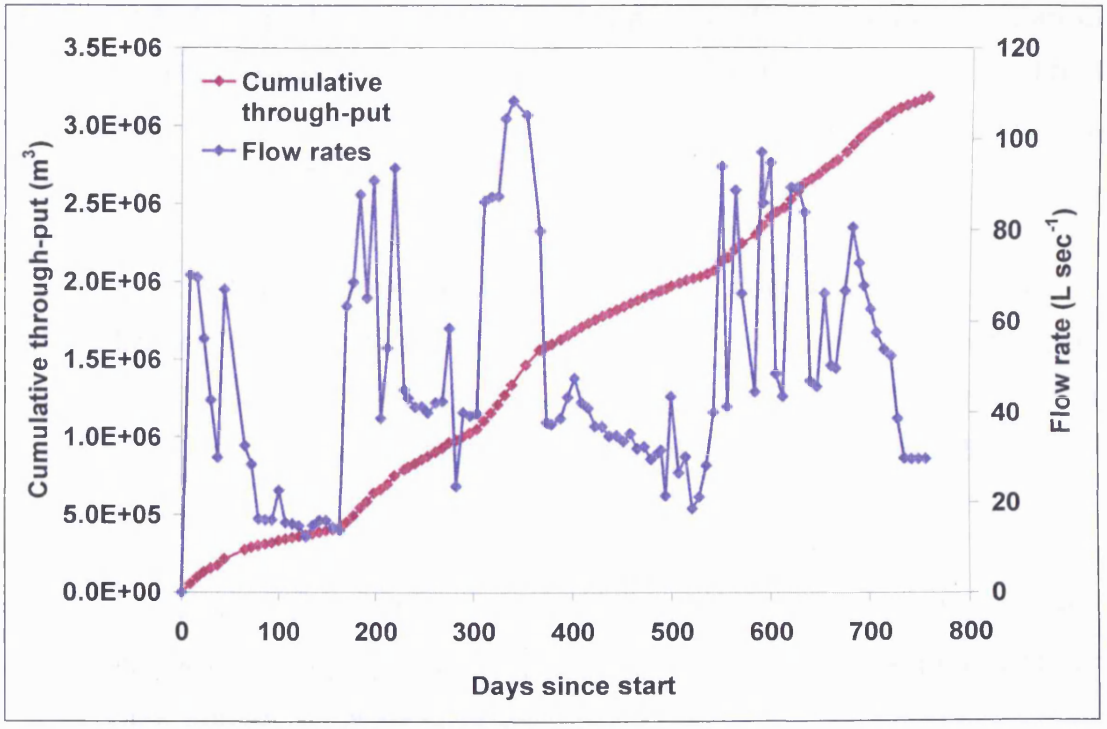

Figure 8-1: Flow rate and cumulative through-put for the combined L1 and L2 settlement lagoons

The data are characterised by periods of steady low "base" flow inter-dispersed by periods of much higher more variable "storm" flow. An eight fold

variation exists between the minimum flow of approximately 15 L sec^{-1} after 100 days to maximum mean weakly flow of over 108 L sec^{-1} at 338 days. The mean flow determined from all available data is 43.86 L sec^{-1} with a SD of 24.9 L sec^{-1} and a total yearly through-put of $1.39x10^6$ m^3. This equates to a mean HRT of 22.7 hours with a SD of 14.4 hours.

In the VFR system, inlet flows were partially controlled by adjustment of an in-line ball valve. However it was not possible to control the flow into the VFR accurately as flow was also dependant on the frequency of pumping into the distribution weir. Approximate adjustments were made and therefore measured values represent both anthropogenic and natural factors.

Figure 8-2 shows the averaged mine water flow rates in L sec^{-1} and cumulative through-puts in m^3 through the 20 mm VFR. Averaged flow rates were calculated by assuming a linear relationship between flow rates determined at the end of a sampling day and those determined at the start of the next sampling day. In each case, flow rates were determined by direct measurement at the outlet, or by correction of inlet flow rates using the calculated pump on/off ratio.

For the first 100 days it was attempted to fix the flow at approximately 1 L sec^{-1}. This was followed by a further period where the flow control valve was opened fully and flows of up to 3.27 L sec^{-1} were attained. This resulted in some bed scour. After this point flows were maintained between 0.5 and 1 L sec^{-1}.

Overall mean flow rates of 0.91 L sec^{-1} were attained with an SD 0.67 L sec^{-1} and a total yearly through-put of $2.44x10^4$ m^3. This equates to a mean HRT of 19.66 hours with an SD of 10.77 hours.

Figure 8-3 shows the averaged mine water flow rates in L sec^{-1} through the 6 mm VFR against the time in days since sampling started. Cumulative through-puts in m^3 are also shown. Initially, it was attempted to maintain the flow rate

at 1 L sec^{-1}, however, significant problems were encountered after 430 days due to ochre build up in the inlet pipe. This resulted in two periods where the flow into the VFR was minimal to zero between 450 and 500 days and at approximately 550 days.

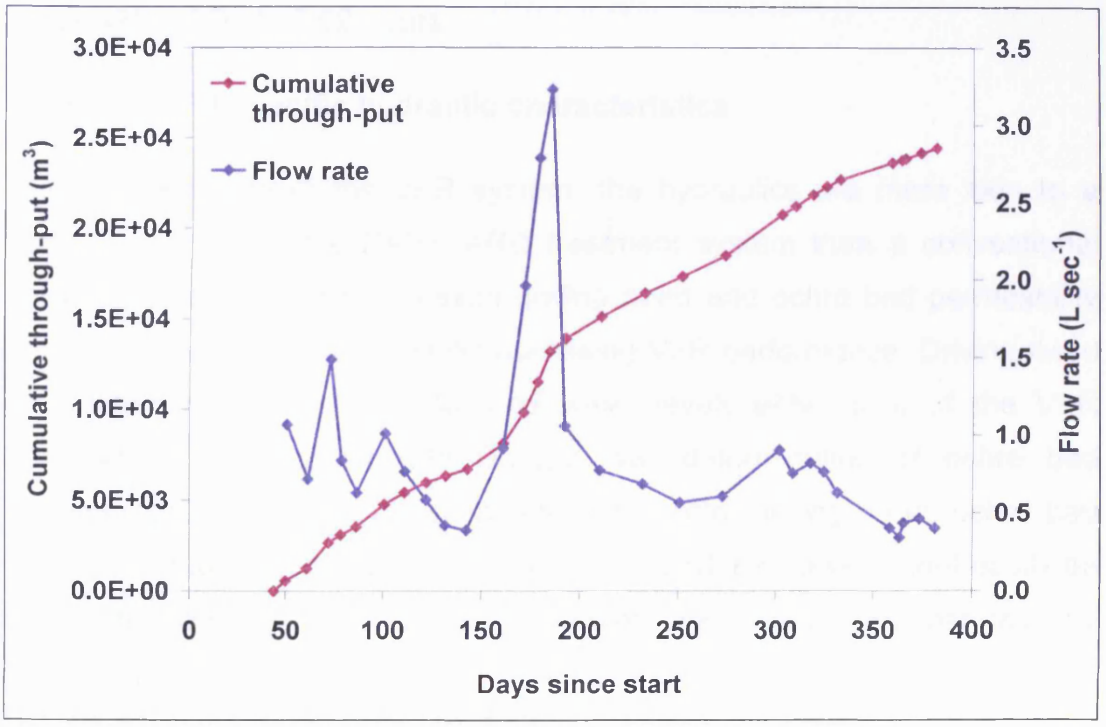

Figure 8-2: Flow rate and cumulative through-put for the 20 mm VFR

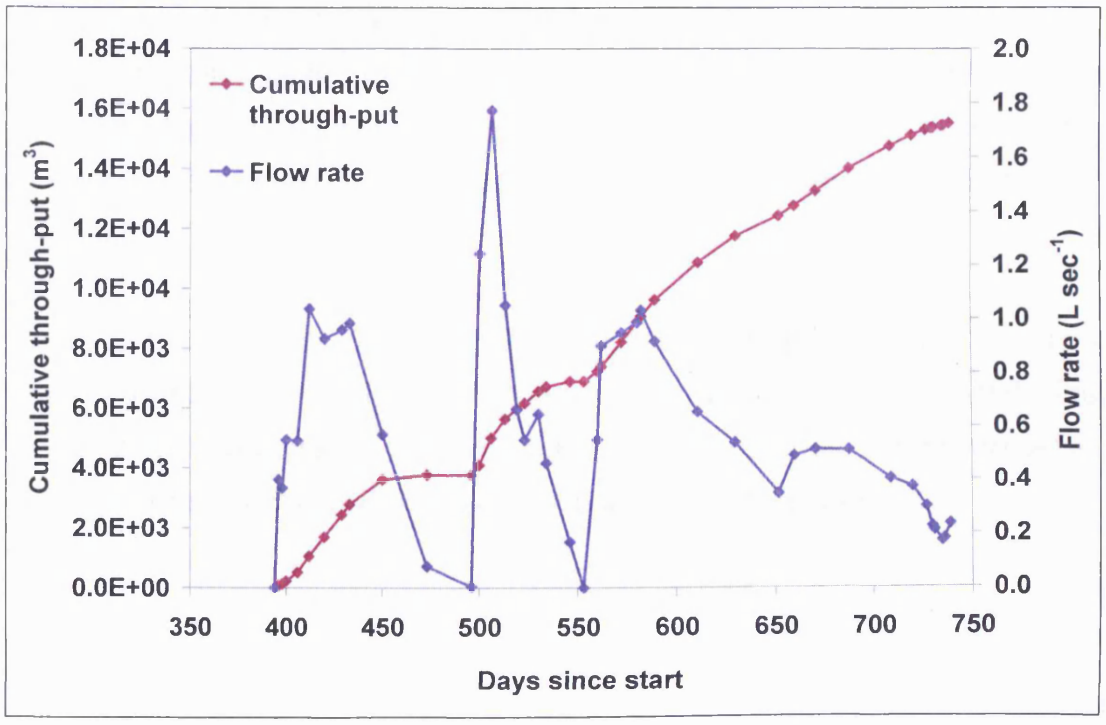

Figure 8-3: Flow rate and cumulative through-put for the 6 mm VFR

Due to problems with the pipe blocking, the maximum determined averaged flow rate was 1.8 L sec^{-1} and flow rates were highly variable. Overall mean flow rates of 0.57 L sec^{-1} were attained with a SD of 0.38 L sec^{-1} and total yearly through-put of $1.64x10^4$ m^3. This equates to a mean HRT of 26.17 hours with a SD of 16.62 hours.

8.2.2 VFR specific hydraulic characteristics

Due to the nature of the VFR system, the hydraulics are more akin to a vertical sand filter or a RAPS ARD treatment system than a conventional settlement lagoon. For this reason driving head and ochre bed permeability must be taken into account whilst assessing VFR performance. Driving head was determined from the measured water levels either side of the VFR bulkhead. In accordance with Darcy's law, determination of ochre bed permeability is reliant on the parameters flow rate, driving head, ochre bed surface area and ochre bed thickness. Ochre bed thickness cannot easily be determined directly and remains a master unknown in any permeability calculation.

An adaptation of Darcy's law to include cumulative ochre mass allowed for a relationship between ochre removal and permeability to be formulated. Also an approximation of the hydraulic conductivity was possible by determining the ochre depth from the cumulative ochre removal and solids concentration with ochre depth determined in Section 7.2. This will be discussed further in Section 8.7.

Figure 8-4 shows the recorded water levels in meters Below Tank Top (mBTT) in the 20 mm VFR against time in days since sampling started. The level in the up-flow chamber was controlled with weir boards and initially set at 0.18 mBTT to give a maximum HRT in the treatment chamber.

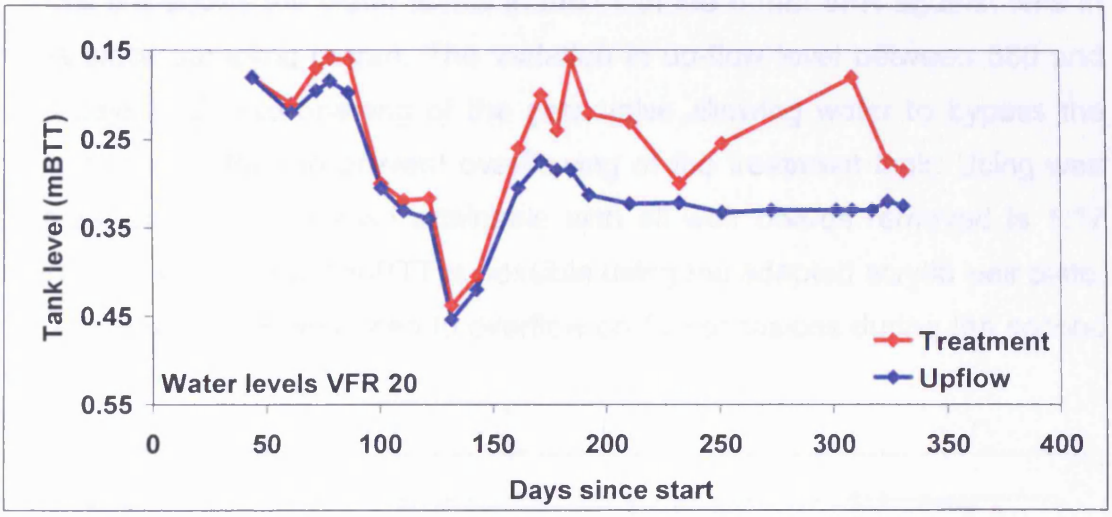

Figure 8-4: Water levels against time for the 20 mm VFR

Figure 8-5 compares hydraulic head difference (ΔH) in m and Bed Thickness Independent coefficient of permeability (BTI)[1] in sec^{-1} for the 20 mm VFR against time in days since sampling started. Both the ΔH and BTI values show a high variation which reflects the variable mine water flow rate. A maximum ΔH of 0.13 m and minimum BTI of $1.76x10^{-4}$ sec^{-1} was attained during operation of the 20 mm VFR.

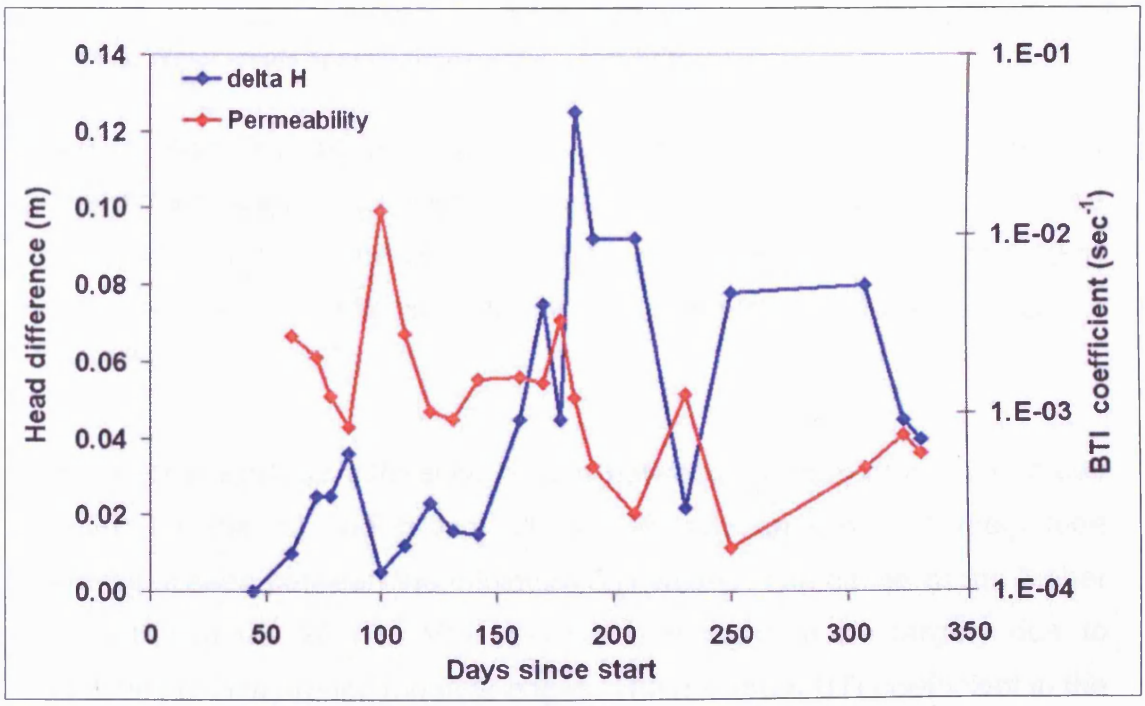

Figure 8-5: BTI coefficient of permeability and head difference for the 20 mm VFR

[1] see Section 5.2.4 for explanation of BTI permeability coefficient

Figure 8-6 shows the water levels in mBTT in the 6 mm VFR against time in days since sampling began. The variation in up-flow level between 580 and 660 days is due to opening of the gate valve allowing water to bypass the weir; this was done to prevent overflowing of the treatment tank. Using weir boards, the minimum level attainable with all weir boards removed is 1.17 mBTT. However, only 1 mBTT is possible using the adapted acrylic weir plate. The treatment tank was seen to overflow on five occasions during the second year.

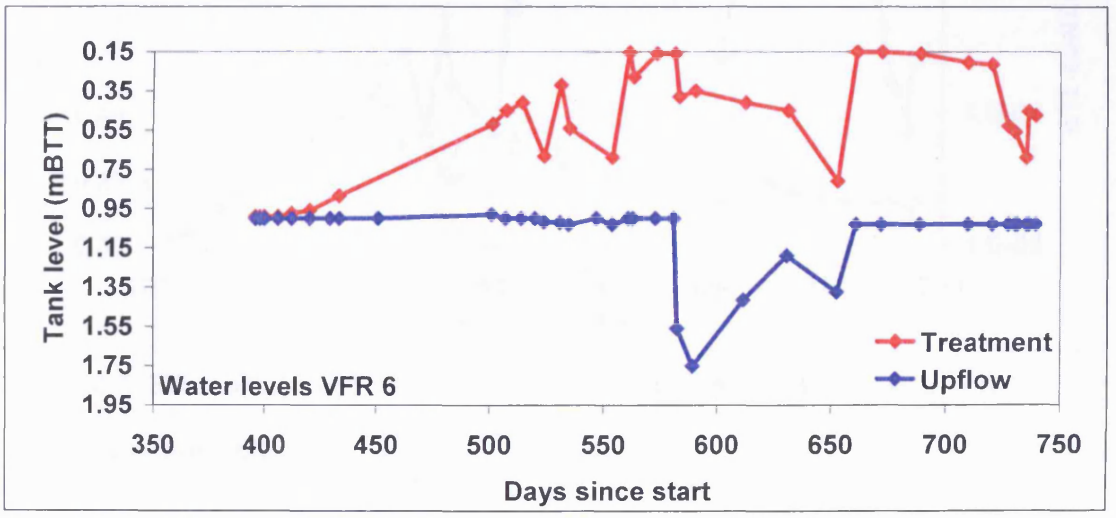

Figure 8-6: Water levels against time for the 6 mm VFR

Figure 8-7 compare values of ΔH in m and BTI in sec^{-1} for the 6 mm VFR against time in days since sampling began. ΔH values show high variance reflecting the variable mine water flow rate. A maximum ΔH value of 1.40 m was reached. The BTI shows a steady decrease with time to a minimum of 1.77×10^{-5} sec^{-1}.

An order of magnitude difference occurs between the maximum ΔH values recorded for the 20 and 6 mm VFRs. Similarly an order of magnitude difference is seen between the minimum BTI values. The cause of the higher permeability in the 20 mm VFR system is thought to be largely due to shortcutting of flow around the tank edges. The minimum BTI coefficient in the 20 mm VFR reflects the throttling effect of the short circuiting routes rather than the true bed permeability. Short circuiting was largely eliminated in the 6

mm VFR bed by emplacement of a sand fillet around the tank edges. In this case the BTI should be representative of the actual ochre bed BTI.

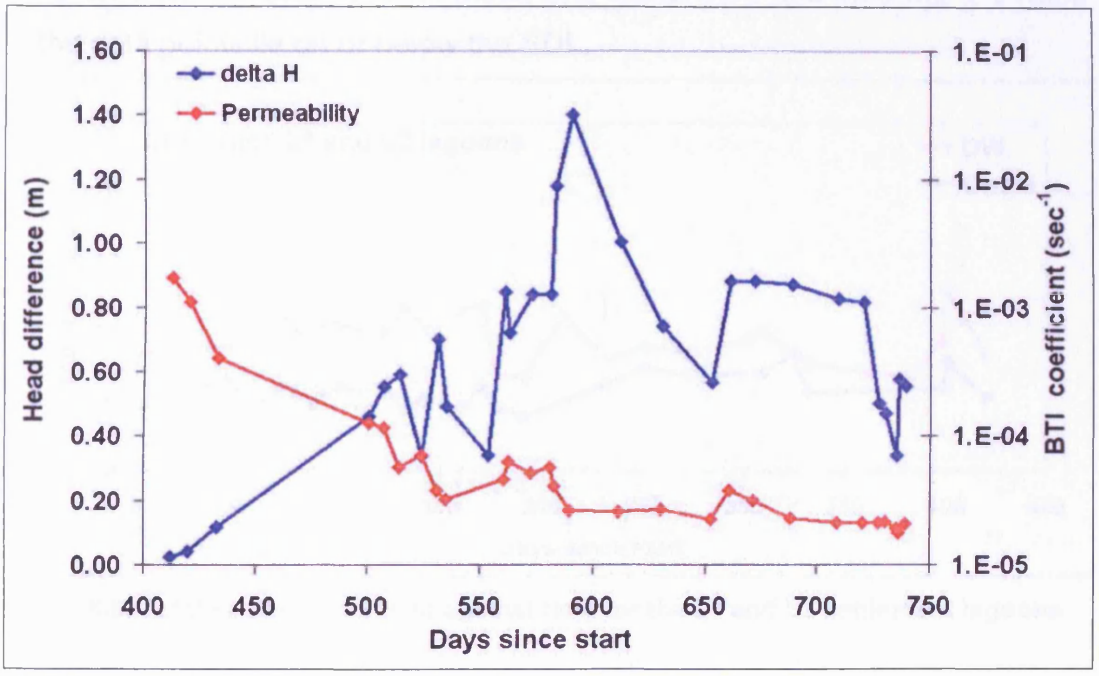

Figure 8-7: BTI coefficient of permeability and head difference in the 6 mm VFR

8.3 Iron removal

Recorded values for inlet and outlet mine water, total, filtered and ferrous (Fe(II)) Fe, for the lagoons, 20 mm VFR and 6 mm VFR are presented. In each case individual data points are marked with solid diamonds and are connected with lines purely to aid interpretation and are not intended as an indication of the values of missing data. The horizontal red dashed lines show the Taff Merthyr consent Specified Discharge Limit (SDL) for total Fe of 1 mg L^{-1}.

8.3.1 Total iron

Figure 8-8 shows the concentrations of total Fe in mg L^{-1} against time in days since sampling began. Values were recorded at the inlet distribution weir (DW) and outlet from the combined L1 and L2 settlement lagoons. The DW data shows a drop in total Fe at 177 days with mean values decreasing from 10.2 mg L^{-1} with an SD of 1.0 mg L^{-1} before 177 days to 9.0 mg L^{-1} with a SD of 1.85 mg L^{-1} after 177 days, a mean decrease of 1.2 mg L^{-1}. Variation in the

inlet concentrations is highest in the data after 177 days with minimum and maximum values of 6.6 and 13.0 mg L^{-1}. Outlet total Fe concentrations are fairly consistent with an overall mean and SD of 5.81 and 1.09 mg L^{-1}. None of the data points lie on or below the SDL.

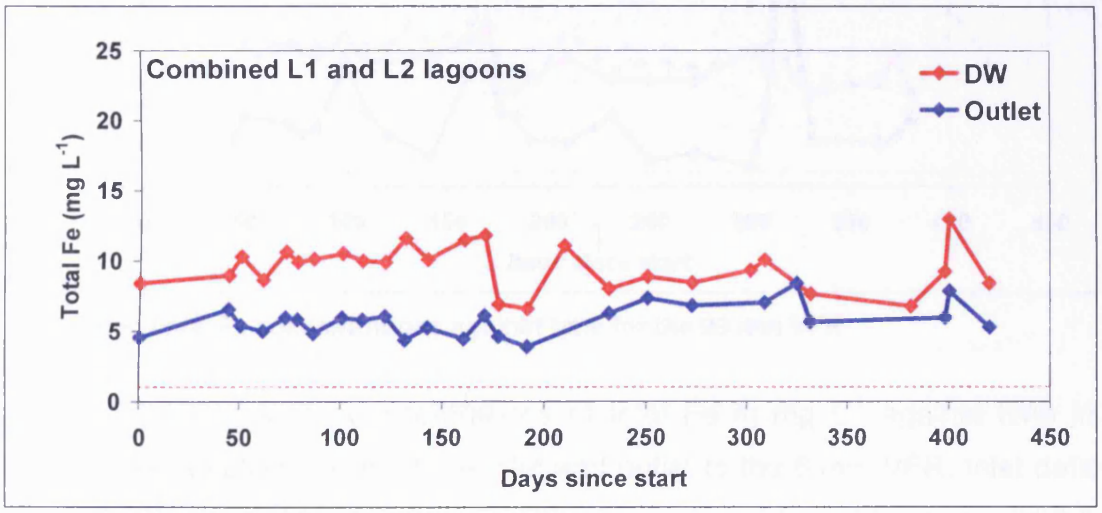

Figure 8-8: Total Fe concentrations against time for the L1 and L2 settlement lagoons

Figure 8-9 shows the concentrations of total Fe in mg L^{-1} against time in days since sampling began. Samples were taken at the inlet and outlet to the 20 mm VFR and data from the DW is included for comparison. As with the DW, a step down in Fe concentrations at 177 days is observed. Mean and SD values before and after 177 days were determined as 9.9 mg L^{-1} with an SD of 0.8 mg L^{-1} before 177 days and 7.8 mg L^{-1} with a SD of 3.74 mg L^{-1} after 177 days. This equates to a mean decrease of 2.1 mg L^{-1}. A peak value 18.63 mg L^{-1} is observed at 317 days data.

Mean and SD values were determined for the whole data set with the 317 days data point omitted. Mean concentrations of 9.22 and 4.27 mg L^{-1} were determined for the inlet and outlet total Fe concentrations respectively and correspond to SD values of 2.94 and 3.32 mg L^{-1}. None of the outlet values were at or below the SDL.

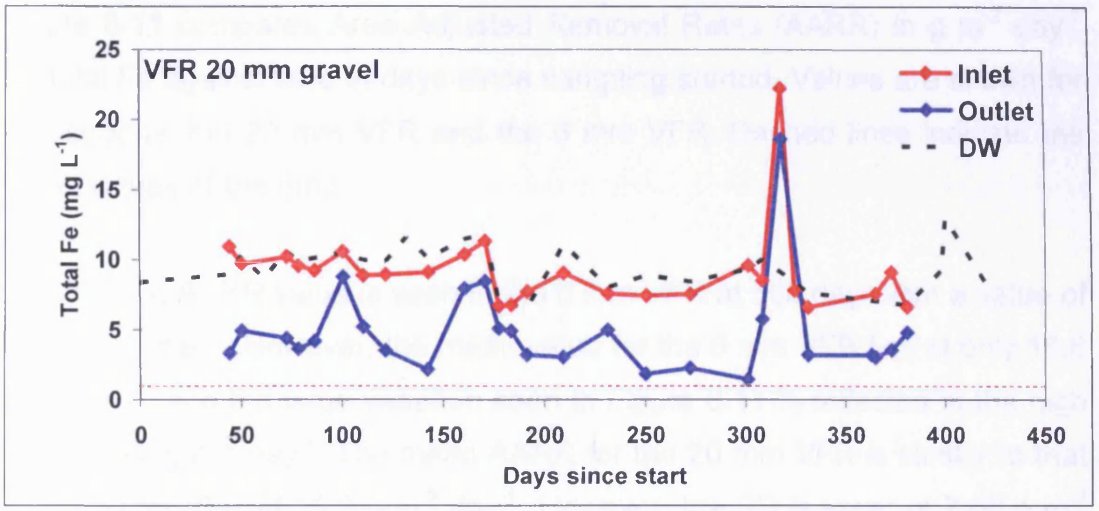

Figure 8-9: Total Fe concentrations against time for the 20 mm VFR

Figure 8-10 shows the concentrations of total Fe in mg L^{-1} against time in days since sampling began at the inlet and outlet to the 6 mm VFR. Inlet data determined prior to 500 days shows little variance and is stable at around 8.5 mg L^{-1}. Between 500 and 570 days, a concave trend is observed with a steady decrease from 8.5 to 5.1 mg L^{-1} followed by a gradual increase to 7.2 mg L^{-1}after 660 days. A peak value of 13.62 mg L^{-1} is seen at 660 days. The peak is not observed in the outlet data indicating that the load has been largely removed. A mean inlet concentration of 7.24 mg L^{-1} is calculated with an SD of 1.74 mg L^{-1}. 75.8 % of the outlet data points lie at or below the SDL which equates to a mean and SD of 0.7 and 1.0 mg L^{-1}.

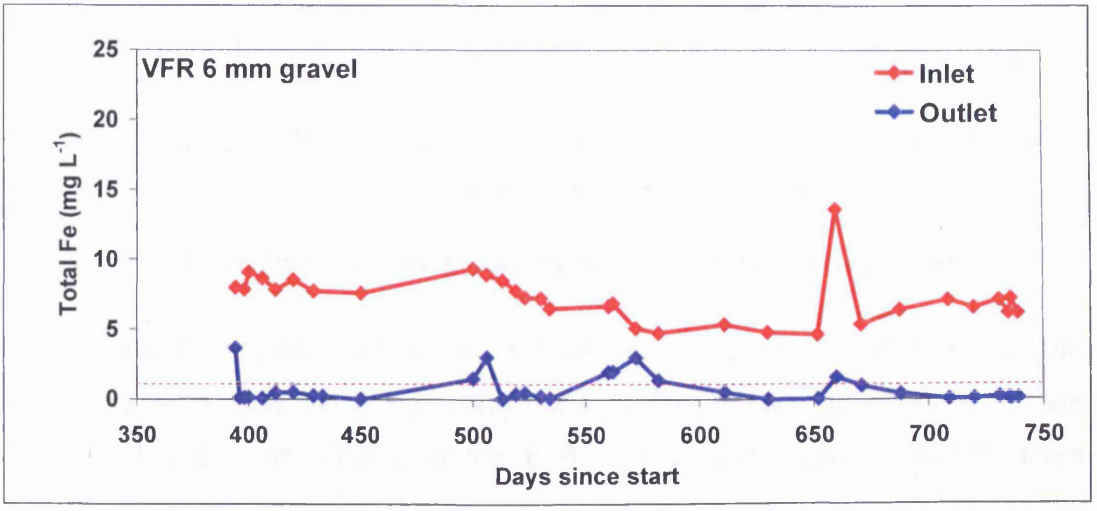

Figure 8-10: Total Fe concentrations against time for the 6 mm VFR

Figure 8-11 compares Area Adjusted Removal Rates (AARR) in g m^{-2} day^{-1} for total Fe against time in days since sampling started. Values are shown for the lagoons, the 20 mm VFR and the 6 mm VFR. Dashed lines indicate the mean values of the data.

The highest AARR value is seen in the 6 mm VFR at 500 days with a value of 69.1 g m^{-2} day^{-1}. However, the mean value for the 6 mm VFR lies at only 16.6 g m^{-2} day^{-1} and the large variation seen in Figure 8-11 is reflected in the high SD of 13.0 g m^{-2} day^{-1}. The mean AARR for the 20 mm VFR is similar to that of the 6 mm VFR at 15.6 g m^{-2} day^{-1}. However, the SD is lower at 7.68 g m^{-2} day^{-1} reflecting the lower variability of the data. The AARR value for the combined lagoons is roughly 1/3 of the VFR at 4.6 g m^{-2} day^{-1} and shows a lower variance with a SD of 2.6 g m^{-2} day^{-1}.

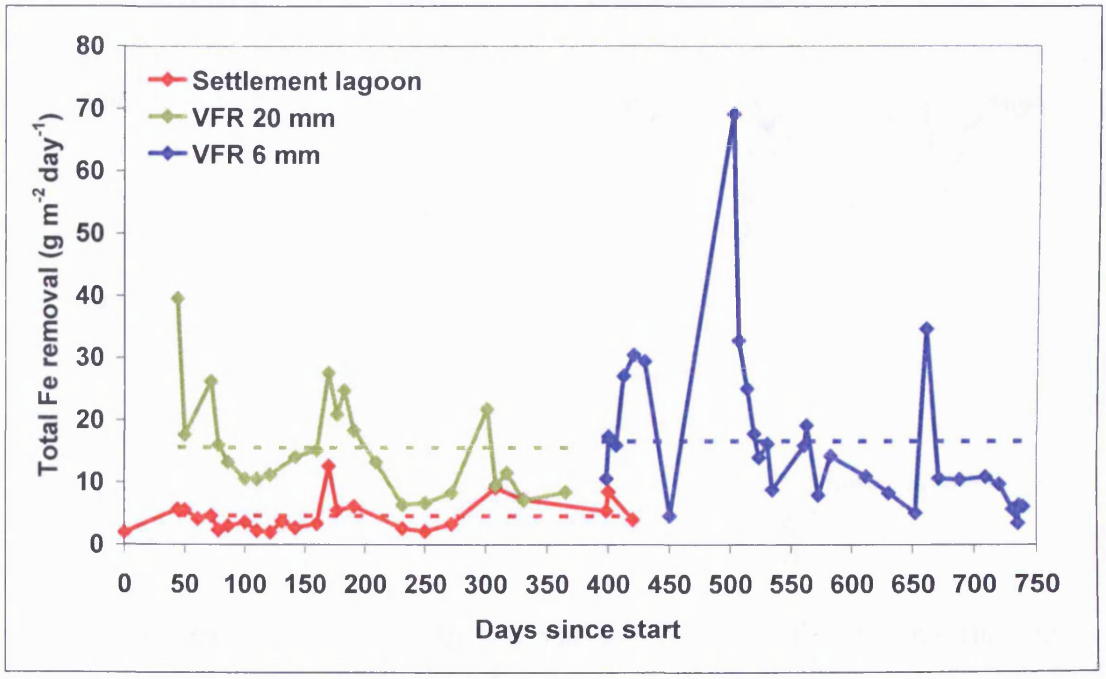

Figure 8-11: Total Fe area adjusted removal rates for the settlement lagoon and VFR

Figure 8-12 compares the total Fe removal as a % of the initial total Fe load against time in days since sampling started. The values determined for the lagoons, the 20 mm VFR and the 6 mm VFR are shown. Dashed lines indicate the mean values of the data.

The % removal of total Fe is highest in the 6 mm VFR followed by the lagoons, with mean values of 96 and 93 % respectively. % oxidation is lower in the 20 mm VFR at only 75 %, and with an SD of 18.9 %. The 6 mm VFR and the lagoons show a more consistent removal with SD values of 6.4 and 8.2 % respectively.

Figure 8-13 shows the % of total Fe removed against the calculated nominal HRT. Results for the settlement lagoons, 20 mm VFR and 6 mm VFR are shown for comparison. The 6 mm VFR gives the best overall performance and, above 30 hours HRT, greater than 95 % of the total Fe load is consistently removed. At high HRT most of the Fe(II) load will be homogeneously oxidised above the bed and the Fe load will be predominantly in the form of particulate Fe(III) (hydroxy)oxides. In this case the removal efficiency is a reflection of the ochre bed's filtration characteristics.

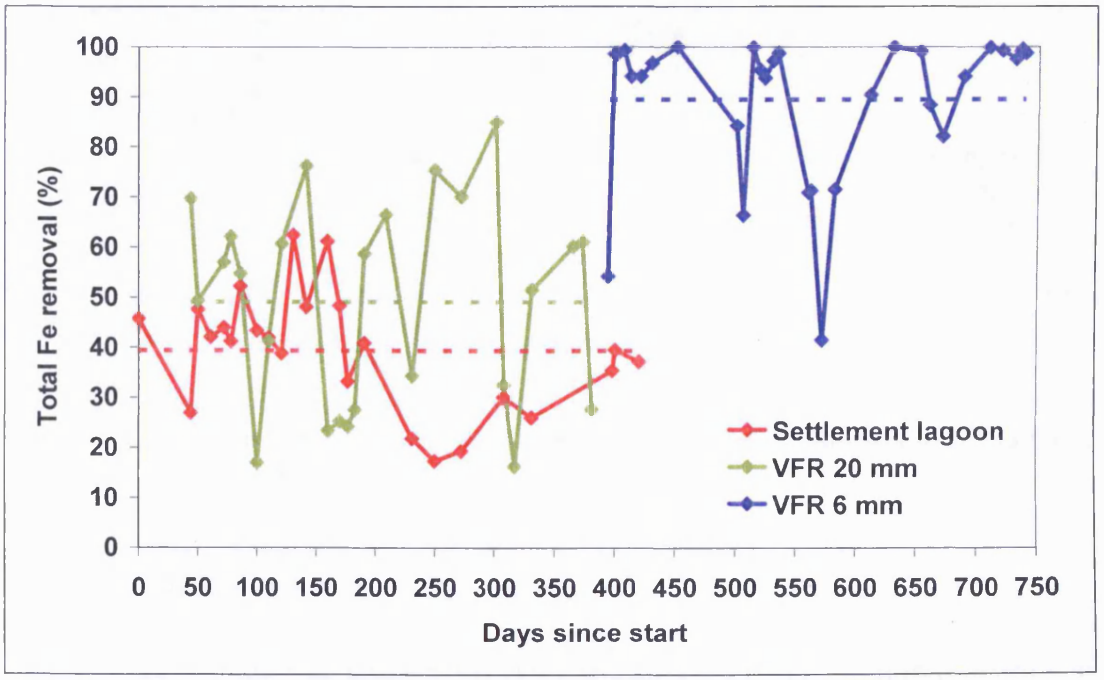

Figure 8-12: Percentage of initial total Fe removed in the settlement lagoon and VFR

Maximum removal efficiencies of 80 % are seen in the 20 mm VFR at HRT greater than 30 hours which is significantly lower than the 6 mm VFR. This is thought to be due to incomplete filtration of particulate Fe due to shortcutting

around the tank edges. This is supported by the high BTI and the low head difference observed in the 20 mm VFR (see Section 8.2.2).

The lagoons show the lowest total Fe removal performance. This is due to the reliance on gravity separation of the suspension of ochre particulates rather than physical separation via filtration as in the VFR. The lower Fe removal performance at HRT less than 30 hours in the 6 mm VFR is due to either transport of dissolved Fe(II) through the bed and or due to scouring of particulate ochre from the base of the bed.

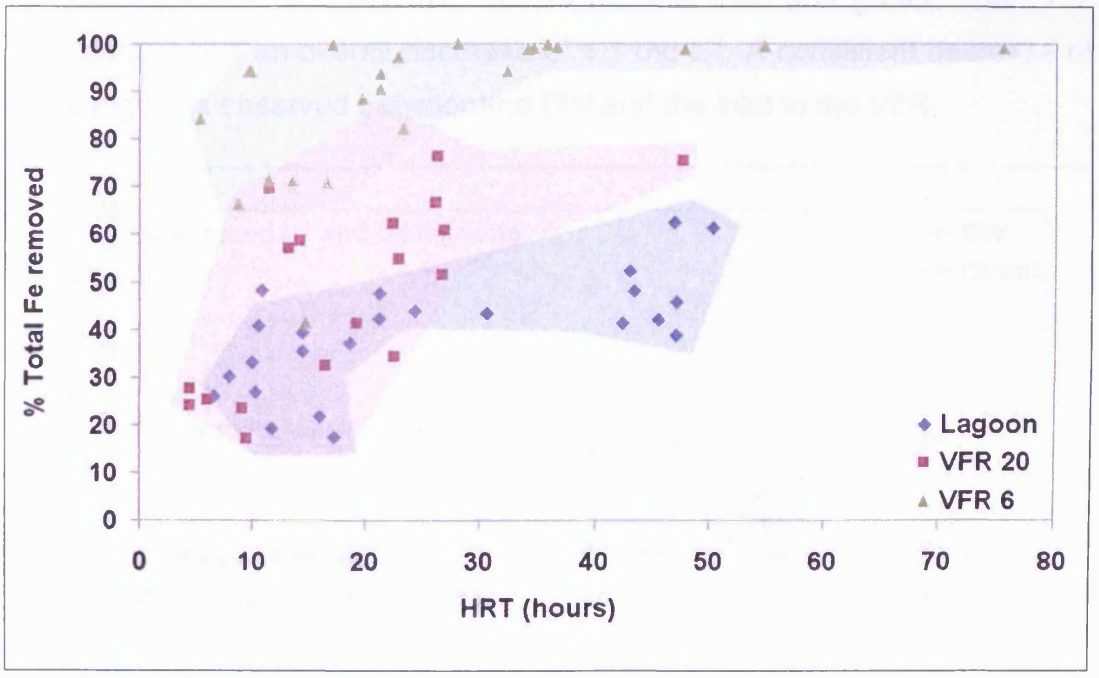

Figure 8-13: Comparison between nominal HRT and % total Fe removal in the lagoon, 20mm VFR and 6 mm VFR

8.3.2 Dissolved iron

Figure 8-14 shows the filtered Fe concentrations in mg L^{-1} against time in days since sampling began. Concentrations were determined at the Distribution Weir (DW) and outlet to the combined L1 and L2 settlement lagoons. The red dashed line indicates the Standard Discharge Limit (SDL) of 1 mg L^{-1}. A decrease in measured concentrations is observed between 170 and 177 days in DW data. Mean and SD values of 9.6 and 0.4 mg L^{-1} were determined for less than 177 days data, whilst values of 8.0 and 1.08 mg L^{-1}

were determined for greater than 177 days data, a difference of 1.6 mg L-1. Outlet filtered Fe is consistently low with 85 % of data points at or below the SDL.

Figure 8-15 shows the filtered Fe concentrations in mg L^{-1} against time in days since sampling began for the 20mm VFR. Concentrations were determined at the inlet and outlet. Concentration determined at the DW is included for comparison and the red dashed line indicates the SDL of 1 mg L^{-1}. The Inlet data show the familiar step down at 177 days as seen in the DW data. Comparison of mean inlet values for less than and greater than 177 days data shows an overall decrease of 1.1 mg L^{-1}. A consistent decrease of 1 to 2 mg L^{-1} is observed between the DW and the inlet to the VFR.

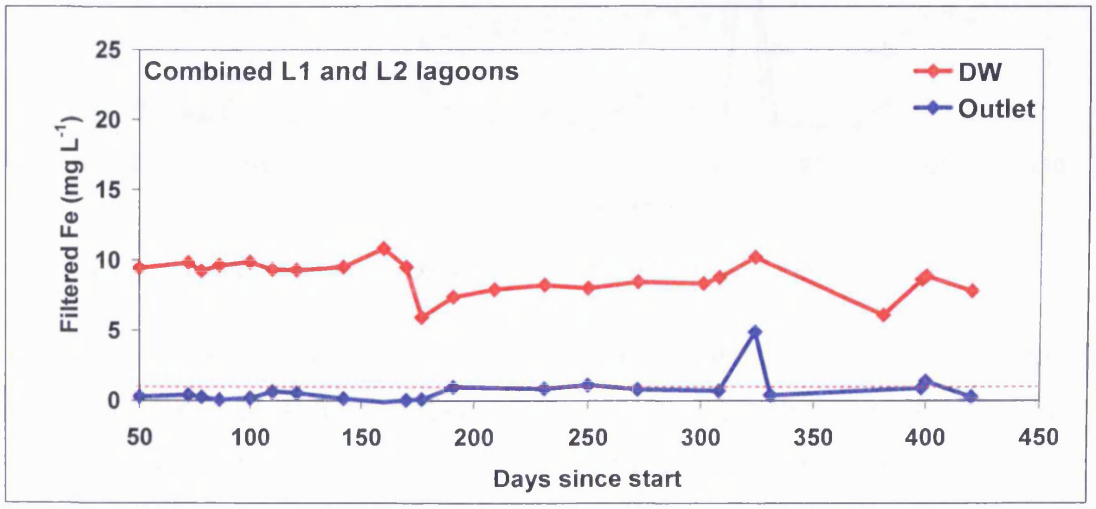

Figure 8-14: Filtered Fe concentrations against time for the L1 and L2 settlement lagoons

A peak is observed in the 20 mm VFR data on day 317, with inlet and outlet values of 21.5 and 16.2 mg L^{-1} respectively. These data points are absent in the lagoon data as samples were not taken on this date. Outlet data are inconsistent with mean and SD values of 2.2 and 3.2 mg L^{-1} respectively. Only 41.7 % of outlet data points lie at or below the SDL.

Figure 8-16 shows the filtered Fe concentrations in mg L^{-1} against time in days since sampling began for the 6mm VFR. The red dashed line indicates the SDL of 1 mg L^{-1}. Inlet concentrations of filtered Fe are lower for the 6 mm

VFR than for the 20 mm VFR, with mean and SD values of 6.3 and 1.3 mg L^{-1} respectively. A concave trend is evident in the inlet data with a minimum value of 3.8 mg L^{-1} occurring at 582 days. Values increase before and after this point with highs of 8.47 mg L^{-1} at 500 days and 7.23 mg L^{-1} at 739 days. Outlet data have a low mean and SD values of 0.3 and 0.5 mg L^{-1} and reflect the observed consistency of the data. 92 % of the data points are at or below the SDL.

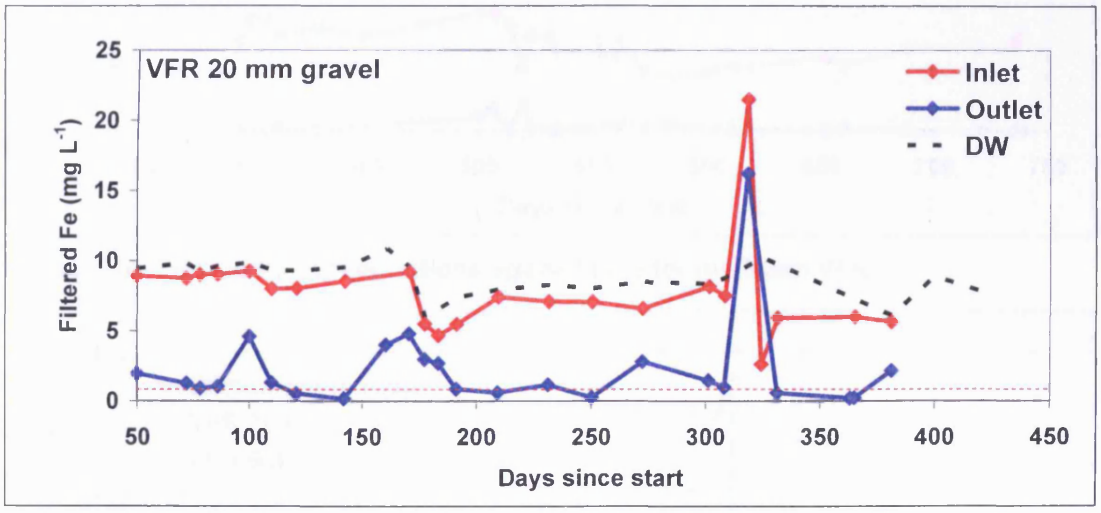

Figure 8-15: Filtered Fe concentrations against time for the 20 mm VFR

Figure 8-17 compares Area Adjusted Removal Rates (AARR) in g m^{-2} day^{-1} for filtered Fe against time in days since sampling started. Values are shown for the lagoons, the 20 mm VFR and the 6 mm VFR. Dashed lines indicate the mean values of the data.

The highest AARR value is seen in the 6 mm VFR at 500 days with a value of 66.4 g m^{-2} day^{-1} consistent with the observations for Fe(II). It can be seen that the highest mean AARR is associated with the 20 mm VFR with a mean AARR of 20 g m^{-2} day^{-1}. Mean AARR values for the 6 mm VFR and the lagoons are 16.8 and 10.9 g m^{-2} day^{-1}. Large variations in the data are seen for both VFR data sets with correspondingly high SD values of 8.7 and 12.9 g m^{-2} day^{-1} for the 20 and 6 mm VFRs respectively.

Figure 8-18 compares the total Fe removal as a % of the initial total Fe load against time in days since sampling started. The values determined for the

lagoons, the 20 mm VFR and the 6 mm VFR are shown. Dashed lines indicate the mean values of the data.

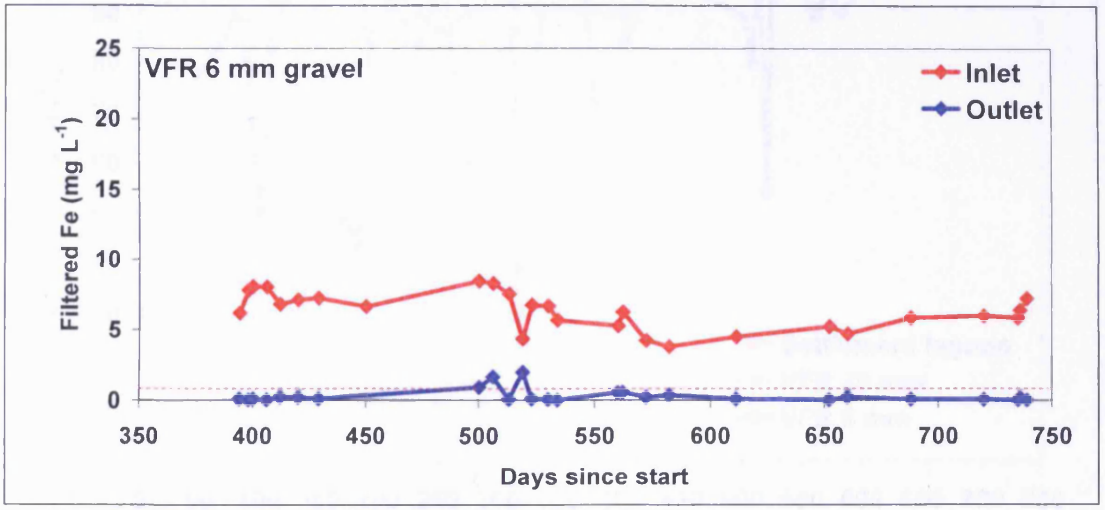

Figure 8-16: Filtered Fe concentrations against time for the 6 mm VFR

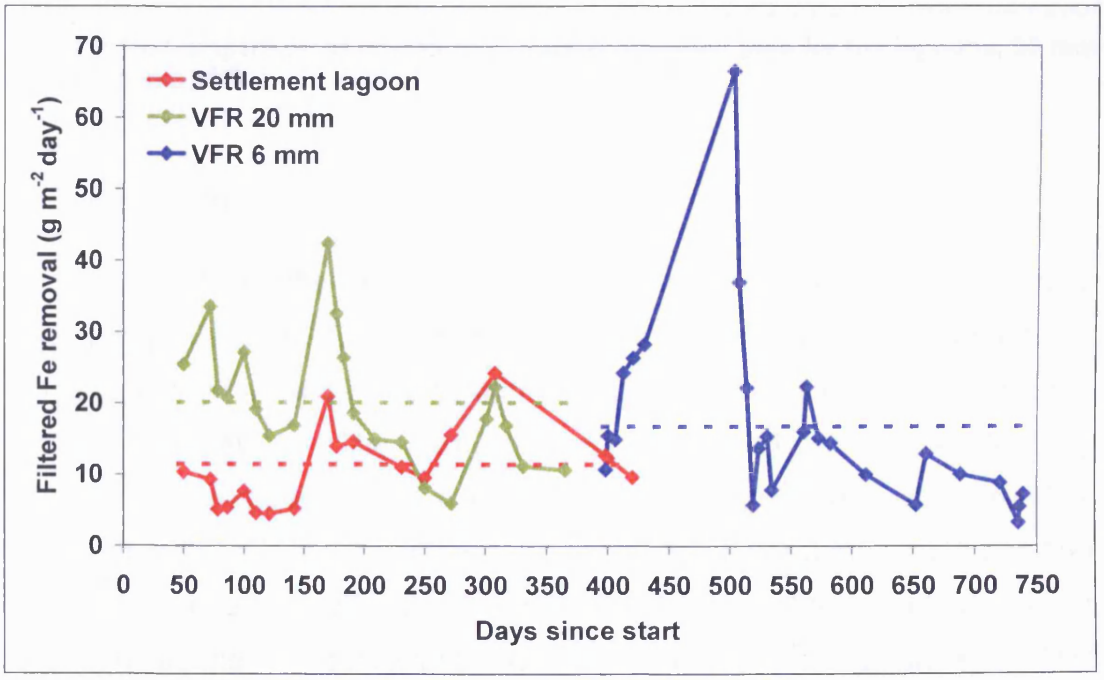

Figure 8-17: Comparison of filtered Fe area adjusted removal rates for the lagoons, 20mm VFR and 6 mm VFR

Percentage removal of filtered Fe is highest in the 6 mm VFR and the lagoons, with mean values of 94.7 and 93.6 % respectively. Percentage oxidation is lower in the 20 mm VFR at only 75.3 % and also shows the highest variance with mean and SD values of 20.7 % (as compared to 9.3 and 4.7 % for the 20 mm VFR and lagoons respectively).

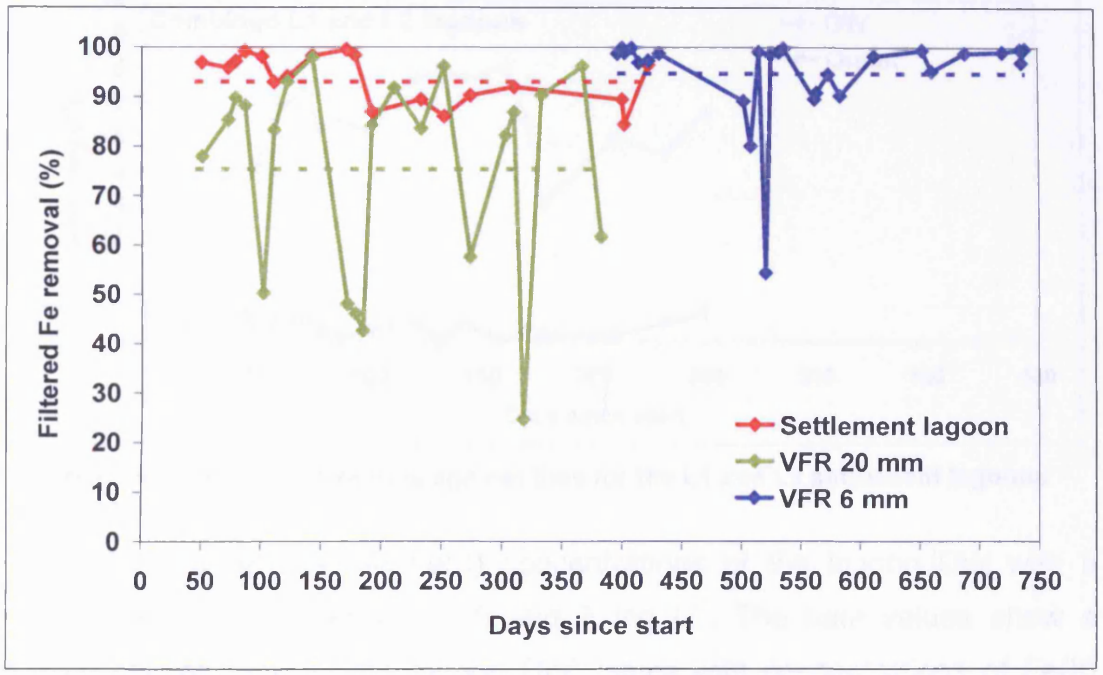

Figure 8-18: Comparison of filtered Fe % removal against time for the lagoons, 20 mm VFR and 6 mm VFR

8.3.3 Fe(II)

Figure 8-19 shows the Fe(II) concentrations in mg L^{-1} against time in days since sampling began. Concentrations were determined at the DW and outlet to the combined L1 and L2 settlement lagoons. The red dashed line indicates the SDL of 1 mg L^{-1}. The Fe(II) concentrations recorded at the DW vary between a maximum of 8 and a minimum of 4 mg L^{-1}. A convex trend is observed, with Fe(II) concentrations increasing from 4 to 8 mg L^{-1} prior to 150 days, then decreasing after this point. Fe(II) recorded at the combined outlet from the lagoons is consistently less than 1 mg L^{-1} regardless of DW concentrations with a mean and SD of 0.39 mg L^{-1} and 0.29 respectively. All of the data points are at or below the SDL.

Figure 8-20 shows the Fe(II) concentrations in mg L^{-1} against time in days since sampling began for the 20 mm VFR. Concentration determined at the DW is included for comparison and the red dashed line indicates the SDL of 1 mg L^{-1}.

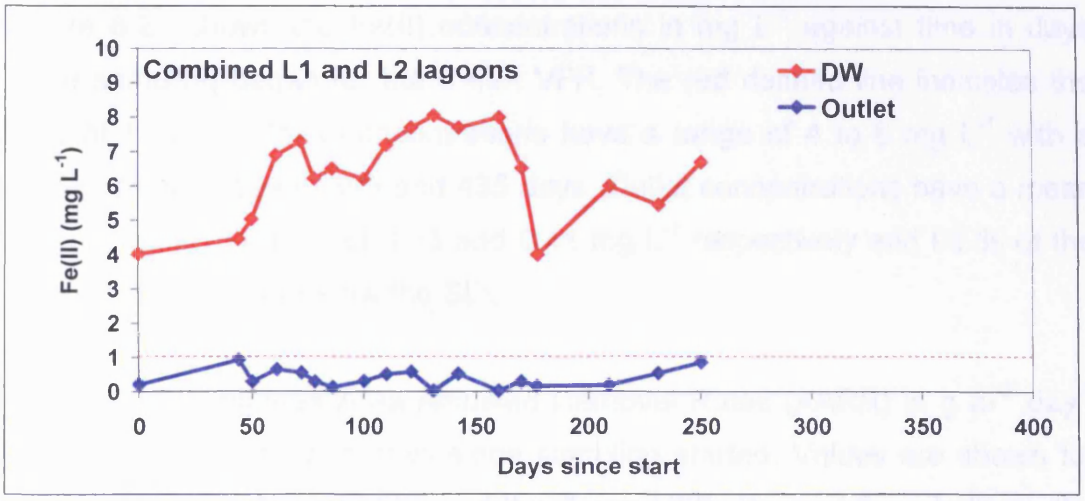

Figure 8-19: Fe(II) concentrations against time for the L1 and L2 settlement lagoons

The inlet flow reflects the Fe(II) concentrations of the lagoon DW with a concentration range between 7.5 and 3 mg L^{-1}. The data values show a similar convex trend to the lagoon DW values with concentrations of Fe(II) showing an overall increase between 60 and 130 days. This is followed by an overall decrease after this point. Some oxidation of Fe(II) in the inlet feed pipe is evident with DW Fe(II) often being higher than the VFR 20 inlet concentrations. Sparse data between 250 and 370 days does not allow interpretation. The final data point is at 4 mg L^{-1}, this is at the low end of the concentration range. Outlet Fe(II) concentrations have mean and SD values of 1.34 and 0.23 mg L^{-1} respectively with 65 % of the data points are at or below the SDL.

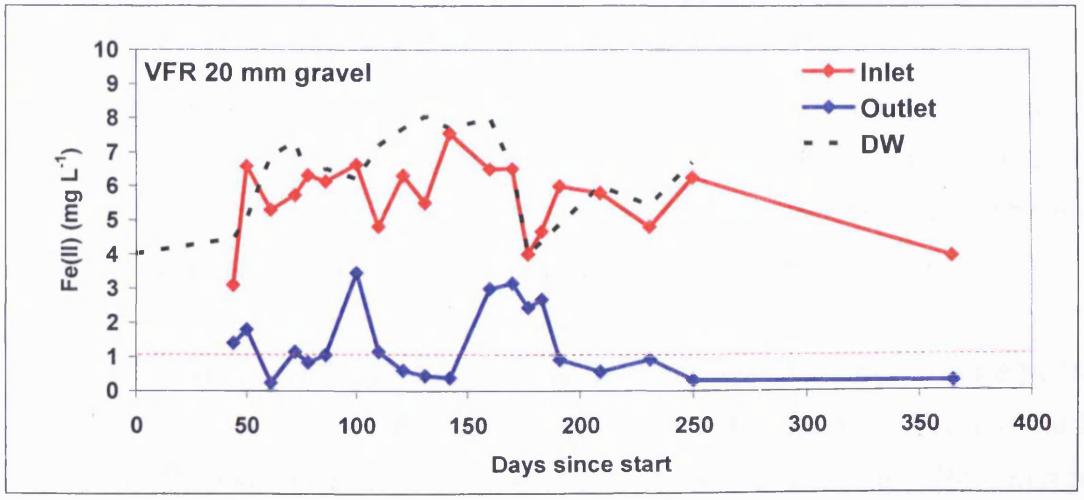

Figure 8-20: Fe(II) concentrations against time for the 20 mm VFR

Figure 8-21 shows the Fe(II) concentrations in mg L^{-1} against time in days since sampling began for the 6 mm VFR. The red dashed line indicates the SDL of 1 mg L^{-1}. Inlet concentrations have a range of 4 to 8 mg L^{-1} with a convex trend between 395 and 435 days. Outlet concentrations have a mean and standard deviation of 0.23 and 0.41 mg L^{-1} respectively and 93 % of the data points are at or below the SDL.

Figure 8-22 compares Area Adjusted Removal Rates (AARR) in g m^{-2} day^{-1} for Fe(II) against time in days since sampling started. Values are shown for the lagoons, the 20 mm VFR and the 6 mm VFR. Dashed lines indicate the mean values of the data.

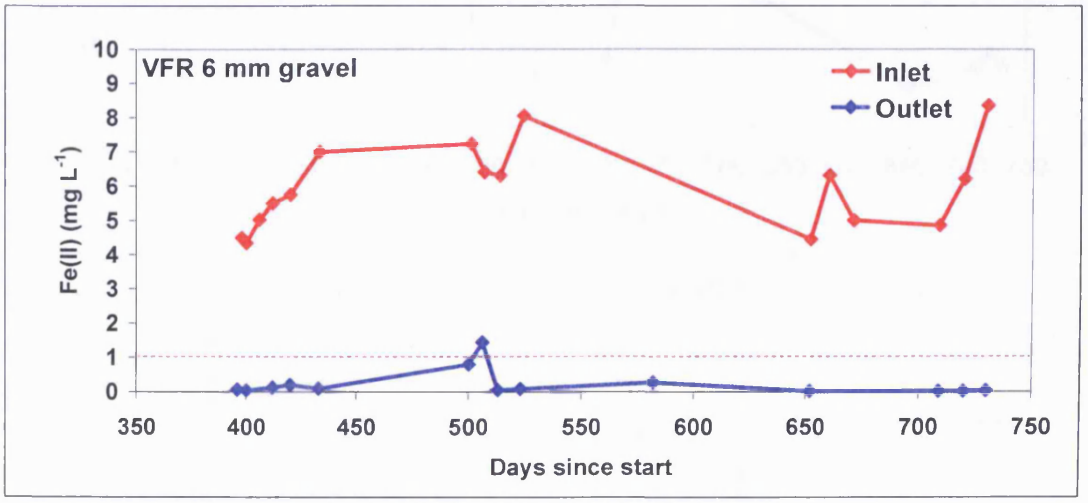

Figure 8-21: Fe(II) concentration against time for the 6 mm VFR

The highest AARR value is seen in the 6 mm VFR at 500 days with a value of 56 g m^{-2} day^{-1}. However, the mean value for the 6 mm VFR lies at 10.6 g m^{-2} day^{-1} and the large fluctuations seen in Figure 8-22 are reflected in the SD of 7.37 g m^{-2} day^{-1}. Both the mean values for the 20 mm VFR and the lagoons are of a similar magnitude at 6.4 and 6.1 g m^{-2} day^{-1} respectively and show a lower variance than the 6 mm VFR with SD of 2.8 and 3.0 g m^{-2} day^{-1}.

Figure 8-23 compares Fe(II) decrease as a % of the initial Fe(II) load against time in days since sampling started for the lagoons, the 20 mm VFR and the 6 mm VFR. Dashed lines indicate the mean values of the data. Percentage oxidation of Fe(II) is highest in the 6 mm VFR and the lagoons with mean

values of 96 and 93 % respectively. It is lower in the 20 mm VFR at only 75 % and shows a high %SD of 18.9. The 6 mm VFR and the lagoons show a more consistent removal with %SD values of 6.4 and 8.2 respectively.

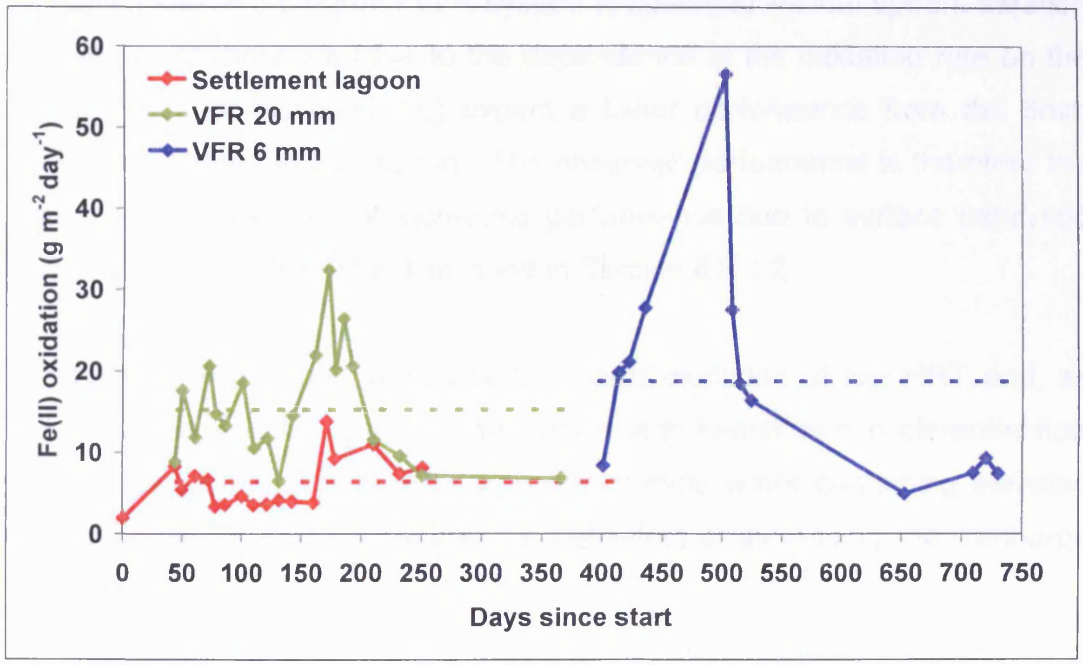

Figure 8-22: Fe(II) area adjusted oxidation rates for the settlement lagoons

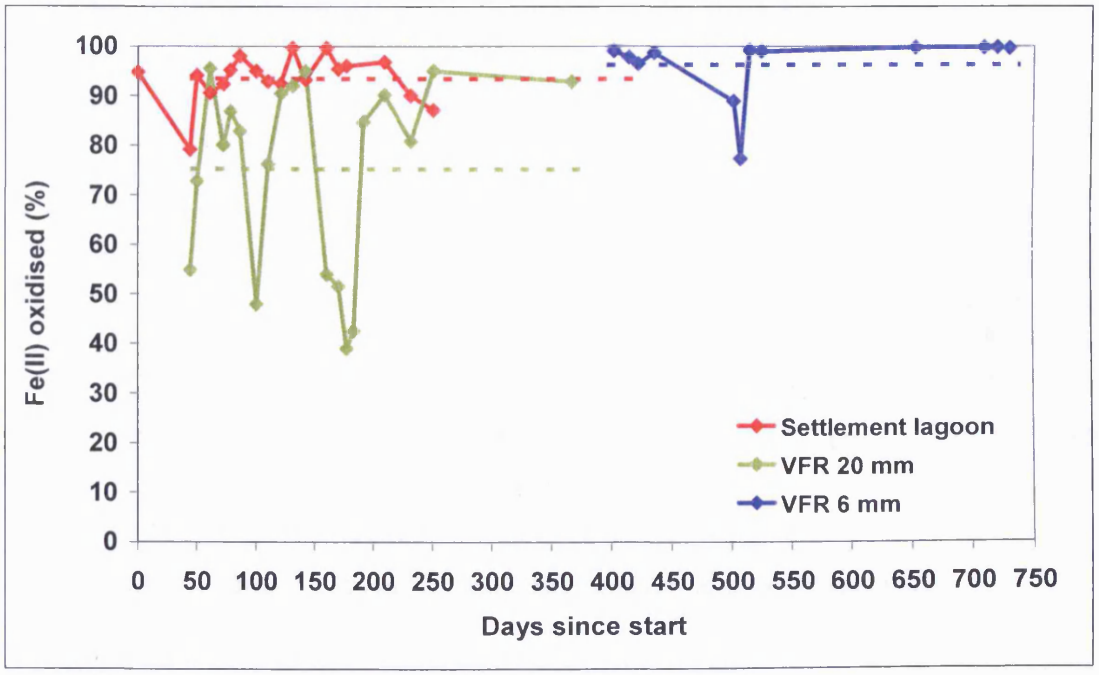

Figure 8-23: Comparison of percent Fe(II) decrease for the lagoons, 20 mm VFR and 6 mm VFR

Figure 8-24 shows the consolidated data for the % decrease in Fe(II) against HRT in hours for the lagoons, 20 mm VFR and 6 mm VFR. It is evident that both the lagoons and the 6 mm VFR perform equally well as Fe(II) oxidising systems. However, the 6mm VFR system is operating without upfront aeration and we would therefore (due to the dependence of the oxidation rate on the concentration of dissolved O_2) expect a lower performance from the 6mm VFR as compared to the lagoon. The observed performance is therefore the first indication we have of increased performance due to surface catalysed Fe(II) oxidation. This will be discussed in Section 8.8.1.2.

The 20 mm VFR shows generally low Fe(II) oxidation at low HRT and, as indicated before, is thought to be primarily due to formation of preferential flow paths. These permit the fast through put of mine water containing elevated concentrations of Fe(II). This has the net effect of increasing the discharge concentration.

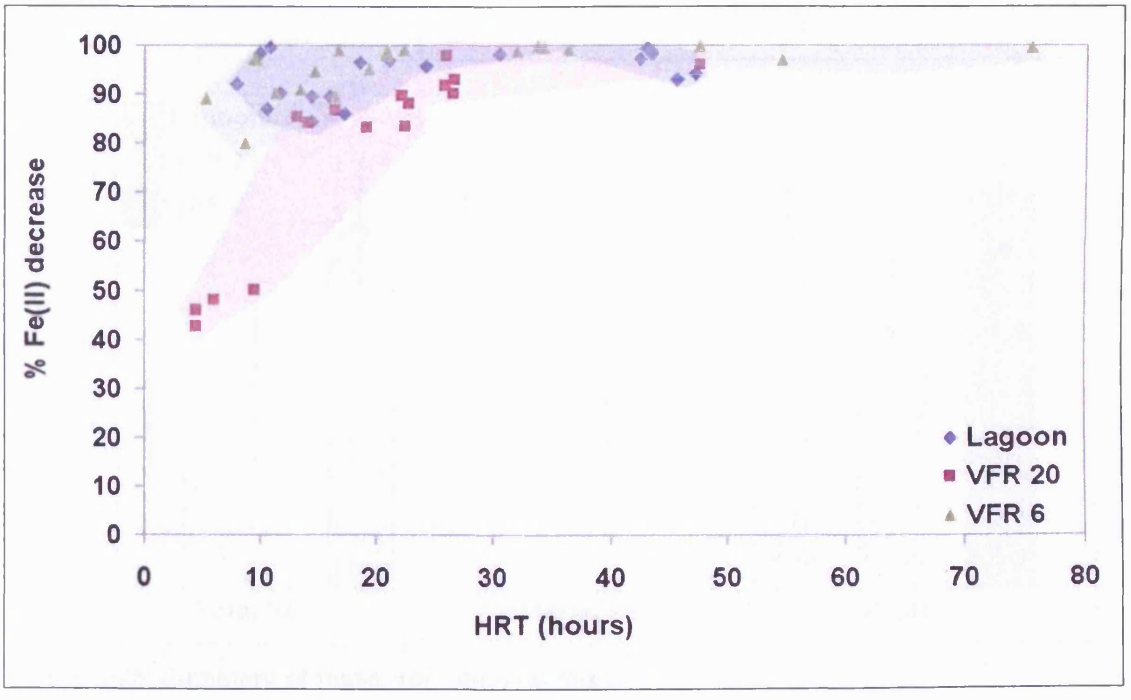

Figure 8-24: Comparison between nominal HRT and percent Fe(II) decrease

8.3.4 Summary of iron removal performance

Figure 8-25 shows the mean removal of total Fe, filtered Fe and Fe(II) as a % of the initial concentration for the lagoons , 20 mm VFR and 6 mm VFR. Mean values are indicated by the columns and SD values by the black bars.

There is no significant difference between filtered Fe and Fe(II) mean % removal values for all three systems. Values for both filtered Fe and Fe(II) for the lagoons and the 6 mm VFR are comparable and all values occur within 94.5 ± 1.8 %, the SD values are also low for these datasets at 6.3 ± 3 %. The 20 mm VFR has the lowest % removal for filtered Fe and Fe(II) and the highest SD at 75.3 ± 0.03 and 19.8 ± 0.9 % respectively.

Mean values for the % removal of total Fe from the lagoons and the 20 mm VFR are similar with values of 39.4 and 49.1 % respectively. The 6 mm VFR shows by far the highest mean % removal at 89.5 % with a low SD of 14.7 %.

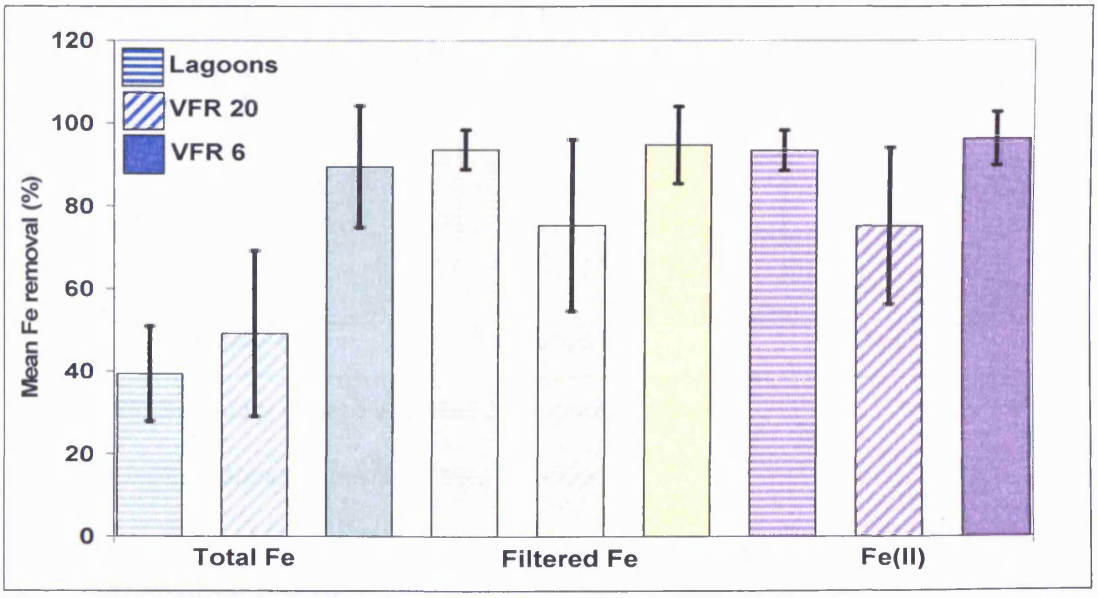

Figure 8-25: Summary of mean iron removal rates.

Error bars indicate standard deviation from the mean.

Figure 8-26 shows the mean AARR values for total Fe, filtered Fe and Fe(II) as g m^{-2} day^{-1} for the combined L1 and L2 lagoons and the 20 mm and 6 mm

VFRs. Mean values are indicated by columns and SD is indicated by the black bars. The total Fe AARR values for both the VFRs are roughly triple those of the lagoons at about 16 g m^{-2} day^{-1}. The high SD values in the VFR datasets are largely due to flow variation and associated fluctuation in inlet flux of Fe. It would be expected that a full scale system, once established would show much lower variability in performance.

From comparison of total, filtered and Fe(II) iron concentrations, it can be seen that the 6 mm VFR gives the best overall performance. The lagoon gives the poorest performance in terms of total Fe removal, but shows an equal performance to the 6 mm VFR for Fe(II) removal.

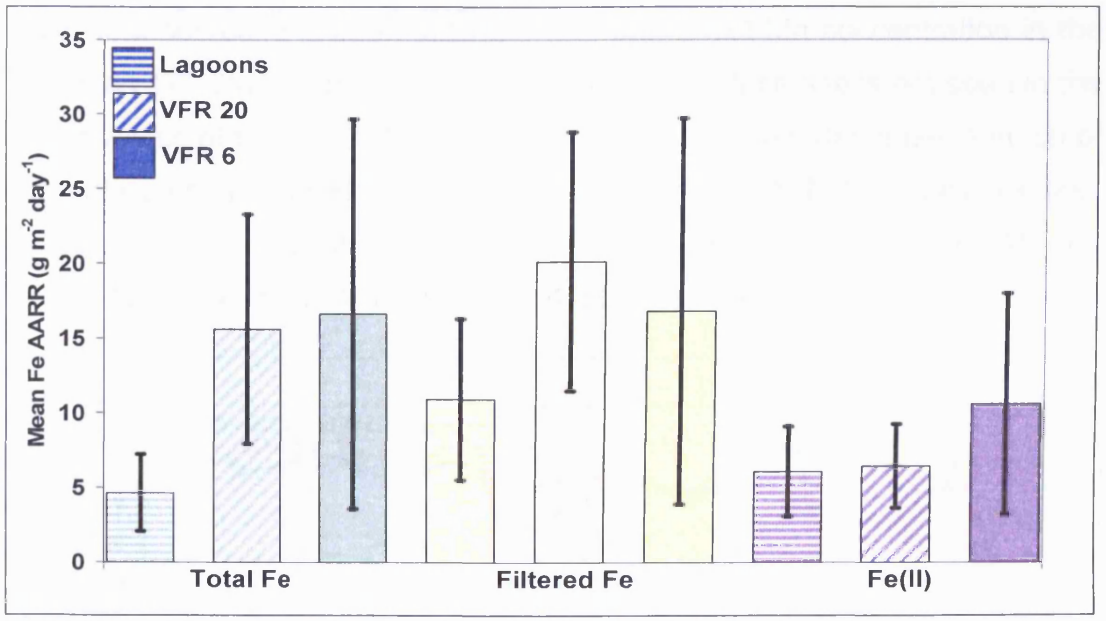

Figure 8-26: Summary of area adjusted iron removal rates.

Error bars indicate standard deviation from the mean.

8.4 Manganese removal

Recorded values for, total manganese concentrations for the lagoons, 20 mm VFR and 6 mm VFR are presented. Filtered Mn data are generally not presented as it was found that the relationship between total and filtered Mn was roughly 1:1. In each case individual data points are marked with solid

diamonds and are connected with lines purely to aid interpretation and are not intended as an indication of the values of missing data.

8.4.1 Total manganese

Figure 8-27 shows the concentrations of total Mn in mg L^{-1} determined at the DW and lagoon outlet, against time in days since sampling began. Filtered Mn data are also shown at the outlet from the VFR for comparison. As with Fe results a characteristic drop in Mn concentrations is observed at 177 days. Data up to 177 days show low variance with mean and SD value of 0.87 and 0.02 mg L^{-1} at the DW and 0.79 and 0.07 mg L^{-1} at the outlet. After 177 days, a mean DW value to 0.77 mg L^{-1} was determined.

Overall, a decrease is seen between DW and outlet Mn concentration in the less than 177 days data of 0.08 mg L^{-1}. The same decrease is not seen in the mean values of the ≥ 177 days data despite an apparent decrease in much of the data presented in Figure 8-27. The greater than 177 days data are less consistent and do not show the consistent reduction in Mn between DW and outlet. An overall mean Mn removal of 0.03 mg L^{-1} can be determined.

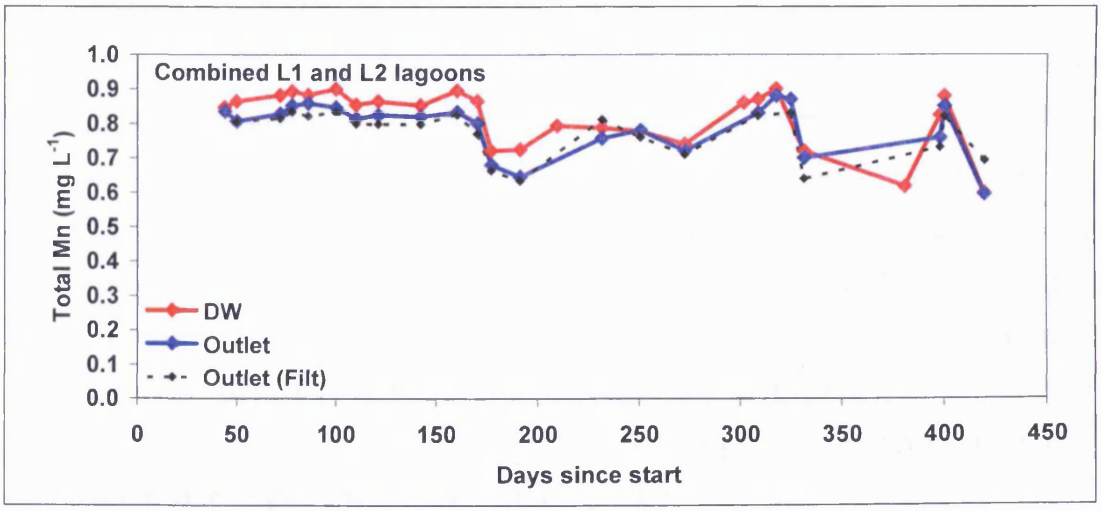

Figure 8-27: Total Mn concentration against time for the lagoons

Filtered outlet Mn concentrations are included for comparison.

Figure 8-28 shows the inlet and outlet total Mn concentrations for the 20 mm VFR against time in days since sampling started. DW concentrations are also

shown for comparison. Inlet Mn concentrations closely follow the DW values. As is evident in the DW values a step can be seen at approximately 170 days which corresponds to the start of November 2005. A recovery from a low of 0.6 mg L^{-1} up to 0.9 mg L^{-1} is evident between 150 and 300 days before a further step down to 0.7 mg L^{-1}. Mn concentrations in the outlet are variable with a SD of 0.17 mg L^{-1} mainly due to HRT within the system at the time of sampling.

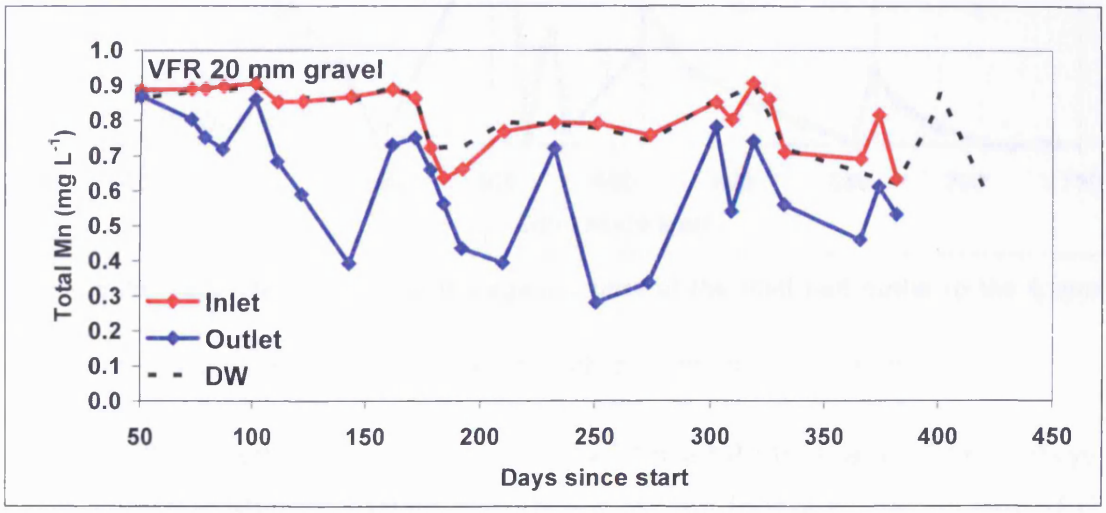

Figure 8-28: Total Mn concentrations against time at the inlet and outlet to the 20 mm VFR

Distribution weir values are included for comparison.

Figure 8-29 shows the inlet and outlet total Mn concentrations for the 6 mm VFR against the time in days since sampling started. Inlet Mn concentrations are stable at approximately 0.75 mg L^{-1} up to 575 days (which again fall on the start of November) where a step is seen and a decrease in Mn concentrations to a mean of 0.6 mg L^{-1} can be seen. Mean and SD values for inlet Mn are 0.7 and 0.07 mg L^{-1}. Mn concentrations in the outlet are variable reflecting flow rates through the VFR system, this is shown with a high SD value of 0.22 mg L^{-1} from a mean of 0.23 mg L^{-1}. However, they are consistently and significantly lower than the feed.

On comparison of Figure 8-27 to Figure 8-29 with Figure 8-1 it can be seen that the inlet Mn concentration steps down at 175 and 575 days correspond with an increase in flow rates through the Taff Merthyr treatment system. This

indicates dilution of the mine water with either increased surface runoff or increased mine water discharge.

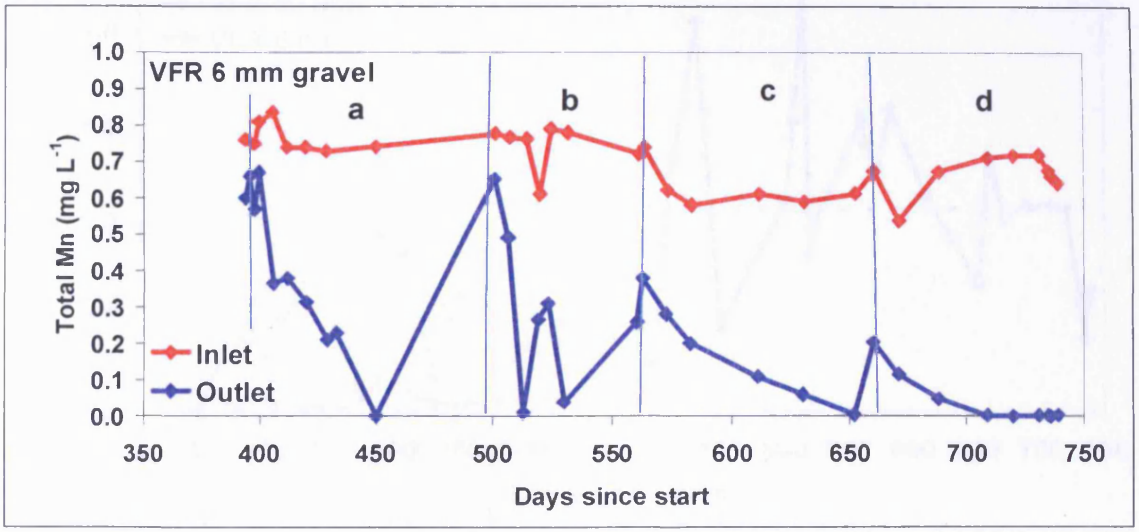

Figure 8-29: Total Mn concentrations against time at the inlet and outlet to the 6 mm VFR

Zones a, b, c, and d indicate flow zones of consistently increasing Mn removal

Figure 8-30 compares AARR in g m^{-2} day^{-1} for total Mn against time in days since sampling started. Values are shown for the lagoons, the 20 mm VFR and the 6 mm VFR. Dashed lines indicate the mean values of the data. Mean AARR values increase in the order: lagoons, 20 mm VFR, and 6 mm VFR. This corresponds with mean values of 0.06, 0.57 and 1.07 g m^{-2} day^{-1} and SD's of 0.05, 0.31, and 0.49 g m^{-2} day^{-1} respectively.

Figure 8-31 compares Fe(II) decrease as a % of the initial total Mn load, against time in days since sampling started for the lagoons, the 20 mm VFR, and the 6 mm VFR. Dashed lines indicate the mean values of the data. Mean % removal increases in the order: lagoons, 20 mm VFR and 6 mm VFR. This corresponds with mean values of 4.49, 23.11, and 69.21 % and with SD's of 2.57, 17.02, and 27.62 % respectively.

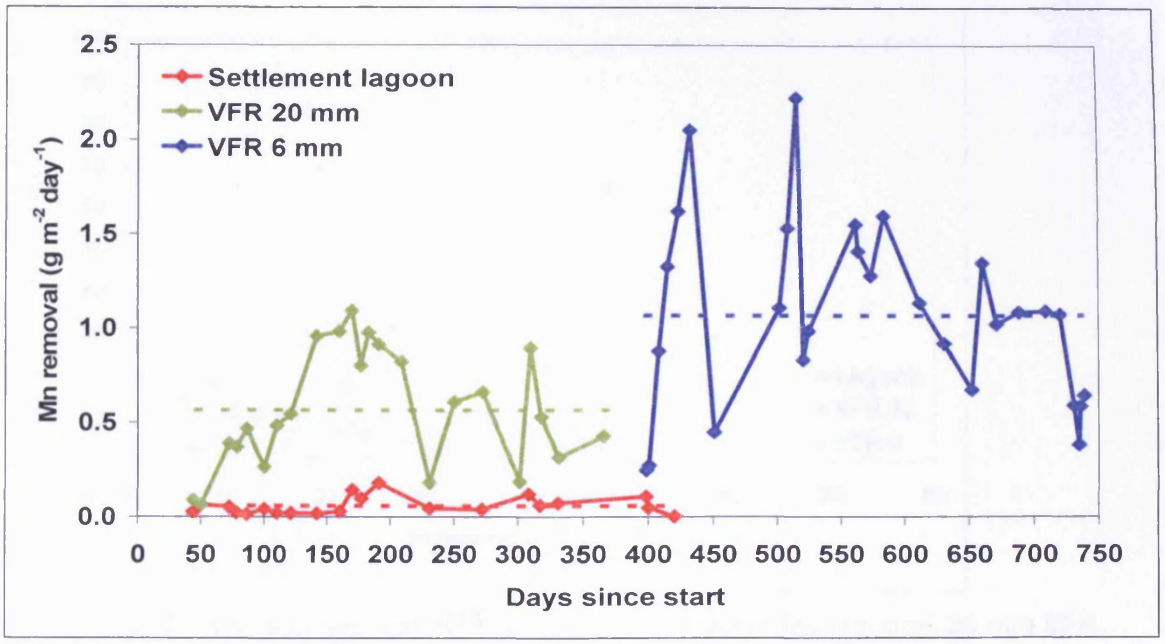

Figure 8-30: Total Mn area adjusted removal rates for the lagoons, 20 mm VFR and 6 mm VFR

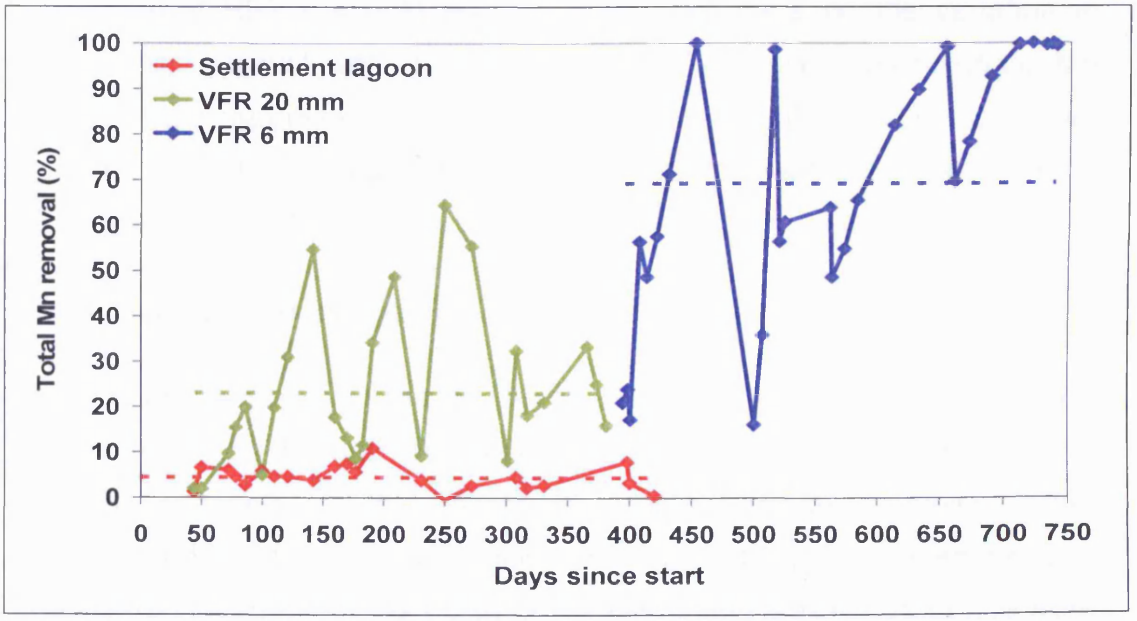

Figure 8-31: Percentage of initial total Mn removed against time in the lagoons, 20 mm VFR and 6 mm VFR

Figure 8-32 shows the % total Mn removal against HRT in hours determined for the combined L1 and L2 lagoons, 20 mm VFR and 6 mm VFR. The 6 mm VFR gives the best removal performance with upwards of 95 % Mn removal at HRT > 30 hours.

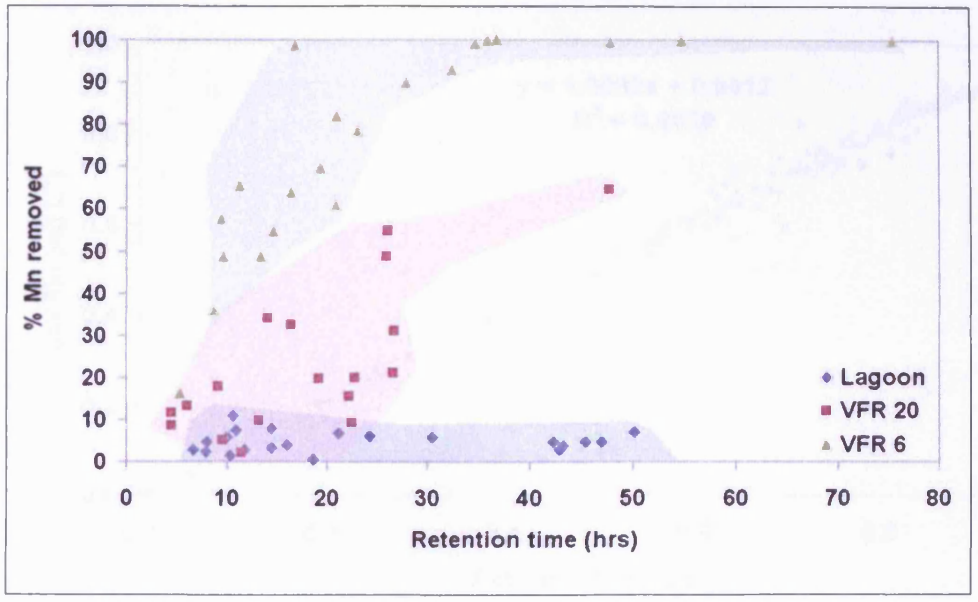

Figure 8-32: Comparison between HRT and % Mn removal in the lagoons, 20 mm VFR and 6 mm VFR

The lagoons give the lowest performance with < 10 % of Mn removed irrespective of HRT it should also be noted that there is little variation in lagoonal Mn removal with HRT. The 20 mm VFR gives intermediate Mn removal with a maximum of 60 % removed at HRT > 30. At HRT < 30 hours the 6 mm VFR Mn removal performance drops rapidly with less than 70 % of Mn removed if the HRT is less than 20 hours.

8.4.2 Dissolved manganese

Figure 8-33 compares values of filtered and total Mn in mg L^{-1}. The red dashed line marks a linear trend with an R^2 value at 0.984. Due to the close correlation between total and filtered Mn only total Mn concentrations have been reported and filtered data is included in Appendix 2. The exception is in the case of filtered Mn in the outlet of the lagoons in which divergence from the total Mn values was observed.

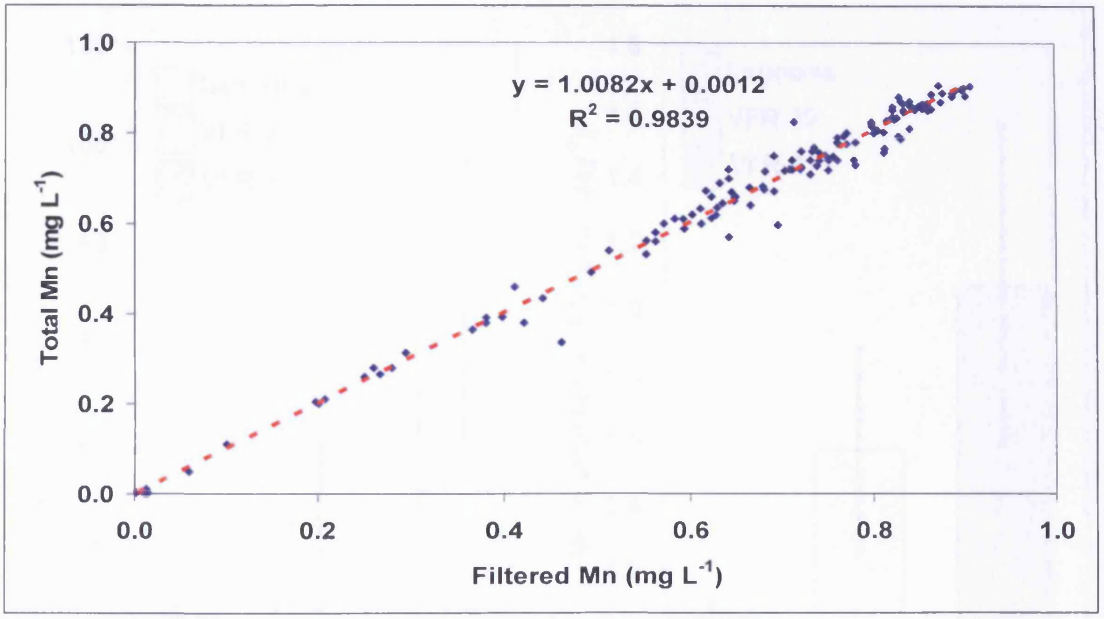

Figure 8-33: Comparison of total and filtered Mn concentrations

Red dashed line indicates an ideal 1:1 relationship

8.4.3 Summary of Mn removal performance

Figure 8-34a shows the mean total Mn removal from the lagoons, the 20 mm VFR and the 6 mm VFR as a percentage of the inlet concentration. SD values for the % removal dataset are shown as black bars. Mean % removal values increase in the order of lagoon, 20 mm VFR and 6 mm VFR. These correspond with values of 4.5, 23.1 and 69.2 % respectively with corresponding SD values of 2.6, 17.0 and 27.6 %.

Figure 8-34b shows the mean Mn removal rates from the lagoons, the 20 mm VFR and the 6 mm VFR as AARR in g m^{-2} day^{-1}. SD values for the AARR dataset in g m^{-2} day^{-1} are shown as black bars. Mean vales increase as with the % removal dataset from lagoons through 20 mm and 6 mm VFR systems. This corresponds to values of 0.06, 0.57 and 1.07 g m^{-2} day^{-1} with SD's of 0.05, 0.31 and 0.49 g m^{-2} day^{-1} respectively.

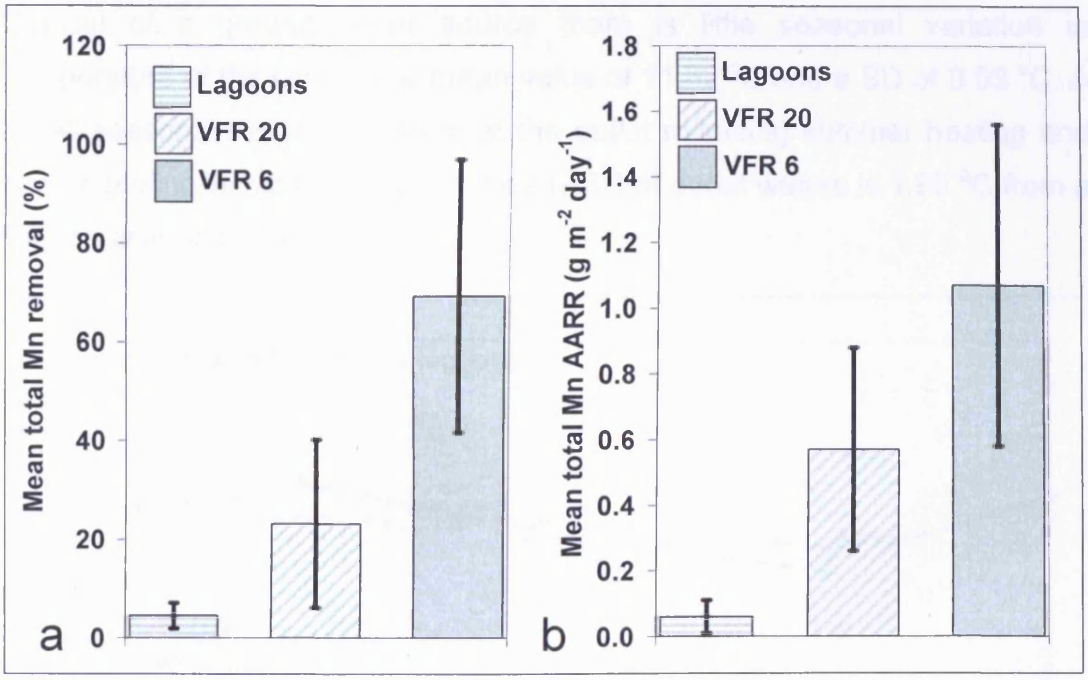

Figure 8-34: a) Summary of mean % Mn removal and b) summary of mean area adjusted removal rates for the lagoons, 20 mm VFR and 6 mm VFR.

Error bars indicate standard deviation from the mean

8.5 Temperature, pH, Eh, dissolved oxygen and alkalinity

Recorded values for inlet and outlet mine water temperature, pH, Eh, dissolved O_2 (DO) and alkalinity, for the lagoons, 20 mm VFR and 6 mm VFR are presented. In each case individual data points are marked with solid diamonds and are connected with lines purely to aid interpretation and are not intended as an indication of the values of missing data.

8.5.1 Temperature

Figure 8-35, Figure 8-36 and Figure 8-37 show mine water temperature recorded in the lagoons, 20 mm VFR and 6 mm VFR. The light red shaded area within the charts marks the monthly average daily minimum and maximum air temperatures recorded at the Met Office's, Cardiff Bute park weather station (data courtesy of the Met Office, 2007).

Figure 8-35 shows the temperature in °C of the mine water at the DW and the outlet from the lagoons against the time in days since sampling began.

Typical of a ground water source there is little seasonal variation in temperature at the DW with a mean value of 11.62 °C and a SD of 0.58 °C. A small seasonal variation is seen at the outlet reflecting summer heating and winter cooling within the lagoons. Yearly SD of outlet waters is 1.95 °C from a mean value of 12.19 °C.

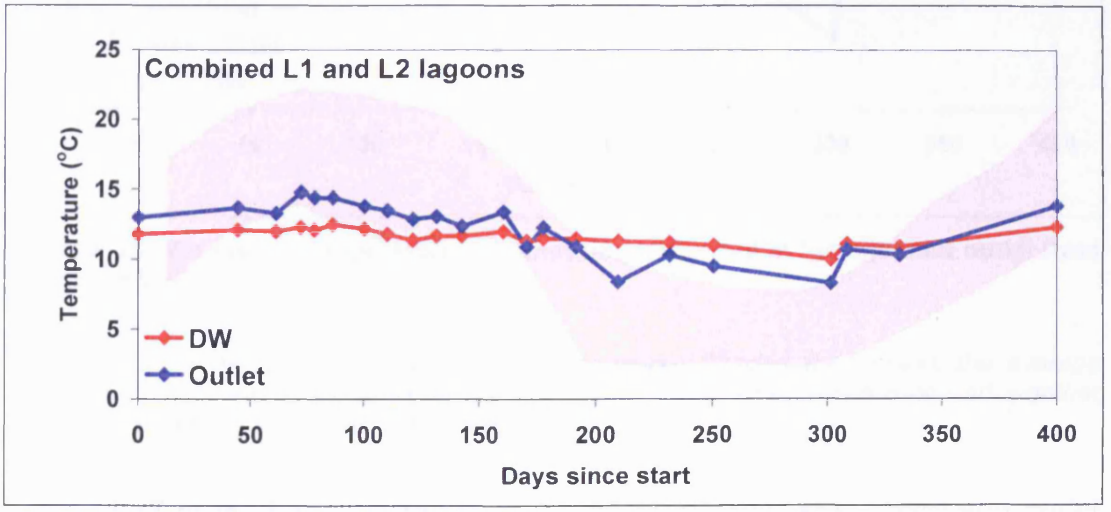

Figure 8-35: Mine water temperature against time recorded at the distribution weir and outlet from the L1 and L2 lagoons

Shaded area marks the average monthly maximum and minimum air temperatures as determined at Cardiff Bute Park weather station (data courtesy of the Met Office, 2007)

Figure 8-36 gives the temperature in °C for mine water at the inlet and outlet from the 20 mm VFR against the time in days since sampling began. The inlet temperature closely follows the trend of the distribution weir with a mean of 11.79 °C and a SD of 0.94 °C. The outlet temperature shows seasonal SD of 2.58 °C from a mean of 12.05 °C.

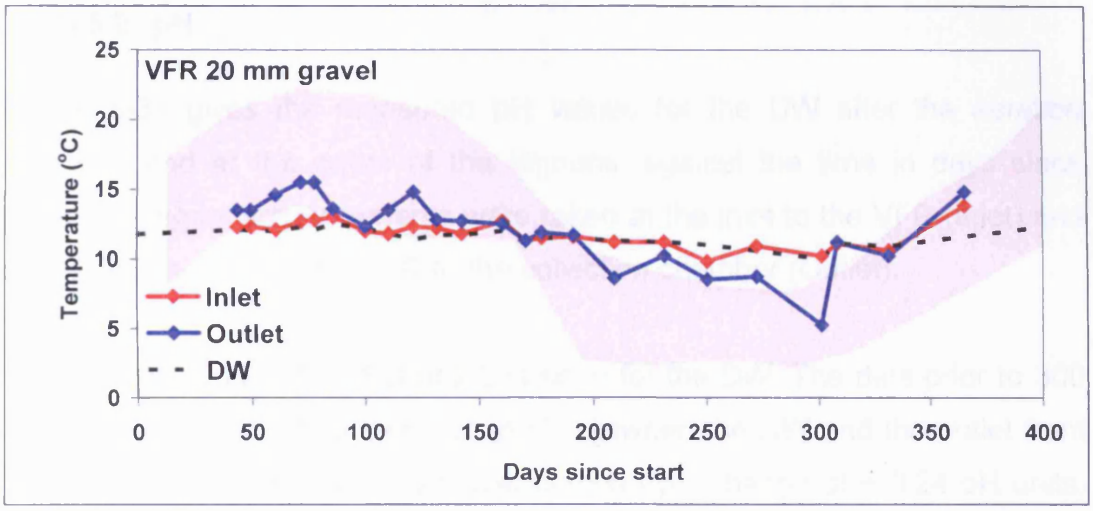

Figure 8-36: Mine water temperatures against time recorded at the inlet and outlet from the 20 mm VFR.

The distribution weir values are shown for comparison. Shaded area marks the average monthly maximum and minimum air temperatures as determined at Cardiff Bute Park weather station (data courtesy of the Met Office, 2007).

Figure 8-37 gives the temperature in °C for mine water at the inlet and outlet to the 6 mm VFR, against the time in days since sampling began. The inlet temperature shows only slight variation with a mean value of 11.6 °C and an SD of 0.6 °C. The outlet temperature shows a seasonal SD of 1.18 °C from a mean of 11.62 °C.

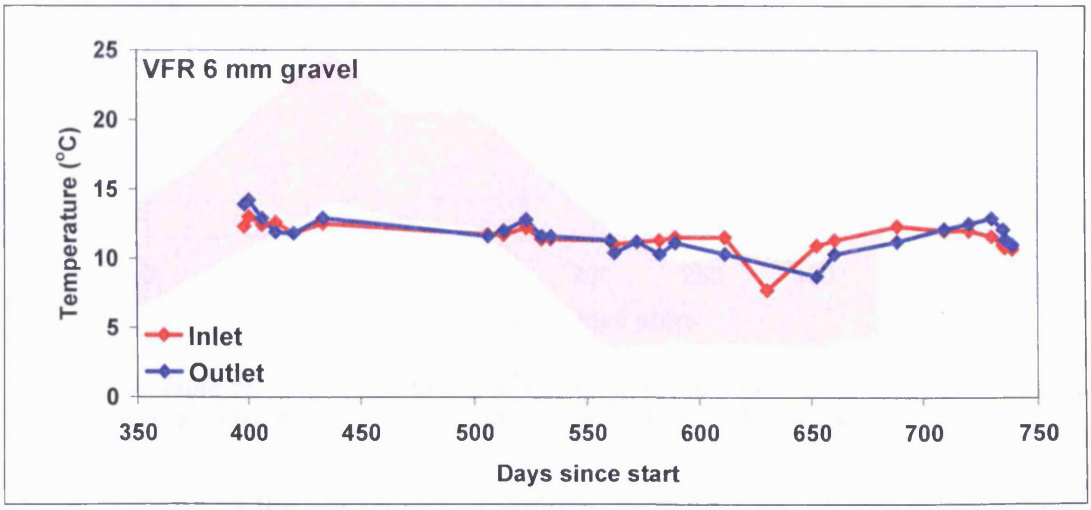

Figure 8-37: Mine water temperatures against time recorded at the inlet and outlet from the 6 mm VFR.

Shaded area marks the average monthly maximum and minimum air temperatures as determined at Cardiff Bute Park weather station (data courtesy of the Met Office, 2007).

8.5.2 pH

Figure 8-38 gives the measured pH values for the DW after the aeration cascade, and at the outlet of the lagoons, against the time in days since sampling began. Measurements were taken at the inlet to the VFR (Inlet) and at the discharge from the VFR to the collection chamber (Outlet).

A mean pH of 6.9 with a SD of 2.3 is seen for the DW. The data prior to 300 days shows a consistent increase in pH between the DW and the outlet from the lagoons which equate to an overall mean pH change of + 0.24 pH units. Of this total increase, + 0.08 units is accounted for by the aeration cascade and the remaining 0.16 unit rise occurs between the cascade and the lagoon outlet. The data points after 300 days are not consistent with the previous data and show an overall fall in pH. In addition a decrease in pH is observed between the DW and the discharge. The mean discharge pH is 7.2 with a SD of 0.1 units. The pH increase observed at the aeration cascade is thought to be due to degassing of dissolved CO_2.

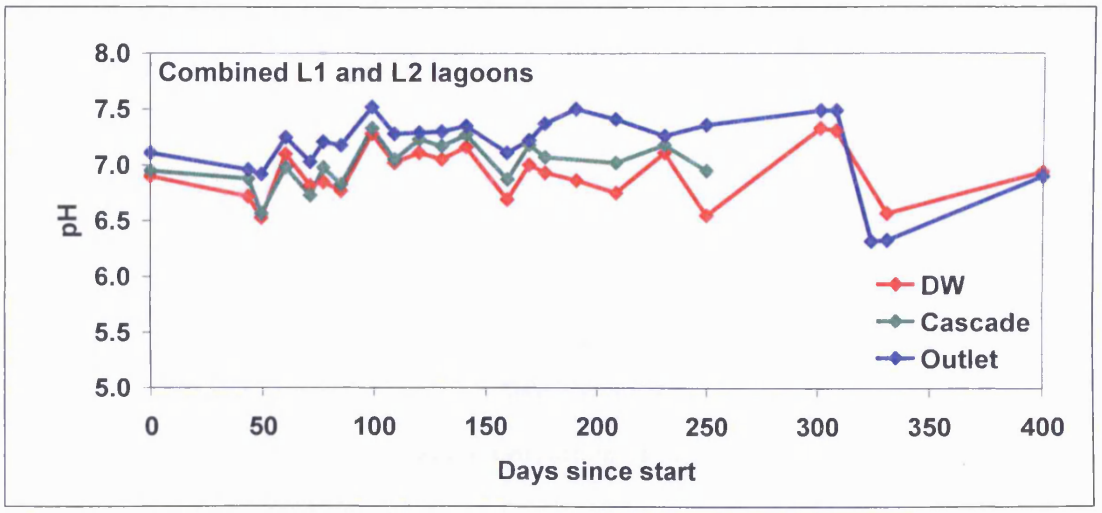

Figure 8-38: Mine water pH against time recorded at the distribution weir, distribution channel (to the L2 lagoon) and outlet from the combined L1 and L2 settlement lagoons

Figure 8-39 gives the measured pH values for mine water flowing through the 20 mm VFR, against the time in days since sampling began. Measurements were taken at the inlet to the VFR (Inlet) and at the discharge from the VFR to

the collection chamber (Outlet) values recorded at the distribution weir are included for comparison.

Recorded pH values between 100 and 250 days show only minor deviation from the mean. This is consistent with the trend of an increase in pH between the inlet and outlet as seen in the lagoons and is thought to be due to degassing of CO_2 however, the increase is much lower than observed in the lagoons which is thought to be due to a) there is no aeration cascade and b) the vertical flow through the system partially confines the system and minimises water / gas interactions. Recorded data prior to 100 days is variable and the inlet data is lower than the data from the distribution weir, however, it is consistent with the trend of lower inlet pH values than outlet pH values. Recorded data after 250 days again shows a large deviation from the mean and also lacks the trend of a pH increase from inlet to outlet. The post 300 days inlet data closely matches the distribution weir data.

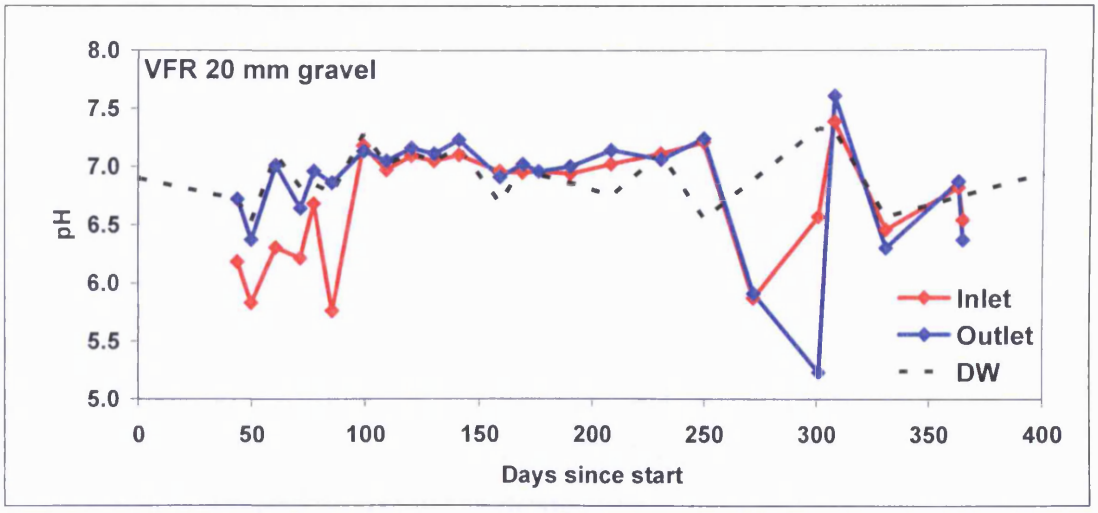

Figure 8-39: Mine water pH against time recorded at the inlet and outlet from the 20 mm VFR.

Distribution weir pH values shown for comparison

Figure 8-40 shows the measured pH values for mine water flowing through the 6 mm VFR, against time in days since sampling began. Measurements were taken at the inlet to the VFR (Inlet) and at the discharge from the VFR to the collection chamber (Outlet).

The trend of an increase in pH from inlet to the outlet is apparent but is not consistent throughout the dataset. The data between 590 and 700 days shows the trend consistently whilst the post 700 days and 500 to 590 days data does not show this trend. At the beginning of the operational period a large number of visits were made. Mean and SD values of 6.7 and 0.3 for the inlet and 6.8 and 0.3 for the outlet show a change in pH of only + 0.1 units across the whole data set.

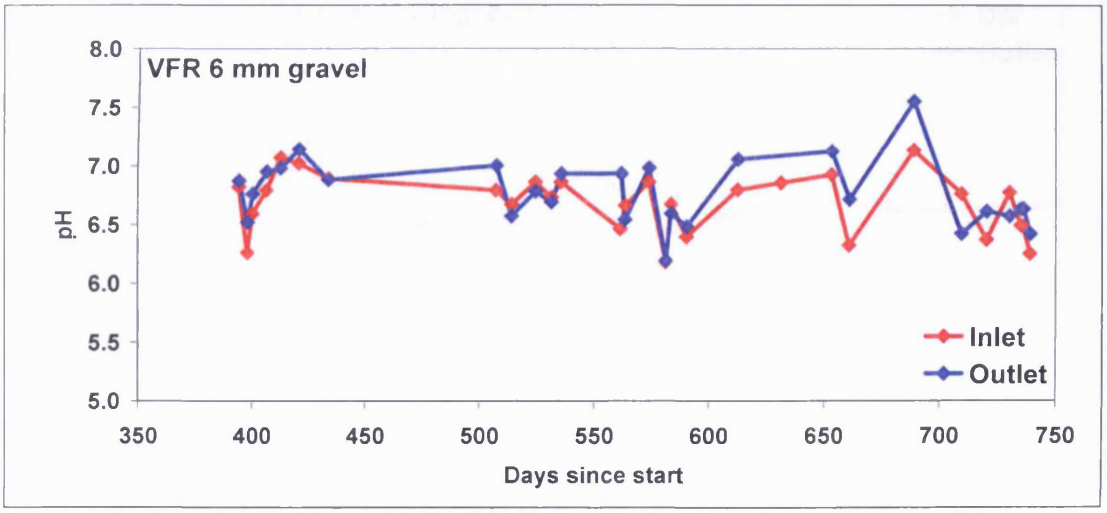

Figure 8-40: Mine water pH against time recorded for the inlet and outlet from the 6 mm VFR

8.5.3 Eh

Figure 8-41, Figure 8-42 and Figure 8-43 show mine water redox potential (Eh) recorded in the lagoons, 20 mm VFR and 6 mm VFR. 200 mV have been added to all field readings to allow for the reference electrode potential against the Standard Hydrogen Electrode (SHE).

Figure 8-41 shows the recorded Eh values in mV determined at the DW and lagoon outlet, against the time in days since sampling began. The Eh recorded at the DW is consistently lower than the outlet with a mean Eh change through the system of + 45.8 mV. The mean and standard deviation of the Eh readings at the DW are 170.0 and 41.7 mV respectively. The Eh measured at the DW was seen to decrease from approximately 250 mV, to around 100 mV between 0 and 100 days which corresponds to a change in

meters (this therefore indicates that the meter was defective). Values are seen to increases to 150 mV after 140 days. The mean and standard deviation of Eh values at the outlet were 215.8 and 42.3 mV respectively. Overall, there is an initial decrease in Eh corresponding with a change in meters. This is followed by a slight increase before stabilisation at approximately 200 mV.

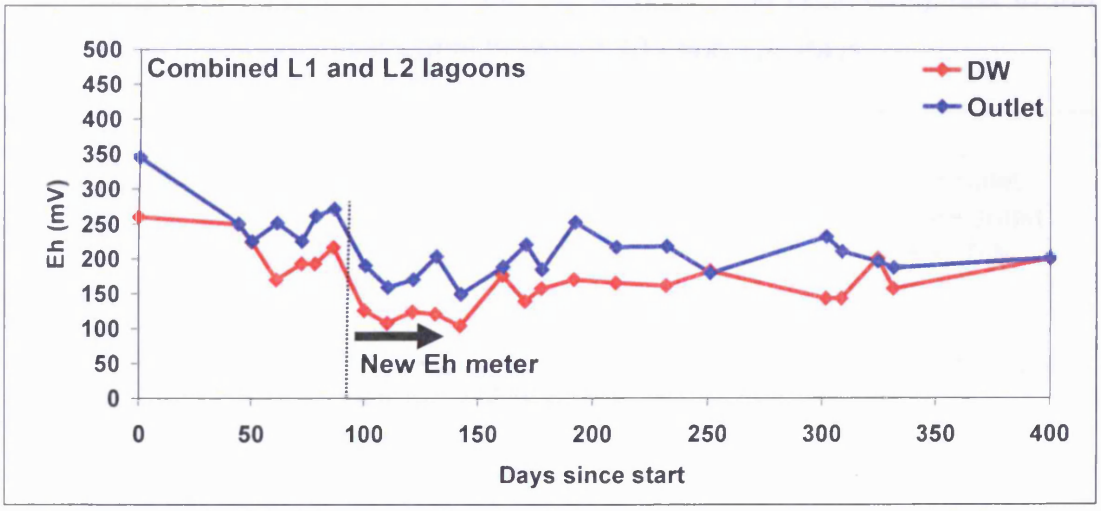

Figure 8-41: Mine water Eh against time recorded at the distribution weir and outlet from the combined L1 and L2 settlement lagoons.

Figure 8-42 sows the recorded Eh values in mV for the 20 mm VFR, against the time in days since sampling began. Recorded values for inlet and outlet data are shown. As with the lagoons, an overall apparent decrease of 60 mV is observed after 100 days which again corresponds with a change of Eh meter. For the greater than 100 days data, the trend of increasing Eh values between the inlet and outlet is consistent with the data from the lagoon, with a mean increase of + 51.8 mV. This trend is not apparent for the less than 100 days data which shows a mean decrease between inlet and outlet of - 20.1 mV. The consistency of 20 mm VFR inlet, and distribution weir values is good for greater than 100 days data. However, the DW values are up to 125 mV lower than the 20 mm VFR inlet values for the less than 100 days data.

Figure 8-43 shows the recorded Eh values in mV for the 6 mm VFR, against the time in days since sampling began. Recorded values for inlet and outlet data are shown. Mean values for the inlet and outlet data are 219.1 and 296.6

mV respectively. Due to peaks in the inlet data the SD is high at 73.7 mV and the outlet SD is higher still at 113.1 mV. The high SD's observed in the inlet and outlet data are primarily due to the high Eh values at 580 and 582 days. High values are also observed in the outlet between 709 and 739 days. The trend of increasing Eh values between the inlet and outlet to the VFR is again seen with a mean increase of + 77.4 mV. This is higher than the values reported for both the 6mm VFR and the lagoons, and is primarily due to the high values observed in the outlet between 709 and 739 days.

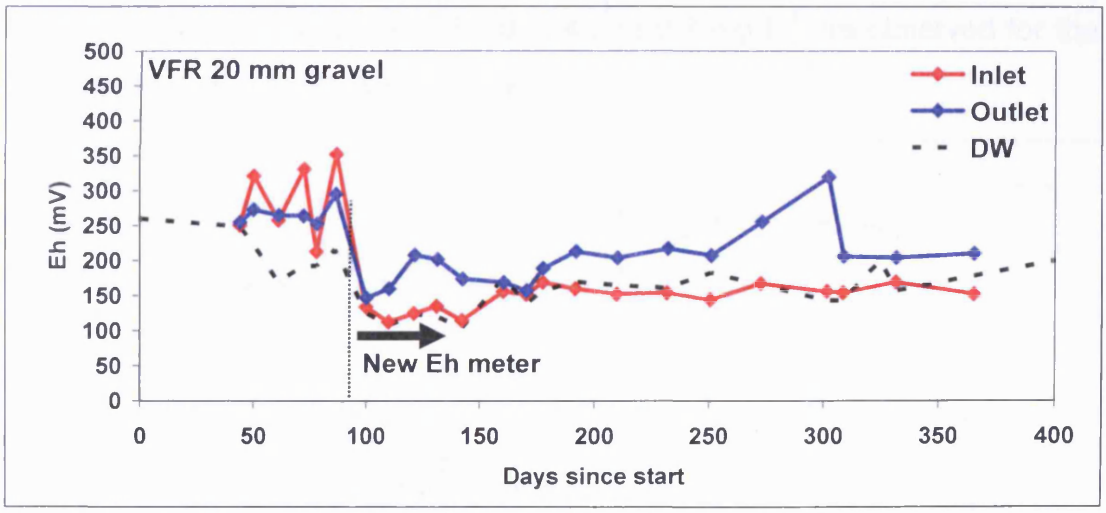

Figure 8-42: Mine water Eh against time recorded at the inlet and outlet from the 20 mm VFR

Distribution weir Eh shown for comparison

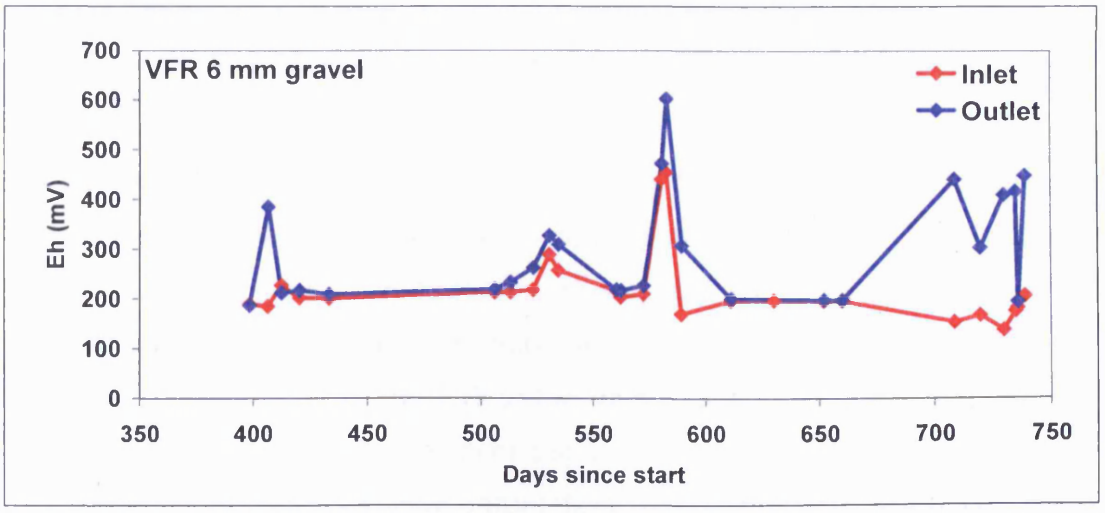

Figure 8-43: Mine water Eh against time recorded at the inlet and outlet from the 6 mm VFR

8.5.4 Dissolved Oxygen

Figure 8-44 shows the DO values in mg L^{-1} for the lagoons, against time in days since sampling began. Values are reported at the DW, after the aeration cascade in the distribution channel to lagoon L2 (Cascade), and for the lagoons outlet (Outlet). It is clear from the differences in values recorded for the DW, cascade and outlet that most oxygenation of the mine water occurs in the aeration cascade with mean values increasing from 3.5 to 7.0 mg L^{-1}. A further increase to 8.0 mg L^{-1} is observed between the cascade and the outlet from the lagoons. SD values of 1.0, 0.4 and 0.7 mg L^{-1} are observed for the DW, cascade and outlet respectively.

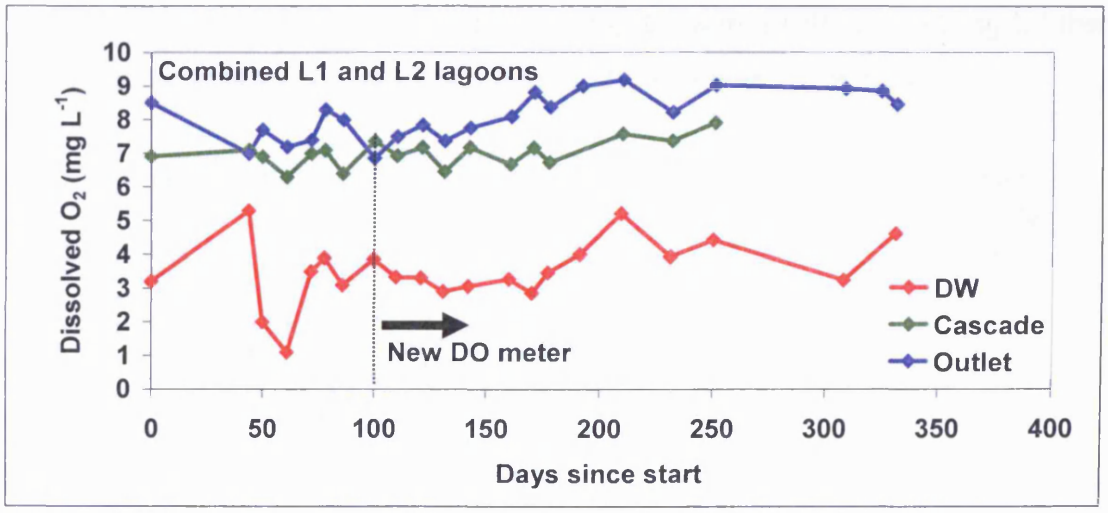

Figure 8-44: Mine water dissolved O_2 concentration against time for the combined L1 and L2 lagoons

Recorded at the distribution weir (DW), distribution channel (Cascade) and outlet from the L1 and L2 settlement lagoons

Figure 8-45 shows the DO values in mg L^{-1} for the 20 mm VFR, against time in days since sampling began. Values are reported for the inlet and outlet to the VFR and the DW concentrations are included for comparison. The inlet concentrations are often higher than the DW concentrations even though mine water travelling from the DW to the VFR inlet should not be exposed to oxygen in the feed pipe. The inconsistency is due largely to difficulties in monitoring inlet electrochemical parameters, where, unlike at the outlet, mine water must be collected in a suitable vessel (usually a 10 L bucket). Electrochemical probes are then placed into the bucket and readings taken.

Unfortunately this method was not consistent throughout the sampling period and on some occasions the bucket was slung below the inlet and probes inserted directly into the circulating mine water pool in the bucket. On other occasions the bucket was filled and removed. Also the heights at which the bucket was slung varied at different times. In this situation it is certain that some dissolution of O_2 will have occurred and therefore the recorded concentration will be higher than the concentration in the feed pipe.

Outlet DO concentrations were more consistent as they were recorded by submerging the DO probe by the V notch outlet from the VFR. IT was found that the flow of water at this point was adequate to keep a steady reading. Outlet DO concentrations averaged 4.46 mg L^{-1} with an SD of 1.21 mg L^{-1} the mean increase in DO between the inlet and outlet was + 0.9 mg L^{-1}.

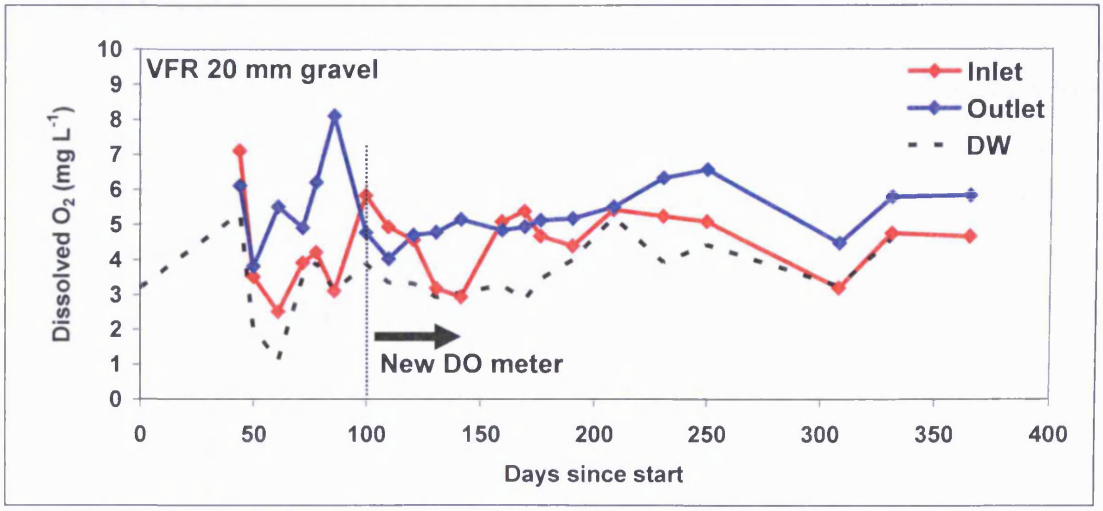

Figure 8-45: Mine water dissolved O_2 concentration against time for the inlet and outlet from the 20 mm VFR

The distribution weir values are shown for comparison

Figure 8-46 shows the inlet and outlet DO concentrations in mg L^{-1} against days since sampling began for the 6 mm VFR. During 6 mm VFR operation a bucket was permanently hung at approximately 50 cm beneath the inlet feed pipe and mine water flowed from the swan-neck, into the bucket and then overflowed from the bucket into the VFR treatment tank. Mean values of 3.68 and 5.16 mg L^{-1} and SD values of 1.10 and 1.14 mg L^{-1} were determined for

the inlet and outlet respectively equating to a mean increase of +1.48 mg L^{-1} through the system.

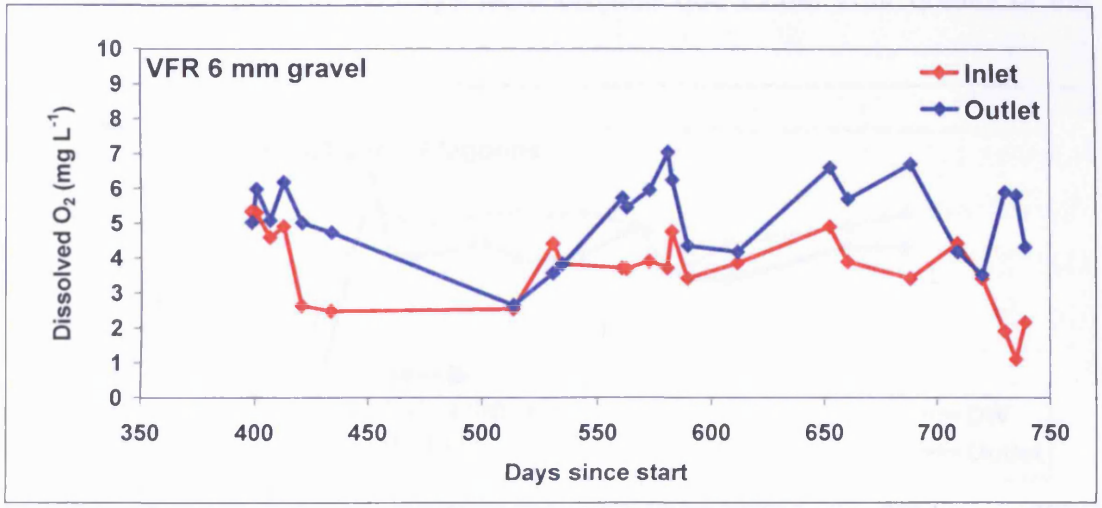

Figure 8-46: Mine water dissolved O_2 concentration against time for the inlet and outlet from the 6 mm VFR

The concentrations of DO in the outlet from the VFR should be less than the maximum concentration, due to DO consumption by the oxidation of Fe(II) and Mn(II) in the VFR system. Although DO consumption in the lagoon will occur it is likely to be harder to observe in the outlet due to a) a greater mass transfer of O_2 due to a greater surface area and b) and initially higher DO concentration.

8.5.5 Alkalinity

Figure 8-47 and Figure 8-48 show the recorded alkalinity in mg L^{-1} as $CaCO_3$ for the 20 mm VFR and lagoons. Initially alkalinity was determined with a HACH test kit which was found to underestimate the alkalinity by approximately 40 mg L^{-1}. After 75 days a HACH digital titrator was used and gave more consistent results.

Figure 8-47 shows the determined alkalinity in mg L^{-1} as $CaCO_3$ for the lagoons, against time in days since the start of sampling. After the introduction of the digital titrator, consistent results are seen relative to previous readings and a general trend of lower outlet concentrations than inlet concentrations can is observed. Mean values of 244.2 and 227.3 mg L^{-1} and SD values of 9.1

and 8.8 mg L^{-1} were determined at the DW and outlet respectively. This equates to a mean decrease in alkalinity of 16.9 mg L^{-1}. In each case the recorded vales prior to 75 days were omitted due to the poor quality of the data.

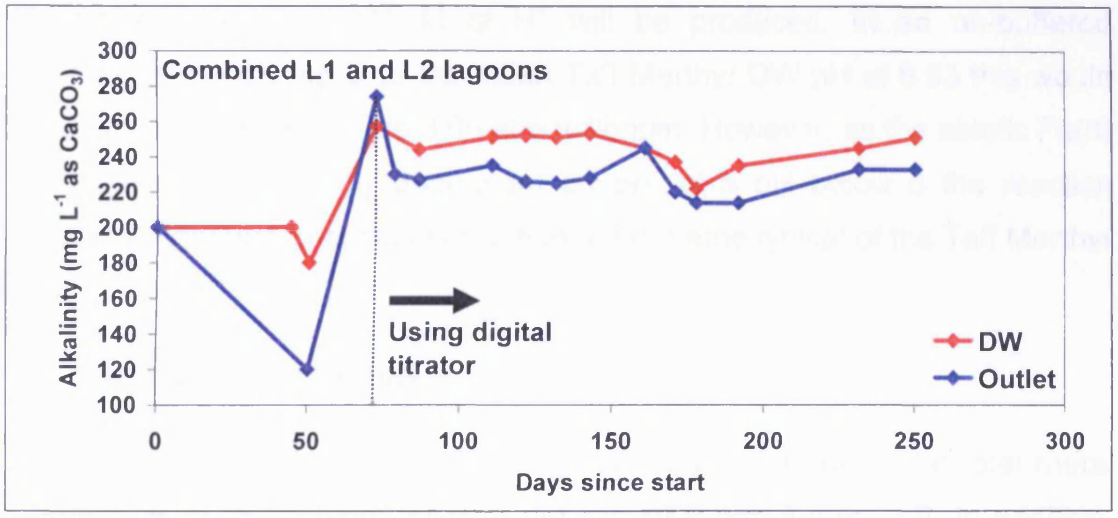

Figure 8-47: Mine water alkalinity against time recorded at the distribution weir and outlet from the combined L1 and L2 settlement lagoons

Figure 8-48 shows the alkalinity in mg L^{-1} as $CaCO_3$ for the 20 mm VFR, against time in days since the start of sampling. As with the lagoons a general decrease in alkalinity is seen between inlet and outlet values. Mean values for the inlet and outlet were determined as 243.9 and 228.8 mg L^{-1} with SD values of 9.2 and 7.7 mg L^{-1} respectively. This equates to a mean decrease of 15.1 mg L^{-1} with pre 75 day values omitted.

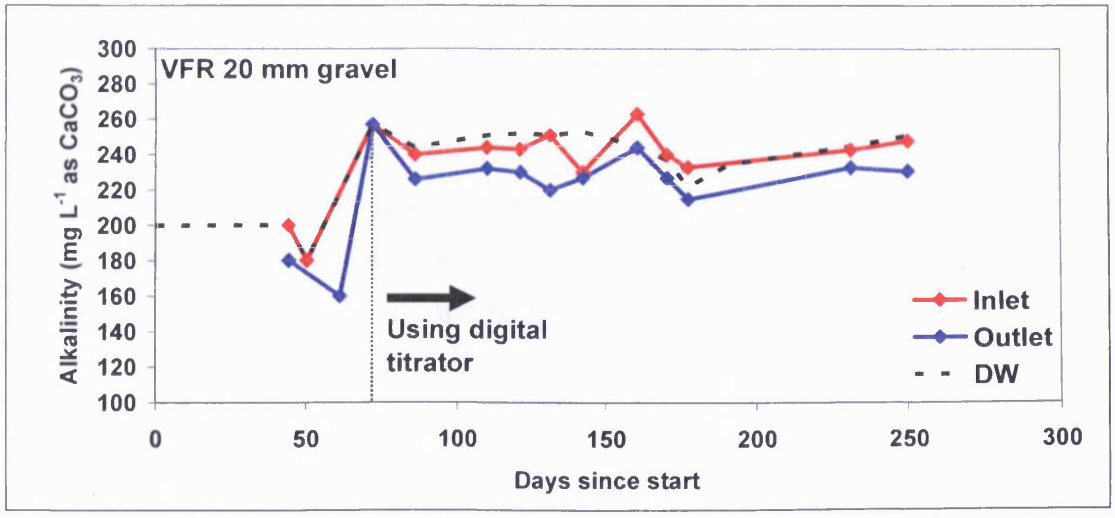

Figure 8-48: Mine water alkalinity against time recorded at the inlet and outlet from the 20 mm VFR

The distribution weir values are shown for comparison

The general reduction in alkalinity can be attributed to acidity produced during oxidation of Fe(II) and associated precipitation of hydrous Fe(III) oxides which releases 2 moles of protons to every mole of Fe(II) oxidised. Using the average Fe(II) concentration of $1.13x10^{-4}$ M (6.33 mg L^{-1}), it can be determined that $2.26x10^{-4}$ M of H^+ will be produced. In an un-buffered solution, with a pH equal to the mean Taff Merthyr DW pH of 6.93 this would result in a reduction in pH to 3.65 at equilibrium. However, as the abiotic Fe(II) oxidation rate is strongly dependant on pH, at a pH below 6 the reaction would not continue to completion within a timeframe typical of the Taff Merthyr HRT.

8.6 Metals concentrations

Figure 8-49 shows the mean difference between inlet and outlet total metal concentrations through the lagoons, 20 mm VFR and 6 mm VFR. In addition, Figure 8-50 shows the same results as percentages of the initial concentrations. Fe and Mn are shown primarily for comparison with the other non-redox sensitive metals, calcium, magnesium, sodium, potassium, silicon and strontium. Of the non redox sensitive metals, the difference between inlet and outlet Ca is highest with a general reduction in concentrations; this is followed by Mg, Na, Si and K in order of decreasing removal. Sr concentrations appear to be conservative through all systems.

Despite Ca removal being dominant (reflecting over-saturation of $CaCO_3$ minerals), Si is removed disproportionately with 6.9 % removal averaged across all systems. In the PhreeqC equilibrium model described in section 7.3.3, Si was calculated to be over-saturated with respect to the mineral phase quartz. It should also be noted that removal is not uniform across all systems and that Ca, Mg, Na and K removal is not evident in the 6 mm VFR.

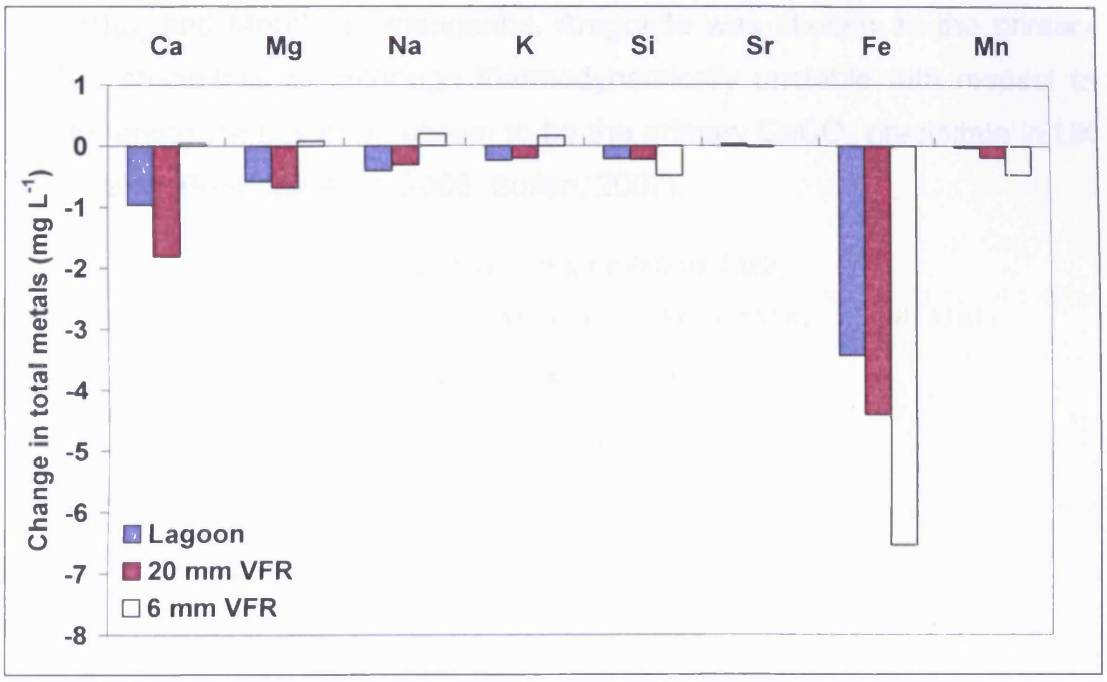

Figure 8-49: Mean change in total metal concentrations during passage through the lagoons, 20 mm VFR and 6 mm VFR

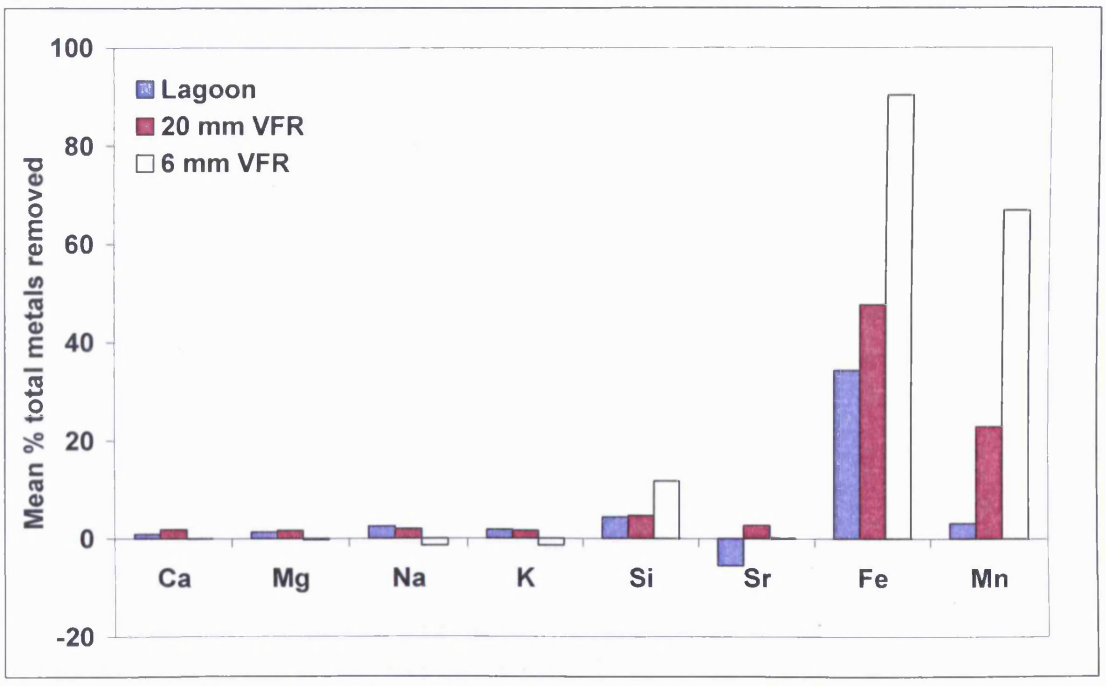

Figure 8-50: Mean % total metal removal during passage through the lagoons, 20 mm VFR and 6 mm VFR

To determine the proportion of Ca that could precipitate in the Taff Merthyr mine-water a PhreeqC simulation (simulation TM2) was carried out. In this the average mine-water composition was equilibrated with both atmospheric CO_2 and O_2. $CaCO_3$ was then precipitated as aragonite, as well as Fe(III) as

$Fe(OH)_{3(a)}$ and Mn(III) as manganite. Aragonite was chosen as the primary $CaCO_3$ precipitate as, although thermodynamically unstable with respect to calcite, aragonite has been shown to be the primary $CaCO_3$ precipitate in UK mine water (Bearcock et al, 2006; Bullen, 2007).

The following is the input script used in simulation TM2:

```
TITLE Taff Merthyr O2/CO2 equilibration. Aragonite, Fe(OH)3(a),
Manganite ppt (TM2).
SOLUTION 1 Mean Taff Merthyr DW composition
    temp      11.6
    pH        6.93
    pe        3.0171
    redox     pe
    units     mg/L
    density   1
    Si        4.78
    K         13.04
    Na        15.87
    Ca        101.58
    Mg        42.11
    Mn        0.8
    Sr        0.59
    Cl        10
    S(6)      226.33 as SO4
    Alkalinity 297.7286 as HCO3
    O(0)      3.5
    Fe(2)     6.3
    Fe(3)     2.59
    -water    1 # kg
End
Use solution 1
EQUILIBRIUM_PHASES 2
    Aragonite 0 0
    CO2(g)    -2.523 10
    Fe(OH)3(a) 0 0
    O2(g)     -0.678 10
    Manganite 0 0

End
```

The following is a summary of the output for simulation TM2

```
----------------------------Description of solution----------------

                    pH  =   7.722      Charge balance
                    pe  =  14.095      Adjusted to redox equilibrium
                         Activity of water  =   1.000
                            Ionic strength  =  1.240e-002
                        Mass of water (kg)  =  1.000e+000
                 Total alkalinity (eq/kg)   =  3.304e-003
                        Total CO2 (mol/kg)  =  3.436e-003
                       Temperature (deg C)  =  11.600
                    Electrical balance (eq) = -2.029e-006
 Percent error, 100*(Cat-|An|)/(Cat+|An|)   =  -0.01
                                 Iterations  =  18
                                    Total H  = 1.110172e+002
                                    Total O  = 5.552742e+001
----------------------------Distribution of species----------------
```

Using the above simulation a reduction in Ca concentrations from 101.7 to 76.1 mg L^{-1} was determined at equilibrium, a reduction of 25%. This is much greater than shown in the lagoons or VFR. However, an intensive study of the Taff Merthyr project site on the 11/11/05 (see appendix 2) found that Ca decreased from 94 to 61 mg L^{-1} through one section (section A) of the reed beds. It should also be noted that significantly reduced flow through the reed bed due to a blockage gave elevated retention times, possibly allowing for equilibrationto be fully attained.

The PhreeqC simulations have also shown the Taff Merthyr mine-water to be over-saturated with respect to quartz. This was not included as an equilibrium phase in the model as quartz precipitation is thought to be unlikely in the conditions of the study. Si removal is thought to be more likely attributed to co-precipitation with Fe(III) (hydroxy)oxides.

8.7 VFR performance and System longevity

8.7.1 Determination of VFR ochre depth

Figure 8-51 and Figure 8-52 show the cumulative total Fe and Fe as ochre removed from the 20 mm and 6 mm VFR systems. Due to the difficulties involved in the direct determination of the VFR ochre bed depth, it was necessary to estimate the depth from the cumulative Fe removed as ochre and the ochre solids content. This was done by conversion from cumulative Fe to cumulative ochre removed using the Fe:Ochre ratio of 0.536 determined in section 7.4.1.

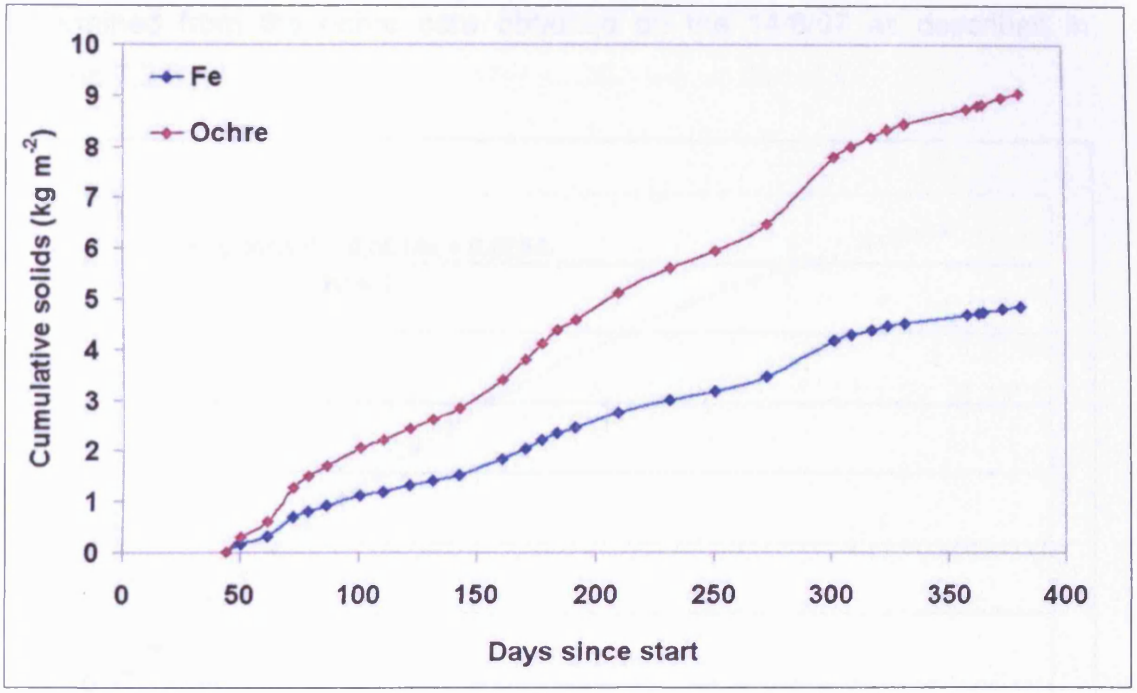

Figure 8-51: Cumulative total Fe and Fe as ochre, removed by the 20 mm VFR

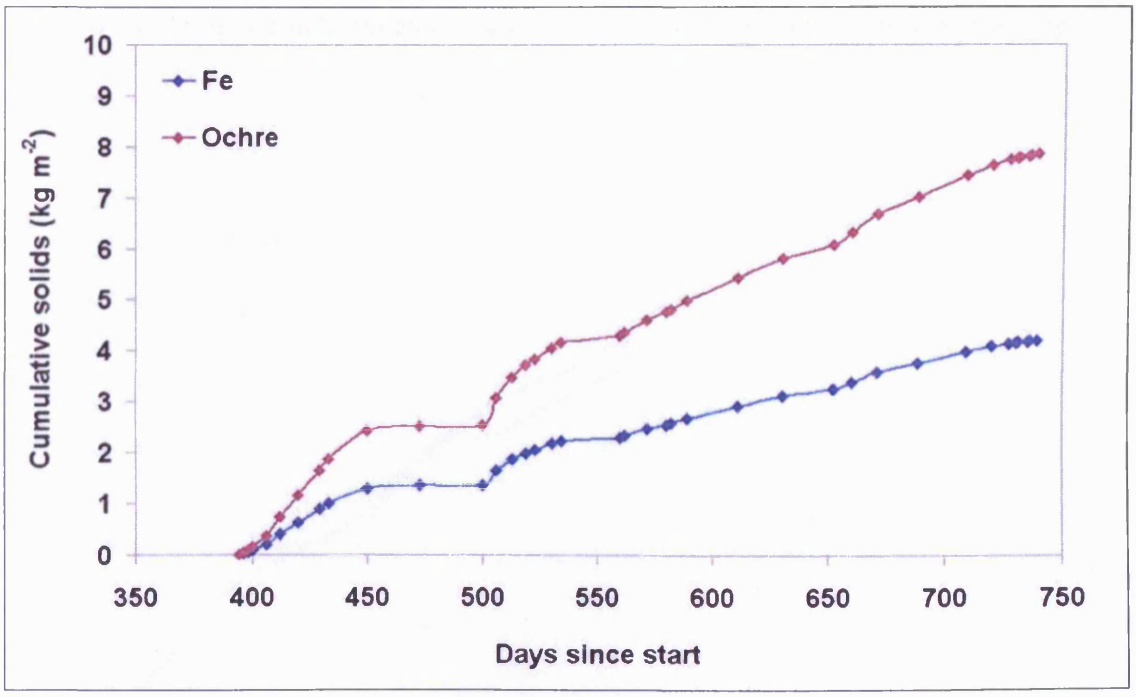

Figure 8-52: Cumulative total Fe and Fe as ochre removed by the 6 mm VFR

Conversion from cumulative ochre removal to ochre depth was achieved using the ochre depth:ochre solids relationship shown in Figure 8-53 and

determined from the ochre core obtained on the 14/6/07 as described in section 7.2.3.

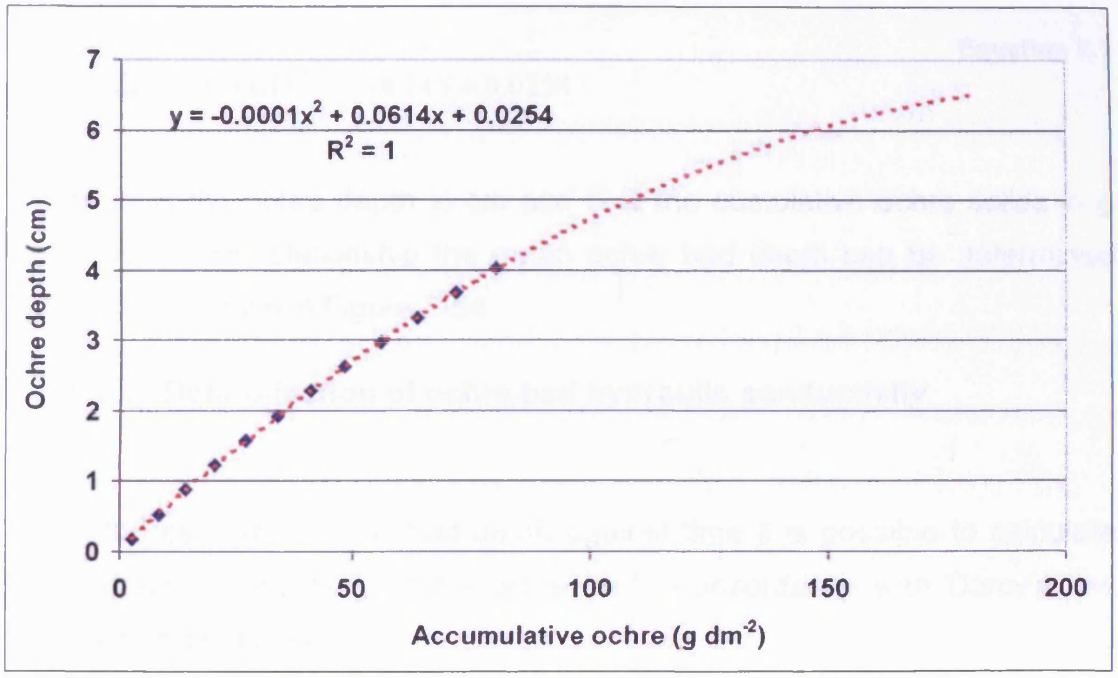

Figure 8-53: Comparison between ochre depth and cumulative ochre from ochre core

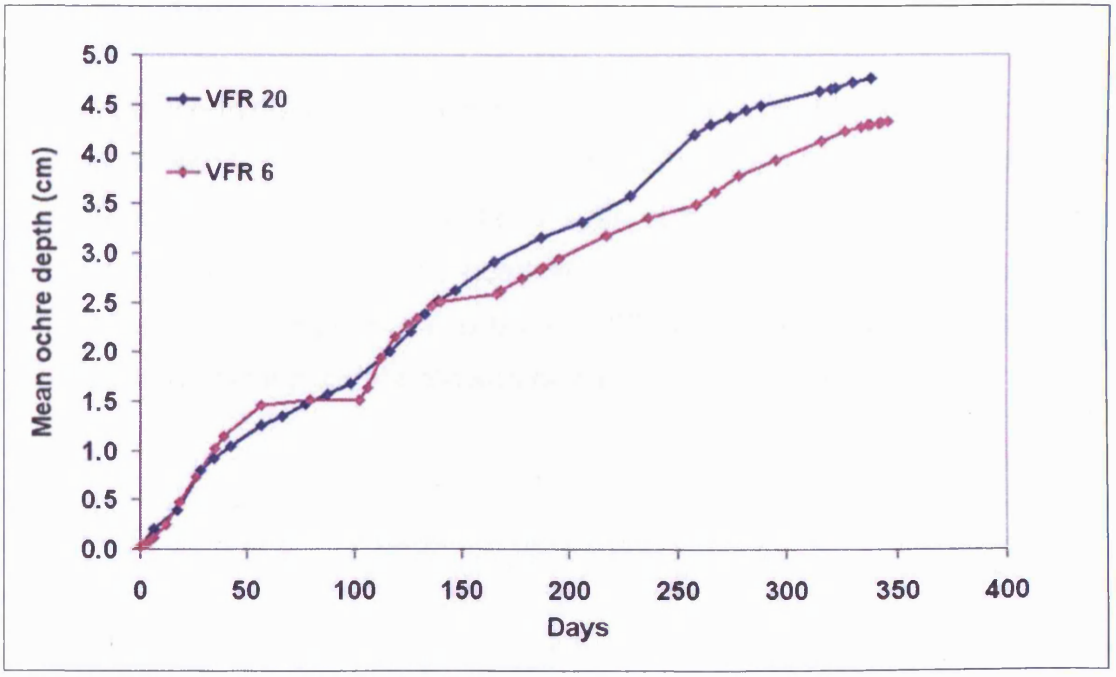

Figure 8-54: Mean bed depth against time for the 20 mm VFR and 6 mm VFR

Where Days are days since first operation of the VFR with either 6 mm or 20 mm gravel beds

The red trend line in Figure 8-53 indicates a second order polynomial fit obtained using Microsoft Excel with the following relationship:

Equation 8.1

$$L_h = -0.0001S^2 + 0.0614S + 0.0254$$

where L_b is the ochre depth in cm and S is the cumulative ochre solids in g dm^{-2}. Using this relationship the mean ochre bed depth can be determined with time as shown in Figure 8-54.

8.7.2 Determination of ochre bed hydraulic conductivity

Using the estimate of VFR bed depth against time it is possible to calculate the hydraulic conductivity of the ochre bed in accordance with Darcy's law using Equation 8.2 as:

Equation 8.2

$$k = \frac{QL_h}{A\Delta H}$$

where k is the hydraulic conductivity in m sec^{-1}, Q is the flow rate through the VFR in m^3 sec^{-1}, L_b is the thickness of the VFR ochre bed in m determined from Equation 8.1, A is the x-sectional area of the VFR ochre bed in m^2 and ΔH is the change in hydraulic head across the ochre bed in m. Hydraulic conductivities for the 20 mm and 6 mm VFR beds are shown in Figure 8-55 where the availability of data allowed calculation.

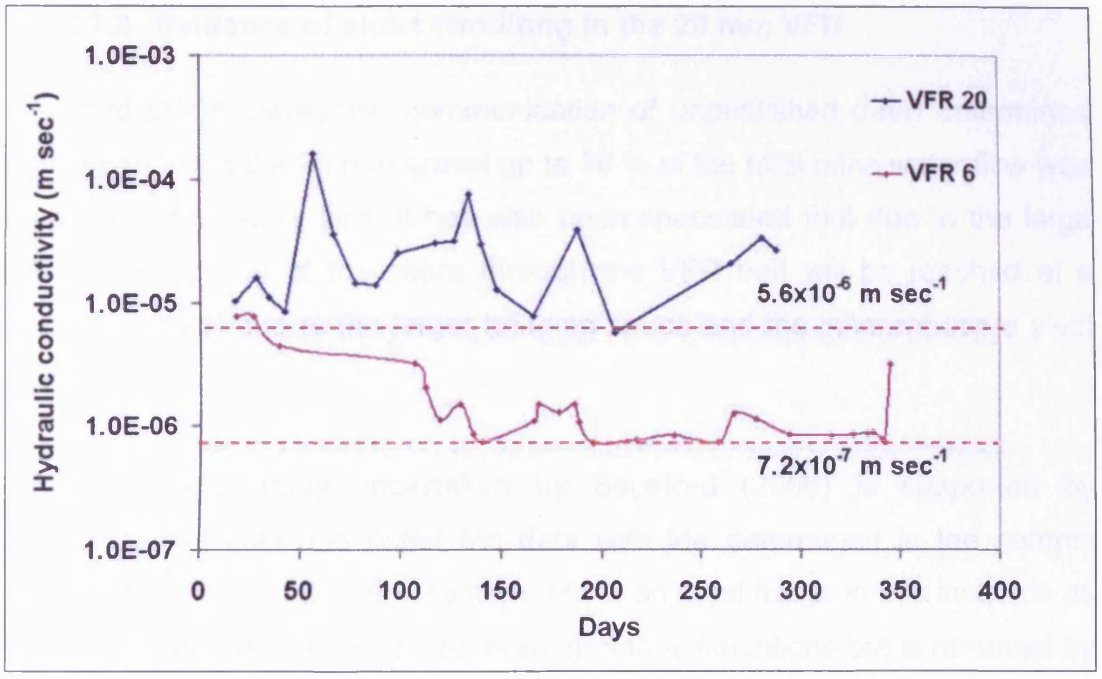

Figure 8-55: Hydraulic conductivity determined for the 20 mm VFR and 6 mm VFR

Mean values of k for the 20 mm and 6 mm VFR systems were determined as $3.14x10^{-5}$ and $1.83x10^{-6}$ m sec^{-1} respectively. A large variability is seen in the 20 mm VFR k value with an SD value of $3.49x10^{-5}$ m sec^{-1}. This is thought to be due to the development of piping and short circuiting around the ochre bed. Therefore, the observed minimum k value of $5.6x10^{-6}$ m sec^{-1} is thought not to reflect the true ochre hydraulic conductivity but to be an artificially high value that takes into account additional permeability of the short circuits. The minimum k value of $7.2x10^{-7}$ m sec^{-1} determined for the 6 mm VFR ochre bed, is thought to be a more realistic determination of the true ochre bed permeability. The 6 mm VFR k value shows greater consistency in measurements and only low variability after 125 days. It is possible that the lower 6 mm VFR k value after 125 days is due to compression of the ochre bed corresponding to high flow rates at 106 days. This would act to increase the vertical bed load and decrease the voids ratio, as k is directly dependant on the voids ratio.

8.7.3 Evidence of short circuiting in the 20 mm VFR

Sapsford (2006, personnel communication of unpublished data) determined that, when using the 20 mm gravel up to 30 % of the total mine water flow was by-passing the ochre bed. It has also been speculated that due to the large gravel size, piping of the ochre through the VFR bed will be reached at a much lower ΔH due to the larger bridging space and the inherent ochre yield strength.

The theoretical study undertaken by Sapsford (2006) is supported by comparison of inlet and outlet Mn data with Mn determined in the sample ports installed within the VFR system. Mn is an ideal tracer in this instance as it is a conservative element under homogeneous conditions but is removed by the VFR bed. Figure 8-56 shows the mean concentrations of total Mn recorded on different sampling days for the VFR sample ports. High indicates the high level sample ports, 0.5 m above the VFR ochre bed, low indicates the low sample ports positioned within the VFR gravel bed and below the ochre bed. Inlet and outlet concentrations are reported for comparison as is the surface water concentrations when determined.

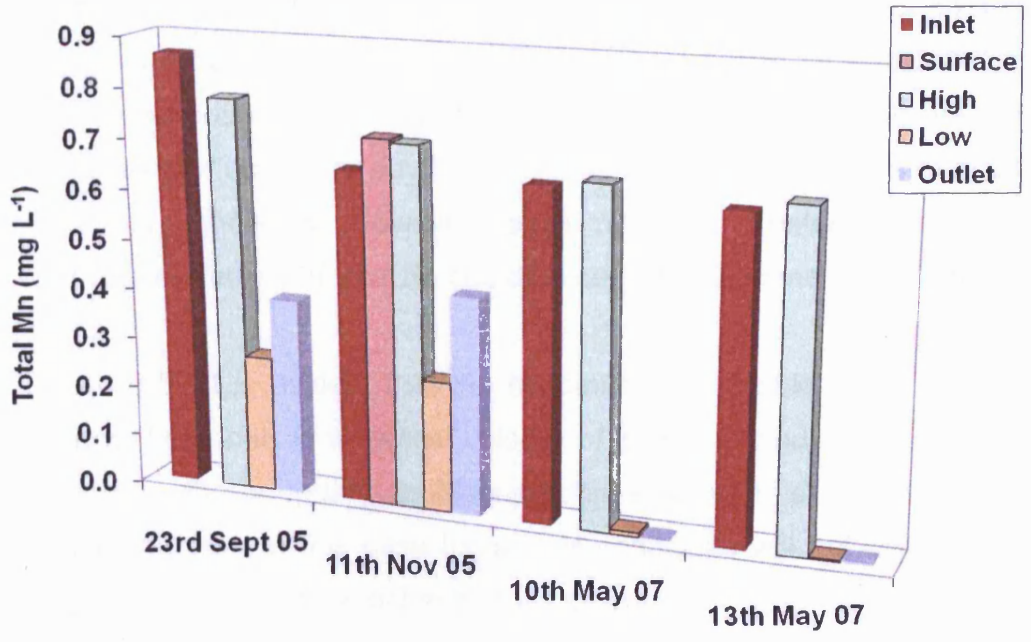

Figure 8-56: Mean VFR sample port data for total Mn

Samples taken on the 23/9/05 and the 11/11/05 are taken during VFR operation with the 20 mm gravel support whilst 10/5/07 and 13/5/07 are during operation with 6 mm gravel. It can be seen that, in the 20 mm VFR the outlet concentrations are higher than the low sample port concentrations. If all flow was passing through the ochre bed it would be expected that the observed outlet Mn concentration would be equal to, or lower than, the mean low sample port concentrations. Therefore, there is clearly a proportion of the mine water by-passing the VFR ochre bed. In the 6 mm VFR data the outlet Mn is lower than the mean low sample port concentrations. This indicates that all of the flow is passing through the ochre bed. In addition, in the 20 mm VFR, outlet Mn concentrations are roughly 25-30 % higher than the low sample port data. This strongly supports the findings of Sapsford (2006).

8.7.4 Estimating VFR size requirements

Figure 8-57 shows the relationship between vertical velocities in m day^{-1}, head difference (delta H) in m and the total Fe concentration (expressed as the relative bubble size) for the 6 mm VFR. The red line indicates the hypothesised boundary above which all data points show evidence of bed scour and associated high total Fe concentrations. Below this boundary all data point show low total Fe concentrations however the edges of this boundary have not been proven in the field and a blue boundary is included to show the proven boundary conditions. It can be seen that in the current trial vertical velocities of up to 4 m day^{-1} were attained with good total Fe removal under low ΔH conditions. However, once ΔH was greater than 0.6m, significant concentrations of total Fe could be seen at this same flow regime.

From Figure 8-57 it is evident that the maximum sustainable flow condition without further field trials is a vertical velocity of 2 m day^{-1} and a ΔH of 1 m. It is unknown how the boundary conditions behave above this point and may well decrease further. In this case higher ΔH conditions will not be attained without significant scour of the ochre bed via piping.

Using the maximum vertical velocity of 2 m day^{-1} it is possible to determine the required treatment area for a particular discharge using the following relationship:

Equation 8.3

$$A = \frac{Q}{V}$$

where A is the required treatment area in m^2, Q is the maximum mine water discharge in m^3 day^{-1} and V is the maximum vertical velocity allowable for the VFR system. This is presuming a 6 mm gravel support bed is used with a vertical velocity of 2 m day^{-1}.

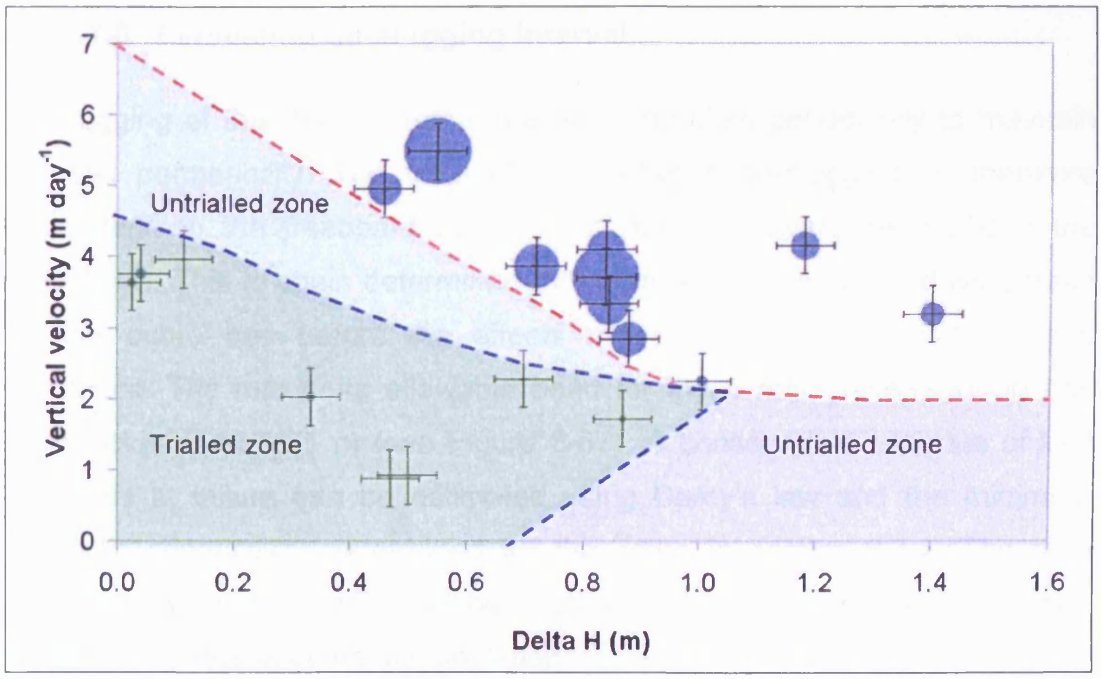

Figure 8-57: Comparison of vertical velocity (Area Adjusted Flow Rate) against head difference for the 6 mm VFR

Size estimates for a VFR system for treatment of the total Taff Merthyr discharge have been determined as follows. First a conservative estimate for the maximum mine water flow through the Taff Merthyr treatment site was determined. This was calculated by taking the maximum recorded mean weekly flow rate (180.46 L sec^{-1} determined from weekly pumping hours run) and multiplying by 1.25 (to give a 25 % contingency limit). This equates to a maximum flow of 225.57 L sec^{-1} or 19489.68 m^3 day^{-1}.

Using Equation 8.3 a value for A can be calculated at 9,744.84 m^2 for the required treatment area of a VFR system to treat the entire Taff Merthyr mine water discharge. This would take into account worst case conditions, and removal of Fe and Mn concentrations to less than 1 and 0.5 mg L^{-1} respectively. The current Taff Merthyr treatment site occupies 30,000 m^2 (Coal Authority, 2002), 3 times the area required by an equivalent VFR treatment system. In this model no allowance has been taken into account for additional water volume from rainfall events. However, it is thought that the contribution by rainfall would be negligible and a maximum of 1000 m^3 day^{-1} of extra throughput could be expected. This would be covered by the 25 % contingency limit.

8.7.5 Estimating de-slugging interval

De-slugging of the VFR system must be undertaken periodically to maintain the bed permeability. The time interval between de-slugging, is therefore dependant on the freeboard available to develop driving head above the gravel bed. This is again determined by the maximum allowable driving head for the ochre bed before the effects of bed scour and piping become significant. The maximum allowable head for the 6 mm gravel support has been determined as 1 m (see Figure 8-57). A conservative estimate of bed thickness at failure can be estimated using Darcy's law and the minimum hydraulic conductivity determined for the ochre in section 8.7.2. The time interval between de-slugging will be dictated by the inlet Fe concentration and therefore the rate of ochre accumulation.

In accordance with Sapsford (2007), and using the field data determined in this chapter, Figure 8-58 was constructed. This shows the relationship between the BTI coefficient of permeability and the cumulative Fe removed from the VFR system with the following relationship:

Equation 8.4

$$BTI = kFe_{(\cdot}^{-\beta}$$

where BTI is the Bed Thickness Independent coefficient of permeability (see Section 5.2.4) in sec^{-1}, k is a constant in $m^2\ kg^{-1}\ sec^{-1}$ with a value of $3x10^{-4}$, Fe_c is the cumulative Fe removed in kg m^{-2} and β is the fitting constant with a value of 1.9327. Figure 8-58 shows determined values of BTI coefficient of permeability in sec^{-1} against the cumulative Fe removed from the 6 mm VFR system in kg m^{-2} of ochre bed.

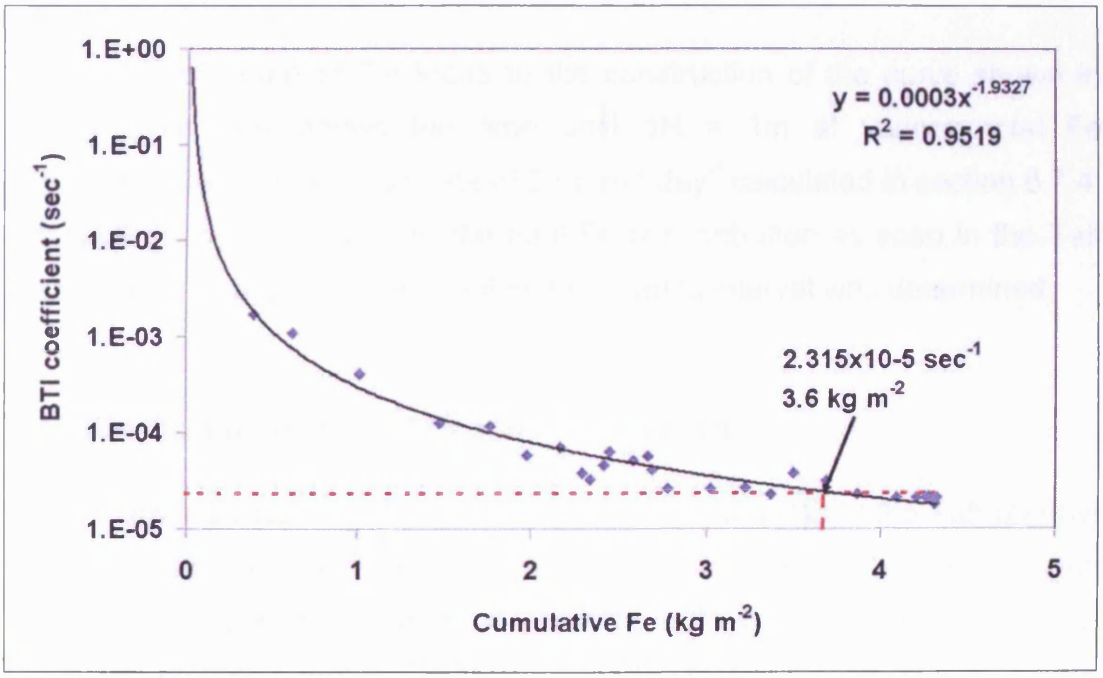

Figure 8-58: BTI permeability coefficient against Fe removed in the 6 mm VFR

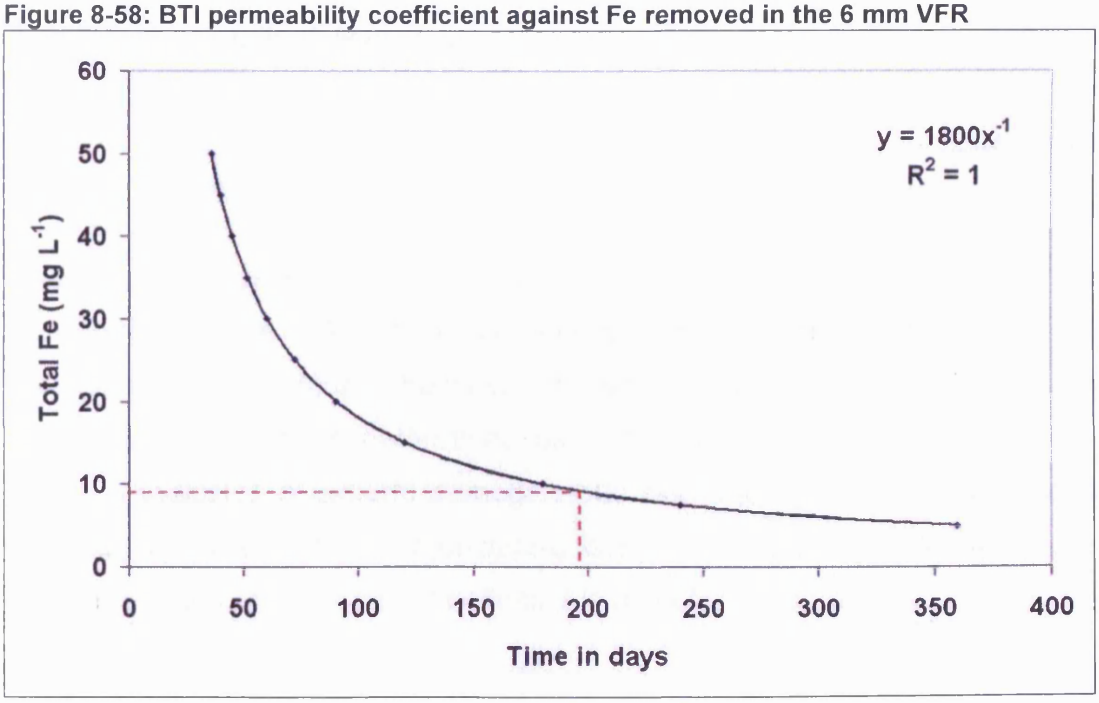

Figure 8-59: Calculated time until the head difference = 1 m for an area adjusted flow rate of 2 $m^3\ m^{-2}\ day^{-1}$

The red dashed line in Figure 8-58 shows the interception point and value of the BTI and Fe_c at which system overtopping will occur. This is calculated using the ideal parameters of, 1 m of available freeboard, a total inlet Fe concentration of 9.6 mg L^{-1}, and a flow of 2 m^3 m^{-2} day^{-1}, as determined for the Taff Merthyr discharge. In this case, the BTI coefficient of permeability at overtopping is $2.315x10^{-5}$ sec^{-1} equating to 3.6 kg m^{-2} of ochre solids.

Application of Equation 8.4 leads to the construction of the curve shown in Figure 8-59. This shows the time until ΔH = 1m at varying total Fe concentrations using the flow rate of 2 m^3 m^{-2} day^{-1} calculated in section 8.7.4. On application of the curve to the total Fe concentration as seen in the Taff Merthyr site, an approximate 200 day de-slugging interval was determined.

8.8 Kinetic assessment of Fe and Mn oxidation

In the following section, the rate of oxidation of Fe and Mn in the Taff Merthyr treatment systems is examined. In each case both pH and oxygen concentrations are presumed to be constant and oxidationto be pseudo first order with respect to Fe(II) and Mn(II). Pseudo first order rate constant were determined using the following equation

Equation 8.5

$$k_x = \frac{-\ln(C_{out}/C_{in})}{t}$$

where k_x is the pseudo first order rate constant in sec^{-1}, C_{in} and C_{out} are the concentration of Fe or Mn at the inlet and outlet to the system in M and t is the reaction time in sec. In this thesis k_x can either be, k_{HRT}, k_1 or k_2, where k_{HRT} is used where the rate is determined using the nominal Hydraulic Retention Time, k_1 indicates a generic homogeneous rate and k_2 indicates a generic heterogeneous rate. The nomenclature is not defined independently for Fe and Mn and the same constant definition is used for simplicity.

8.8.1 Fe(II) oxidation kinetics

8.8.1.1 Kinetics of homogeneous Fe(II) oxidation at Taff Merthyr lagoons and VFR

Homogeneous pseudo first order oxidation rates for Fe(II) in the Taff Merthyr mine water were determined using two methods a) from monitoring data obtained from the lagoons (using Equation 8.5), and b) by means of field oxidation rate experiments as determined by Sapsford (2007) in accordance with Section 5.4. From the Equation 8.5 second order rate constants were determined using the associated rate expression:

Equation 8.6

$$-\frac{d[Fe(II)]}{dt} = \frac{k_1'[Fe(II)][O_2]}{[H^+]^2}$$

where [ ] indicates concentration in M and k_1' is the rate constant in M sec^{-1}.

In general the agreement between rates determined by the above two methods was good and within the limits of the standard deviation of each method (see Table 8.1; Section 8.8.1.2 and Appendix 2). In comparison the pseudo first order rate constant as determined in this work (Section 10.2.1) and in the literature (for example, Stumm and Morgan, 1996) is approximately one order of magnitude greater than the field rate determined in this study. Reasons for the differences between field and laboratory rates are discussed fully in Chapter 3. However, possible reasons could be due to elevated sulfate and organic acid concentrations in the field as opposed to the laboratory.

8.8.1.2 Kinetics of heterogeneous Fe(II) oxidation at Taff Merthyr VFR

Both homogeneous and heterogeneous oxidation rates must be taken into account in the VFR system. The homogeneous rate constant (k_1) determined by Sapsford (2007) was shown to hold true for the settlement lagoons, and is therefore considered to be applicable for the homogeneous oxidation in the VFR system (above and below the ochre bed).

Determination of the heterogeneous rate constant (k_2) for Fe(II) oxidation in the VFR ochre bed has been treated thoroughly by Sapsford (2007) who split the VFR system into three separate reactors (as shown in Figure 8-60). These were the treatment tank above the ochre bed (Reactor 1), the ochre bed itself (Reactor 2), and the under-drain and up-flow tank (Reactor 3), and it is assumed that flow within the ochre bed is of plug flow type. Computational Fluid Dynamics (CFD) modelling work of flow through the VFR conducted by Reid (2006) has shown that the treatment tank above the ochre bed is almost completely mixed and behaves in analogous to a Constantly Stirred Tank Reactor (CSTR). This is confirmed by spatial comparison of Fe(II) and Mn(II) concentrations within the VFR which show Reactor 1 concentrations to be relatively uniform (see Section 8.7.3 and Appendix 2)

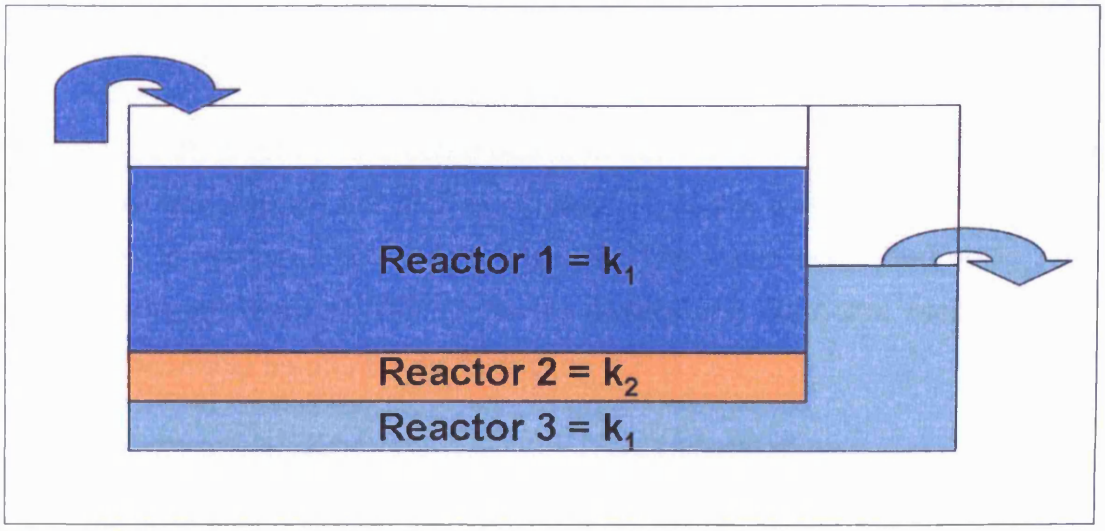

Figure 8-60: Schematic cross section through the VFR showing three idealised reactors

(after Sapsford, 2007)

In accordance with Sapsford (2007) the concentration of Fe(II) at the outlet from reactor 1 was determined using the CSTR equation as follows:

Equation 8.7

$$C_1 = \frac{QC_{in}}{Q + k_1 V_1}$$

where C_1 is the concentration of Fe(II) in the Reactor 1 effluent in mg L^{-1}, C_{in} is the influent concentrationto reactor 1 in mg L^{-1}, Q is the flow rate through

the VFR in L sec^{-1}, k_1 is the pseudo first order homogeneous rate constant in sec^{-1} and V_1 is the volume of reactor 1 in L. Reactor 2 was treated as a plug flow type reactor in each case, and the following equation was used:

Equation 8.8

$$C_2 = C_1 e^{-k_2 t_b}$$

where C_1 is the effluent concentration from Reactor 1 in mg L^{-1}, C_2 is the effluent concentration from the ochre bed (reactor 2) in mg L^{-1}, k_2 is the pseudo first order oxidation rate for Fe(II) in the VFR bed in sec^{-1} and t_b is the VFR bed travel time in sec. t_b was determined as follows:

Equation 8.9

$$t_b = \frac{L_b}{Q / A_b} e_b$$

where L_b is the depth of the ochre bed in m determined using Equation 8.1, Q is the flow rate through the VFR in m^3 sec^{-1}, A_b is the area of the VFR bed in m^2 and e_b is the mean VFR bed voids ratio. The mean ochre bed voids ratio was determined from the VFR ochre dry density and the ochre depth - ochre solids relationship as mentioned in section 8.7.1.

Reactor 3 was modelled as both plug flow and CSTR type reactors. Plug flow uses the plug flow equation as used for the VFR ochre bed but substitutes t_b with the nominal HRT (determined for Reactor 3, in sec^{-1}). Also, k_2 is substituted with k_1. The Solver tool included with Microsoft Excel was used to determine k_2 in each example for the field data as shown below:

Equation 8.10

$$C_{1Field} \xrightarrow{k1} C_2 \xrightarrow{k2} C_3 \xrightarrow{k1} C_{4Calc} \cong C_{4Field}$$

Solver was set to adjust the value of k_2 until $(C_{4Calc}-C_{4Field})^2$ was equal to zero. This was done for both the 20 mm and 6 mm VFR beds. It was not possible to reach a conclusion with the 20 mm VFR due to the extensive short circuiting around the ochre bed and therefore discrepancies in the concentration

retention time relationship. The results of k_2 determined using the above method are shown in Figure 8-61. Pseudo first order rates determined using the three modelling methods (CSTR-PLUG-CSTR, CSTR-PLUG-PLUG, and PLUG-PLUG-PLUG) and the overall pseudo first order rate determined using the HRT are included for comparison.

It is evident that the CSTR-PLUG-PLUG and CSTR-PLUG-CSTR rate constants generally agree well indicating that the model has a low sensitivity to the way in which to Reactor 3 is modelled, and further confirms the findings of Reed (2007) and data from the current study that Reactor 1 behaves as a CSTR. In addition, the PLUG-PLUG-PLUG rate constants generally do not agree well with the CSTR-PLUG-PLUG and CSTR-PLUG-CSTR models. This is expected as it has been shown that Reactor 1 does not behave as a plug flow system and this will therefore not be discussed further.

It has been found that the values of k_2 calculated using the above models decrease with increasing ochre depth. A similar decrease is observed in the overall rate constant (k_{HRT}) which Sapsford (2007) attributed to a reduction in the intimacy of the contact between mine water and ochre, with increasing compression of the ochre bed.

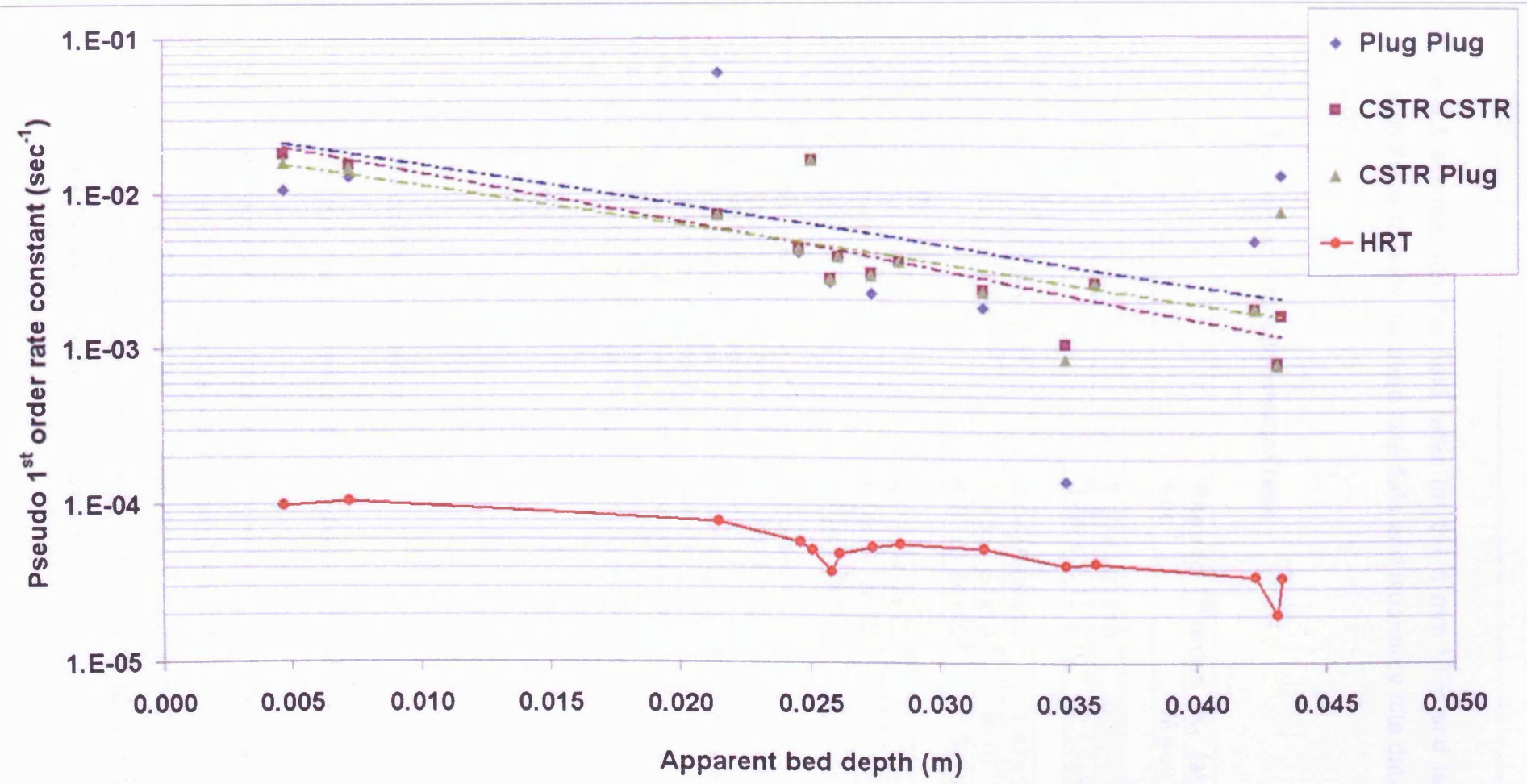

Figure 8-61: Heterogeneous pseudo first order rate constants determined in the 6 mm VFR using CSTR-CSTR, CSTR-PLUG and PLUG-PLUG models.

Where CSTR-CSTR is CSTR-PLUG-CSTR; CSTR-Plug is CSTR-PLUG-CSTR; and Plug-Plug is PLUG-PLUG-PLUG configurations for Reactors 1, 2 and 3 respectively. HRT indicates the pseudo first order rate constant determined using the nominal Hydraulic Retention Time within the entire VFR.

Table 8.1 summarises the field rates for the 6 mm VFR and lagoons and compares these to both literature rate data and laboratory rate data derived in this study.

Table 8.1: Summary of VFR Fe(II) oxidation rates

	Pseudo 1st order	**K_1' (at 25°C)**
	sec^{-1}	**M sec^{-1}**
HRT		
6 mm VFR k_{HRT}	$7.37\pm3.02\times10^{-5}$	
Lagoon k_{HRT}	$3.66 \pm 2.15 \times 10^{-5}$	$2.13\pm6.13 \times 10^{-14}$
Homogeneous (k_1)		
Sapsford (2007) – lagoonal [a,c]	$4.04\pm5.98\times10^{-5}$	$1.47\pm1.4\times10^{-14}$
Stumm and Morgan (1996) [b,c]	$3.45\pm2.84\times10^{-4}$	5×10^{-14}
This study [d,c]	$4.07\pm3.34\times10^{-4}$	5.897×10^{-14}
Heterogeneous (k_2)		
VFR Bed PP method [e]	$4.79\pm14.7\times10^{-2}$	
VFR Bed CC method [f]	$5.69\pm5.75\times10^{-3}$	
VFR Bed CP method [g]	$5.86\pm5.29\times10^{-3}$	

± error indicates standard deviation of multiple measurements
[a] k_1 calculated using the rate constant k_1' from Sapsford (2007) for field conditions and temperatures determined during lagoonal monitoring
[b] k_1 calculated using the rate constant k_1' from Stumm and Morgan (1996) for field conditions and temperatures determined during lagoonal monitoring
[c] k_1 determined from k_1' at the Taff Merthyr mine water temperature using the activation energy of 25500 Cal/mol as reported by Dempsey et al, 2001.
[d] k_1' determined in this study from homogeneous laboratory experimentation (see Section 10.2.1)
[d] PLUG-PLUG-PLUG
[e] CSTR-PLUG-CSTR
[f] CSTR-PLUG-PLUG

8.8.2 Mn oxidation kinetics

8.8.2.1 Kinetics of homogeneous Mn oxidation at Taff Merthyr

Pseudo first order oxidation rates were determined for Mn using Equation 8.5 and as with Fe(II), the lagoons were treated analogous to a homogeneous reactor (method a; Section 8.8.1.1). This data were compared to the pseudo first order rate calculated using the constant devised by Morgan (1964) (see Table 8.2) and the associated rate expression:

Equation 8.11

$$\frac{-d[Mn]}{dt} = \frac{k_1'[Mn][O_2]}{[H^+]^2}$$

where [Mn] is the aqueous concentration of Mn in M and k_1' is the second order rate constant in M sec^{-1}, which is taken to be $4.63x10^{-21}$ M sec^{-1} at 25°C (Morgan, 1964, 1967). In this study aqueous Mn is taken to be equal to Mn(II) Interestingly k_1 determined using dissolved Mn concentrations in the Taff Merthyr lagoons is 3 orders of magnitude greater than predicted using Equation 8.11 (see Table 8.2).

Table 8.2 also shows the literature values as determined by Diem and Stumm, 1984; and Zhang et al, 2002 for microbial catalysed Mn oxidation. Interestingly the value of k_1 determined in the field at the Taff Merthyr site is within the range of readings reported by Diem and Stumm (1984) and Zhange et al (2002) and is not consistent with direct abiotic homogeneous oxidation of Mn and precipitation of Mn(III,IV) (hydroxy)oxides (where half lives are in the order of 183 years; Morgan, 1964, 1967).

In laboratory experiments Hem (1963), found a significant reduction in dissolved Mn(II) in the presence of freshly precipitated $Fe(OH)_3$ above pH 7. He attributed this to co-precipitation of Mn(II) with Fe. Nuttal (2003) also observed that up to 20 % of an initial 1 to 4 mg L^{-1} Mn load was removed in a conventional settlement lagoon, with a nominal HRT of 24 hours and 40 mgL^{-1} of influent Fe. He attributed this removal to adsorption of Mn(II) onto precipitating Fe(III) (hydroxy)oxide particles.

Qualitatively the 20 % removal of 1 mg L^{-1} Mn observed by Nuttal (2003) in the presence of 40 mg L^{-1} Fe is equivalent to the 5 % removal of 0.8 mg L^{-1} Mn in the presence of 10 mg L^{-1} of total Fe as observed here. For this reason it is possible that Mn removal from the lagoons may be by adsorption alone. Indeed, based on the mean value of 3.74 mg L^{-1} total Fe removal, and an Fe to ochre content of roughly 50 %, it can be assumed that approximately 7.5 mg L^{-1} of ochre solid is removed from the mine-water within the lagoons.

Based on the BET surface area of 247 m^2 g^{-1} (see Table 7.1) and the surface site concentration of 2.27 sites per nm^{-2} (Liger et al, 1999), it is possible to calculate the concentration of surface sites as available per L of Taff Merthyr mine water in the lagoons to be $7x10^{-6}$ M. As the molar concentration of Mn removed from the system is $9x10^{-7}$ M, and therefore there is 7.7 moles of surface sites removed from the system to every mole of Mn.

A similar portion of suspended Fe(III) (hydroxy)oxide leaves the lagoon as is retained in it, and could explain the difference of $1x10^{-6}$ M between total and filtered Mn in the discharge. The ratio of Mn removed to Fe removed as ochre in the lagoons is 5.34 mg(Mn) g^{-1}(Ochre) which agrees well with the ratio of Mn to Ochre in ochre samples collected from the base of the lagoons (4.2 mg(Mn) g^{-1}(Ochre) see Section 7.4.1).

Without determination of the valance of the potentially adsorbed Mn species, it is not possible to determine whether adsorption promotes rapid oxidation of Mn. Work by Sung and Morgan (1981) showed γ-FeOOH (lepidocrocite) at a concentration of $1x10^{-3}$ M to be an effective catalyst for Mn(II) oxidation. He studied the effect at pH between 8 and 9, and found that the oxidation rate increased with increasing pH and γ-FeOOH concentration.

Some important considerations that should be taken into account when discussing Mn removal from the settlement lagoons is that the total removal is only in the order of 5 % of the total Mn load and that measured differences are within the ± 10 % range of the ICP-AES error, however the observed vales do form a trend that was observed in 18 out of 21 cases of filtered samples and 20 out of 21 case of total samples making the observed removal to be unlikely caused by experimental or human error.

8.8.2.2 Kinetics of Heterogeneous Mn oxidation at Taff Merthyr

The calculation of Mn oxidation within the VFR bed is simplified by the slow kinetics of homogeneous oxidation (as determined in the lagoons). Due to the slow homogeneous rate it is possible to allocate greater than 95 % of the

removal to mechanisms occurring in the ochre bed itself. As with the lagoons, pseudo first order kinetics were assumed and Mn removal rate constants were determined from calculated nominal HRT.

Figure 8-62 shows k_{HRT} in sec^{-1} plotted on a log scale against cumulative ochre in g m^{-2} for the 20 mm and 6 mm VFR systems. The mean k_{HRT} for the lagoons is also plotted for comparison. The exponential trend line shows that k_{HRT} increases exponentially with increasing ochre removed.

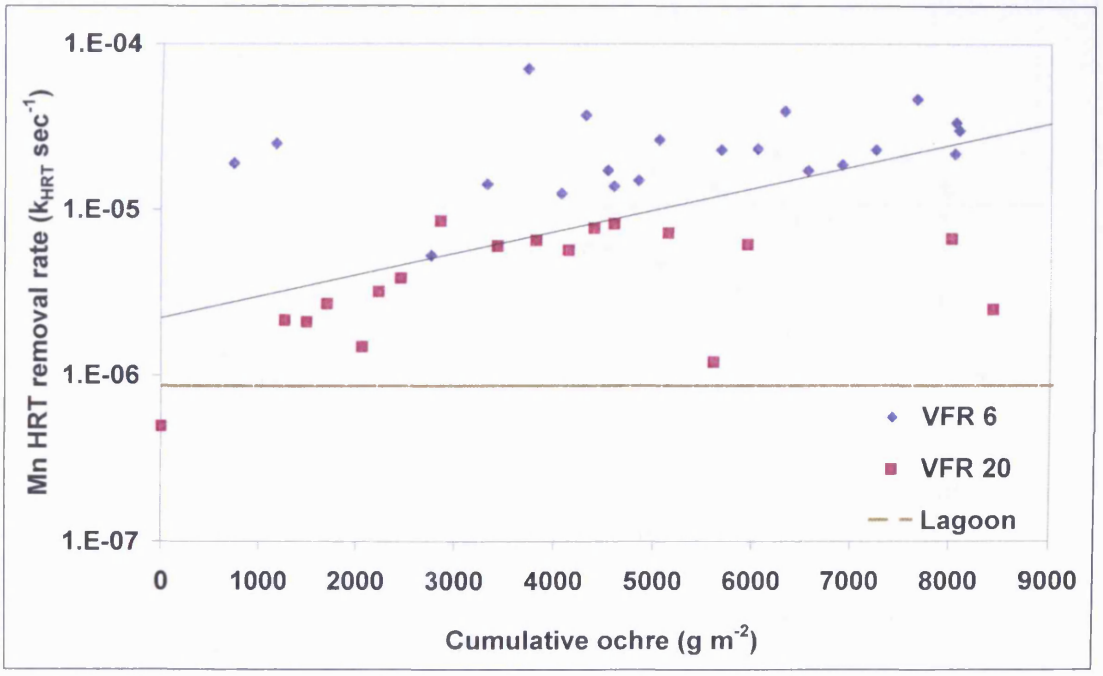

Figure 8-62: Pseudo first order removal rate constants (k_{HRT}) against cumulative ochre removed for the 20 mm VFR and 6 mm VFR

Allowing for the accumulation of ochre in the VFR the rate expression can be adjusted to incorporate an ochre corrected rate constant k'_{HRT} in g^{-1} m^2 sec^{-1} and in accordance with the expression:

Equation 8.12

$$\frac{-d[Mn]}{dt_{HRT}} = k'_{HRT}\,[Mn]Ochre$$

Where Ochre is the amount of ochre per unit area of bed in g m^{-2} and where k'_{HRT} in g^{-1} m^2 sec^{-1} is related to k_{HRT} in sec^{-1} as follows:

Equation 8.13

$$k'_{HRT} = \frac{k_{HRT}}{Ochre}$$

Figure 8-63 shows k'_{HRT} in g^{-1} m^2 sec^{-1} plotted against the cumulative ochre removed for the 6 mm and 20 mm VFR systems.

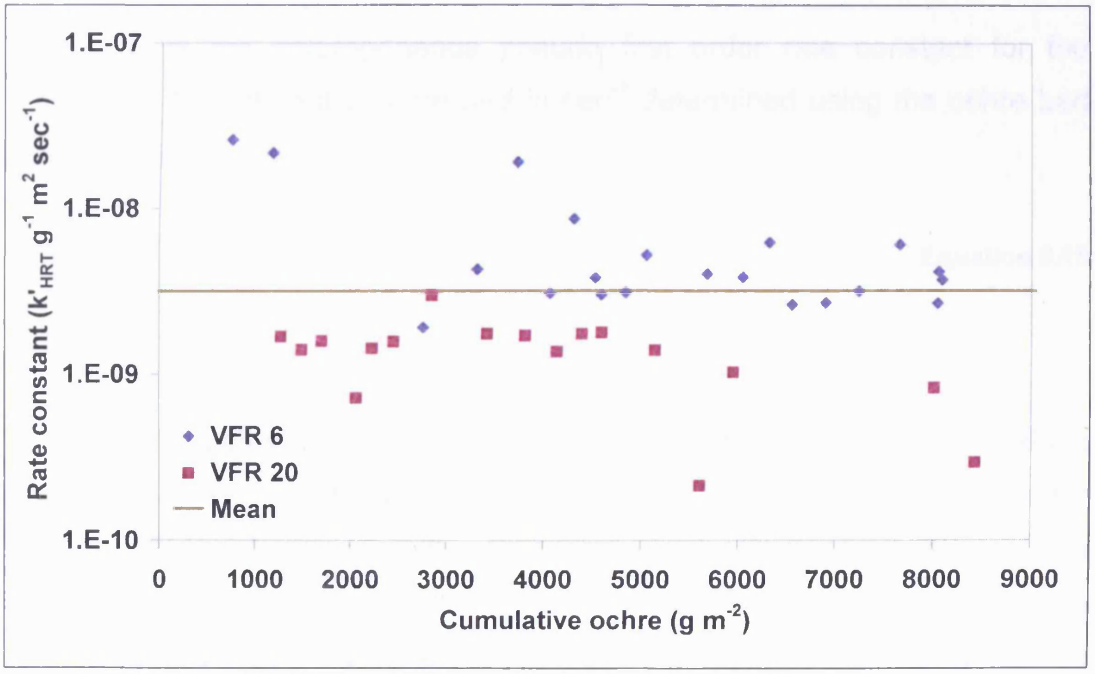

Figure 8-63: Ochre corrected Mn removal rate constant against cumulative ochre removed for the 20 mm VFR and 6 mm VFR

The ochre corrected value of k'_{HRT} is fairly constant and independent of cumulative ochre with a mean and SD of $2.69 \pm 2.01 \times 10^{-9}$ g^{-1} m^2 sec^{-1}. The slightly lower values of k'_{HRT} recorded for the VFR 20 mm bed are probably due to short circuiting (see Section 4.5.9) as this would lead to less Mn being removed than would be expected if flow was primarily through the bed.

From the evaluation of the relationship between k_{HRT} and cumulative ochre, it is possible to determine that removal of Mn from the system is due almost exclusively to processes occurring within the ochre bed. As the rate constants $k_{HRT,}$ and k'_{HRT} are true only for the Taff Merthyr VFR system as they take in to account the total VFR HRT. Using these constants within a system with a

larger water to bed volume ratio, would greatly overestimate removal (and vice versa). A true rate constant, for universal use, takes into account HRT within the ochre bed itself and can be formulated as follows:

Equation 8.14

$$\frac{-d[Mn]}{dt} = k_2[Mn]$$

Where k_2 is the heterogeneous pseudo first order rate constant for the removal of Mn within the ochre bed in sec^{-1} determined using the ochre bed travel time as follows:

Equation 8.15

$$t_h = \frac{l}{V} R_v$$

where l is the ochre depth in m, V is the vertical velocity in m sec^{-1} and R_V is the ochre voids ratio. The value l was determined from the cumulative ochre removal and determined ochre solids content. R_V was determined in accordance with the methods listed in Section 6.3.1. A mean and SD for k_2 was determined as $1.9 \pm 0.87 \times 10^{-3}$ sec^{-1}. In the narrow range of conditions encountered in the VFR system, this value was found to be largely independent of pH, temperature and dissolved oxygen.

Figure 8-64 shows k_2 in sec^{-1} against cumulative ochre removal in g m^{-2} for the 20 mm and 6 mm VFR systems, together with the mean value of k_2. As with the values of k'_{HRT} in Figure 8-63 the calculated rate constants are largely independent of cumulative ochre. Interestingly the Mn oxidation rates do not share the same trend of decreasing removal rate with increasing ochre removed as with Fe(II) removal.

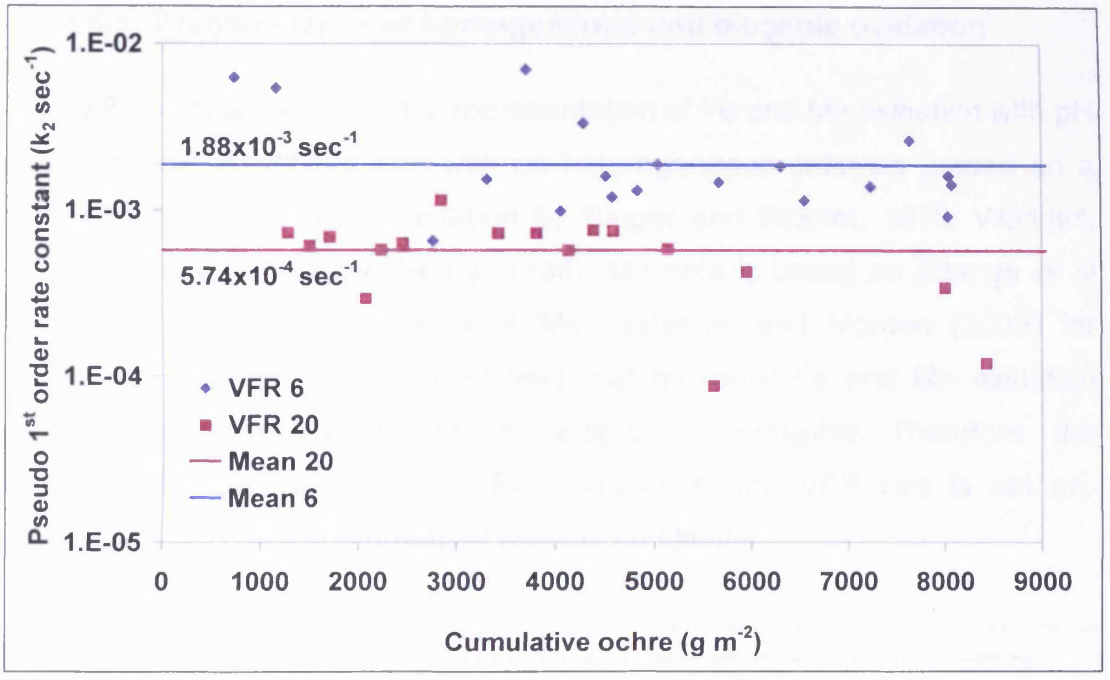

Figure 8-64: Mn bed removal rate (k_2) against cumulative ochre for the 20 mm VFR and 6 mm VFR

The lines indicate mean values for each data set (where Mean 20 is for the 20 mm VFR and Mean 6 is for the 6 mm VFR)

Table 8.2 summarises the rate constants obtained in the lagoons and VFR. Literature values for abiotic homogeneous oxidation and homogeneous microbial oxidation are shown for comparison.

Table 8.2 Summary of VFR Mn removal rates

	Pseudo 1st order	K_2' (25°C)
Homogeneous	**sec^{-1}**	**M sec^{-1}**
L1 and L2 Lagoons (k_{HRT})	$8.64 \pm 7.23 \times 10^{-7}$	
Morgan (1964, 67) [a]	1.2×10^{-10}	4.63×10^{-21}
Heterogeneous		
6 mm VFR bed rate (k_2)	$5.74 \pm 0.87 \times 10^{-3}$	
20 mm VFR bed rate (k_2)	$1.88 \pm 0.87 \times 10^{-3}$	
Homogeneous microbial oxidation		
Diem and Stumm (1984) [b,c]	2.43×10^{-7}	
Diem and Stumm (1984) [b,d]	8.17×10^{-7}	

[a] *Conditions pH 6.93, $O_{2(aq)}$ 8.5 mg L^{-1}, 25°C.*
[b] *values of k' determined for solutions of lake water from Lake Zurich, Switzerland with addition of suspensions of "Mn oxidising bacteria" of*
[c] *1 mL per L and*
[d] *5 mL per L*

8.8.3 Predominance of homogeneous and biogenic oxidation

Figure 8-65 shows a schematic representation of Fe and Mn oxidation with pH under aerobic conditions and with no heterogeneous catalysis (based on a similar diagrams of Fe(II) oxidation by Singer and Stumm, 1970, Waddell, 1978, and Kirby and Elder Brady, 1998). Mn data is based on Zhange et al (2002) for circum-neutral microbial Mn oxidation, and Morgan (2005) for abiotic Mn oxidation. It demonstrated that microbial Fe and Mn oxidation predominates when homogeneous oxidation is negligible. Therefore, the absence of significant microbial Fe oxidation in the VFR bed is not un-expected due to the circum-neutral aerobic conditions.

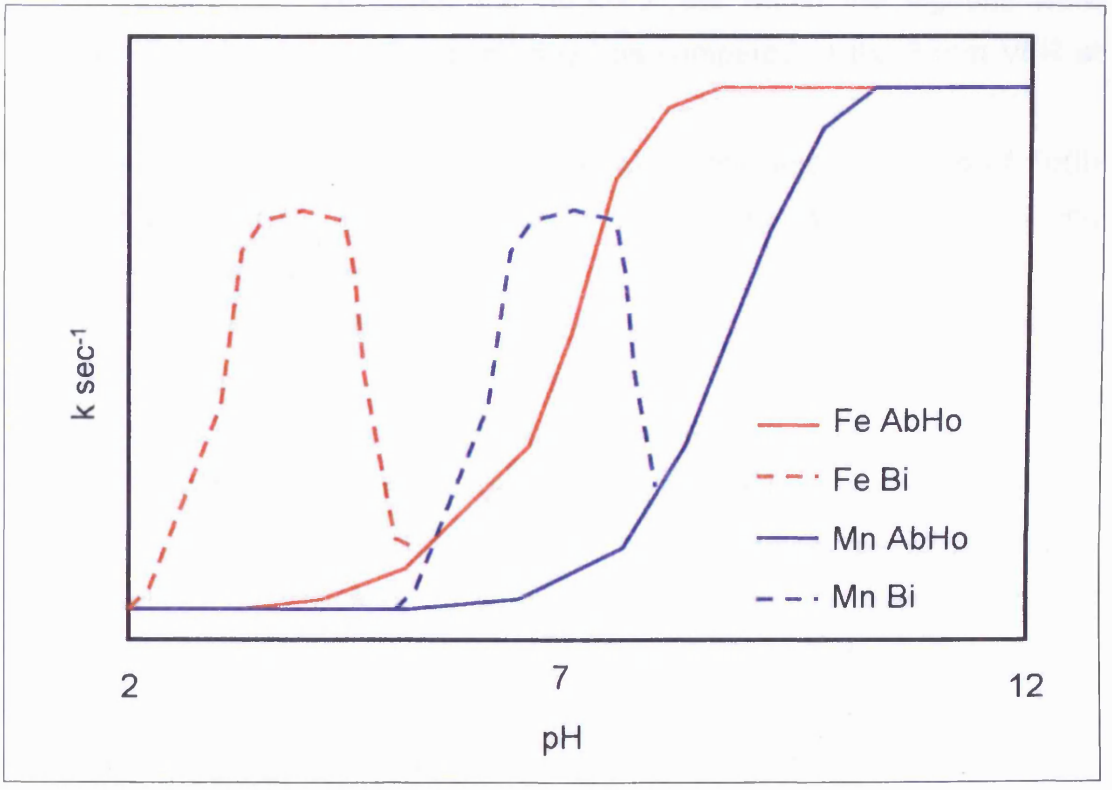

Figure 8-65: Predominance of abiotic and microbial oxidation of Fe and Mn, under aerobic conditions against pH

8.9 Chapter summary and conclusions

This chapter has presented the hydraulic and geochemical data determined during the monitoring of the Taff Merthyr VFR and L1 and L2 settlement lagoons.

From the data presented the following conclusions can be drawn.

- The 6 mm VFR out performs the existing settlement lagoons at the Taff Merthyr site in terms of overall total iron removal. Mean values for % Fe removal are 89.5 % in the 6 mm VFR and 39.4 % in the lagoons. This corresponds to area adjusted removal rates of 16.6 and 4.6 g m^{-2} day^{-1}.
- Total iron removal from the 20 mm gravel VFR gave mean values of 49.1 % and 15.6 g m^{-2} day^{-1}. The relatively high removal rate despite the lower % removal is a reflection of the generally higher flow rates through the 20 mm VFR as compared to the 6 mm VFR.
- Both the 6 mm VFR and the lagoons oxidised a similar percentage of Fe(II) with % difference between inlet and outlet Fe(II) of 96.3 and 93.5 % respectively. However, the removal rate within the lagoons were significantly lower at 6.1 g m^{-2} day^{-1} as compared to the 6 mm VFR at 10.58 g m^{-2} day^{-1}.
- The 20 mm VFR had the worst overall performance in terms of Fe(II) oxidation with %, and area adjusted removal rate values of 75.3 % and 6.4 g m^{-2} day^{-1} respectively.
- Pseudo first order oxidation rate constants of $3.66\pm2.15\times10^{-5}$ sec^{-1} for homogeneous and $5.69\pm5.75\times10^{-3}$ sec^{-1} for heterogeneous Fe(II) oxidation have been calculated within the VFR
- Both the 20 mm and 6 mm VFRs outperformed the lagoons in terms of manganese removal. The 6 mm VFR performed best overall with mean values of 69.2 % and 1.1 g m^{-2} day^{-1}. The lagoons gave the lowest removal with a mean removal of 4.5 % at 0.06 g m^{-2} day^{-1}. The highest removal rate achieved was 2.25 g m^{-2} day^{-1} in the 6 mm VFR.
- As shown above It has been demonstrated that the homogeneous manganese oxidation rate is negligible in the Taff Merthyr mine water resulting in a very low Mn removal rate in the lagoon system. However, Mn oxidation within the VFR system has been shown to be an order of magnitude greater than that of the lagoons. This is thought to be due to heterogeneous catalysis of the oxidation rate as a near linear dependence is observed between Mn removal and cumulative Fe removal. However, the proportion of this rate that can be attributed to

microbial mediated processes is not known. Pseudo first order heterogeneous Mn oxidation rates of $5.74\pm0.87\times10^{-3}$ sec^{-1} have been determined for the 6mm VFR bed. This is thought to be representative for Mn oxidation within a VFR ochre bed and has been found to be largely independent of fluctuations in pH and dissolved oxygen concentrations within the VFR.

- Formation of Mn rich bands within the VFR ochre bed suggests that Mn oxidation is predominantly autocatalytic and that Mn precipitates are responsible for the majority of the oxidation. Further work is required to determine the proportions of Mn oxidation that can be attributed to a) autocatalytic oxidation on Mn precipitates b) catalytic oxidation by Fe(III) (hydroxy)oxide precipitates and c) microbial catalysed oxidation.

9 Laboratory experimentation

9.1 Introduction

A laboratory study was undertaken to investigate the rates and mechanisms of the oxidation of Fe(II) by dissolved O_2. This Chapter describes the laboratory reagents, apparatus and methods used in the experiments, and is subdivided into the following sections:

Section 9.2: Reagent selection and preparation – describes the chemical reagents used in the study.

Section 9.3: Fe(II) analytical method – describes the method used for the determination of both total and dissolved Fe(II) in experiments and the elimination of interference caused by high concentrations of dissolved Fe(III).

Section 9.4: Homogeneous and heterogeneous behaviour of Fe(II) *in bicarbonate buffered systems* – describes the materials and methods used for the determination of oxidation rates, adsorption and redox potential in Fe(II) / bicarbonate buffer systems with and without Fe(III) (hydroxy)oxide surfaces.

Section 9.5: Fe(II) *adsorption and oxidation pH 4 and 6* – Describes the materials and methods used for the determination of Fe(II) adsorption and oxidation in contact with Fe(III) (hydroxy)oxide surfaces at pH 4 and 6 using Na-acetate buffer in the light.

9.2 Reagent selection and preparation

9.2.1 Laboratory chemicals and deionised water

Reagents used were Analytical Reagent grade (AR grade) or better. In most cases reagents were used directly from the containers and used without further preparation. Deionised water was Millipore Millis 18.2 MΩ. Volumetric

solutions were prepared from minimum AR grade chemicals and deionised water.

9.2.2 Fe(III) (hydroxy)oxide

9.2.2.1 Fe(III) (hydroxy)oxide selection

Ferrihydrite forms the predominant secondary mineral phase in circum-neutral ferruginous mine water discharges (Murad and Rojik, 2004) It has also been shown that relatively amorphous ferrihydrite forms a stable phase in mine water discharges due to the adsorption and co-precipitation of sulfate, inhibiting crystalline iron oxide formation (Brady et al, 1986). Under laboratory conditions ferrihydrite is unstable with respect to goethite and rapidly re-crystallises by way of dissolution / re-crystallisation in the presence of Fe(II) with goethite forming the stable end product (Park and Dempsey, 2005 and references therein). Bingham et al (1992) and Schwertmann et al (1995) showed that goethite is the stable mineral phase formed in mine water discharges characterised by pH below 6 and SO_4^{2-} concentrations below 1000 mg L^{-1}. Bingham et al (1992) also describes how ferrihydrite was generally only detectable at pH greater than 5.

As it was intended to conduct experiments at pH 4, goethite was used as the principle mineral surface in the laboratory investigation. A commercially available synthetic goethite pigment (Bayferrox 930) was sourced from Lanxess (Germany) to eliminate the complications of lab synthesis of large quantities of a uniform product. Experiments were also conducted using a synthetic lepidocrocite (Bayferrox 943) and a Fe(III) (hydroxy)oxide produced

9.2.2.2 Fe(III) (hydroxy)oxide preparation

Before using the goethite powder, it was first cleaned to remove effervescent salts and adsorbed ions and anion contaminants. Washing was carried out in two 750 mL polypropylene centrifuge bottles and 250 g of goethite powder was added to each bottle. After each washing stage the suspensions were centrifuged at 3000 rpm for 20 minutes to separate the solid from the wash

solution and the supernatant was decanted. The washing steps were as follows.

- The powder was first suspended in 0.1 N NaOH for 2 hours to remove adsorbed ligands then rinsed once with deionised water.
- It was then re-suspended twice in 0.1 N HCl to remove adsorbed metals.
- The suspension was then rinsed seven times with deionised water and the pH and conductivity of the solution were recorded.
- After the final rinse the pH was adjusted to approximately 7 with 0.1 N NaOH.

The final slurry was poured onto four A3 sheets of Whatman number 1 filter paper in a shallow tray, and a further sheet was placed ontop. The sandwich was put in an oven at 60 °C and left for approximately 18 hours. During this time the filter paper acted as a wick drawing moisture and any remaining effervescing salts away from the goethite onto the filter paper. The final dried sandwich was ground with a mortar and rolled to disaggregate the goethite cake and the resulting powder was then poured into a sealable bag and stored in a desicator.

9.2.3 Anoxic Fe(II) stock

An approximately 1000 mg L^{-1} (18.25 mM) Fe(II) stock solution was prepared by dissolving 4.9778 g of Fe(II)SO4.7H_2O in nitrogen purged deionised water. The stock was stored in a 1.5 L borosilicate glass vessel with a 30 mm neck and 10 mm side access port both of which were sealed with rubber septums. Two PTFE tubes of 1 mm internal diameter were fitted through the top septum of the vessel and allowed wetted nitrogen gas to be continuously bubbled through the solution and exit via a gas bubbler to prevent oxygen ingress. The side port allowed for extraction of stock solution using a syringe and stainless steel needle.

The stock solution was calibrated by adding 1 mL of the solutionto a 100 mL class A volumetric flask and making up to mark with 2.6 N H_2SO_4. The stock concentration was then determined using the 1,10-phenathroline method described in Section 9.3.3.

Although all attempts were made to prevent oxidation of the stock solution it was found that a yellowy precipitate formed on dissolution of the solid $Fe(II)SO_4.7H_2O$ to the nitrogen purged water. This was presumed to be some form of Fe(III) (hydroxy)oxide and could either be due to oxidation of Fe(II) by residue oxygen or, as is more likely, to precipitation of $Fe(III)SO_4$ contaminates in the $Fe(II)SO_4.7H_2O$ reagent. In either case before use the stock solution was syringe-filtered through a 0.2 µm membrane to remove solid particulates.

9.3 Fe(II) analytical method

9.3.1 Fe(II) extraction procedure

Due to the presence of Fe(III) (hydroxy)oxide surfaces in the experimental work Fe(II) existed in both the dissolved and sorbed phases. In accordance with previous work (Jeon et al, 2003a, 2003b; Park and Dempsey, 2005) both dissolved and total Fe(II) were determined with sorbed Fe(II) being the difference between these two. Dissolved Fe(II) was operationally defined as all Fe(II) detected after filtration though 0.2 µm Millipore cellulose nitrate membrane filters. Total Fe(II) was defined as the Fe(II) recoverable by filtration after 20 hours extraction with either 0.5 N HCl or 0.8 N H_2SO_4.

In some cases due to high concentrations of goethite in reaction mixtures, centrifugation of solids was preferred to filtration as it was found that the small pore size filters clogged rapidly under such conditions. It this case samples were spun for 15 minutes at 3500 rpm in a bench-top centrifuge and the centrifugate was then pipetted off from the surface.

It was assumed that actual dissolved Fe(II) and experimentally determined dissolved Fe(II) using phase separation either by filtration or centrifugation was identical. It was however acknowledged that the concentration of experimentally determined Fe(II) would possibly be lower than the actual concentration due to adsorption of Fe(II) onto the filter and by formation of a filter cake of filterable solid on the surface of the filter. By filtration of large (10 mL) volumes, it was possible to minimise the effect of Fe(II) adsorption onto the filter of pre and post filtered Fe(II) concentrations as Adsorption onto the filter cake will increase with increasing filter cake concentration (in accordance with the law of mass balance). No attempt was made to minimise this effect.

9.3.2 The spectrophotometric determination of Fe(II)

Concentrations of Fe(II) were determined spectrophotometrically using an adapted 1,10-phenanthroline method first described by Tamura et al (1974) and used in several studies following this (Tamura et al, 1976b, 1980; Sung and Morgan, 1980; Jeon et al, 2001, 2003a, 2003b, 2004; Park and Dempsey, 2005) (see Table 9.1). The method enables determination Fe(II) despite the presence of up to 2500 mg L^{-1} Fe(III) which would otherwise form a positive interference with the 1,10-phenanthroline reagent used in the determination of Fe(II). The coloured Fe(III) 1,10-phenanthroline complex is masked by an excess of fluoride ions which strongly complex Fe(III). Accelerated oxidation of Fe(II) in the presence of fluoride is prevented by ensuring the pH of the sample is < 2 after fluoride addition and prior to 1,10-phenanthroline addition. The Fe(II) 1,10-phenanthroline complex is stable at pH greater than 3 with respect to oxidation even in the presence of a large excess of fluoride.

Table 9.1: 1,10 Phenanthroline method as given in Tamura et al (1974)

Reagent description in order of addition	Amount (mL)
Sample	15
H_2SO_4 "14+"[a] (3.6 M[b], 25 %[c] or 80 %[d])	1
2M NH_4F solution	2
1 % w/v 1,10-Phenanthroline monohydrochloride monohydrate solution	2
3 M Hexamethylantramine buffer solution	3
Deionised water	2

[a] *Stipulated by Tamura et al (1974),* [b] *as used by Sung and Morgan (1980),* [c] *as used by Demir and Tufekci (2002) and references there in,* [d] *as used in this study.*

Tamura et al (1974) stipulate that the resulting solution is buffered with ammonium acetate / acetic acid buffer at approximately pH 4 at which colour development is rapid in the presence of Fe(II). The sample absorbance is measured against a reagent deionised water blank at a wavelength of 520 or 510 nm using either a Perkin Elmer Lambda EZ150 or a Hitachi U1900 spectrophotometer and 10 mm path-length disposable polystyrene cells. In some cases it was not possible to use either of the above instruments and instead a portable HACH DR890 colorimeter was used and the absorbance was measured at 520 nm using either disposable polystyrene test-tubes of approximately 10 mm path-length or HACH cylindrical sample cells made of optical glass with a 20 mm path-length. It was found that the Beer-Lambert law was obeyed up to a concentration of 7.3 mg L^{-1} of Fe(II) in the analytical solution when either 520 or 510 nm wavelength were used.

9.3.3 Further development of the analytical method in the present work

The method developed by Tamura et al (1974) was proven to be effective at masking Fe(III) concentrations up to 2500 mg L^{-1}, after this point the method breaks down and significant interference is seen from the Fe(III) ions. It is stipulated by Tamura et al (1974) that "larger quantities of acid and fluoride should be added if the Fe(III) concentration is higher than 2500 ppm". A study was undertaken to investigate the effectiveness of the procedure above the 2500 mg L^{-1} threshold as accurately and precisely measuring Fe(II) in the presence of dissolved Fe(III) at concentrations > than 2500 mg L^{-1} would be beneficial in the characterisation of acid digested field and laboratory ochre.

Nine standards were prepared in 100 mL class A volumetric flasks. Each flask contained final concentrations of 12 mg L^{-1} Fe(II) (added as 1 mL of filtered anoxic Fe(II) stock solution), and either 0, 2.5, 5, 10, 15, 20, 30, 40 or 50 g L^{-1} total Fe(III) (as $NH_4Fe(III)SO_4$). 9.1 mL of 80 % H_2SO_4 was added to each of the flasks and the solution was made up to the mark with deionised water. The solutions were covered and left overnight in order for the Fe(III) salts to

completely dissolve. The solutions were then topped up to the mark after approximately 24 hours with deionised water and inverted several times to ensure the solution is homogeneous..

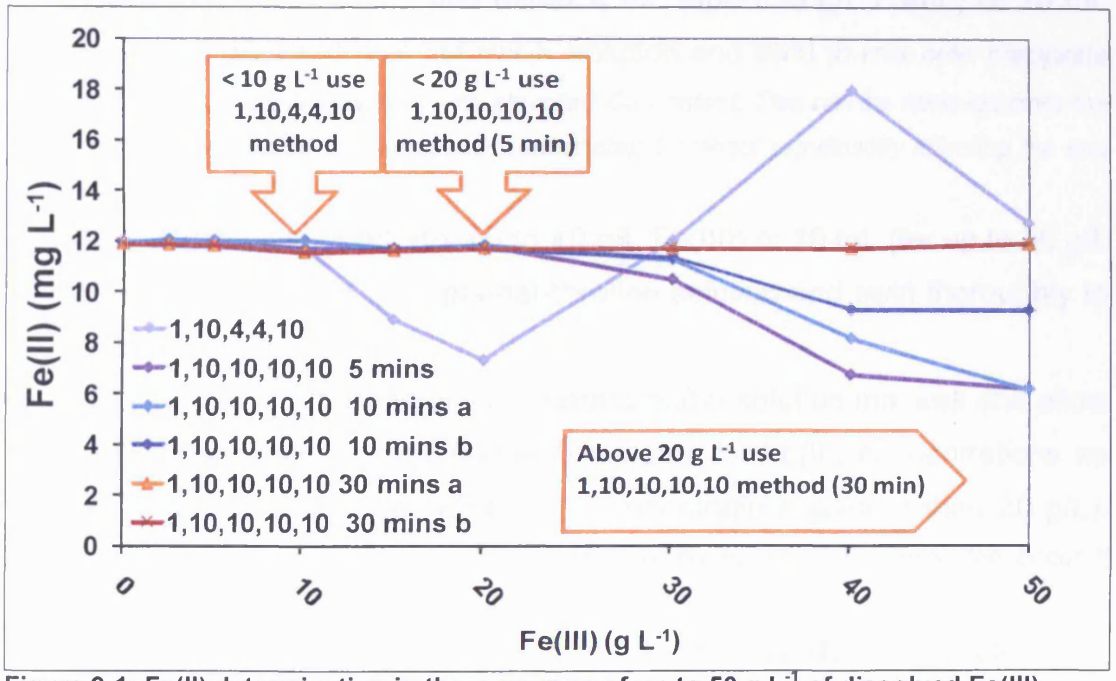

Figure 9-1: Fe(II) determination in the presence of up to 50 g L^{-1} of dissolved Fe(III)

Using the Tamura et al (1974) method as a base line, concentrations and amounts of reagents were systematically varied in order that the concentration of 10 mg L^{-1} of Fe(II) could be accurately detected with minimal interference from Fe(III)-phenanthroline complexes. Tamura et al (1974) states that ammonium acetate buffer can be used in substitution for the 3 M hexamethylantramine buffer used during their study and was used here. Ammonium acetate buffer was prepared in accordance with the method described in AWWA (1995) for Fe analysis. A 1 % 1,10-phenanthroline solution was prepared from 1,10-phenanthroline monohydrate (1 g per 100 mL) and dissolved in 2 % HCl. Rather than the 2 M NH_4F solution used by Tamura et al (1974), an 8 M solution was used here to allow delivery of a large quantity of fluoride without excessive sample dilution. Likewise, 80 % H_2SO_4 was used to acidify the sample prior to reagent addition. A summary of the finalised reagent volumes are shown in Figure 9-1 and Table 9.2 and should be used in accordance with the following procedure:

1. In to a 60 mL sterilin bottle (or other suitable container) add 10 mL of raw sample.
2. To this add 1 mL of 80% H_2SO_4 and swirl to mix
3. Once thoroughly mixed add either 4 mL (up to 10 g/L Fe(III)) or 10 mL (up to 50 g/L Fe(III)) of 8M NH_4F solution and swirl to mix *note: precipitate of CaF_2 may occur in waters with elevated Ca content. This can be removed from the solution by filtration or centrifugation after step 5 without significantly affecting the end result*
4. Add to this either 4 mL (for up to 10 g/L Fe(III)) or 10 mL (for up to 50 g/L Fe(III)) of 1% w/v 1,10 – phenanthroline solution and swirl thoroughly to mix
5. Add 10 mL of 12M Ammonium acetate buffer solution mix well and allow appropriate reaction time (either 5 minutes for Fe(III) concentrations up to 20 g/L or 30 minutes for Fe(III) concentrations greater than 20 g/L). *note: ensure that the mixture is thoroughly mixed as significant error can occur if density differences exist within the solution*
6. Measure absorbance at 510nm using a suitable spectrophotometer.

Table 9.2: 1,10 Phenanthroline method developed in this study

Reagent description in order of addition	Amount (mL) for Fe(III) method (g L^{-1})		
	(0) 2.5 to 10	10 to 20	20 to 50
Sample	10	10	10
80 % H_2SO_4	1	1	1
8 M NH_4F solution	4	10	10
1 % w/v 1,10-phenanthroline solution in 2 % HCl	4	10	10
12 M Ammonium acetate buffer[a]	10	10	10
Reaction time	5 min	5 min	30 min

[a] *as used in 1,10-phenanthroline method described in AWWA, (1995)*

9.3.4 Standardisation of the Fe(II) secondary standard

A secondary standard Fe(II) solution was prepared by dissolving 49.7521 g of $Fe(II)SO_4.7H_2O$ in 1 L of 2.6 N H_2SO_4 in a class A volumetric flask equating to a Fe(II) concentration of approximately 10 g L^{-1}. The Fe(II) stock solution was transferred to a Nalogene Pyrex threaded bottle, capped tightly and wrapped

in aluminium foil to exclude light and prevent any photo redox effects whilst the low pH of the solution effectively retards aerial oxidation of Fe(II).

Standardisation of the Fe(II) stock was performed using a method adapted from a chemical oxygen demand test (AWWA, 1995) and previously used for this purpose by Park and Dempsey (2005) in which the primary redox standard $K_2Cr_2O_7$ is titrated with Fe(II) to the ferroin end point. Titrations were carried out in triplicate and the mean values were used for further calculations. The procedure is outlined below:

1. 3 x 25 mL solutions of the primary standard $K_2Cr_2O_7$ (41.75 mM) were measure into 250 mL acid washed wide neck conical flasks using 25 mL class B volumetric pipette.
2. To this approximately 75 mL of deionised water and 30 mL (3 x 10 mL pipette) of concentrated H_2SO_4 was added along with a PTFE magnetic stirrer bar, swirled to mix and left to cool to room temperature in a fume cupboard. The dichromate solutions are orange in colour at this stage.
3. The initial secondary standard Fe(II) solution (at approximately 10 gL^{-1}) was diluted to 50 % by pipetting 50 mL of the standard (using a class B volumetric pipette) into 100 mL class A volumetric flasks and making this up to mark with 2.6 N H_2SO_4. *note: using 2.6 N H_2SO_4 simulates the 1:10 ratio of sample to 80% H_2SO_4 as used in the analytical procedure and matches the solution used in the preparation of the original secondary standard*
4. 3 drops of ferroin redox indicator (1.485 g 1,10-phenanthroline monohydrate and 0.695 g Fe(II)$SO_4.7H_2O$ in 100 mL deionised water, AWWA, 1995) were added to the cooled $K_2Cr_2O_7$ solutions and the solution was placed on a magnetic stirrer under the burette containing the 50% secondary standard solution.
5. The solutions were titrated with the 50 % Fe(II) standard solution through the green transitionto the ferroin end point which is marked by a dark red colour.

9.3.5 Calibration of the spectrophotometer

Calibration of the spectrophotometric method was performed using a set of standard dilutions. These were made from an initial 1 in 1000 dilution of the original secondary Fe(II) standard described in the previous section. Dilution concentrations were as follows (as % of the 1 in 1000 dilution) 50 %, 20 %, 10 % and 1 %. All dilutions were performed using class A volumetric flasks and 2.6 N H_2SO_4. The Fe(II) standard dilutions were analysed for Fe(II) in triplicate using the spectrophotometric method as described in Section 9.3.3. A calibration curve was generated and a linear relationship between absorbance at 510 nm and the standard concentration was found. Using Microsoft Excel linear trend line, and with the interception point set to zero, the relationship is as follows:

Equation 9.1

$$[Fe(II)] = 4.8972\,ABS_{510}$$

where [Fe(II)] is the Fe(II) concentration in mg L^{-1}, Abs_{510} is the absorbance of light at a 510 nm wavelength (using 10 mm path length disposable polystyrene cuvettes) determined against a reagent blank. The R^2 value for the linear trend line was 0.9997.

Previously, instrument calibration was carried out at a wavelength of 520 nm in which case the relationship was:

Equation 9.2

$$[Fe^{2+}] = 5.2366\,ABS_{520}$$

where Abs_{520} is the absorbance of light in the 520 nm wavelength across a 10 mm path length cuvette. Using this method, and with the intercept set as zero using Microsoft Excel linear trend function, an R^2 value of 0.9997 was achieved

Due to failure of the Perkin Elmer Lambda EZ150 instrument, it was necessary to use a portable HACH DR/890 colorimeter for a number of laboratory measurements. In this case, measurements were made in either HACH cylindrical sample cells of approximately 20 mm path length, or disposable polystyrene test tube with a path length of approximately 10 mm.

9.4 Heterogeneous and homogeneous oxidation of Fe(II) in bicarbonate buffered solutions

A set of experiments were undertaken to determine the homogeneous and heterogeneous oxidation rates of Fe(II) under thermostatically controlled conditions. pH was set using a bicarbonate / CO_2 buffer system, a method which had been used by a number of previous authors for the determination Fe(II) oxidation kinetics in homogeneous (e.g. Stumm and Lee, 1961; Tamura et al, 1976a; Sung and Morgan, 1980; Millero et al, 1987) and heterogeneous (e.g. Tamura et al, 1976b, 1980; Sung and Morgan, 1980; Tufekci and Sarikaya, 1996, 1980) systems.

9.4.1 Apparatus

Experiments were conducted inside a 1 L Pyrex borosilicate glass reaction vessel with an integral water jacket as shown in Figure 9-2. Temperature was maintained at 25.0 ± 0.05 °C by circulating water through the water jacket from a Grant water bath via a centrifugal pump. A Neslab Cryocool refrigerating probe was inserted into the water bath to balance the heating element. The reaction mixture was intensively mixed from overhead using a PTFE coated anchor stirrer bar powered by a Heidolph stirrer motor supported on a heavy duty clamp stand. The reaction vessel was covered with a specifically machined 5 mm Perspex lid that was sealed to the ground glass rim of the reaction vessel using a smear of silicon grease and a wire clamp and butterfly bolt assembly.

A Pyrex stirrer gland (using deionised water lubricant), was used to allow stirring through the reaction vessel lid and prevent gas escape. The Perspex

lid had one central 30 mm hole for the stirrer gland and a further 6 20 mm holes arranged in a circle around the outside, the diameters of the holes corresponded to the diameters of commercially available 30 and 20 mm natural rubber septums. A hole was bored through a 30 mm septum to allow the insertion of the stirrer gland, further holes were bored through 20 mm septums to fit electrochemical probes and a fritted glass tube for gas bubbling. The septum assemblies' then push fit into the holes of the reaction vessel lid forming a low pressure gas tight head assembly. The rubber septums also allow the withdrawal of sample from the reaction mixture without disturbing the atmosphere inside the reaction vessel by way of 200 mm stainless steel hypodermic needles and Plastipak polyethylene Syringes.

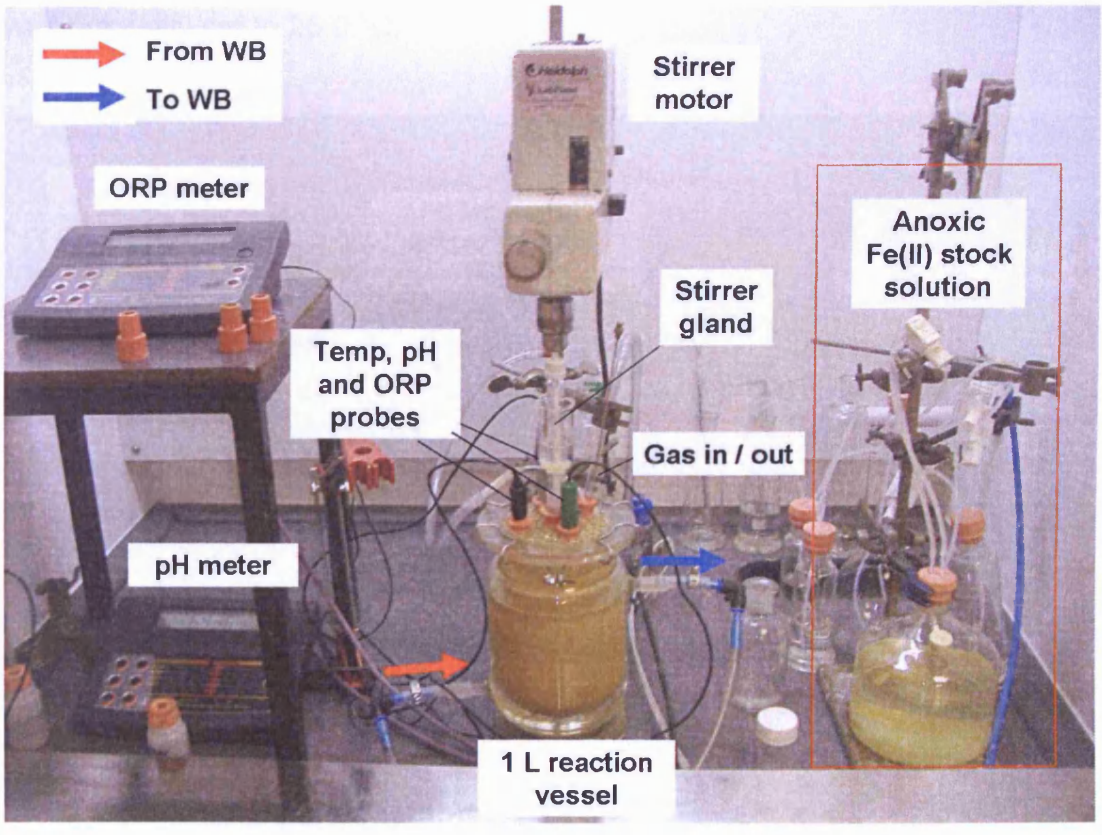

Figure 9-2: Reaction vessel apparatus used for Fe(II) oxidation experiments

pH was controlled by altering a mixture of N_2, O_2 and CO_2 bubbled through the reaction mixture by way of fine bubble diffusion using a Pyrex glass tube with a fine sintered glass end. Proportions of gasses were mixed using a set of variable area flow meters as shown in Figure 9-3 ,

Two Hanna Instruments pH 213 meters were used for the determination of pH, temperature and ORP and readings were automatically logged every 10 seconds to a PC running Hanna Instruments HI9913 software as shown in Figure 9-3. The pH meter was calibrated using NIST certified buffers at pH 4.01 and 7.01. The buffers were equilibrated in the water bath at 25 °C prior to calibration and the probe was rinsed with deionised water and buffer before the calibration was set. The ORP cell potential was determined against Lights solution equilibrated to 25 °C (AWWA, 1995) to allow correctionto the Standard Hydrogen Electrode (SHE). The meter measuring pH also had a stainless steel thermocouple temperature probe (accurate to ± 0.1 °C) to allow Automatic Temperature Compensation (ATC) and was used to monitor the temperature within the reaction vessel. The temperature of the ORP meter was manually set to 25.0 °C.

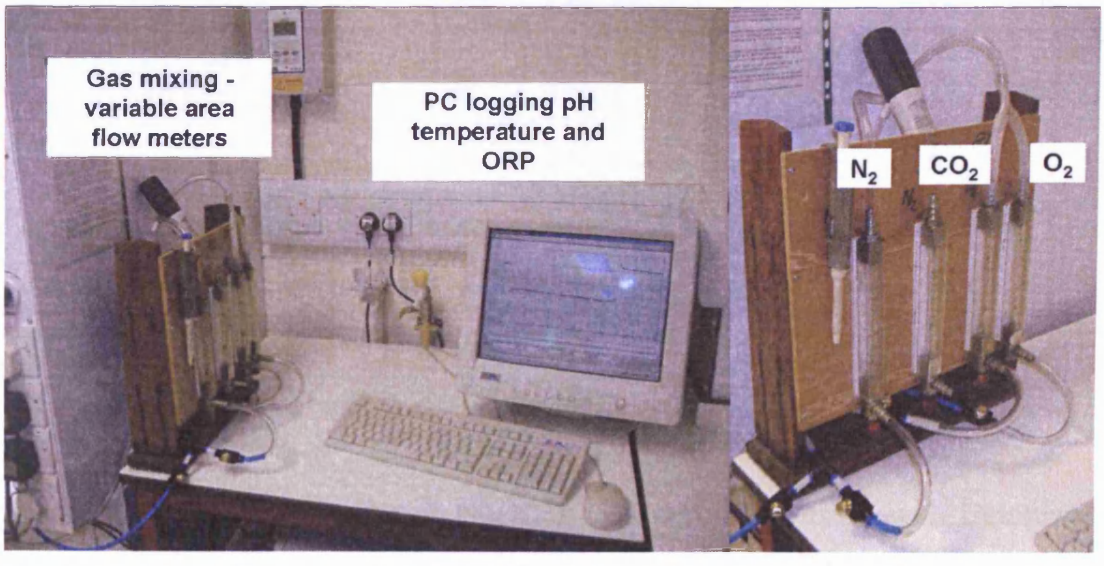

Figure 9-3: Gas mixing apparatus and PC logging pH, temperature and Eh

9.4.2 Materials and methods

Four experiments (Experiments 1 to 4) were carried out to verify homogenous Fe(II) oxidation constants, and rate expressions reported in the literature (e.g. Sung and Morgan, 1980; Wehrli, 1990) between pH 5.6 and 7.4. A second set of experiments (6a and 6b) were conducted in the presence of Fe(III) (hydroxy)oxide (type A) to determine compliance with heterogeneous rate

laws as reported by Tamura et al, 1976b and 1980. Finally, a third set of experiments were conducted under anoxic conditions to determine the behaviour of Fe(II) adsorptionto lepidocrocite. Details of the reaction conditions are shown in Table 9.3.

Table 9.3: Experimental parameters used in bicarbonate buffered experiments

Exp No	pH	$NaHCO_3$	Fe(II)#	Temp	$O_{2(aq)}$	SO_4#	FeOOH
		mg/L	mg/L	°C	mg/L	mg/L	mg/L
1	5.6±0.02	420	10	25±0.06	8.4±0.5	18	0
2	6.48±0.056	420	10	25±0.06	8.4±0.5	18	0
3	6.50±0.089	420	12	22.3±1.1	9.17±0.5	22	0
4	7.11±0.0195	420	10	25.1±0.06	8.54±0.5	18	0
5a	6.455±0.006	450	10	25.05±0.05	8.245±0.5	18	200 [a]
5b	6.591±0.03	1000	10	24.95±0.05	8.33±0.5	18	200 [a]
6a	6.48±0.0155	510	10	25.05±0.05	0	18	200 [b]
6b	6.49±0.024	503	10	25.0±0.0	0	18	200 [b]
9	6.013±0.012	501	5	25.0±0.1	0 to 8.52	9.5	10000 [c]

± error indicates standard deviations determined during experimental runs
[a] Using type A Fe(III) (hydroxy)oxide added as a slurry
[b] Using Bayferrox 943 lepidocrocite added as a slurry
[c] Using Bayferrox 930 goethite added as a washed powder
Approximate initial concentrations

The experimental procedure is as follows:

1. The required quantity of $NaHCO_3$ reagent was mixed with deionised water in a 1 L volumetric flask. In the case of the heterogeneous reactions a 10 mL slug of the required Fe(III) (hydroxy)oxide slurry (equalling 200 mg/L in the final solution) was added via a PlastiPak syringe. This was then made up to the mark with deionised water.
2. The bicarbonate (and Fe(III) (hydroxy)oxide) solution was added to the reaction vessel assembly and the lid was sealed with a smear of silicon grease and the manufacturers clamps. The pH, temperature, and redox probe were then inserted and the mixer was set to 80 rpm.

3. The water bath was set to the desired temperature and the water was circulated through the reaction vessels water jacket.
4. The gas flow rates were set to attain the suitable partial pressure for oxygen of (*p*0.21 for Experiments 1 to 5, 0 for Experiments 6a and 6b then initially 0 for Experiment 9 before oxidationto *p*0.21). The desired pH should was attained by adjusting the partial pressure of CO_2 and balancing this with N_2.
5. Once equilibrium was attained with regards to temperature, and pH the logging system was initiated.
6. A 10mL slug of anoxic Fe(II) solution was then removed from the reservoir using a plastic syringe and hypodermic needle. This was then injected into the reaction vessel through the rubber septum. This initiated the reaction.
7. At least 30 seconds was left prior to removal of the first 20mL subsample for Fe(II) determination. This was done using a plastic syringe and hypodermic needle at each sample period as determined prior to initiation. The first 10 mL of this was quenched directly in 1 mL of 80% H_2SO_4, the second 10 mL sample was filtered through a 0.2 µm cellulose nitrate membrane syringe filter tip prior to quenching in 1 mL of 80% H_2SO_4. After a 24 hour dissolution period Fe(II) was determined in accordance with the method in Section 9.3.3.

9.4.3 Analysis

10 mL samples were removed at pre-determined intervals using a 5 mL calibrated re-pipette and total Fe(II) was determined using the 0.82 N H_2SO_4 extraction method as described in Section 9.3.1. Dissolved Fe(II) was only determined on the 04-04, 15-05 and the 04-06-2007 in accordance with the procedure described in Section 9.3.1. Experiments 1, 3 and 4; a, b and c were run for the full 67 days whilst Experiment 2 was stopped after 24 days as it was found that all of the goethite solid in the reaction mixture had adhered to the neck of the flask due to the swirling action of the orbital shaker and therefore no difference was observed between this and Experiment 1.

9.4.4 Reaction rate determination

The rate of oxidation of Fe(II) was assumed to be first order with respect to Fe(II) and dissolved O_2. During the experimental runs the dissolved oxygen concentration was assumed to be constant. Therefore, pseudo first order rate constants were determined using the exponential trend line fitting in Microsoft Excel. These were compared to pseudo first order rate constants determined from successive half life analysis which confirmed the first order dependence on Fe(II).

Due to the rapid oxidative surface cycling of the dissolved Fe(II) in Experiment 9, the determination of pseudo first order oxidation rate constant based on the dissolved Fe(II) portion was not possible. However, it was possible to determine a rate constant for the oxidisable sorbed Fe(II) portion. The rate was determined from the 5700 sample point up to the 8400 seconds sample point for the oxidisable portion of the sorbed Fe(II). This was done by subtracting the mean determined non-oxidisable sorbed Fe(II) portion (as determined from sample points 9000, 10800 and 13020) from the 5700 to 8400 seconds data to effectively return only the oxidisable Fe(II) portion.

9.5 Iron adsorption and oxidation pH 4 and 6

A set of experiments was conducted to determine the characteristics of adsorption of Fe(II) onto goethite at pH 4 and 6. The experiment differed from a standard adsorption isotherm experiment such as those reported by Zhang et al (1992), Liger et al (1999) and Vikesland and Valentine (2002) in that only two pH conditions were chosen, the concentration of Fe(II) was the same for all experiments and that the concentration of goethite solid was varied. Therefore these experiments effectively represent adsorption isotherms for Fe(II) onto goethite surfaces with emphasis on the concentration of surface adsorption sites. The adsorption experiments were carried out in a glove box which was continuously purged with oxygen-free nitrogen to maintain a positive pressure and prevent oxygen ingress. Once analysis had been undertaken to determine adsorption of Fe(II) the anoxic Fe(II) mixtures were

allowed to aerate and were left for 48 hours to determine the reaction rates of Fe(II) oxidation by oxygen.

9.5.1 Apparatus

Reaction vessels consisted of 60 mL polypropylene centrifuge tubes with screw cap lids which were used as received. Complete mixing was achieved using a rotational type end over end mixer and was performed at approximately 30 rpm inside a Plaslabs Petite glove-box (see Figure 9-4). The glove box had a side airlock for degassing of samples and transfer of materials. The glove-box was used in accordance with the manufacturer's guidelines for purging and airlock use. A pressure release valve was devised for the outlet of the box and the inlet was fitted with a variable area flow meter to monitor inlet nitrogen flow which was maintained at > 1 L min^{-1}.

Oxygen concentrations were monitored periodically from the outlet of the glove box using a Servomex 570A oxygen analyser which confirmed O_2 to be 0.0% therefore O_2 is assumed to be < 0.06% (as the machine would round values > 0.06% to 0.1%) or a PO_2 of 0.0006 atm. Using Henrys law the maximum $O_{2(aq)}$ concentration can be determined as follows:

Equation 9.3

$$[O_{2(aq)}] = K_H PO_2$$

Where $[O_{2(aq)}]$ is the aqueous concentration of O_2 in mol L^{-1}, K_H is the oxygen gas / water equilibrium (Henrys) constant (1.26×10^{-3} mol L^{-1} atm^{-1} at 25 °C) and PO_2 is the partial pressure of oxygen in atm. The above equation gives a dissolved O_2 concentration of 0.024 mg L^{-1}.

Temperature was controlled near 25 °C using a hot plate, heat exchanger and thermostat assembly, measured temperatures of final solutions were slightly above the desired temperature of 25 °C with a mean of 25.47 °C and a SD of 0.37 °C.

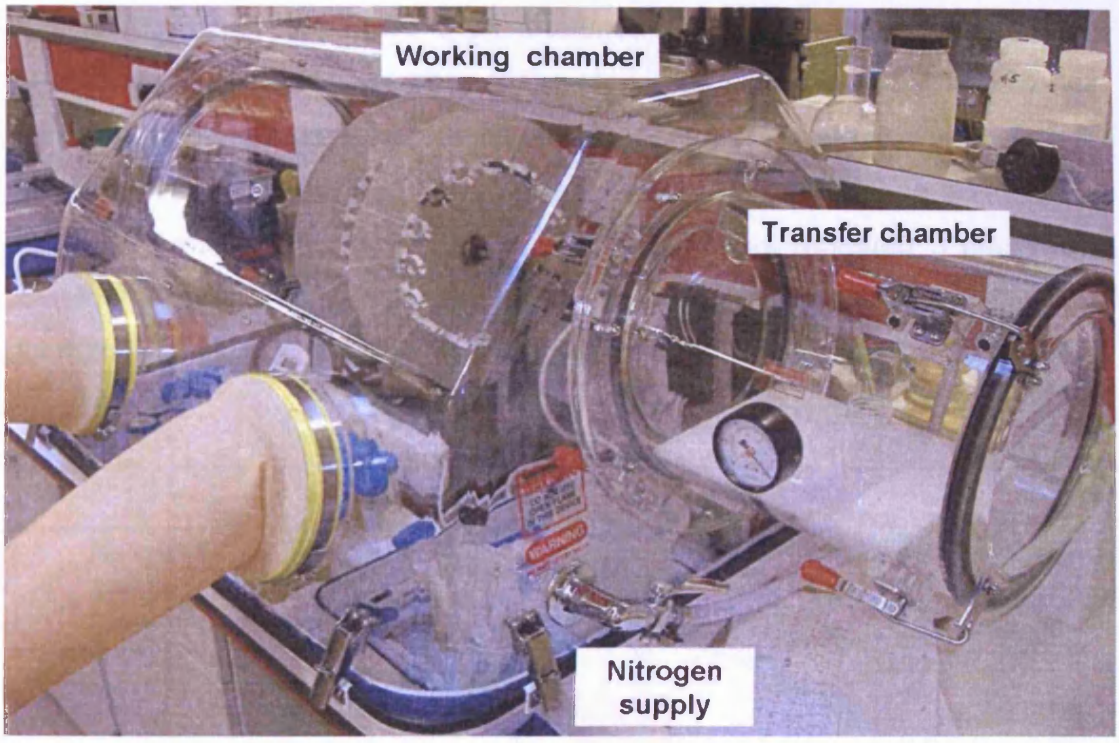

Figure 9-4: Glove box used in Fe(II) adsorption and oxidation experiments

9.5.2 Materials and methods

1 L each of either pH 4 or 6 sodium acetate / acetic acid buffer was prepared to acetate concentration of 10 mM. Buffers were prepared in 1 L class A volumetric flasks using the amounts of reagent as shown in Table 9.4 and made up to the mark with deionised water.

Table 9.4: Acetate buffer preparation

pH	Acetic acid (glacial) (g)	Sodium acetate rehydrate (g)
4	0.5112	0.2053
6	0.0324	1.2886

All weights are amounts added to 1 L of deionised water to make a 10 mM solution

Washed goethite was used in its dry form as described in Section.9.2.2.2 Goethite was weighed directly into the reaction vessels using an analytical balance. To the weighed solid, 20 mL of either pH 4 or pH 6 buffer was added using a class B volumetric pipette, the reaction vessels were then capped and shaken vigorously. The reaction vessels were placed in test tube holders and partially immersed in an ultrasonic bath for 10 minutes to break up

aggregates. The caps were then loosened and the reaction vessels were placed into the transfer chamber of the glove box to degas under vacuum at -90 knag below atmospheric for approximately 10 minutes. The vessels were then removed from the transfer chamber and shaken to release any bubbles that had formed in the solution. The procedure was repeated 3 times. The transfer chamber was then purged in accordance with the manufacturers guidelines and the reaction vessels were passed through to the working chamber.

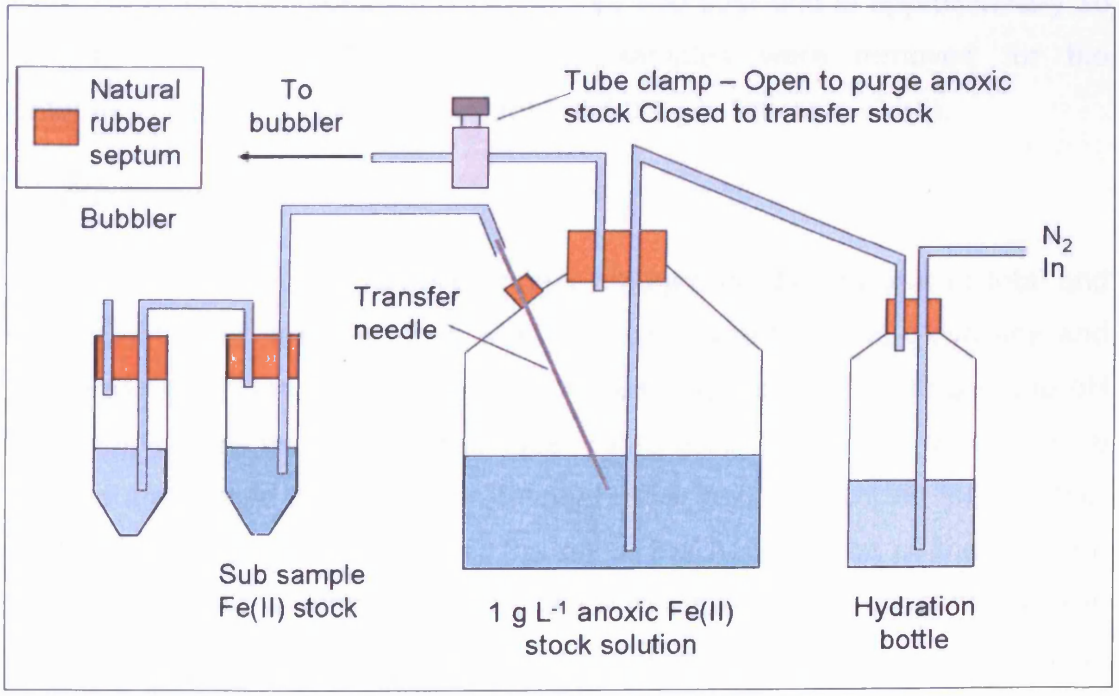

Figure 9-5: Anoxic Fe(II) stock solution transfer

Anoxic Fe(II) stock was transferred from the N_2-purged reservoir into a 50 mL centrifuge tube using the apparatus as shown in Figure 9-5. The centrifuge tube was sealed with a rubber septum through which two 3 mm ID PTFE tubes where passed as shown in Figure 9-5, one to a bubbler assembly and the other to the anoxic stock solution.

The reaction vessels containing buffer solution and weighed solids were left loosely capped in the glove box for approximately 72 hours (over one weekend) under 0.5 L min^{-1} flow of N_2 in order for as much dissolved O_2 as possible to be removed from the solutions. It was found that the N_2 supply had

run down towards the end of the weekend and that constant purging had not taken place. However, the glove box had remained at a positive pressure despite loss of through flow and a fresh N_2 supply was fitted on discovery of the problem.

After further purging for 2 hours, 2 x 0.1 mL (0.2 mL) of anoxic Fe(II) stock solution was transferred to each of the 48 reaction vessels using a calibrated re-pipette and the tubes were capped tightly and attached to the rotational mixer. The reaction tubes were then mixed end over end at approximately 30 rpm for 24 hours after which time samples were removed for the determination of 0.5 N HCl extractable and 0.2 μm filterable Fe(II).

9.5.3 Oxidation

After samples had been removed under nitrogen for the analysis of total and filtered Fe(II) the reaction tubes were then removed from the glove box and the remaining 7.5 mL of reaction mixture was exposed to the air and the pH and temperature were measured (see Table 9.5). The tubes were then re capped and placed back on the rotational mixer and left aerated for a further 48 hours. It was determined that the air in the head space of the reaction tubes would have a sufficient excess of O_2 to elevate $O_{2(aq)}$ concentrations in the reaction mixture to near saturation without significantly lowering the partial pressure.

Table 9.5: pH 4 and pH 6 adsorption / oxidation experimental conditions

	pH 4			pH 6		
	goethite $g\ L^{-1}$	Mean pH	Mean Temp °C	goethite $g\ L^{-1}$	Mean pH	Mean Temp °C
1 a, b, c	0.00	3.912	25.70	0.00	5.848	26.37
2 a, b, c	1.00	3.917	25.70	0.06	5.816	25.53
3 a, b, c	5.00	3.886	25.23	0.11	5.749	25.67
4 a, b, c	10.01	3.887	25.33	0.51	5.724	25.63
5 a, b, c	25.01	3.904	25.13	0.99	5.655	25.23
6 a, b, c	50.04	3.888	25.07	4.99	5.665	25.37
7 a, b, c	100.02	3.912	25.10	10.00	5.734	25.77
8 a, b, c	200.01	4.027	24.90	50.04	5.866	25.80

The letters a, b and c refer to the triplicate runs for each of the 8 goethite concentrations used at both pH.

9.5.4 Analysis

Two sets of 48 polystyrene disposable test tubes were prepared one set with 0.5 mL of 5.5 N HCl and one set with 0.5 mL of 80% H_2SO_4. These were transferred into the glove box. The rotator was stopped and the reaction tubes were removed individually. For each tube 5 mL of the reaction mixture was removed and pipetted into a labelled test tube containing HCl. A further 7 mL (approximately measured) was poured into a disposable Plastipak 20 mL syringe with a disposable Millipore 0.22 µm syringe filter attached. The plunger was then inserted and the suspension was filtered into a clean test tube. 5 mL of the filtered suspension was then pipetted into a labelled test tube containing H_2SO_4. The test tubes containing filtered and total samples with acid were transferred out of the glove box and sealed with lab film.

The test tubes were placed at an angle on an orbital shaker in test tube racks at 200 rpm for 20 hours. After 20 hours the HCl extractions were centrifuged at 3000 rpm for 20 minutes to separate the suspension. 1 mL of the centrifugate was then pipetted into a separate test tube containing 0.1 mL of 80 % H_2SO_4. Both filtered and HCl extracted (total) Fe(II) were then analysed using the 1,10-phenanthroline method described in section 9.3. Due to unforeseen circumstances analysis had to be performed using a HACH DR 890 colorimeter with a test tube adapter at 520 nm. In this case reagents were added directly to the test tubes which were then inserted directly into the colorimeter.

After 48 hours oxidation the same procedures were undertaken to determine filtered and total Fe(II) however only 2 mL of mixture was removed and added to 0.2 mL of 5.5 N HCl for determination of total Fe(II). In addition rather than using filtrationto separate the remaining 5.5 mL of reaction mixture prior to the determination of Fe(II) (dissolved) centrifugation at 2500 rpm for 20 minutes was used. Of the centrifugate 1 mL was removed and added to 0.1 mL of 80 % H_2SO_4 for Fe(II) analysis.

9.5.5 Reaction rate determination

Reaction rates for the oxidation of Fe(II) were determined from the colorimetric absorbance after 48 hours of oxidation and were therefore determined from two points, Fe(II) concentration at time (T) = 0 hours and Fe(II) concentration at T = 48 hours. A first order dependence on Fe(II) and saturated dissolved O_2 conditions was assumed throughout the experimental run. A pseudo first order rate constant, k in sec^{-1} was calculated as follows:

Equation 9.4

$$k = \frac{-\ln([Fe(II)]_{48}\ [Fe(II)]_0)}{\Delta t}$$

where $[Fe(II)]_0$ is the Fe(II) concentration at T = 0 hours in mol L^{-1}, $[Fe(II)]_{48}$ is the Fe(II) concentration at T = 48 hours in mol L^{-1}, Δt is the change in time between time 0 and time 48 in seconds and k is the first order rate constant in sec^{-1}.

10 Results of the laboratory studies

10.1 Introduction

This chapter presents and discusses the results of a laboratory investigation into the rates and mechanisms of Fe(II) oxidation by dissolved O_2. The chapter is split into the following sections:

Section 10.2: Fe(II) oxidation kinetics pH 5.5 – 7.5 – presents the results of both homogeneous and heterogeneous batch kinetic experiments for Fe(II) oxidation rates in carbonate buffered systems. Data are also included from a number of "redox" experiments in which Eh was monitored in differing media to determine if extended contact time between Fe(II) and goethite solids produced more reducing conditions.

Section 10.3: Experiments 7 and 8 – Adsorption and oxidation of Fe(II) on goethite at pH 4 and 6 – presents data for the adsorption of Fe(II) under N_2 atmosphere then subsequent inferred oxidation rates after 48 hours of exposure to atmospheric oxygen. These experiments were carried out in a Na Acetate / Acetic acid buffer solution.

Section 10.4: Experiment 9 – pH 6 batch oxidation run - details the results of batch pre-equilibration and adsorption followed by oxidation of Fe(II) on goethite.

Section 10.5: Comparison of field and laboratory kinetic data - compares laboratory and field homogeneous and heterogeneous Fe(II) oxidation rates determined in this work.

Section 10.6: Chapter summary and conclusions

10.2 Fe(II) oxidation kinetics pH 5.5 – 7.1

A series of experiments were undertaken to determine the rates of homogeneous and heterogeneous Fe(II) oxidation in the mildly acidic to circum-neutral pH range. Experiments were undertaken in bicarbonate buffered solutions and were carried out in accordance with the method devised in Section 9.4.

10.2.1 Homogeneous oxidation pH 5.5 – 7.1

Figures 10.1 to 10.4 show reaction profiles determined for the homogeneous oxidation of Fe(II) by dissolved O_2 at pH between 5.6 and 7.1. In each case concentrations of both total and filtered Fe(II) are shown in mg L^{-1} (as determined using the method shown in Section 9.3) along with the logged pH and Eh (mV) values. The values given below the figure for pH and temperature are mean values, and the ± gives the SD of all readings taken.

10.2.1.1 Experiment 1 – pH 5.6

Figure 10-1 shows Eh in mV, pH, total and filtered Fe(II) in mg L^{-1} against time in seconds for Fe(II) oxidation by dissolved O_2. Reaction conditions are pH 5.6±0.02, 25±0.06 °C, 8.4±0.5 mg L^{-1} dissolved O_2 (DO), 420 mg L^{-1} $NaHCO_3$, approximately 18 mg L^{-1} SO_4^{2-}, and an initial Fe(II) concentration of 10 mg L^{-1}.

A decrease in Fe(II) concentration of 1 mg L^{-1} was observed during the duration of the experiment. Due to the initial absence of particulate Fe(III) (hydroxy)oxide, it would be expected that all Fe(II) would be recoverable in the filtered portion. However, the experiment shows that total Fe(II) is consistently approximately 0.1 mg L^{-1} higher than the filtered Fe(II). This discrepancy is possibly caused by adsorption of Fe(II) onto the filter during filtration, or due to error incurred during correction of analytical results. The difference seen is within the experimental error of ± 1 %. The erroneous filtered Fe(II) reading at 12359 seconds is likely due to human error.

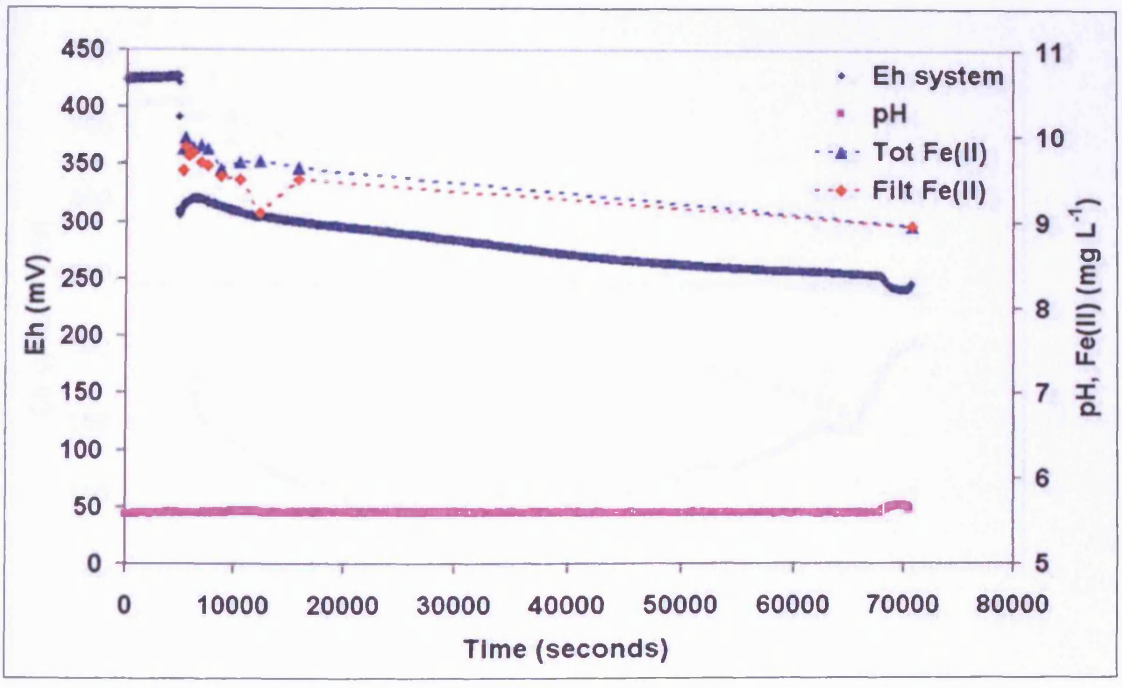

Figure 10-1: Experiment 1 – Homogeneous oxidation of Fe(II) at pH 5.6

Experimental conditions – pH 5.6±0.02, 25±0.00 °C, DO 8.4±0.5 mg L^{-1}, $NaHCO_3$ 420 mg L^{-1}, SO_4^{2-} ~ 18 mg L^{-1}.

The initial Eh of the system in the presence of 8.4 mg L^{-1} of O_2 and without the addition of Fe(II) is 430 mV. With addition of Fe(II) aliquot, the Eh drops instantaneously to 305 mV, which is followed by a gradual decrease to 250 mV throughout the duration of the experiment. It is not known if this gradual decrease in Eh is a real effect, or due to slow poisoning of the platinum electrode or porous junction. If it is a real effect it could be due to formation of reactive surface bound Fe(II) species on freshly precipitated Fe(III) (hydroxy)oxide surfaces. They are shown to be stronger reducing agents than dissolved Fe(II) alone.

10.2.1.2 Experiment 2 – pH 6.5

Figure 10-2 shows Eh in mV, pH, total and filtered Fe(II) in mg L^{-1} against time in seconds for Fe(II) oxidation by dissolved O_2. Reaction conditions are pH 6.48±0.056, 25±0.06 °C, 8.4±0.5 mg L^{-1} DO, 420 mg L^{-1} $NaHCO_3$, approximately 18 mg L^{-1} SO_4^{2-}, and initially approximately 10 mg L^{-1} Fe(II).

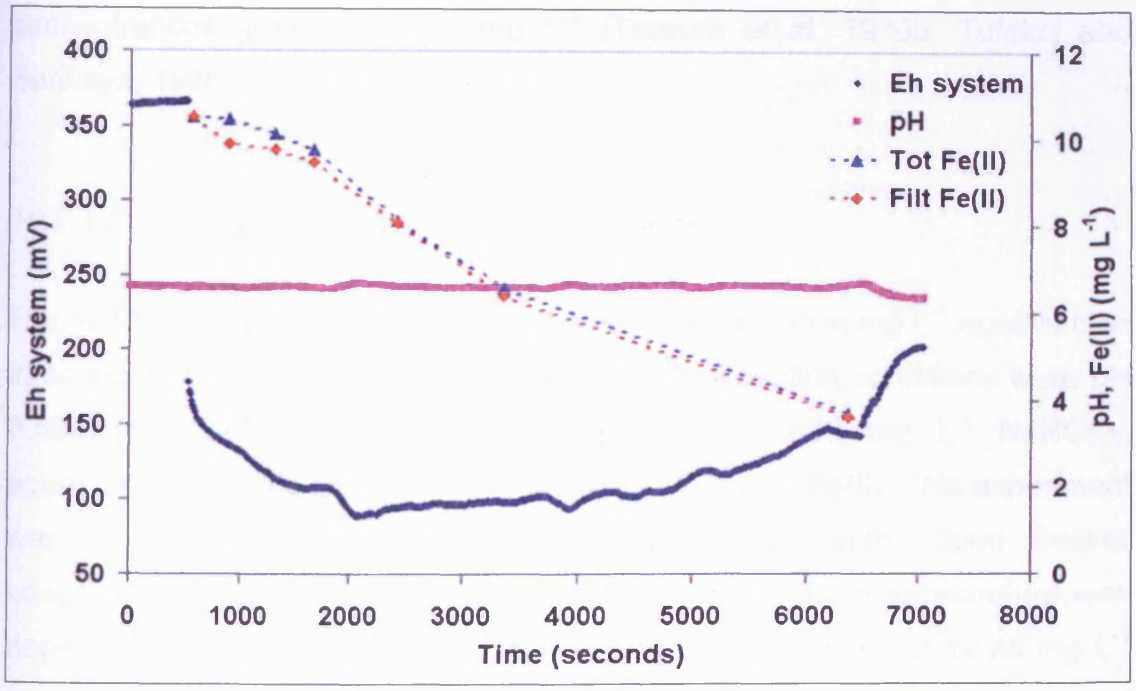

Figure 10-2: Experiment 2 – Homogeneous oxidation of Fe(II) at pH 6.5

Experimental conditions – pH 6.48±0.056, 25±0.06 °C, DO 8.4±0.5 mg L^{-1}, $NaHCO_3$ 420 mg L^{-1}, SO_4^{2-} ~ 18 mg L^{-1}.

The concentration of Fe(II) is seen to decrease from 10.43 to 3.68 mg L^{-1} in 1.52 hours, a reduction of 6.75 mg L^{-1}. As with the experiment at pH 5.6, the filtered Fe(II) is seen to be consistently below the concentration of the total Fe(II) for the first four sample points. After this point, total and Filtered Fe(II) are within experimental error of each other, despite increasing Fe(III) (hydroxy)oxide surfaces.

System Eh is recorded at 370 mV prior to addition of the Fe(II) aliquot. At this point the Eh drops instantaneously to around 170 mV before a more gradual decrease, to a minimum of 90 mV at 2000 seconds. This equates to a net decrease of 280 mV. Eh is then seen to recover with a decrease in Fe(II) concentration. On closer inspection of the reaction profile it can be seen that the initial concentration of Fe(II) decreases at a slower rate during the first four samples and then increases after this point, demonstrating autocatalytic behaviour. It has been indicated that autocatalysis of Fe(II) oxidation is not apparent below a pH of ~ 7 (Sung and Morgan, 1980). However, other studies have shown that autocatalysis does occur at pH below 7, with initial Fe(II)

concentrations greater than 3 mg L^{-1} (Tamura et al, 1976b; Tufekci and Sarikaya, 1996).

10.2.1.3 Experiment 3 – pH 6.5 (open beaker)

Figure 10-3 shows Eh in mV, pH, total and filtered Fe(II) in mg L^{-1} against time in seconds for Fe(II) oxidation by dissolved O_2. Reaction conditions were pH 6.50±0.089, 22.3±1.1 °C, 9.17±0.5 mg L^{-1} DO, 420 mg L^{-1} $NaHCO_3$, approximately 22 mg L^{-1} SO_4^{2-}, and initially ~ 12 mg L^{-1} Fe(II). This experiment was a repeat of the previous Experiment 2, but under Open Beaker conditions. As no temperature control was used, the given temperature was dependant on room temperature. Initial Fe(II) concentrations of 12.25 mg L^{-1} are seen to decrease to 3.36 mg L^{-1} over 2.05 hours. This is a reduction of 8.89 mg L^{-1} in Fe(II).

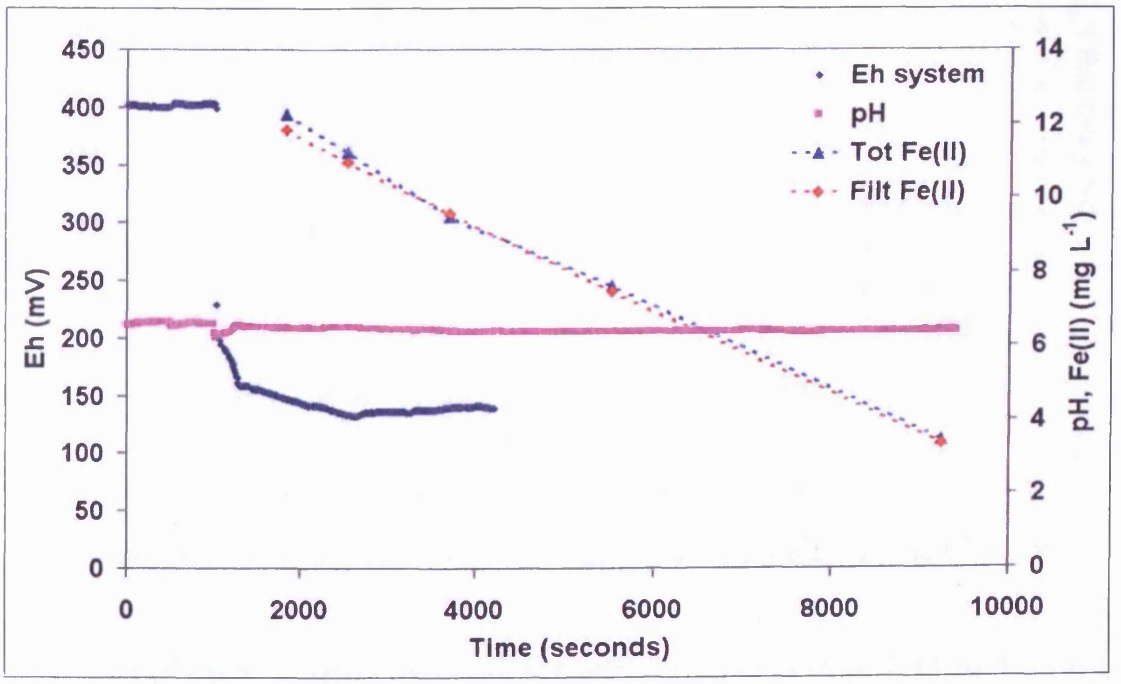

Figure 10-3: Experiment 3 – Homogeneous oxidation of Fe(II) at pH 6.5, Open beaker

Experimental conditions - pH 6.50±0.089, 22.3±1.1 °C, DO 9.17±0.5 mg L^{-1}, $NaHCO_3$ 420 mg L^{-1}, SO_4^{2-} ~ 18 mg L^{-1}.

As with Experiments 1 and 2 a slight difference is seen between initial total and filtered Fe(II) concentrations, but they are within experimental error from

the third point on. Initial Eh conditions are slightly higher than in Experiment 2 at 400 mV, which may be a consequence of the higher DO concentration in this experiment. A similar Eh drop is seen on addition of the Fe(II) aliquot to 200 mV, which then declines rapidly to a minimum of 133 mV after 2665 seconds. This equates to a net decrease of 267 mV.

10.2.1.4 Experiment 4 – pH 7.1

Figure 10-4 shows Eh in mV, pH, total and filtered Fe(II) in mg L^{-1} against time in seconds for Fe(II) oxidation by dissolved O_2. Reaction conditions were, pH 7.11±0.02, 25.1±0.06 °C, 8.54±0.5 mg L^{-1} DO, 420 mg L^{-1} $NaHCO_3$, approximately 18 mg L^{-1} SO_4^{2-}, and initially ~ 10 mg L^{-1} Fe(II).

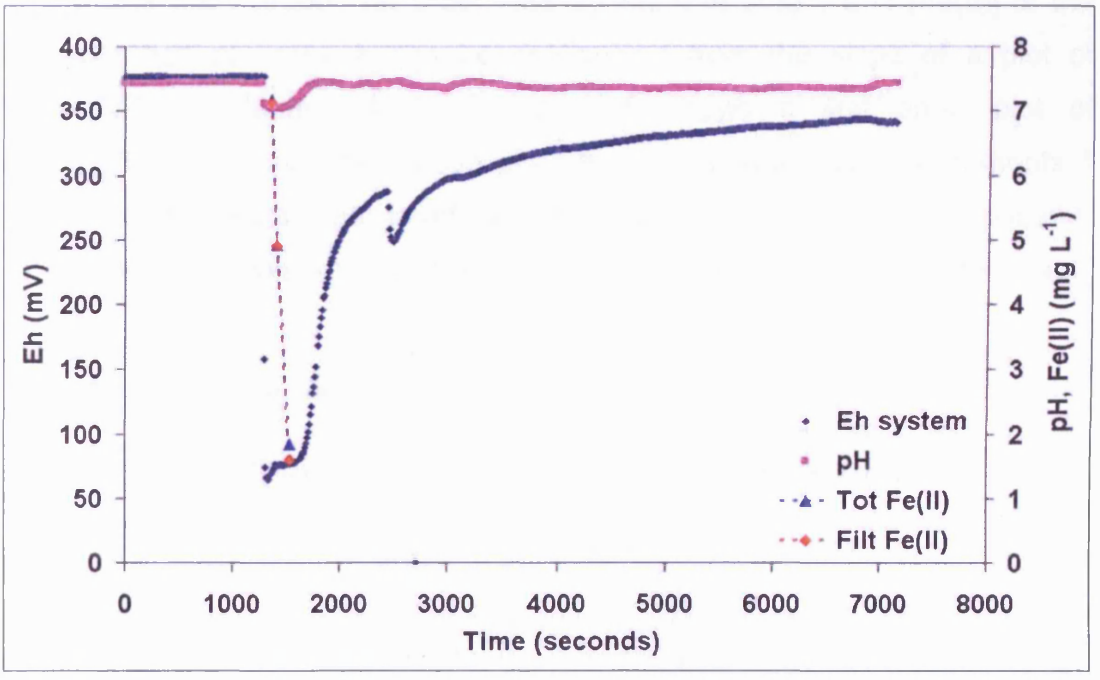

Figure 10-4: Experiment 4 – Homogeneous oxidation of Fe(II) at pH 7.1

Experimental conditions – pH(rate) 7.11±0.0195, 25.1±0.0 °C, DO 8.54±0.5 mg L^{-1}, $NaHCO_3$ 420 mg L^{-1}, SO_4^{2-} ~ 18 mg L^{-1}.

Oxidation of Fe(II) is rapid with concentrations reducing from 7.11 to 1.83 mg L^{-1} in 160 seconds, a net reduction of 5.28 mg L^{-1}. pH is reported as pH(rate). This is the mean pH over which reliable Fe(II) concentration data was obtained between 1330 and 1600 seconds. Initial Eh 375 mV decrease instantaneously on addition of the Fe(II) aliquot to 70 mV, before a gradual increase after this point.

10.2.2 Homogeneous oxidation rates

At constant pH and DO, the homogeneous oxidation of Fe(II) has been shown to be pseudo first order with respect to the concentration of Fe(II) (as shown by previous authors; Stumm and Lee, 1961; Sung and Morgan, 1980 etc). These authors have shown that the rate of oxidation of Fe(II) can be expressed by the equation:

Equation 10.1

$$\frac{-d[Fe(II)]}{dt} = k[Fe(II)]$$

where k is the pseudo first order rate constant in time^{-1}, and [Fe(II)] is the concentration of Fe(II). k can be determined from the slope of a plot of $\ln(Fe(II)/Fe(II)_o)$ against time. Figure 10-5 shows a first order plot of $\ln(Fe(II)/Fe(II)_o)$ against time in seconds for the homogeneous experiments 1 to 4 . In each case a linear trend line and R^2 value is included for comparison. The slope is equivalent to the inverse pseudo first order rate constant k in sec^{-1}.

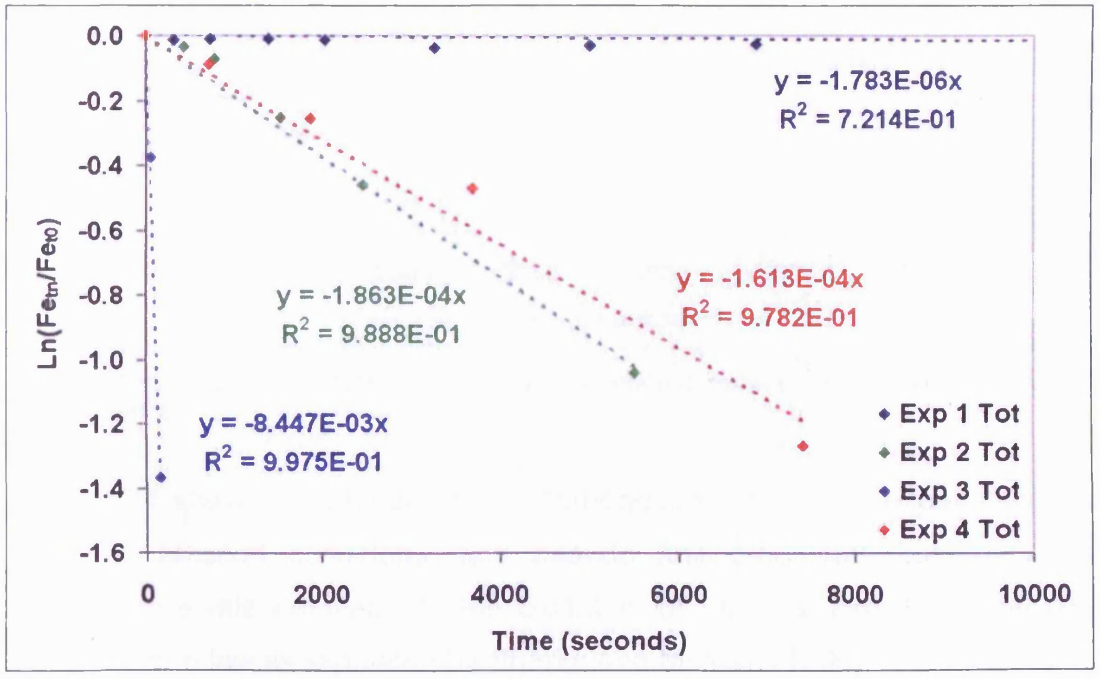

Figure 10-5: First order plot of $\ln(Fe_{tn}/Fe_{to})$ against time for homogeneous Fe(II) oxidation experiments

Although the R^2 value for Experiment 2 is high at 0.988, it can be seen that the initial rate (first three data points), and the rate determined towards the end of the experimental run diverge, as shown in Figure 10-6. This shows $\ln(Fe(II)/Fe(II)_O)$ against time determined for Experiment 2. Comparison of the slopes determined for the initial and end rate show that the end rate is 2.2 times faster than the initial oxidation rate, with vales of 1.97×10^{-4} and 8.82×10^{-5} sec^{-1} respectively. This is thought to be due to oxidation catalysed by freshly precipitated Fe(III) (hydroxy)oxides, which has been shown to occur at pH greater than 7 (Sung and Morgan, 1980). The effect is not so clear in Experiment 4. This could be due to compounded variable as the reaction conditions were not as tightly restrained, and fluctuations in temperature make determination of data difficult.

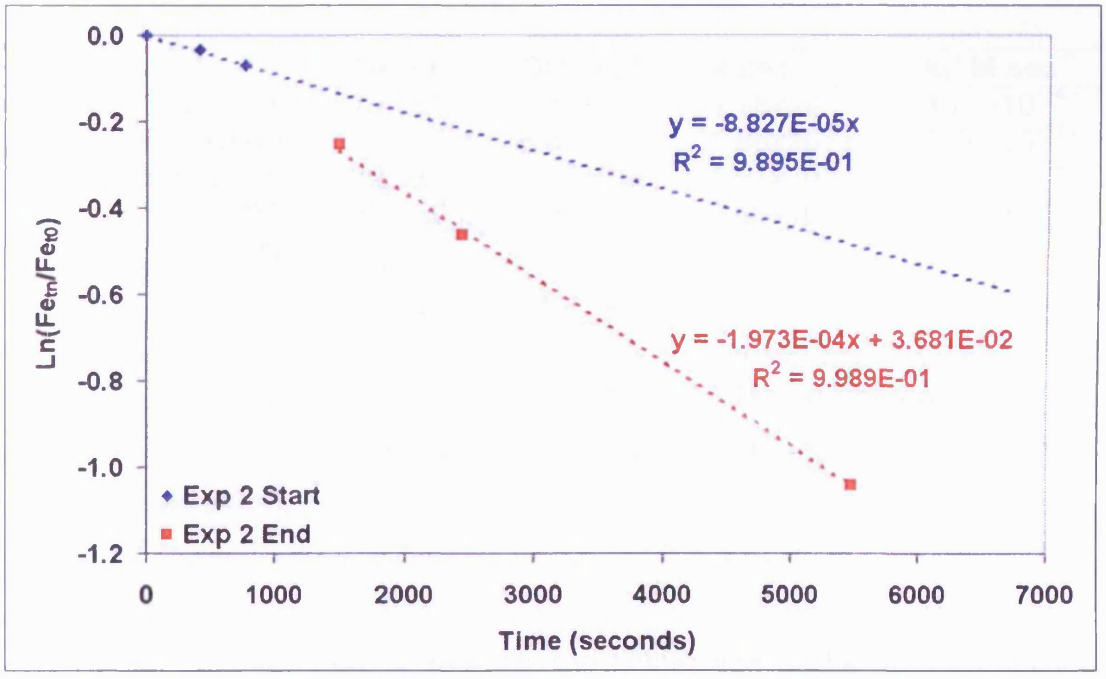

Figure 10-6: First order plot of $-Ln(Fe_{tn}/Fe_{to})$ against time for the start and end of experiment 2

Table 10.1 shows a summary of the homogeneous oxidation experiments in terms of reaction conditions, and pseudo first order rate constants. k_H indicates the rate constant for the oxidation of Fe(II) at circum-neutral pH, using the rate law as stipulated by Stumm and Morgan (1996):

Equation 10.2

$$\frac{d[Fe(II)]}{dt} = \frac{k_{II}[O_2(aq)]}{[H^+]^2}[Fe(II)]$$

where k_H is a constant in M sec^{-1} and [ ] indicates concentration in molar (M) and k_H is related to k via:

Equation 10.3

$$k_{II} = \frac{k[H^+]^2}{[O_2(aq)]}$$

Table 10.1: Homogeneous oxidation rate summary

Exp ID	pH [a]	Temp ^{O}C	DO mg L^{-1}	k sec^{-1}	k_1' M sec^{-1}
1	5.60±0.020	25.0±0.0	8.40±0.5	$1.78x10^{-6}$	$4.28x10^{-14}$
2	6.48±0.056	25.0±0.1	8.40±0.5	$1.86x10^{-4}$ [b]	$7.78x10^{-14}$ [c]
3	6.50±0.089	22.3±1.1	9.17±0.5	$1.61x10^{-4}$	$5.63x10^{-14}$
4	7.37±0.078	25.1±0.0	8.54±0.5	$8.45x10^{-3}$	$5.63x10^{-14}$

[a] *Stirred pH readings 800 rpm*
[b] *Initial k_1' $8.83x10^{-5}$ end k_1' $1.97x10^{-4}$ sec^{-1}*
[c] *Initial k_1' $3.68x10^{-14}$ End k_1' $8.23x10^{-14}$*

From the above data a mean value of $5.83x10^{-14}$ M sec^{-1} can be obtained. This is within the range of k_H values given by Davison and Seed (1983), from an extensive review of the literature (and from their own study) of 1.95 to $9.59x10^{-14}$ M sec^{-1} with a universal constant of $2.96x10^{-14}$.

The value presented here is towards the higher end of the range of values reported by Davison and Seed (1983), and above the values reported by Millero et al (1987), Tamura et al (1976a), and Ghosh (1974). It should be noted that pH was continuously monitored in this study, and therefore measurements are of a continuously stirred systems. Therefore a stirring error will be introduced into the system. Galster (1991) stated that the error incurred between stirring and not stirring should not exceed +0.02 pH units. In this study a negative error of -0.01 pH units was found between stirring and not stirring at pH 6. Adjustments of k_H to take account of the observed -0.01 pH

unit shift yields a mean value of $5.56x10^{-14}$ M sec^{-1}. It can be seen that the observed elevated rate cannot be accounted for by the stirring effect alone.

10.2.3 Experiments 5a and 5b - Heterogeneous oxidation, pH 6.5

Figure 10-7 and Figure 10-8 show reaction profiles determined for the heterogeneous oxidation of Fe(II) by dissolved oxygen at pH 6.5, in the presence of 200 mg L^{-1} of lepidocrocite using a bicarbonate / CO_2 buffer system. In each case concentrations of both total and filtered Fe(II) are shown in mg L^{-1} (as determined using the method shown in Section 9.3) along with the logged pH and Eh (mV) values. The values given below the figure for pH and temperature are mean values, and the ± are the SD of all readings taken. The Fe(III) (hydroxy)oxide used in Experiments 5a and 5b (termed Precipitate A) was sourced from a previous mine-water treatment experiment in the carried out at Cardiff University. Although the exact methods used in the study are not recorded, the Fe(III) (hydroxy)oxide was probably precipitated at pH greater than 9, using either NaOH or $Ca(OH)_2$ from a synthetic minewater solution. Precipitate A was identified as lepidocrocite with some calcite using XRD (see Appendix 1.1), although the exact proportions of $CaCO_3$ to γ-FeOOH where not determined. It should be noted that calcite is not easily distinguishable from the lepidocrocite trace using XRD analysis. Particle sizing of Precipitate A was determined using a Malvern instruments Version 2.19 long bed MasterSizer X laser sizer. The surface area using particle sizing data (Appendix 1) and assuming spherical particles leads to a mean particle size of 1.66 m^2 g^{-1} (using the lepidocrocite density of 4.09 g cm^{-1} as given by Cornell and Schwertmann, 2003).

10.2.3.1 Experiments 5a - lepidocrocite, pH 6.5

Figure 10-7 shows Eh in mV, pH, total and filtered Fe(II) in mg L^{-1} against time in seconds for Fe(II) oxidation by dissolved O_2. Reaction conditions were pH 6.455±0.006. 25.05±0.05 °C, 8.245±0.5 mg L^{-1} DO, 450 mg L^{-1} $NaHCO_3$, approximately 18 mg L^{-1} SO_4^{2-}, initially ~ 10 mg L^{-1} Fe(II), and 200 mg L^{-1} Fe(III) as lepidocrocite.

Filtered Fe(II) is seen to decrease rapidly from an initial 7.55 mg L^{-1} at the first sample to 0.069 mg L^{-1}, over a reaction time of 1935 seconds. This equates to a net decrease of 7.481 mg L^{-1}. Filtered samples taken after this point are below the detection limit of the analytical procedure used. Total Fe(II) show a reduction in concentration from 7.73 mg L^{-1} to 0.71 over the same 1935 second time period, equating to a net reduction of 7.02 mg L^{-1}. Divergence is seen between the total and filtered Fe(II) samples after the first sample point, with the lower filtered Fe(II) concentrations attributed to adsorption of Fe(II) at the lepidocrocite particle water interface. The reduction in total Fe(II) concentrations between 2610 and 4350 seconds can largely be attributed to oxidation of the remaining filterable Fe(II) portion, and beyond 4350 only negligible reduction in total Fe(II) is observed, (0.607 to 0.594 mg L^{-1} at 8580 seconds).

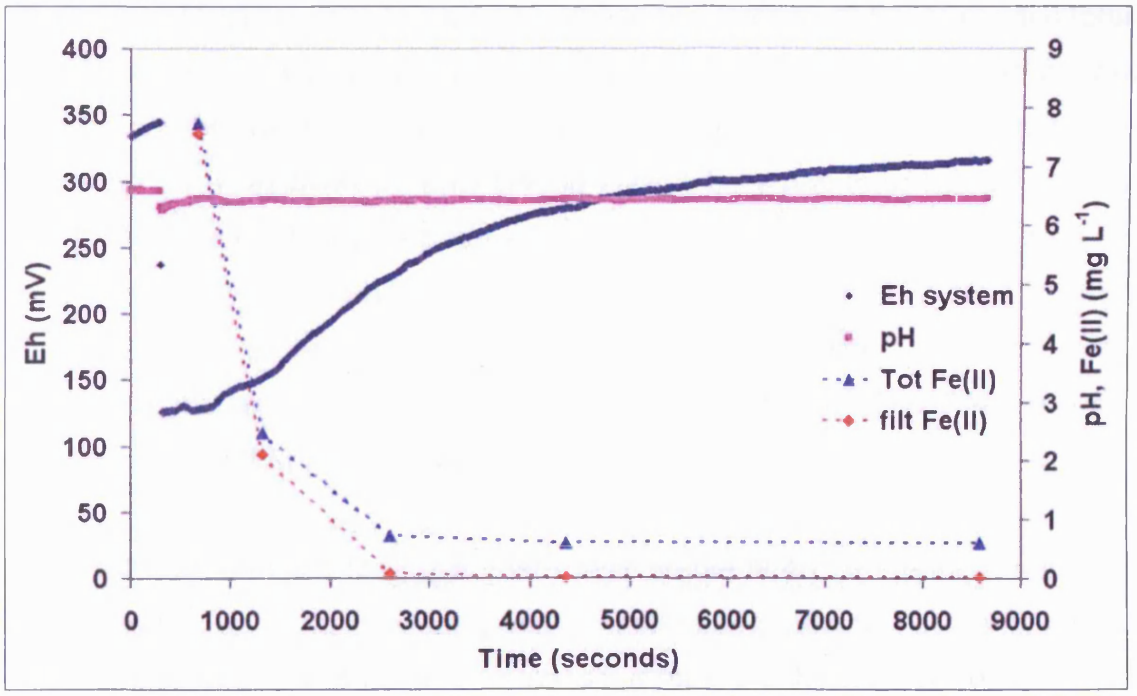

Figure 10-7: Experiment 5a – Heterogeneous oxidation of Fe(II) at pH 6.5

Experimental conditions – pH 6.455±0.006, 25.05±0.05 °C, DO 8.245±0.5 mg L^{-1}, $NaHCO_3$ 450 mg L^{-1}, SO_4^{2-} ~ 18 mg L^{-1}, initial Fe(III) 200 mg L^{-1} as lepidocrocite

System Eh has an initial high of 350 mV which decreases rapidly on addition of the Fe(II) stock aliquot to 126 mV. Eh is then shown to recover to 316 mV after 8540 seconds.

10.2.3.2 Experiments 5b - lepidocrocite, pH 6.5 (repeat)

Figure 10-8 shows Eh in mV, pH, total and filtered Fe(II) in mg L^{-1} against time in seconds for Fe(II) oxidation by dissolved O_2. Reaction conditions were pH 6.591±0.03, 24.95±0.05 °C, 8.33±0.5 mg L^{-1} DO, 1000 mg L^{-1} $NaHCO_3$, approximately 18 mg L^{-1} SO_4^{2-}, initially ~ 10 mg L^{-1} Fe(II), and 200 mg L^{-1} Fe(III) as lepidocrocite.

The experimental conditions are similar in all respects to Experiment 5a apart from a higher $NaHCO_3$ concentration. The intention of this was to see if increasing HCO_3^- concentration affects the observed results. However this was found to be inconclusive, and Experiment 5b proves more useful to qualitatively support the findings of Experiment 5a.

Experiment 5b shows similar trends to those of Experiment 5a. The initial total and filtered Fe(II) are comparable at 8.69 and 9.04 mg L^{-1} respectively. The discrepancy between total and filtered is likely to be caused by experimental or human error, as filtered Fe(II) should always be equal to or less than total Fe(II). After the third sample point at 2323 seconds, dissolved Fe(II) is seen to be largely below detection, whilst total Fe(II) is detectable at 0.74 mg L^{-1}. After 2323 seconds a reduction in total Fe(II) concentrations is seen, with concentrations reducing to 0.56 mg L^{-1} by 5948 seconds. The 5948 second value is comparable with the 8580 value of Experiment 5a.

System Eh determined for Experiment 5b is stable at 407 mV prior to addition of Fe(II) stock solution, at which point an instant decrease to 184.3 mV with a minimum of 168 mV after 270 seconds is seen. Whilst a full recovery of system Eh to levels prior to Fe(II) addition is not seen to the same extent as in Experiment 5a, system Eh is observed to recover. However, the initial system Eh was higher in Experiment 5b than Experiment 5a. The comparison of Eh values after 7000 seconds shows that the recovered Eh values are comparable at 307 and 329 mV respectively. The difference in initial Eh is

thought to be due to the difficulties in reproducible measurements of Eh in poorly poised solutions.

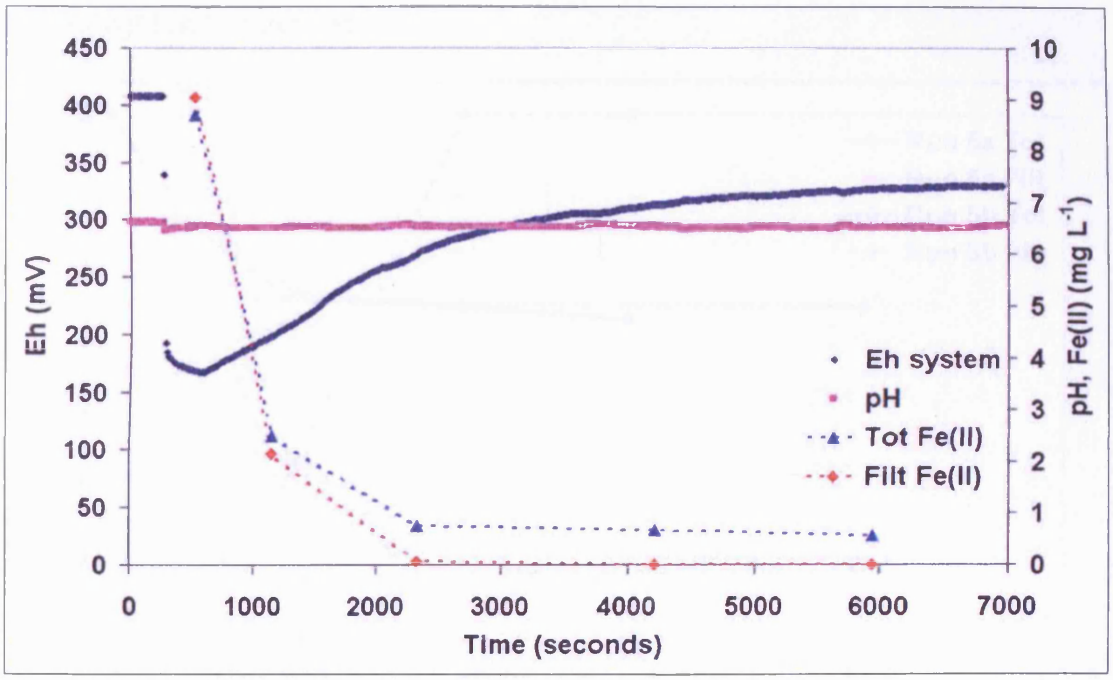

Figure 10-8: Experiment 5b- Heterogeneous oxidation of Fe(II) at pH 6.5

Experimental conditions – pH 6.591±0.03, 24.95±0.05 °C, DO 8.33±0.5 mg L^{-1}, $NaHCO_3$ 1000 mg L^{-1}, SO_4^{2-} ~ 18 mg L^{-1}, initial Fe(III) 200 mg L^{-1} as lepidocrocite.

10.2.4 Heterogeneous oxidation rates, pH 6.5

Figure 10-9 and Figure 10-10 show $\ln(Fe(II)/Fe(II)_O)$ determined for the total and filtered Fe(II) concentrations in Experiments 5a and 5b against time in seconds. Figure 10-9 shows $\ln(Fe(II)/Fe(II)_O)$ against time, determined for the full dataset. It can be seen that the linear relationship breaks down after the third data point at approximately 2000 seconds.

It can be seen that the rate of total Fe(II) oxidation slows considerably after this point and coincides with the observed increase in total non-oxidisable Fe(II) as shown in Figure 10-7 and Figure 10-8. It was found to be not present in the filtered portion and therefore can be attributed to the sorbed Fe(II). The breakdown of the linear relationship of $\ln(Fe(II)/Fe(II)_O)$ with time determined for the filterable Fe(II) portion, can be attributed to the sensitivity of the

analytical method used and it would be expected that the near linear dependence of $\ln(Fe(II)/Fe(II)_O)$ against time for filterable Fe(II) would continue, if the detection limit of the analytical technique was enhanced using longer light path cuvettes.

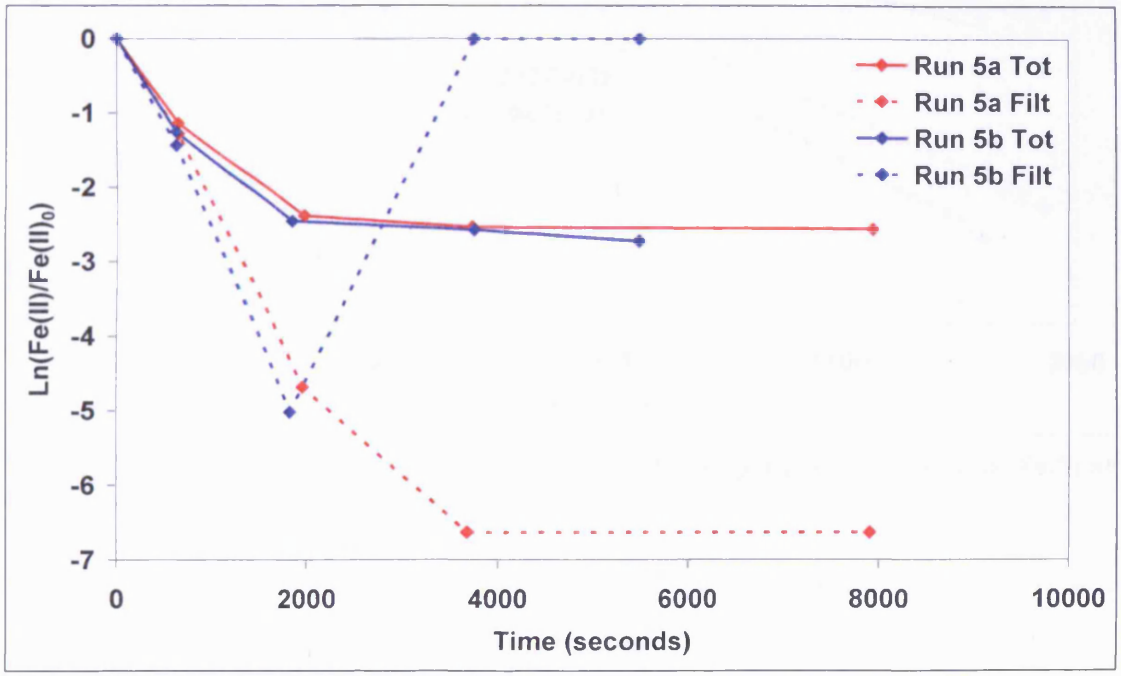

Figure 10-9: Pseudo first order reaction plot for the heterogeneous oxidation of Fe(II) at pH 6.5 in Experiments 5a and 5b

Figure 10-10 shows $\ln(Fe(II)/Fe(II)_O)$ against time for the linear part (first three data points) of the data shown in Figure 10-9. It is evident that the oxidation rates determined in experiment 5b are slightly higher than those determined in experiment 5a, which would correspond with the slightly higher mean values of pH and DO. On close examination of the initial data it can be seen that initial rates determined from both filtered and total Fe(II) are similar. However they quickly diverge with increasing non-oxidisable sorbed Fe(II). It can be assumed that the true rate of Fe(II) oxidation is represented by the total Fe(II) concentration. The filtered Fe(II) rate takes into account both true oxidation and also removal from solution as non-oxidisable sorbed Fe(II).

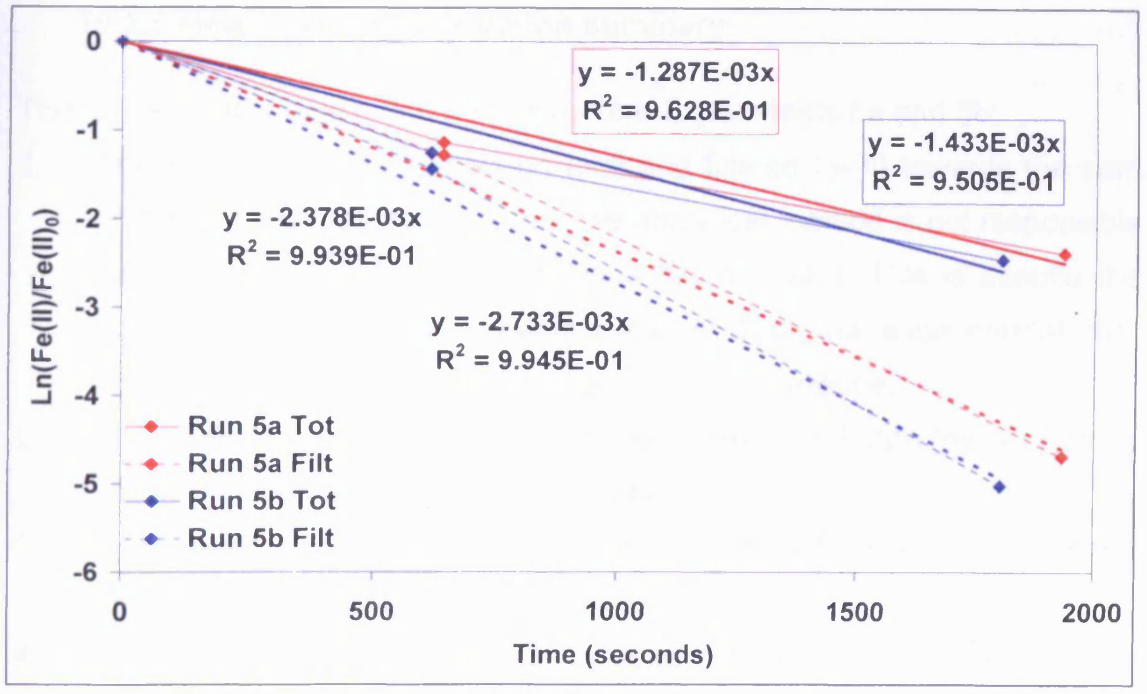

Figure 10-10: Pseudo first order reaction plot for heterogeneous oxidation of Fe(II) at pH 6.5 in Experiments 5a and 5b for Initial data points

In order to determine the true oxidation rate for Fe(II) removal from the system it would be necessary to pre-equilibrate Fe(II) with the Fe(III) (hydroxy)oxide surface prior to the commencement of the oxidation experiment. In Experiments 5a and 5b it is evident that the detectable sorbed Fe(II) is non-oxidisable. This indicates that if a reactive surface species forms, it is rapidly oxidised at a rate greater than or equal to the rate of its formation. Park and Dempsey (2005) found that no oxidation of sorbed Fe(II) took place during their experiments, in which Fe(II) was pre-equilibrated with freshly precipitated Fe(III) (hydroxy)oxide. The heterogeneous oxidation rates are summarised in Table 10.2.

Table 10.2: Heterogeneous oxidation rate summary determined using filtered Fe(II)

Exp ID	pH [a]	Temp ^{O}C	DO mg L^{-1}	k sec^{-1} All data	k sec^{-1} Initial	k sec^{-1} End
					$x10^{-3}$	
5a	6.455±0.01	25.05±0.05	8.24±0.5	2.378	1.985	2.64
5b	6.591±0.03	24.95±0.05	8.33±0.5	2.733	2.318	3.026

10.2.5 Heterogeneous oxidation summary

The following key points can be drawn from Experiments 5a and 5b:

1. The close agreement between total and filtered Fe(II) towards the start of the experiments, indicate that the analytical method is not responsible for the difference between total and filtered Fe(II). This is despite the lack of adsorbed Fe(II) towards the end of the experimental run. Therefore the total Fe(II) observed is a real occurrence.
2. The surface bound Fe(II) does not desorb from the Fe(III) (hydroxy)oxide surface in the absence of Fe(II) in solution.
3. The Fe(III) (hydroxy)oxide surface acts as an effective catalyst for the oxidation of Fe(II) from solution by DO.
4. A portion of surface bound Fe(II) does not oxidise rapidly despite the presence of oxygen.
5. System Eh recovers to pre Fe(II) addition levels, indicating that residual sorbed Fe(II) is not strongly reducing.

The results observed here are consistent with the results of Park and Dempsey (2005). They observed residual Fe(II) on the surface of freshly precipitated ferrihydrite, and ferrihydrite partially converted to goethite at pH 6.8 to 7.

10.2.6 Experiments 6a and 6b - Adsorption of Fe(II) onto lepidocrocite, pH 6.5

Two duplicate experiments were undertaken to determine the behaviour of Fe(II) adsorptionto lepidocrocite under circum-neutral pH conditions in a bicarbonate buffer system. Experiments were carried out under anoxic conditions in a nitrogen atmosphere. Details of the experimental procedure are given in Section 9.4.

The Fe(III) (hydroxy)oxide used in the adsorption experiments was a synthetic lepidocrocite (Bayferrox 943) obtained from Lanexess (Germany), and used

previously in a study of Fe(II) adsorption (Zhang et al, 1992). The Bayferrox 943 was fully characterised as shown in Table 10.3. The ochre used in Experiments 5a and 5b was unfortunately not fully characterised. Therefore the lepidocrocite constituents of this ochre are assumed to share identical properties to that of Bayferrox 943.

Table 10.3: Characterisation of Bayferrox 943 and 930

Analyte	Method	Units	Bayferrox 943	Bayferrox 930
Mineralogy	XRD		Lepidocrocite	Goethite
Fe	Digest	%	71	69
SA*	BET	$m^2 g$	17	15
Shape	EM#		Acicular	Acicular
Size	EM#	µm	0.05x0.3	0.2x0.8
Density	DIN+	$g\ mL^{-1}$	3.8	4.1

SA – Specific surface Area EM – Electron Micrograph # Lanxess (2005) + DIN EN ISO 787 Teil 10 (1995) from Lanxess (2005)

10.2.6.1 Experiment 6a – Adsorption of Fe(II) onto lepidocrocite, pH 6.5

Figure 10-11 shows Eh in mV, pH, total and filtered Fe(II) in mg L^{-1} against time in seconds for the adsorption of Fe(II) onto 200 mg L^{-1} of Bayferrox 943 (lepidocrocite) in Experiment 6a. The lepidocrocite was added as a slurry and the reaction conditions were, pH 6.48±0.0155, 25.05±0.05 °C, ~0 mg L^{-1} DO (N_2 atmosphere), 510 mg L^{-1} $NaHCO_3$, approximately 18 mg L^{-1} SO_4^{2-}, and initially ~ 10 mg L^{-1} Fe(II).

Logging started 7461 seconds after addition of an aliquot of Fe(II) stock. Therefore time 0 in Figure 10-11 represents 7461 seconds after Fe(II) addition. Filter Fe(II) concentrations are not seen to decrease significantly during the duration of sampling, and variation in Fe(II) is reflected in both total and filtered Fe(II) concentrations. Mean values of 10.68 and 9.21 mg L^{-1} can be ascertained for the total and filtered samples respectively, which equates to a mean sorbed concentration of 1.473 mg L^{-1}.

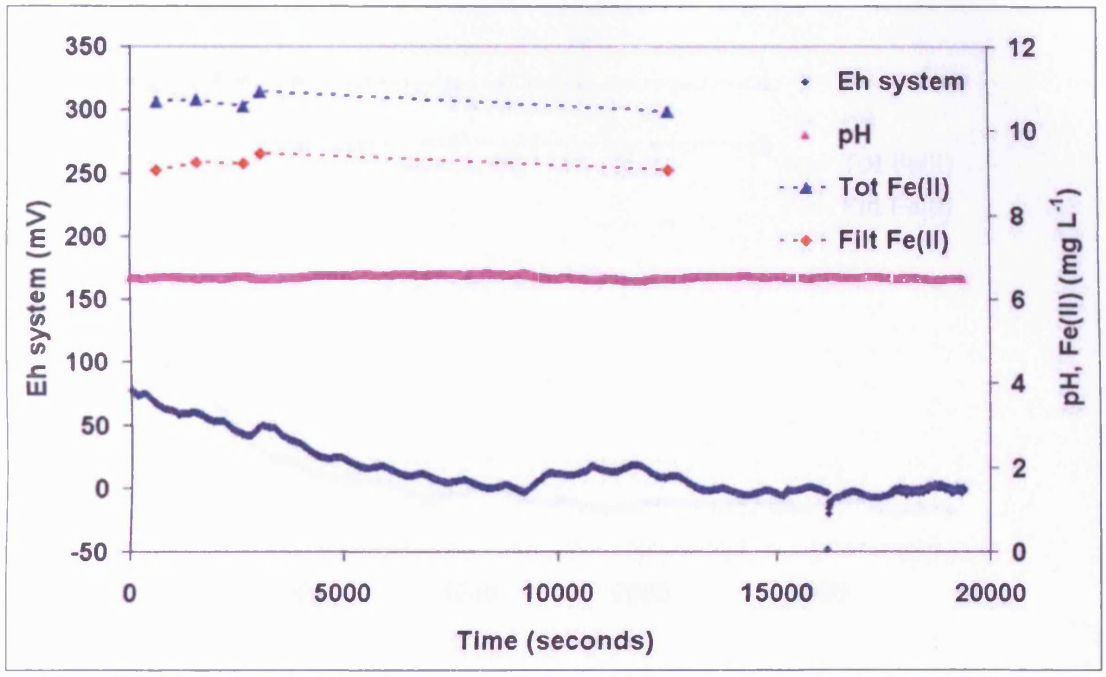

Figure 10-11: Experiment 6a - Fe(II) adsorption under N_2 pH 6.5

Experimental conditions – pH 6.48±0.0155, 25.05±0.05 °C, DO ~ 0 mg L^{-1}, $NaHCO_3$ 510 mg L^{-1}, SO_4^{2-} ~ 18 mg L^{-1}, Fe(III) 200 mg L^{-1} as Bayferrox 943 (lepidocrocite).

System Eh values are seen to decrease from an initially recorded value (although not a pre Fe(II) addition value) of 75 mV, to a minimum of – 7 mV. Local variation in the system Eh is largely due to small scale pH variation and the dependence of Eh on pH.

10.2.6.2 Experiment 6b – Adsorption of Fe(II) onto lepidocrocite pH 6.5 (repeat)

Figure 10-12 shows Eh in mV, pH, total and filtered Fe(II) in mg L^{-1} against time in seconds for the adsorption of Fe(II) onto 200 mg L^{-1} of Bayferrox 943 (lepidocrocite) in Experiment 6b. In this experiment lepidocrocite was added as a dried powder, and the reaction conditions were, pH 6.49±0.024, 25.0±0.0 °C, ~0 mg L^{-1} DO (N_2 atmosphere) , 503 mg L^{-1} $NaHCO_3$, approximately 18 mg L^{-1} SO_4^{2-}, and initially ~ 10 mg L^{-1} Fe(II).

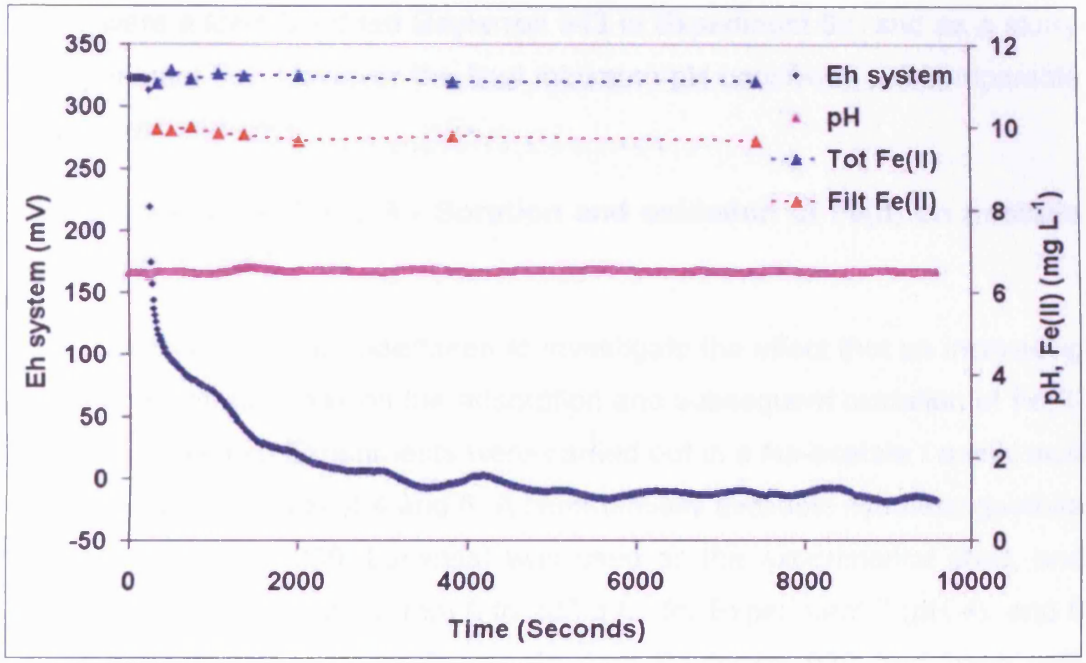

Figure 10-12: Experiment 6b - Fe(II) adsorption under N_2 at pH 6.5

Experimental conditions – pH 6.49±0.024, 25.0±0.0 °C, DO ~ 0 mg L^{-1}, $NaHCO_3$ 503 mg L^{-1}, SO_4^{2-} ~ 18 mg L^{-1}, Fe(III) 200 mg L^{-1} as Bayferrox 943 (lepidocrocite).

Experiment 6b was carried out under identical conditions to Experiment 6a, and Eh and pH logging was undertaken prior to addition of Fe(II). Samples were also removed for the determination of Fe(II) immediately after the addition of the Fe(II) aliquot. Mean total and filtered Fe(II) concentrations were determined as 11.19 and 9.84 mg L^{-1} respectively, which equates to a sorbed Fe(II) concentration of 1.35 mg L^{-1}. Filtered Fe(II) concentrations do not show a significant decrease after the first sample point. This suggests that sorption of Fe(II) to the lepidocrocite surface is rapid, and is largely complete within the 110 seconds time span between Fe(II) addition, and the taking of the first sample. System Eh is 325 mV prior to Fe(II) addition which drops sharply to 126 mV in the 120 seconds following Fe(II) addition. A gradual decrease in Eh is then observed, with Fe(II) decreasing to a minimum of – 16 mV at approximately 5300 seconds. After this no further decrease is seen. The time taken for minimum system Eh conditions to be reached in Experiment 6b, is considerably shorter following Fe(II) addition than in Experiment 6a. There is no clear reason for this. It is possible that the effect could be due to the state of the platinum combination electrode, or possibly due to the form in which the

solids were added (as dried Bayferrox 943 in Experiment 6a, and as a slurry in Experiment 6b). However the final minimum pH conditions are comparable for both experiments.

10.3 Experiments 7 and 8 - Sorption and oxidation of Fe(II) on goethite at pH 4 and 6

Two experiments were undertaken to investigate the effect that an increasing solids concentration has on the adsorption and subsequent oxidation of Fe(II) at mildly acidic pH. Experiments were carried out in a Na-acetate / acetic acid buffered solution at pH of 4 and 6. A commercially available synthetic goethite pigment (Bayferrox 930, Lanxess) was used as the experimental solid, and concentrations were varied from 0 to 200 g L^{-1} for Experiment 7 (pH 4), and 0 to 50 g L^{-1} for Experiment 8 (pH 6). The Bayferrox 930 had been well characterised, and the materials properties are included in Table 10.3.

As described in detail in Section 9 experiments were undertaken in a nitrogen atmosphere to prevent Fe(II) oxidation and were degassed under vacuum prior to addition of Fe(II). Experiments were undertaken in 60 mL centrifuge tubes and reaction solutions were de-gassed under vacuum to remove dissolved oxygen. Reaction mixtures containing goethite, buffer and Fe(II) stock solution were then allowed to equilibrate for 24 hours under nitrogen. Samples were subsequently taken for the determination of dissolved (as determined by filtration or centrifugation) and total (as determined by filtration or centrifugation after a 24 hour extraction in 0.5 N HCl) Fe(II).

The reactor tubes were then removed from the nitrogen glove box, and exposed to atmospheric oxygen (to allow sample oxygenation) and a further 48 hour reaction period was allowed. After this, further samples were taken for the determination of dissolved and total Fe(II). pH and temperature readings were also taken. All experiments were carried out in triplicate.

10.3.1 Experiment 7 - Heterogeneous oxidation and adsorption of Fe(II) to goethite pH 4

Figure 10-13 and Figure 10-14 show the mean concentrations of dissolved and total Fe(II) in mg L^{-1}, against goethite concentration in g L^{-1} both before and after the 48 hour oxidation period. Error bars (where visible) represent SD from the mean of singular readings, from triplicate experiments. The calculated values of the total minus dissolved Fe(II) are included for comparison, and represent the recoverable sorbed Fe(II) portion. Initial conditions were 10.75 mg L^{-1} total Fe(II) in a 10 mM Na-acetate / acetic acid buffer solution, pH 3.917±0.012, and temperature 25.27±0.125 °C. pH and temperature are means of individual values determined at the end of the experimental run, and ± error indicate SD of measurements from the triplicate experiments.

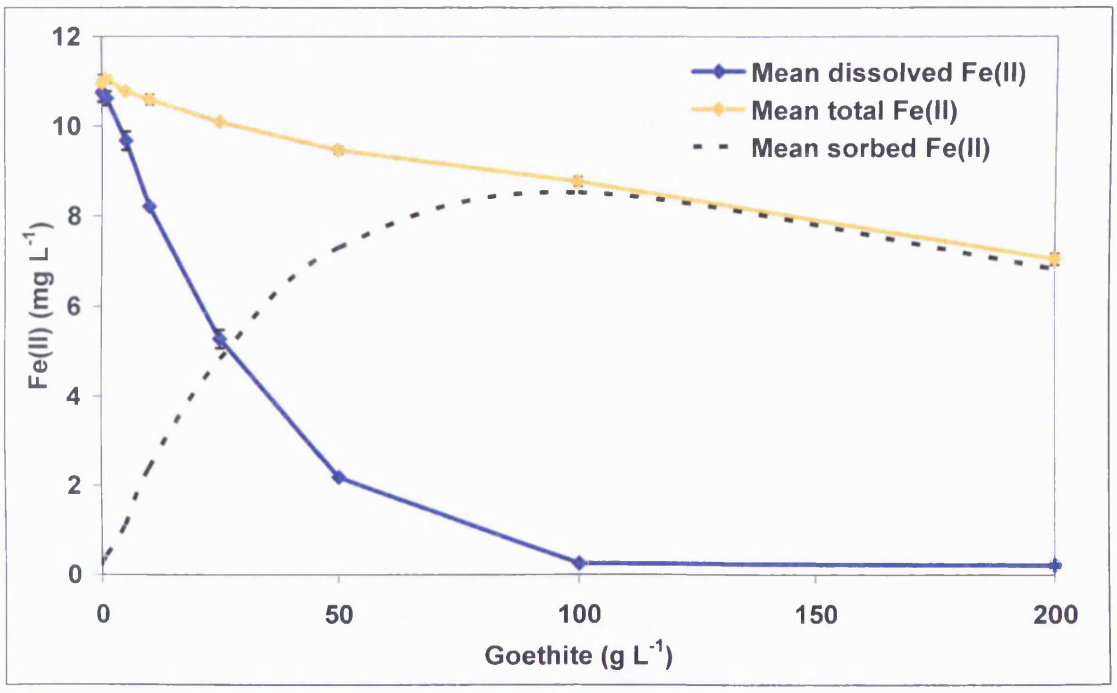

Figure 10-13: Mean total, filtered and sorbed Fe(II) concentrations against goethite concentration Experiment 7 after 24 hours equilibration under N_2

Examination of the data presented in Figure 10-13 shows that the concentration of total Fe(II) is not constant throughout the experiments. It is seen to decrease from 10.75 mg L^{-1} in the absence of goethite, to 6.72 mg L^{-1} in the presence of 200 g L^{-1} of goethite. This equates to a reduction of 4.03

mg L^{-1}. This could be due tp incomplete recovery of sorbed Fe(II) from the goethite surface or to the presence of trace dissolved oxygen concentrations.

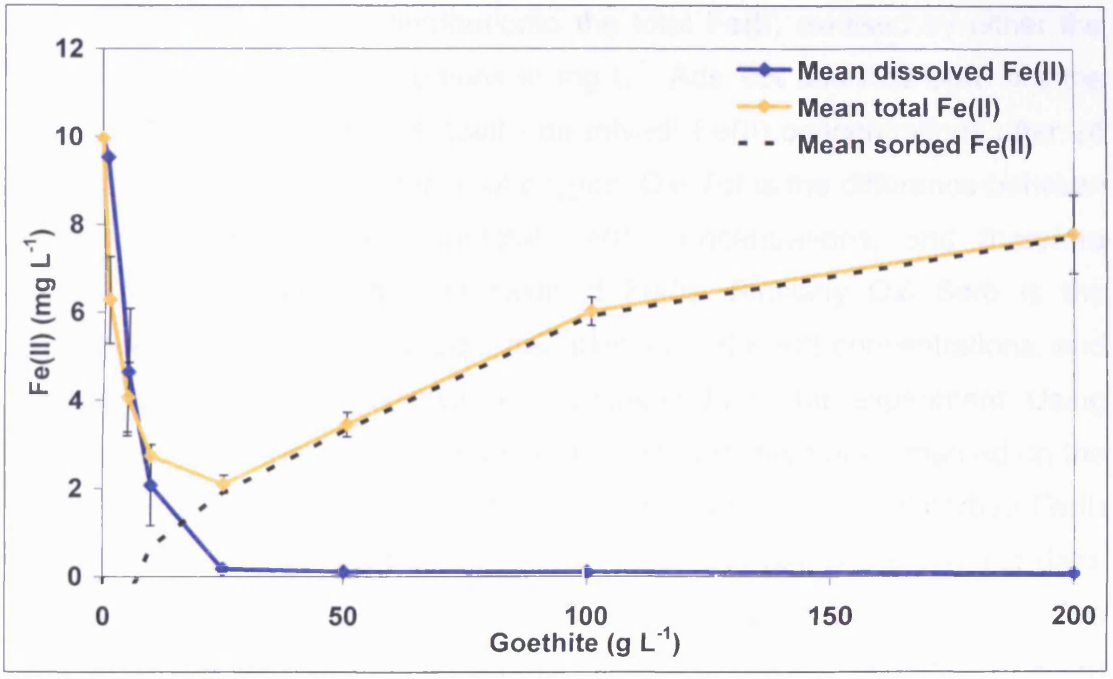

Figure 10-14: Mean total, filtered and sorbed Fe(II) concentrations against goethite concentration in Experiment 7 48 hours aerial oxidation

Complete adsorption of Fe(II) was not found in the pH 4 experiments, and a detectable residual Fe(II) was present even at 200 g L^{-1} goethite. Dissolved concentrations in Figure 10-13 are shown to decrease with increasing goethite concentration. There was an initial mean value of 10.75 mg L^{-1} in the goethite free experiment, to 0.25 mg L^{-1} at 100 g L^{-1} goethite and 0.21 mg L^{-1} at 200 g L^{-1} goethite. After 48 hours aeration, no detectable dissolved Fe(II) is evident above goethite concentrations of 50 g L^{-1}. It is also evident that complete oxidation of total Fe(II) did not occur at any goethite concentration as shown in Figure 10-14. Initial concentrations of total Fe(II) with no added goethite are shown to have decreased from 10.75 to 9.96 mg L^{-1}, a reduction of 0.79 mg L^{-1} after 48 hours oxidation. Post oxidationtotal Fe(II) is shown to reduce with increasing goethite concentrationto a minimum at 25 g L^{-1}, with total Fe(II) concentrations decreasing from 10.03 to 2.079 mg L^{-1}. It is evident that a significant portion of sorbed Fe(II) is not oxidised during the 48 hour oxidation period. The proportion of this increases with increasing goethite

concentration until, at 200 g L^{-1}, the non-oxidisable portion represents 100 % of the total Fe(II).

Figure 10-15 shows the contributionto the total Fe(II) oxidised by either the dissolved or sorbed Fe(II) portions in mg L^{-1}. Ads Tot and Ads Sorb are the determined total, and sorbed (total - dissolved) Fe(II) concentrations after 24 hour equilibration in the absence of oxygen. Oxi Tot is the difference between initial total and post oxidationtotal Fe(II) concentrations, and therefore represents the total portion of oxidised Fe(II). Similarly Oxi Sorb is the difference between initial and post oxidation sorbed Fe(II) concentrations, and represents the portion of sorbed Fe(II) oxidised during the experiment. Using the above criteria three regions can be defined, and have been marked on the chart. The area below the Oxi Sorb data indicates the portion of sorbed Fe(II) oxidised. The area above the Oxi Sorbed data and below the Oxi Tot data, indicates the contribution of dissolved Fe(II) to the total oxidised Fe(II). The area above the Oxi Tot and below the Ads Tot line, show the portion of Fe(II) remaining in the experiments. The areas above the Oxi Sorb data and below the Ads Sorb data represents the portion of non-oxidisable sorbed Fe(II).

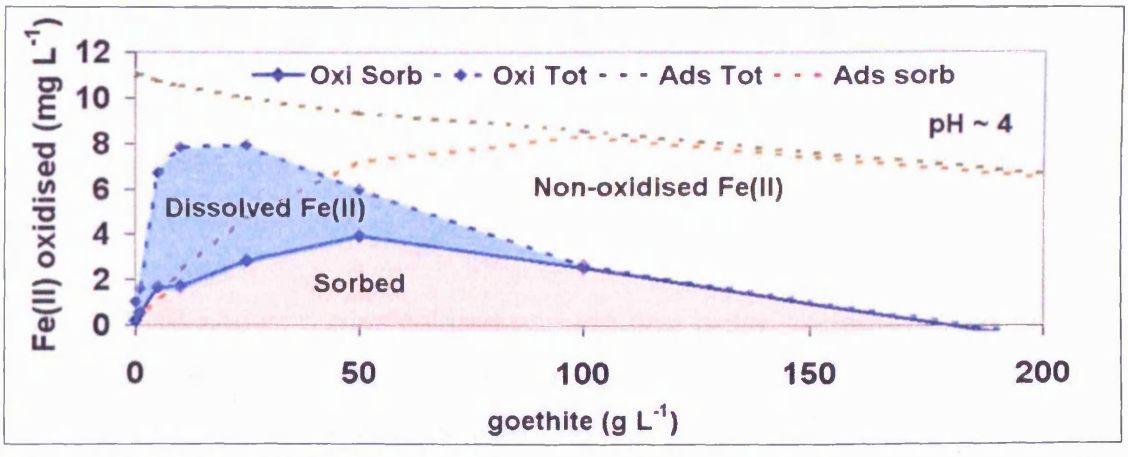

Figure 10-15: Proportions of dissolved and sorbed Fe(II) oxidised against goethite concentration in Experiment 7.

Ads Tot and Ads Sorb are the determined total, and sorbed (total - dissolved) Fe(II) concentrations after 24 hour equilibration in the absence of oxygen. Oxi Tot is the difference between initial total and post oxidationtotal Fe(II) concentrations, and therefore represents the total portion of oxidised Fe(II). Similarly Oxi Sorb is the difference between initial and post oxidation sorbed Fe(II) concentrations, and represents the portion of sorbed Fe(II) oxidised during the experiment.

The contribution made by reductions in dissolved and sorbed Fe(II) to the total Fe(II) oxidised, changes with increasing goethite concentration. Below 25 gL^{-1} goethite, the total Fe(II) oxidised is dominated by a reduction in the dissolved Fe(II) portion, as the amount of sorbed Fe(II) is low (< 35 %) in comparisonto the dissolved Fe(II) portion. It is evident that the portion of non-oxidisable sorbed Fe(II) increases with increasing goethite concentration, and that the maximum contribution of sorbed Fe(II) to the overall Fe(II) reduction is ~ 65 % at goethite concentrations of 50 g L^{-1}. Above this point the ratio of oxidisable to total sorbed Fe(II) decreases to zero at 200 g L^{-1} goethite.

From analysis of the data presented in Figure 10-13 to Figure 10-15 a number of key observations can be drawn:

1. The total Fe(II) determined by 0.5 N HCl extraction decreases with increasing goethite concentration in absence of oxygen
2. There is incomplete oxidation of Fe(II) after aeration for 48 hours.
3. The amount of Fe(II) oxidised in the 48 hour aeration period increases with increasing goethite concentration, up to a goethite concentration of 25 g L^{-1}, where 79.3 % total and 96.6 % dissolved Fe(II) oxidised in 48 hours.
4. Above 25 g L^{-1} goethite amount of total Fe(II) oxidised in 48 hours decreases to 63.7 % at 50 g L^{-1}, 31.44 % at 100 g L^{-1} and ~ 0 % at 200 mg L^{-1}.

Figure 10-16 shows the calculated pseudo first order oxidation rates in sec^{-1} for the pH 4 adsorption-oxidation experiments determined for mean dissolved and total Fe(II) concentrations over the 48 hour oxidation period, against goethite concentrations in g L^{-1}. Error bars (where visible) represent the range of maximum and minimum k values determined from adsorption maximum to post oxidation minimum Fe(II) data (maximum k), and from adsorption minimum to post oxidation maximum Fe(II) data (minimum k). Post 25 g L^{-1} goethite concentration k values determined for filterable Fe(II), are minimum rates as in each case dissolved Fe(II) (as determined via centrifugation) was

below the detection limit of the analytical procedure. In each case values of k were determined as follows

Equation 10.4

$$k = \frac{-\ln(Fe(II)_{Oxi} / Fe(II)_{Ads})}{Time}$$

Where k is the pseudo first order rate constant in sec^{-1}, $Fe(II)_{Oxi}$ is the concentration of Fe(II) after oxidation for 48 hours, $Fe(II)_{Ads}$ is the concentration of Fe(II) prior to oxidation, and Time is the time in seconds. In each case Fe(II) can be either the total, or dissolved Fe(II) concentrations.

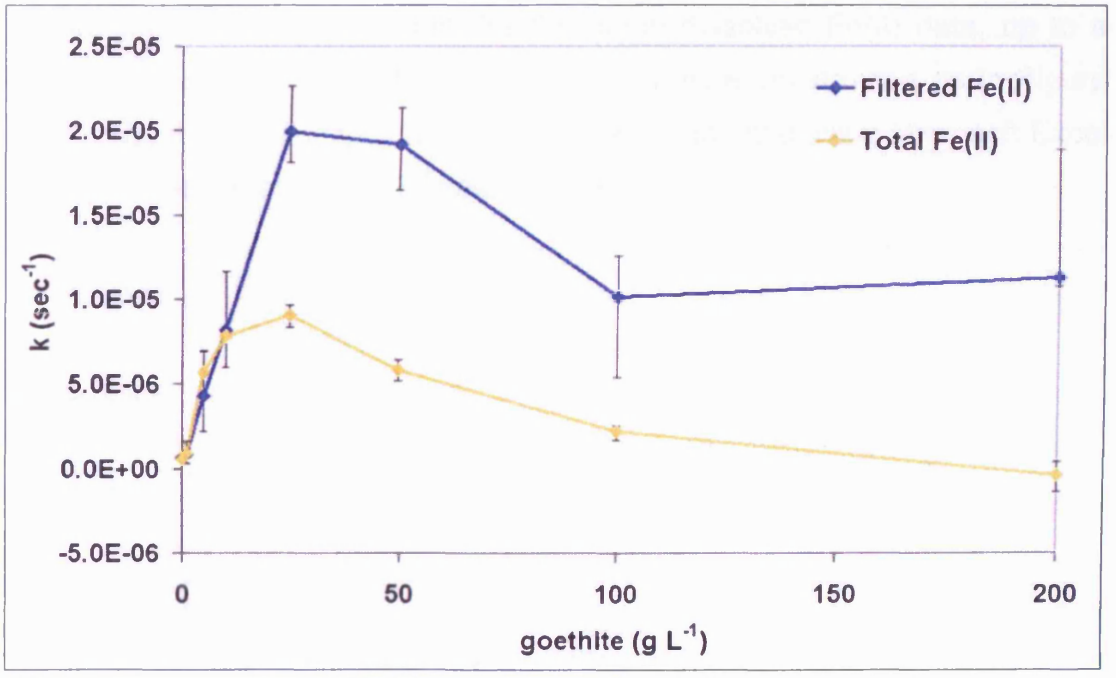

Figure 10-16: Pseudo first order Fe(II) oxidation rate constants determined for filtered and HCl extractable Fe(II) against goethite concentration in Experiment 7

It can be seen that up to 10 g L^{-1} of Bayferrox 930 the calculated pseudo first order oxidation rates, determined for both the HCl extractable and filterable Fe(II) portions, increases linearly with increasing solids concentration. The calculated rates for each of these portions are within experimental error. The 25 g L^{-1} filtered Fe(II) value follows closely the linear trend observed in the previous data points, whilst there is a considerable difference observed between the total and dissolved Fe(II) oxidation rates. The observed reduction

in the filterable Fe(II) oxidation rates in the post 25 g L^{-1} data, is due to the near complete sorption of the initial Fe(II), or to the near complete oxidation of Fe(II) at the end of the 48 hour oxidation timescale. It should be noted that pseudo first order kinetics are assumed during the determination of rate constants, and cannot be proven as only two data points are determined e.g. initial and post 48 hours. Constant saturated DO conditions were assumed during these experiments, and should be expected. This is because the reaction vessels were mixed end over end and sufficient head space to liquid ratio allowed for a considerable excess of O_2.

Figure 10-17 shows the pseudo first order rate determined for the pH 4 adsorption-oxidation experiment for the mean dissolved Fe(II) data, up to a goethite concentration of 25 g L^{-1}. Error bars were constructed as in Figure 10-16. The dashed line indicates a linear trend line fitted using Microsoft Excel and the slope equation and R^2 values are shown.

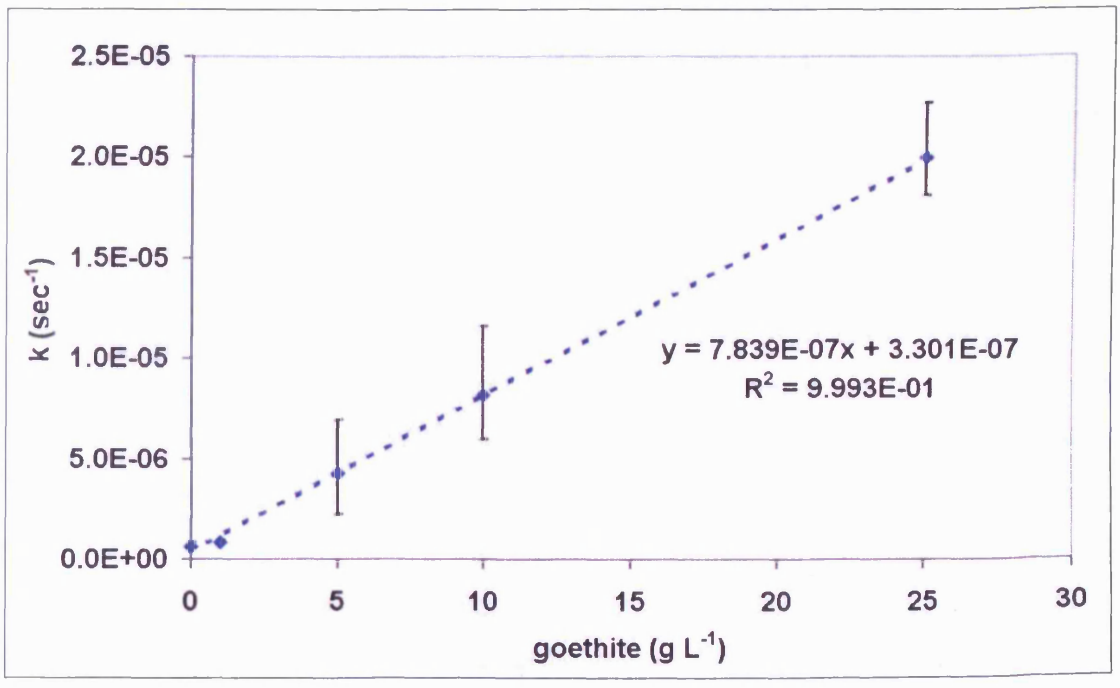

Figure 10-17: Pseudo first order rate constants determined for dissolved Fe(II) in the presence of goethite from Experiment 7

At pH 4 the rate of oxidation determined using the concentration of dissolved Fe(II), has a linear dependence on goethite concentration, with the following relationship found up to goethite = 25 g L^{-1} :

Equation 10.5

$$k = \beta_1 [Fe(III)] + k_1$$

where k is the pseudo first order constant in sec^{-1} determined from filterable Fe(II) concentrations, β_1 is the slope constant for the dependence of the oxidation rate on goethite concentration (7.84×10^{-7} L g^{-1} sec^{-1}), [Fe(III)] is the concentration of Bayferrox 930 (goethite) in g L^{-1}, and k_1 is the homogeneous pseudo first order rate constant for the oxidation of Fe(II) (3.301×10^{-7} sec^{-1}). The linear trend was found to have a very high correlation with an R^2 value of 0.9993. The rate constant can be normalised for goethite concentration as follows:

Equation 10.6

$$k_{Gt} = \frac{k}{[Fe(III)]}$$

where k_{Gt} is the goethite solids concentration normalised rate constant in sec^{-1} g^{-1} L, k is the pseudo first order rate constant for the oxidation of dissolved Fe(II) in sec^{-1}, and [Fe(III)] is the concentration of goethite in g L^{-1}.

Figure 10-18 shows k_{Gt} in sec^{-1} g^{-1} L, against goethite concentration in g L^{-1}. The pseudo first order rate for the homogeneous oxidation of Fe(II) is also shown as a red diamond. Error bars are determined as in the method described for Figure 10-16. The dashed line indicates the mean value determined for k_{Gt}.

As shown in Figure 10-18, a mean value for k_{Gt} of $8.19 \pm 0.213 \times 10^{-7}$ sec^{-1} g^{-1} L can be determined, where the ± error is the SD of all ascertained mean values. However the maximum range is 0.4 to 1.35×10^{-6} sec^{-1} g^{-1} L as determined from the range of maximum and minimum rate data. Using the data previously described the following rate law can be devised:

Equation 10.7

$$\frac{-d[Fe(II)_{diss}]}{dt} = (k + k_{Gt}[Fe(III)])[Fe(II)_{diss}]$$

where k is determined as 6.1×10^{-7} sec^{-1}, k_{Gt} is 8.19×10^{-6} sec^{-1} g^{-1} L, $[Fe(II)_{diss}]$ is the dissolved Fe(II) concentration of molar, and [Fe(III)] is the goethite solids concentration in g L^{-1}, assuming first order behaviour of filterable Fe(II). This rate law in this form is shown to be valid for [Fe(III)] as Bayferrox 930 up to 25 g L^{-1} at pH 3.917±0.012 and temperature 25.27±0.125 °C, and DO saturated solutions of 10 mM Na-acetate / acetic acid buffer.

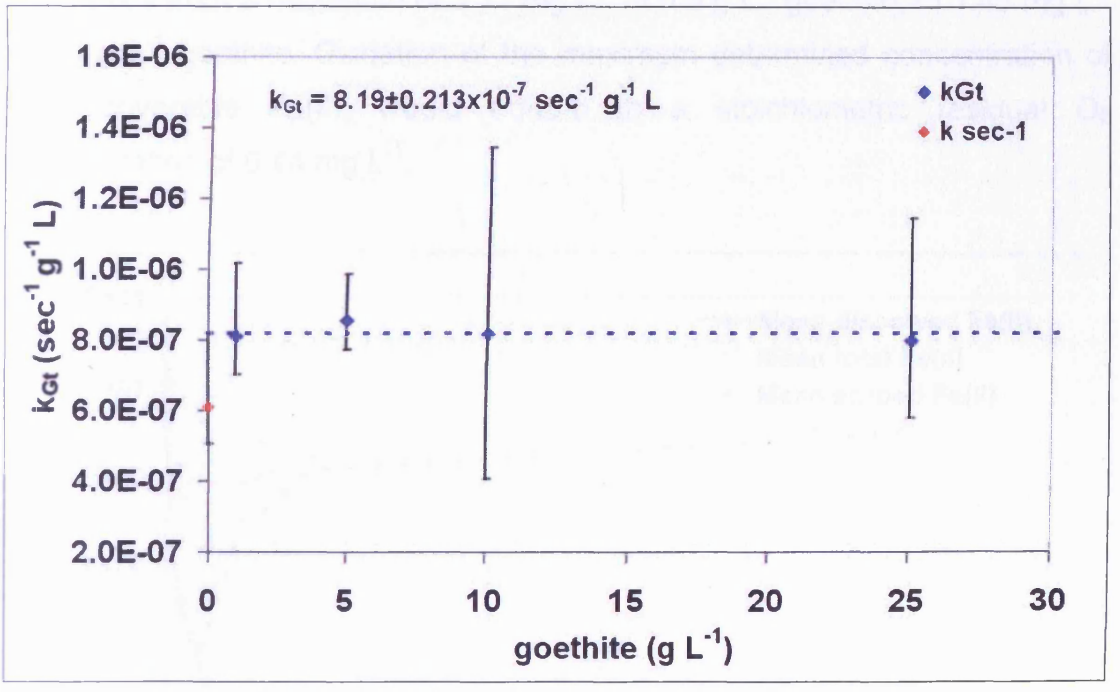

Figure 10-18: Goethite normalised rate constant determined using filtered Fe(II) concentrations against goethite concentration in Experiment 7

10.3.2 Experiment 8 - Heterogeneous oxidation and adsorption of Fe(II) to goethite pH 6

Figure 10-19 and Figure 10-20 show the mean concentrations of 0.2 µm filterable (dissolved), and 0.5 N HCl extractable (total) Fe(II) in mg L^{-1}, against Bayferrox 930 (goethite) concentration in g L^{-1}, in Experiment 8. Figure 10-19 shows determined values after 24 hours equilibration under nitrogen, whilst Figure 10-20 shows the same experiment after 48 hours aeration. Error bars (where visible) represent SD from the mean of singular readings, in triplicate experiments. The calculated value of total minus dissolved Fe(II), is included for comparison, and represents the recoverable sorbed Fe(II) portion.

As with Experiment 7, a significant portion of the initial Fe(II) is not recoverable via 0.5 N HCl extraction. In fact, up to a goethite concentration of 0.5 g L^{-1}, less than 50 % of the difference between homogeneous dissolved Fe(II) (as determined in the goethite free control experiments), and dissolved Fe(II) determined in experiments with goethite, cannot be recovered via HCl extraction. Above 0.5 g L^{-1} the overall concentration of non-recoverable Fe(II) decreases from a maximum of 3.11 mg L^{-1} at 0.5 g L^{-1} goethite, to 1.46 mg L^{-1} at 50 g L^{-1} goethite. Oxidation of the maximum determined concentration of non-recoverable Fe(II), would equate to a stoichiometric residual O_2 concentration of 0.44 mg L^{-1}.

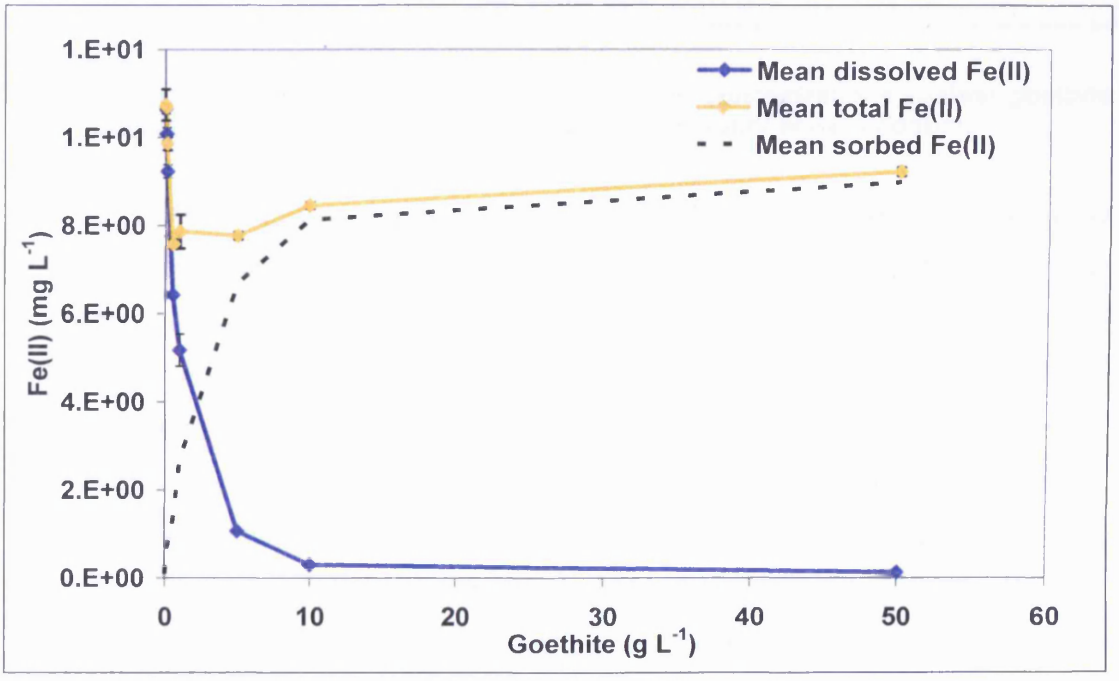

Figure 10-19: Mean filtered and HCl extractable Fe(II) concentrations against goethite concentration in pH 6 adsorption experiments after 24 hours equilibration under N_2

Complete adsorption of Fe(II) is not seen in Figure 10-19, and a residual dissolved Fe(II) concentration of 0.12 mg L^{-1} is seen at goethite concentrations of 50 g L^{-1}. However mean dissolved Fe(II) concentrations are seen to decrease exponentially between 0 and 10 g L^{-1} from an initial 10.68 mg L^{-1} to 0.30 mg L^{-1} Fe(II) respectively.

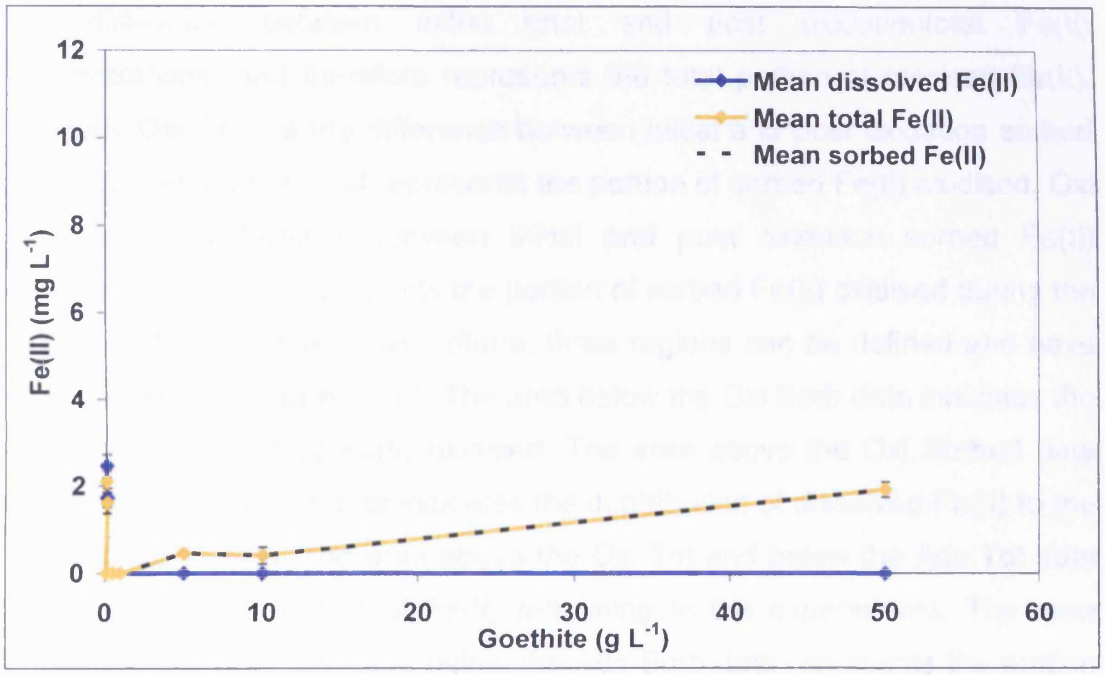

Figure 10-20: Mean filtered and HCl extractable Fe(II) concentrations against goethite concentration in pH 6 adsorption experiments after 48 hours aerial oxidation

Following 48 hours aeration, dissolved Fe(II) concentrations are only detectable in goethite concentrations of less than 0.05 g L^{-1}. Data above this concentration are consistently below the detection limit of the analytical procedure used (apart from the 1 g L^{-1} data, in which one of the three readings showed a higher value, which slightly skewed the mean concentration). However, the other two measurements were below detection, and it is thought that the high reading is due to experimental error and should be disregarded. Total Fe(II) is evident at goethite concentrations less than or equal to 0.05 g L^{-1}, at which points total and dissolved Fe(II) are equal to within experimental error. Total Fe(II) is below detection across an order of magnitude range of goethite concentrations (between 0.1 and 1 g L^{-1}). At higher concentrations total Fe(II) is evident at concentrations of 0.47 mg L^{-1}, at 5 g L^{-1} to 1.82 mg L^{-1}, at 50 g L^{-1} of goethite respectively.

Figure 10-21 shows the contributionto the total Fe(II) oxidised by the dissolved and sorbed Fe(II) portions in mg L^{-1}, in Experiment 8. Ads Tot and Ads Sorb are the determined total, and sorbed (total - dissolved) Fe(II) concentrations after 24 hour equilibration, in the absence of oxygen. Oxi Tot is

the difference between initial total and post oxidationtotal Fe(II) concentrations, and therefore represents the total portion of oxidised Fe(II). Similarly Oxi Sorb is the difference between initial and post oxidation sorbed Fe(II) concentrations, and represents the portion of sorbed Fe(II) oxidised. Oxi Sorb is the difference between initial and post oxidation sorbed Fe(II) concentrations, and represents the portion of sorbed Fe(II) oxidised during the experiment. Using the above criteria, three regions can be defined and have been marked on Figure 10-21. The area below the Oxi Sorb data indicates the total portion of sorbed Fe(II) oxidised. The area above the Oxi Sorbed data and below the Oxi Tot data indicates the contribution of dissolved Fe(II) to the total oxidised Fe(II). The area above the Oxi Tot and below the Ads Tot data points shows the portion of Fe(II) remaining in the experiments. The area above the Oxi Sorb data and below the Ads Sorb data represents the portion of non-oxidisable sorbed Fe(II).

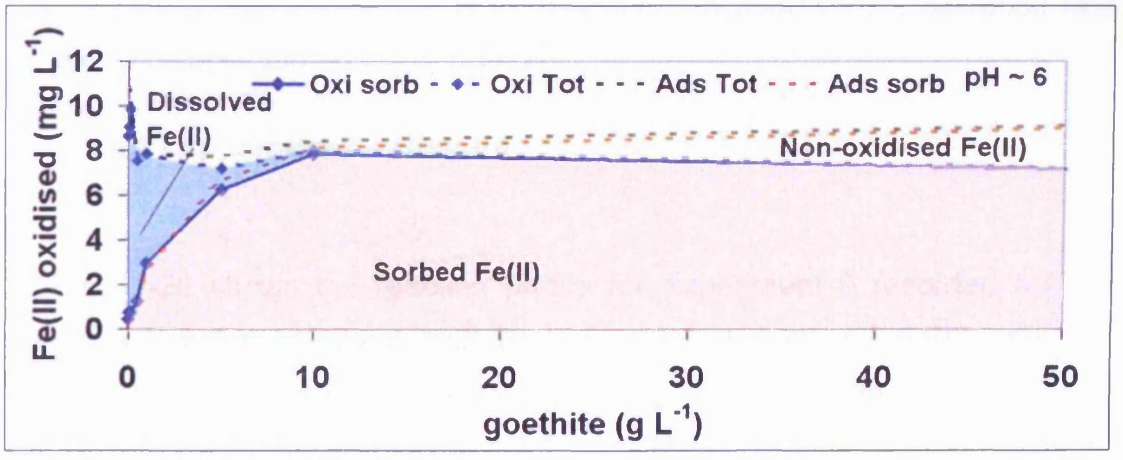

Figure 10-21: Proportions of dissolved and sorbed Fe(II) oxidised against goethite concentration in pH 6 adsorption – oxidation experiments

Ads Tot and Ads Sorb are the determined total, and sorbed (total - dissolved) Fe(II) concentrations after 24 hour equilibration in the absence of oxygen. Oxi Tot is the difference between initial total and post oxidationtotal Fe(II) concentrations, and therefore represents the total portion of oxidised Fe(II). Similarly Oxi Sorb is the difference between initial and post oxidation sorbed Fe(II) concentrations, and represents the portion of sorbed Fe(II) oxidised during the experiment.

From a comparison of Figure 10-19 and Figure 10-20 and consolidated Figure 10-21, it can be seen that the contributionto overall Fe(II) oxidation of sorbed and dissolved Fe(II) changes with increasing goethite concentration as is the case with Experiment 7 an pH 4. Initially oxidation of the dissolved Fe(II)

portion in the absence of significant sorbed Fe(II) is responsible for the observed reduction in total Fe(II) concentrations. In addition, unlike at pH 4 in Experiment 7, at goethite concentrations of 10 g L^{-1}, almost all sorbed Fe(II) was oxidised.

10.4 Experiment 9 - pH 6 batch oxidation run

An experiment was undertaken to determine the oxidation rate of sorbed Fe(II) at pH 6 in a bicarbonate buffer system after pre-equilibration with 10 g L^{-1} of goethite (Bayferrox 930). Pre-equilibration was done under constant nitrogen gas bubbling in a sealed reaction vessel to prevent oxygen ingress. The details of the experimental method are given in Section 9.4. This experiment was in response to the results determined in Experiment 8 in which significant sorbed Fe(II) is oxidised during the experimental run. The aim of Experiment 9 therefore is to determine an approximate oxidation rate for the oxidisable sorbed Fe(II) portion.

10.4.1 Experiment 9 – Results

Figure 10-22 shows the reaction profile for Experiment 9 recorded for the adsorption and subsequent oxidation of an initial 5 mg L^{-1} Fe(II) onto the surface of 10 g L^{-1} of Bayferrox 930 (goethite). Total and filtered Fe(II) in mg L^{-1}, system Eh in mV and DO in mg L^{-1} are shown against time in seconds. The reaction conditions were pH 6.013±0.012, 25.0±0.1 °C, $NaHCO_3$ 501 mg L^{-1}, SO_4^{2-} ~ 18 mg L^{-1}, Fe(II) 5 mg L^{-1}, Fe(III) 10 g L^{-1} (as Bayferrox 930 - goethite).

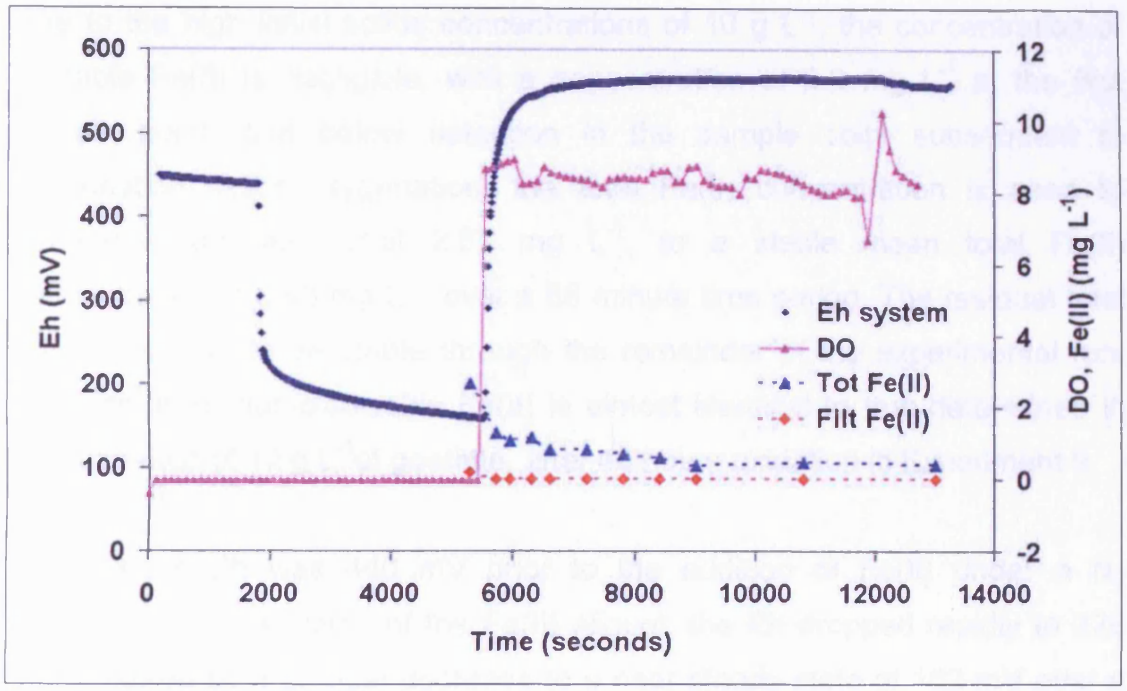

Figure 10-22: Experiment 9 – Heterogeneous oxidation of Fe(II) after pre-equilibration with goethite at pH 6

Experimental conditions – pH 6.013±0.012, 25.0±0.1 °C, $NaHCO_3$ 501 mg L^{-1}, SO_4^{2-} ~ 9.5 mg L^{-1}, Fe(II) 5 mg L^{-1}, Fe(III) 10 g L^{-1} as Bayferrox 930 (goethite). DO 0 to 8.52±0.12 mg L^{-1}

The first sample point shown in Figure 10-22 was taken prior to the introduction of oxygen into the system. Therefore the total Fe(II) determined at this point should be identical to the initial Fe(II) added to the system. However, it was found that the total Fe(II) concentration was only 2.66 mg L^{-1}, rather than the 5 mg L^{-1} target concentration. As the first sample was taken after 58 minutes of nitrogen bubbling following the addition of the Fe(II) aliquot, it is unclear as to what mechanism can account for the discrepancy observed. Possibilities include:

- Oxidation by trace concentrations of O_2
- Oxidation of Fe(II) during sample handling prior to acidification
- Error in initial addition of Fe(II) resulting In an initially lower concentration
- Incomplete recovery of Fe(II) from the goethite surface during acid extraction
- Interfacial electron transfer with the underlying goethite solid.

Due to the high initial solids concentrations of 10 g L^{-1}, the concentration of filterable Fe(II) is negligible, with a concentration of 0.2 mg L^{-1} at the first sample point, and below detection in the sample point subsequent to oxygenation. After oxygenation, the total Fe(II) concentration is seen to decrease from the initial 2.67 mg L^{-1}, to a stable mean total Fe(II) concentration of 0.43 mg L^{-1}, over a 58 minute time period. The residual total Fe(II) is shown to be stable through the remainder of the experimental run. The portion of non-oxidisable Fe(II) is almost identical to that determined in the presence of 10 g $L^{-1}$of goethite, after 48 hours oxidation in Experiment 9.

The system Eh was 440 mV prior to the addition of Fe(II) under a N_2 atmosphere. On addition of the Fe(II) aliquot, the Eh dropped rapidly to 228 mV, followed by a gradual decrease to a near steady state of 162 mV over a 60 minute period. This could possibly be indicative of surface reorganisation of Fe(II) species including IET mechanisms, however, probe equilibration cannot be discounted. After the system was oxygenated the Eh rose rapidly to 565 mV and remained constant after this point indicating complete oxidation of the system.

10.4.2 Experiment 9 – Heterogeneous kinetics

Due to the rapid oxidative surface cycling of the dissolved Fe(II) in Experiment 9, the determination of pseudo first order oxidation rate constant based on the dissolved Fe(II) portion was not possible. However, it was possible to determine a rate constant for the oxidisable sorbed Fe(II) portion. The rate was determined from the 5700 sample point up to the 8400 seconds sample point for the oxidisable portion of the sorbed Fe(II). This was done by subtracting the mean determined non-oxidisable sorbed Fe(II) portion (as determined from sample points 9000, 10800 and 13020) from the 5700 to 8400 seconds data to effectively return only the oxidisable Fe(II) portion. The pseudo first order rate constant was determined from the reaction plot shown

in Figure 10-23 and was determined to be 5.60×10^{-4} seconds^{-1} which is equal to a half life of approximately 20.6 minutes.

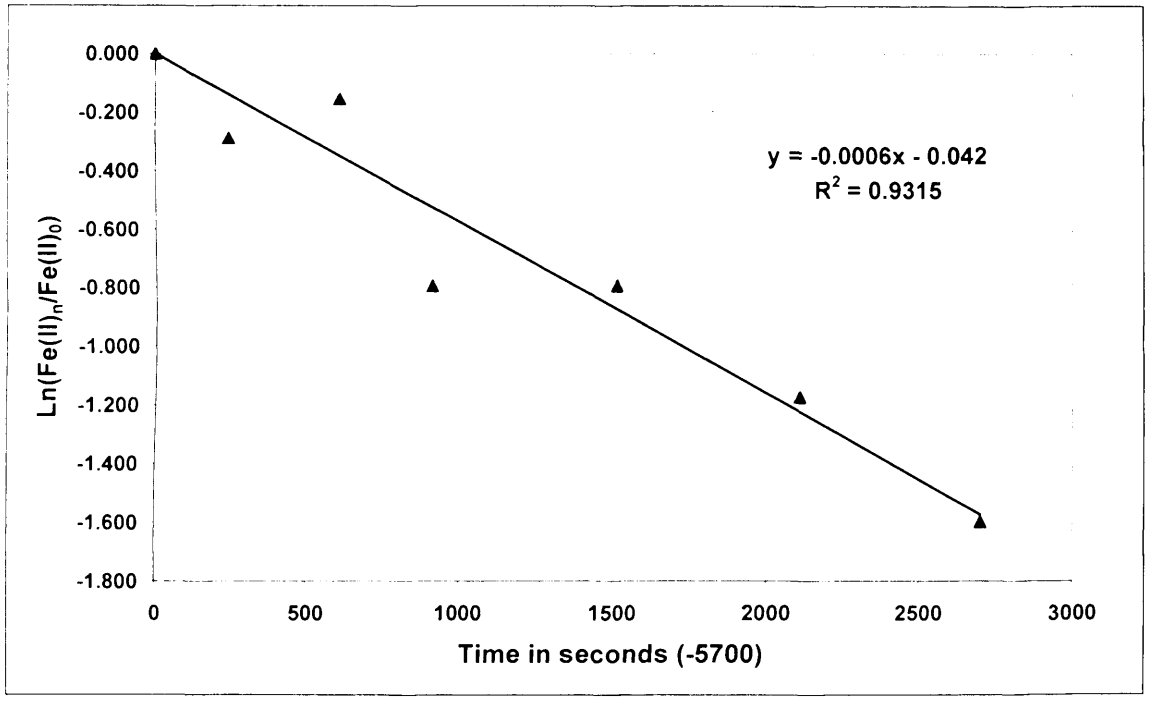

Figure 10-23: Pseudo first order reaction plot of $\ln(Fe(II)_n/Fe(II)_0)$ against time in seconds for oxidisable sorbed Fe(II) in Experiment 9.

5700 seconds are deducted from the total reaction time to set the zero to the 5700 data point

As far as the author is aware this is the first time a rate constant has been determined for the oxidation of oxidisable sorbed Fe(II) in the absence of detectable dissolved Fe(II). This result appears to be further evidence for strong and weak site adsorption on the goethite surface, and that the strong site sorbed Fe(II) appears to be resistant to oxidation by dissolved oxygen.

10.5 Comparison of field and laboratory kinetic data

Figure 10-24 compares the pseudo first order oxidation rate constants determined in this study for both field and laboratory conditions. Also shown is the pseudo first order rate as calculated using the composite rate law as devised by King (1998) (dashed red line); the data determined for the Taff Merthyr field oxidation rate (as determined by Sapsford, 2007). The blue filled squares are determined from the homogeneous experiments (1 to 4) whilst

the blue filled triangles and from the heterogeneous experiments (5a and 5b). The red filled triangles are oxidation rates determined using data obtained from the field sample ports (See Appendix 2.5).

The blue dashed line in Figure 10-24 marks the maximum heterogeneous rates determine in the current study and this is thought to be a potential ceiling for abiotic heterogeneous Fe(II) oxidation. Homogeneous field oxidation rates are noticeable slower than those predicted by the King (1998) rate law. This is mainly due to the lower dissolved oxygen condition in the VFR system. In addition the elevated sulfate in the Taff Merthyr minewater may also act to inhibit the overall oxidation rate. Heterogeneous rates determined in the VFR using the VFR tank numerical model (see Section 8.8.1.2) as devised by Sapsford (2007) are greater than those determined using the upper and lower sample ports as the upper sample port is elevated with respect to the top of the bed, therefore overestimating the heterogeneous rate.

Figure 10-24 shows that, using heterogeneous catalysis, an oxidation rate in the same order of magnitude to the homogeneous rate determined for the Taff Merthyr VFR is possible at a pH around 4. In addition this rate is almost 3 orders of magnitude faster than the homogeneous rate at the same pH. This therefore forms a viable treatment option. The pH conditions determined in the laboratory work cover the majority of the pH conditions observed for net-alkaline coal mine drainage in the UK. Therefore the VFR may be an applicable system to the majority of UK coal mine water discharges.

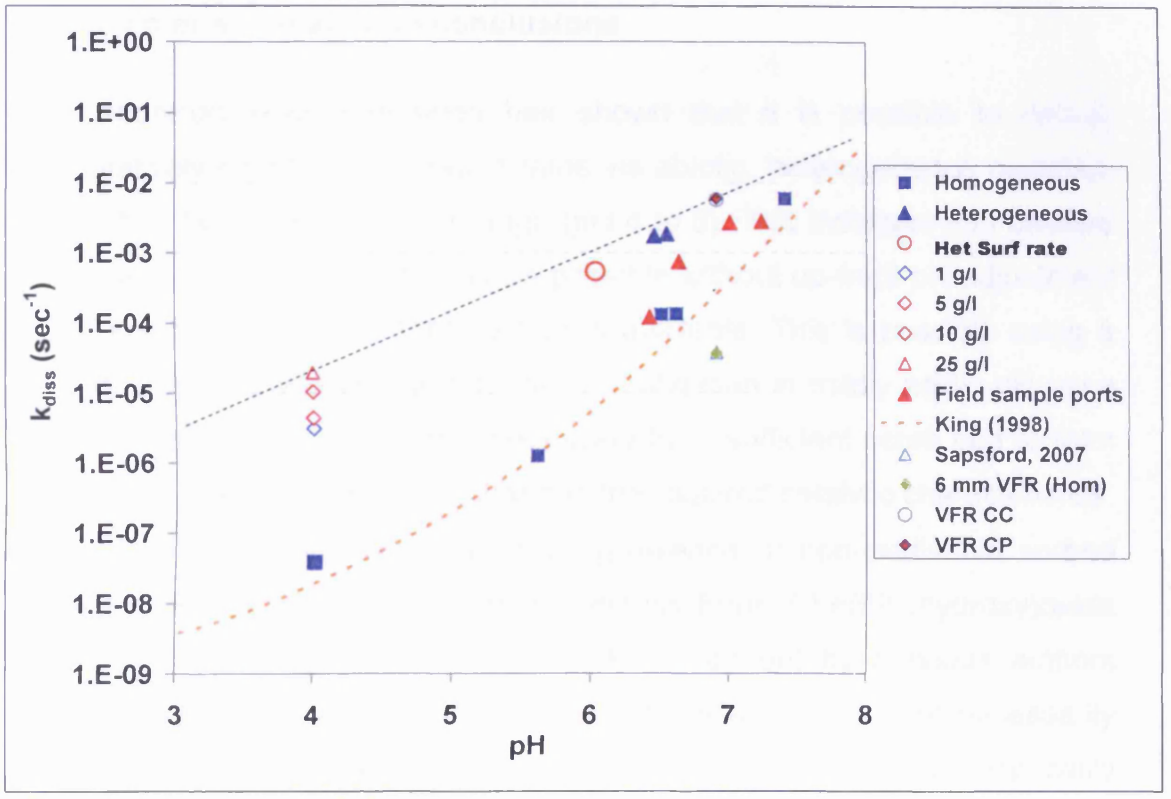

Figure 10-24: Comparison of laboratory results with VFR field data.
where King (1998) is the Pseudo first order rate calculated using the King (1998) (dashed red line) rate law. Sapsford, 2007 is the rate determined for the Taff Merthyr field oxidation rate by Sapsford, 2007. The blue filled squares above pH 5 are determined from the homogeneous experiments (1 to 4) whilst the blue filled triangles are from the heterogeneous experiments (5a and 5b). 1, 5, 10, and 25 g/l indicate the goethite concentrations and pseudo first order rates determined in experiment 7 as was the pH 4 homogeneous rate. Het surf rate indicates the pseudo first order rate determined in Experiment 9 for Fe(II) adsorbed to goethite. The 6 mm VFR (Hom) is the rate calculated for the homogeneous oxidation using the average 6 mm VFR chemistry. VFR CC is the heterogeneous oxidation rate determined in the 6 mm VFR using CSTR above and below the bed (in accordance with Sapsford, 2007). VFR CP is the heterogeneous oxidation rate determined in the 6 mm VFR using CSTR above the bed and Plug flow below the bed (in accordance with Sapsford, 2007). Finally the dark blue dashed line indicates maximum rates determined in the current study.

10.6 Chapter summary and conclusions

- Laboratory experimentation has shown that it is possible to deliver relatively high Fe(II) oxidation rates via abiotic, heterogeneous oxidation within the mildly acidic pH range (pH 4 to 6). This indicates that passive treatment of mine water may be possible without up-front pH adjustment if sufficient solid liquid interaction is available. This is possible using a VFR system and warrants further investigation in mildly acidic pH mine water to identify a) the time necessary for a sufficient ochre bed to form and b) if naturally formed ochre has the required catalytic characteristics.
- During laboratory experiments the presence of non-oxidisable sorbed Fe(II) is ubiquitous in the heterogeneous Fe(II) / Fe(III) (hydroxy)oxide system. This agrees well with work carried out by previous authors although the mechanisms offered by these authors do not necessarily give an adequate explanation for the observed behaviour, especially under mildly acidic pH conditions. A speculative discussion of this matter is given in Appendix 5.
- The presence of non-oxidisable sorbed Fe(II) in the VFR has not been definitively proven. It is possible that the non-oxidisable sorbed Fe(II) may be consumed in microbial mediated processes (Dr D Sapsford, personal communication).
- The pH conditions determined in the laboratory work cover the majority of the pH conditions observed for net-alkaline coal mine drainage in the UK. Therefore the VFR may be an applicable system to the majority of UK coal mine water discharges. However, many discharges from metal mines are commonly net-acidic and low pH. Therefore further work needs to be carried out to determine if the VFR is effective at treating these minewaters.

11 Conclusions and recommendations

11.1 Key Conclusions

Based on the research carried during this study, the following key conclusions can be drawn:

- In respect to the VFR performance: The 6mm gravel bed in the VFR gave the best performance and managed to prevent bed scour and piping. The 6mm gravel bed was also found to give the best overall performance in terms of iron and manganese removal as follows:

  1 Average total iron removal. 89.5 % or 16.6 g m^{-2} day^{-1} in the 6 mm VFR 49.1 % or 15.6 g m^{-2} day^{-1} in the 10mm VFR and 39.4 % or 4.6 g m^{-2} day^{-1}in the lagoons.
  2 Average Fe(II) oxidation: 6 mm VFR 93% or 10.58 g m^{-2} day^{-1}, 20mm VFR 75.3 % or 6.4 g m^{-2} day^{-1} and the lagoons 93.5% or 6.1 g m^{-2} day^{-1}.
  3 Average total manganese removal: 6 mm VFR 69.2 % and 1.1 g m^{-2} day^{-1} (max 2.25 g m^{-2} day^{-1}). 20mm VFR 23.11% or 0.57 g m^{-2} day^{-1}, and the lagoons 4.5 % or 0.06 g m^{-2} day^{-1}.

- The bulk of the VFR ochre was found to be largely amorphous 2-line ferrihydrite under XRD. No conversion of the VFR ferrihydrite to goethite was detected. This is thought to be due to the inhibitory effect of Si and SO42- ions in the mine-water. Conversion of ferrihydrite to goethite was evident in the lagoonal ochre. Suspected reducing conditions in the lagoonal ochre opens a possible pathway for the formation of goethite via bio-reduction of ferrihydrite to green rust followed by re-oxidation and re-crystallisation as goethite. The zeta potential of VFR ochre was found to be -8.5 mV at the pH of Taff Merthyr mine water (pH 6.9). In addition the IEP was found to be at pH 4. The low IEP in relationto PPZC is thought to be due to sulfate

adsorptionto the ferrihydrite surface. The low magnitude of the zeta potential is thought to be due to the prevalence of divalent counter ions. The low magnitude of zeta potential means particle aggregation is likely as is seen under electron and light microscope.

- The specific cake resistance of the 6mm VFR ochre is lower than that of single pass active treatment sludge and within the same order of magnitude as that determined in the High Density Sludge (HDS) active treatment process. It was also found that the lagoon ochre has a greater mass per volume ratio than the VFR ochre. However, it was also found that both VFR and lagoon ochres contain almost identical mass per volume proportions of iron with calculated ferrihydrite making up 80 % of the dry mass of the VFR ochre and only 48 % of the lagoon ochre dry mass. This results in a much higher dry density in the VFR ochre of 3.71 as compared to 2.34 g/cm3 in the lagoon.

- PhreeqC modelling has demonstrated that the Taff Merthyr mine-water is oversaturated with respect to the carbonate mineral phases aragonite, calcite and dolomite upon equilibration with atmospheric CO2. In addition modelled atmospheric equilibration with respect to CO2(g) acts to increase pH and supersaturate calcium carbonate mineral phases.

- In cross section the VFR bed contained four distinct dark grey layers. Geochemical and mineralogical characterisation of these layers has shown them to contain elevated manganese concentrations and to have XRD peaks associated with barium manganese oxide hydrate and birnessite. It was also found that as well as Mn, the elements Tl, Ti, Cr, Co, Ni, Zn and Ba were also elevated within these layers. However, it was found that only 40% of the total carbon content of the lagoon could be accounted for as Ca carbonates. The remainder is thought to be present as organic carbon.

- Formation of Mn rich bands within the VFR ochre bed suggests that Mn oxidation is predominantly autocatalytic and that Mn precipitates are responsible for the majority of the oxidation.

- It has been shown that both oxidisable and non-oxidisable sorbed Fe(II) exists on the goethite surface. It has also been shown that, at a fixed pH, and total initial Fe(II), that with increasing goethite solids, there was a near linear increase in the concentration of the non-oxidisable sorbed Fe(II) species. The portion of Fe(II) oxidised is shown to increase with increasing goethite concentration. This demonstrates that goethite effectively catalyses the oxidation of Fe(II) even in the mildly acidic pH. This opens up the possibility of using a VFR treatment system (or other "Ochre Accretion" based system) in the mildly acidic pH region. The residual Fe(II) adsorbed to the surface of the Fe(III) (hydroxy)oxide surface as found in this study and the study of Park and Dempsey (2005) seems to indicate that, if it is attributed to IET, that it is unavailable for oxygen reduction. However, non-oxidisable sorbed Fe(II) has not yet been observed in the field which may be due to potential exhaustion by microbial catalysis (Dr D Sapsford, personal communication).

- Macroscopic observations at pH 4 show possible evidence for the existence of strong and weak site adsorption of Fe(II) on the surface of goethite. In addition, Fe(II) adsorbed to the strong sorption sites may be resistant to oxidation by dissolved O2.

- The pH conditions determined in the laboratory work cover the majority of the pH conditions observed for net-alkaline coal mine drainage in the UK. Therefore the VFR system should be an effective treatment system for the majority of UK coal mine drainages.

11.2 Key Recommendations

Based on the research carried during this study, the following recommendations for future work can be made:

- Many discharges from metal mines are commonly net-acidic and low pH. Therefore further work needs to determine if the VFR is effective at treating these minewaters.

- Further demonstration of the VFR system is required on other coal mine water discharges. Ideally these should be of mildly acidic, yet net-alkaline type. Coal mine water discharges within the range observed in the UK and b) on metal laden Acid Mine Drainage. Conditions determined in the laboratory work cover the majority of the pH conditions observed for net-alkaline coal mine drainage in the UK. Therefore the VFR may be an applicable system to the majority of UK coal mine water discharges. However, many discharges from metal mines are commonly net-acidic and low pH. Therefore further work needs to be carried out to determine if the VFR is effective at treating these minewaters.

- Further work is needed to determine how residual Fe(II) affects the reducing potential of the system to give a better indication of why the unreactive sorbed Fe(II) is not available for oxygen reduction. Further work is also needed to determine the stability of the non-reactive sorbed Fe(II) in the presence of stronger oxidising agents and microbes.

- Further work is needed to determine if the proton release observed during adsorption experiments of Fe(II) onto Fe(III) (hydroxy)oxides is due to a) formation of ≡FeOFeOHo surface species (as is commonly interpreted or b) due to surface hydrolysis of surface Fe(III) formed

during Interfacial Electron Transfer (IET) between adsorbed Fe(II) and underlying structural Fe(III) centres.

- Further work is needed to determine the proportions of Mn oxidation that can be attributed to a) autocatalytic oxidation on Mn precipitates b) catalytic oxidation by Fe(III) (hydroxy)oxide precipitates and c) microbial catalysed oxidation.

References

Amonette J.E., Workman D.J., Kennedy D.W., Fruchter J.S., Gorby Y.A. 2000. Dechlorination of carbon tetrachloride by Fe(II) associated with goethite. Envirnmental Science and Technology 34. 4606-4613.

Anderson C.R., Pedersen K. 2003. In situ growth of Gallionella biofilms and partitioning of lanthanides and actinides between biological material and ferric oxyhydroxides. Geobiology 1. 169-178.

Andersson H., Johansson J. 2002. Iron Removal from Groundwater in Rakai District, Uganda: A minor field study. Masters Thesis 2002:292, Lulea University of Technology. ISSN: 1402-1617 Karlstads University, Sweden (http://epubl.luth.se/1402-1617/2002/292/LTU-EX-02292-SE.pdf)

Appelo C.A.J., Van Der Weiden M.J.J., Tournassat C., Charlet L. 2002. Surface complexation of ferrous iron and carbonate on ferrihydrite and the mobilization of arsenic. Environmental Science and Technology 36. 3096-3103.

AWWA, APHA, WEF. 1995. Standard methods for the examination of water and wastewater, 19th ed. APHA, Washington DC.

Baes C.F and Mesmer R.E. 1976. The hydrolysis of cations. John Wiley and Sons, London. ISBN: 0-471-03985-3.

Ball J.W., Nordstrom D.K. 1991. WATEQ4F - User's manual with revised thermodynamic data base and test cases for calculating speciation of major, trace and redox elements in natural waters: U.S. Geological Survey Open-File Report 91-183, 189 p. (Revised and reprinted August 1992.)

Bangor 2007. Bangor university unpublished preliminary report on microbial poulation of Taff Merthyr ochre.

Banks D., Burke S.P., Gray C. 1997. The hydrogeochemistry of coal mine drainage and other ferrouginous waters in North Derbyshire and South Yorkshire, UK. Quarterly Journal of Engineering Geology 30. 257-280.

Barry R.C., Schnoor J.L., Sulzberger B., Sigg L., Stumm W. 1994. Iron oxidation kinetics in an acidic alpine lake. Water Research 28. 323-333.

Bearcock J.M., Perkins W.T., Dinelli E., Wade S.C. 2006. Fe(II)/Fe(III) 'green rust' developed within ochreous coal mine drainage sediment in South Wales, UK. Mineralogical Magazine 70. 731-741.

Best G.A., Aikman D.L. 1983. The treatment of ferruginous groundwater from an abandoned colliery. Water Pollution Control 82. 537-566.

Bethke C.M. 2005. The Geochemists Workbench Software. University of Illonois. Distributed by Rockware Inc.

Betlem G., Brans E., Santamaria L., Kroll A. 2004. ERMITE (Environmental Regulation of Mine Waters in the European Union). Deliverable D8; Guidelines. Kroll A. (Ed). European Commission Fifth framework programme. Energy, Environment and Sustainable development.

Bielski B.H.J., Cabelli D.E., Arudi R.L. 1985. Reactivity of H2O/O2- radicals in aqueous-solutions. Journal of Physical and Chemical Reference Data 14(4). 1041-1100.

Bingham J.M., Schwertmann U., Carlson L. 1992. Mineralogy of precipitates formed by the biogeochemical oxidation of Fe(II) in mine drainage. In Skinner H.C.W., Fitzpatrick R.W. (Eds). Biomineralization processes of Iron and Manganese – Modern and Ancient Environments. Catena Supplement 21. 219-232.

Bowell R.J., Williams K.P., Grifiths L. 1997. Acid generation and leachate chemistry fron sulfide rich spoil heaps, Avoca mine, Ireland. SRK Ltd unpublished report.

Brady K.S., Bigham J.M., Jaynes W.F., Logan T.J. 1986. Influence of sulfate on Fe-oxide formation: Comparison with a stream receiving acid mine drainage. Clays and Clay Minerals. 34, 266-274.

Buerge I.J., Hug S.J. 1999. Influence of mineral surfaces on chromium(VI) reduction by iron2+. Environmental Science and Technology 33. 4285-4291.

Bullen C.J. 2007. An investigation into the mechanisms controlling the formation of Nigh Density Sludge. Ph.D thesis. Cardiff University, Cardiff.

Burke S.P., Banwart S.A. 2002. A geochemical model for removal of iron(II)(aq) from mine water discharges. Applied Geochemistry 17. 431-443.

Charlet L., Liger E., Gerasimo P. 1998. Decontamination of TCE- and U-rich waters by granular iron: role of sorbed Fe(II). Journal of Environmental Engineering 124. 25-30.

Cher M., Davidson N. The kinetics of the oxygenation of ferrous iron in phosphoric acid solution. Journal of the American Water Works Association 77(3). 793-798.

Coal Authority. 2002. The Taff Merthyr Mine water treatment scheme. PDF download available from http://www.coal.gov.uk/resources/environment/taffmerthyrminewatertreatmentscheme.cfm

Cornell R.M., Schneider W. 1988. Formation of goethite from ferrihydrite at physiological pH under the influence of Cystein. Polyhedron 8. 149-155.

Cornell R.M., Schwertmann U. 2003. The iron oxides: Structure, Properties, Reactions, Occurrences and Uses. 2nd Edition. Wiley-VCH, Weinheim, Germany. 658 p.

Coughlin B.R., Stone A.T. 1995. Nonreversible adsorption of divalent metal ions (MnII, CoII, NiII, CuII and PbII) onto goethite: Effects of acidification, FeII addition and picolinic acid addition. Environmental Science and Technology 29. 2445-2455.

Coulson J.M., Richardson J.F., Backhurst J.R., Harker J.H. 1991. Chemical Engineering: Fluid Flow, Heat Transfer, and Mass Transfer. Pergamon Press ISBN 0080379575, 9780080379579. 708p.

Darwent J.R. 1983. Photochemical reduction of oxygen catalysed by colloidal cadmium selenide. Journal of the Chemical Society – Faraday Transactions 80. 183-189.

Davies C.C., Chen H-W., Edwards M. 2002. Modelling silica sorptionto iron hydroxide. Environmental Science and Technology 36. 582-587.

Davies S.H.R., Morgan J.J. 1989. Manganese(II) oxidation-kinetics on metal-oxide surfaces. Journal of Colloid and Interface Science 129(1). 63-77.

Davis J.A., Leckie J.O. 1978. Surface ionization and complexation at oxide-water interface 2. Surface properties of amorphous iron oxyhydroxide and adsorption of metal ions. Journal of Colloid and Interface Science 67(1). 90-107.

Davison W., Seed G. 1983. The kinetics of the oxidation of ferrous iron in synthetic and natural waters. Geochimica et Cosmochimica Acta 47. 67-79.

Demir G., Tufekci N. 2002. Investigation of the catalytic reaction kinetics of Fe(III) on Fe(II) oxidation at various pH values. Fresenius Environmental Bulletin 11. 868-873.

Dempsey B.A. Fu L-T., Liu W. 1995. Control of Nucleation/Crystal Growth Rates to Produce High-Density Sludges from Acid Mine Drainage and Coal Pile Runoff. National Mine Land Reclamation Centre.

Dempsey B.A., Dietz J., Jeon B-H., Roscoe H.C., Ames R. 2002. Heterogeneous oxidation of ferrous iron for treatment of mine drainage. Proceedings of the National Meeting of the American Society of Mining and Reclamation (ASMR), Lexington KY, June 9-13, 2002. Published by the ASMR.

Dempsey B.A., Jeon B-H. 2001. Characteristics of sludge produced from passive treatment of mine drainage. Geochemistry: Exploration and Environmental Analysis 2. 1-6.

Dempsey B.A., Roscoe H.C., Ames R., Hedin R., Jeon B-H. 2001. Ferrous oxidation chemistry in passive abiotic systems for the treatment of mine drainage. Geochemistry: Exploration, Environment, Analysis 1. 81-88.

Dempsey B.A. 1993. Control of Nucleation / Crystal Growth Rates to Produce High-Density Sludges from Acid Mine Drainage and Coal Pile Runoff. U.S. National Mine Land Reclamation Centre.

Dey M., Sadler P.J.K., Williams K.P. 2003. A novel approach to mine water treatment. Land Contamination and Reclamation 11. 967 – 0513.

Dey M., Williams K.P. 2000. Observations on Whitworth A SAPS, Constructed Wetlands for Minewater Treatment R & D Project Steering Group Meeting 10th October. Cardiff University Report No. 2680.

Dey M., Williams K.P. 2001. Worsley Delph and Bridgewater Canal Options for Minewater Discharge. Cardiff University Report No. 2800.

Diebler H., Sutin N. 1964. Kinetics of some oxidation-reduction reactions involving manganese(3). Journal of Physical Chemistry 68(1). 174-178.

Diem D., Stumm W. 1984. Is dissolved Mn(II) being oxidized by O2 in absence of Mn-bacteria or surface catalysts?. Geochimica et Cosmochimica Acta 48. 1571-1573.

Dixit S., Hering J.G. 2006. Sorption of Fe(II) and As(III) on goethite in single- and dual-sorbate systems. Chemical Geology 228. 6-15.

Dzombak D.A., Morel F.M.M. 1990. Surface complexation modelling – hydrous ferric oxide. John Wiley and Sons, London. ISBN: 0-471-63731-9.

Eckenfelder W.W. 2000. Industrial water pollution control. McGraw-Hill, Boston.

Emerson D., Rivsbech N.P. 1994. Investigation of an iron-oxidizing microbial mat community located neat Aarhus Denmark: Field studies. Applied Environmental Microbiology 60. 4022-4031.

Emerson D., Weiss V. 2004. Bacterial iron oxidation in circum-neutral freshwater habitats: Findings from the fields and the laboratory. Geomicrobiology Journal 21. 405-414.

Evans T.D., Leal J.R., Arnold P.W. 1979. The interfacial electrochemistry of goethite (alpha-FeOOH) especially the effects of CO2 contamination. Journal of Electroanalytical Chemistry 105. 161-167.

Fackler J.P., Chawla I.D. 1964. Spectra of Manganese(3) complexes + Aquomanganese(3) ion + hydroxide, flouride and chloride complexes. Inorganic Chemistry 3(8). 1130-1138.

Fox R.K., Swinehart D.F., Garrett A.B. 1941. The equilibria of manganese hydroxide, Mn(OH)(II), in solutions of hydrochloric acid and sodium hydroxide. Journal of the American Chemical Society 63. 1779-1782.

Furrer G., Sollins P., Westall J. 1990. The study of soil chemistry through quasi-steady-state models: acidity of soil solution. Geochimica et Cosmochimica Acta 54. 2363–2374.

Galster, H. 1991. pH measurement: Fundamentals, Methods, Applications, Instrumentation. VCH, Cambridge. 356 p.

George P. 1954. The oxidation of ferrous perchlorate by molecular oxygen. Journal of the Chemical Society (December 1954). 4349-4359.

Ghosh M.M. 1974. Oxygenation of ferrous iron(II) in highly buffered solutions. In: Rubin A.J. (Ed). Aqueous Environmental Chemistry of Metals, Chapter 5. 193-217. Ann Arbor Science.

Ghosh M.M., O'Connor J.T., Engelbrecht R.S. 1966. Precipitation of Iron in aerated groundwaters. Journal of the Sanitary Engineering Division of the American Society of Civil Engineers 16(SA1). 199-213.

Giovanoli R., Cornell R.M. 1992. Crystallisation of metal substituted ferrihydrite. Zeitschrift Fur Pflanzenernahrung Und Bodenkunde 155(5-6). 455-460.

Good N.E., Winget D., Winter W., Connolly T.N., Izawa S., Singh M.M. 1966. Hydrogen ion buffers for biological research. Biochemistry 5. 467-477.

Gregory K.B., Larese-Casanova P.,Parkin G.F., Scherer M.M. 2004. Abiotic transformation of hexahydro-1,3,5-trinitro-1,3,5-triazine by FeII bound to magnetite. Environmental Science and Technology 38. 1408-1414.

Haber F., Weiss J. 1934. The catalytic decomposition of hydrogen peroxide by iron salts. Proceedings of the Royal Society (London) A147. 332 – 351.

Hedin R.S., Nairn R.W., Kleinmann R.L.P. 1994. Passive treatment of Coal Mine Drainage. U.S. Bureau of Mines I.C. 9389. 35 pages.

Hem J. 1963. Chemical Equilibria and rate of manganese oxidation: Chemistry of manganese in natural waters. US Geological Survey Water-Supply paper 1667-A.

Herbert R.B. 1999. MiMi - Sulfide oxidation in mine waste deposits: A review with emphasis on dysoxic weathering. The MISTRA program MiMi: Mitigation of the environmental impact from mining waste. Stokholm, Sweeden.

Hiemenz P.C., 1986. Principles of colloid and surface chemistry. Marcel and Decker, New York.

Holluta J., Kolle W. 1964. Das Cas und Wasserfach 18. 471-480.

Huisman L., Wood W.E. 1974. Slow Sand Filtration. World Health Organisation, Geneva. ISBN 92 4 154037 0.

Jarvis A.P., England A. 2002. Operational and treatment performance of an unique Reducing and Alkalinity Producing System (RAPS) for acidic leachate remediation in Lancashire, UK. Proceedings of the International Conference on Uranium Mining and Hydrogeology III and the International Mine Water Association Symposium. Freiberg, Germany, 15-21 September 2002. 1003-1010.

Jarvis AP, Younger PL. 2001. Passive treatment of ferruginous mine waters using high surface area media Water Research 35, 3643-3648.

Jeon B-H., Dempsey B.A., Burgos W.D. 2003. Kinetics and Mechanisms for reactions of Fe(II) with Iron(III) oxides. Environmental Science and Technology 37. 3309-3315.

Jeon B-H., Dempsey B.A., Burgos W.D. 2003a. Kinetics and mechanisms for reactions of Fe(II) with iron(III) oxides. Environmental Science and Technology 37. 3309-3315.

Jeon B-H., Dempsey B.A., Burgos W.D., Royer B.R. 2001. Reactions of ferrous iron with hematite. Colloids and Surfaces; A: Physicochemical and Engineering Aspects 191. 41-55.

Jeon B-H., Dempsey B.A., Burgos W.D., Royer B.R. 2003b. Sorption kinetics of Fe(II), Zn(II), Co(II), Cd(II) and Fe(II)/Me(II) onto hematite. Water Research 37. 4135-4142.

Jeon B-H., Dempsey B.A., Royer R.A. Burgos W.D. 2004. Journal of Environmental Engineering 130. 1407-1410.

Jimenez-Lopez C., Romanek C.S. 2004. Precipitation kinetics and carbon isotope partitioning of inorganic siderite at 25oC and 1 atm. Geochimica et Cosmochimica Acta 68(3). 557-571.

Jobin R., Ghosh MM. 1972. Effect of buffer intensity and organic-matter on oxygenation of Ferrous Iron. Journal of the American Water Works Association 64(9). 590-598.

Johnson K.L., Younger P.L. 2005. Rapid manganese removal from mine waters using an aerated packed-bed bioreactor. Journal of Environmental Quality 34. 987-993.

Kepler D.A., McCleary E.C. 1994. Successive Alkalinity Producing Systems (SAPS) for the treatment of Acid Mine Drainage. Proceedings of the International Land Reclamation and Mine Drainage Conference and the 3rd international conference on the Abatement of Acidic Drainage. Pittsburgh, P.A; April 1994. Volume 1: Mine Drainage. 195-204.

Kester D.R., Byrne R.H. Liang Y.Y. 1975. Redox reactions and solution complexes of Iron in marine Systems. ACS Symposium Series 18. 59-79.

King D.W. 1998. Role of carbonate speciation on the oxidation rate of Fe(II) in aquatic systems. Environmental Science and Technology 32. 2997-3003.

King D.W., Lounsbury H.A., Millero F.J. 1995. Rates and mechanisms of Fe(II) oxidation at nanomolar total iron concentrations. Environmental Science and Technology 29. 818-824.

King J., Davidson N. 1958. Kinetics of the Ferrous Iron-oxygen reaction in acidic phosphate-pyrophosphate solutions. Journal of the American Chemical Society 80(7). 1542-1545.

Kirby C.S., Elder Brady J.A. 1998. Field determination of Fe(II) oxidation in acid mine drainage using a continuously-stirred tank reactor. Applied Geochemistry 13. 509-520.

Kirby C.S., Thomas H.M., Southam G., Donald R. 1999. Relative contributions of abiotic and biological factors in Fe(II) oxidation in mine drainage. Applied Geochemistry 14. 511-530.

Klausen J., Trober S.P., Haderlein S.B., Schwarzenbach R.P. 1995. Reduction of substituted Nitrobenzene's by Fe(II) in Aqueous Mineral suspensions. Environmental Science and Technology 29. 2396-2404.

Lamb A.B., Elder L.W. 1931. The electromotive activation of oxygen. Journal of the American Chemical Society 53(1). 137-163.

Langmuir D. 1997. Aqueous environmental chemistry. Prentice-Hall, London.

Larese-Casanova P., Scherer M.M. 2007. Fe(II) sorption on Hematite: New insight based on spectroscopic measurements. Environmental Science and Technology 41. 471-477.

Liang L., McCarthy J.F., Jolley L.W., McNabb J.A., Mehlhorn T.L. 1993. Iron dynamics: Transformation of Fe(II)/Fe(III) during injection of natural organic matter in a sandy aquifer. Geochemica et Cosmochimica Acta 57. 1987-1999.

Liang L., McNabb J.A., Paulk J.M., Gu B., McCarthy J.F. 1993. Kinetics of Fe(II) oxygenation at low partial pressures of oxygen in the presence of natural organic matter. Environmental Science and Technology 27. 1864-1870.

Liger E., Charlet L., Cappellen P.V. 1999. Surface catalysis of uranium(VI) reduction by iron2+. Geochimica et Cosmochimica Acta 63. 2939-2955.

Light T.S. 1972. Standard Solution for redox potential measurements, Analytical Chemistry 44. 1038-1039.

Luoma S.N., Davis J.A. 1983. Requirements for modelling trace-elements partitioning in oxidized estuarine sediments. Marine Chemistry 12(2-3). 159-181.

Marsh McBirney. 2007. Open channel profiling methods- 0.9 x V-Max method. [WWW] Url: Accessed:17-10-2007 [17:17] http://www.marshmcbirney.com/classes/oc_profiling/profiling_06.htm

Mathews, C.T., Robins, R.G. 1972. The oxidation of aqueous ferrous sulfate solutions by molecular oxygen. Proceedings of the Australian Institute of Mining and Metallurgy 242. 47-55.

McBain J.W. 1901. Oxidation of ferrous solutions by free oxygen. Journal of Physical Chemistry 5(9). 623-638.

MEND (Mine Environment Neutral Drainage program). 1996. Review of systems for treatment of acid mine drainage. MEND report 3.14.1. Revised 1999.

Millero F. 1985. The effect of ionic interactions on the oxidation of metals in natural waters. Geochimica et Cosmochimica Acta 49. 547-554.

Millero F., Sotolongo S., Izaguirre M., 1987. The oxidation kinetics of Fe(II) in seawater. Geochimica et Cosmochimica Acta 51. 793-801.

Millero F.J., Yao W., Aicher J. 1995. The speciation of Fe(II) and Fe(III) in natural waters. Marine Chemistry 50. 21-39.

Mogan J.J. 1967. Chemical equilibria and kinetic properties of manganese in natural waters. In Faust S.D., Hunter J.V. (Eds). Principles and applications of water chemistry. Wiley interscience.

Morgan J.J. 1964. Chemistry of Aqueous equilibria and kinetic properties of manganese(II) and (IV). Ph.D. thesis. Harvard University, U.S.A.

Morgan J.J. 2005. Kinetics of reactions between O2 and Mn(II) species in aqueous solutions. Geochimica et Cosmochimica Acta 69. 35-48.

Morgan J.J., Stumm W.1964. The role of multivalent metal oxides in limnological transformations, As exemplified by iron and manganese. Journal Water Pollution Control Federation 36(3). 276-277.

Murad E., Rojik P. 2004. Jarosite, schwertmannite, goethite, ferrihydrite and lepidocrocite: the legacy of coal and sulfide ore mining. Proceedings of 3rd Australian New Zealand Soils Conference, 5-9th December 2004. University of Sydney. Australia. Published on CDROM. WWW [URL] http://www.regional.org.au/asssi/

Nano G.V., Strathmann T.J. 2006. Ferrous iron sorption by hydrous metal oxides. Journal of Colloid and Interface Science 297. 443-454.

Nishizawa M., Sasaki Y., Saito K. 1985. Kinetics and mechanisms of the outer-sphere oxidation of CIS-Aquaoxovanadium(IV) complexes containing quadridentate amino polycarboxykates – Interpretation of the difference in activation parameters with the charge type of reactants. Inorganic Chemistry 24(5), 767–772.

O'Loughlin E.J., Larese-Casanova P., Scherer M., Cook R. 2007. Green rust formation from the bioreduction of gamma-FeOOH (lepidocrocite): Comparison of several Shewanella Species. Geomicrobiology Journal 24. 211-230.

Pacini V.A., Ingallinella A.M., Sanguinetti G. 2005. Removal of iron and manganese using biological roughing up flow filtration technology. Water Research 39. 4463-4475.

Park B., Dempsey B.A. 2005. Heterogeneous oxidation of Fe(II) on ferric oxide at neutral pH and a low partial pressure of O2. Environmental Science and Technology 39. 6494-650.

Parker K. 2003. Mine water management on a national scale - Experience from the coal authority. Land Contamination and Reclamation 11(2). 181-190.

Parkhurst D.L., Appelo C.A.J. 1999. User's guide to PHREEQC (Version 2) - A computer program for speciation, batch-reaction, one-dimensional transport, and inverse geochemical calculations: U.S. Geological Survey Water-Resources Investigations Report 99-4259, 310 p.

Pecher K., Handerlaein S.B., Schwerzenbach R.P. 2002. Reduction of polyhalogenated methanes by surface-bound Fe(II) in Aqueous suspensions of iron oxides. Environmental Science and Technology 36. 1734-1741.

Perrin D.D. 1962. Hydrolysis of manganese(II) ion. Journal of the Chemical Society (June 1962). 2197-2202.

PIRAMID consortium. 2003. Engineering guidelines for the passive remediation of acidic and/or metaliferous mine drainage and similar wastewaters. PIRAMID: Passive In-situ Remediation of Acidic Mine / Industrial Drainage. European Commission 5th framework programme.

Posner A.M. 1953. The kinetics of autoxidation of ferrous ions in concentrated HCl solutions. Transactions of the Faraday Society 49(4). 382-388.

Pound J.R. 1939. The oxidations of solutions of ferrous salts. Journal of Physical Chemistry 43(8). 955-967.

Ratke L., Voorhees P.W. 2002. Growth and Coarsening: Ripening in material processing. Springer-Verlag, London. 299 pp.

Reid, G. 2006. CFD modelling of a passive mine water treatment system. MEng Thesis. Cardiff University, UK.

Reilly N. 2001. The internal processes and sustainability of a constructed wetland system treating mine drainage at Tonmawr, South Wales. Unpublished MSc thesis, University of Manchester.

Rosso K.M., Morgan J.J. 2002. Outer-sphere electron transfer kinetics of metal ion oxidation by molecular oxygen. Geochemica et Cosmochimica Acta 66. 4223-4233.

Santana-Casiano J.M., Gonzalez-Davila M., Millero F.J. 2004. The oxidation of Fe(II) in NaCl-HCO3- and seawater solutions in the presence of phthalate and salicylate ions: a kinetic model. Marine Chemistry 85. 27-40.

Santana-Casiano J.M., Gonzalez-Davila M., Millero F.J. 2005. Oxidation of Nanomolar levels of Fe(II) with oxygen in natural waters. Environmnetal Science and Technology 39. 2073-2079.

Santana-Casiano J.M., Gonzalez-Davila M., Rodriguez M.J., Millero F.J. 2000. The effect of organic compounds in the oxidation kinetics of Fe(II). Marine Chemistry 70. 211-222.

Sapsford D.J, Barnes A., Dey M., Williams K.P. 2007. Low Footprint Mine Water Treatment: Field Demonstration and Application. Proceedings of the International Mine Water Association Symposium, 2007. Cagliari, 27-31 May, 2007. Italy.

Sapsford D.J. 2003. Generation of acid mine drainage in the laboratory: Influence of experimental procedure. Unpublished Ph.D. thesis. Cardiff University, UK.

Sapsford, D.J. 2007. Design concepts and guidelines for aerobic vertical flow reactors for low-footprint passive treatment of mine waters. Cardiff University unpublished report No: 3154. Cardiff University, Cardiff, UK.

Sapsford, D.J., Barnes A., Dey, M., Liang, L., Williams, K.P. 2005. A novel method for passive treatment of mine water using a vertical flow accretion system. In: Loredo J. and Pendás (eds.), Proceedings of the 9th International Mine Water Association Congress (1), Oviedo, 5-7th Sept 2005, pp. 389-394, Spain. Oviedo University (ISBN 84-689-3415-1).

Sapsford, D.J., Barnes, A., Dey, M., Williams, K.P., Jarvis, A., Younger, P., Liang, L. 2006. Iron and Manganese Removal in a Vertical Flow Reactor for Passive Treatment of Mine Water. In: Proceedings of the 7th International Conference on Acid Rock Drainage, St. Louis, March 26-30, 2006. pp 1831-1843, USA. Published by ASMR, Lexington.

Sarikaya H.Z. 1980. Interactions between ferrous iron oxidation and phosphate. In Curi, K. (Ed). Treatment and disposal of liquid and solid industrial waste. 143-160. Pergamon Press, New York.

Sarikaya H.Z. 1990. Contact aeration for iron removal - A theoretical assessment. Water Research 24. 329-331.

Sawyer T.S., Valentine J.S. 1981. How super is superoxide? Accounts of Chemical Research 14. 393-400.

Schwertmann U., Bingham J.M., Murad E. 1995. The 1st occurrence of schwertmannite in a natural stream environment. European Journal of Mineralogy 7(3). 547-552.

Silvester E., Charlet L., Tournassat C., Gehin A., Greneche J-M., Liger E. 2005. Redox potential measurements and Mossbauer spectrometry of Fe(II) adsorbed onto Fe(III) (oxyhydr)oxides. Geochemica et Cosmochemica Acta 69. 4801-4815.

Singer P.C., Stumm W. 1968. Kinetics of oxidation of ferrous iron. Proceedings of the 2nd symposium on coal mine drainage. 12–34.

Sobolev D., Roden E.E. 2001. Suboxic deposition of ferric iron by bacteria in

opposing gradients of Fe(II) and oxygen at circum-neutral pH. Applied and Environmental Microbiology 67. 1328-1334.

Søgaard, E.G., Medenwaldt, R., Abraham-Peskir, J.V. 2000. Conditions and rates of biotic and abiotic iron precipitation in selected Danish freshwater plants and microscopic analysis of precipitate morphology. Water Research. 34(10), 2675-2682.

Søgaard, E.G., Remigijus, A., Abraham-Peskir, J.V., Koch, C.B. 2001. Conditions for biological precipitation of iron by Gallionella ferruginea in a slightly polluted ground water. Applied Geochemistry 16. 1129-1137.

Sorensen J., Thorling L. 1991. Stimulation by lepidocrocite (γ-FeOOH) of Fe(II) dependant nitrite reduction. Geochimica et Cosmochimica Acta 55. 1289-1294.

Strawn, D.G., Hickney, P., Knudsen, A., Baker, L. 2006. Geochemistry of lead contaminated wetland soils amended with phosphorus. Environmental Geology 52(1). 109-122.

Stumm W. 1997. Catalysis of redox processes by hydrous oxide surfaces. Croatica Chemica Acta 70. 71-93.

Stumm W., Lee G.F. 1961. Oxygenation of Ferrous iron. Industrial and engineering chemistry 53.143-147.

Stumm W., Morgan J.J. 1996. Aquatic Chemistry: Chemical equilibria and rates in natural systems. Third edition. John Willey and Sons, Chichester.

Stumm W., Sulzberger B. 1992. The cycling of iron in natural environments: Considerations based on laboratory studies of heterogeneous redox processes. Geochimica et Cosmochimica Acta 56. 3233-3257.

Sung W., Morgan J.J. 1980. Kinetics and Products of Ferrous Iron Oxygenation in Aqueous Systems. Environmental Science and Technology 14. 561-568.

Sung W., Morgan J.J. 1981. Oxidative removal of Mn(II) from solution catalysed by the gamma-FeOOH (lepidocrocite) surface. Geochimica et Cosmochimica Acta 45. 2377-2383.

Takeno, N. 2005. Atlas of Eh – pH diagrams: Intercomparison of thermodynamic databases. Geological Survey of Japan, Open file report number. 419. Available for download from URL www.gsj.jp/GDB/openfile/... files/no0419/openfile419e.pdf

Tamura H., Goto K., Nagayama M. 1976a. Effects of anions on the

oxygenation of ferrous ion in neutral solutions. Journal of Inorganic Nucl Chemistry 38. 113-117.

Tamura H., Goto K., Nagayama M. 1976b. The effect of ferric hydroxide on the oxygenation of ferrous ions in neutral solutions. Corrosion Science 16(4). 197-207.

Tamura H., Kawamura S., Hagayama M. 1980. Acceleration of the oxidation of Fe(II) ions by Fe(III)-(hydroxy)oxides. Corrosion Science 20. 963-971.

Tamura, H., Goto, K., Yotsuyanagi, T., Nagayama, M. 1974. Spectrophotometric determination of iron(II) with 1,10-phenanthroline in the presence of large amounts of iron(III). Talanta 21, 314-318.

Theis T.L., Singer P.C. 1974. Complexation of Iron(II) by organic matter and its effect on Iron(II) oxygenation. Environmental Science and Technology 8. 569-573.

Tufekci N., Sarikaya H.Z. 1996. Catalytic effects of high Fe(III) concentrations on Fe(II) oxidation. Water, Science and Technology 34. 389-396.

Tufekci N., Sarikaya H.Z. 1998. Influence of ageing on the catalytic activity of ferric sludge for oxidation of Fe(II). Water Science and Technology 38. 129-137.

Tufekci N., Sarikaya H.Z., Ozturk I. 2000. An experimental study on iron removal with ferric sludge recycling. Water Science and Technology 42. 393-397.

U.S. Department of the Interior – Bureau of Reclamation. 2001. Water measurement manual. 3rd Revised edition. U.S. Government printing office, Washington. 272 p. Available for download from: http://www.usbr.gov/pmts/hydraulics_lab/pubs/manuals/WMM_3rd_2001.zip

US Environmental Protection Agency (EPA). 2000. Abandoned mine site characterization and cleanup handbook. US EPA

Vikesland P.J., Valentine R.L. 2002. Iron oxide surface-catalyzed oxidation of ferrous iron by monochloramine: Implications of oxide type and carbonate on reactivity. Environmental Science and Technology 36. 512-519.

Villalobos M., Leckie J.O. 2000. Carbonate adsorption on goethite under closed and open CO2 conditions. Geochimica et Cosmochimica Acta 64. 3787-3802.

Villasenor Nano, G., Strathmann, T.J. 2006. Ferrous iron sorption by hydrous metal oxides. Journal of Colloid and Interface Science 297. 443-454.

Waddell R.K. 1978. Evaluation of a Surficial Application of limestone and flue dust in the abatement of acidic mine drainage: Jonathon Run drainage basin at interstate 80, Centre County, Pennsylvania. Ph.D. dissertation, The Pennsylvania State University.

Watzlaf G.R., Schroeder K.T., Kleinmann R.L.P., Kairies C.L. Nairn R.W. 2003. The passive treatment of coal mine drainage. Nationak Energy Technology Laboratory, U.S. Department of Energy, and University of Oklahoma. U.S.A.

Wehrli B. 1990. Redox reactions of metal ions at mineral surfaces. In: Stumm W. (Ed). Aquatic Chemical Kinetics. John Wiley and Sons, Chichester.

Wells C.F., Davies G. 1967. A spectrophotometric investigation of aquomanganese(III) ion in perchlorate media. Journal of the Chemical Society: A Inorganic, Physical and Theoretical 11. 1858-1863.

Welsh Coal Mines. (2009). Taff Merthyr. A Welsh coal mines webpage. WWW [URL] http://www.welshcoalmines.co.uk/GlamEast/TaffMerthyr.htm Accessed 19-04-2009 [10:31 GMT].

Williams A.G.B., Scherer M.M. 2000. Chromate reduction by hydroxycarbonate green rust. Proceedings of the 2000 conference on Hazardous Waste Research. WWW [URL] http://www.engg.ksu.edu/hsrc/00proceed/williams1.pdf. Accessed 30-10-2006 [16:25 GMT].

Williams A.G.B., Scherer M.M. 2004. Spectroscopic evidence for Fe(II)-Fe(III) electron transfer at the Iron Oxide-water interface. Environmental Science and Technology 38. 4782-4790.

Wiseman I. 2002. Constructed wetlands for mine water treatment. R&D Technical report P2-181/TR. Published by the Environment Agency, Bristol UK. ISBN 1844320731.

Wolkersdorfer C. 2006. Water management at abandoned flooded underground mines: Fundamentals, tracer tests, modelling, water treatment. http://www.wolkersdorfer.info/publication/pdf/MineAbandonment.pdf

Wolthoorn A., Temminghoff E.J.M., Weng L., van Riemsdijk W.H. 2004. Colloid formation in groundwater: effect of phosphate, manganese, silicate and dissolved organic matter on the dynamic heterogeneous oxidation of ferrous iron. Applied Geochemistry 19. 611-622.

Younger, P. 2000. The adoption and adaptation of passive treatment technologies for mine waters in the United Kingdom. Mine Water and the Environment 19. 84 – 97.

Younger, P.L., Banwart, S.A., Hedin, R.S. 2002. Mine Water: Hydrology, Pollution, Remediation. Kluwer Academic Publishers, Dordrecht, Netherlands. 442 pages.

Zänker, H., Ritchter, W., Huttig, G. 2003. Scavenging and immobilization of trace contaminants by colloids in the waters of abandoned mines. Colloids and Surfaces A: Physiochemical and Engineering Aspects 217, 21-31.

Zänker H., Richter W., Huttig G. 2003. Scavenging and immobilization of trace contaminants by colloids in the waters of abandoned ore mines. Colloids and surfaces A: Physicochemical Engineering Aspects 217. 21-31.

Zeltner, W.A., Anderson, M.A. 1988. Surface charge development at the goethite / aqueous solution interface: Effects of CO2 adsorption. Langmuir 4. 469-474.

Zhang Y., Charlet L., Schindler P.W. 1992. Adsorption of protons, Fe(II) and Al(III) on lepidocrocite. Colloids and Surfaces 63. 259-268.

Zhang, J., Lion, W.L., Nelson, Y.M., Shuler, M.L., Ghiorse, W.C. 2002. Kinetics of Mn(II) oxidation by Leptothrix discophora SS1. Geochimica et Cosmochimica Acta 65(5). 773-781.

Zhang, Y., Charlet, L., Schindler, P.W. 1992. Adsorption of protons, Fe(II) and Al(III) on lepidocrocite. Colloids and Surfaces 63. 259-268.

Appendix 1 – (CD-ROM) Ochre characterisation

Appendix 1.1 - XRD data

Appendix 1.2 - Sequential extraction

Appendix 1.3 – Whole rock digest

Appendix 1.4 – Specific resistance to filtration

Appendix 1.5 – Surface area determination

Appendix 2 – (CD-ROM) Field data

Appendix 2.1 - Routine lagoon monitoring data

Appendix 2.2 - Routine 20 mm VFR monitoring data

Appendix 2.3 - Routine 6 mm VFR monitoring data

Appendix 2.4 - Intensive sampling of the Taff Merthyr site

Appendix 2.5 – Zeta titrations

Appendix 3 – (CD-ROM) Laboratory data

Appendix 3.1 – Fe(II) analytical method development

Appendix 3.2 – Spectrophotometer calibration

Appendix 3.2 – Experiments 1 to 6 and 9

Appendix 3.3 – Experiments 7 and 8

Appendix 4 – (CD-ROM) PhreeqC input code

Appendix 4.1 – Model TM1

Appendix 4.2 – Model TM2

Appendix 4.3 – Model TM3

Appendix 4.4 – Surface speciation determined for experiment 7

Appendix 5 – Discussion on the possible significance of laboratory work

A5.1 Site densities determined for goethite

In Experiments 5a and b, 7, 8 and 9 (Section 10 of the main report), it was found that both oxidisable and non-oxidisable sorbed Fe(II) exists on the goethite surface. It was also shown in Experiments 7 and 8 that, at a fixed pH, and total initial Fe(II), that with increasing goethite solids, there was a near linear increase in the concentration of non-oxidisable sorbed Fe(II). This behaviour is consistent with adsorption of Fe(II) to both high and low affinity cation sites on the goethite surface if the Fe(II) adsorbed to the high affinity cation sites is not capable of reducing dissolved Fe(II).

The presence of high and low affinity adsorption sites has been used extensively to explain observed non ferrous cation adsorption onto hydrous ferric oxide (HFO) (Dzombak and Morel, 1990; and references therein), and for Fe(II) adsorptionto HFO (Appelo et al, 2002). However, previous studies of Fe(II) adsorptionto lepidocrocite (Zhang et al, 1992), goethite (Vikesland and Valentine, 2002a,b; Dixit and Hering, 2006), hematite (Liger et al, 1999), and magnetite (Klausen et al, 1995; Charlet et al, 1998), have not found high affinity cation sites to have been necessary to describe the adsorption data.

A5.1.1 Determination of total surface site densities

Figure A5-1 shows the theoretical sorption densities as Fe(II) per nm^{-2} determined from the total sorbed Fe(II) concentration (prior to oxidation) in Experiments 7, 8 and 9. Results are shown against goethite concentration in g L^{-1}.

In all cases, the maximum sorption densities occur at the minimum goethite concentrations and the densities decrease with increasing goethite concentration. When the ratio of goethite to Fe(II) is at its lowest, the

maximum total sorbed Fe(II) densities of 7.7 Fe(II) nm^{-2} was determined in Experiment 8, at a goethite concentration of 0.06 g L^{-1}. Concentrations then decreased to 0.13 Fe(II) nm^{-2} at 50 g L^{-1} of goethite. Due to the lower total Fe(II) sorbed per g of goethite (as determined to be 0.31 Fe(II) nm^{-2} at 1 g L^{-1}), the initial sorbed Fe(II) densities in Experiment 7 are lower than in Experiments 8 and 9.

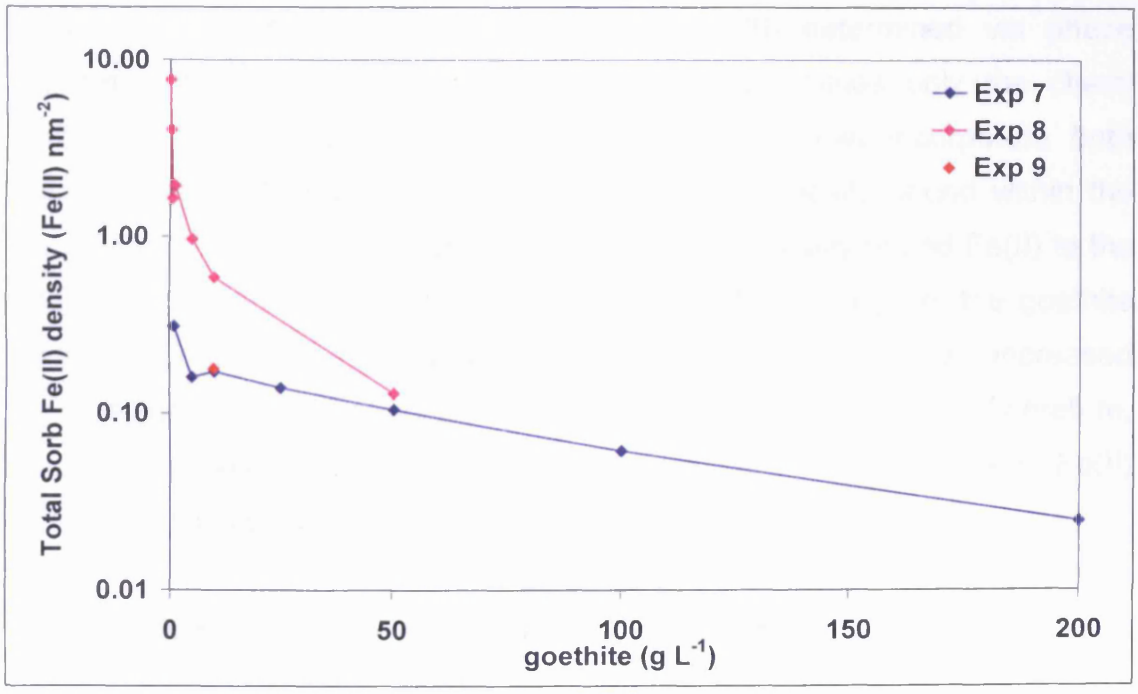

Figure A5-1: Adsorption density determined from the total sorbed Fe(II) in Experiments 7, 8 and 9 (Chapter 10 of main report).

Using a surface area of 15 m^2 g^{-1} (as determined by BET surface area analysis, Table 10.2, Section 10 of main report); the analytically determined total sorbed Fe(II) concentration; and assuming saturation with respect to Fe(II). A total site density can be determined as follows:

Equation A5-1

$$\{Fe(II)_t\} = \frac{[Fe(II)_{Sorb}]N}{[SA][S]}$$

where $\{Fe(II)_t\}$ is the total sorbed Fe(II) density in molecules per nm^{-2}, $[Fe(II)_{Sorb}]$ is the molar concentration of total sorbed Fe(II), N is Avogadro's

constant ($6.022x10^{23}$ mol^{-1}), [SA] is the specific surface area of solid in nm^2 g^{-1}, and [S] is the solids concentration in g L^{-1}. Using Equation A5-1 and the maximum total sorbed Fe(II) density, a maximum total sorption site density of 7.7 sites per nm^{-2} can be calculated for the Bayferrox 930 (goethite).

A site density of 7.7 sites per nm^{-2} assumes a monolayer surface coverage of Fe(II) on goethite. This also assumes that the method for the determination of sorbed Fe(II) (e.g. subtraction of dissolved Fe(II) determined via phase separation from total acid extractable Fe(II)), determines only the chemi sorbed Fe(II) portion. In reality total minus filtered Fe(II) will incorporate both truly chemisorbed Fe(II), as well as Fe(II) electrostatically bound within the stern layer of the EDL. The contribution of electrostatically bound Fe(II) to the total sorbed Fe(II) will vary depending on the surface charge of the goethite particle. Generally, a negative surface charge will favour increased electrostatic adsorption of positively charged ions (including Fe(II)). Therefore, due to the positive charge on the goethite surface, electrostatic Fe(II) adsorption should be negligible.

A5.1.2 Determination of high affinity site densities

If it is assumed that all non-oxidisable sorbed Fe(II) determined in Experiments 7, 8 and 9, (Section 10 of main report) is sorbed to high affinity sorption sites then a relationship between the two can be determined as follows. Using a surface area of 15 m^2 g^{-1} (as determined by BET surface area analysis, Table 10.2, Section 10 of main report); the analytically determined concentrations of surface bound non-oxidised Fe(II); and assuming that strong sites, where present are at near saturation with respect to Fe(II). A high affinity site density can be determined as follows:

EquationA5-2

$$\{Fe(II)_{D}\} = \frac{[Fe(II)_{OxiSorb}]N}{[SA][S]}$$

where $\{Fe(II)_D\}$ is the non-oxidisable sorbed Fe(II) density in molecules per nm^{-2}, $[Fe(II)_{OxiSorb}]$ is the molar concentration of non-oxidisable sorbed Fe(II), N is Avogadro's constant ($6.022x10^{23}$ mol^{-1}), [SA] is the specific surface area of solid in nm^2 g^{-1}, and [S] is the solids concentration in g L^{-1}. Figure A5-2 shows the calculated non-oxidisable sorbed Fe(II) densities as Fe(II) molecules nm^{-2} determined for Experiments 7, 8 and 9 against goethite concentration in g L^{-1}.

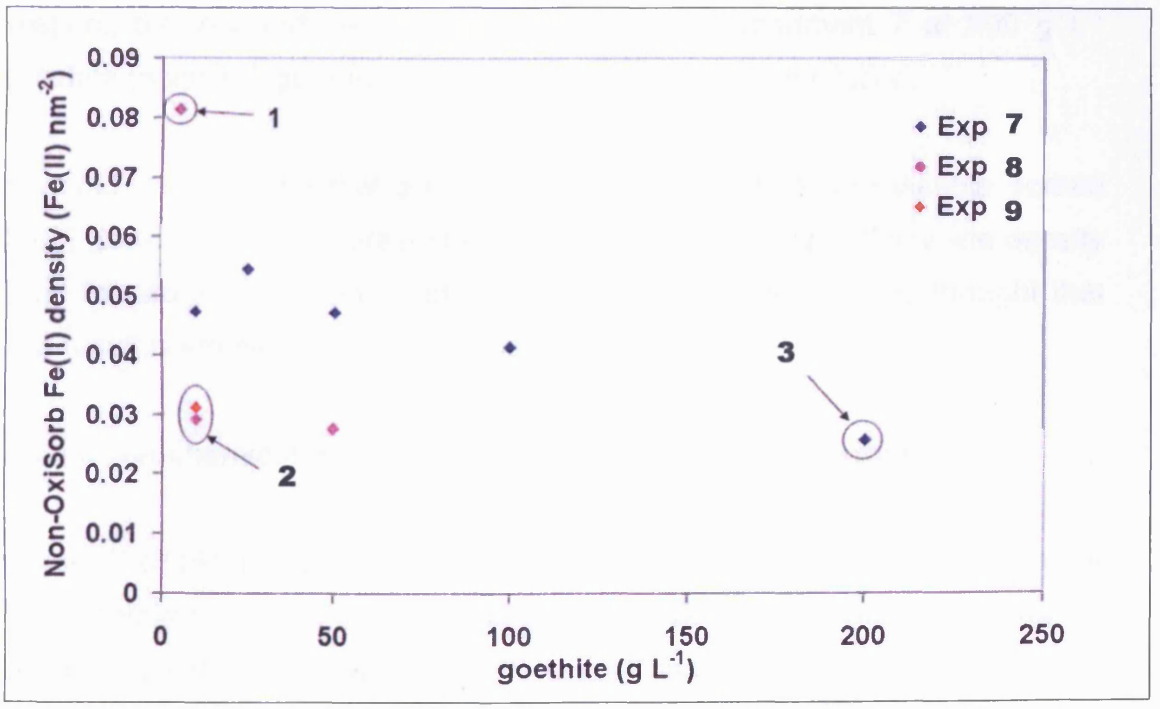

Figure A5-2: Adsorption density of non-oxidised sorbed Fe(II) on the goethite surface

From Figure A5-2 a range for non-oxidisable sorbed Fe(II) densities of 0.026 to 0.081 molecules of Fe(II) nm^{-2} is evident. Point 2 in Figure A5-2 highlights the density of 0.029 and 0.031 Fe(II) nm^{-2} as determined at 10 g L^{-1} goethite in Experiments 8 and 9 which are almost identical despite the different initial Fe(II) conditions. However, strong site densities determined in Experiments 8 and 9, at 10 g L^{-1} goethite (and Experiment 8 at 50 g L^{-1}) are significantly lower than the strong site densities determined at pH 4 for comparable goethite concentrations. This indicates that the weak site compete more favourably for the available Fe(II) at higher pH conditions. The high non-oxidisable sorbed Fe(II) density of 0.081 Fe(II) nm^{-2} determined for

Experiment 8 at 5 g L^{-1} goethite (point 1, Figure A5-2) is unusual and does not correctly fit the model.

In Experiment 7, 8, and 9, adsorption of Fe(II) to the goethite surface was approaching completion at 10 g L^{-1} (Experiments 8 and 9) and 100 g L^{-1} (Experiment 7). The non-oxidisable sorbed Fe(II) density determined at goethite concentrations approaching, and above these concentrations will be below saturation (effectively diluted by an excess of surface sites). In this respect, the low surface density determined in Experiment 7 at 200 g L^{-1} goethite (point 3, Figure A5-2) is probably due to surface dilution.

It would be expected that the maximum determined non-oxidisable sorbed Fe(II) density will best represent the most likely actual high affinity site density (and therefore a site density of 0.08 sites nm^{-2}). However, it is thought that this result is erroneous

A5.1.3 Geochemical modelling of Fe(II) adsorptionto goethite

PhreeqC (Parkhurst and Appello, 1999) was used to model the adsorption of Fe(II) onto the goethite surface in accordance with Experiment 7 (Chapter 10 of main report). The Wateq4F geochemical database (Ball and Nordstrom, 1991) was used with the addition of the aqueous species as shown in Table 3.5 (Chapter 3 of main report), the surface species shown in Table A5-1 and the site densities for strong and weak sites as determined in Section A5.1.1 and A5.1.2 and summarised in Table A5-1. The full PhreeqC input script is included in Appendix 4.4.

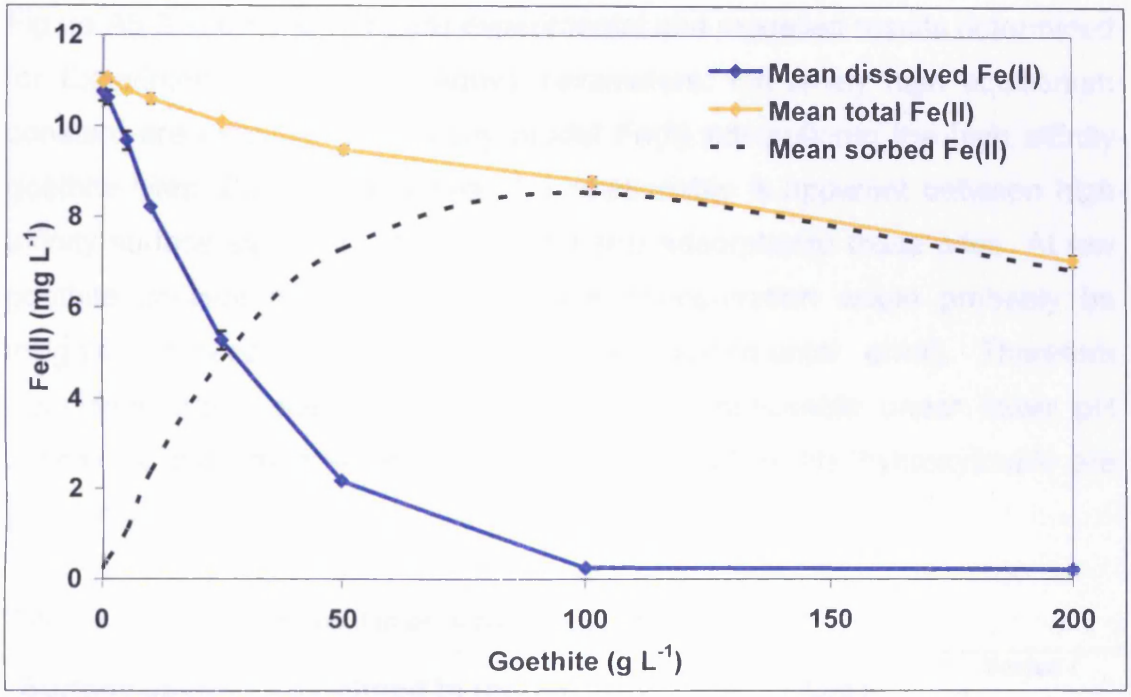

Figure A5-3: Mean filtered and HCl extractable Fe(II) concentrations against goethite concentration in pH 3.92 adsorption Experiment 9 after 24 hours equilibration under N_2.

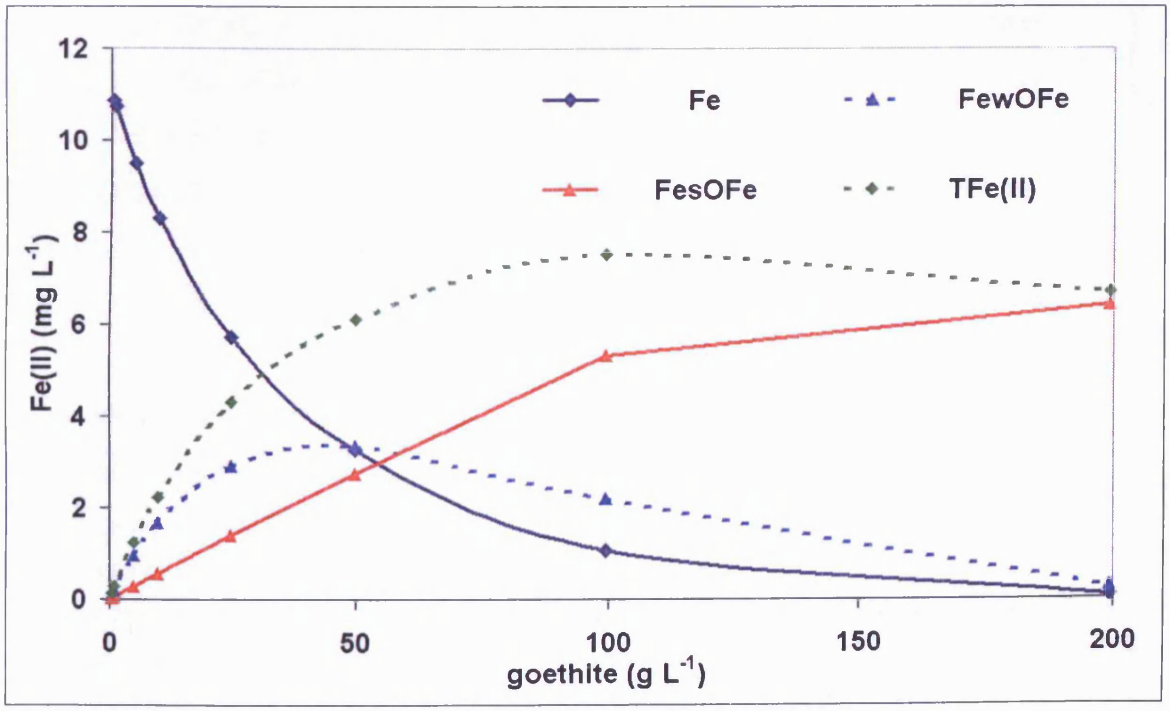

Figure A5-4: Modelled adsorption of Fe(II) at the goethite surface in accordance with Experiment 9

Where FesOFe is Fe(II) adsorbed to high affinity sites on the goethite surface, FewFe is Fe(II) adsorbed to low affinity sites on the goethite surface Fe is the concentration of dissolved Fe(II) and TFe(II) is the total sorbed Fe(II) concentration (both strong and weak site.

Figure A5-3 and A5-4 compare experimental and modelled results determined for Experiment 7 using the above parameters. Extremely high equilibrium constant are required to correctly model Fe(II) adsorptionto the high affinity goethite sites. Due to this a near 1:1 relationship is apparent between high affinity surface site concentration and Fe(II) adsorptionto these sites. At low goethite concentrations, the strong site concentration would probably be insignificant (and within the realms of experimental error). Therefore significant strong site adsorption will only be noticeable under lower pH conditions and where significant concentrations of Fe(III) (hydroxy)oxide are present.

Table A5-1: Parameters used in pH 4 adsorption model

Surface species as defined in model	**Log k [a]**	**Varied / Fixed**
$Gt\_sOH = Gt\_sOH$	0.0	Fixed
$Gt\_sOH + H^+ = Gt\_sOH^{2+}$	7.29 [b]	Fixed
$Gt\_sOH = Gt\_sO^- + H^+$	-8.93 [b]	Fixed
$Gt\_wOH = Gt\_wOH$	0.0	Fixed
$Gt\_wOH + H^+ = Gt\_wOH_2^+$	7.29 [c]	Fixed
$Gt\_wOH = Gt\_wO^- + H^+$	-8.93 [c]	Fixed
$Gt\_sOH + Fe^{+2} = Gt\_sOFe^+ + H^+$	6 [d]	Varied
$Gt\_wOH + Fe^{+2} = Gt\_wOFe^+ + H^+$	1 [d]	Varied
	Sites nm^{-2}	
Low affinity site density	7.063 [e]	Fixed
High affinity site density	0.06 [e]	Fixed

[a] *Surface equilibrium constant*

[b] *As given by Liger et al (1999)*

[c] *Same hydrolysis constants used for high affinity sites as used for low affinity site (reported by Liger et al, 1999)*

[d] *Adjusted manually to best fit the adsorption data as determined in Experiment 9*

[e] *As determined in Section* A5.1.1

A5.2 Site densities determined for lepidocrocite

Due to the experimental procedure, total and non-oxidisable sorbed Fe(II) was not determined directly in the lepidocrocite solid experiments (Experiments 5a and b and 6a and b, Chapter 10 of main report). For this reason determination of non-oxidisable and total sorbed Fe(II) has been treated separately.

A5.2.1 Experiments 5a and 5b – Non-oxidisable surface site densities

A specific BET surface area was not determined for the lepidocrocite used in Experiments 5a and 5b and therefore a definite sorption density cannot be determined for non-oxidisable sorbed Fe(II). However, laser particle sizing was undertaken using a Malvern instruments Version 2.19 long bed MasterSizer X. Determination of surface area using particle sizing data and assuming spherical particles leads to a specific surface area of 1.66 m^2 g^{-1} (using the lepidocrocite density of 4.09 g cm^{-1} as given by Cornell and Schwertmann, 2003). Calculation of surface area in this way generally leads to an underestimation due to the assumption of sphericity, whilst lepidocrocite crystals are acicular in nature. Despite this, it is unlikely that the lepidocrocite used in Experiments 5a and 5b has a surface area significantly greater than either the Bayferrox 930 (goethite) or the Bayferrox 943 (lepidocrocite).

Assuming a surface area of 17 m^2 g^{-1} for the lepidocrocite used in Experiments 5a and 5b (as determined for the Bayferrox 943, lepidocrocite), a non-oxidisable sorbed Fe(II) density of 1.88 Fe(II) nm^{-2} can be determined. This is over 25 times greater than that determined for goethite. In addition, calculation of non-oxidisable sorbed Fe(II) density using the surface area determined using particle sizing data results in a much greater density of 19.2 Fe(II) per nm^{-2}.

A5.2.2 Experiments 6a and 6b – Total surface site densities

Using the method described in Section A5.1.2 and the BET surface area determined for Bayferrox 943 (lepidocrocite), a mean total Fe(II) surface density of 4.41 Fe(II) per nm^{-2} was determined for Experiments 6a and 6b. Comparison of this total sorbed density with the non-oxidisable sorbed Fe(II) density of between 1.88 to 19.2 Fe(II) per nm^{-2} determined for Experiments 5a and 5b shows that, despite the many uncertainties in respect to the surface area of the lepidocrocite used in Experiments 5a and 5b, it is evident that a large proportion of sorbed Fe(II) on the lepidocrocite surface, at circum-neutral pH, is non-oxidisable.

Assuming the saturation of surface sites with Fe(II), a site density of 4.41 sites nm^{-2} can be calculated. This value is higher than the value of 1.67 sites nm^{-2} determined by Zhang et al (1992) using proton saturation data on the same Bayferrox 943 solid. However, the value determined here lies within the range of values reported in Zhang et al (1992) between 1.67 to 9.6 sites per nm^{-2}. The lower site density determined for Experiments 5a and 5b could be due to the differences in the specific surface areas of the two solids, that pre equilibration between the lepidocrocite and Fe(II) was not allowed, or due to the larger experimental uncertainty. In the second case, a degree of competition between adsorption and oxidation of Fe(II) would have taken place (possibly reducing the final sorbed Fe(II) concentration). Unfortunately experiments 6a and 6b were not aerated after adsorption and the proportions of oxidisable and non-oxidisable Fe(II) were not directly determined.

A5.3 Possible implications for heterogeneous Fe(II) oxidation mechanisms

A5.3.1 High affinity sites, low affinity sites and IET

It is clear that the same high affinity site cannot be used to explain the non-oxidisable sorbed Fe(II) in lepidocrocite as was calculated for goethite (as the

density of non-oxidisable Fe(II) is much higher). Zhang et al (1992), found that the adsorption of Fe(II) to lepidocrocite was best described using two surface species (those of ≡FeOFe$^+$, and ≡FeOFeOH), adsorbing to a single surface site type (≡FeO$^-$). Zhang et al (1992) found the dominant surface species to be ≡FeOFeOH and that the contribution of the ≡FeOFe$^+$ species was negligible. The high density of non-oxidisable sorbed Fe(II) as determined for Experiments 5a and 5b could potentially be explained if it is assumed that the ≡FeOFeOH surface species is stable in the presence of dissolved O_2. The single site, two surface species model has been used extensively to describe experimental Fe(II) adsorption data. Examples include, adsorption of Fe(II) onto; lepidocrocite (Zhang et al, 1992), goethite (Coughlin and Stone, 1995), magnetite (Charlet et al, 1998), hematite, and ferrihydrite (Liger et al, 1999).

As discussed in Chapter 3, Liger et al (1999) found the rate of reduction of U(VI) by Fe(II) adsorbed on hematite, to be directly proportional to the modelled concentration of the ≡FeOFeOH surface species and not to the overall concentration of surface Fe(II). This indicates that the ≡FeOFeOH species is an effective reductant for U(VI), and that the ≡FeOFe$^+$ species did not contribute to the overall oxidation. They also showed that no detectable reduction of U(VI) occurred in a homogeneous solution containing dissolved Fe(II).

It is expected that the mechanism of heterogeneous oxidation of Fe(II) by U(VI) is different from the oxidation by dissolved O_2, as U(VI) specifically adsorbs to Fe(III) (hydroxy)oxide surfaces (Liger et al, 1999). Specific adsorption of O_2 is assumed not to take place due to the non-ionic nature of the oxygen dimmer (however, heterogeneous photocatalytic reduction of dissolved O_2 in the presence of Fe(III) (hydroxy)oxides has been reported indicating some possible di-oxygen surface interaction; for examples see Darwent, 1983). Reduction of adsorbed U(VI) by adsorbed Fe(II) indicates that oxidation occurs at spatially distributed sites on the Fe(III) (hydroxy)oxide surface. Park and Dempsey (2005) suggested a semi conductor mechanism for heterogeneous oxidation of Fe(II) by dissolved O_2. In this, oxidation and

reduction occurred at discreetly different sites, and the Fe(III) (hydroxy)oxide surface acted as a semiconductor facilitating electron transfer.

It is known that Interfacial Electron Transfer (IET) can occur between adsorbed Fe(II) and underlying Fe(III) centres in Fe(III) (hydroxy)oxide minerals (Stone and Morgan, 1987; Wehrli, 1990). Studies by Williams and Scherer (2004), Silvester et al (2005), and Larese-Casanova and Scherer (2007) have found spectroscopic evidence for heterogeneous electron transfer between adsorbed Fe(II) and underlying Fe(III). In the case of Silvester et al (2005), and Larese-Casanova and Scherer (2007), almost all of the adsorbed Fe(II) was found to undergo heterogeneous electron transfer forming a surface Fe(III) layer.

As disused in Chapter 3 of the main report, Nano and Strathmann (2006) stated that the Intrinsic stability constants determined by acid base titrations of Fe(II) solutions, in the presence of Fe(III) (hydroxy)oxide, will not have taken into account IET (as proved to exist by Williams and Scherer, 2004; Silvester et al, 2005; and Larese-Casanova and Scherer, 2007). It is possible that the observed proton release (historically attributed to the formation of a hydrolysed Fe(II) surface species) may actually be due to hydrolysis of the fresh IET formed Fe(III) surface species. This is feasible as the log of the first hydrolysis constant for Fe(III) in solution is -2.19 as compared to -9.5 for Fe(II) (Baes and Mesmer, 1976) and a similar relationship would be expected to be observed with surface species. This is supported by the behaviour of non-redox sensitive cations on the Fe(III) (hydroxy)oxide surface. For instance, Dzombak and Morel (1990) (re-processing previous data) found that no hydrolysed surface species were required to model divalent transition metal cations adsorption by hydrous ferric oxide. However, hydrolysed surface species were found to be necessary to model Cr(III) adsorption on HFO (Dzombak and Morel, 1990) and Al(III) adsorption on lepidocrocite (Zhang et al, 1992).

When these findings are applied to the conventional surface model for adsorption of Fe(II) onto Fe(III) (hydroxy)oxides and for the prediction of surface catalysed oxidation rates this will have a marked effect on the prediction of Fe(II) surface speciation. It should also be noted that Larese-Casanova and Scherer (2007) only detected truly adsorbed Fe(II) species (Fe(II) that had not undergone IET) after theoretical monolayer surface coverage had been achieved. However, the residual Fe(II) adsorbed to the surface of the Fe(III) (hydroxy)oxide surface (as found in this study and the study of Park and Dempsey, 2005) seems to indicate that, if it is attributed to IET, that it is unavailable for oxygen reduction. However the residual Fe(II) can also be attributed to an un-reactive $\equiv FeOFe^{+}$ species and to significant hysteresis in surface species equilibration.

A5.3.2 Evidence of semiconductor / IET as a plausible oxidation mechanism

As well as the evidence presented by Park and Dempsey (2005) further evidence can be found in the literature for the above mechanism. For instance, the reliance of the surface catalysed rate on the concentration of the hydrolysed Fe(II) surface species (as observed by Liger et al, 1999; see Figure A5-6), could be due to the increasing degree of thermodynamic stability of magnetite or other mixed valence Fe (hydroxy)oxides as indicated by Jeon et al (2003) and shown in Figure 5-5, would give false evidence for adsorbed Fe(II) hydrolysis. An increasing degree of electron transfer in the newly formed Fe(III) (hydroxy)oxides phase would support the semiconductor mechanism as proposed by Park and Dempsey (2005).

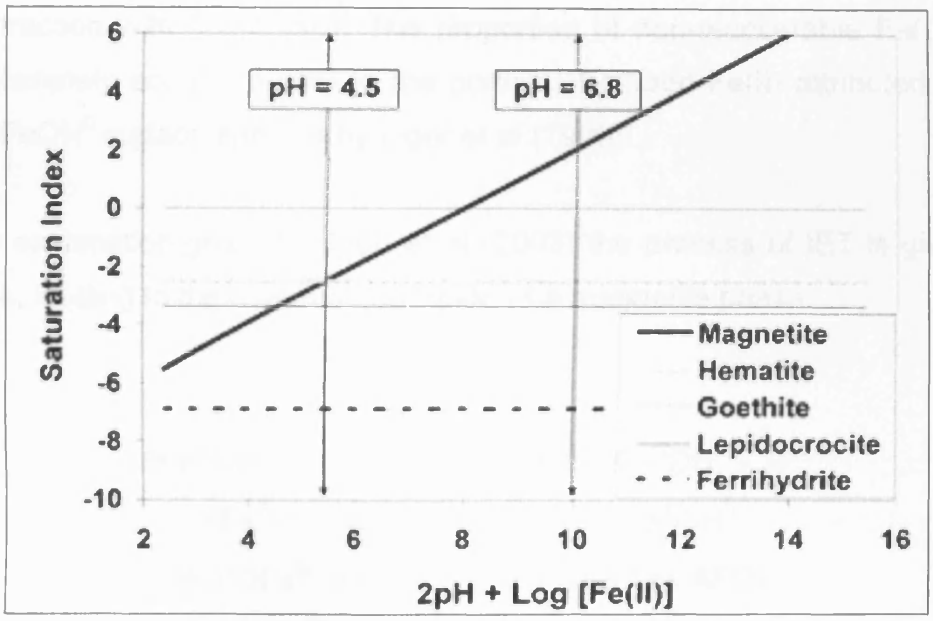

Figure A5-5: Stability of Fe(III) (hydroxy)oxides in the presence of 0.1 – 0.25 mM Fe(II) and hematite in 0.01M NaCl solution at 25°C (from Jeon et al, 2003)

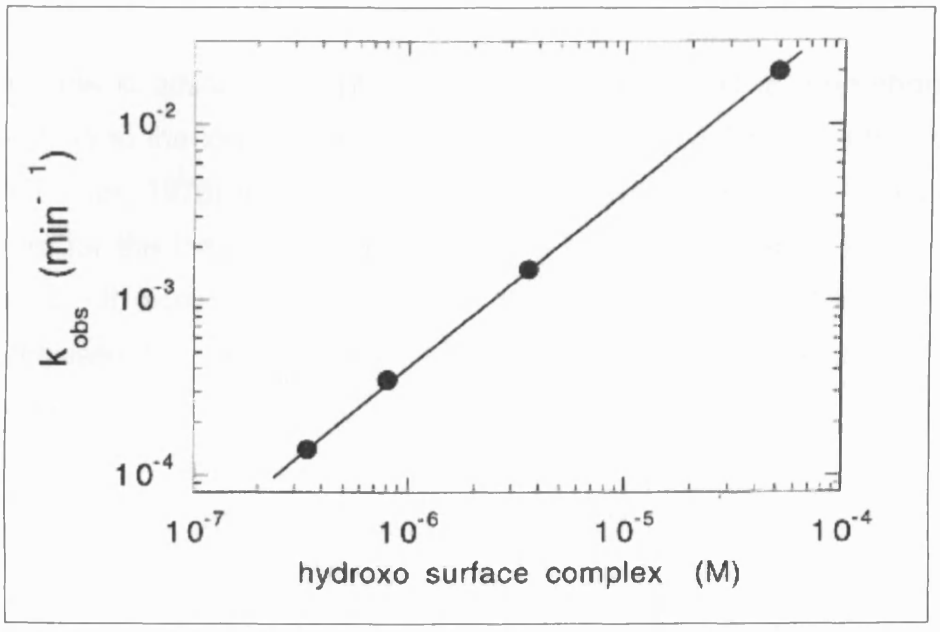

Figure A5-6: Plot of the pseudo first order rate of reduction of U(VI) in min^{-1} by Fe(II) against the calculated concentration of the surface complex ΞFeOFeOH (from Liger et al, 1999)

The pseudo-first-order rate constant for U(VI) reduction by Fe(II) in the presence of hematite nanoparticles depends linearly on the concentration of the hydroxo surface complex.

Furthering the above discussion, Jeon et al (2003) used IET to explain the observed results of the adsorption of Fe(II) onto hematite at pH 6.8. They found a significant portion of the sorbed Fe(II) to be fixed and not recoverable

by extraction with 0.5 N HCl. The proportion of non-recoverable Fe(II) was approximately equal (~50 %) to the portion of sorbed Fe(II) attributed to the $\equiv FeOFeOH^0$ surface species by Liger et al (1999).

In the explanation given by Jeon et al (2003) the process of IET is given as follows, leading to the eventual formation of a magnetite phase:

$$\equiv Fe^{III}OH + FeOH^+ \xleftrightarrow{ads} \equiv Fe^{III}OFe^{II}OH^0 + H^+$$

$$\equiv Fe^{III}OFe^{II}OH^0 \xleftrightarrow{IET} \equiv Fe^{II}OFe^{III}OH^0$$

$$\equiv Fe^{II}OFe^{III}OH^0 \xleftrightarrow{ppt} \equiv Fe^{II}OFe^{III}(\text{as AFO})$$

$$\equiv Fe^{II}OFe^{III}(\text{as AFO}) \xleftrightarrow{MT} \equiv[\text{Magnetite}]$$

Where ads is adsorption, ppt is precipitation and AFO is amorphous ferric oxide. Due to the low aqueous concentration of $FeOH^+$ below pH ~ 8 (Baes and Mesmer, 1976) it is unlikely that direct sorption of $FeOH^+$ species can account for the initial adsorption step and that a hydrolysis step should be included. It would be more feasible that for IET of $\equiv Fe^{III}OFe^+$ It can be hypothesised that the $\equiv Fe^{III}OFe^{II}OH^0$ surface species is a product of IET itself as follows:

$$\equiv Fe^{III}OH + Fe(II) \xleftrightarrow{ads} \equiv Fe^{III}OFe^{II+} + H^+$$

$$\equiv Fe^{III}OFe^{II+} \xleftrightarrow{IET} \equiv Fe^{II}OFe^{III+}$$

$$\equiv Fe^{II}OFe^{III+} + H_2O \xleftrightarrow{Hyd} \equiv Fe^{II}OFe^{III}OH^0 + H^+$$

$$\equiv Fe^{II}OFe^{III}OH^0 \xleftrightarrow{MT} \equiv[\text{Magnetite}]$$

The wealth of evidence for an IET mechanism has significant implications for Fe(II) oxidation as it explains a number of previous findings. For instance in previous studies (Zhang et al, 1992; Charlet et al, 1998; Liger et al, 1999; Silvester et al, 2005) of adsorption of Fe(II) to Fe(III) (hydroxy)oxides, two surface species have generally been invoked to best fit the experimental data, ($\equiv FeOFe^+$ and $\equiv FeOFeOH^0$ respectively. ≡FeO represents a single adsorption

site on the Fe(III) (hydroxy)oxide surface). Also reduction of various pollutants has been shown to occur only at pH above where the $\equiv FeOFeOH^0$ (potential IET / semi conductor) species becomes significant as is apparent with U(VI) (Liger et al, 1999) and U(VI), trichloroethene and tetrachloroethene (Charlet et al, 1998).

A5.3.3 Possible conceptual model of the Fe(III) (hydroxy)oxide surface

Conceptually, three separate sorption behaviours and relative reduction potentials for aqueous Fe(II) on Fe(III) (hydroxy)oxide surface can be used to describe the observed behaviour:

Behaviour	**Reduction potential**
▪ Adsorption of Fe(II) to Low density high affinity sorption sites	Low
▪ Adsorption of Fe(II) to High density low affinity sorption sites	Medium
▪ Adsorption of Fe(II) to High density low affinity sorption sites followed by Interfacial Electron Transfer with underlying Fe(III) centres followed by subsequent formation, and hydrolysis of Surface Fe(III) groups	High

in which case the corresponding relative reduction potentials can be evoked for each mechanism.

A5.3.4 Stability of Fe(II) sorbed to high affinity sites

The proposed Fe(II) species adsorbed to the high affinity sites in the presence of dissolved O_2 have been shown to be highly stable and resistant to oxidation. A recent discussion by Park and Dempsey (2005) highlighted the research of Rosso and Morgan (2002) who showed hydrolysed aqueous Fe(II) species to undergo oxidation via inner sphere mechanism (contrary to

previous belief that oxidation occurred via outer sphere electron transfer for examples see Wehrli, 1999). Park and Dempsey (2005) stated that inner-sphere electron transfer would suggest that the most strongly sorbed Fe(II) would be most resistant to oxidation whilst outer sphere oxidation would favour the more strongly bound Fe(II). This is consistent with the data presented here.

A5.3.5 Evidence against the semi conductor / IET mechanism

Barry et al (1994) studied the heterogeneous catalytic oxidation of Fe(II) on Fe_2O_3, TiO_2, MnO_2, Al_2O_3 and SiO_2 and found that, on an area adjusted basis, oxidation rates on Fe_2O_3, TiO_2 and MnO_2 were approximately equal and three orders of magnitude greater than those for Al_2O_3 and SiO_2. Nano and Strathmann (2006) determined surface complexation parameters for Fe(II) on TiO_2, Al_2O_3 and AlOOH and found adsorption onto TiO_2 was best described by single site adsorption with two surface Fe(II) species ($\equiv TiOFe^+$ and $\equiv TiOFeOH^o$) in agreement with surface Fe(II) species used for Fe(III) (hydroxy)oxides. On AlOOH and Al_2O_3 however no evidence was found for the hydrolysed surface species. The above evidence would appear to support the historic mechanism in which a hydrolysed surface Fe(II) species is formed, unless heterogeneous electron transfer also takes place on TiO_2 (It should also be noted that Fe_2O_3, TiO_2 and MnO_2 can all act a semi conductors; Stumm and Morgan, 1996). However, Nano and Strathmann (2006) found complete recovery of all adsorbed Fe(II) after acidificationto pH 4.5 indicating that IET had not taken place. They also state that TiO_2 enhances the surface hydrolysis of many other divalent metal ions therefore it may be an exception and behave differently to Fe(III) (hydroxy)oxides

A5.2 Conclusions and recommendations

Based on the above discussions the following tentative conclusions can be drawn:

- Intrinsic surface constants determined for the adsorption of Fe(II) to goethite do not adequately explain the observed adsorption at pH 4 in the presence of high concentrations of goethite using only one surface adsorption site type.
- The results shown here are best described using a two site adsorption model as previously described by Dzombak and Morel, 1990 and references therein. These types of sites have been used extensively for the description of experimental data for the adsorption of divalent metal ions on hydrous ferric oxide. However, high and low affinity type sites have not previously been reported for goethite or lepidocrocite.
- From the data presented a strong adsorption site density of ~0.034 sites nm^{-2} can be determined for the Bayferrox 930 (goethite) solid used in the pH 4 adsorption-oxidation experiments and the pH 6 heterogeneous oxidation experiment.
- It has been shown that the incorporation of a site type with a very high affinity for Fe(II) (log k ~ 6) and possibly other cations (as used by Dzombak and Morel, 1990) at a surface concentration of 0.067 sites nm^{-2} can be used to model fit the experimental data. This was determined by assuming that the Fe(II) adsorbed to high affinity sites is not available for oxygen reduction (as has been indicated by previous authors). Unfortunately no attempt was made to determine surface hydrolysis constants for high affinity cation sites on the goethite surface. Therefore the same hydrolysis constants were used for high affinity sites as were used for low affinity sites. Therefore the model presented here is only meant to indicate the viability of the theory and is not meant to be definitive. Further work is required to correctly determine Fe(II) adsorptionto goethite (and other Fe(III) (hydroxy)oxide surfaces) in light of the current evidence.

Clearly more work must be done to determine the plausibility of the mechanisms discussed here. However, they are plausible mechanisms and may well present a potential explanation for the observed behaviour of Fe(II) on the surface of Fe(III) (hydroxy)oxides. What is apparent is that the

likelihood of a single mechanisms that explains the behaviour of Fe(II) across the entire pH range is unlikely and that it is more likely a composite of a number of mechanisms the influence of each is governed by solution pH and surface area. Of course other factors may well influence this such as competing cations or complexing ligands. Also, as indicated in a personal communication with Professor S Banwart, in the experiments conducted in the present study, contamination with carbonates cannot be ruled out and until the effects of these are known the results of experiments undertaken in this study cannot be satisfactorily prove or disprove these mechanisms. However, I do think the results of these experiments open up a line of investigation that should be eagerly pursued.